MARINE POLLUTION - EMERGING ISSUES AND CHALLENGES

EDITED BY: Elisabeth Marijke Anne Strain, Laura Airoldi, Kenneth Mei Yee Leung, Allyson O'Brien and Camille White

PUBLISHED IN: Frontiers in Marine Science

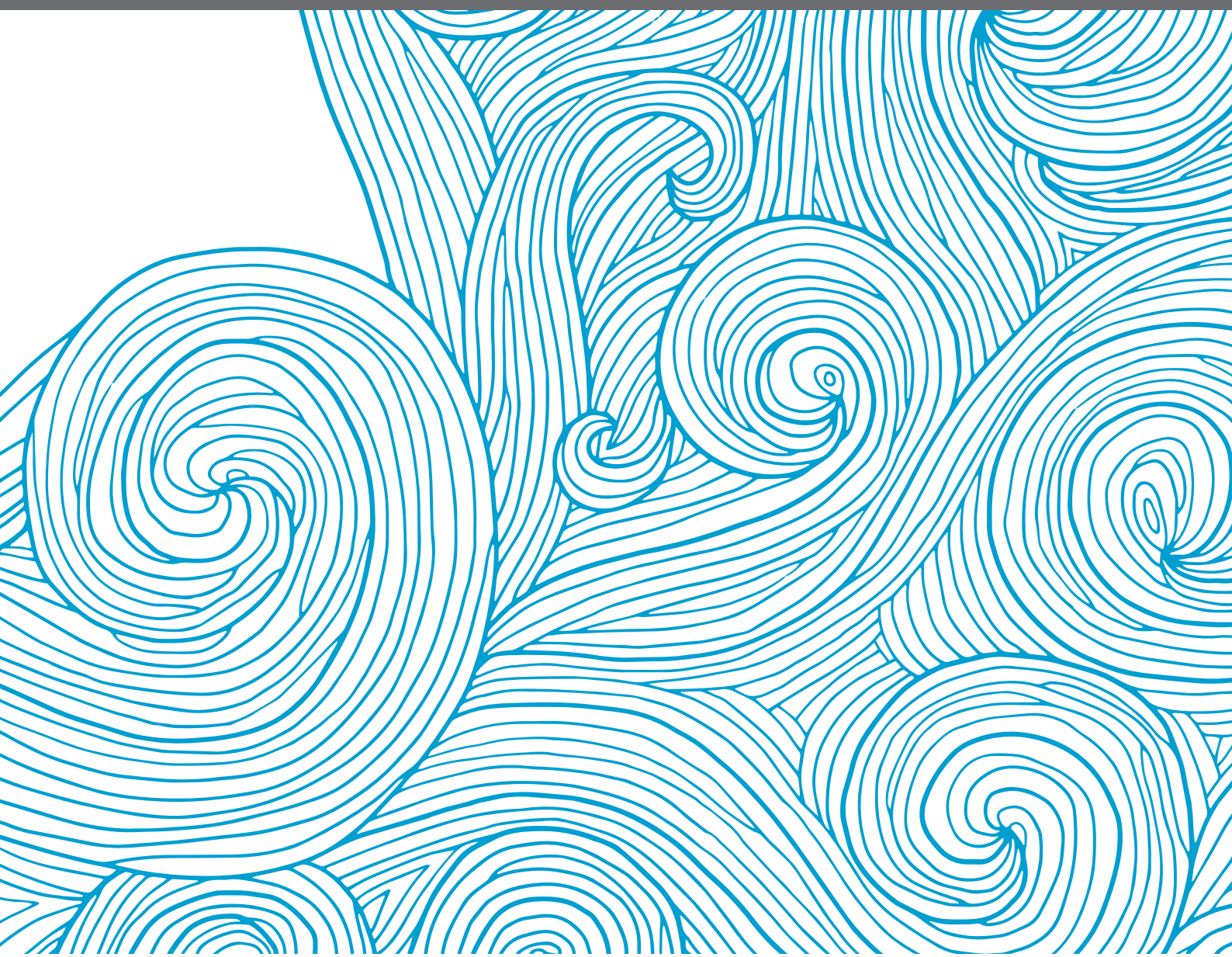

frontiers Research Topics

frontiers

ISSN 1664-8714
ISBN 978-2-88976-490-7
DOI 10.3389/978-2-88976-490-7

About Frontiers

Frontiers is more than just an open-access publisher of scholarly articles: it is a pioneering approach to the world of academia, radically improving the way scholarly research is managed. The grand vision of Frontiers is a world where all people have an equal opportunity to seek, share and generate knowledge. Frontiers provides immediate and permanent online open access to all its publications, but this alone is not enough to realize our grand goals.

Frontiers Journal Series

The Frontiers Journal Series is a multi-tier and interdisciplinary set of open-access, online journals, promising a paradigm shift from the current review, selection and dissemination processes in academic publishing. All Frontiers journals are driven by researchers for researchers; therefore, they constitute a service to the scholarly community. At the same time, the Frontiers Journal Series operates on a revolutionary invention, the tiered publishing system, initially addressing specific communities of scholars, and gradually climbing up to broader public understanding, thus serving the interests of the lay society, too.

Dedication to Quality

Each Frontiers article is a landmark of the highest quality, thanks to genuinely collaborative interactions between authors and review editors, who include some of the world's best academicians. Research must be certified by peers before entering a stream of knowledge that may eventually reach the public - and shape society; therefore, Frontiers only applies the most rigorous and unbiased reviews.
Frontiers revolutionizes research publishing by freely delivering the most outstanding research, evaluated with no bias from both the academic and social point of view. By applying the most advanced information technologies, Frontiers is catapulting scholarly publishing into a new generation.

What are Frontiers Research Topics?

Frontiers Research Topics are very popular trademarks of the Frontiers Journals Series: they are collections of at least ten articles, all centered on a particular subject. With their unique mix of varied contributions from Original Research to Review Articles, Frontiers Research Topics unify the most influential researchers, the latest key findings and historical advances in a hot research area! Find out more on how to host your own Frontiers Research Topic or contribute to one as an author by contacting the Frontiers Editorial Office: frontiersin.org/about/contact

MARINE POLLUTION - EMERGING ISSUES AND CHALLENGES

Topic Editors:
Elisabeth Marijke Anne Strain, University of Tasmania, Australia
Laura Airoldi, University of Padova Chioggia Hydrobiological Station, Italy
Kenneth Mei Yee Leung, City University of Hong Kong, SAR China
Allyson O'Brien, The University of Melbourne, Australia
Camille White, University of Tasmania, Australia

Citation: Strain, E. M. A., Airoldi, L., Leung, K. M. Y., O'Brien, A., White, C., eds. (2022). Marine Pollution - Emerging Issues and Challenges. Lausanne: Frontiers Media SA. doi: 10.3389/978-2-88976-490-7

Table of Contents

frontiers | Frontiers in Marine Science

EDITORIAL
published: 08 June 2022
doi: 10.3389/fmars.2022.918984

Editorial: Marine Pollution - Emerging Issues and Challenges

Elisabeth Marijke Anne Strain[1,2*], *Racliffe Weng Seng Lai*[3], *Camille Anna White*[1], *Stefania Piarulli*[4], *Kenneth Mei Yee Leung*[3,5], *Laura Airoldi*[6,7] *and Allyson O'Brien*[8]

[1] Institute for Marine and Antarctic Studies, University of Tasmania, Hobart, TAS, Australia, [2] Centre for Marine Socioecology, University of Tasmania, Hobart, TAS, Australia, [3] State Key Laboratory of Marine Pollution and Department of Chemistry, City University of Hong Kong, Kowloon, Hong Kong SAR, China, [4] Department of Climate and Environment, Stiftelsen for industriell og teknisk forskning (SINTEF) Ocean, Trondheim, Norway, [5] Southern Marine Science and Engineering Guangdong Laboratory (Zhuhai), Zhuhai, China, [6] Chioggia Hydrobiological Station "Umberto D'Ancona", Department of Biology, University of Padova, UO CoNISMa), Chioggia, Italy, [7] Department for the Cultural Heritage, University of Bologna, Ravenna, Italy, [8] School of BioSciences, University of Melbourne, Parkville, VIC, Australia

Keywords: nutrient enrichment, heavy metals, persistent organic pollutants, plastic debris, artificial structures, multiple stressors, management options

Editorial on the Research Topic

Marine Pollution - Emerging Issues and Challenges

OPEN ACCESS

Edited by:
Ilaria Corsi,
University of Siena, Italy

Reviewed by:
Julian Alberto Gallego Urrea,
Horiba Europe, Sweden
Julian Blasco,
Spanish National Research Council (CSIC), Spain

****Correspondence:***
Elisabeth Marijke Anne Strain
elisabeth.strain@utas.edu.au

Specialty section:
This article was submitted to Marine Pollution, a section of the journal Frontiers in Marine Science

Received: *13 April 2022*
Accepted: *16 May 2022*
Published: *08 June 2022*

Citation:
Strain EMA, Lai RWS, White CA, Piarulli S, Leung KMY, Airoldi L and O'Brien A (2022) Editorial: Marine Pollution - Emerging Issues and Challenges. Front. Mar. Sci. 9:918984. doi: 10.3389/fmars.2022.918984

INTRODUCTION: CLASSIC AND EMERGING RESEARCH TRENDS IN MARINE POLLUTION

With the rapid development of human society, there is an increasing diversity and geographic spread of substances being released into the marine environment. Above threshold values these substances can have negative effects on the biological component of these systems and are therefore classified as pollutants (Cabral et al., 2019). Pollutants can be introduced to marine environments directly through human activities, indirectly through runoff such as discharges of untreated or partially treated wastewater, and or by exchange with the atmosphere (Noone et al., 2013). The relative contribution of different pollutants from these pathways varies substantially between substances and also spatially and temporally (Bierman et al., 2011). In this editorial we conducted a review of current and emerging trends in marine pollution research based on a keyword search of the literature in Web of Science. Our aim was to provide context to the articles published in the special issue.

Research on marine pollution is an important component of marine science, with the number of studies on this topic rapidly increasing through time (**Figure 1A**). Most of these studies have been conducted in shallow nearshore environments of sheltered estuaries and bays where human activities are concentrated (Halpern et al., 2008) whereas only very few studies have been conducted in open oceans and deep seas (Van Cauwenberghe et al., 2013; Cózar et al., 2014; Tournadre, 2014). The research effort is not evenly distributed across the globe, with much of the published literature being produced in China, followed closely by the USA and various countries in Europe (**Figure 1B**). This reflects the substantial impacts of these nations on the marine environment (Halpern et al., 2019; Bhuyan et al., 2021) and their leading role in producing scientific outputs (Marginson, 2021). Alarmingly, recent research on pollution in many developing regions such as Africa, Asia, and South America (**Figure 1B**), has demonstrated high levels of pharmaceuticals (Wilkinson et al., 2022). Hence, more research on marine pollution in these little-

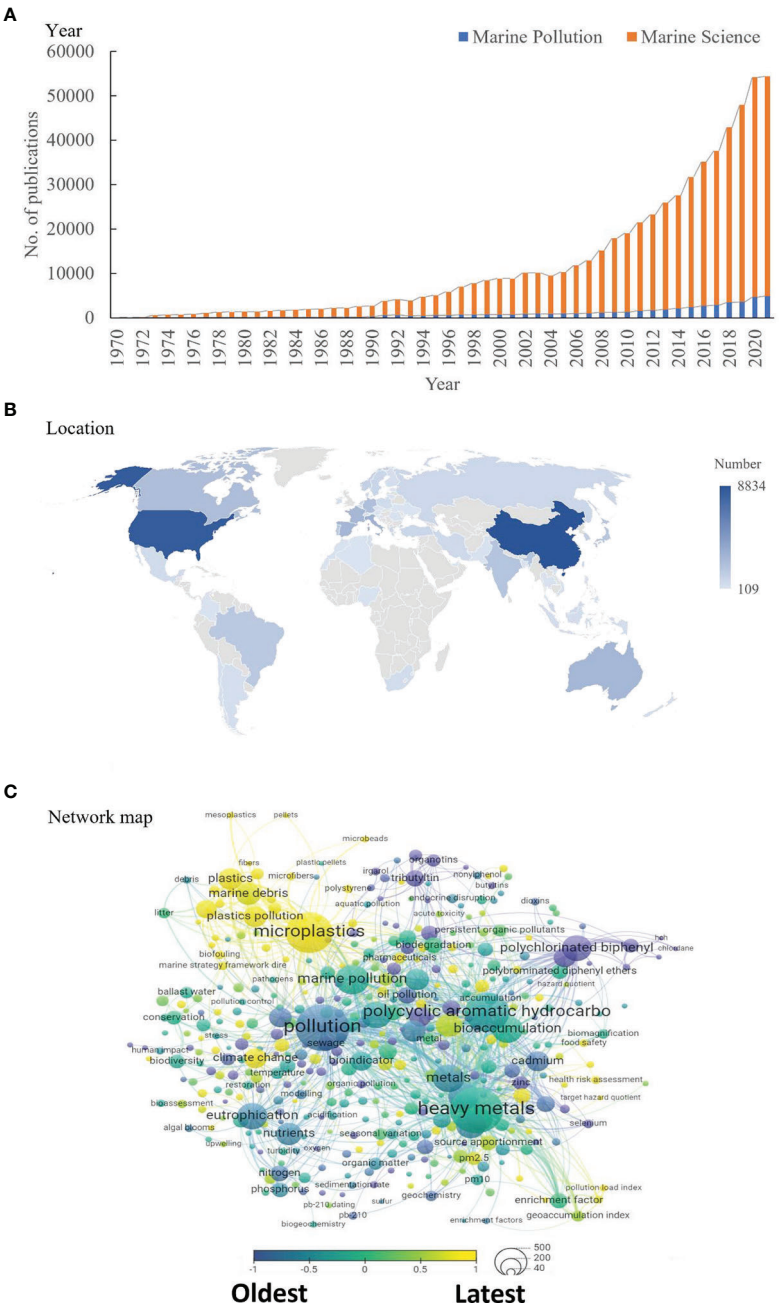

FIGURE 1 | The total number of studies **(A)** on marine pollution and marine science by year and **(B)** by country (with more than 100 results) and **(C)** a network map (online version at https://bit.ly/31Z88uo) showing the most research topics in marine pollution during 1970 to 2021 based on keyword searches in the search engine Web of Science. The search for studies on "marine pollution" and "marine science" was conducted on 23rd August 2021. A total of 39,550 research articles on "marine pollution" and 568,755 on "marine science" were identified.

studied regions is necessary to gain a greater understanding of the spatial footprint of anthropogenic activities.

Traditionally, research on marine pollution has focused on studying how the release of hazardous or waste substances in particular heavy metals and nutrients affects individual organisms (O'Brien and Keough 2014). More recently, however, research on marine pollution has highlighted how the input and spread of other substances including debris, microplastics, antibiotics and persistent organic pollutants (POPs) Shamskhany et al., antibiotics (Dahms, 2014) can influence populations, assemblages and ecosystems (**Figure 1C**). The range of topics in this special issue suggests the definition for marine pollution should be expanded to include the individual and interactive impacts of these substances with other forms of pollution from energy transfer (e.g., heat, noise

and light) and artificial structures (e.g., sea cages, oil rigs, coastal infrastructure) or from the construction of marine artificial structures (e.g., sea cages, oil rigs, coastal infrastructure).

Melbourne-Thomas et al.; Georgiades et al.. We also highlight that the high uncertainty about effects of multiple substances entering the marine environment has important repercussions for developing effective monitoring, management, and mitigation solutions.

EFFECTS OF POLLUTANTS AND THEIR IMPACTS

Nutrient Enrichment

High nitrogen and phosphorus concentrations are common sources of pollution in the marine environment, with inputs derived from various point and diffuse sources. Resultant eutrophication has many undesirable ecological effects, for example phytoplankton blooms and/or shifts toward noxious cyanobacteria (Wurtsbaugh et al., 2019), replacement of ecosystem engineers including kelps and scleractinian corals with structurally less complex foliose or turf-algae (D'Angelo and Wiedenmann, 2014; Strain et al., 2014) and increases in the occurrence and severity of marine diseases. Most devastatingly, nutrient pollution has been linked to low levels of dissolved oxygen in marine environments, or hypoxia conditions which create large areas devoid of macrofauna, due to emigration or mortality, leading to the creation of dead zones (Altieri and Diaz, 2019). Understanding the impacts of nutrients, through time and across multiple locations and marine habitats remains an ongoing challenge in marine science.

Heavy Metals

Heavy metals (the group of metals and metalloids of relatively high atomic mass, that can cause toxicity problems) are primarily brought into marine environments through industrial, urban runoff and shipping activities, where they disperse into the water column or are incorporated into sediments (Birch, 2017). Some metals such as Fe, Zn and Cu play vital roles in marine organism's metabolism and only become toxic at high concentrations. Other metals, including Hg, Pb, Cd and Cr are detrimental to marine organisms even at low concentrations. As pollutants, heavy metals have known effects on the physiological and individual performance of seaweeds (Baumann et al., 2009; Costa et al., 2020), invertebrates (Fowles et al., 2018) and invertebrates with knock on effects on fishes Tamburini et al. In sheltered locations, heavy metals are particularly hazardous pollutants in the marine environment because they do not degrade and can bioaccumulate through the food chain with potential detrimental effects to human health *via* consumption of contaminated seafood (Lavoie et al., 2018). Rare earth elements (e.g. lanthanides and + yttrium) and nanoparticles of Ag, ZnO and TiO have also been increasingly detected in the marine environment (Gwenzi et al., 2018). However, the extent and impact of these rare elements and nanoparticles on marine organisms and ecosystems have yet to be determined (Piarulli et al., 2021).

Persistent Organic Pollutants

POPs are a broad range of organic chemicals that are persistent, bioaccumulative and toxic substances in the environment and include some polycyclic aromatic hydrocarbons (PAHs). They are a relatively diverse group of pollutants derived from multiple sources. For example, PAHs are mainly derived from activities related to the petrochemical industry, combustion, and oil spills (Ghosal et al., 2016). These chemicals have an extremely long half-life in the marine environment and have been found from coastal beaches to the deepest ocean trenches (Jamieson et al., 2017). POPs accumulate in the tissues of marine flora and fauna, where they may cause damage, with effects exacerbated *via* bioaccumulation and biomagnification in marine food webs (Andrady, 2011; Matthies et al., 2016). There is increasing scientific interest in the presence of newly identified POPs in the marine environment such as perfluoroalkyl and polyfluoroalkyl substances, polychlorinated naphthalenes, flame retardants and paraffins (e.g. Lee et al.). Often the use of these emerging compounds has not regulated and their effects on the surrounding marine environment are still being investigated.

Plastic Debris

Inefficient land-based waste management and human negligence have led anthropogenic litter entering and accumulating in the marine environment. Plastic litter is omnipresent across polar regions to the equator and persistent in the marine environment both in the water column and sediments (Barnes et al., 2009; Rosevelt et al., 2013). More than 200 species, including marine megafauna such as seabirds, cetaceans, pinnipeds, and sea turtles, are negatively affected by large plastic debris through entanglement or ingestion (Derraik, 2002; Gregory, 2009). The smaller particle size may pose greater risk, as the particles can be ingested by a wider range of invertebrate and vertebrate species, enter the food chain and transfer across different trophic levels (de Souza Machado et al., 2018). Recent research has demonstrated that microplastics (plastic particles between 1 μm and 5 mm) can have physical, chemical, and biological impacts on organisms either directly or indirectly through associated additives (plasticisers) and adsorbed chemical contaminants. Adverse effects include physical damages such as obstructions, abrasions and inflammation and physiological alterations such as decreased food consumption, weight loss, decreased growth rate and fecundity and energy depletion (Zhang et al., 2019). Despite growing research interest, the broader ecological effects of macro-, micro- and nano plastic debris in different marine compartments and ecosystem remain largely unexplored. Also, the role of different biological processes in affecting the dynamics and fate of these particles necessitates further study.

Artificial Structures

Urbanisation of coastal areas (Small and Nicholls, 2003; Strain et al., 2019), and growth in the blue economy have resulted in the proliferation of artificial structures (e.g. breakwaters, reefs,

sewage/storm water outflows and offshore platforms etc) in the marine environment (Bugnot et al., 2021). Artificial structures are not traditionally considered a pollutant, but they are included in the broader definition of pollution established by this special issue (see definition above). Artificial structures include contamination associated with the discharge of toxins and nutrients and increased noise and light pollution (Heery et al., 2017; Komyakova et al., 2022). These structures frequently destroy and fragment natural habitats but also provide novel surfaces for colonising marine organisms (Firth et al., 2016). Artificial structures can facilitate the establishment and spread of non-native species (Airoldi et al., 2015, https://research-topic-management-app.frontiersin.org/manage/17385/manuscript) and in some cases form ecological traps which reduce organism fitness (Swearer et al., 2021) and reduce ecological connectivity by acting as physical barriers to the movement of organisms within and among habitats (Bishop et al., 2017). Globally it was estimated that in 2018 the footprint of marine artificial structures $1.0–3.4 \times 10^6\,km^2$ was greater than the extent of some natural vegetated habitats and predicted to increase by at least 23% over the next twenty years (Bugnot et al., 2021).

EFFECTS OF MULTIPLE POLLUTANTS AND SECONDARY FEEDBACK LOOPS

Given the broad connectivity of the marine environment, there is the general assumption that various forms of marine pollution will be in some way interactive (Crain et al., 2008; Black et al., 2015). As the diversity of pollutants in the marine environment increases, so does the complexity of interactions. Thus, our ability to interpret and manage such complex and interacting impacts should be enhanced as well. Complex interactions occur between mixtures of chemicals (Belden et al., 2007) but also between artificial infrastructure, nutrients, and other sources of pollution (e.g. Rivero et al., 2013). Although studies on the effect of multiple pollutants and secondary or indirect pathways are complex, their outcomes are more realistic and aligned with management actions (Adams, 2005)

The current challenge is to establish a framework to assess the effects of multiple pollutants that is realistic and can be used to guide management decisions. This is partly constrained by the lack of research on multiple pollutants in urban marine and estuarine environments (Van den Brink et al., 2019). On a global scale, research has focussed over the last 10 years on understanding the effects of individual sources of pollutants (O'Brien et al., 2019), occasionally two pollutants (Black et al., 2015) but rarely more (e.g. Martin et al., 2021). Climate change, although not a source of pollution, is also stressor that can influence the effects of pollution (e.g. Wang et al., 2019) and should also be considered a component in the context of multiple stressors and marine pollution research (Cabral et al., 2019, https://research-topic-management-app.frontiersin.org/manage/17385/manuscript).

The effects of multiple pollutants are commonly categorised as additive, antagonistic or synergistic (Piggott et al., 2015). Additive effects are those where the combined effect is equal to the sum of their individual effects, antagonistic effects occur when the interactions between stressors result in a lesser combined effect and synergistic effects result in an amplification of effects (Orr et al., 2020). The effects of marine pollutants can accumulate over time (Jackson et al., 2001) or occur at different frequencies and intensities making the overall impacts difficult to predict (e.g. Blasco et al., 2016). A recent review identified synergistic or antagonistic interactions for specific chemical combinations were not consistent (Martin et al., 2021) and often did not exceed the magnitude of the effect predicted by an additive model (e.g. Boobis et al., 2011).

Another option for understanding the effects of multiple pollutants is to consider the severity of the impact based on the magnitude of the interactive effects. The magnitude of the effect could be measured by the extent of the deviation from the expected additive model (Martin et al., 2021) or other null models depending on the stressor mode of action or species sensitivities (Schäfer and Piggott, 2018). For example, an antagonistic interaction is predicted for nutrients and metal contamination whereby the effects of the individual pollutants are greater than the interactive effects. This type of interactive effect has been shown to occur in coastal marine microbial communities. However, the direction and magnitude of the antagonistic interactive effect can change at higher levels of biological organisation. This approach is useful as it can identify different magnitudes of the additive, antagonistic or synergistic interactive effects, and potentially more flexible to multiple sources and definitions of marine pollution.

APPROACHES TO MONITORING MARINE POLLUTION

The development of novel techniques and methods is critical for monitoring the impacts of marine pollutants. Studies on the effects of emerging and multiple pollutants often require innovative models, equipment, or methods to detect impacts. Here we briefly provide an overview of some of the emerging approaches and techniques that are currently being used or proposed for monitoring marine pollutants.

Environmental Risk Assessment

Conventional quantitative environmental risk assessment (ERA) focuses on characterising the exposure and effect of a specific chemical substances in the environment, with their ratio used to estimate risk (Environmental Risk Assessment, 1998). In the marine environment, however, organisms are simultaneously exposed to a cocktail of various anthropogenic chemicals. This discrepancy between the real environment and ERA presents a challenge for monitoring and management (Backhaus and Faust, 2012; Kortenkamp and Faust, 2018). Recent studies have developed more complicated ERA frameworks such as (1) summing up the toxicity thresholds derived from the species sensitivity distribution based on either

the concentration addition or independent action models and (2) deriving the mixture toxicity for each species separately based on the mode of action before fitting species sensitivity distribution and deriving the overall toxicity threshold. However, none of methods consider the potential non-additive interactions among the environmental pollutants (Warne and Hawker, 1995; Belden et al., 2007). Therefore, future ERAs probably require a case-by-case assessments of the interactions between chemicals and other sources of pollution by trained specialists, instead of using standard protocols for risk assessments (Heys et al., 2016).

Molecular Approaches and eDNA

Metabolomics, proteomics, and transcriptomics are, high-throughput technologies that are used for environmental genomics and eDNA monitoring (Leung, 2018, https://research-topic-management-app.frontiersin.org/manage/17385/manuscript). These approaches can be used to detect individual-level responses (e.g. metabolomics; Jeppe et al., 2017; Sinclair et al., 2019), populations changes (e.g. eDNA; Smart et al., 2015), and occasionally community-level effects of pollution (e.g. metabarcoding; Chariton et al., 2010). More recently, novel applications that combine multiple molecular approaches to detect the effects of pollution on ecosystem functioning have emerged. For example, using metabolomics combined with metabarcoding to detect the effects of pollution on microbial community function (Morris et al., 2018). Despite the broad knowledge and potential use of molecular approaches to detect impacts that align with management goals, barriers adopting them in routine monitoring and pollution assessments remain (Cordier et al., 2021).

Unmanned Platforms

Mooring, satellites, and vehicles have great potential to measure the effects of marine pollutants over a wide range of spatial and temporal scales, and in difficult to assess environments including open oceans and deeper waters (Verfuss et al., 2019; Salgado-Hernanz et al., 2021). However, much of the research on developing and testing sensors has been targeted to specific pollutant types and terrestrial settings (e.g. detection of litter along beaches) (Salgado-Hernanz et al., 2021). In water, the application of these newly developing technologies is often limited to specific locations and depths, and subject to biofouling and maritime growth, which can influence the measurement outcomes (Verfuss et al., 2019; Salgado-Hernanz et al., 2021, Part et al.). Further development of sensor technologies and subsequent reductions in costs, will allow these platforms to become increasingly important monitoring tools in marine environments.

Artificial Intelligence/Machine Learning

Machine learning, a subset of artificial intelligence, refers to the ability of machines to learn and understand relationships between inputs and outputs from a full set of representative training samples (He et al., 2021). Monitoring approaches that use machine learning to monitor marine pollution are still relatively conceptual, although it is a field of research where progress is being made very quickly. There have been successful applications in the context of oil spill detection (Al-Ruzouq et al., 2020), benthic monitoring (Mohamed et al., 2018) and monitoring of fish populations (Ditria et al., 2021) while machine learning has been incorporated widely into bioinformatics associated with molecular approaches (Cordier et al., 2017; Fruhe et al., 2021). There is clear application where monitoring techniques generate thousands of images or video, or where large data sets are produced. With ongoing improvement and development in computing and technology, there is clear potential for progress in this space.

SOLUTIONS FOR MARINE POLLUTIONS

Reducing marine pollution is a global challenge that needs to be addressed for the health of the oceans and the maintenance of its ecosystem goods and services. Solutions to reduce marine pollution at local scales can be applied singularly or in combination and include 1) detection and prevention; 2) sustainable management; 3) habitat restoration and reconciliation. We suggest a combined approach may be more appropriate given the broadening definition of marine pollution and the complexity of interactions. Here we explore the application of these strategies in the context of nutrients enrichment, plastic litter, and artificial structures. More research in this area is needed to address the complex interactions between marine pollutants and the global nature of impacts.

Case Study 1: Nutrient Pollution

Chesapeake Bay is an example of where the combined approach of scientific monitoring, sustainable management, and targeted habitat restoration has successfully been implemented to restore estuarine health (Lefcheck et al., 2018). Concerns about the loss of large areas of submerged aquatic vegetation (SAV) within the estuary during the 1970s and 80's, resulted in development of a key goals and comprehensive scientific monitoring program for monitoring changes in water quality through time (Orth et al., 2017). Local management measures which included reduction of land-based nonpoint sources, improved design of watersheds, technological implementation of sewage treatment plants and restoration of the SAV area in the Bay were applied by multiple agencies to reduce the amount of nutrients and sediments entering and concentrating in the Bay (Orth et al., 2017; Lefcheck et al., 2018) A scientific monitoring program developed and reported on in an "Annual Ecological Report Card" (AERC) that provides quantitative measurements of (1) water quality through chlorophyll-*a*, dissolved oxygen, and Secchi depth assessments (2) biological measures of phytoplankton diversity and abundance and (3) quantifies the area of SAV which are combined to determine performance-driven numeric grades of the ecosystem health (Bay Health Index) (Williams et al., 2009). The AERC is important for communicating the results of the monitoring to decision-makers and stakeholders (Williams et al., 2009). Through time,

the AERC has been used to document substantial improvements in water quality and recovery of tens of thousands of hectares of SAV in the estuarine with flow on benefits for biodiversity and other ecosystems services (Lefcheck et al., 2018).

Case Study 2: Plastic Debris

Globally marine plastic pollution has become a significant environmental concern for multiple stakeholder groups (Seltenrich, 2015). Effective solutions to reduce marine plastic debris are still under development at international level, but focus on combing detection, prevention and sustainable management using four main categories (Chen, 2015):

1. Source prevention based on the 3R rule (i.e. reuse, reduce and recycle) and accompanied by land-based management actions to prevent plastic debris to enter the marine environment;
2. Removal based on the environmental monitoring of the marine debris followed by local initiatives at both at institutional and citizenship for plastic clean-up;
3. Regulative and sustainable management frameworks developing and implementing regulations for production of single use plastics, litter disposal, reuse and recycling;
4. Educational which covers campaigns to raise societal awareness and economic/incentive approaches.

The beaches of Cijin, Kaohsiung (Taiwan) have demonstrated that the reduction, reuse and recycling of plastics in terrestrial environments can abated the transfer of these pollutants into marine environments (Liu et al., 2013). In 2001, plastic constituted the 21.1% of household waste (Liu et al., 2013). In 2002, TEPA developed the Plastic Restriction Policy under the Waste Disposal Act which prohibited the use of plastic shopping bags and disposable plastic tableware in all government agencies and public facilities. Through time, the quantity of shoppers using recyclable shopping bags increased considerably, resulting in a substantial reduction of plastic waste. In 2002 and 2005, Taiwan implemented the Resource Recycling Act (RRA) and the Compulsory Trash-sorting Policy (CTP) which required the use of recycling bins in all public places and encouraged users to sort their waste. An economic penalty of 1200–6000 NT was applied for unsorted trash. These policies reduced the waste disposal rate from 2001 to 2010, by 50% (from 0.9 to 0.48 kg per capita) (Liu et al., 2013). Over ten years, the development and implementation of a stricter waste-management programs and associated policies has successfully reduced the amount of plastic debris on the surrounding beaches by approximately 20% (Liu et al., 2013).

Case Study 3: Artificial Structures

Coastal artificial structures are typically built to protect infrastructure and assets but can have negative impacts on natural intertidal habitats (Morris et al., 2019). The artificial structures in Caress Bush Park, NSW, Australia represent a key example of where sustainable management or habitat restoration solutions have been applied during construction to allow natural processes and tidal inundation to occur (Heath, 2017). The development contains a mixture of habitats, rock pools, crevices, mudflats for colonising mangroves and planted saltmarshes. This simultaneously protects public land from flooding and erosion and improves native biodiversity (Heath and Moody, 2013; Strain et al., 2018b) and habitat connectivity (Strain et al., 2018a). This approach to habitat restoration also has the potential to restore other ecosystem services (e.g. nutrient cycling and carbon sequestration), while developing relationships with the community through educational and recreational engagement (Heath, 2017).

CONCLUSION

The study of marine pollution has traditionally focused on understanding the detrimental effects of human wastes and hazardous substances on living resources, human health, and activities, at various spatial and temporal scales. More recently, studies have also considered the input of energy including heat, light, and noise, and changing environmental conditions (e.g. acidification), as sources of pollution. Apart from direct discharges from untreated and partially treated sewage, inputs of pollutants can also be transferred into the marine environment indirectly through surface runoff, freshwater inputs, and atmospheric processes. However, research on marine pollution is rapidly expanding, this special issue highlights, new and emerging types of marine pollution, the complexity of their interactions, and approaches for monitoring with a specific focus on scientific papers published over the last five years. We provide three key examples of solutions to address the hot or emerging topics in marine pollution, focusing on nutrients, plastics, and artificial structures. A combination of scientific monitoring, sustainable management and restoration solutions will be fundamental to addressing the UN sustainable development goal 14.1. "*preventing and significantly reduce marine pollution of all kinds*" and the UN Decade of Ocean Science for Sustainable Development (2021-2030) (https://www.oceandecade.org/) that supports all international efforts to reverse the cycle of decline in ocean health, making the ocean cleaner and safer for all.

AUTHOR CONTRIBUTIONS

ES, CW and RL and AO'B conceived of the presented ideas. All authors discussed the concepts and contributed to the final manuscript.

FUNDING

Support for LA was from project MUR EMME - PRIN 2017-2018.

REFERENCES

Adams, S. M. (2005). Assessing Cause and Effect of Multiple Stressors on Marine Systems. *Marine Pollution Bull.* 51, 649–657. doi: 10.1016/j.marpolbul.2004.11.040

Airoldi, L., Turon, X., Perkol-Finkel, S., and Rius, M. (2015). Corridors for Aliens But Not for Natives: Effects of Marine Urban Sprawl at a Regional Scale. *Diversity Distributions* 21, 755–768. doi: 10.1111/ddi.12301

Altieri, A. H., and Diaz, R. J. (2019). "Dead Zones: Oxygen Depletion in Coastal Ecosystems," in *World Seas: An Environmental Evaluation* (Oxford, UK: Elsevier), Pages 453–473.

Al-Ruzouq, R., Gibril, M. B. A, Shanableh, A., Kais, A., Hamed, O., Al-Mansoori, S., et al. (2020). Sensors, Features and Machine Learning for Oil Spill Detection and Monitoring: A Review. *Remote Sensing* 12 (20), 3338. doi: 10.3390/rs12203338

Andrady, A. L. (2011). Microplastics in the Marine Environment. *Marine Pollution Bull.* 62, 1596–1605. doi: 10.1016/j.marpolbul.2011.05.030

Backhaus, T., and Faust, M. (2012). Predictive Environmental Risk Assessment of Chemical Mixtures: A Conceptual Framework. *Environ. Sci. Technol.* 46, 2564–2573. doi: 10.1021/es2034125

Barnes, D. K., Galgani, F., Thompson, R. C., and Barlaz, M. (2009). Accumulation and Fragmentation of Plastic Debris in Global Environments. *Philos. Trans. R. Soc. B: Biol. Sci.* 364, 1985–1998. doi: 10.1098/rstb.2008.0205

Baumann, H. A., Morrison, L., and Stengel, D. B. (2009). Metal Accumulation and Toxicity Measured by PAM—Chlorophyll Fluorescence in Seven Species of Marine Macroalgae. *Ecotoxicol. Environ. Saf.* 72, 1063–1075. doi: 10.1016/j.ecoenv.2008.10.010

Belden, J. B., Gilliom, R. J., and Lydy, M. J. (2007). How Well can We Predict the Toxicity of Pesticide Mixtures to Aquatic Life? *Integrated Environ. Assess. Management: Int. J.* 3, 364–372. doi: 10.1002/ieam.5630030307

Bhuyan, M. S., Venkatramanan, S., Selvam, S., Szabo, S., Hossain, M. M., Rashed-Un-Nabi, M., et al. (2021). Plastics in Marine Ecosystem: A Review of Their Sources and Pollution Conduits. *Regional Stud. Marine Sci.* 41, 101539. doi: 10.1016/j.rsma.2020.101539

Bierman, P., Lewis, M., Ostendorf, B., and Tanner, J. (2011). A Review of Methods for Analysing Spatial and Temporal Patterns in Coastal Water Quality. *Ecol. Indic.* 11, 103–114. doi: 10.1016/j.ecolind.2009.11.001

Birch, G. (2017). Determination of Sediment Metal Background Concentrations and Enrichment in Marine Environments–a Critical Review. *Sci. Total Environ.* 580, 813–831. doi: 10.1016/j.scitotenv.2016.12.028

Bishop, M. J., Mayer-Pinto, M., Airoldi, L., Firth, L. B., Morris, R. L., Loke, L. H., et al. (2017). Effects of Ocean Sprawl on Ecological Connectivity: Impacts and Solutions. *J. Exp. Marine Biol. Ecol.* 492, 7–30. doi: 10.1016/j.jembe.2017.01.021

Black, J. G., Reichelt-Brushett, A. J., and Clark, M. W. (2015). The Effect of Copper and Temperature on Juveniles of the Eurybathic Brittle Star Amphipholis Squamata–Exploring Responses Related to Motility and the Water Vascular System. *Chemosphere* 124, 32–39. doi: 10.1016/j.chemosphere.2014.10.063

Blasco, J., Chapman, P. M., Campana, O., and Hampel, M. (2016). *Marine Ecotoxicology: Current Knowledge and Future Issues* (Amsterdam, Netherlands: Elsvier).

Boobis, A., Budinsky, R., Collie, S., Crofton, K., Embry, M., Felter, S., et al. (2011). Critical Analysis of Literature on Low-Dose Synergy for Use in Screening Chemical Mixtures for Risk Assessment. *Crit. Rev. Toxicol.* 41, 369–383. doi: 10.3109/10408444.2010.543655

Bugnot, A., Mayer-Pinto, M., Airoldi, L., Heery, E., Johnston, E., Critchley, L., et al. (2021). Current and Projected Global Extent of Marine Built Structures. *Nat. Sustainability* 4, 33–41. doi: 10.1038/s41893-020-00595-1

Cabral, H., Fonseca, V., Sousa, T., and Costa Leal, M. (2019). Synergistic Effects of Climate Change and Marine Pollution: An Overlooked Interaction in Coastal and Estuarine Areas. *Int. J. Environ. Res. Public Health* 16, 2737. doi: 10.3390/ijerph16152737

Chariton, A. A., Court, L. N., Hartley, D. M., Colloff, M. J., and Hardy, C. M. (2010). Ecological Assessment of Estuarine Sediments by Pyrosequencing Eukaryotic Ribosomal DNA. *Front. Ecol. Environ.* 8, 233–238. doi: 10.1890/090115

Chen, C. L. (2015). "Regulation and Management of Marine Litter," in *Marine Anthropogenic Litter* (Cham: Springer), Pages 395–428.

Costa, G. B., Koerich, G., d. Ramos, B., Ramlov, F., Martínez-Crego, B., Costa, M. M., et al. (2020). A Review of Common Parameters and Descriptors Used in Studies of the Impacts of Heavy Metal Pollution on Marine Macroalgae: Identification of Knowledge Gaps and Future Needs. *Acta Botanica Brasilica* 34, 460–477. doi: 10.1590/0102-33062020abb0072

Cózar, A., Echevarría, F., González-Gordillo, J. I., Irigoien, X., Úbeda, B., Hernández-León, S., et al. (2014). Plastic Debris in the Open Ocean. *Proc. Natl. Acad. Sci.* 111, 10239–10244. doi: 10.1073/pnas.1314705111

Crain, C. M., Kroeker, K., and Halpern, B. S. (2008). Interactive and Cumulative Effects of Multiple Human Stressors in Marine Systems. *Ecol. Lett.* 11, 1304–1315. doi: 10.1111/j.1461-0248.2008.01253.x

Cordier, T., Alonso-Sáez, L., Apothéloz-Perret-Gentil, L., Aylagas, E., Bohan, D. A., Bouchez, A, et al. (2021). Ecosystems Monitoring Powered by Environmental Genomics: A Review of Current Strategies With an Implementation Roadmap. *Mol. Eco.* 30(13), 2937–2958

Cordier, T., Esling, P., Lejzerowicz, F., Visco, J., Ouadahi, A., Martins, C., et al. (2017). Predicting The Ecology quality Status of Marine Environments From eDNA Metabarcoding Data Using Supervised Machine Learning. *Enviror. Sci. Tech.* 51(16), 9118–26. doi: 10.1021/acs.est.7b01518

Dahms, H. U. (2014). The Grand Challenges in Marine Pollution Research. *Front. Marine Sci.* 1, 9. doi: 10.3389/fmars.2014.00009

D'Angelo, C., and Wiedenmann, J. (2014). Impacts of Nutrient Enrichment on Coral Reefs: New Perspectives and Implications for Coastal Management and Reef Survival. *Curr. Opin. Environ. Sustainability* 7, 82–93. doi: 10.1016/j.cosust.2013.11.029

Derraik, J. G. (2002). The Pollution of the Marine Environment by Plastic Debris: A Review. *Marine Pollution Bull.* 44, 842–852. doi: 10.1016/S0025-326X(02)00220-5

de Souza Machado, A. A., Kloas, W., Zarfl, C., Hempel, S., and Rillig, M. C. (2018). Microplastics as an Emerging Threat to Terrestrial Ecosystems. *Global Change Biol.* 24, 1405–1416. doi: 10.1111/gcb.14020

Ditria, E. M, Connolly, R. M, Jinks, E. L, and Lopez-Marcano, S. (2021). Annotated Video Footage for Automated Identification and Counting of Fish in Unconstrained Seagrass Habitats. *Front. Mar. Sci.* 54. doi: 10.3389/fmars.2021.629485

Environmental Risk Assessment. (1998). *Guidelines for Ecological Risk Assessment*. (Washington, DC, United States: Environmental Protection Agency).

Firth, L. B., Knights, A. M., Bridger, D., Evans, A., Mieskowska, N., Moore, P. J., et al. (2016). Ocean Sprawl: Challenges and Opportunities for Biodiversity Management in a Changing World. *Oceanography Marine Biol.: an Annu. Rev.* 54, 189–191.

Fowles, A. E., Stuart-Smith, R. D., Stuart-Smith, J. F., Hill, N. A., Kirkpatrick, J. B., and Edgar, G. J. (2018). Effects of Urbanisation on Macroalgae and Sessile Invertebrates in Southeast Australian Estuaries. *Estuarine Coastal Shelf Sci.* 205, 30–39. doi: 10.1016/j.ecss.2018.02.010

Fruhe, L., Cordier, T., Dully, V., Breiner, H., Lentendu, G., Pawlowski, J., et al. (2020). Supervised Machine Learning is Superior to Indicator Value Inference in Monitoring the Environmental Impacts of Salmon Aquaculture Using eDNA Metabarcode. *Mol. Eco.* doi: 10.1111/mec.15434

Ghosal, D., Ghosh, S., Dutta, T. K., and Ahn, Y. (2016). Current State of Knowledge in Microbial Degradation of Polycyclic Aromatic Hydrocarbons (Pahs): A Review. *Front. Microbiol.*, 1369. doi: 10.3389/fmicb.2016.01369

Gregory, M. R. (2009). Environmental Implications of Plastic Debris in Marine Settings—Entanglement, Ingestion, Smothering, Hangers-on, Hitch-Hiking and Alien Invasions. *Philos. Trans. R. Soc. B: Biol. Sci.* 364, 2013–2025. doi: 10.1098/rstb.2008.0265

Gwenzi, W., Lynda, M., Concilia, D., Nhamo, C., Nothando, D., and Edmond, S. (2018). Sources, Behaviour, and Environmental and Human Health Risks of High-Technology Rare Earth Elements as Emerging Contaminants. *Sci Environ* 636, 299–313.

Halpern, B. S., Frazier, M., Afflerbach, J., Lowndes, J. S., Micheli, F., O'Hara, C., et al. (2019). Recent Pace of Change in Human Impact on the World's Ocean. *Sci. Rep.* 9, 1–8. doi: 10.1038/s41598-019-47201-9

Halpern, B. S., Walbridge, S., Selkoe, K. A., Kappel, C. V., Micheli, F., D'Agrosa, C., et al. (2008). A Global Map of Human Impact on Marine Ecosystems. *Science* 319, 948–952. doi: 10.1126/science.1149345

Heath, T. (2017). *Carss Bush Park Environmentally Friendly Seawall–Stage 1* (Sydney, Australia: Fish Friendly Marine Infrastructure).

Heath, T., and Moody, G. (2013). "Habitat Development Along a Highly Urbanised Foreshore", in *Proceedings of New South Wales Coastal Conference 2003*. Sydney, Australia.

He, L., Bai, L., Dionysiou, D. D., Wei, Z., Spinney, R., Chu, C., et al. (2021). Applications of Computational Chemistry, Artificial Intelligence, and Machine Learning in Aquatic Chemistry Research. *Chem. Eng. J.* 426, 131810. doi: 10.1016/j.cej.2021.131810

Heery, E. C., Bishop, M. J., Critchley, L. P., Bugnot, A. B., Airoldi, L., Mayer-Pinto, M., et al. (2017). Identifying the Consequences of Ocean Sprawl for Sedimentary Habitats. *J. Exp. Marine Biol. Ecol.* 492, 31–48. doi: 10.1016/j.jembe.2017.01.020

Heys, K. A., Shore, R. F., Pereira, M. G., Jones, K. C., and Martin, F. L. (2016). Risk assessment of environmental mixture effects.. *RSC advances* 6, 47488–57. doi: 10.1039/C6RA05406D

Jackson, J. B., Kirby, M. X., Berger, W. H., Bjorndal, K. A., Botsford, L. W., Bourque, B. J., et al. (2001). Historical Overfishing and the Recent Collapse of Coastal Ecosystems. *Science* 293, 629–637. doi: 10.1126/science.1059199

Jamieson, A. J., Malkocs, T., Piertney, S. B., Fujii, T., and Zhang, Z. (2017). Bioaccumulation of Persistent Organic Pollutants in the Deepest Ocean Fauna. *Nat. Ecol. Evol.* 1, 1–4. doi: 10.1038/s41559-016-0051

Jeppe, K. J., Yang, J., Long, S. M., Carew, M. E., Zhang, X., Pettigrove, V., et al. (2017). Detecting Copper Toxicity in Sediments: From the Subindividual Level to the Population Level. *J. Appl. Ecol.* 54, 1331–1342. doi: 10.1111/1365-2664.12840

Komyakova, V., Jaffrés, J. B., Strain, E. M., Cullen-Knox, C., Fudge, M., Langhamer, O., et al. (2022). Conceptualisation of Multiple Impacts Interacting in the Marine Environment Using Marine Infrastructure as an Example. *Sci. Total Environ.*, 154748. doi: 10.1016/j.scitotenv.2022.154748

Kortenkamp, A., and Faust, M. (2018). Regulate to Reduce Chemical Mixture Risk. *Science* 361, 224–226. doi: 10.1126/science.aat9219

Lavoie, R. A., Bouffard, A., Maranger, R., and Amyot, M. (2018). Mercury Transport and Human Exposure From Global Marine Fisheries. *Sci. Rep.* 8, 1–9. doi: 10.1038/s41598-018-24938-3

Lefcheck, J. S., Orth, R. J., Dennison, W. C., Wilcox, D. J., Murphy, R. R., Keisman, J., et al. (2018). Long-Term Nutrient Reductions Lead to the Unprecedented Recovery of a Temperate Coastal Region. *Proc. Natl. Acad. Sci.* 115, 3658–3662. doi: 10.1073/pnas.1715798115

Leung, K. M. (2018). Joining the Dots Between Omics and Environmental Management. *Integrated Environ. Assess. Manage.* 14, 169–173. doi: 10.1002/ieam.2007

Liu, T. K., Wang, M. W., and Chen, P. (2013). Influence of Waste Management Policy on the Characteristics of Beach Litter in Kaohsiung, Taiwan. *Marine Pollution Bull.* 72, 99–106. doi: 10.1016/j.marpolbul.2013.04.015

Marginson, S. (2021). 'All Things are in Flux': China in Global Science. *Higher Educ.* 83, 1–30. doi: 10.1007/s10734-021-00712-9

Martin, O., Scholze, M., Ermler, S., McPhie, J., Bopp, S. K., Kienzler, A., et al. (2021). Ten Years of Research on Synergisms and Antagonisms in Chemical Mixtures: A Systematic Review and Quantitative Reappraisal of Mixture Studies. *Environ. Int.* 146, 106206. doi: 10.1016/j.envint.2020.106206

Matthies, M., Solomon, K., Vighi, M., Gilman, A., and Tarazona, J. V. (2016). The Origin and Evolution of Assessment Criteria for Persistent, Bioaccumulative and Toxic (PBT) Chemicals and Persistent Organic Pollutants (Pops). *Environ. Sci.: Processes Impacts* 18, 1114–1128. doi: 10.1039/C6EM00311G

Mohamed, H., Nadaoka, K., and Nakamura, T. (2018). Assessment of Machine Learning Algorithms for Automatic Benthic Cover Monitoring and Mapping Using Towed Underwater Video Camera and High-Resolution Satellite Images. *Remote Sensing* 10 (5), 773. doi: 10.3390/rs10050773

Morris, R. L., Heery, E. C., Loke, L. H., Lau, E., Strain, E., Airoldi, L., et al. (2019). Design Options, Implementation Issues and Evaluating Success of Ecologically Engineered Shorelines. *Oceanography Marine Biol.: an Annu. Rev.* 57, 169–228.

Morris, L., O'brien, A., Natera, S. H., Lutz, A., Roessner, U., and Long, S. M. (2018). Structural and Functional Measures of Marine Microbial Communities: An Experiment to Assess Implications for Oil Spill Management. *Marine Pollution Bull.* 131, 525–529. doi: 10.1016/j.marpolbul.2018.04.054

Noone, K. J., Sumaila, U. R., and Diaz, R. J. (2013). *Managing Ocean Environments in a Changing Climate: Sustainability and Economic Perspectives* (St Louis: Newnes).

O'Brien, A. L., and Keough, M. J. (2014). Ecological response to contamination: A meta-analysis of experimental marine studies. *Environmental Pollution* 195, 185–191.

O'Brien, A., Dafforn, K., Chariton, A., Johnston, E., and Mayer-Pinto, M. (2019). After Decades of Stressor Research in Urban Estuarine Ecosystems the Focus is Still on Single Stressors: A Systematic Literature Review and Meta-Analysis. *Sci. Total Environ.* 684, 753–764. doi: 10.1016/j.scitotenv.2019.02.131

Orr, J. A., Vinebrooke, R. D., Jackson, M. C., Kroeker, K. J., Kordas, R. L., Mantyka-Pringle, C., et al. (2020). Towards a Unified Study of Multiple Stressors: Divisions and Common Goals Across Research Disciplines. *Proc. R. Soc. B* 287, 20200421. doi: 10.1098/rspb.2020.0421

Orth, R. J., Wilcox, D. J., Whiting, J. R., Nagey, L. S., Kenne, A. K., and Smith, E. R. (2017). *2016 Distribution of Submerged Aquatic Vegetation in Chesapeake Bay and Coastal Bays* (Virginia, USA: Virginia Institute of Marine Science, College of William and Mary).

Piarulli, S., Hansen, B. H., Ciesielski, T., Zocher, A. L., Malzahn, A., Olsvik, P. A., et al. (2021). Sources, Distribution and Effects of Rare Earth Elements in the Marine Environment: Current Knowledge and Research Gaps. *Environ. Pollution* 291, 118230. doi: 10.1016/j.envpol.2021.118230

Piggott, J. J., Townsend, C. R., and Matthaei, C. D. (2015). Reconceptualizing Synergism and Antagonism Among Multiple Stressors. *Ecol. Evol.* 5, 1538–1547. doi: 10.1002/ece3.1465

Rivero, N. K., Dafforn, K. A., Coleman, M. A., and Johnston, E. L. (2013). Environmental and Ecological Changes Associated With a Marina. *Biofouling* 29, 803–815. doi: 10.1080/08927014.2013.805751

Rosevelt, C., Los Huertos, M., Garza, C., and Nevins, H. (2013). Marine Debris in Central California: Quantifying Type and Abundance of Beach Litter in Monterey Bay, CA. *Marine Pollution Bull.* 71, 299–306. doi: 10.1016/j.marpolbul.2013.01.015

Salgado-Hernanz, P. M., Bauzà, J., Alomar, C., Compa, M., Romero, L., and Deudero, S. (2021). Assessment of Marine Litter Through Remote Sensing: Recent Approaches and Future Goals. *Marine Pollution Bull.* 168, 112347. doi: 10.1016/j.marpolbul.2021.112347

Schäfer, R. B., and Piggott, J. J. (2018). Advancing Understanding and Prediction in Multiple Stressor Research Through a Mechanistic Basis for Null Models. *Global Change Biol.* 24, 1817–1826. doi: 10.1111/gcb.14073

Seltenrich, N. (2015). *New Link in the Food Chain? Marine Plastic Pollution and Seafood Safety* (USA: NLM-Export).

Sinclair, G. M., O'Brien, A. L., Keough, M., De Souza, D. P., Dayalan, S., Kanojia, K., et al. (2019). Using Metabolomics to Assess the Sub-Lethal Effects of Zinc and Boscalid on an Estuarine Polychaete Worm Over Time. *Metabolomics* 15, 1–13. doi: 10.1007/s11306-019-1570-x

Small, C., and Nicholls, R. J. (2003). A Global Analysis of Human Settlement in Coastal Zones. *Journal of Coastal Research*, 584–99.

Smart, A. S., Tingley, R., Weeks, A. R., Van Rooyen, A. R., and McCarthy, M. A. (2015). Environmental DNA Sampling is More Sensitive Than a Traditional Survey Technique for Detecting an Aquatic Invader. *Ecol. Appl.* 25, 1944–1952. doi: 10.1890/14-1751.1

Strain, E., Alexander, K., Kienker, S., Morris, R., Jarvis, R., Coleman, R., et al. (2019). Urban Blue: A Global Analysis of the Factors Shaping People's Perceptions of the Marine Environment and Ecological Engineering in Harbours. *Sci. Total Environ.* 658, 1293–1305. doi: 10.1016/j.scitotenv.2018.12.285

Strain, E., Heath, T., Steinberg, P., and Bishop, M. (2018a). Eco-Engineering of Modified Shorelines Recovers Wrack Subsidies. *Ecol. Eng.* 112, 26–33. doi: 10.1016/j.ecoleng.2017.12.009

Strain, E. M., Olabarria, C., Mayer-Pinto, M., Cumbo, V., Morris, R. L., Bugnot, A. B., et al. (2018b). Eco-Engineering Urban Infrastructure for Marine and Coastal Biodiversity: Which Interventions Have the Greatest Ecological Benefit? *J. Appl. Ecol.* 55, 426–441. doi: 10.1111/1365-2664.12961

Strain, E. M., Thomson, R. J., Micheli, F., Mancuso, F. P., and Airoldi, L. (2014). Identifying the Interacting Roles of Stressors in Driving the Global Loss of Canopy-Forming to Mat-Forming Algae in Marine Ecosystems. *Global Change Biol.* 20, 3300–3312. doi: 10.1111/gcb.12619

Swearer, S. E., Morris, R. L., Barrett, L. T., Sievers, M., Dempster, T., and Hale, R. (2021). An Overview of Ecological Traps in Marine Ecosystems. *Front. Ecol. Environ.* 19, 234–242. doi: 10.1002/fee.2322

Tournadre, J. (2014). Anthropogenic Pressure on the Open Ocean: The Growth of Ship Traffic Revealed by Altimeter Data Analysis. *Geophysical Res. Lett.* 41, 7924–7932. doi: 10.1002/2014GL061786

Van Cauwenberghe, L., Vanreusel, A., Mees, J., and Janssen, C. R. (2013). Microplastic Pollution in Deep-Sea Sediments. *Environ. Pollution* 182, 495–499. doi: 10.1016/j.envpol.2013.08.013

Van den Brink, P. J., Bracewell, S. A., Bush, A., Chariton, A., Choung, C. B., Compson, Z. G., et al. (2019). Towards a General Framework for the Assessment of Interactive

Effects of Multiple Stressors on Aquatic Ecosystems: Results From the Making Aquatic Ecosystems Great Again (MAEGA) Workshop. *Sci. Total Environ.* 684, 722–726. doi: 10.1016/j.scitotenv.2019.02.455

Verfuss, U. K., Aniceto, A. S., Harris, D. V., Gillespie, D., Fielding, S., Jiménez, G., et al. (2019). A Review of Unmanned Vehicles for the Detection and Monitoring of Marine Fauna. *Marine Pollution Bull.* 140, 17–29. doi: 10.1016/j.marpolbul.2019.01.009

Wang, W., Gao, H., Jin, S., Li, R., and Na, G. (2019). The Ecotoxicological Effects of Microplastics on Aquatic Food Web, From Primary Producer to Human: A Review. *Ecotoxicol. Environ. Saf.* 173, 110–117. doi: 10.1016/j.ecoenv.2019.01.113

Warne, M. S. J., and Hawker, D. W. (1995). The Number of Components in a Mixture Determines Whether Synergistic and Antagonistic or Additive Toxicity Predominate: The Funnel Hypothesis. *Ecotoxicol. Environ. Saf.* 31, 23–28. doi: 10.1006/eesa.1995.1039

Wilkinson, J. L., Boxall, A. B., Kolpin, D. W., Leung, K. M., Lai, R. W., Galbán-Malagón, C., et al. (2022). Pharmaceutical Pollution of the World's Rivers. *Proc. Natl. Acad. Sci.* 119, e2113947119. doi: 10.1073/pnas.2113947119

Williams, M., Longstaff, B., Buchanan, C., Llansó, R., and Dennison, W. (2009). Development and Evaluation of a Spatially-Explicit Index of Chesapeake Bay Health. *Marine Pollution Bull.* 59, 14–25. doi: 10.1016/j.marpolbul.2008.11.018

Wurtsbaugh, W. A., Paerl, H. W., and Dodds, W. K. (2019). Nutrients, Eutrophication and Harmful Algal Blooms Along the Freshwater to Marine Continuum. *Water* 6, e1373. doi: 10.1002/wat2.1373

Zhang, S., Wang, J., Liu, X., Qu, F., Wang, X., Wang, X., et al. (2019). Microplastics in the Environment: A Review of Analytical Methods, Distribution, and Biological Effects. *Trends Analytical Chem.* 111, 62–72. doi: 10.1016/j.trac.2018.12.002

Conflict of Interest: The authors declare that the research was conducted in the absence of any commercial or financial relationships that could be construed as a potential conflict of interest.

Publisher's Note: All claims expressed in this article are solely those of the authors and do not necessarily represent those of their affiliated organizations, or those of the publisher, the editors and the reviewers. Any product that may be evaluated in this article, or claim that may be made by its manufacturer, is not guaranteed or endorsed by the publisher.

frontiers in Marine Science

HYPOTHESIS AND THEORY
published: 28 April 2021
doi: 10.3389/fmars.2021.660125

The Role of Vessel Biofouling in the Translocation of Marine Pathogens: Management Considerations and Challenges

Eugene Georgiades[1], Chris Scianni[2], Ian Davidson[3], Mario N. Tamburri[4], Matthew R. First[5], Gregory Ruiz[6], Kevin Ellard[7], Marty Deveney[8] and Daniel Kluza[1]*

[1] Ministry for Primary Industries, Wellington, New Zealand, [2] Marine Invasive Species Program, California State Lands Commission, Long Beach, CA, United States, [3] Cawthron Institute, Nelson, New Zealand, [4] Chesapeake Biological Laboratory, University of Maryland Center for Environmental Science, Solomons, MD, United States, [5] U.S. Naval Research Laboratory, Washington, DC, United States, [6] Smithsonian Environmental Research Center, Edgewater, MD, United States, [7] Invasive Species Branch, Biosecurity Tasmania, Department of Primary Industries, Parks, Water and Environment, Hobart, TAS, Australia, [8] SARDI Aquatic Sciences and Marine Innovation Southern Australia, South Australian Research and Development Institute, West Beach, SA, Australia

OPEN ACCESS

Edited by:
Elisabeth Marijke Anne Strain, University of Tasmania, Australia

Reviewed by:
Thomas W. Therriault, Pacific Biological Station, Department of Fisheries and Oceans (Canada), Canada
Gordon James Watson, University of Portsmouth, United Kingdom

***Correspondence:**
Eugene Georgiades
Eugene.Georgiades@mpi.govt.nz

Specialty section:
This article was submitted to Marine Pollution, a section of the journal Frontiers in Marine Science

Received: *28 January 2021*
Accepted: *01 April 2021*
Published: *28 April 2021*

Citation:
Georgiades E, Scianni C, Davidson I, Tamburri MN, First MR, Ruiz G, Ellard K, Deveney M and Kluza D (2021) The Role of Vessel Biofouling in the Translocation of Marine Pathogens: Management Considerations and Challenges. Front. Mar. Sci. 8:660125. doi: 10.3389/fmars.2021.660125

Vessel biofouling is a major pathway for the introduction, establishment, and subsequent spread of marine non-indigenous macro-organisms. As a result, national and international regulations and guidelines have been implemented to manage the risks associated with this pathway, yet widespread enforcement and uptake are still in their infancy. By comparison, translocation of marine pathogens by vessel biofouling has received little attention despite a mounting body of evidence highlighting the potential importance of this pathway. Using molluscan pathogens as a model, this paper examines the potential for translocation of marine pathogens via the vessel biofouling pathway by reviewing: (1) examples where vessel biofouling is suspected to be the source pathway of non-indigenous pathogen introduction to new areas, and (2) the association between pathogens known to have detrimental effects on wild and farmed mollusk populations with species known to foul vessels and anthropogenic structures. The available evidence indicates that vessel biofouling is a viable and important pathway for translocating marine pathogens, presenting a risk to marine values (i.e., environmental, economic, social, and cultural). While preventive measures to minimize the translocation of macro-organisms are the most efficient way to minimize the likelihood of associated pathogen translocation, the application of reactive management measures to biofouled vessels, including post-filtration treatment, requires further and explicit consideration.

Keywords: vessel biofouling, pathogens, mollusks, in-water cleaning, marine biosecurity

INTRODUCTION

The International Maritime Organization (IMO) defines biofouling as the growth and accumulation of organisms on immersed ship surfaces or structures (International Maritime Organization [IMO], 2011). Typically, any substrate placed in natural waters is quickly colonized by micro-organisms (creating a biofilm, also known as the slime layer) that is followed by a succession

of diverse sessile or sedentary micro- and macro-organisms (Flemming, 2002; Aldred and Clare, 2008; Amara et al., 2018). Vessel biofouling is acknowledged as a major, and perhaps the most important, pathway for the introduction, establishment, and subsequent spread of marine non-indigenous macro-organisms (Drake and Lodge, 2007; Hewitt and Campbell, 2010; Bell et al., 2011; Ruiz et al., 2015; Bailey et al., 2020). Similar to the concerns over the transport of human pathogens in ships' ballast water (McCarthy and Khambaty, 1994; Ruiz et al., 2000a; Cohen et al., 2012), the potential for vessel biofouling to act as a vector for non-indigenous pathogens has been highlighted for some time (e.g., Howard, 1994). Pathogens have been found in biofilms growing on vessel surfaces (e.g., Drake et al., 2007; Shikuma and Hadfield, 2010), and mature organisms within vessel biofouling assemblages are more likely to harbor pathogens than their younger or larval planktonic stages associated with ballast water (Hine, 1995). For the purpose of this document, the term pathogen is used to include viruses, bacteria, protists, and fungi that cause disease in other organisms; the term vessel is used to include every description of ship, boat, or other craft used in water navigation, i.e., both recreational and commercial vessels are included.

The role of anthropogenic vectors in global scale biotic exchange is largely based on patterns and processes linked to macro-organism translocations and biogeography (Ruiz et al., 2000b; Pagenkopp-Lohan et al., 2020), thus the magnitude and impacts of marine micro-organism translocations are likely "vastly underestimated" (Pagenkopp-Lohan et al., 2020). Practical difficulties in micro-organism identification and detection, and a lack of baseline knowledge about native organism geographical ranges, however, have hampered research efforts (Davidson et al., 2013; Pagenkopp-Lohan et al., 2020).

In the risk analysis to support implementation of New Zealand's biofouling regulations (Ministry for Primary Industries New Zealand [MPI], 2018), Bell et al. (2011) identified recent changes to shipping patterns including increased shipping volumes, expansion of trade routes, and increased vessel speeds were providing a greater likelihood of translocation of marine non-indigenous macro-organisms. The delivery rate of micro-organisms associated with vessel biofouling may be similarly increasing over time (Pagenkopp-Lohan et al., 2020). The role of shipping, particularly vessel biofouling, in pathogen translocations may, therefore, undermine regulations and improved management practices aimed at addressing the major anthropogenic vectors for historical pathogen translocations, such as aquaculture and fisheries stocking (Williams et al., 2013; Georgiades et al., 2016; Pagenkopp-Lohan et al., 2020). While vessel biofouling has also been subject to increased scrutiny and management in some jurisdictions (Georgiades et al., 2020; Scianni et al., in press), it remains a largely unregulated broad-scale vector of organisms both domestically and internationally.

The threats posed by non-indigenous pathogens are similar to marine non-indigenous macro-organisms: once established they are difficult to control, and eradication is often infeasible or unsuccessful (Centre for Environment, Fisheries and Aquaculture Science [CEFAS], 2009; Georgiades et al., 2020). Prevention is therefore the only effective measure (Centre for Environment, Fisheries and Aquaculture Science [CEFAS], 2009; Georgiades et al., 2016). This is particularly the case for shellfish aquaculture and fisheries, where the introduction and establishment of novel pathogens can have devastating effects. For example, *Bonamia ostreae* and *Marteilia refringens* drastically reduced European production of cultured flat oysters (*Ostrea edulis*) from 29,595 t in 1961 to 5,921 t in 2000 (Culloty and Mulcahy, 2007). Between 1980 and 1983 alone, estimated losses in France included a 20% reduction of employment within the industry, US$ 240 million turn-over, and US$ 200 million of added value [Meuriot and Grizel (1984) in Arzul et al., 2006]. European flat oyster production has stabilized but at low levels (< 3,000 t; Goulletquer, 2004), using modified husbandry techniques with lower employment than the industry had historically provided (Arzul et al., 2006; Culloty and Mulcahy, 2007). Based on these impacts, introduction of *B. ostreae* to New Zealand in 2015 led to the pre-emptive depopulation of all farmed flat oyster (*O. chilensis*) stock to protect uninfected areas, particularly the Bluff wild oyster fishery at the southern tip of the South Island (Farnsworth et al., 2020).

The ostreid herpes virus microvariant 1 (OsHV-1) has caused mass mortalities in spat and juvenile Pacific oysters (*Crassostrea gigas*) in France (Ségarra et al., 2010), Australia (Paul-Pont et al., 2014), and New Zealand (Bingham et al., 2013). During initial outbreaks, stock losses of up to 100% were recorded (Keeling et al., 2014; European Food Safety Authority [EFSA], 2015), and the disease halved New Zealand's Pacific oyster production (Johnston, 2014). The immediate impacts to industry and biosecurity response costs for OsHV-1 and *B. ostreae* in New Zealand have far outweighed those related to marine non-indigenous macro-organisms (Georgiades et al., 2020).

The introduction of *Haplosporidium nelsoni* to the mid-Atlantic coast of the United States in the 1950s also had extensive impacts on *Crassostrea virginica* populations, with mortality exceeding 90% in Delaware and Chesapeake Bays (Haskin and Ford, 1982; Haskin and Andrews, 1988). Between 1958 and 1983, it was estimated that *H. nelsoni* had reduced oyster landings in Delaware Bay by two-thirds (Haskin and Ford, 1982). The introduction of *H. nelsoni*, combined with pollution and oyster overharvesting, drove large-scale ecological impacts on Chesapeake Bay (Kemp et al., 2005), and extensive management and restoration efforts have achieved relatively modest success (National Research Council., 2004). The fishery in Chesapeake Bay declined to 2% of its historical catch in 30 years, and introduction and culture of non-native oyster species (including *C. gigas* and *C. ariakensis*) was seriously considered (Mann et al., 1991; Calvo et al., 1999; Tamburri et al., 2008).

While vessel biofouling regulations have been enacted by some jurisdictions (California Code of Regulations, 2017; Ministry for Primary Industries New Zealand [MPI], 2018; Georgiades et al., 2020), these are focused largely on preventing the translocation of marine non-indigenous macro-organisms (e.g., Bell et al., 2011). New information on translocation of pathogens associated with biofouling is emerging, however (e.g., Lane et al., 2018; Itoh et al., 2019; Costello et al., 2020; Lane and Jones, 2020; Pagenkopp-Lohan et al., 2020). Biofouling management measures routinely

applied to vessels, such as in-water cleaning of macrofouling [i.e., reactive in-water cleaning (RIC)], are also cause for concern as they may increase the likelihood of pathogen release and establishment into new areas (Scianni and Georgiades, 2019).

In light of the major negative consequences novel pathogen introductions have thus far caused, understanding the risk of pathogen translocation by vessel biofouling is critical to inform biosecurity guidelines, regulations, and management approaches to protect marine values such as biodiversity, customary and recreational practices, fisheries, and aquaculture. This analysis reviews the literature to investigate the likelihood of this translocation pathway, including the ramifications for vessel maintenance, and discusses potential risk management options, as appropriate.

ANALYSIS

Analysis Scope

This analysis primarily focuses on the pathogens of mollusks as a model. There are numerous World Organization for Animal Health (OIE) listed or emerging molluscan pathogens that are of major concern for jurisdictions worldwide (Bower, 2017; OIE, 2020). The implications, conclusions, and recommendations drawn from the molluscan model may have broad application to other marine and human pathogens.

Pathogen Translocation Associated With Vessel Biofouling

Howard (1994) noted that the domestic transfer of *B. ostreae* from Cornwall to Plymouth (England) likely occurred with biofouling, which included live mollusks, on concrete barges. This conclusion was based on Plymouth having no history of the disease nor any reason to receive live oyster transfers for aquaculture purposes (Howard, 1994). The spread of *B. ostreae* has also been linked to vessel biofouling in the Netherlands (van Banning, 1991) and Ireland (Culloty and Mulcahy, 2007).

Bonamia ostreae was detected in the Southern Hemisphere (New Zealand) in 2015 (Georgiades, 2015; Lane et al., 2016) and was most likely introduced by vessel biofouling (Lane et al., 2020). The spread of *B. exitiosa*, from southern New Zealand to the Northern Hemisphere (Bishop et al., 2006; Abollo et al., 2008; Longshaw et al., 2013) and Argentina (Kroeck and Montes, 2005), has similarly been associated with shipping (Hill-Spanik et al., 2015; Lane et al., 2018). *B. ostreae* and other molluscan pathogens are associated with non-indigenous ascidians (Costello et al., 2020), highlighting the potential role of non-molluscan biofouling species as vectors of this pathogen.

Vessel biofouling is suggested as responsible for the introduction of OsHV-1 into New Zealand (Lane et al., 2020) and Australia (Fisheries Research and Development Corporation, 2011; Whittington et al., 2018), and its subsequent Australian spread to Tasmania and South Australia (Deveney et al., 2017). Fuhrmann and Hick (2020) found that laboratory transmission of OsHV-1 between donor and naive Pacific oysters via a simulated biofouling scenario was plausible but complex. While transmission from other biofouling species was not observed by Fuhrmann and Hick (2020), the association of OsHV-1 with some biofouling organisms (i.e., bryozoan species) suggested that they may protect the virus from degradation (Martenot et al., 2015; Hick et al., 2016). OsHV-1 transmission to naive Pacific oysters has also been shown following cohabitation with exposed wild crabs (*Carcinus maenas*; Bookelaar et al., 2018) and mussels (*Mytilus* spp.; O'Reilly et al., 2018). These taxa have previously been identified within vessel biofouling assemblages (Visscher, 1928; Apte et al., 2000; Moshchenko and Zvyagintsev, 2001; Coutts et al., 2003). The mechanisms by which marine non-indigenous species can affect pathogen-host interactions are complex (Goedknegt et al., 2016), which has possible implications for their association and transport by vessels.

Vessel movements have also been linked to the introduction of *H. nelsoni* to the United States and Canada either through biofouling or release of *H. nelsoni* spores by ballast water discharges (National Research Council., 2004; Stephenson and Petrie, 2005). Hine (1996) highlighted the biofouling pathway as a risk for spreading *Perkinsus marinus*, and Pagenkopp-Lohan et al. (2018) and Itoh et al. (2019) further demonstrated the potential for shipping to contribute to the long-range dispersal of *Perkinsus* species.

In addition to pathogens, it is also noteworthy that parasitic invertebrates may be translocated by vessel biofouling (Davidson et al., 2013). Parasitic invertebrates were found to infect 7.8% of mussels sampled from 23 vessels operating on the U.S. West Coast, including the parasitic copepods *Pseudomyicola spinosus* and *Modiolicola gracilis*. Transport of infected mussels by international shipping has also been implicated in the intercontinental spread of a molluscan transmissible neoplasia (Yonemitsu et al., 2019).

In assessing pathogen risks associated with translocation of mollusk shells for reef restoration, Diggles (2020) noted the potential of molluscan pathogens, including iridoviruses, OsHV-1, and *Bonamia* species, to be introduced to Australia by vessel biofouling specifically and others, including *H. nelsoni* and *Perkinsus* species, by shipping more generally. The Australian Government Field Identification Guide for Aquatic Animal Diseases (Department of Agriculture, Water and the Environment, 2020) also recognizes vessel biofouling as a potential pathway for translocating various *Bonamia* species and OsHV-1. These examples show that the role of shipping, and more specifically vessel biofouling, in pathogen translocation is increasingly recognized as a serious risk factor for increasing the incidence of infection and disease outbreaks at various scales (within regions and over long-distance oceanic scales).

Associations of OIE-Listed and Other Important Pathogens With Known Biofouling Species

The OIE is an intergovernmental organization established to promote global animal health (OIE, 2019). To facilitate health certification and reduce risk in the trade of aquatic animals and their products, the OIE Aquatic Animal Health Standards Commission compiles the *Manual of Diagnostic Tests for Aquatic Animals* (the Aquatic Manual), records species known to be

susceptible to listed pathogens, and provides standardized, validated approaches for diagnosis.

The chapters of the OIE Aquatic Manual (OIE, 2019) specific to molluscan pathogens show that many known susceptible species are associated with biofouling of vessels, anthropogenic structures within harbors, hard substrates, or offshore installations (**Table 1**). Further, many of these pathogens either have poorly understood life cycles (e.g., *B. exitiosa*) or have been shown to survive outside the host for periods of weeks to months (e.g., *B. ostreae*, *P. marinus*, and *P. olseni*; OIE, 2019). There are also many molluscan pathogens that, although not listed by the OIE, cause substantial impacts and are associated with biofouling species (**Table 2**).

Pathogen translocation via the biofouling pathway adds further layers of complexity to factors that influence pathogen transmission and disease dynamics (Fuhrmann and Hick, 2020; Lane et al., 2020). These parameters include pathogen life cycles, host specificity and susceptibility, infective dose, survival outside host, and susceptible host life stages (OIE, 2019; Pagenkopp-Lohan et al., 2020). To understand the translocation dynamics of these pathogens, presence of host or carrier species on vessel submerged surfaces, exposure of those species to pathogens prior to transit, prevalence and intensity of infection, and time of year (i.e., both seasonal dynamics and environmental conditions encountered) need to be considered.

Introduction of pathogens to new environments is influenced by vessel itinerary (i.e., places visited and duration of stay) and the type and duration of exposure of hosts in recipient environments. For example, exposure may occur as a result of pathogen shedding from organisms on a vessel, release of macro-organisms from the vessel surface, or an uncontained release of biofouling and pathogens following in-water cleaning. Characteristics of the recipient environment also need to be considered, including temperature, salinity, pollution, and—importantly—the presence, proximity, and density of susceptible host or carrier species (OIE, 2019; Lane et al., 2020; Pagenkopp-Lohan et al., 2020).

Receiving environments for vessels are typically ports and marinas which, being heavily modified, offer a variety of habitats for colonization by sessile and mobile taxa, including non-indigenous species (Ruiz et al., 1997; Johnston et al., 2017). These environments are often enclosed, leading to high particle retention (Gadd et al., 2011; Morrisey et al., 2013), thus, if released, pathogens may stay in contact with host species that are present for longer periods at potentially infective doses. The presence of artificial and modified habitats, combined with relatively high retention, enhances conditions for introduction, establishment, and spread of new non-indigenous macro-organisms (Floerl et al., 2009; Ruiz et al., 2009; Johnston et al., 2017) and associated pathogens. Following arrival and colonization, domestic vessels provide a vital link for spread from primary infected areas via movement of associated ballast water (Inglis et al., 2013) and biofouling, including fouled vessels that transit aquaculture zones (Sim-Smith et al., 2016).

Not every mollusk that is translocated with vessel fouling will cause a novel pathogen to establish with subsequent consequences (e.g., Gias and Johnston, 2010; Davidson et al., 2013; Fuhrmann and Hick, 2020). Mounting evidence from laboratory and field observations as well as documented consequences, however, indicates that the risks associated with this pathway are non-negligible and that risk management measures may be justified. The evidence chain outlined here is consistent with the criteria applied to assess the risks associated with vessel biofouling for marine non-indigenous macro-organism translocations (Bell et al., 2011), which was a key step that led to biofouling regulations in New Zealand (Georgiades et al., 2020).

Mollusks are, importantly, not the only taxa associated with vessel biofouling that may translocate pathogens of concern. The invasive crabs *Eriocheir sinensis* and *C. maenas* are associated with fouled vessels (Peters and Panning, 1933 in Herborg et al., 2003; Coutts et al., 2003) and are susceptible hosts or carriers of several pathogens with well-documented consequences to marine values, including fisheries and aquaculture (**Table 3**). Parasitic invertebrates can also be translocated by barnacles, including the castrating isopod *Hemioniscus balani* (Davidson et al., 2013). Human pathogens, such as *Vibrio cholerae*, *Vibrio parahaemolyticus*, and *Escherichia coli*, have also been found in the surface biofilms of vessels (Shikuma and Hadfield, 2010; Revilla-Castellanos et al., 2015).

Potential Management Options

Pathogens can be released from vessel biofouling by being: (a) sloughed from the attached biofilm, (b) dispersed by proactive in-water cleaning (PIC), (c) shed from macrofouling that remains intact on the vessel, (d) shed with macrofouling released during normal vessel operations (i.e., drop-off of attached species or active escape of mobile species), or (e) dispersed with or without their hosts during application of RIC. We have identified a two-pronged approach to protect marine values from pathogen introductions associated with vessel biofouling by: (1) limiting the volume and frequency of pathogen translocations via ongoing vessel transportation (i.e., propagule pressure; Lockwood et al., 2005) and (2) avoiding pathogen releases by reactive management activities. The methods used to achieve these approaches all have associated advantages and disadvantages (**Table 4**).

The maritime antifouling industry is established to prevent and manage biofouling on vessels. The primary focus has been on surface paints or coatings on the immersed surfaces of ships to prevent macrofouling growth (using biocides, such as copper- and zinc-based compounds) and/or restrict macrofouling adhesion (non-biocidal or fouling-release, such as silicone-based coatings; Dafforn et al., 2011; Lewis, 2020). The use of biocidal coatings represents a trade-off between vessel fuel efficiency, reduced exhaust emissions, and reduced translocation of non-indigenous species, versus environmental impacts of the biocides (Dafforn et al., 2011; Scianni and Georgiades, 2019; Richir et al., 2021). Even though these coatings have evolved toward more sophisticated, cost effective, and environmentally acceptable products, antifoulants do not prevent biofilm formation (Dobretsov, 2010) or incidental macrofouling that establishes during vessel in-service periods (i.e., the time between vessel dry-docking; Georgiades and Kluza, 2017). There are areas of ships that cannot be painted

TABLE 1 | OIE-listed molluscan pathogens associated with known fouling species and their size (Bower, 2017; OIE, 2019).

Pathogen and OIE chapter	Susceptible species associated with fouling	Fouling type	Fouling reference	Particle size (μm)
Bonamia exitiosa	*Ostrea chilensis*	Vessels	Smith et al. (2016)	2.4 ± 0.5
OIE (2019)	*O. angasi*	Harbors	Lewis (1982, 1986)	
Chapter 2.4.2	*O. edulis*	Vessels	Howard (1994)	
	O. stentina	Settlement plates	Hamaguchi et al. (2017)	
Bonamia ostreae	*O. edulis*	Vessels	Howard (1994)	3 ± 0.3
OIE (2019)	*O. chilensis*	Vessels	Coutts and Dodgshun (2007)	
Chapter 2.4.3	*O. puelchana**	Harbors	Schwindt et al. (2014)	
	*O. angasi**	Harbors	Lewis (1982, 1986)	
Marteilia refringens	*O. edulis*	Vessels	Howard (1994)	4–40
OIE (2019)	*Mytilus edulis*	Vessels	Visscher (1928)	
Chapter 2.4.4	*M. galloprovincialis*	Vessels	Apte et al. (2000)	
	O. stentina	Settlement plates	Hamaguchi et al. (2017)	
	Xenostrobus securis	Vessels	Barbieri et al. (2011)	
	*O. chilensis**	Vessels	Coutts and Dodgshun (2007)	
	*O. puelchana**	Harbors	Schwindt et al. (2014)	
	*O. angasi**	Harbors	Lewis (1982, 1986)	
	*O. denselamellosa**	Offshore structures	Tao and Wenxia (2002)	
Ostreid herpesvirus 1 μvar	*Crassostrea gigas*	Vessels	Brock et al. (1999)	0.07–0.35
OIE (2019)	*C. angulata*	Vessels	Ojaveer et al. (2018)	
Chapter 2.4.5				
Perkinsus marinus	*C. virginica*	Vessels	Woods Hole Oceanographic Institution	2–15
OIE (2019)	*C. gigas*	Vessels	(WHOI) (1952)	
Chapter 2.4.6	*C. ariakensis*	Vessels	Brock et al. (1999)	
	C. rhizophorae	Vessels	National Research Council. (2004)	
	C. corteziensis	Hard substrate	Farrapeira et al. (2010)	
	*Mya arenaria***	Vessels	Angell (1986)	
			Carlton (1999)	
*Perkinsus olseni***	*C. ariakensis*	Vessels	National Research Council. (2004)	5–15
OIE (2019)	*C. sikamea*	Hard substrate	Hamaguchi et al. (2013)	
Chapter 2.4.7	*Pinctada margaritifera*	Offshore structures	Yan et al. (2006)	
	P. martensii	Offshore structures	Yan et al. (2006)	
	P. fucata	Hard substrate	Alagarswami (1977)	
Mikrocytos mackini	*C. gigas*	Vessels	Brock et al. (1999)	2–3
OIE (2019)	*C. virginica*	Vessels	Woods Hole Oceanographic Institution	
Chapter 2.4.9	*O. edulis*	Vessels	(WHOI) (1952)	
	O. lurida	Vessels	Howard (1994)	
			Brock et al. (1999)	

**Infected when deployed in a known infected area although pathogen identification not completed to molecular level.*
***Perkinsus olseni has an extremely wide host range. Members of the families Arcidae, Malleidae, Isognomonidae, Chamidae, and Veneridae are particularly susceptible.*
****Primarily an infaunal clam. Associated (nestled) in a biofouling community but not sessile or attached in this sense.*

(e.g., anodes), are difficult to paint (e.g., dry-dock support strips), or experience sub-optimal coating performance because of surface or hydrodynamic issues (e.g., sea chests, gratings, rudders, and projections). These "niche areas" are hotspots of biofouling accumulation (Coutts and Taylor, 2004; Davidson et al., 2009, 2016) that require ongoing vigilance and maintenance (California Code of Regulations, 2017; Georgiades et al., 2018; Ministry for Primary Industries New Zealand [MPI], 2018). While biocide release rates from coatings can be estimated and environmental concentrations predicted (e.g., Morrisey et al., 2013), no quantitative assessments or estimates have been made of the release rates or quantities of live micro- or macrofouling organisms into coastal ecosystems as a result of normal vessel operations.

In-water cleaning has emerged as the principal approach to address limitations in coating performance and operational impacts of biofouling that accumulate while in-service. In-water cleaning typically involves use of diver or remotely operated cleaning or cart systems that remove biofouling from hull surfaces (McClay et al., 2015; Morrisey and Woods, 2015; Tamburri et al., 2020). While in-water cleaning is often performed in response to fundamental operational factors, such as increasing fuel consumption (to reset hull surfaces to a more hydrodynamic state), it can have unintended consequences including: (a) increased release of antifouling biocides to ambient waters; (b) active liberation of live biofouling organisms or their propagules into local habitats, with increased risk of non-indigenous species introduction; and (c) diminished coating condition that reduces antifouling performance and longevity (Scianni and Georgiades, 2019; Tamburri et al., 2020). There is growing consensus internationally that steps should be taken to minimize these environmental impacts,

TABLE 2 | Examples of non-OIE listed molluscan pathogens that have caused substantial impacts and are associated with known fouling species (per Bower, 2017).

Pathogen and reference	Susceptible species associated with fouling	Fouling type	Fouling reference	Particle size (μm)
Oyster velar virus Bower (2001d)	*Crassostrea gigas*	Vessels	Brock et al. (1999)	0.228 + 0.007
Gill necrosis virus Bower (2001a)	*C. angulata* *C. gigas*	Vessels	Ojaveer et al. (2018) Brock et al. (1999)	0.350–0.380
Haemocytic infection virus Bower et al. (1994)	*C. angulata* *C. gigas*	Vessels Vessels	Ojaveer et al. (2018) Brock et al. (1999)	0.380
Roseovarius crassostreae Bower (2010)	*C. virginica*	Vessels	Woods Hole Oceanographic Institution (WHOI) (1952)	4.8 × 1.2
Marteilioides chungmuensis Itoh et al. (2004)	*C. gigas* *C. nippona*	Vessels Hard substrate	Brock et al. (1999) Wang and Li (2020)	6.3 × 4 Initial sporulation stage
Virus-like particles Bower (2001e)	*Perna canaliculus* *Mytilus galloprovincialis*	Vessels Vessels	Smith et al. (2016) Apte et al. (2000)	0.025–0.047
Vibrio spp. Bower (2009) Lopez-Joven et al. (2018)	*C. gigas* *C. virginica* *C. sikamea* *O. edulis* *O. conchaphila*	Vessels Vessels Hard substrate Vessels Hard substrate	Brock et al. (1999) Woods Hole Oceanographic Institution (WHOI) (1952) Hamaguchi et al. (2013) Howard (1994) Groth and Rumrill (2009)	<5
Cytophaga spp. Bower (2001b) Dungan et al. (1989)	*C. gigas* *C. virginica* *Ostrea edulis*	Vessels Vessels Vessels	Brock et al. (1999) Woods Hole Oceanographic Institution (WHOI) (1952) Howard (1994)	>5
Nocardia crassostreae Bower (2006)	*C. gigas* *O. edulis*	Vessels Vessels	Brock et al. (1999) Howard (1994)	<10
Plectonema terebrans *Hyella caespitose* *Mastigocoleus testarum* *Mastigocoleus* sp. (Nostochopsidaceae *Pleurocapsa* sp.) Bower et al. (2002)	*M. galloprovincialis* *Choromytilus meridionalis* *Aulacomya ater*	Vessels Hard substrate Hard substrate	Apte et al. (2000) Barkai and Branch (1989) Barkai and Branch (1989)	<8
Kidney coccidia *Pseudoklossia semilunar* Bower (2001c)	*M. edulis/galloprovincialis/ trossulus* species complex	Vessels	Visscher (1928) Apte et al. (2000) Moshchenko and Zvyagintsev (2001)	6 × 3 Sporocysts
Haplosporidium costale Bower (2014a)	*C. virginica*	Vessels	Woods Hole Oceanographic Institution (WHOI) (1952)	3–4 2.6 × 3.1
Haplosporidium nelsoni Bower (2014b)	*C. virginica*	Vessels	Woods Hole Oceanographic Institution (WHOI) (1952)	7.5 × 5.4 Spores 4–100 Multi-nucleate plasmodia
Minchinia occulta Bower (2014c)	*Saccostrea cuccullata*	Vessels	Yan and Huang (1993)	4.5–6.7 × 3.3–4.1 Spores (micro) 4.5–5.0 × 3.5–4.1 Spores (EM)
Marteilia sydneyi Bower and Kleeman (2011) Green and Barnes (2010)	*S. glomerata*	Vessels	Ulman et al. (2017)	<10 diameter Mature sporonts
Bonamia roughleyi Bower (2015)	*S. glomerata*	Vessels	Ulman et al. (2017)	1–2
Marteilia maurini Bower (2019)	*M. galloprovincialis*	Vessels	Apte et al. (2000)	9.9 8.4
Marteilia pararefringens Bower (2019)	*M. edulis*	Vessels	Visscher (1928)	

by moving away from in-water cleaning of macrofouling that does not attempt to capture debris (i.e., RIC), and toward RIC that capture, contain, and treat debris (RICC), or PIC to prevent macrofouling establishment and growth. For all in-water cleaning systems, there are two main processes that can release biological material including pathogens: (a) application of the cleaning unit to the vessel surface (either through incomplete or ineffective capture of debris by the cleaning head)

TABLE 3 | Notable pathogens and parasitic invertebrates associated with *Eriocheir sinensis* and *Carcinus maenas*.

Species	Pathogen	Particle size (μm)	References
Eriocheir sinensis	*Hepatospora eriocheir*	1.8 × 0.9	Stentiford et al. (2011)
	Spiroplasma eriocheir	0.1–0.35 diameter 0.1–0.2 diameter 3–12 length	Wang et al. (2004a,b) Wang et al. (2011)
	E. sinensis ronivirus	0.060– 0.110 × 0.024– 0.042	Zhang and Bonami (2007)
	White spot syndrome virus	0.080–0.150 diameter 0.250–0.380 length	Ding et al. (2015) OIE (2019) (Chapter 2.2.8)
	Aphanomyces astasci (freshwater)	Hyphae 7–9 width Secondary zoospores 8 × 12	OIE (2019) Chapter 2.2.2
	Paragonimus westermani (secondary host)	>100 Metacercariae diameter	Peters and Panning (1933) Habe et al. (1993)
Carcinus maenas	*Hematodinium perezi* *Hematodinium* sp.	15–100 length multinucleate plasmodium 6–22 diameter Single cell trophont	Bower (2013a,b) Davies et al. (2019)
	White spot syndrome virus	0.080–0.150 diameter 0.250–0.380 length	Bateman et al. (2012)
	Ostreid herpesvirus 1 μvar	0.07–0.35	Bookelaar et al. (2018) OIE (2019)

and (b) release of untreated or incompletely treated effluent (Scianni and Georgiades, 2019).

Pathway Management Approach

Few jurisdictions have enacted biofouling regulations to limit the translocation of marine non-indigenous macro-organisms (Georgiades et al., 2020; Scianni et al., in press). New Zealand's Craft Risk Management Standard for Biofouling on Vessels Arriving to New Zealand (CRMS-BIOFOUL) defines "clean hull" thresholds which are governed by the vessel's itinerary (Ministry for Primary Industries New Zealand [MPI], 2018). These thresholds, while acknowledging issues of feasibility and practicality, were designed to limit macro-organism species richness and density, constraining reproduction, and limiting establishment (Georgiades and Kluza, 2017). The holistic "level of fouling" approach applied by New Zealand manages risk but avoids difficulties, costs, and time associated with taxonomic identifications (Bell et al., 2011). This approach also protects against species not yet known to be invasive and does not require formation and ongoing maintenance of lists of "risk species" or the ongoing cost of surveillance and reporting against such lists.

The likelihood of pathogen translocation from vessels is most efficiently reduced by limiting the amount of macrofouling, which includes susceptible hosts and carrier species, on incoming international or inter-regional vessels. Similar to predicting invasive marine macro-organisms (Bell et al., 2011), identifying future high-risk marine pathogens is difficult; further, the relative dearth of information in this area (Lane et al., 2020; Pagenkopp-Lohan et al., 2020) and the complexities related to pathogen introduction and establishment (section "Associations of OIE-Listed and Other Important Pathogens With Known Biofouling Species") create challenges and uncertainty in determining risk. A pathway management approach to holistically manage pathogen translocations associated with vessel biofouling is therefore likely to be more effective than a pathogen-specific approach.

In-water cleaning plays an important role in managing risks associated with the vessel biofouling pathway (Georgiades et al., 2018; Scianni et al., in press). There are, however, multiple approaches to consider in advancing a "cleaning strategy" to explicitly minimize the transfer of pathogens and micro-organisms. The following sections build on existing tools while identifying challenges, knowledge gaps, and possible solutions.

Proactive In-Water Cleaning (PIC) to Support Ongoing Vessel Maintenance

Proactive in-water cleaning (PIC) is an emerging approach used to prevent biofilm formation, to remove it from the hull (including microscopic life stages of macrofouling organisms), and ultimately to prevent or reduce the establishment and growth of macrofouling (Scianni and Georgiades, 2019). Because of its application early in the biofouling process, less abrasive techniques that are more consistent with the recommendations of antifouling system manufacturers may be used. While a substantial amount of microscopic material is released into the marine environment, PIC is viewed as a relatively low-risk activity because it minimizes the translocation of macrofouling species (Department of Agriculture [DOA] et al., 2015) and therefore minimizes potential translocation of pathogens replicating in macrofouling organisms (Hine, 1995; Lallias et al., 2008; Fuhrmann and Hick, 2020).

Harmful microalgae (including diatoms and dinoflagellates) and pathogens *can* occur in the biofilm of vessels (Drake et al., 2005, 2007; Molino and Wetherbee, 2008; Shikuma and Hadfield, 2010; Revilla-Castellanos et al., 2015). Biofilm formation and its subsequent sloughing from submerged vessel areas during normal operations (including interactions with tugs, bunkering barges, pilot boats, fenders, lines, etc.), however, cannot be prevented (Dobretsov, 2010; Morrisey et al., 2013) without near continual maintenance (Tribou and Swain, 2017; Amara et al., 2018). It may be conceivable to treat liberated biofilm associated micro-organisms during PIC [e.g., exposing the cleaning unit effluent to ultraviolet (UV) radiation], however, the role of the biofilm in pathogen and non-indigenous species translocations requires clarification, thus decisions about the utility and efficacy of PIC require consideration of this uncertainty.

The "Clean Before You Leave" Approach

To further limit the potential for pathogen translocation, adopting the reactive in-water cleaning (RIC) approach of "clean before you leave" could be especially useful, considering that the geographic origin of accumulated fouling dictates the

TABLE 4 | High-level approach for management of pathogen translocation via vessel biofouling.

Approach	Advantages	Disadvantages	Level of maturity/ availability	Key references
Pathway management	Protects against known and unknown risks	Some areas on vessels are difficult to access and maintain	High	Bell et al. (2011) Georgiades et al. (2018) Georgiades et al. (2020)
	Consistent with international fuel efficiency and emissions reduction policies			
	Practicality/feasibility and low cost of implementation			
	Not reliant on species lists and ongoing international surveillance and reporting activities			
Proactive cleaning	Prevents or reduces establishment of macrofouling	Can release substantial amounts of biological material (pathogens and other microbes) of unknown risk into the environment	Low to medium* *Depending on the need for recapture	Schultz et al. (2011) Inglis et al. (2012) Morrisey et al. (2013) Tribou and Swain (2017) Hunsucker et al. (2019) Scianni and Georgiades (2019)
	Consistent with some antifouling system (AFS) manufacturer's recommendations	Some areas on vessels are difficult to access and maintain		
	More convenient and cost effective than fouling penalties and dry-docking	Upfront costs for predicted future benefits		
	Lower environmental risk both chemically and biologically (macrofouling) than reactive cleaning	Some potential for increased release of biocides and macrofouling into the environment		
Reactive cleaning				
Clean before you leave	Little or no biological risk depending on vessel history/itinerary	Potential release of biocides into the environment	High	Inglis et al. (2012) Department of Agriculture [DOA] et al. (2015) Scianni and Georgiades (2019)
	Potentially more convenient and cost effective than dry-docking	Some areas on vessels are difficult to access and maintain		
	Generally applies to a wide range of vessel types (includes most recreational boats) and a subset of other vessels that are high-risk (work barges/platforms, idle/lay-ups, etc.)	Removal of hard fouling associated with AFS damage Does not apply to a majority of commercial vessels		
Reactive in-water cleaning with capture	Potentially more convenient and cost effective than dry-docking	Some potential release of macrofouling and pathogens into the environment	Low	Schultz et al. (2011) Inglis et al. (2012) Morrisey et al. (2013) Morrisey and Woods (2015) Scianni and Georgiades (2019) Tamburri et al. (2020)
	Costs only incurred if/when macrofouling removal is clearly beneficial	Some potential release of biocides into the environment Some areas on vessels are difficult to access and maintain		
		Removal of hard fouling associated with AFS damage		

biosecurity risk (Department of Agriculture [DOA] et al., 2015). This approach recognizes that the most effective focal point for management is prevention, and thus looks to manage the risk of pathogen translocation at the source to limit spread and downstream impacts (Ricciardi et al., 2020). The applicability of this practice depends on the vessel's prior itinerary, pathogen status of the recipient area and areas visited earlier, and proximity to high-value areas. Management of environmental contamination by antifouling biocides is a key consideration if such an approach is to be used (Scianni and Georgiades, 2019).

Reactive In-Water Cleaning With Capture (RICC)

Reactive in-water cleaning of vessel biofouling includes methods to capture, contain, and treat associated organisms [i.e., RICC, also referred to as in-water cleaning with capture (IWCC)]. The efficacy of RICC systems is uncertain in many cases and

may vary by organism size and local conditions (Davidson et al., 2008; Scianni and Georgiades, 2019; Tamburri et al., 2020). To date, cleaning units are designed primarily to capture macrofouling organisms, with some attention to treatment of chemical effluent (Scianni and Georgiades, 2019). Vessel surveys to assess if RICC of macro-organisms is required are limited to detection and identification of macrofouling, while pathogens that may be associated with biofouling organisms have seldom been considered (Georgiades et al., 2020).

Removal of macrofouling by RICC is likely to kill the hosts and, where appropriate treatment of waste is not applied, release pathogens if present. Infected mollusks that are dead or moribund are known pathogen sources, for example: OsHV-1 (see Sauvage et al., 2009), *P. olseni* (see Raynard et al., 2007), and *P. marinus* (see Bobo et al., 1997). The reactive removal of macrofouling can release infective material, potentially in large amounts, into receiving environments with high particle retention. A single oyster can contain 4.4×10^8 *B. ostreae* parasites (Lallias et al., 2008), and Arzul et al. (2009) observed 58% survival of *B. ostreae* parasites after 7 days exposure to seawater at 15°C. OsHV-1 has been observed at 10^7 DNA copies per mg of clinically affected Pacific oyster tissue (Pepin et al., 2008). Hick et al. (2016) found that OsHV-1 remained infectious in seawater for 2 days at 20°C and in non-viable oyster tissues (wet or dry) for at least 7 days at 20°C. Vigneron et al. (2004) detected OsHV-1 DNA released into seawater from macerated larvae for 22 days at 4°C and 12 days at 20°C, although it was not determined if this DNA was viable. *P. olseni* loads in infected host tissues can exceed 2×10^6 parasites per gram (Choi and Park, 2010), and *P. olseni* can survive outside a host for at least several months (Casas et al., 2002). All life stages of *P. olseni* are considered infective (Villalba et al., 2004). While elevated concentrations of antifouling biocides in the treatment stream (Tamburri et al., 2020) may render some pathogens non-viable (Dupont et al., 2011), these can also impact the health of organisms in the receiving environment (Dafforn et al., 2011; Amara et al., 2018), and potentially increase their susceptibility to disease (Moreau et al., 2015).

Direct releases of biofouling from the cleaning head can be assessed by analyzing the total suspended solids (TSS) in water sampled from the surrounding environment during equipment operation (Alliance for Coastal Technologies Maritime Environmental Resource Center [ACT/MERC], 2019; Tamburri et al., 2020). Inclusion of this analysis is a useful addition to the technical advice released by MPI on testing in-water cleaning and treatment systems for external hull and niche areas (Morrisey et al., 2015) and internal seawater systems (Growcott et al., 2019). Similar to direct video observations of the cleaning unit during operations, TSS may serve as a proxy for propagule release into the marine environment.

Recommendations for biosecure effluent treatment standards for surface-based waste processing systems associated with RICC are typically based on physical separation (typically settling tanks followed by filtration) to remove live organisms and propagules associated with macro-organisms (Scianni and Georgiades, 2019). Targeted particle size thresholds range between 2 μm (Morrisey et al., 2013), 5 μm (California Water Boards, 2013), 10 μm (Lewis, 2020), 12.5 μm (Morrisey et al., 2015; Growcott et al., 2019), 50 μm (Department of Agriculture [DOA] et al., 2015), and 60 μm (Morrisey et al., 2013). Assessments of filtration technologies associated with ballast water management systems (BWMS) that use similar designs and functions as those incorporated in RICC systems have shown that they are far from 100% effective at removing live organisms above the stated target particle size, or even the specific physical mesh or sieve size employed (e.g., Gregg et al., 2009; Briski et al., 2014; Cangelosi et al., 2014). Although filtration and settlement can be effective in removing the proportion of pathogens contained within infected material, physical separation of particles, even down to 2–5 um, is unlikely to completely remove many known pathogens, including smaller protists, bacteria, and viruses (**Tables 1–3**), or dissolved biocides (Terraphase Engineering Inc, 2012; Tamburri et al., 2020), from the effluent. Additional effluent treatment options (i.e., a disinfection step) should therefore be considered where the prevention of pathogen translocation associated with vessel biofouling is a concern.

Additional effluent treatment options for reactive in-water cleaning

For high risk international vessels or vessels from regions with different biosecurity conditions, additional measures to the physical separation of captured debris alone include, *but are not limited to*, treatment using biocides, UV radiation, or heat to render propagules non-viable (**Table 5**), or direct disposal of the liquid effluent into municipal sewerage where permitted (Morrisey and Woods, 2015). Pre-filtration to reduce the particulate and organic material present is still required to improve the treatment efficacy of UV, ozone, or oxidants (Chahal et al., 2016; Hess-Erga et al., 2019). Depending on the treatment purpose, pre-filtration recommendations vary between 7 μm (Fraser et al., 2006), 20 μm (Sassi et al., 2005), and 50 μm (Department of Agriculture, Fisheries and Forestry [DAFF], 2008). High flow velocities, however, such as those associated with fouling removal by RICC systems, may decrease filtration efficacy by reducing the contact time between pathogens and particles, and increasing hydraulic shear which can disrupt pathogen-to-particle binding (Chahal et al., 2016). While this may lead to increase in the exposure to subsequent treatments resulting improved efficacy, it also results increased load on this stage of the treatment process.

The concept of appropriate effluent treatment from RICC systems is challenging because:

a) The macrofouling species and pathogens present on submerged surfaces of any given vessel will be largely unknown, therefore any treatments employed should have a wide range of efficacy across a number of pathogen types (e.g., viruses, bacteria, and protists).
b) The efficacy of some treatments (e.g., biocides and UV) is dictated by the amount of organic and particulate matter present and the size of some pathogens (i.e., viruses) is far smaller than any filter size that can be practically achieved. The main purpose of physical separation will, therefore, be to reduce the amount of particulate and

TABLE 5 | Recommended dose/fluence for efficacy of common water treatment agents.

Disinfecting agent	Application	Recommended dose/fluence	References
Chlorine	Drinking water	1 mg/L, 30 min	Henze et al. (2008)
	Effluent (aquaculture)	2 mg/L, 5 min	Meyers (2010)
	Effluent (Processing facilities)	5 mg/L, 30 min An initial concentration of 1,000 mg/L of sodium hypochlorite is sufficient	Fraser et al. (2006)
	Wastewater (aquaculture) (Decontamination)	30 mg/L, 24 h (maintain residual 5 mg/L)	Department of Agriculture, Fisheries and Forestry [DAFF] (2008)
	Wastewater	20–40 mg/L	Henze et al. (2008)
	Wastewater (Cryptosporidium)	20–40 mg/L, 90 min	Henze et al. (2008)
	OSHV-1	50 mg/L, 15 min	Hick et al. (2016)
	Marteilia sydneyi	200 mg/L, 4 h	Wesche et al. (1999)
	Perkinsus marinus	300 mg/L, 30 min	OIE (2019) Chapter 2.4.6
	P. olseni	6 mg/L, 30 min	OIE (2019) Chapter 2.4.7
	Bonamia exitiosa	40 g/L, 10 min	Buss et al. (2020)
Ultraviolet radiation	Effluent (aquaculture)	> 25 mJ/cm^2	Department of Agriculture, Fisheries and Forestry [DAFF] (2008)
	Effluent (aquaculture) (including Mxyosporideans)	> 35 mJ/cm^2	Department of Agriculture, Fisheries and Forestry [DAFF] (2008)
	OsHV-1	42 mJ/cm^2	Stavrakakis et al. (2017)
	P. marinus	> 28 mJ/cm^2	OIE (2019) Chapter 2.4.6
	P. olseni	60 mJ/cm^2	OIE (2019) Chapter 2.4.7
	Influent (freshwater aquaculture) Infectious pancreatic necrosis virus (IPNV)	122 mJ/cm^2	Fraser et al. (2006)
	Effluent (freshwater aquaculture) (Nodavirus)	290 mJ/cm^2	Fraser et al. (2006)
	Effluent (processing facilities)	120 mJ/cm^2	Fraser et al. (2006)
	Influent/effluent (aquaculture) High flow/heavy particulates (99.9% reduction fish viruses)	175 mJ/cm^2	Meyers (2010)
Ozone	Influent/effluent (aquaculture)	8 mg/L, 3 min (Corresponding to redox potential 600–750 mV)	Fraser et al. (2006)
	Emergency disease events (Residual level)	0.5 mg/L,10 min 1 mg/L, 1 min	Department of Agriculture, Fisheries and Forestry [DAFF] (2008)
	OsHV-1	1 mg/L, 30 min	Stavrakakis et al. (2017)
Heat	Wastewater (aquaculture) (Decontamination)	60°C, 10 min 70°C, 6 min 75°C, 5 min 80°C, 4 min Most pathogens Enveloped viruses and some bacteria may be resistant	Department of Agriculture, Fisheries and Forestry [DAFF] (2008)
	Treatment of hard surfaces and equipment	Steam cleaning at 115–130°C for 5 min	Department of Agriculture, Fisheries and Forestry [DAFF] (2008)
	Treatment of gear and steam cleaning non-porous surfaces	70°C, 2 h (IPNV)	Fraser et al. (2006)
	P. marinus	50°C, 1 h (Filtered seawater) 60°C, 1 h (Tissues)	OIE (2019) Chapter 2.4.7

(Continued)

TABLE 5 | Continued

Disinfecting agent	Application	Recommended dose/fluence	References
	Iridoviruses of mollusks (VL) OsHV-1 Malacoherpesviruses Oyster edema disease *Haplosporidium nelsoni* (VL?) *Marteilia* spp. (?) *M. sydneyi* (VL?) *Marteiloides* spp. (?) *M. chungmuensis* (VL?) *Perkinsus* spp. (VL) *P. olseni* (VL) *P. chesapeaki* (VL)	55°C, > 10 min VL = very low risk (= appropriate level of protection) ? = uncertainty due to lack of information	Diggles (2020)
	OsHV-1 Malacoherpesviruses Oyster edema disease *Bonamia* spp. (VL?) *B. exitiosa* (VL?) *B. ostreae* (VL?) *Haplosporidium nelsoni* (?) *Marteilia* spp. (?) *M. refringens* (VL?) *M. sydneyi* (?) *M. roughleyi* (VL?) *Marteiloides* spp. (?) *M. chungmuensis* (?) *Mikrocytos* spp. (VL?) *M. mackini* (VL?) *Minchinia* spp. (VL?) *M. occulta* (VL?) *Perkinsus* spp. (VL?) *P. olseni* (VL?) *P. chesapeaki* (VL?) *P. marinus* (VL?) Akoya oyster disease (VL?)	80°C, > 5 min VL = very low risk (= appropriate level of protection) ? = uncertainty due to lack of information	Diggles (2020)

organic matter present to assist the efficacy of any subsequent treatment(s).

c) The efficacy of some subsequent treatments (e.g., biocides and UV) will be difficult to ascertain without some form of indicator. That is, approaches for disinfecting effluent prior to discharge should demonstrate their efficacy in removing viral, bacterial, and protistan pathogens (or surrogates for pathogens).
d) Biocidal treatments may be subject to local water quality regulations and may require neutralization prior to effluent discharge.

Effluent treatment for the in-water removal of high-risk biofouling can be guided by lessons learned from municipal sewage treatment (Henze et al., 2008; Chahal et al., 2016), the influent and effluent treatment for land-based aquaculture (Fraser et al., 2006; Department of Agriculture, Fisheries and Forestry [DAFF], 2008; Meyers, 2010; Baulch et al., 2013; Whittington et al., 2020), and the development of BWMS (Balaji et al., 2014; First and Drake, 2014; Batista et al., 2017; Hess-Erga et al., 2019).

While the fundamental goal for management of both the biofouling and ballast water pathways is to minimize the risk of non-indigenous species introductions from vessels, discharge thresholds and management approaches for ballast water regulations (e.g., International Maritime Organization [IMO], 2004) are not directly applicable to RICC of vessel biofouling because:

a) Ballast water brought onboard ships has fewer suspended solids and smaller particle sizes than wastewater produced and treated by RICC.
b) The planktonic organisms treated by BWMS are dissimilar in many ways to micro- and macro-organisms observed within biofouling assemblages.
c) The IMO ballast water regulations do not consider organisms less than 10 μm in size, apart from a few target taxa (*E. coli*, Enterococci, and toxigenic *V. cholerae*).
d) RICC systems use large volumes of ambient water in the cleaning process, and RICC effluent therefore requires treatment of biofouling organisms removed from ship surfaces and substantial biomass of local planktonic organisms.
e) Ballast water effluent treatment methods are unlikely to address the environmental risk of releasing antifouling biocides associated with vessel coatings.

In-water cleaning systems do not have the same physical space and power limitations as shipboard BWMS, which could facilitate broader treatment options, such as those used in land-based water treatment, including sewage treatment facilities and aquaculture establishments. While all RICC systems incorporate some form(s) of physical separation (e.g., settling tank, filter, hydrocyclone, and flocculation), decisions about the incorporation of subsequent treatment to either remove dissolved antifouling biocides (e.g., selective metal-binding or adsorption media) or kill pathogens should carefully consider a number of factors including, but not limited to: the marine values requiring protection, risk reduction outcomes, treatment feasibility and practicality, and cost (see Inglis et al., 2012). The following are examples of possible subsequent treatment and disinfection approaches, but not an exhaustive list.

Chlorine. A common disinfectant for wastewater, municipal water, and ballast water (see Ghernaout, 2017), "chlorine"—used here to represent the suite of reactive halogens derived from chlorine—may be suited to disinfect effluent from in-water cleaning operations (**Table 5**). Chlorine can be injected from an external source, or it may be produced on-site, through electrolytic chlorine generation. Regardless of the chlorine compound, and irrespective of whether it is introduced as a solid, liquid, or a gas, a series of cascading reactions occur based upon the water characteristics following the injection of the compound into the effluent. For example, an electrolytic chlorine generator introduces chlorine as a gas, which upon dissolution in water, reacts to form hypochlorous acid (HOCl). In seawater, HOCl is unstable and quickly dissociates to form hypochlorite (OCl^-) and then hypobromous acid, which is also an effective germicide and more stable than HOCl at the pH of seawater (Wong and Davidson, 1977; Abarnou and Miossec, 1992). When ammonia is present in seawater, the oxidants produced through electrolysis form mono-, di-, or tri-chloramines. While these are not considered the primary biocidal agent, some organisms (including invertebrates such as copepods and crab larvae) are sensitive to chloramines (Capuzzo, 1979).

Some BWMS use chlorine to treat large volumes of natural water (Joint Group of Experts on the Scientific Aspects of Marine Environmental Protection [GESAMP], 2019). Generally, ballast water is treated upon uptake, i.e., entry into the ship prior to transit. Treated water is typically held in ballast tanks for at least 1 day, and residual oxidants are neutralized prior to discharge into the environment. In-water cleaning operations require rapid treatment of large volumes, but—relative to ships' ballasting operations—reservoir volumes are small and hold times are minimal. Adapting a BWMS-like approach for in-water cleaning operations would require large tanks and other infrastructure, which may not be practicable. For active substances, treatment would have to occur following the final filtration, as to minimize organic particulates that consume oxidants. In an in-water cleaning operation, treated water would almost immediately be neutralized thus limiting system efficacy, as short treatment times limit the dispersion of chlorine and the reactivity of the primary oxidizing species. Biocidal concentrations required for high flow, small reservoir systems will exceed those for treating ballast water, and the effective doses would vary based upon a variety of factors including temperature, pH, light, salinity, presence of organic matter (Chahal et al., 2016; Batista et al., 2017; Hess-Erga et al., 2019), and contact time. These factors emphasize the importance of measuring the residual dose of chlorine in the system and assessing efficacy using validated methods.

Chlorine may be effective for effluent treatment if on-site or nearby reservoirs are used to hold treated water, allowing time for the reaction and dissipation of chlorine prior to neutralization. Other strategies to improve the biocidal efficacy of chlorine will allow for shorter residence times in the treatment system. For example, combinations of chlorine and other reagents (e.g., CO_2) have shown improved efficacy (Growcott et al., 2017; Hess-Erga et al., 2019). Likewise, mixed-oxidant systems have demonstrated improved biocidal efficacy relative to chlorine alone (Venczel et al., 1997). Finally, an approach for the in-water treatment of hull surfaces has been envisioned: this suggestion would use chlorine produced directly on the hull surfaces by electrolytic chlorination as an antifouling treatment (Iliopoulos et al., 2014). For this approach, ships' existing cathodic protection systems would be reengineered so that chlorine—naturally produced at the anodes—is dispersed to prevent fouling on the hull and other wetted surfaces. This approach would guard against both macrofouling organisms and their pathogens. However, "in-water chlorination" would potentially introduce high concentrations of chlorine (and disinfection byproducts) into natural water systems which would likely violate the local water quality standards of many jurisdictions.

While chlorination appears to be an obvious candidate for secondary treatment of in-water cleaning effluent, its efficacy remains unresolved (Cahill et al., 2019a), the effluent would need to be neutralized prior to discharge to satisfy local water quality standards, and it is not yet incorporated in any commercially available RICC system.

Ultraviolet (UV) radiation. Ultraviolet radiation is used to disinfect drinking, waste, and ballast water (see Chen et al., 2006). By contrast to chlorine, UV radiation is readily adaptable for an in-line system for effluent treatment: treatment occurs during the short period that suspended organism transits through a chamber. Reactive chemicals are not required, nor are neutralizing agents. Effluent water could be discharged immediately following treatment, given that the dose is sufficient. To achieve the prescribed ballast water discharge standards, Oemcke et al. (2004) and Kim et al. (2019) recommended doses of 60–70 mJ/cm^2 to treat most bacteria and viruses (**Table 5**). Oemcke et al. (2004) further recommended that a dose of 120 mJ/cm^2 would remove most micro-organisms except for resistant cysts and viruses. Much higher doses are required to treat the cysts of *Cryptosporidium* spp. ($>$ 200 mJ/cm^2) and diatoms such as *Gymnodinium catenatum* ($>$ 1,600 mJ/cm^2) (Gregg et al., 2009). For many micro-organisms, the effect of UV irradiation may not be immediate, raising the issue of organism viability (i.e., treatment efficacy). This issue has introduced a variety of complications when determining the efficacy of BWMS (First and Drake, 2014; Batista et al., 2017; Peperzak et al., 2020). For example, damage to organisms, in certain cases,

may be repairable (e.g., Zimmer and Slawson, 2002). Similar to chlorine, UV radiation efficacy varies based upon the water characteristics, particularly the concentration of particulate and dissolved material (primarily organic matter), which reduce the UV transmissivity (%UVT), but may also scavenge reactive oxidation species (Ou et al., 2011). At least one commercially available RICC system includes the option of secondary UV treatment of captured debris (Lewis, 2013).

Ozone. Ozone is an established water treatment (see Langlais et al., 1991) and is effective against a range of micro-organisms (Gregg et al., 2009; Chahal et al., 2016). Similar to chlorine, ozone is an oxidizing compound that may be generated on-site. For ballast water treatment > 5 mg/L, total residual oxidants for 10 h appear to be a broad-spectrum treatment for free-living bacteria, dinoflagellates, and diatoms; however, 8–14 mg/L for 24 h was required to effectively treat the spore-forming bacteria *Bacillus subtilis* (see Gregg et al., 2009; **Table 5**). Ozone—when used as a disinfectant for effluent from a land-based RICC treatment system—has some of the same limitations and caveats as chlorine. Treatment efficacy is a product of both dose concentration and exposure time, and for a flow-through system, exposure time will be limited. Likewise, residual oxidants will require neutralization. Ozone is not yet incorporated into RICC systems.

Heat. Some in-water cleaning technologies use heat as an approach for removing fouling, particularly the algal and biofilm fouling on easily accessible areas of ships' hulls (Morrisey and Woods, 2015). In this case, heat treatment would be effective against free-living pathogens. Heat may also be used in shore-side treatment systems to kill organisms remaining prior to discharge. For treatment of macrofouled vessel internal seawater systems, Cahill et al. (2019b) and Growcott et al. (2019) recommended exposure to 60°C for 60 min. Such a treatment would appear to be effective against all but the hardiest pathogens, e.g., birnaviruses such as infectious pancreatic necrosis virus (IPNV; Fraser et al., 2006). Aquatic birnaviruses have been found in oysters and mussels located near salmon farms (Mortensen, 1993; Rivas et al., 1993). IPNV has had substantial impacts on global salmonid aquaculture (Munro and Midtlyng, 2011) and has been experimentally transmitted from *Mytilus edulis* to *Salmo salar* by cohabitation (Molloy et al., 2013). When considering the range of pathogens of biosecurity relevance to Australia, Diggles (2020) concluded that heating (80°C in water, > 5 min) would meet the acceptable level of protection (i.e., an annual probability of establishment between 1 in 20 and 1 in 100 years) for all identified risk pathogens despite uncertainty from data deficiency (**Table 5**).

For BWMS, chlorine and UV radiation are common disinfectants, but heat is also used in some cases. For one particular BWMS, the heat source is primarily waste heat from the ship engines and cargo pumps. Treatment occurs in a section of heated pipe, designed so that flowing water meets minimal hold time and temperature limits for disinfection. Note that this system, while shown in Type Approval testing to meet limits on regulated groups of organisms (e.g., Coast Guard Maritime Commons, 2020), was not evaluated for its efficacy in treating pathogenic bacteria, protists < 10 μm, and viruses. While heat treatment is not sensitive to most water characteristics (such as dissolved organic material, salinity, etc.), its efficiency does depend upon the temperature of the input water, i.e., more energy is required to meet the minimum effective temperature in cold and temperate waters relative to tropical waters. On ships, heat-based BWMS may be coupled with heat generating systems, but on a shore-side operation, it is likely that a dedicated, intentional heat source is necessary. The feasibility for using heat to treat the effluent from in-water cleaning operations, therefore, rests on the characteristics of a specific location, including water temperatures, access to fuel or energy for boilers, and opportunities for capturing waste heat. Heat is not yet incorporated into RICC systems.

CONCLUSION

The long history of devastating impacts to marine values caused by cross-boundary translocation of marine pathogens has resulted in improved practices from regulatory and non-regulatory controls that apply to established pathways, such as fisheries and aquaculture. Available evidence indicates that vessel biofouling is also a viable and important pathway for translocating marine pathogens which presents a risk to marine values. This largely unmanaged pathway, therefore, represents a considerable gap in the biosecurity measures of jurisdictions committed to the prevention and control of aquatic disease. Preventive measures, such as those used in New Zealand and Californian biofouling regulations, lower the likelihood of pathogen translocation by reducing diversity, population size, and total mass of susceptible hosts and carrier species on vessels. Reactive measures, such as in-water removal of macrofouling, may, however, exacerbate the problem and will likely need modification to manage the risk associated with pathogens. While lessons learned from ballast water management, sewage treatment, and aquaculture industries should be considered when developing cleaning and effluent treatment criteria for reactive approaches, preventing or greatly reducing the translocation of pathogens using proactive measures for vessel biofouling is likely to be more effective. Both proactive and reactive solutions, however, have their own unique challenges. The balance between marine protection and risk reduction versus treatment feasibility and cost requires careful consideration.

DATA AVAILABILITY STATEMENT

The original contributions presented in the study are included in the article. Further inquiries can be directed to the corresponding author/s.

AUTHOR CONTRIBUTIONS

EG and DK conceived the idea for the manuscript which was drafted by EG. DK, CS, ID, MT, MF, GR, KE, and MD revised the manuscript draft and contributed sections based on their areas of expertise. All authors contributed to manuscript revision and read and approved the submitted version.

FUNDING

Preparation of this article was funded by the Risk Assessment Group, Ministry for Primary Industries, New Zealand. The New Zealand Ministry for Business Innovation and Employment's Endeavour Fund: Aquaculture Health Strategies to Maximise Productivity and Security (CAWX1707) funded ID's contribution. The U.S. Department of Transportation's Maritime Administration supported MT's and MF's contributions.

ACKNOWLEDGMENTS

Draft versions of this manuscript were reviewed by Oliver Quinn, Michael Ormsby, Enrico Perotti (MPI), and Nicole Dobroski (CSLC). Jonathan Thompson (CSLC) provided useful discussions and assistance regarding ballast water management. The authors thank the two reviewers for their constructive feedback which greatly improved the manuscript.

REFERENCES

Abarnou, A., and Miossec, L. (1992). Chlorinated waters discharged to the marine environment: Chemistry and environmental impact - An overview. *Sci. Total Environ.* 126, 173–197. doi: 10.1016/0048-9697(92)90490-j

Abollo, E., Ramilo, A., Casas, S. M., Comesaña, P., Cao, A., Carballal, M. J., et al. (2008). First detection of the protozoan parasite *Bonamia exitiosa* (*Haplosporidia*) infecting flat oyster *Ostrea edulis* grown in European waters. *Aquaculture* 274, 201–207. doi: 10.1016/j.aquaculture.2007.11.037

Alagarswami, K. (1977). "Larval Transport and Settlement of Pearl Oysters (genus Pinctada) in the Gulf of Mannar," in *Proceedings of the Symposium on Warm Water Zooplankton*, (Goa: National Institute of Oceanography).

Aldred, N., and Clare, A. S. (2008). The adhesive strategies of cyprids and development of barnacle-resistant marine coatings. *Biofouling* 24, 351–363. doi: 10.1080/08927010802256117

Alliance for Coastal Technologies Maritime Environmental Resource Center [ACT/MERC] (2019). *Evaluation of Subsea Global Solutions in-Water Cleaning and Capture Technology for Ships*. Baltimore, MD: ACT/MERC, ACT/MERC IWCC Evaluation Report ER01-19. Available online at: http://www.maritime-enviro.org/Downloads/Reports/Other_Publications/ACT_MERC_SGS_IWCC_Evaluation_Report.pdf (accessed April, 2021).

Amara, I., Miled, W., Slama, R. B., and Ladhari, N. (2018). Antifouling processes and toxicity effects of antifouling paints on marine environment. *Environ. Toxicol. Pharm.* 57, 115–130. doi: 10.1016/j.etap.2017.12.001

Angell, C. L. (1986). *he Biology and Culture of Tropical Oysters. ICLARM Studies and Reviews. Vol. 13. International Center for Living Aquatic Resources Management*. Philippines: Manila.

Apte, S., Holland, B. S., Godwin, L. S., and Gardner, J. P. A. (2000). Jumping ship: A stepping stone event mediating transfer of nonindigenous species via a potentially unsuitable environment. *Biol. Invas.* 2, 75–79.

Arzul, I., Gagnaire, B., Bond, C., Chollet, B., Morga, B., Ferrand, S., et al. (2009). Effects of temperature and salinity on the survival of *Bonamia ostreae*, a parasite infecting flat oysters *Ostrea edulis*. *Dis. Aquat. Organ.* 85, 67–75. doi: 10.3354/dao02047

Arzul, I., Moissec, L., Blanchet, E., Garcia, C., Francois, C., and Joly, J.-P. (2006). "*Bonamia ostreae* and *Ostrea edulis*: a Stable Host–parasite System in France?," in *Proceedings of the 11th International Symposium on Veterinary Epidemiology and Economics*. Cairns.

Balaji, R., Yaakob, O., and Koh, K. K. (2014). A review of developments in ballast water management. *Environ. Rev.* 22, 298–310. doi: 10.1139/er-2013-0073

Bailey, S. A., Brown, L., Campbell, M. L., Carlton, J. T., Castro, N., Chainho, P., et al. (2020). Trends in the detection of aquatic non-indigenous species across global marine, estuarine and freshwater ecosystems: A 50—year perspective. *Diver. Distribut.* 26, 1780–1797. doi: 10.1111/ddi.13167

Barbieri, M., Maltagliati, F., Di Giuseppe, G., Cossu, P., Lardicci, C., and Castelli, A. (2011). New records of the pygmy mussel *Xenostrobus securis* (Bivalvia: Mytilidae) in brackish-water biotopes of the western Mediterranean provide evidence of its invasive potential. *Mar. Biodiv. Rec.* 2011:4.

Barkai, A., and Branch, G. M. (1989). Growth and mortality of the mussels *Choromytilus meridionalis* (Krauss) and *Aulacomya ater* (Molina) as indicators of biotic conditions. *J. Molluscan Stud.* 55, 329–342. doi: 10.1093/mollus/55.3.329

Bateman, K. S., Tew, I., French, C., Hicks, R. J., Martin, P., Munro, J., et al. (2012). Susceptibility to infection and pathogenicity of White Spot Disease (WSD) in non-model crustacean host taxa from temperate regions. *J. Invert. Pathol.* 110, 340–351. doi: 10.1016/j.jip.2012.03.022

Batista, W. R., Fernandes, F. C., Lopes, C. C., Lopes, R. S., Miller, W., and Ruiz, G. (2017). Which ballast water management system will you put aboard? Remnant anxieties: A mini-review. *Environments* 4:54. doi: 10.3390/environments4030054

Baulch, T., Ellard, K., and Bradshaw, M. (2013). Tasmanian abalone biosecurity project: Implementation phase 1: Biosecurity strategies for abalone processors. *J. Shellfish Res.* 32, 33–35. doi: 10.2983/035.032.0107

Bell, A., Philipps, S., Denny, C., Georgiades, E., and Kluza, D. (2011). *Risk Analysis: Vessel Biofouling. Ministry of Agriculture and Forestry Biosecurity*. New Zealand: Wellington.

Bingham, P., Brangenberg, N., Williams, R., and van Andel, M. (2013). Investigation into the first diagnosis of ostreid herpesvirus type 1 in Pacific oysters. *Surveillance* 40, 20–24.

Bishop, M. J., Carnegie, R. B., Stokes, N. A., Peterson, C. H., and Burreson, E. M. (2006). Complications of a non-native oyster introduction: facilitation of a local parasite. *Mar. Ecol. Prog. Series* 325, 145–152. doi: 10.3354/meps325145

Bobo, M. Y., Richardson, D. L., Coen, L. D., and Burrell, V. G. (1997). *A Report on the Protozoan Pathogens Perkinsus marinus (Dermo)* and *Haplosporidium nelsoni (MSX)* in South Carolina Shellfish Populations. South Carolina Marine Resources Division Technical Report No. 86. Columbia: South Carolina State Library.

Bookelaar, B. E., Reilly, A. O., Lynch, S. A., and Culloty, S. C. (2018). Role of the intertidal predatory shore crab *Carcinus maenas* in transmission dynamics of ostreid herpesvirus-1 microvariant. *Dis. Aquat. Organ.* 130, 221–233. doi: 10.3354/dao03264

Bower, S. M. (2019). *Synopsis of Infectious Diseases and Parasites of Commercially Exploited Shellfish: Marteilia refringens/maurini* of mussels. Available online at: https://www.dfo-mpo.gc.ca/science/aah-saa/diseases-maladies/mrmaurmu-eng.html (accessed September 2020)

Bower, S. M. (2017). *Synopsis of Infectious Diseases and Parasites of Commercially Exploited Shellfish: Table of Contents*. Available online at: https://www.dfo-mpo.gc.ca/science/aah-saa/diseases-maladies/toc-eng.html#mol (accessed September 2020)

Bower, S. M. (2015). *Synopsis of Infectious Diseases and Parasites of Commercially Exploited Shellfish: Bonamia* (=*Mikrocytos*) *roughleyi* (Australian winter disease) of oysters. Available online at: https://www.dfo-mpo.gc.ca/science/aah-saa/diseases-maladies/mikrouoy-eng.html (accessed September 2020)

Bower, S. M. (2014a). *Synopsis of Infectious Diseases and Parasites of Commercially Exploited Shellfish: Haplosporidium costale* (SSO) of Oysters. Available online at: https://www.dfo-mpo.gc.ca/science/aah-saa/diseases-maladies/hcoy-eng.html (accessed September 2020)

Bower, S. M. (2014b). *Synopsis of Infectious Diseases and Parasites of Commercially Exploited Shellfish: Haplosporidium nelsoni* (MSX) of oysters. Available online at: https://dfo-mpo.gc.ca/science/aah-saa/diseases-maladies/hapneloy-eng.html (accessed September 2020).

Bower, S. M. (2014c). *Synopsis of Infectious Diseases and Parasites of Commercially Exploited Shellfish: Haplosporidium* sp. of rock oysters.Available online at: https://www.dfo-mpo.gc.ca/science/aah-saa/diseases-maladies/haprockoy-eng.html (accessed September 2020)

Bower, S. M. (2013a). *Synopsis of Infectious Diseases and Parasites of Commercially Exploited Shellfish: Hematodinium* sp. (Bitter Crab Disease). Available online

at: https://www.dfo-mpo.gc.ca/science/aah-saa/diseases-maladies/hematcb-eng.html (accessed September 2020)

Bower, S. M. (2013b). *Synopsis of Infectious Diseases and Parasites of Commercially Exploited Shellfish: Hematodinium perezi* and *Hematodinium* sp. of Atlantic Crabs. Available online at: https://www.dfo-mpo.gc.ca/science/aah-saa/diseases-maladies/hphacb-eng.html (accessed September 2020)

Bower, S. M., and Kleeman, S. N. (2011). *Synopsis of Infectious Diseases and Parasites of Commercially Exploited Shellfish: Marteilia sydneyi* of oysters. Available online at: https://www.dfo-mpo.gc.ca/science/aah-saa/diseases-maladies/marsydoy-eng.html (accessed September 2020)

Bower, S. M. (2010). *Synopsis of Infectious Diseases and Parasites of Commercially Exploited Shellfish: Juvenile disease of Eastern oysters*. Available online at: https://dfo-mpo.gc.ca/science/aah-saa/diseases-maladies/jdeoy-eng.html (accessed September 2020).

Bower, S. M. (2009). *Synopsis of Infectious Diseases and Parasites of Commercially Exploited Shellfish: Vibrio* spp. (larval and juvenile vibriosis) of oysters. Available online at: https://www.dfo-mpo.gc.ca/science/aah-saa/diseases-maladies/vibrioy-eng.html (accessed September 2020)

Bower, S. M. (2006). *Synopsis of Infectious Diseases and Parasites of Commercially Exploited Shellfish: Nocardiosis of Oysters*. Available online at: https://dfo-mpo.gc.ca/science/aah-saa/diseases-maladies/nocardoy-eng.html (accessed September 2020).

Bower, S. M. (2001a). *Synopsis of Infectious Diseases and Parasites of Commercially Exploited Shellfish: Gill disease of Portuguese oysters*. Available online at: https://dfo-mpo.gc.ca/science/aah-saa/diseases-maladies/gilldpoy-eng.html (accessed September 2020).

Bower, S. M. (2001b). *Synopsis of Infectious Diseases and Parasites of Commercially Exploited Shellfish: Hinge Ligament Disease of Juvenile Oysters*. Available online at: https://www.dfo-mpo.gc.ca/science/aah-saa/diseases-maladies/hldjoy-eng.html (accessed September 2020)

Bower, S. M. (2001c). *Synopsis of Infectious Diseases and Parasites of Commercially Exploited Shellfish: Kidney coccidia of mussels*. Available online at: https://www.dfo-mpo.gc.ca/science/aah-saa/diseases-maladies/kidcocmu-eng.html (accessed September 2020)

Bower, S. M. (2001d). *Synopsis of Infectious Diseases and Parasites of Commercially Exploited Shellfish: Oyster velar virus disease (OVVD)*. Available online at: https://dfo-mpo.gc.ca/science/aah-saa/diseases-maladies/ovvdoy-eng.html (accessed September 2020).

Bower, S. M. (2001e). *Synopsis of Infectious Diseases and Parasites of Commercially Exploited Shellfish: Virus-like disease of mussels*. Available online at: https://www.dfo-mpo.gc.ca/science/aah-saa/diseases-maladies/virldmu-eng.html (accessed September 2020)

Bower, S. M., Korrûbel, J. L., and Webb, S. C. (2002). *Synopsis of Infectious Diseases and Parasites of Commercially Exploited Shellfish: Phototrophic endolith invasion of mussel shells*. Available online at: https://www.dfo-mpo.gc.ca/science/aah-saa/diseases-maladies/bgasimu-eng.html (accessed September 2020)

Bower, S. M., McGladdery, S. E., and Price, I. M. (1994). *Synopsis of Infectious Diseases and Parasites of Commercially Exploited Shellfish: Haemocytic infection virus disease of oysters*. Available online at: https://dfo-mpo.gc.ca/science/aah-saa/diseases-maladies/hivoy-eng.html (accessed September 2020).

Briski, E., Linley, R. D., Adams, J., and Bailey, S. A. (2014). Evaluating efficacy of a ballast water filtration system for reducing spread of aquatic species in freshwater ecosystems. *Manag. Invas.* 5, 245–253. doi: 10.3391/mbi.2014.5.3.08

Brock, R., Bailey-Brock, J. H., and Goody, J. (1999). A case study of efficacy of freshwater immersion in controlling introduction of alien marine fouling communities: the USS Missouri. *Pacific Sci.* 53, 223–231.

Buss, J., Wiltshire, K. H., Harris, J. O., and Deveney, M. R. (2020). Decontamination of *Bonamia exitiosa*. *Aquaculture* 2020:735210. doi: 10.1016/j.aquaculture.2020.735210

Cahill, P., Hickey, C., Lewis, P., Tait, L., and Floerl, O. (2019a). *Treatment Agents for Biofouling in Internal Pipework of Recreational Vessels*. Available online at: https://www.mpi.govt.nz/dmsdocument/33606-treatment-agents-forbiofouling-in-internal-pipework-of-recreational-vessels-a-review-ofpipework-configurations-biofouling-risk-and-operational-considerations (accessed March 2019).

Cahill, P., Tait, L., Floerl, O., Bates, T., Growcott, A., and Georgiades, E. (2019b). Design and assessment of a thermal treatment system for fouled internal pipework of recreational vessels. *Mar. Pollut. Bull.* 139, 65–73. doi: 10.1016/j.marpolbul.2018.12.032

California Code of Regulations (2017). *Biofouling Management to Minimize the Transfer of Nonindigenous Species from Vessels Arriving at California Ports*. California, CA: California Code of Regulations.

California Water Boards. (2013). *In-water Vessel Hull Cleaning. Best Management Practice Fact Sheet – July 2013*. Available online at: http://www.waterboards.ca.gov/sanfranciscobay/publications_forms/documents/In-water_vessel_hull_cleaning_fact_sheet.pdf (accessed September 2020)

Calvo, G. W., Luckenbach, M., and Burreson, E. M. (1999). *A Comparative Field Study of Crassostrea gigas* and *Crassostrea virginica* in Relation to Salinity in Virginia. Special Reports in Applied Marine Science and Ocean Engineering (SRAMSOE) No. 349. Williamsburg: Virginia Institute of Marine Science, William and Mary.

Cangelosi, A., Aliff, M., Allinger, L., Balcer, M., Beesley, K., Desai, M., et al. (2014). *Results of Shipboard Approval Tests of Ballast Water Treatment Systems in Freshwater (No. CG-D-05-15)*. New London: Coast Guard Research and Development Center.

Capuzzo, J. M. (1979). Effect of temperature on the toxicity of chlorinated cooling water to marine animals: A preliminary review. *Mar. Pollut. Bull.* 10, 45–47. doi: 10.1016/0025-326x(79)90267-4

Carlton, J. T. (1999). Molluscan invasions in marine and estuarine communities. *Malacologia* 41, 439–454.

Casas, S. M., Villalba, A., and Reece, K. S. (2002). Study of perkinsosis in the carpet shell clam Tapes decussatus in Galicia (NW Spain). I. Identification of the aetiological agent and in vitro modulation of zoosporulation by temperature and salinity. *Dis. Aquat. Organ.* 50, 51–65. doi: 10.3354/dao050051

Centre for Environment, Fisheries and Aquaculture Science [Cefas]. (2009). *Shellfish Biosecurity Measures Plan. Guidance and Templates for Shellfish Farmers and Traders*. Weymouth: Fish Health Inspectorate, Centre for Environment, Fisheries and Aquaculture Science.

Chahal, C., Van Den Akker, B., Young, F., Franco, C., Blackbeard, J., and Monis, P. (2016). Pathogen and particle associations in wastewater: Significance and implications for treatment and disinfection processes. *Adv. Appl. Microb.* 97, 63–119.

Chen, J. P., Yang, L., Wang, L. K., and Zhang, B. (2006). "Ultraviolet Radiation for Disinfection," in *Advanced Physicochemical Treatment Processes. Handbook of Environmental Engineering*, Vol. 4, eds L. K. Wang, Y. T. Hung, and N. K. Shammas (Totowa, NY: Humana Press).

Choi, K. S., and Park, K. I. (2010). "Review on the Protozoan Parasite *Perkinsus olseni* (Lester and Davis 1981) Infection in Asian Waters," in *Coastal Environmental and Ecosystem Issues of the East China Sea*, eds A. Ishimatsu and H.-J. Lie (Japan: Hiroshima University Press), 269–281.

Coast Guard Maritime Commons (2020). *Marine Safety Center issues Ballast Water Management System Type Approval Certificate to BAWAT A/S. Maritime Commons web posting, 3/4/2020*. Available online at: https://mariners.coastguard.blog/2020/03/04/marine-safety-center-issues-ballast-water-management-system-type-approval-certificate-to-bawat-a-s/ (accessed January 2021).

Cohen, N. J., Slaten, D. D., Marano, N., Tappero, J. W., Wellman, M., Albert, R. J., et al. (2012). Preventing maritime transfer of toxigenic *Vibrio cholerae*. *Emerg. Infect. Dis.* 18, 1680–1682.

Costello, K. E., Lynch, S. A., McAllen, R., O'Riordan, R. M., and Culloty, S. C. (2020). The role of invasive tunicates as reservoirs of molluscan pathogens. *Biol. Invas.* 2020, 1–15.

Coutts, A. D., and Dodgshun, T. J. (2007). The nature and extent of organisms in vessel sea-chests: A protected mechanism for marine bioinvasions. *Mar. Pollut. Bull.* 54, 875–886. doi: 10.1016/j.marpolbul.2007.03.011

Coutts, A. D., and Taylor, M. D. (2004). A preliminary investigation of biosecurity risks associated with biofouling on merchant vessels in New Zealand. *N. Zeal. J. Mar. Freshwater Res.* 38, 215–229. doi: 10.1080/00288330.2004.9517232

Coutts, A. D. M., Moore, K. M., and Hewitt, C. L. (2003). Ships' sea-chests: an overlooked transfer mechanism for non-indigenous marine species? *Mar. Pollut. Bull.* 46, 1504–1515.

Culloty, S. C., and Mulcahy, M. F. (2007). Bonamia ostreae in the Native Oyster *Ostrea edulis*. *Mar. Environ. Health Series* 2007:29.

Dafforn, K. A., Lewis, J. A., and Johnston, E. L. (2011). Antifouling strategies: History and regulation, ecological impacts and mitigation. *Mar. Pollut. Bull.* 62, 453–465. doi: 10.1016/j.marpolbul.2011.01.012

Davidson, I., Scianni, C., Hewitt, C., Everett, R., Holm, E., Tamburri, M., et al. (2016). Mini-review: Assessing the drivers of ship biofouling management–aligning industry and biosecurity goals. *Biofouling* 32, 411–428. doi: 10.1080/08927014.2016.1149572

Davidson, I., Ashton, G., Ruiz, G., Scianni, C., Brown, C., Pagenkopp-Lohan, K., et al. (2013). *Richness, Extent, Condition, Reproductive Status, and Parasitism of Fouling Communities on Commercial Vessels*. California: Report to the California State Lands Commission, Marine Invasive Species Program.

Davidson, I. C., Brown, C. W., Sytsma, M. D., and Ruiz, G. M. (2009). The role of containerships as transfer mechanisms of marine biofouling species. *Biofouling* 25, 645–655. doi: 10.1080/08927010903046268

Davidson, I. C., McCann, L. D., Sytsma, M. D., and Ruiz, G. M. (2008). Interrupting a multi-species bioinvasion vector: The efficacy of in-water cleaning for removing biofouling on obsolete vessels. *Mar. Pollut. Bull.* 56, 1538–1544. doi: 10.1016/j.marpolbul.2008.05.024

Davies, C. E., Batista, F. M., Malkin, S. H., Thomas, J. E., Bryan, C. C., Crocombe, P., et al. (2019). Spatial and temporal disease dynamics of the parasite *Hematodinium* sp. in shore crabs. *Carc. Parasit. Vect.* 12:472.

Deveney, M., Roberts, S., Moody, N., Crane, M., and Ellard, K. (2017). "Biofouling as a Long Distance Vector for Pathogens," in *Proceedings of the 4th Fisheries Research and Development Corporation Australasian Aquatic Animal Health and Biosecurity Scientific Conference*, ed. M. S. J. Crane (Cairns, Australia).

Department of Agriculture, Fisheries and Forestry [DAFF] (2008). *Operational Procedures Manual - Decontamination* (Version 1.0). In: Australian Aquatic Veterinary Emergency Plan (AQUAVETPLAN). Canberra, ACT: Australian Government Department of Agriculture, Fisheries and Forestry.

Department of Agriculture, Water and the Environment (2020). *Aquatic Animal Diseases Significant to Australia: Identification Field Guide, 5th Edition*. Canberra: Australian Government Department of Agriculture, Water and the Environment. Available online at: https://www.agriculture.gov.au/sites/default/files/documents/field-guide-5th-edition.pdf (accessed September 2020)

Department of Agriculture [DOA], Department of the Environment [DOE], and New Zealand Ministry for Primary Industries [MPI]. (2015). *Antifouling and in-Water Cleaning Guidelines*. Canberra: Department of Agriculture.

Diggles, B. K. (2020). *Risk Analysis: Biosecurity Risks Related to Recycling of Mollusc Shell Waste for Shellfish Reef Restoration*. New Zealand: DigsFish Services Report DF20-03b for Fisheries Research and Development Corporation.

Ding, Z., Yao, Y., Zhang, F., Wan, J., Sun, M., Liu, H., et al. (2015). The first detection of white spot syndrome virus in naturally infected cultured Chinese mitten crabs, *Eriocheir sinensis* in China. *J. Virolog. Methods* 220, 49–54. doi: 10.1016/j.jviromet.2015.04.011

Dobretsov, S. (2010). "Marine biofilms," in *Biofouling*, eds S. Dürr and J. C. Thomasson (Oxford: Wiley-Blackwell), 123–136.

Drake, J. M., and Lodge, D. M. (2007). Hull fouling is a risk factor for intercontinental species exchange in aquatic ecosystems. *Aquat. Invas.* 2, 121–131. doi: 10.3391/ai.2007.2.2.7

Drake, L. A., Doblin, M. A., and Dobbs, F. C. (2007). Potential microbial bioinvasions via ships' ballast water, sediment, and biofilm. *Mar. Pollut. Bull.* 55, 333–341. doi: 10.1016/j.marpolbul.2006.11.007

Drake, L. A., Meyer, A. E., Forsberg, R. L., Baier, R. E., Doblin, M. A., Heinemann, S., et al. (2005). Potential invasion of micro-organisms and pathogens via 'interior hull fouling': Biofilms inside ballast water tanks. *Biol. Invas.* 7, 969–982. doi: 10.1007/s10530-004-3001-8

Dungan, C. F., Elston, R. A., and Schiewe, M. H. (1989). Evidence for colonization and destruction of hinge ligaments in cultured juvenile Pacific oysters (*Crassostrea gigas*) by *cytophaga*-like bacteria. *Appl. Env. Microb.* 55, 1128–1135. doi: 10.1128/aem.55.5.1128-1135.1989

Dupont, C. L., Grass, G., and Rensing, C. (2011). Copper toxicity and the origin of bacterial resistance—new insights and applications. *Metallomics* 3, 1109–1118.

European Food Safety Authority [Efsa]. (2015). European Food Safety Authority Panel on Animal Health Welfare. Scientific Opinion on Oyster Mortality. *EFSA J.* 13:59.

Farnsworth, M., Culloty, S., Carnegie, R., Diggles, B., Deveney, M., and Michael, K. (2020). *Report of the Technical Advisory Group 2019 on a Return to Flat Oyster Farming. 23-27 September 2019*. Wellington: Produced for Biosecurity New Zealand.

Farrapeira, C. M. R., Ferreira, G. F. D. A., and Tenório, D. D. O. (2010). Intra-regional transportation of a tugboat fouling community between the ports of Recife and Natal, northeast Brazil. *Brazilian J. Oceanogr.* 58, 1–14.

First, M. R., and Drake, L. A. (2014). Life after treatment: detecting living micro-organisms following exposure to UV light and chlorine dioxide. *J. Appl. Phycol.* 26, 227–235. doi: 10.1007/s10811-013-0049-9

Fisheries Research and Development Corporation (2011). *Final Report, OsHV-1 μ-var International Workshop*, Australi: Fisheries Research and Development Corporation.

Flemming, H. C. (2002). Biofouling in water systems–cases, causes and countermeasures. *Appl. Microb. Biotechnol.* 59, 629–640. doi: 10.1007/s00253-002-1066-9

Floerl, O., Inglis, G. J., Dey, K., and Smith, A. (2009). The importance of transport hubs in stepping-stone invasions. *J. Appl. Ecol.* 46, 37–45. doi: 10.1111/j.1365-2664.2008.01540.x

Fraser, D. I., Munro, P. D., and Smail, D. A. (2006). *Disinfection Guide Version IV. Practical steps to prevent the introduction and minimise the transmission of diseases of fish. Fisheries Research Services Internal Report No. 13/06. In: Code of Good Practice Management Group (2015). The Code of Good Practice for Scottish Finfish Aquaculture*. Scotland: Scottish Salmon Producer's Organisation. Available online at: http://www.thecodeofgoodpractice.co.uk/ (accessed September 2020)

Fuhrmann, M., and Hick, P. M. (2020). *Vessel Biofouling and Aquatic Pathogens. Biosecurity new Zealand Technical Paper*. New Zealand: Ministry for Primary Industries.

Gadd, J., Depree, C., and Hickey, C. (2011). *Relevance to New Zealand of the OECD Emission Scenario Document for Antifouling Paints: Phase 2 Report. Report for the Environmental Protection Authority (EPA)*. Hamilton: National Institute of Water and Atmospheric Research Ltd.

Georgiades, E. (2015). *Risk Assessment: Pathways Associated with Domestic Spread of Bonamia ostreae*. Prepared for Animal and Marine Biosecurity Response Team. New Zealand: Ministry for Primary Industries.

Georgiades, E., and Kluza, D. (2017). Evidence-based decision making to underpin the thresholds in New Zealand's CRMS: biofouling on vessels arriving to New Zealand. *J. Mar. Sci. Technol.* 51, 76–88. doi: 10.4031/mtsj.51.2.5

Georgiades, E., Kluza, D., Bates, T., Lubarsky, K., Brunton, J., Growcott, A., et al. (2020). Regulating vessel biofouling to support New Zealand's marine biosecurity system – A blue print for evidence-based decision making. *Front. Mar. Sci.* 7:390.

Georgiades, E., Growcott, A., and Kluza, D. (2018). *Technical Guidance on Biofouling Management for Vessels Arriving to New Zealand*. Wellington: Ministry for Primary Industries, 16.

Georgiades, E., Fraser, R., and Jones, B. (2016). *Options to Strengthen On-farm Biosecurity Management for Commerical and Non-commercial Aquaculture. Technical Paper No. 2016/47*. Wellington: Ministry for Primary Industries.

Ghernaout, D. (2017). Water treatment chlorination: An updated mechanistic insight review. *Chem. Res. J.* 2, 125–138.

Gias, E., and Johnston, C. (2010). Molecular tools for diagnosis of mollusc pathogens. *Surveillance* 37, 44–48.

Goedknegt, M. A., Feis, M. E., Wegner, K. M., Luttikhuizen, P. C., Buschbaum, C., Camphuysen, K., et al. (2016). Parasites and marine invasions: Ecological and evolutionary perspectives. *J. Sea Res.* 113, 11–27.

Goulletquer, P. (2004). *Cultured Aquatic Species Information programme. Ostrea edulis*. Rome: FAO Fisheries Division [online].

Green, T. J., and Barnes, A. C. (2010). Bacterial diversity of the digestive gland of Sydney rock oysters, *Saccostrea glomerata* infected with the paramyxean parasite, *Marteilia sydneyi*. *J. Appl. Microb.* 109, 613–622.

Gregg, M., Rigby, G., and Hallegraeff, G. M. (2009). Review of two decades of progress in the development of management options for reducing or eradicating phytoplankton, zooplankton and bacteria in ship's ballast water. *Aquat. Invas.* 4, 521–565. doi: 10.3391/ai.2009.4.3.14

Groth, S., and Rumrill, S. (2009). History of Olympia oysters (*Ostrea lurida* Carpenter 1864) in Oregon estuaries, and a description of recovering populations in Coos Bay. *J. Shellfish Res.* 28, 51–58. doi: 10.2983/035.028.0111

Growcott, A., Kluza, D., and Georgiades, E. (2019). *Technical Advice: Evaluation of In-Water Systems to Reactively Treat or Remove Biofouling within Vessel Internal*

Niche Areas. Technical Paper No. 2019/02. Wellington: Ministry for Primary Industries.

Growcott, A., Kluza, D., and Georgiades, E. (2017). Review: in-water systems to reactively manage biofouling in sea chests and internal pipework. *J. Mar. Sci. Technol.* 51, 89–104. doi: 10.4031/mtsj.51.2.3

Habe, S., Lai, K. P., Agatsuma, T., Ow-Yang, C. K., and Kawashima, K. (1993). Crab hosts for *Paragonimus westermani* (Kerbert, 1878) in Malaysia. *Japan. J. Trop. Med. Hygiene* 21, 137–142. doi: 10.2149/tmh1973.21.137

Hamaguchi, M., Manabe, M., Kajihara, N., Shimabukuro, H., Yamada, Y., and Nishi, E. (2017). DNA barcoding of flat oyster species reveals the presence of *Ostrea stentina* Payraudeau, 1826 (Bivalvia: Ostreidae) in Japan. *Mar. Biodiv. Rec.* 10:4.

Hamaguchi, M., Shimabukuro, H., Kawane, M., and Hamaguchi, T. (2013). A new record of the Kumamoto oyster *Crassostrea sikamea* in the Seto Inland Sea, Japan. *Mar. Biodiv. Rec.* 2013:6.

Haskin, H. H., and Andrews, J. D. (1988). Uncertainties and speculations about the life cycle of the eastern oyster pathogen *Haplosporidium nelsoni* (MSX). *Am. Fisheries Soc. Special Public.* 18, 5–22.

Haskin, H. H., and Ford, S. E. (1982). *Haplosporidium nelsoni* (MSX) on Delaware Bay seed oyster beds: A host–parasite relationship along a salinity gradient. *J. Invertebr. Pathol.* 40, 388–405. doi: 10.1016/0022-2011(82)90178-1

Henze, M., van Loosdrecht, M. C. M., Ekama, G. A., and Brdjanovic, D. (eds) (2008). *Biological Wastewater Treatment - Principles, Modelling and Design*. London: IWA Publishing.

Herborg, L. M., Rushton, S. P., Clare, A. S., and Bentley, M. G. (2003). *Spread of the Chinese Mitten Crab (Eriocheir sinensis* H. Milne Edwards) in Continental Europe: Analysis of a Historical Data Set. In Migrations and Dispersal of Marine Organisms. Dordrecht: Springer, 21–28.

Hess-Erga, O. K., Moreno-Andrés, J., Enger, Ø, and Vadstein, O. (2019). Micro-Organisms in ballast water: Disinfection, community dynamics, and implications for management. *Sci. Total Environ.* 657, 704–716. doi: 10.1016/j.scitotenv.2018.12.004

Hewitt, C. L., and Campbell, M. (2010). *The Relative Contribution of Vectors to the Introduction and Translocation of Invasive Marine Species. Commissioned by The Department of Agriculture*. Canberra: Fisheries and Forestry (DAFF).

Hick, P., Evans, O., Looi, R., English, C., and Whittington, R. J. (2016). Stability of ostreid herpesvirus-1 (OsHV-1) and assessment of disinfection of seawater and oyster tissues using a bioassay. *Aquaculture* 450, 412–421. doi: 10.1016/j.aquaculture.2015.08.025

Hill-Spanik, K. M., McDowell, J. R., Stokes, N. A., Reece, K. S., Burreson, E. M., and Carnegie, R. B. (2015). Phylogeographic perspective on the distribution and dispersal of a marine pathogen, the oyster parasite *Bonamia exitiosa*. *Mar. Ecol. Prog. Series* 536, 65–76. doi: 10.3354/meps11425

Hine, P. M. (1996). Southern hemisphere mollusc diseases and an overview of associated risk assessment problems. *Revue Sci. Tech.-Off. Int. des Èpizooties* 15, 563–571. doi: 10.20506/rst.15.2.940

Hine, P. M. (1995). Other mechanisms of marine organism transfer. In: Ballast Water a Marine Cocktail on the Move. *R. Soc. N. Zealand Miscell. Series* 30, 95–101.

Howard, A. E. (1994). The possibility of long-distance transmission of *Bonamia* by fouling on boat hulls. *Bull. Eur. Assoc. Fish Pathol.* 14, 211–212.

Hunsucker, K. Z., Ralston, E., Gardner, H., and Swain, G. (2019). "Specialized grooming as a mechanical method to prevent marine invasive species recruitment and transport on ship hulls," in *Impacts of Invasive Species on Coastal Environments*, eds C. Makowski and C. W. Finkl (Berlin: Springer), 247–265. doi: 10.1007/978-3-319-91382-7_7

Iliopoulos, A., Michopoulos, J. G., DeGiorgi, V., and Policastro, S. (2014). "Towards a Computational Multiphysics Framework for Modeling Antibiofouling Processes," in *Proceedings of the International Design Engineering Technical Conferences and Computers and Information in Engineering Conference*. New York, NY, Vol. 1A.

Inglis, G. J., Morrisey, D., Woods, C., Sinner, J., and Newton, M. (2013). *Managing the Domestic Spread of Harmful Marine Organisms. Part A: Operational Tools for Management*. Wellington: Ministry for Primary Industries.

Inglis, G. J., Floerl, O., and Woods, C. (2012). *Scenarios of Vessel Biofouling Risk and their Management: An Evaluation of Options. Technical Paper No: 2012/07*. Wellington: Ministry of Agriculture and Forestry.

International Maritime Organization [Imo]. (2011). *Guidelines for the Control and Management of Ships' Biofouling to Minimize the Transfer of Invasive Aquatic Species*. London: International Maritime Organization.

International Maritime Organization [Imo]. (2004). *International Convention for the Control and Management of Ships' Ballast Water and Sediments*. London: International Maritime Organization.

Itoh, N., Komatsu, Y., Maeda, K., Hirase, S., and Yoshinaga, T. (2019). First discovery of *Perkinsus beihaiensis* in Mediterranean mussels (*Mytilus galloprovincialis*) in Tokyo Bay, Japan. *J. Invertebr. Pathol.* 166, 107226. doi: 10.1016/j.jip.2019.107226

Itoh, N., Komiyama, H., Ueki, N., and Orawa, K. (2004). Early developmental stages of a protozoan parasite, *Marteilioides chungmuensis* (Paramyxea), the causative agent of the ovary enlargement disease in the Pacific oyster, *Crassostrea gigas*. *Internat. J. Parasitol.* 34, 1129–1135. doi: 10.1016/j.ijpara.2004.06.001

Johnston, C. J. (2014). *Statement of Evidence on Behalf of Fisheries Submitters before the Environmental Protection Authority*, Victoria: Environmental Protection Authority.

Johnston, E. L., Dafforn, K. A., Clark, G. F., Rius, M., and Floerl, O. (2017). Anthropogenic activities promoting the establishment and spread of marine non-indigenous species post-arrival. *Oceanogr. Mar. Biol. Ann. Rev.* 55, 389–420. doi: 10.1201/b21944-6

Joint Group of Experts on the Scientific Aspects of Marine Environmental Protection [GESAMP] (2019). *Methodology for the evaluation of ballast water management systems using Active Substances*. Reports and Studies GESAMP No. 101.

Keeling, S. E., Brosnahan, C. L., Williams, R., Gias, E., Hannah, M., Bueno, R., et al. (2014). New Zealand juvenile oyster mortality associated with ostreid herpesvirus 1 - An opportunistic longitudinal study. *Dis. Aquat. Organ.* 109, 231–239. doi: 10.3354/dao02735

Kemp, W. M., Boynton, W. R., Adolf, J. E., Boesch, D. F., Boicourt, W. C., Brush, G., et al. (2005). Eutrophication of Chesapeake Bay: Historical trends and ecological interactions. *Mar. Ecol. Prog. Series* 303, 1–29. doi: 10.3354/meps303001

Kim, Y., Snow, S. D., Reichel-Deland, V., Maghsoodi, M., Langlois, G. M., Tarabara, V. V., et al. (2019). Current status and recommendations toward a virus standard for ballast water. *Manag. Biol. Invasions* 10, 267–284. doi: 10.3391/mbi.2019.10.2.04

Kroeck, M. A., and Montes, J. (2005). Occurrence of the haemocyte parasite *Bonamia* sp. in flat oysters *Ostrea puelchana* farmed in San Antonio Bay (Argentina). *Dis. Aquat. Organ.* 63, 231–235. doi: 10.3354/dao063231

Lallias, D., Arzul, I., Heurtebise, S., Ferrand, S., Chollet, B., Robert, M., et al. (2008). *Bonamia ostreae*-induced mortalities in one-year old European flat oysters *Ostrea edulis*: Experimental infection by cohabitation challenge. *Aquat. Living Res.* 21, 423–439. doi: 10.1051/alr:2008053

Lane, H. S., Brosnahan, C. L., and Poulin, R. (2020). Aquatic disease in New Zealand: Synthesis and future directions. *N. Zealand J. Mar. Freshwater Res.* 2020, 1–42. doi: 10.1080/00288330.2020.1848887

Lane, H. S., and Jones, J. B. (2020). Low internal transcribed spacer rDNA variation in New Zealand *Bonamia ostreae*: Evidence for a recent arrival. *Dis. Aquat. Organ.* 139, 121–130.

Lane, H. S., Jones, B., and Poulin, R. (2018). Comparative population genetic study of an important marine parasite from New Zealand flat oysters. *Mar. Biol.* 165:9.

Lane, H. S., Webb, S. C., and Duncan, J. (2016). *Bonamia ostreae* in the New Zealand oyster *Ostrea chilensis*: A new host and geographic record for this haplosporidian parasite. *Dis. Aquat. Organ.* 118, 55–63. doi: 10.3354/dao02960

Langlais, B., Reckhow, D. A., and Brink, D. R. (1991). *Ozone in Water Treatment, Application and Engineering*. Boca Raton: CRC Press.

Lewis, J. A. (2020). *Chemical Contaminant Risks Associated with In-water Cleaning of Vessels. Department of Agriculture*. Canberra: Water and the Environment.

Lewis, J. A. (1986). *Fouling Settlement at HMAS Stirling (Cockburn Sound, Western Australia) - A Review (No. MRL-R-995)*. Australia: Defence Science and Technology Organisation Materials Research Laboratories, Ascot Vale.

Lewis, J. A. (1982). *A Guide to the Principal Marine Fouling Organisms, with Particular Reference to Cockburn Sound, WA (No. MRL-R-858)*. Australia: Defence Science and Technology Organisation Materials Research Laboratories, Ascot Vale.

Lewis, J. A. (2013). *In-Water Hull Cleaning and Filtration System: in-Water Cleaning Trials – 26–28 November 2012*. Available online at: http://www.fish.wa.gov.au/Documents/occasional_publications/fop114.pdf (accessed July 2013).

Lockwood, J. L., Cassey, P., and Blackburn, T. (2005). The role of propagule pressure in explaining species invasions. *Trends Ecol. Evol.* 20, 223–228. doi: 10.1016/j.tree.2005.02.004

Longshaw, M., Stone, D. M., Wood, G., Green, M. J., and White, P. (2013). Detection of *Bonamia exitiosa* (*Haplosporidia*) in European flat oysters *Ostrea edulis* cultivated in mainland Britain. *Dis. Aquat. Organ.* 106, 173–179. doi: 10.3354/dao02643

Lopez-Joven, C., Rolland, J. L., Haffner, P., Caro, A., Roques, C., Carré, C., et al. (2018). Oyster farming, temperature, and plankton influence the dynamics of pathogenic Vibrios in the Thau Lagoon. *Front. Microb.* 9:2530.

Mann, R. L., Burreson, E. M., and Baker, P. K. (1991). The decline of the Virginia oyster fishery in Chesapeake Bay considerations for introduction of a non-endemic species, *Crassostrea gigas* (Thunberg, 1793). *J. Shell. Res.* 10, 379–388.

Martenot, C., Denechere, L., Hubert, P., Metayer, L., Oden, E., Trancart, S., et al. (2015). Virulence of ostreid herpesvirus 1 mu Var in sea water at 16 degrees C and 25 degrees C. *Aquaculture* 439, 1–6. doi: 10.1016/j.aquaculture.2015.01.012

McCarthy, S. A., and Khambaty, F. M. (1994). International dissemination of epidemic *Vibrio cholerae* by cargo ship ballast and other nonpotable waters. *Appl. Env. Microb.* 60, 2597–2601. doi: 10.1128/aem.60.7.2597-2601.1994

McClay, T., Zabin, C., Davidson, I., Young, R., and Elam, D. (2015). *Vessel biofouling prevention and management options report*. Available online at: https://apps.dtic.mil/dtic/tr/fulltext/u2/a626612.pdf (accessed January 2021).

Meuriot, E., and Grizel, H. (1984). Note sur l'impact économique des maladies de l'huître plate en Bretagne. *Rapports Techniques de lŠInstitut Scientifique and Technique des Pêches Maritimes* 12, 1-20. France.

Meyers, T. (2010). *Regulation Changes, Policies and Guidelines for Alaska Fish and Shellfish Health and Disease Control. Alaska Department of Fish and Game*, Regional Information Report 5J10-01, *Juneau*.

Ministry for Primary Industries New Zealand [Mpi]. (2018). *Craft Risk Management Standard: Biofouling on Vessels Arriving to New Zealand. CRMS - BIOFOUL*. Wellington: Ministry for Primary Industries.

Molino, P. J., and Wetherbee, R. (2008). The biology of biofouling diatoms and their role in the development of microbial slimes. *Biofouling* 24, 365–379. doi: 10.1080/08927010802254583

Molloy, S. D., Pietrak, M. R., Bricknell, I., and Bouchard, D. A. (2013). Experimental transmission of infectious pancreatic necrosis virus from the blue mussel, *Mytilus edulis*, to cohabitating Atlantic salmon (*Salmo salar*) smolts. *Appl. Environ. Microb.* 79, 5882–5890. doi: 10.1128/aem.01142-13

Moreau, P., Faury, N., Burgeot, T., and Renault, T. (2015). Pesticides and ostreid herpesvirus 1 infection in the Pacific oyster, *Crassostrea gigas*. *PLoS One* 10:e0130628. doi: 10.1371/journal.pone.0130628

Morrisey, D., Inglis, G., Tait, L., Woods, C., Lewis, J., and Georgiades, E. (2015). *Procedures for Evaluating In-Water Systems to Remove or Treat Vessel Biofouling. New Zealand Ministry for Primary Industries Technical Paper No. 2015/39*. Wellington: Ministry for Primary Industries.

Morrisey, D., and Woods, C. (2015). *In-Water Cleaning Technologies: Review of Information. New Zealand Ministry for Primary Industries Technical Paper No. 2015/38*. Wellington: Ministry for Primary Industries.

Morrisey, D., Gadd, J., Page, M., Lewis, J., Bell, A., and Georgiades, E. (2013). *In-Water Cleaning of Vessels: Biosecurity and Chemical Contamination Risks. New Zealand Ministry for Primary Industries Technical Paper No. 2013/11*. Wellington: Ministry for Primary Industries.

Mortensen, S. H. (1993). Passage of infectious pancreatic necrosis virus (IPNV) through invertebrates in an aquatic food chain. *Dis. Aquat. Organ.* 16, 41–45. doi: 10.3354/dao016041

Moshchenko, A. V., and Zvyagintsev, A. Y. (2001). Composition and structure of macrofouling communities on ocean-going ships of Far East Sea Basin. *Ocean Polar Res.* 23, 63–75.

Munro, E. S., and Midtlyng, P. J. (2011). "Infectious Pancreatic Necrosis and Associated Aquatic Birnaviruses," in *Fish Diseases and Disorders. Volume 3: Viral, Bacterial and Fungal Infections, Second Edition*, eds P. T. K. Woo and D. W. Bruno Wallingford: CABI Publishing. 1–65. doi: 10.1079/9781845935542.0001

National Research Council. (2004). *Non-native Oysters in the Chesapeake Bay*. Washington, DC: The National Academies Press.

OIE (2020). *OIE-Listed diseases, infections and infestations in force in 2020*. Available online at: https://www.oie.int/animal-health-in-the-world/oie-listed-diseases-2020/ (accessed September 2020)

OIE (2019). *Aquatic Manual*. Available online at: https://www.oie.int/en/standard-setting/aquatic-manual/ (accessed September 2020)

Ojaveer, H., Galil, B. S., Carlton, J. T., Alleway, H., Goulletquer, P., Lehtiniemi, M., et al. (2018). Historical baselines in marine bioinvasions: Implications for policy and management. *PLoS One* 13:e0202383. doi: 10.1371/journal.pone.0202383

Oemcke, D., Parker, N., and Mountfort, D. (2004). Effect of UV irradiation on viability of micro scale and resistant forms of marine organisms: Implications for the treatment of ships' ballast water. *J. Mar. Env. Eng.* 7, 153–171.

O'Reilly, A., Laide, C., Maloy, A., Hutton, S., Bookelaar, B. K., Lynch, S. A., et al. (2018). *Parasitology* 145, 1095–1104.

Ou, H., Gao, N., Deng, Y., Wang, H., and Zhanga, H. (2011). Inactivation and degradation of *Microcystis aeruginosa* by UV-C irradiation. *Chemosphere* 85, 1192–1198. doi: 10.1016/j.chemosphere.2011.07.062

Pagenkopp-Lohan, K. M., Ruiz, G. M., and Torchin, M. E. (2020). "Invasions Can Drive Marine Disease Dynamics," in *Marine Disease Ecology*, eds D. C. Behringer, K. D. Lafferty, and B. D. Silliman (Oxford: Oxford University Press)115–138. doi: 10.1093/oso/9780198821632.003.0007

Pagenkopp-Lohan, K. M., Hill-Spanik, K. M., Torchin, M. E., Fleischer, R. C., Carnegie, R. B., Reece, K. S., et al. (2018). Phylogeography and connectivity of molluscan parasites: *Perkinsus* spp. in Panama and beyond. *Int. J. Parasitol.* 48, 135–144. doi: 10.1016/j.ijpara.2017.08.014

Paul-Pont, I., Evans, O., Dhand, N. K., Rubio, A., Coad, P., and Whittington, R. J. (2014). Descriptive epidemiology of mass mortality due to ostreid herpesvirus-1 (OsHV-1) in commercially farmed Pacific oysters (*Crassostrea gigas*) in the Hawkesbury River estuary. Australia. *Aquaculture* 422, 146–159. doi: 10.1016/j.aquaculture.2013.12.009

Peperzak, L., Zetsche, E.-M., Gollasch, S., Artigas, L. F., Bonato, S., Creach, V., et al. (2020). Comparing flow cytometry and microscopy in the quantification of vital aquatic organisms in ballast water. *J. Mar. Eng. Tech.* 19, 68–77. doi: 10.1080/20464177.2018.1525806

Pepin, J. F., Riou, A., and Renault, T. (2008). Rapid and sensitive detection of ostreid herpesvirus 1 in oyster samples by real-time PCR. *J. Virol. Methods* 149, 269–276. doi: 10.1016/j.jviromet.2008.01.022

Peters, N., and Panning, A. (1933). *Zoologischer Anzeiger* 104, Amsterdam: Elsevier 180.

Raynard, R., Wahli, T., Vatsos, I., and Mortensen, S. (eds) (2007). *Review of Disease Interactions and Pathogen Exchange between Farmed and Wild Finfish and Shellfish in Europe.* Work package 1, deliverable 1.5. Disease Interactions and Pathogen Exchange Between Farmed and Wild Aquatic Animal Populations - a European Network. Issued by Veterinærmedisinsk Oppdragssenter AS. Project number: 1655. Oslo: Veterinrrnedisink Oppdragssenter AS

Revilla-Castellanos, V. J., Guerrero, A., Gomez-Gil, B., Navarro-Barrón, E., and Lizárraga-Partida, M. L. (2015). Pathogenic *Vibrio parahaemolyticus* isolated from biofouling on commercial vessels and harbor structures. *Biofouling* 31, 275–282. doi: 10.1080/08927014.2015.1038526

Ricciardi, A., Iacarella, J. C., Aldridge, D. C., Blackburn, T. M., Carlton, J. T., Catford, J. A., et al. (2020). Four priority areas to advance invasion science in the face of rapid environmental change. *Env. Rev.* 2020:0088.doi: 10.1139/er-2020-0088

Richir, J., Bray, S., McAleese, T., and Watson, G. J. (2021). Three decades of trace element sediment contamination: The mining of governmental databases and the need to address hidden sources for clean and healthy seas. *Env. Int.* 149:106362. doi: 10.1016/j.envint.2020.106362

Rivas, C., Cepeda, C., Dopazo, C. P., Novoa, B., Noya, M., and Barja, J. L. (1993). Marine environment as reservoir of birnaviruses from poikilothermic animals. *Aquaculture* 115, 183–194. doi: 10.1016/0044-8486(93)90135-l

Ruiz, G. M., Fofonoff, P. W., Steves, B. P., and Carlton, J. T. (2015). Invasion history and vector dynamics in coastal marine ecosystems: A North American

perspective. *Aquat. Ecosyst. Health Manag.* 18, 299–311. doi: 10.1080/14634988.2015.1027534

Ruiz, G. M., Freestone, A. L., Fofonoff, P. W., and Simkanin, C. (2009). "Habitat Distribution and Heterogeneity in Marine Invasion Dynamics: The Importance of Hard Substrate and Artificial Structure," in *Marine Hard Bottom Communities*, ed. M. Wahl (Berlin: Springer-Verlag), 321–332. doi: 10.1007/b76710_23

Ruiz, G. M., Fofonoff, P. W., Carlton, J. T., Wonham, M. J., and Hines, A. H. (2000b). Invasion of coastal marine communities in North America: Apparent patterns, processes, and biases. *Ann. Rev. Ecol. Syst.* 31, 481–531. doi: 10.1146/annurev.ecolsys.31.1.481

Ruiz, G. M., Rawlings, T. K., Dobbs, F. C., Drake, L. A., Mullady, T., Huq, A., et al. (2000a). Global spread of micro-organisms by ships. *Nature* 408, 49–50. doi: 10.1038/35040695

Ruiz, G. M., Carlton, J. T., Grosholz, E. D., and Hines, A. H. (1997). Global invasions of marine and estuarine habitats by non-indigenous species: mechanisms, extent, and consequences. *Am. Zool.* 37, 621–632. doi: 10.1093/icb/37.6.621

Sassi, J., Viitasalo, S., Rytkönen, J., and Leppäkoski, E. (2005). Experiments with Ultraviolet Light,Ultrasound and Ozone Technologies for Onboard Ballast Water Treatment. Espoo 2005. *VTT Tiedotteita. Res.* 2005:7.

Sauvage, C., Pepin, J. F., Lapegue, S., Boudry, P., and Renault, T. (2009). Ostreid herpes virus 1 infection in families of the Pacific oyster, *Crassostrea gigas*, during a summer mortality outbreak: differences in viral DNA detection and quantification using real-time PCR. *Virus Res.* 142, 181–187. doi: 10.1016/j.virusres.2009.02.013

Schultz, M. P., Bendick, J. A., Holm, E. R., and Hertel, W. M. (2011). Economic impact of biofouling on a naval surface ship. *Biofouling* 27, 87–98. doi: 10.1080/08927014.2010.542809

Schwindt, E., Gappa, J. L., Raffo, M. P., Tatián, M., Bortolus, A., Orensanz, J. M., et al. (2014). Marine fouling invasions in ports of Patagonia (Argentina) with implications for legislation and monitoring programs. *Mar. Env. Res.* 99, 60–68. doi: 10.1016/j.marenvres.2014.06.006

Scianni, C., Lubarsky, K., Ceballos-Osuna, L., and Bates, T. (in press). Yes, we CANZ: Initial compliance and lessons learned from regulating vessel biofouling management in California and New Zealand. *Manag. Biol. Invas.*

Scianni, C., and Georgiades, E. (2019). Vessel in-water cleaning or treatment: Identification of environmental risks and science needs for evidence-based decision making. *Front. Mar. Sci.* 6:467.

Ségarra, A., Pépin, J. F., Arzul, I., Morga, B., Faury, N., and Renault, T. (2010). Detection and description of a particular ostreid herpesvirus 1 genotype associated with massive mortality outbreaks of Pacific oysters, *Crassostrea gigas*, in France in 2008. *Virus Res.* 153, 92–99. doi: 10.1016/j.virusres.2010.07.011

Shikuma, N. J., and Hadfield, M. G. (2010). Marine biofilms on submerged surfaces are a reservoir for *Escherichia coli* and *Vibrio cholerae*. *Biofouling* 26, 39–46. doi: 10.1080/08927010903282814

Sim-Smith, C., Faire, S., and Lees, A. (2016). *Managing Biosecurity for Business Benefit. Aquaculture Biosecurity Practices Research. Technical Paper No. 2016/14*. Wellington: Ministry for Primary Industries.

Smith, M., Inglis, G. J., Wilkens, S., and McDonald, S. (2016). Emergency surveillance for marine pests after the grounding of the container vessel, MV Rena. *N. Zealand J. Mar. Freshwater Res.* 50, 42–55. doi: 10.1080/00288330.2015.1127828

Stavrakakis, C., Papin, M., Dupuy, B., Riou, K., Penisson, C., and Nourry, M. (2017). *Désinfection de l'eau de mer–DESIMER Etude des sous-produits de désinfection*. France: Département Ressources Biologiques et Environnement.

Stentiford, G. D., Bateman, K. S., Dubuffet, A., Chambers, E., and Stone, D. M. (2011). *Hepatospora eriocheir* (Wang and Chen, 2007) gen. et comb. nov. infecting invasive Chinese mitten crabs (*Eriocheir sinensis*) in Europe. *J. Invertebr. Pathol.* 108, 156–166. doi: 10.1016/j.jip.2011.07.008

Stephenson, M., and Petrie, B. (2005). Oceanographic influences on the management of MSX disease of American oysters (*Crassostrea virginica*) in Atlantic Canada. *Bull. Aquac. Assoc. Can.* 105, 67–78.

Tamburri, M. N., Davidson, I. C., First, M. R., Scianni, C., Newcomer, K., Inglis, G. J., et al. (2020). In-water cleaning and capture to remove ship biofouling: An initial evaluation of efficacy and environmental safety. *Front. Mar. Sci.* 7:437.

Tamburri, M. N., Luckenbach, M. W., Breitburg, D. L., and Bonniwell, S. M. (2008). Settlement of *Crassostrea ariakensis* larvae: Effects of substrate, biofilms, sediment and adult chemical cues. *J. Shellfish Res.* 27, 601–608. doi: 10.2983/0730-8000(2008)27[601:socale]2.0.co;2

Tao, Y., and Wenxia, Y. (2002). *Study of offshore fouling in China – now and in the future. Studia Marina Sinica*. Available online at: http://en.cnki.com.cn/Article_en/CJFDTotal-HKJK200200011.htm (accessed September 2020)

Terraphase Engineering Inc (2012). *In-Water Hull Cleaning Summary Report*. Alameda, CA: US-Department of Transportation – Maritime Administration, 48.

Tribou, M., and Swain, G. (2017). The effects of grooming on a copper ablative coating: A six year study. *Biofouling* 33, 494–504. doi: 10.1080/08927014.2017.1328596

Ulman, A., Ferrario, J., Occhipinti-Ambrogi, A., Arvanitidis, C., Bandi, A., Bertolino, M., et al. (2017). A massive update of non-indigenous species records in Mediterranean marinas. *PeerJ* 5:e3954. doi: 10.7717/peerj.3954

van Banning, P. (1991). Observations on bonamiasis in the stock of the European flat oyster, *Ostrea edulis*, in the Netherlands, with special reference to the recent developments in Lake Grevelingen. *Aquaculture* 93, 205–211. doi: 10.1016/0044-8486(91)90232-v

Venczel, L. V., Arrowood, M., Hurd, M., and Sobsey, M. D. (1997). Inactivation of *Cryptosporidium parvum* oocysts and *Clostridium perfringens spores* by a mixed-oxidant disinfectant and by free chlorine. *Appl. Env. Microb.* 63, 1598–1601. doi: 10.1128/aem.63.4.1598-1601.1997

Vigneron, V., Solliec, G., Montanié, H., and Renault, T. (2004). Detection of ostreid herpesvirus 1 (OsHV-1) DNA in seawater by PCR: Influence of water parameters in bioassays. *Dis. Aquat. Organ.* 62, 35–44. doi: 10.3354/dao062035

Villalba, A., Reece, K. S., Ordás, M. C., Casas, S. M., and Figueras, A. (2004). Perkinsosis in molluscs: A review. *Aquat. Living Resour.* 17, 411–432. doi: 10.1051/alr:2004050

Visscher, J. P. (1928). Nature and extent of fouling of ships' bottoms. *Bull. Bureau Fisheries* 43, 193–252.

Wang, T., and Li, Q. (2020). Effects of temperature, salinity and body size on the physiological responses of the Iwagaki oyster *Crassostrea nippona*. *Aquac. Res.* 51, 728–737. doi: 10.1111/are.14423

Wang, W., Gu, W., Gasparich, G. E., Bi, K., Ou, J., Meng, Q., et al. (2011). Spiroplasma eriocheiris sp. nov., associated with mortality in the Chinese mitten crab, *Eriocheir sinensis*. *Int. J. Syst. Evol. Microb.* 61, 703–708. doi: 10.1099/ijs.0.020529-0

Wang, W., Chen, J., Du, K., and Xu, Z. (2004a). Morphology of spiroplasmas in the Chinese mitten crab *Eriocheir sinensis* associated with tremor disease. *Res. Microb.* 155, 630–635. doi: 10.1016/j.resmic.2004.04.010

Wang, W., Wen, B. H., Gasparich, G. E., Zhu, N. N., Rong, L. W., Chen, J. X., et al. (2004b). A spiroplasma associated with tremor disease in the Chinese mitten crab (*Eriocheir sinensis*). *Microbiology* 150, 3035–3040. doi: 10.1099/mic.0.26664-0

Wesche, S. J., Adlard, R. D., and Lester, R. J. G. (1999). Survival of spores of the oyster pathogen *Marteilia sydneyi* (Protozoa, Paramyxea) as assessed using fluorogenic dyes. *Dis. Aquat. Organ.* 36, 221–226. doi: 10.3354/dao036221

Whittington, R. J., Hick, P., Fuhrmann, M., Liu, O., and Paul-Pont, I. (2020). Removal of oyster pathogens from seawater. *Environ. Int.* 2020:106258. doi: 10.1016/j.envint.2020.106258

Whittington, R. J., Paul-Pont, I., Evans, O., Hick, P., and Dhand, N. K. (2018). Counting the dead to determine the source and transmission of the marine herpesvirus OsHV-1 in *Crassostrea gigas*. *Veter. Res.* 49:34.

Williams, S. L., Davidson, I. C., Pasari, J. R., Ashton, G. V., Carlton, J. T., Crafton, R. E., et al. (2013). Managing multiple vectors for marine invasions in an increasingly connected world. *Bioscience* 63, 952–966. doi: 10.1525/bio.2013.63.12.8

Wong, G. T. F., and Davidson, J. A. (1977). The fate of chlorine in seawater. *Water Res.* 11, 971–978.

Woods Hole Oceanographic Institution (WHOI) (1952). *Marine fouling and its prevention*. Maryland: United States Naval Institute.

Yan, S. K., and Huang, Z. G. (1993). "Biofouling of Ships in Daya Bay, China. In: The Marine Biology of the South China Sea," in *Proceedings of the First International Conference on the Marine Biology of Hong Kong and the South China Sea*, (Hong Kong).

Yan, T., Yan, W., Dong, Y., Wang, H., Yan, Y., and Liang, G. (2006). Marine fouling of offshore installations in the northern Beibu Gulf of China. *Int. Biodeter. Biodegr.* 58, 99–105. doi: 10.1016/j.ibiod.2006.07.007

Yonemitsu, M. A., Giersch, R. M., Polo-Prieto, M., Hammel, M., Simon, A., Cremonte, F., et al. (2019). A single clonal lineage of transmissible cancer identified in two marine mussel species in South America and Europe. *Elife* 2019:8.

Zhang, S., and Bonami, J. R. (2007). A roni—like virus associated with mortalities of the freshwater crab, *Eriocheir sinensis* Milne Edwards, cultured in China, exhibiting 'sighs disease'and black gill syndrome. *J. Fish Dis.* 30:181. doi: 10.1111/j.1365-2761.2007.00796.x

Zimmer, J. L., and Slawson, R. M. (2002). Potential repair of *Escherichia coli* DNA following exposure to UV radiation from both medium- and low-pressure UV sources used in drinking water treatment. *Appl. Env. Microb.* 68, 3293–3299. doi: 10.1128/aem.68.7.3293-3299.2002

Conflict of Interest: The authors declare that the research was conducted in the absence of any commercial or financial relationships that could be construed as a potential conflict of interest.

frontiers in Marine Science

ORIGINAL RESEARCH
published: 28 June 2021
doi: 10.3389/fmars.2021.669329

Heavy Metal, Rare Earth Element and Pb Isotope Dynamics in Mussels During a Depuration Experiment in the Gulf of Aqaba, Northern Red Sea

Tal Benaltabet[1,2], Eldad Gutner-Hoch[2,3] and Adi Torfstein[1,2]*

[1] The Fredy and Nadine Herrmann Institute of Earth Sciences, Hebrew University of Jerusalem, Jerusalem, Israel, [2] The Interuniversity Institute for Marine Sciences, Eilat, Israel, [3] School of Zoology, George S. Wise Faculty of Life Sciences, Tel Aviv University, Tel Aviv, Israel

OPEN ACCESS

Edited by:
Kenneth Mei Yee Leung, City University of Hong Kong, Hong Kong, SAR China

Reviewed by:
Chee Kong Yap, Putra Malaysia University, Malaysia
Paula Sánchez Marín, Spanish Institute of Oceanography, Spain

***Correspondence:**
Tal Benaltabet
tal.benaltabet@mail.huji.ac.il

Specialty section:
This article was submitted to Marine Pollution, a section of the journal Frontiers in Marine Science

Received: *18 February 2021*
Accepted: *11 May 2021*
Published: *28 June 2021*

Citation:
Benaltabet T, Gutner-Hoch E and Torfstein A (2021) Heavy Metal, Rare Earth Element and Pb Isotope Dynamics in Mussels During a Depuration Experiment in the Gulf of Aqaba, Northern Red Sea. Front. Mar. Sci. 8:669329. doi: 10.3389/fmars.2021.669329

Mussels are considered highly efficient marine biomonitors, tracing anthropogenic and natural variations in heavy metals and various organic compounds. While heavy metals depuration processes in biomonitors are of growing interest, less knowledge is available regarding their Pb isotopes and rare earth elements (REEs) accumulation-release dynamics, and their response to short-term anthropogenic and terrigenous perturbations. Here, we report the results of a relocation experiment where a group of mussels (*Brachidontes pharaonis*) were extracted from a contaminated lagoon in the Gulf of Aqaba, northern Red Sea, and placed in water tanks that were flushed continuously with fresh, uncontaminated seawater. Specimens were removed periodically from the water table over a period of 13 weeks and trace and REEs and Pb isotopic compositions were determined separately for mussel's shells and soft tissues. The results display a clear decrease over time in the concentrations of various heavy metals and REEs in the soft tissue, in concert with a similar shift in the Pb isotopic compositions toward seawater values. By contrast, the elemental and Pb isotopic composition of the shell presents little change over time. Coupling between the Pb isotopic composition of corresponding soft tissue and shell samples allows back-calculation of the timing and magnitude of abrupt pollution events and presents a novel approach for monitoring short-term pollution events. Nevertheless, given the coastal setting of the studied samples, it is important to consider the effects of terrigenous material on the results. Accordingly, Al-normalized element concentrations, Pb isotopes and calculated Ce anomalies, are used to identify two distinct terrigenous end members controlling the contaminated lagoon and the pristine site. The study demonstrates the potential of using mussels as robust biomonitors of natural and anthropogenic environmental perturbations through the combination between elemental concentrations and the isotopic composition of Pb.

Keywords: biomonitoring, mussels, depuration, heavy metals, Pb isotopes, rare earth elements, red sea, pollution

INTRODUCTION

Concentrations of heavy metals in the oceans, perturbated by anthropogenic processes, are particularly high in coastal areas (e.g., Steding et al., 2000; Buck et al., 2005; Xu et al., 2014), especially those proximal to big cities, where the discharge of untreated industrial and human waste is most significant (Van Geen et al., 1997; Boyle, 2019). Yet, evaluating the degree of contamination in coastal environments remains challenging because of the complexity in sampling and analyzing water samples and the short residence times of some contaminants in seawater following pollution events. Alternatively, it is possible to use the abundances of contaminants in solid phases within the marine environment as temporal and spatial tracers of pollution. These could be suspended or deposited sediment particles that may adsorb dissolved elements onto their surface from surrounding water, or living organisms that actively circulate seawater and hence incorporate dissolved elements internally, i.e., biomonitors (Rainbow, 2002). An advantage of using marine biomonitors is the ease of processing and analyses (relative to seawater) and their supposedly short response time to local changes in seawater heavy metal contents, whereas solid sediment particles tend to accumulate surrounding elements overtime but do not respond to short term perturbations in the seawater composition. Various species have been recognized to serve as reliable biomonitors, including ascidians, polychaetes, copepods, mussels, clams, oysters, snails and fish (e.g., Hutchinson et al., 1995; Van der Oost et al., 2003; Horiguchi, 2006; Cebrian et al., 2007; Raisuddin et al., 2007; Zhou et al., 2008; Zega et al., 2009; Moloukhia and Sleem, 2011; Carmichael et al., 2012; Tzafriri-Milo et al., 2019). Of these, mussels have been recognized as particularly reliable biomonitors because they have the ability to filter high volumes of water, allowing for the relatively significant accumulation of pollutants in their tissue (Phillips, 1976; Roditi et al., 2000). The use of mussels as biomonitors was introduced in the mid-1970s by Goldberg (1975), who proposed that specimens from coastal and open ocean sites could be beneficial to assess the spatial and temporal trends of various compound concentrations, such as halogenated hydrocarbons, transuranics, heavy metals, and petroleum. This resulted in the establishment of the global program known as "Mussel Watch" (Goldberg et al., 1978; Farrington et al., 1983), which widely uses mussels from the genus Mytilus for marine biomonitoring. The intertidal mussel *Brachidontes pharaonis* from the family *Mytilidae* is present in the coasts of the western Pacific Ocean, Indian Ocean, Red Sea, and Mediterranean Sea (Taylor, 1971; Sasekumar, 1974; Barash and Danin, 1986; Morton, 1988). Several studies have demonstrated the metal bio-accumulation capacity of *B. pharaonis* at polluted and pristine locations along the coasts of the Mediterranean Sea (Göksu et al., 2005; Karayakar et al., 2007; Dar et al., 2018; Hamed et al., 2020). However, to the best of our knowledge, none has presented the depuration dynamics of this species.

Despite numerous studies of the accumulation of heavy metals in mussels (e.g., Chan, 1989; Naimo, 1995; Yap et al., 2003; Fung et al., 2004; Zuykov et al., 2013; Liu and Wang, 2016), their elemental retention and depuration dynamics are still of growing interest. In addition to anthropogenic inputs, terrigenous sources such as atmospheric deposition, rivers and sediments are a prominent source of heavy metals and other elements to the marine environment (Turekian, 1977; Bruland et al., 2013). Similar to anthropogenic pollution such as discrete events of oil pollution and industrial or sewage discharge, terrigenous inputs can also have an abrupt nature, with relatively short episodes of increased fluxes such as dust storms (Mahowald et al., 2009; Ternon et al., 2010), flash floods (Katz et al., 2015), and large-scale sediment resuspension events (Bruland et al., 2008; Torfstein et al., 2020). The terrigenous components may also contribute anthropogenic sourced metals, as these may adsorb heavy metals onto their surfaces during transportation (Nriagu and Pacyna, 1988; Cziczo et al., 2009). Due to the complexity of sampling these and other anthropogenic driven events, examples of the use of mussels as biomonitors for abrupt pulses of marine pollution are scarce.

The Gulf of Aqaba (GoA) is a deep oligotrophic water body connected to the Red Sea across the shallow Straits of Tiran in its southern part (**Figure 1**). The regional climate is extremely arid (rainfall <30 mm/year), therefore freshwater input from precipitation and fluvial run-off are quantitatively insignificant, with only a few rain events and associated flashfloods each winter, compared to high fluxes of atmospheric dust deposition (Genin et al., 1995; Almogi-Labin et al., 2008; Genin, 2008; Lazar et al., 2008). Two major cities reside in the northern tip of the GoA: Eilat (Israel) and Aqaba (Jordan) (**Figure 1**). Marine based commerce activity, together with the environmental impacts of big cities, are often in conflict with the well-being of natural resources, making the GoA marine habitats highly sensitive to anthropogenic contamination (Abelson et al., 1999; Wielgus et al., 2004). A man-made inland lagoon (the "Peace Lagoon", **Figure 1**) was constructed to support the development of tourism along the seashore. Yet overestimates of the water exchange rates with the open sea had resulted in an almost isolated inland lagoon with very little water exchange with the open waters. Consequently, the lagoon accumulated contaminants and organic material over time, and its interstitial waters became anoxic. At present, the lagoon is considered contaminated and unfit for recreation activities.

Several previous studies have provided information about metals in, or near, the GoA, ranging between analyses of seawater (Chase et al., 2011, 2006; Chien et al., 2019; Benaltabet et al., 2020), atmospheric dust (Chen et al., 2008; Torfstein et al., 2017; Chien et al., 2019) and studies of surface sediments (Al-Taani et al., 2014; Barakat et al., 2015). Despite these efforts, we still lack a clear understanding of the sources of contamination, their spread range and their long and short-term impact on the GoA and its marine ecosystem.

In addition to the use of heavy metal distributions as tracers of anthropogenic contamination processes, lead (Pb) isotopes (^{204}Pb, ^{206}Pb, ^{207}Pb, and ^{208}Pb), whose relative abundances often differ between natural and anthropogenic sources, make it possible to infer the source of Pb pollution in the environment (e.g., Boyle et al., 1986; Erel et al., 2002; Komárek et al., 2008). Indeed, the Pb isotopic composition of mussels has previously

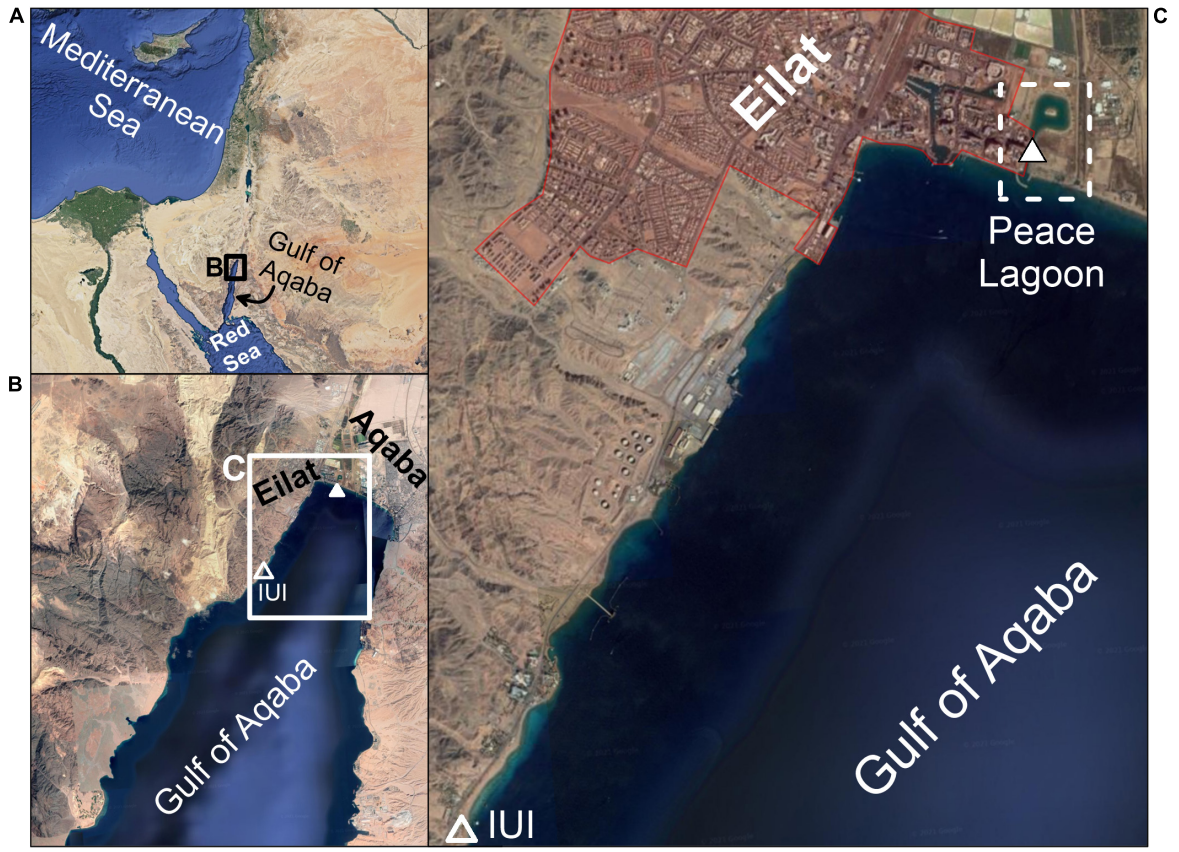

FIGURE 1 | (A) Location map. The location of the Interuniversity Institute (IUI) for Marine Sciences, where the mussels were relocated to, is marked by an empty triangle in panel **(B)**. The location of the Peace Lagoon is presented in panel **(C)**, including the exact site of sampling (white triangle). Map taken from Google Maps.

been used to trace the source of environmental pollution in coastal environments (Labonne et al., 2001, 1998; Richardson et al., 2001; Dang et al., 2015).

The distribution of Rare Earth Elements (REEs) in seawater has been shown to be a useful proxy for quantifying and distinguishing between terrigenous and anthropogenic inputs to the oceans (de Baar et al., 1985; Elderfield, 1988; Hatje et al., 2016). In recent years, the increasing use of REEs in industrial (La, Ce, Pr, Sm, Nd, and Tm) and medical (Gd) fields have resulted in their intrusion into the marine environment and subsequent accumulation in marine biota (Gwenzi et al., 2018; Squadrone et al., 2019). The low concentrations of REEs in seawater hamper their application as *in-situ* marine-environmental monitors. By contrast, elevated abundances in various marine organisms renders them useful biomonitor for REEs in the marine environment (Bonnail et al., 2017; Ma et al., 2019; Wang et al., 2019).

In this study, we explore the depuration process of heavy metals, REEs and Pb isotopes in mussels (*B. pharaonis*). To this end, a native population living in the Peace Lagoon (**Figure 1**) were relocated to pristine seawater tanks in the Interuniversity Institute (IUI) for Marine Sciences (**Figure 1**) where heavy metals concentrations were shown to be lower compared with the north shore, in the vicinity of the lagoon (Herut et al., 1999; Chase et al., 2011, 2006; Chien et al., 2019). The shell and soft tissues were analyzed for their heavy metal and REEs concentrations and Pb isotopic composition over a period of 13 weeks in order to demonstrate the depuration trends from highly contaminated values to the low and natural baseline.

MATERIALS AND METHODS

Experimental Setup and Sample Processing

A batch of 18 adult (∼3 cm in length) Red Sea mussels *B. pharaonis* were collected from the Peace Lagoon in the north beach of Eilat (32°54′84.4″N 34°96′82.3″E) and translocated to a running seawater tank in the IUI (**Figure 1**) for the rest of the depuration experiment. The water tank volume was 120 liters with a flowing water rate of 8.5 liters per minute. A pair of mussels was removed every week during the first 6 weeks (**Tables 1–3**). The two last samples were removed after 12 and 13 weeks. A pair of mussels was sampled immediately after extraction from the Peace Lagoon (i.e., at "day 0", without being exposed to the water tank).

TABLE 1 | Heavy metal concentrations (μg/g dry weight) in mussel shells and soft tissue.

	Sample	Day	Al	V	Cr	Mn	Fe	Co	Ni	Cu	Zn	Cd	Pb
Soft tissue	**EK-5**	0	1148	3.1	2.1	28.7	1267	1.05	2.4	19.2	53.4	2.2	1.4
	EK-6	0	735	1.6	1.3	33.6	725	0.46	1.1	21.3	41.7	0.6	0.7
	EK-7	5	17.7	0.5	0.8	5.4	106	0.30	0.4	27.2	76.7	0.6	0.4
	EK-8	5	83.8	0.7	1.4	42.8	183	0.31	0.5	28.1	66.3	0.6	0.6
	EK-9	13	240	2.0	3.7	22.6	484	0.58	5.2	81.5	116	2.5	1.6
	EK-10	13	135	2.3	3.9	13.5	487	0.59	2.0	28.2	187	3.8	1.1
	EK-13	21	66.9	1.5	1.1	8.2	206	0.33	1.7	26.1	79.9	1.0	0.4
	EK-14	21	92.1	1.4	1.1	7.1	159	0.26	2.1	26.6	63.2	1.5	0.4
	EK-15	29	60.4	0.9	1.0	4.4	335	0.27	1.5	29.2	93.5	2.0	1.2
	EK-16	29	136	1.0	1.4	5.8	222	0.30	1.3	54.4	59.4	1.2	0.5
	EK-3	35	87.9	1.0	2.6	10.9	354	0.40	2.3	25.9	89.0	1.1	1.4
	EK-4	35	55.5	0.8	0.5	9.8	119	0.16	0.8	5.5	16.2	0.5	0.3
	EK-11	43	63.7	0.7	0.8	3.0	115	0.16	0.4	22.5	27.0	0.4	0.2
	EK-12	43	50.7	0.8	0.9	5.5	133	0.28	0.6	93.5	98.1	1.1	0.4
	EK-2	84	28.0	0.5	0.7	1.9	94.3	0.15	0.5	43.7	28.1	0.7	0.2
	EK-17	91	34.1	0.6	0.5	2.6	105	0.15	0.5	19.4	52.9	0.9	0.5
	EK-18	91	24.2	0.6	0.6	2.4	79.7	0.09	0.4	14.3	19.4	0.2	0.3
Shell	**EK-20**	0	46.3	0.4	n.d	123	336	0.15	n.d.	0.6	n.d.	0.007	0.4
	EK-24	0	38.4	0.3	n.d	68.1	247	0.12	n.d.	0.5	n.d.	0.003	0.3
	EK-22	21	18.8	0.2	n.d	9.2	84.7	0.06	n.d.	0.5	n.d.	0.004	0.2
	EK-19	35	4.9	0.1	n.d	11.2	14.4	0.06	n.d.	0.3	n.d.	0.007	0.3
	EK-21	35	16.9	0.1	n.d	26.8	58.2	0.07	n.d.	0.4	n.d.	0.002	0.2
	EK-23	42	4.6	0.1	n.d	17.3	51.8	0.05	n.d.	0.5	n.d.	0.002	0.2
	EK-25	84	25.3	0.3	n.d	12.1	175	0.09	0.33	0.6	n.d.	0.004	0.3

TABLE 2 | Rare earth element concentrations (ng/g dry weight) in mussel shells and soft tissue.

	Sample	Day	La	Ce	Pr	Nd	Sm	Eu	Gd	Tb	Dy	Ho	Er	Tm	Yb	Lu
Soft tissue	**EK-5**	0	1180	2486	255	985	178	38.7	172	23.3	126	24.9	64.1	9.4	54.6	7.5
	EK-6	0	610	1222	141	525	103	19.8	88.5	12.5	61.4	13.3	33.7	4.5	25.9	4.4
	EK-7	5	80.0	128	10.2	39.6	8.3	1.7	8.2	1.7	6.6	1.7	3.4	0.9	2.9	0.7
	EK-8	5	133	262	23.4	89.9	18.6	2.9	17.5	2.3	11.7	2.4	6.4	0.8	4.5	0.4
	EK-9	13	284	782	66.2	279	48.0	10.4	51.3	6.7	33.4	6.9	17.1	2.2	12.6	1.6
	EK-10	13	321	958	71.8	302	50.7	9.6	52.2	5.6	29.1	5.0	13.8	1.5	9.9	1.2
	EK-13	21	132	228	26.9	105	21.0	3.9	19.7	2.5	11.8	2.8	6.9	0.9	4.3	0.7
	EK-14	21	108	213	21.5	88.1	14.1	2.5	14.5	1.7	11.0	2.2	5.2	0.7	3.5	0.4
	EK-15	29	94.6	206	16.4	62.6	11.4	2.6	11.9	1.5	9.1	1.9	5.7	0.8	3.9	0.6
	EK-16	29	163	321	28.3	106	21.7	4.3	19.2	2.4	12.9	2.9	8.2	1.1	7.0	0.9
	EK-3	35	130	277	23.0	82.1	14.8	2.8	13.0	2.3	10.0	2.1	6.4	0.8	5.0	0.8
	EK-4	35	78.0	120	12.1	49.3	11.2	2.1	8.0	1.4	8.4	1.4	3.8	0.5	2.7	0.5
	EK-11	43	87.6	108	12.1	48.7	11.9	1.7	10.1	1.4	7.3	1.4	4.3	0.5	3.0	0.5
	EK-12	43	100	132	13.2	51.3	9.9	2.0	12.7	1.2	7.2	1.4	3.7	0.3	2.6	0.3
	EK-2	84	66.0	102	9.9	37.3	7.0	1.0	7.0	0.9	3.9	1.1	2.3	0.3	1.2	0.2
	EK-17	91	62.0	96.0	9.0	32.8	6.1	1.1	6.0	0.7	4.1	0.8	2.3	0.3	1.6	n.d.
	EK-18	91	67.7	68.1	8.5	28.8	7.6	0.8	7.2	0.9	5.0	1.2	2.4	0.2	2.2	n.d.
Shell	**EK-20**	0	30.0	86.7	5.8	21.6	4.1	n.d.	3.8	0.5	2.1	0.6	0.8	0.1	0.7	0.2
	EK-24	0	27.0	74.1	4.5	19.6	3.7	0.8	3.5	0.4	2.0	0.6	1.5	0.2	0.8	0.1
	EK-22	21	27.2	64.5	4.6	16.9	2.6	0.7	4.1	0.5	1.8	0.6	1.4	0.2	0.8	0.1
	EK-19	35	14.7	38.6	2.4	8.2	2.6	n.d.	1.3	0.2	0.7	0.1	0.5	0.1	n.d.	n.d.
	EK-21	35	18.4	47.1	3.2	10.4	3.1	n.d.	1.9	0.2	0.8	0.3	1.0	n.d.	0.5	n.d.
	EK-23	42	13.4	35.9	2.0	9.7	3.7	n.d.	1.3	0.2	n.d.	0.2	0.6	0.1	n.d.	n.d.
	EK-25	84	25.2	65.7	4.4	16.1	2.5	0.8	3.5	0.6	1.8	0.6	1.4	0.3	1.2	n.d.

TABLE 3 | Pb isotopes in mussel shells and soft tissue.

	Sample	Day	$^{206}Pb/^{207}Pb$	SD	$^{208}Pb/^{206}Pb$	SD
Soft tissue	**EK-5**	0	1.201	0.003	2.052	0.001
	EK-6	0	1.197	0.003	2.053	0.001
	EK-8	5	1.186	0.003	2.067	0.001
	EK-10	13	1.192	0.003	2.060	0.001
	EK-13	21	1.187	0.003	2.066	0.001
	EK-16	29	1.184	0.003	2.069	0.001
	EK-4	35	1.174	0.003	2.078	0.001
	EK-11	43	1.177	0.003	2.076	0.001
	EK-2	84	1.184	0.003	2.068	0.001
	EK-18	91	1.176	0.003	2.077	0.001
Shell	**EK-24**	0	1.199	0.005	2.051	0.005
	EK-22	21	1.197	0.005	2.054	0.005
	EK-19	35	1.196	0.005	2.055	0.005
	EK-21	35	1.203	0.005	2.048	0.005
	EK-23	43	1.191	0.005	2.060	0.005
	EK-25	84	1.197	0.005	2.053	0.005

After removal from the water tank, the samples were carefully transferred to a clean lab where they were processed in a class 100 environment. Samples were first rinsed in ultrapure MQ water (18.2 MΩ cm) and sonicated over several cycles to remove external debris and particles. The shell and soft tissue were then separated and freeze-dried. After weighing the dry samples, the shell was gently leached with 0.05 N HNO_3, to remove the outer rim that could have potentially been contaminated during the sampling, or contain external residue. We are aware that this might also be the part of the shell that could have formed during the experiment, but in terms of mass balance, this would be negligible and probably not observed when measuring the untreated bulk shell sample.

The soft tissue was digested in acid cleaned Teflon (PFA) beakers (Savillex, United States) through several cycles of heated H_2O_2–HNO_3 mixtures, while the shells were digested using 1 N HNO_3. All reagents used in this study were ultrapure solutions (commercial or in-house double distilled) and their concentrations were adjusted with ultrapure MQ water. Generally, two biological replicates were processed and analyzed for soft tissue elemental abundances while one individual was used for soft tissue and shell Pb isotopic composition. The number of replicates used for elemental abundances and Pb isotopic composition at each sampling date is given in **Tables 1–3**.

Analyses of Trace and Rare Earth Elements Concentrations

The digested samples were dried on a hotplate, re-dissolved in 3% HNO_3, and analyzed for their trace (Al, V, Cr, Mn, Fe, Co, Ni, Cu, Zn, Cd, Pb, and Th) and REE (La, Ce, Pr, Nd, Sm, Eu, Gd, Tb, Dy, Ho, Er, Tm, Yb, and Lu) abundances on an Agilent 7,500cx ICP-MS at the Institute of Earth Sciences, Hebrew University of Jerusalem. A multi-elemental standard solution (3% HNO_3 matrix) was used for instrumental signal calibration. Each sample was spiked online with internal standards (Sc, Re, and Rh) to follow and correct for instrumental drifts. Additional monitoring of the intra- and inter- session drift was achieved through the analyses of an in-house standard solution every 10–15 samples, yielding a long term precision of <2% (2σ). The results were corrected for procedural blank values.

Analyses of Pb Isotopic Composition

The remaining solution after ICP-MS analysis was dried, re-dissolved in 1 N HBr, and then Pb purified using standard ion chromatography (e.g., Torfstein et al., 2018) and the details are summarized hereafter. The HBr solution was taken through a series of purification steps to separate a purified Pb fraction. First, 100 μl of AG1X-8® 100–200 mesh anion resin were loaded onto Teflon micro-columns and cleaned over repeated cycles of MQ water and 6 N HCl. The samples were then loaded to the columns and the matrix was removed using 1 N HBr and 2 N HCl. Pb was eluted into Teflon beakers using 6 N HCl. The samples were then dried and re-dissolved in 3% HNO_3 doped to 50 ppb Tl to account for instrument mass fractionation. These aliquots were analyzed for their Pb isotopic composition on a Neptune *Plus* multi collector ICP-MS, together with repeated measurements of the NIST SRM-981 standard which was used for accuracy and instrumental drifts corrections.

Data Treatment

The uncertainty for elemental concentrations is based on the standard deviation of duplicate samples (i.e., two biological replicates), except when duplicates were not available, in which case the relative uncertainty average of the rest of the samples was applied (**Tables 1**, **2** and **Figure 2**). The detection limits were defined as three-fold the standard deviation of full procedural blanks processed and analyzed with the samples (n = 3). Samples below blank or detection limit values, the higher of the two, are marked by "nd" in **Tables 1**, **2**.

The uncertainty for Pb isotopic ratios was evaluated on the basis of a biological duplicate processing and analyses (sample from day 0 for the soft tissue and sample from day 35 for the shell). The standard deviation from the average of the duplicates was applied to the rest of the samples (**Table 3** and **Figure 3**).

RESULTS

Heavy Metals and REEs

Elemental abundances were measured in a total of 17 soft tissue and seven shell samples (**Tables 1**, **2**). A large suite of elements displays a general ongoing decrease in soft tissue concentrations with time from day 0 to 91. These include Al, V, Cr, Mn, Fe, Co, Ni (**Figure 2**), and the REEs (**Table 2**). Other elements show a more moderate decrease (Pb, Cd, and Zn) or a negligible change with time (Cu) (**Figure 2**). Regardless of the general trend, all elements (besides Mn and Cu) displayed a sharp increase in soft tissue concentrations at day 13, after which concentrations continued to gradually decrease. Compared to the soft tissue, the shell fraction concentration presented little change over time in all elements apart from Mn, which shows a coeval decrease in both fractions.

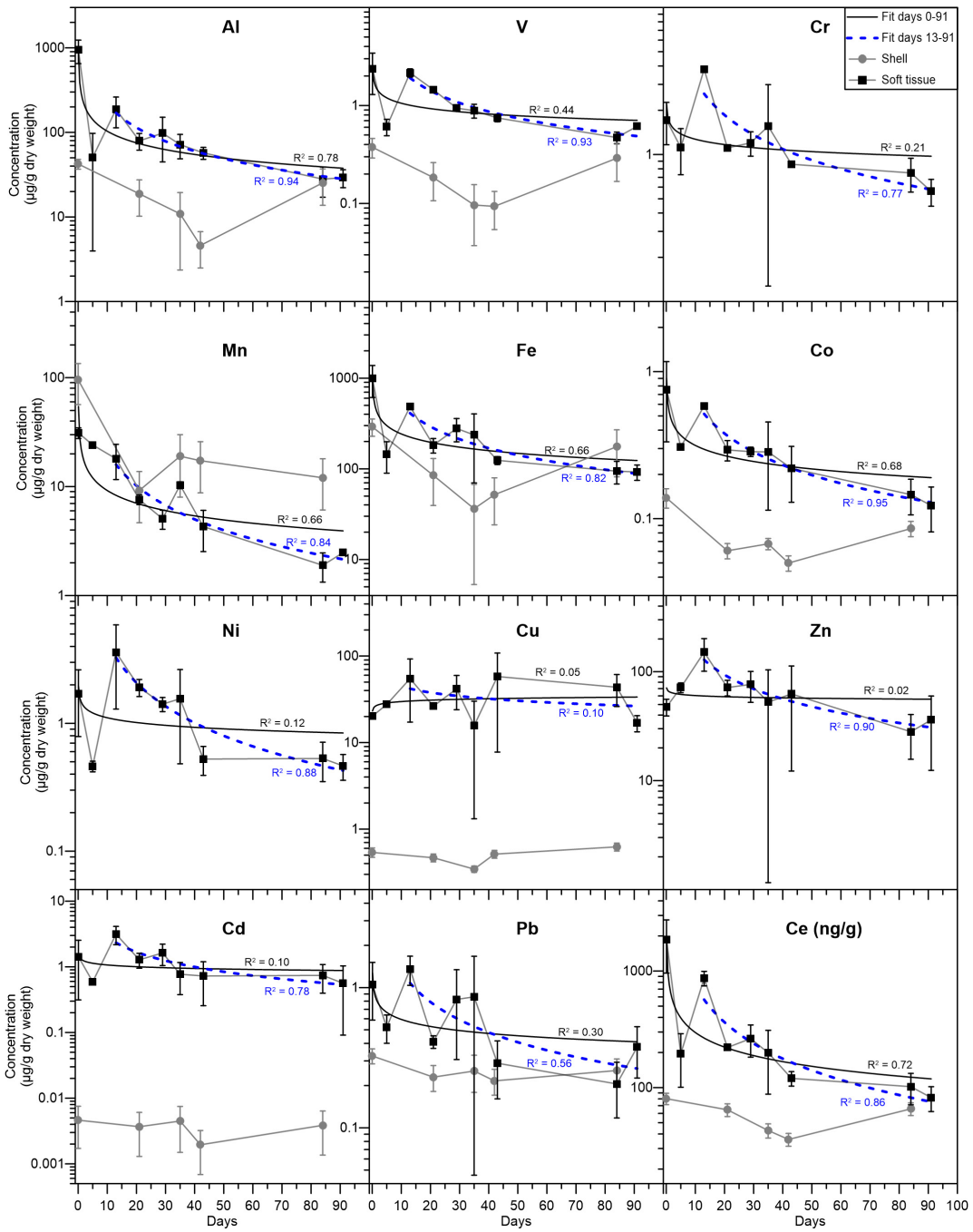

FIGURE 2 | Elemental concentrations (µg/g dry weight) in the soft tissue (black squares) and shell (gray circles). The solid (black) and dashed (blue) curves represent power law fits for the elemental abundances from days 0–91 and 13–91, respectively, with the corresponding R^2 values. Error bars mark the standard deviation of duplicate analyses (see section "Data treatment" for details). Ce is presented as ng/g (dry weight) and its temporal evolution is similar to that of the other REEs (**Table 2**).

Pb Isotopes

The isotopic composition of Pb was measured on a subset of 10 soft tissue and 6 shell samples (**Table 3** and **Figure 3**). The soft tissue samples display a gradual shift in $^{206}Pb/^{207}Pb$ and $^{208}Pb/^{206}Pb$ compositions from 1.199 to 1.176 and 2.052 to 2.077, respectively. At day 13, similar to the elemental abundance patterns, the $^{206}Pb/^{207}Pb$ and $^{208}Pb/^{206}Pb$ soft tissue compositions shift sharply toward higher and lower ratios, respectively. Thereafter, the isotopic ratios continue their initial trend and shift toward lower $^{206}Pb/^{207}Pb$ ratios and

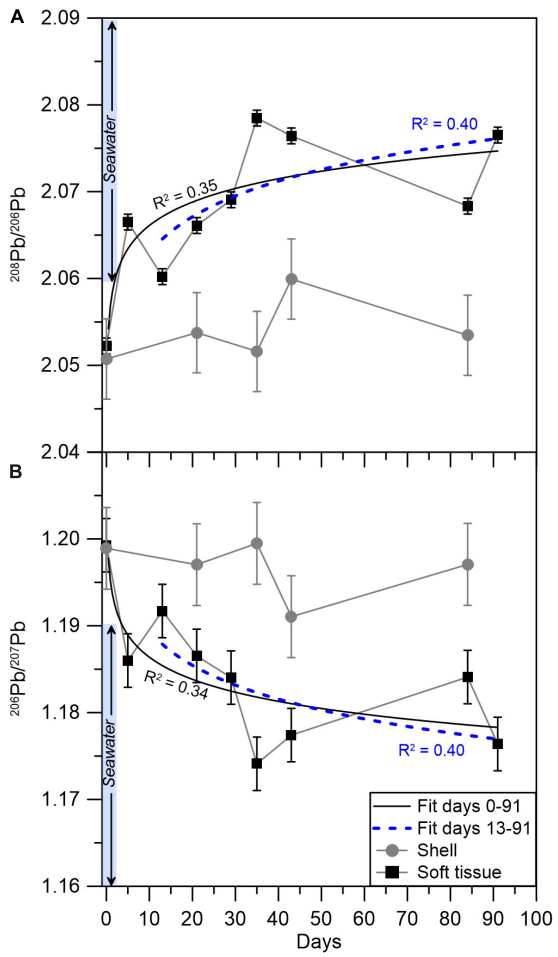

FIGURE 3 | Pb isotopic compositions in the soft tissue (black squares) and shell (gray circles) for **(A)** ^{208}Pb/^{206}Pb and **(B)** ^{206}Pb/^{207}Pb. The solid (black) and dashed (blue) curves represent power law fits for the elemental abundances from days 0–91 and 13–91, respectively, with the corresponding R^2 values. Error bars mark the standard deviation of one duplicate analyses, which was applied to the rest of the samples (see section "Data treatment" for details). The pale blue bar represents the range of seawater Pb isotopic compositions in the GoA (Benaltabet et al., 2020).

higher ^{208}Pb/^{206}Pb ratios. By contrast, and similar to elemental abundance patterns, the shell compositions display little variation regardless of the time the sample was exposed to pristine seawater. Moreover, this unchanging composition corresponds, within uncertainty, to the composition measured in the soft tissue at the start of the experiment, which represents the lagoon environment.

DISCUSSION

Long-Term Depuration Trends in Elemental Abundances

To a first order, all metals (except for Cu) and REEs studied here display a gradual decrease in the soft tissue concentrations (**Tables 1**, **2** and **Figure 2**), from the moment they were moved from the lagoon environment to the water tanks. Although not measured directly in this study, seawater elemental concentrations in the vicinity of the IUI and the lagoon can be estimated based on previous studies (Chase et al., 2011, 2006; Chien et al., 2019). Previously reported surface dissolved Al, Mn, Fe, Co, Cu, Zn, Cd, and Pb concentrations near the IUI coast are generally lower than surface concentrations at the north shore near the lagoon and are more similar to surface concentrations measured at the open sea (**Figure 1**, Station A), further away from shore (**Supplementary Table 1**). Moreover, Herut et al. (1999) have shown that native gastropods (*Cellana rota)* in the vicinity of the IUI presented lower levels of soft tissue Zn, Fe, Cu, and Mn when compared with specimens from the GoA north shore. These observations suggest that the decrease in soft tissue concentrations over time represents the elemental depuration as a result of the relocation from the lagoon to the pristine IUI environment.

The decrease in elemental abundances is observed 5 days after the relocation to the water tanks, as soft tissue concentrations decreased by 51 to 86% between days 0 and 5. These rates are similar to the rapid depuration rates demonstrated by the mussel *Perna virdis* (Yap et al., 2003) and the bivalve *Paphia undulata* (El-Gamal, 2011). No significant decrease trend is observed in the mussel's shells because the fraction of the shell that formed during the experiment is negligible relative to its bulk weight. Hence, it appears that while the soft tissue can biomonitor short-term changes in the organism's environment, the shell represents long-term chronic conditions. It is recognized that the elemental evolution trends are noisy, most likely reflecting the combined natural variability between different specimens, their initial heterogeneity in the lagoon and their individual response to the relocation which could be influenced by their different dry weights (ranging between 10–63 mg) and size, and possibly even their position in the water tank (Phillips, 1980).

To better understand the dynamics of metal concentrations in the soft tissue, the Pearson correlation coefficient (r) was examined between all studied metals in the samples collected after the relocation at days 5–91 (**Table 4**), as any deviation from a linear relationship between metals might suggest a different depuration dynamic modulating soft tissue metal concentrations. Soft tissue Al, V, Cr, Fe, Co, Ni, Zn, Cd, and Pb concentrations between days 5 and 91 present positive correlations with one another (r = 0.76–0.98, $p < 0.03$). When the day 0 samples, which represent the lagoon compositions, are also considered in the calculation, the correlation yields significantly lower values (**Supplementary Table 2**). Regardless of the calculation time span, it appears that the soft tissue passively records the ambient seawater composition of these metals, without an apparent preference. Inversely, poor correlations are presented for Mn and Cu when compared with the other metals suggesting that there might be other controls on their soft tissue abundances.

Soft tissue Cu concentrations do not present the same depuration trend similar to the rest of the metals, as they remain relatively constant over the course of the relocation experiment (**Figure 2**). This could be the result of chronically high dissolved Cu concentrations at the GoA western coast, which may be

TABLE 4 | Pearson correlation coefficient values (r) for soft tissue trace elements concentrations for samples collected between days 5 and 91 with corresponding *p*-values in brackets.

	Al	V	Cr	Mn	Fe	Co	Ni	Cu	Zn	Cd
V	0.93 (0.0007)									
Cr	0.95 (0.0004)	0.88 (0.004)								
Mn	0.44 (0.3)	0.37 (0.4)	0.55 (0.2)							
Fe	0.98 (0.00001)	0.88 (0.004)	0.95 (0.0003)	0.45 (0.3)						
Co	0.95 (0.0003)	0.89 (0.003)	0.95 (0.0003)	0.68 (0.06)	0.93 (0.0007)					
Ni	0.95 (0.0003)	0.97 (0.00007)	0.92 (0.001)	0.36 (0.4)	0.94 (0.0006)	0.90 (0.003)				
Cu	0.44 (0.3)	0.32 (0.4)	0.38 (0.3)	−0.03 (0.9)	0.35 (0.4)	0.37 (0.4)	0.26 (0.5)			
Zn	0.96 (0.0001)	0.90 (0.002)	0.92 (0.001)	0.60 (0.1)	0.92 (0.001)	0.97 (0.00006)	0.87 (0.005)	0.48 (0.2)		
Cd	0.97 (0.00008)	0.92 (0.001)	0.91 (0.002)	0.32 (0.4)	0.94 (0.0004)	0.88 (0.003)	0.93 (0.0008)	0.50 (0.2)	0.92 (0.001)	
Pb	0.90 (0.002)	0.76 (0.03)	0.90 (0.002)	0.52 (0.2)	0.96 (0.0001)	0.88 (0.004)	0.86 (0.007)	0.16 (0.7)	0.83 (0.01)	0.83 (0.01)

similar to those at the lagoon. However, as established before (**Supplementary Table 1**; Chase et al., 2011) high dissolved Cu concentrations are less plausible and a biological mechanism through which the soft tissue retains Cu might explain the constant Cu concentrations throughout the experiment. Similar observations were made by Lorenzo et al. (2003), who transferred mussels (*Mytilus edulis)* from a Cu enriched environment to clean seawater and reported low Cu depuration rates relative to the model expected rates, owing to biological regulation of Cu. It is worth noting that despite the difference in species, the final soft tissue Cu concentrations reported by Lorenzo et al. (2003) were similar to those presented here (**Figure 2**). Furthermore, in a metal depuration experiment performed on the Mediterranean mussel *Mytilus galloprovincialis*, relatively low Cu depuration rates were observed (Anacleto et al., 2015). A possible explanation is that mollusks might actively retain high levels of Cu (and Zn) through metallothioneins, as these are biologically essential metals (Amiard et al., 2006). Similarly, soft tissue Zn, Cd, Fe, and Mn concentrations at day 91 are within the same order of magnitude as the values reported for the gastropod *C. rota* (Herut et al., 1999) near the IUI coast, while Cu concentrations are ∼15–40 times higher. Moreover, while Cr, Mn, Ni, Cd, and Pb soft tissue concentrations at day 91 are similar to the average natural values reported for *in-situ B. pharaonis* by Hamed et al. (2020) in the Mediterranean Sea, Fe, Cu, and Zn are higher by a factor of ∼12, 15, and 10, respectively. It is conceivable that when exposed to high ambient levels of bio-essential metals, *B. pharaonis* will actively retain optimal high soft tissue concentrations (White and Rainbow, 1982; Amiard et al., 2006).

Out of the entire suite of metals studied, Mn is the only metal that presents higher or similar concentrations in the shell compared to the soft tissue (besides Al and Fe, which show similar concentrations at day 84). In addition, only Mn shell and soft tissue concentrations are significantly correlated ($r = 0.97$, $p < 0.01$), implying that they are both modulated by the same mechanism. In their study of the mussel *M. eduils,* Freitas et al. (2016) have shown that shell Mn contents are not directly controlled by ambient dissolved and particulate Mn concentrations nor by kinetic effects, but are mediated by a physiological mechanism associated with the extra-pallial fluid (EPF). It is possible that the decrease in shell Mn after the relocation to the water tanks is coupled to the decrease in soft tissue Mn and related to the connections between the soft tissue and the shell through the EPF (Crenshaw, 1972; Freitas et al., 2016). This might also explain the lack of correlation between soft tissue Mn and other metals, given the high affinity of the EPF to Mn^{2+} (Yin et al., 2005).

Al-Normalized Ratios, REE, and Pb Isotopes as Proxies for Terrigenous Inputs

Terrigenous inputs such as rivers, atmospheric aerosols and terrestrial and marine sediments are the main sources of metals to the oceans (Turekian, 1977; Bruland et al., 2013) with Al being a prominent proxy used to evaluate terrigenous fluxes to the marine environment (Baker et al., 2016; Jickells et al., 2016). To better characterize the controls of terrigenous components over the elemental compositions discussed here, we present the mussel's soft tissue metal concentrations normalized to Al (**Supplementary Figure 1**). The Al-normalized metal ratios allows a better estimation of relative elemental depletion/enrichment in various organic (Bekteshi et al., 2015) and inorganic phases (Shelley et al., 2015; Jickells et al., 2016). Following the relocation of the mussels from the lagoon to the water tanks, all metal/Al ratios between days 0 and 5 displayed a significant increase and remained relatively constant thereafter. This shift clearly depicts the transition from the terrigenous dominated and Al rich shallow lagoon, where exchange with open seawater is limited, to the relatively Al-depleted seawater environment. Moreover, while most metal/Al ratios shifted by up to two order of magnitude, the increase in Fe/Al ratios was smaller (**Supplementary Figure 1**), reflecting the joint association of both Fe and Al with terrigenous material. For comparison, the Al-normalized Th abundances remains relatively stable throughout the entire duration of the experiment, reflecting the strong association of Th with terrigenous inputs.

The transition to a pristine environment is further illustrated in the mussel's soft tissue Pb isotopic composition, which is considered in the context of previously reported GoA seawater Pb compositions (**Figure 4**) and its respective end members (Lee et al., 2015; Chien et al., 2019; Benaltabet et al., 2020). These include seafloor sediments, open Red Sea waters and aerosols,

the latter being the most significant source of anthropogenic Pb to the GoA (Chien et al., 2019; Benaltabet et al., 2020). The initial Pb isotopic composition of both the shell and the soft tissue at day 0 represents the lagoon end member, which presents a mixture between sediments and GoA open seawater. Five days after the translocation, the soft tissue presents open seawater compositions, portraying the organism's rapid response to its ambient seawater Pb composition. However, this trend stops at day 13, when the soft tissue isotopic composition shifts toward the lagoon end member. The sample collected at the following week at day 21 and all subsequent samples, presents Pb compositions similar to open seawater, portraying the organism's prolonged response to ambient pristine waters. The composition of the shell did not overlap with the GoA seawater field throughout the entire experiment, depicting the limited response of the shells to the translocation.

The REE concentrations are normalized to a well-established reference composition, such as the Post Archean Australian Shale (PAAS, Taylor and McLennan, 1985), which helps reveal their relative enrichment and certain REE anomalies (e.g., Ce, Eu, and Gd), providing information regarding sources or sinks of certain elements (Elderfield and Greaves, 1982; de Baar et al., 1983; Hatje et al., 2016). For example, dissolved Ce may be oxidized from Ce^{3+} to Ce^{4+}, resulting in a decrease in solubility and a negative Ce anomaly in seawater (de Baar, 1983). By contrast, anoxic conditions may result in a positive Ce anomaly in sediment's pore-waters (Elderfield and Sholkovitz, 1987). External sources of anthropogenic Gd, associated with medical and industrial wastewaters inputs due to its use in magnetic resonance imaging, may result in a positive Gd anomaly in seawater (Kümmerer and Helmers, 2000; Nozaki et al., 2000; Hatje et al., 2014). The Ce and Gd anomalies are defined as their deviation from an expected, PAAS-normalized ratio, as defined by Eqs 1 (Mclennan, 1989) and 2 (de Baar et al., 1985):

$$Ce\ anomaly = Ce/Ce^* = \frac{Ce_N}{(La_N\ X\ Pr_N)^{0.5}} \quad (1)$$

$$Gd\ anomaly = Gd/Gd^* = \frac{2Gd_N}{(Eu_N + Tb_N)} \quad (2)$$

where the PAAS-normalized concentrations are indicated by subscript $_N$ and * denotes the theoretical interpolated concentration based on neighboring elements. Accordingly, positive and negative Ce and Gd anomalies will feature Ce/Ce^* and Gd/Gd^* ratios higher and lower than 1, respectively.

Figure 5 presents the distribution of soft tissue REEs relative to the composition of PAAS, displaying an enrichment of the light REEs (LREE, La-Eu) relative to the heavy REEs (HREE, Gd-Lu). Similar observations were made for clams (Bonnail et al., 2017), fish, crustaceans, and mollusks (Li et al., 2016; Wang et al., 2019) and were suggested to stem from biological fractionation that favors LREE over HREE (Wang et al., 2019). The samples collected at day 0 display high REE/PAAS ratios (an order of magnitude higher than the rest of the samples) with no anomalies (**Figure 5A**), reflecting the domination of terrigenous sources in the lagoon environment.

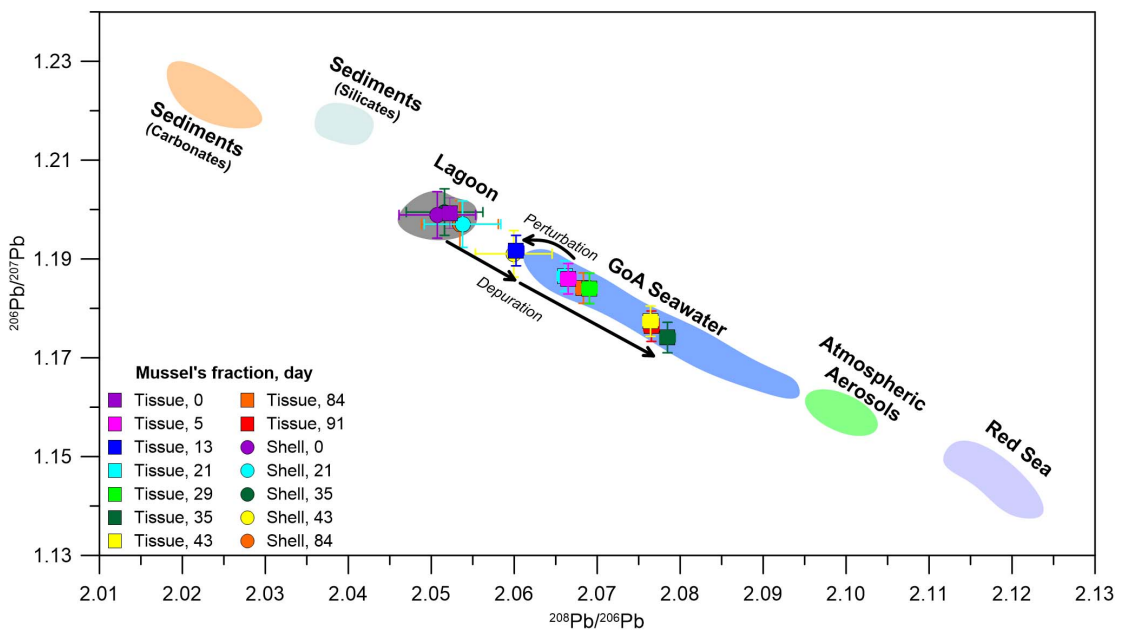

FIGURE 4 | The isotopic composition of $^{208}Pb/^{206}Pb$ versus $^{206}Pb/^{207}Pb$ in soft tissue (squares) and shells (circles). Colored markers represent the different samples through the length of the experiment. Shaded areas represent the regional end members: GoA seawater (blue field; Benaltabet et al., 2020), atmospheric aerosols (Chien et al., 2019), GoA leached and residual sediment fractions (Benaltabet et al., 2020), which represent the carbonate (orange field) and silicate (light blue field) fractions of bottom sediments, respectively. Red Sea seawater compositions (purple field) are assumed to correspond with Arabian Sea compositions (after Lee et al., 2015). For more information regarding the suggested end members the reader is referred to Chien et al. (2019) and Benaltabet et al. (2020). The day 0 shell and soft tissue composition represents the lagoon end member (gray field).

Five days after the translocation, REE concentrations decrease significantly, but shift back to higher values on day 13 while also displaying a positive Ce anomaly (**Figure 5B**). Afterward, the REE concentrations as well as the Ce anomaly at the samples collected at days 21–91, return to values that are similar to day 5. Moreover, following the relocation to the water tanks, the PAAS normalized pattern reveals an increasing positive Gd anomaly (**Figures 5A,C**), which suggests an anthropogenic source of Gd to the GoA waters.

Short-Term Perturbation

During the depuration experiment, the soft tissue samples presented a 2–8-fold increase in elemental concentrations between days 5 and 13 (**Figure 2**), as well as a shift in Pb isotopic composition toward the lagoon and sedimentary end members (**Figures 3**, **4**) and an increase in the PAAS- normalized REE concentrations (**Figure 5**). Moreover, when examining the subsequent samples, soft tissue Al, V, Cr, Mn, Fe, Co, Cd, Zn, Ni, and Pb concentrations gradually decrease from day 13 to 91, following a power law curve, with high R^2 values of 0.56 for Pb to R^2 = 0.95 for Co (**Figure 2**). When compared to the R^2 values for the period between 0 and 91 days, all of the above mentioned R^2 values for the period between 13 and 91 days are significantly higher. The fact that the decrease in soft tissue concentrations after day 13 closely follows a well-defined curve, suggests that the increase in concentrations in day 13 is associated with a compositional perturbation in the water tank's seawater composition (rather than being associated with analytical noise) that effectively reset the experiment at day 13. Moreover, 7 days after the day 13 perturbation, metal levels decreased by 33 to 70%, at rates similar to the initial decrease in concentrations following the relocation to the water tanks (between days 0 to 5) and to previously reported depuration rates (Yap et al., 2003; El-Gamal, 2011). The rate of increase in soft tissue metal abundances in response to the perturbation is comparable with the increases in Cd and Zn reported by Yap et al. (2003), who exposed mussels (*P. virdis)* to high levels of seawater Cd and Zn in a controlled laboratory experiment and followed the change of accumulated metals over time. By contrast, the study carried out by Liu and Wang (2016), who translocated two oyster species from a natural to a contaminated environment and followed metal accumulation with time reported limited increases in the soft tissue metals concentrations after 5 days of exposure. However, the difference in metal accumulation rates compared to our results can probably be attributed to different environmental conditions (Mubiana and Blust, 2007; Casas et al., 2008) and species types (Rainbow, 2002).

The cause of the perturbation between days 5 and 13 is unknown, and could be related to a natural change in the influxing seawater composition, possibly due to sediment resuspension along the coast, or to contamination of the water tank. The relatively high Ce anomaly at day 13 (**Figure 5**) may be indicative of a sedimentary source, as positive Ce anomalies are a common feature in some marine sediments (de Baar, 1983; Toyoda et al., 1990; Pattan et al., 2005). Moreover, several studies suggested that mollusks effectively accumulate LREEs from sediments and suspended particles (Bonnail et al., 2017; Ma et al., 2019; Wang et al., 2019). Hence, a perturbation associated with a terrigenous source will be promptly recorded in the mussel's soft tissue. This, coupled with the shift of the Pb isotopic composition toward sedimentary compositions (**Figure 4**) may suggest that the cause of the perturbation on day 13 is linked to a terrigenous source. Interestingly, the Al normalized ratios of several elements (e.g., Ni, Co, Fe, Cr, V, Pb Cd, Zn, and

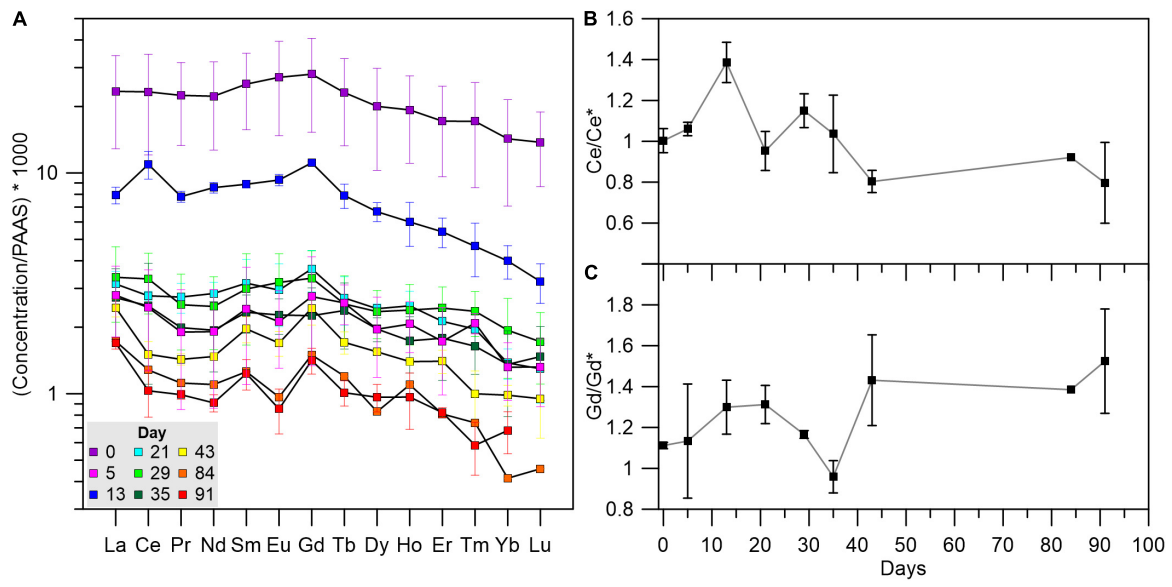

FIGURE 5 | (A) Soft tissue REE concentrations relative to PAAS (Taylor and McLennan, 1985). Colored symbols represent the different sampling days through the length of the experiment. Error bars mark the standard deviation of duplicate analyses (see section "Data treatment" for details). **(B)** Ce/Ce* ratios representing the Ce anomaly throughout the experiment. **(C)** Gd/Gd* ratios representing the Gd anomaly throughout the experiment.

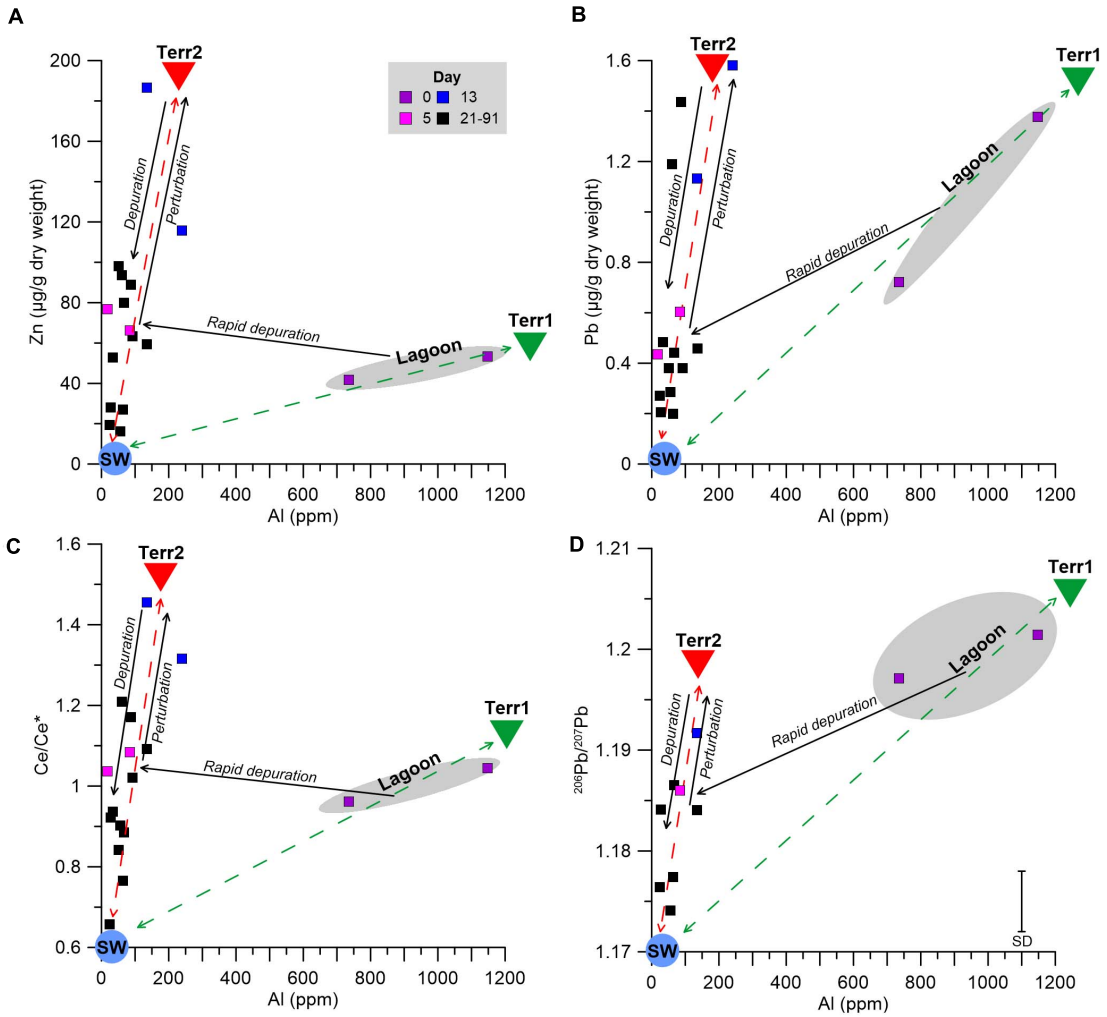

FIGURE 6 | Soft tissue Zn **(A)** and Pb **(B)** concentrations, Ce/Ce* **(C),** and $^{206}Pb/^{207}Pb$ compositions **(D)** versus soft tissue Al concentrations. The dashed lines represent the mixing curves between the two terrigenous (Terr1 and Terr2; green and red triangles, respectively) and seawater (SW; pale blue circle) end members. Solid arrows represent the temporal trend throughout the experiment: the rapid depuration after the relocation from the lagoon environment (gray field, purple squares) to the IUI (pink squares) between days 0 and 5, the brief perturbation toward Terr2 between days 5 and 13 (blue squares), and the long term depuration between days 21 and 91 (black squares).

Cu) display a relatively large shift between day 0 and day 5 but remain stable thereafter (**Supplementary Figure 1**), even after the day 13 perturbation. This implies that the terrigenous end member responsible for the perturbation has a different composition, characterized by a higher metal/Al ratio, compared to the lagoon end member. In other words, one terrigenous end member dominates the lagoon area and a second dominates the IUI coastal waters.

To better characterize the two terrigenous end members, the progress of the soft tissue depuration of various proxies versus Al is outlined in **Figure 6**. Zn and Pb were chosen to represent examples of anthropogenic metals in coastal waters (e.g., John et al., 2007; Boyle, 2019), while the shifts in the Ce anomaly value (Ce/Ce*) and the isotopic composition of Pb ($^{206}Pb/^{207}Pb$) represent the competing influences of terrigenous and seawater end member values. The lagoon environment is dominated by mixing of a terrigenous end member ("Terr1," **Figure 6**) with the seawater end member ("SW," **Figure 6**). While Terr1 features high metal concentrations and high $^{206}Pb/^{207}Pb$ ratios with no Ce anomaly (i.e., Ce/Ce* ≈ 1), the seawater end member is characterized by low metal concentrations (Chase et al., 2011; Chien et al., 2019; Benaltabet et al., 2020), a negative Ce anomaly, a common feature in oxygenated waters (Elderfield and Greaves, 1982; Alibo and Nozaki, 1999) and low $^{206}Pb/^{207}Pb$ ratios (Benaltabet et al., 2020). After the relocation to the water tanks, the mussel's soft tissue composition shifted rapidly to a separate mixing curve, with a different terrigenous end member ("Terr2," **Figure 6**), defined by high metal abundances and lower Al contents relative to Terr1, a positive Ce anomaly and high $^{206}Pb/^{207}Pb$ ratios. Following the day 13 perturbation, the soft tissue compositions shifted toward Terr2, and thereafter subsided toward the composition of the seawater end member,

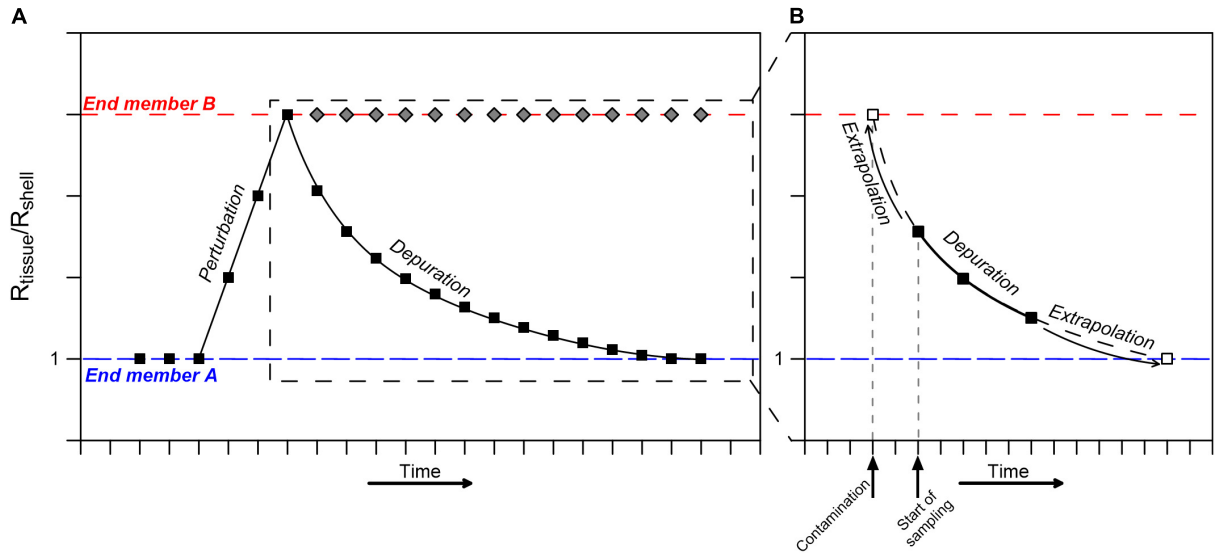

FIGURE 7 | A conceptual representation of a perturbation/pollution event reflected by the ratio between soft tissue (R_{tissue}) and shell (R_{shell}) Pb isotopic compositions. **(A)** A perturbation represented by an exposure to end member B (dashed red line) will result in an increase in the R_{tissue}/R_{shell} ratio. Subsequently, if the contamination persists (chronic contamination), the R_{tissue}/R_{shell} ratio will remain high (until eventually the end member B signal starts dominating the bulk shell composition after a significant period of time not considered here). If the perturbation is brief, the R_{tissue}/R_{shell} ratio will gradually return to a value of 1 (end member A, dashed blue line) following a power law curve. **(B)** R_{tissue}/R_{shell} ratio shortly after a contamination event, depicting how a partial set of observations (e.g., black squares) can be used to extract the timing of the suspected perturbation/contamination event through back extrapolation of the calculated power law depuration curve to the contaminating end member composition (empty square).

as the mussels gradually depurated the accumulated metals from the perturbation.

Long-Term Biomonitoring

Due to biological controls and the variability of elemental partitioning coefficients between seawater, soft tissue and shell (White and Rainbow, 1982; Chong and Wang, 2001; Amiard et al., 2006), metal abundances in the soft tissue and shell are markedly different (**Figure 2**). By contrast, the isotopic composition of the shell and soft tissue at day 0 overlap (**Figures 3**, **4**) because Pb isotopic fractionation during assimilation is negligible (Russell Flegal and Stukas, 1987) and both phases acquired the long term local lagoon composition (**Figure 4**). The ratio between the Pb isotopic composition in the soft tissue and shell is expressed in Eq. 3:

$$\frac{R_{\text{tissue}}}{R_{\text{shell}}} = \frac{\left(\frac{^{206}Pb}{^{207}Pb}\right)_{\text{tissue}}}{\left(\frac{^{206}Pb}{^{207}Pb}\right)_{\text{shell}}} \quad (3)$$

where R_{tissue} and R_{shell} are the $^{206}Pb/^{207}Pb$ ratios (or other Pb isotopic ratios) in the soft tissue and shell, respectively. In the lagoon samples (day 0), the R_{tissue}/R_{shell} ratio presents an approximate value of one and continuously decreases as the soft tissue registers lower $^{206}Pb/^{207}Pb$ seawater compositions (**Figure 3B**).

Thus, mature mussels grown in stable conditions should display an identical Pb isotopic composition in both the shell and soft tissue, i.e., $R_{tissue}/R_{shell} = 1$. Accordingly, the coupled Pb isotopic composition of mussels soft tissue and shell can be used for long-term biomonitoring in coastal environments, even if the initial isotopic composition is unknown, as any deviation from $R_{tissue}/R_{shell} = 1$ will represent a shift toward a new compositional end member (**Figure 7**). If the perturbation is of chronic nature, the R_{tissue}/R_{shell} ratio will remain constant, representing the current long-term composition of surrounding seawater, as is the case here, where the seawater composition changed after their relocation.

This approach can also be applied to other heavy isotopic systems where no isotopic fractionation is associated with the assimilation into the shell and soft tissue (e.g., Nd, U, and Th). However, the isotopic composition of Pb is especially useful for monitoring marine pollution given its sensitivity to anthropogenic inputs and ample reports of natural and anthropogenic end member compositions (e.g., Bollhöfer and Rosman, 2001, 2000; Labonne et al., 2001; Erel et al., 2006; Boyle et al., 2014; Dang et al., 2015).

Biomonitoring of Short-Term Pollution Events

Although serendipitously demonstrated here (i.e., by the perturbation between day 5 and 13), biomonitoring of short-term (daily) events is often challenged by the rapid compositional change in soft tissue compositions in the days following the event, hampering the use of mussels and other marine filter-feeding organisms as biomonitors of abrupt and short pollution events. Nevertheless, our results provide the possibility to overcome this shortcoming by extrapolating observations backward toward the onset of the event.

Consider a pollution event that is identified along a coastline, but evidence (e.g., visual observations, smell, direct seawater analyses) only starts accumulating several days after the actual event. Thus, the exact timing and location of the contamination remain largely unknown. Yet, following alerts of a potential pollution event, it is possible to initiate continuous sampling of *in-situ* living mussels at a daily resolution over a period of 1–2 weeks and analyze the isotopic compositions of their soft tissue and shell. The results will yield a partial segment of the longer-term depuration pattern during which the R_{tissue}/R_{shell} ratio gradually returns to a value of 1 following a power law curve (**Figure 7B**). A backward extrapolation of this curve, allows determining the timing of contamination, as long as the initial contamination value can be estimated, even if only roughly. The latter can be reasonably evaluated in coastal environments where recurring pollution events take place, or by assuming a regional anthropogenic Pb isotope compositional end member. Accordingly, the time of contamination (t) can be determined using Eq. 4 solved for t:

$$\frac{R_c}{R_{shell}} = t^{-m} \quad (4)$$

Where R_c represents the composition of the contaminant, R_{shell} is the measured composition in the shell and m is the power constant given by the depuration curve. Alternatively, if the timing (t) of the pollution event is well known, Eq. 4 can be solved for R_c and cross-referenced with literature report to learn about the source of the contaminant end member (e.g., anthropogenic or natural/terrigenous). This approach assumes that the soft tissue is a sensitive recorder of ambient seawater compositions, as seen here and by others (e.g., Yap et al., 2003; El-Gamal, 2011; Anacleto et al., 2015). Moreover, if coupled with a spatial survey, this approach can also provide information regarding the geographic sources of the contaminants, and how these progress spatially and temporally.

In summary, mussels (*B. pharaonis*) growing in a contaminated lagoon were relocated to a pristine environment for depuration and their soft tissue and shells were analyzed for heavy metal and REE concentrations, as well as the isotopic composition of Pb.

The shell retained its original composition and did not present significant change in metal abundances (apart from Mn) during the experiment. On the other hand, most of the soft tissue metal concentrations (Al, V, Cr, Mn, Fe, Co, Ni, Zn, Cd, and Pb) and the REEs presented a gradual decrease in concentrations in the 91 days following the relocation from the lagoon to the water tanks, with the bulk majority of the decrease (51–86%) restricted to the first 5 days. The decrease trend was disrupted by an abrupt increase in metal and REE concentrations at day 13, after which concentrations decreased gradually following a power law trend (R^2 of up to 0.95).

Pb isotope ratios of both the shells and soft tissue at the lagoon represent a mixture of previously reported seafloor sediment and open seawater compositions. While the composition of the shells remains rather constant throughout the experiment ($^{206}Pb/^{207}Pb$ = 1.191 – 1.199, $^{208}Pb/^{206}Pb$ = 2.051 – 2.060), the soft tissue compositions ($^{206}Pb/^{207}Pb$ = 1.174 – 1.199, $^{208}Pb/^{206}Pb$ = 2.052 – 2.078) shift gradually toward open seawater values from days 5 to 91, while briefly shifting toward the sedimentary end member at day 13. This shift is also illustrated by the REEs pattern relative to PAAS, which features a positive Ce anomaly at day 13. Hence, we conclude that this compositional shift was driven by an environmental perturbation linked to a terrigenous source. By comparing soft tissue metal concentrations, Ce anomaly ratios, Pb isotopic compositions and Al concentrations, it is shown that following the relocation to the water tanks, the mussels were controlled by a separate mixing curve between GoA seawater and a local terrigenous end member (possibly marine sediments), which is different than the terrigenous end member dominating the lagoon environment.

The soft tissue of *B. pharaonis* may be used to biomonitor short-term environmental perturbations or pollution events. The ratio between the Pb isotopic composition of the soft tissue and shell sampled following an event may be used to determine the exact timing and possibly geographic location of the pollution, when both the latter are *a-priori* unknown.

By implementing geochemical tools such as Pb isotopic compositions, Al-normalization and REE patterns, we demonstrated the potential of mussels as biomonitors of short-term fluctuations or alternatively, of long-term seawater compositions. In both cases, the combined suite of geochemical proxies can be used to provide robust quantitative constraints on the sources and magnitude of pollution events, providing important tools for implementing and developing environmental management policies.

DATA AVAILABILITY STATEMENT

The original contributions presented in the study are included in the article/**Supplementary Material**, further inquiries can be directed to the corresponding author/s.

AUTHOR CONTRIBUTIONS

TB, EG-H, and AT wrote the manuscript. EG-H and AT conceived the project and conducted fieldwork and analyses. All authors contributed to the article and approved the submitted version.

FUNDING

Funding was provided by the Israel Science Foundation grants 927/15 and 834/19 and the Hebrew University Ring Foundation to AT, and the Bester and Pfeifer scholarships to TB.

ACKNOWLEDGMENTS

We thank Barak Yarden for his assistance in sample preparation and Ofir Tirosh for his assistance with the instrumental analyses.

SUPPLEMENTARY MATERIAL

The Supplementary Material for this article can be found online at: https://www.frontiersin.org/articles/10.3389/fmars.2021.669329/full#supplementary-material

REFERENCES

Abelson, A., Shteinman, B., Fine, M., and Kaganovsky, S. (1999). Mass transport from pollution sources to remote coral reefs in Eilat (Gulf of Aqaba, Red Sea). *Mar. Pollut. Bull.* 38, 25–29. doi: 10.1016/S0025-326X(98)00081-2

Alibo, D. S., and Nozaki, Y. (1999). Rare earth elements in seawater: particle association, shale-normalization, and ce oxidation. *Geochim. Cosmochim. Acta* 63, 363–372. doi: 10.1016/S0016-7037(98)00279-8

Almogi-Labin, A., Edelman-Furstenberg, Y., and Hemleben, C. (2008). "Variations in the biodiversity of thecosomatous pteropods during the Late Quaternary as a response to environmental changes in the Gulf of Aden–Red Sea–Gulf of Aqaba ecosystem," in *Aqaba-Eilat, the Improbable Gulff: Environment, Biodiversity and Preservation*, ed. F. D. Por (Jerusalem: The Hebrew University Magnes Press), 31–48.

Al-Taani, A. A., Batayneh, A., Nazzal, Y., Ghrefat, H., Elawadi, E., and Zaman, H. (2014). Status of trace metals in surface seawater of the Gulf of Aqaba, Saudi Arabia. *Mar. Pollut. Bull.* 86, 582–590. doi: 10.1016/j.marpolbul.2014.05.060

Amiard, J. C., Amiard-Triquet, C., Barka, S., Pellerin, J., and Rainbow, P. S. (2006). Metallothioneins in aquatic invertebrates: their role in metal detoxification and their use as biomarkers. *Aquat. Toxicol.* 76, 160–202. doi: 10.1016/j.aquatox.2005.08.015

Anacleto, P., Luísa, A., and Leonor, M. (2015). Effects of depuration on metal levels and health status of bivalve molluscs. *Food Control* 47, 493–501. doi: 10.1016/j.foodcont.2014.07.055

Baker, A. R., Landing, W. M., Bucciarelli, E., Cheize, M., Fietz, S., Hayes, C. T., et al. (2016). Trace element and isotope deposition across the air–sea interface: progress and research needs. *Philos. Trans. R. Soc. A Math. Phys. Eng. Sci.* 374:20160190. doi: 10.1098/rsta.2016.0190

Barakat, S. A., Al-Rousan, S., and Al-Trabeen, M. S. (2015). Use of scleractinian corals to indicate marine pollution in the northern Gulf of Aqaba, Jordan. *Environ. Monit. Assess.* 187:42. doi: 10.1007/s10661-015-4275-2

Barash, A., and Danin, Z. (1986). Further additions to the knowledge of Indo-Pacific Mollusca in the Mediterranean Sea. *Spixiana* 9, 117–141.

Bekteshi, L., Lazo, P., Qarri, F., and Stafilov, T. (2015). Application of the normalization process in the survey of atmospheric deposition of heavy metals in Albania through moss biomonitoring. *Ecol. Indic.* 56, 50–59. doi: 10.1016/j.ecolind.2015.03.001

Benaltabet, T., Lapid, G., and Torfstein, A. (2020). Seawater Pb concentration and isotopic composition response to daily time scale dust storms in the Gulf of Aqaba, Red Sea. *Mar. Chem.* 227:103895. doi: 10.1016/j.marchem.2020.103895

Bollhöfer, A., and Rosman, K. J. R. (2000). Isotopic source signatures for atmospheric lead: the southern hemisphere. *Geochim. Cosmochim. Acta* 64, 3251–3262. doi: 10.1016/S0016-7037(00)00436-1

Bollhöfer, A., and Rosman, K. J. R. (2001). Isotopic source signatures for atmospheric lead: the northern hemisphere. *Geochim. Cosmochim. Acta* 65, 1727–1740. doi: 10.1016/S0016-7037(00)00630-X

Bonnail, E., Pérez-López, R., Sarmiento, A. M., Nieto, J. M., and DelValls, T. Á (2017). A novel approach for acid mine drainage pollution biomonitoring using rare earth elements bioaccumulated in the freshwater clam *Corbicula fluminea*. *J. Hazard. Mater.* 338, 466–471. doi: 10.1016/j.jhazmat.2017.05.052

Boyle, E. A. (2019). "Anthropogenic trace elements in the ocean," in *Encyclopedia of Ocean Sciences*, Amsterdam: Elsevier Ltd, 195–202. doi: 10.1016/B978-0-12-409548-9.11592-1

Boyle, E. A., Chapnick, S. D., Shen, G. T., and Bacon, M. P. (1986). Temporal variability of lead in the western North Atlantic. *J. Geophys. Res.* 91, 8573–8593. doi: 10.1029/JC091iC07p08573

Boyle, E. A., Lee, J.-M., Echegoyen, Y., Noble, A., Moos, S., Carrasco, G., et al. (2014). Anthropogenic lead emissions in the ocean: the evolving global experiment. *Oceanography* 27, 69–75. doi: 10.5670/oceanog.2014.10

Bruland, K., Lohan, M. C., Aguilar-Islas, A. M., Smith, G. J., Sohst, B., and Baptista, A. (2008). Factors influencing the chemistry of the near-field Columbia River plume: nitrate, silicic acid, dissolved Fe, and dissolved Mn. *J. Geophys. Res.* 113, 1–23. doi: 10.1029/2007JC004702

Bruland, K., Middag, R., and Lohan, M. C. (2013). "Controls of Trace Metals in Seawater," in *Treatise on Geochemistry: Second Edition*, eds Mottl, J. Michael, Elderfield, and Henry (Philadelphia, PA: Elsevier Ltd), doi: 10.1016/B978-0-08-095975-7.00602-1

Buck, N. J., Gobler, C. J., and Sañudo-Wilhelmy, S. A. (2005). Dissolved trace element concentrations in the East River–Long Island Sound system: relative importance of autochthonous versus allochthonous sources. *Environ. Sci. Technol.* 39, 3528–3537. doi: 10.1021/es048860t

Carmichael, R. H., Jones, A. L., Patterson, H. K., Walton, W. C., Pérez-Huerta, A., Overton, E. B., et al. (2012). Assimilation of oil-derived elements by oysters due to the deepwater horizon oil spill. *Environ. Sci. Technol.* 46, 12787–12795. doi: 10.1021/es302369h

Casas, S., Gonzalez, J.-L., Andral, B., and Cossa, D. (2008). Relation between metal concentration in water and metal content of marine mussels (*Mytilus galloprovincialis*): impact of physiology. *Environ. Toxicol. Chem.* 27, 1543–1552. doi: 10.1897/07-418

Cebrian, E., Uriz, M. J., and Turon, X. (2007). Sponges as biomonitors of heavy metals in spatial and temporal surveys in northwestern Mediterranean: multispecies comparison. *Environ. Toxicol. Chem.* 26, 2430–2439. doi: 10.1897/07-292.1

Chan, H. M. (1989). Temporal and spatial fluctuations in trace metal concentrations in transplanted mussels in Hong Kong. *Mar. Pollut. Bull.* 20, 82–86. doi: 10.1016/0025-326X(89)90231-2

Chase, Z., Paytan, A., Beck, A., Biller, D., Bruland, K. W., Measures, C., et al. (2011). Evaluating the impact of atmospheric deposition on dissolved trace-metals in the Gulf of Aqaba, Red Sea. *Mar. Chem.* 126, 256–268. doi: 10.1016/j.marchem.2011.06.005

Chase, Z., Paytan, A., Johnson, K. S., Street, J., and Chen, Y. (2006). Input and cycling of iron in the Gulf of Aqaba, Red Sea. *Global Biogeochem. Cycles* 20, 1–11. doi: 10.1029/2005GB002646

Chen, Y., Paytan, A., Chase, Z., Measures, C., Beck, A., Sañudo-Wilhelmy, S. A., et al. (2008). Sources and fluxes of atmospheric trace elements to the Gulf of Aqaba, Red Sea. *J. Geophys. Res. Atmos.* 113, 1–13. doi: 10.1029/2007JD009110

Chien, C.-T., Benaltabet, T., Torfstein, A., and Paytan, A. (2019). Contributions of atmospheric deposition to Pb concentration and isotopic composition in seawater and particulate matters in the Gulf of Aqaba, Red Sea. *Environ. Sci. Technol.* 53, 6162–6170. doi: 10.1021/acs.est.9b00505

Chong, K., and Wang, W. X. (2001). Comparative studies on the biokinetics of Cd, Cr, and Zn in the green mussel *Perna viridis* and the Manila clam *Ruditapes philippinarum*. *Environ. Pollut.* 115, 107–121. doi: 10.1016/S0269-7491(01)00087-2

Crenshaw, M. A. (1972). The inorganic composition of molluscan extrapallial fluid. *Biol. Bull.* 143, 506–512. doi: 10.2307/1540180

Cziczo, D. J., Stetzer, O., Worringen, A., Ebert, M., Weinbruch, S., Kamphus, M., et al. (2009). Inadvertent climate modification due to anthropogenic lead. *Nat. Geosci.* 2, 333–336. doi: 10.1038/ngeo499

Dang, D. H., Schäfer, J., Brach-Papa, C., Lenoble, V., Durrieu, G., Dutruch, L., et al. (2015). Evidencing the impact of coastal contaminated sediments on mussels through Pb stable isotopes composition. *Environ. Sci. Technol.* 49, 11438–11448. doi: 10.1021/acs.est.5b01893

Dar, M. A., Belal, A. A., and Madkour, A. G. (2018). The differential abilities of some molluscs to accumulate heavy metals within their shells in the Timsah and the Great Bitter lakes, Suez Canal, Egypt. *Egypt. J. Aquat. Res.* 44, 291–298. doi: 10.1016/j.ejar.2018.11.008

de Baar, H. J. W. (1983). *The Marine Geochemistry of the Rare Earth Elements*. Falmouth, MA: Woods Hole Oceanographic Institution.

de Baar, H. J. W., Bacon, M. P., and Brewer, P. G. (1983). Rare-earth distributions with a positive Ce anomaly in the Western North Atlantic Ocean. *Nature* 301, 324–327. doi: 10.1038/301324a0

de Baar, H. J. W., Brewer, P. G., and Bacon, M. P. (1985). Anomalies in rare earth distributions in seawater: Gd and Tb. *Geochim. Cosmochim. Acta* 49, 1961–1969. doi: 10.1016/0016-7037(85)90090-0

Elderfield, H. (1988). The oceanic chemistry of the rare-earth elements. *Philos. Trans. R. Soc. Lond. Ser. A Math. Phys. Sci.* 325, 105–126.

Elderfield, H., and Greaves, M. J. (1982). The rare earth elements in seawater. *Nature* 296, 214–219. doi: 10.1038/296214a0

Elderfield, H., and Sholkovitz, E.R. t (1987). Rare earth elements in the pore waters of reducing nearshore sediments. *Earth Planet. Sci. Lett.* 82, 280–288. doi: 10.1016/0012-821x(87)90202-0

El-Gamal, M. M. (2011). The effect of depuration on heavy metals, petroleum hydrocarbons, and microbial contamination levels in *Paphia undulata* (Bivalvia: Veneridae). *Czech J. Anim. Sci.* 56, 345–354. doi: 10.17221/2395-cjas

Erel, Y., Axelrod, T., Veron, A., Mahrer, Y., Katsafados, P., and Dayan, U. (2002). Transboundary atmospheric lead pollution. *Environ. Sci. Technol.* 36, 3230–3233. doi: 10.1021/es020530q

Erel, Y., Dayan, U., Rabi, R., Rudich, Y., and Stein, M. (2006). Trans boundary transport of pollutants by atmospheric mineral dust. *Environ. Sci. Technol.* 40, 2996–3005. doi: 10.1021/es051502l

Farrington, J. W., Bowen, V. T., Goldberg, E. D., Risebrough, R. W., and Martin, J. H. (1983). U.S. 'Mussel Watch' 1976-1978: an overview of the trace-metal, DDE, PCB, hydrocarbon, and artificial radionuclide data. *Environ. Sci. Technol.* 17, 490–496. doi: 10.1021/es00114a010

Freitas, P. S., Clarke, L. J., Kennedy, H., and Richardson, C. A. (2016). Manganese in the shell of the bivalve *Mytilus edulis*: seawater Mn or physiological control? *Geochim. Cosmochim. Acta* 194, 266–278. doi: 10.1016/j.gca.2016.09.006

Fung, C. N., Lam, J. C. W., Zheng, G. J., Connell, D. W., Monirith, I., Tanabe, S., et al. (2004). Mussel-based monitoring of trace metal and organic contaminants along the east coast of China using *Perna viridis* and *Mytilus edulis*. *Environ. Pollut.* 127, 203–216. doi: 10.1016/j.envpol.2003.08.007

Genin, A. (2008). "The physical setting of the Gulf of Aqaba: an explanation for a unique occurrence of tropical communities in the subtropics," in *Aqaba-Eilat, the Improbable Gulf: Environment, Biodiversity and Preservation*, ed. F. D. Por (Jerusalem: The Hebrew University Magnes Press), 15–20.

Genin, A., Lazar, B., and Brenner, S. (1995). Vertical mixing and coral death in the Red Sea following the eruption of Mount Pinatubo. *Nature* 377, 507–510. doi: 10.1038/377507a0

Göksu, M. Z. L., Akar, M., Çevik, F., and Findik, Ö (2005). Bioaccumulation of some heavy metals (Cd, Fe, Zn, Cu) in two bivalvia species (*Pinctada radiata* Leach, 1814 and *Brachidontes pharaonis* Fischer, 1870). *Turk. J. Vet. Anim. Sci.* 29, 89–93.

Goldberg, E. D. (1975). The mussel watch–a first step in global marine monitoring. *Mar. Pollut. Bull.* 6:111. doi: 10.1016/0025-326X(75)90271-4

Goldberg, E. D., Bowen, V. T., Farrington, J. W., Harvey, G., Martin, J. H., Parker, P. L., et al. (1978). The mussel watch. *Environ. Conserv.* 5, 101–125. doi: 10.1017/S0376892900005555

Gwenzi, W., Mangori, L., Danha, C., Chaukura, N., Dunjana, N., and Sanganyado, E. (2018). Sources, behaviour, and environmental and human health risks of high-technology rare earth elements as emerging contaminants. *Sci. Total Environ.* 636, 299–313. doi: 10.1016/j.scitotenv.2018.04.235

Hamed, E. S. A. E., Khaled, A., Ahdy, H., Omar Ahmed, H., and Aly Abdelrazek, F. (2020). Health risk assessment of heavy metals in three invertebrate species collected along Alexandria Coast, Egypt. *Egypt. J. Aquat. Res.* 46, 389–395. doi: 10.1016/j.ejar.2020.11.001

Hatje, V., Bruland, K., and Flegal, A. R. (2014). Determination of rare earth elements after pre-concentration using NOBIAS-chelate PA-1® resin: method development and application in the San Francisco Bay plume. *Mar. Chem.* 160, 34–41. doi: 10.1016/j.marchem.2014.01.006

Hatje, V., Bruland, K. W., and Flegal, A. R. (2016). Increases in anthropogenic gadolinium anomalies and rare earth element concentrations in San Francisco Bay over a 20 year record. *Environ. Sci. Technol.* 50, 4159–4168. doi: 10.1021/acs.est.5b04322

Herut, B., Kress, N., Shefer, E., and Hornung, H. (1999). Trace element levels in mollusks from clean and polluted coastal marine sites in the Mediterranean, Red and North Seas. *Helgol. Mar. Res.* 53, 154–162. doi: 10.1007/s101520050021

Horiguchi, T. (2006). Masculinization of female gastropod mollusks induced by organotin compounds, focusing on mechanism of actions of tributyltin and triphenyltin for development of imposex. *Environ. Sci.* 13, 77–87.

Hutchinson, T. H., Jha, A. N., and Dixon, D. R. (1995). The polychaete *Platynereis dumerilii* (audouin and milne-edwards): a new species for assessing the hazardous potential of chemicals in the marine environment. *Ecotoxicol. Environ. Saf.* 31, 271–281. doi: 10.1006/eesa.1995.1074

Jickells, T. D., Baker, A. R., and Chance, R. (2016). Atmospheric transport of trace elements and nutrients to the oceans. *Philos. Trans. R. Soc. A Math. Phys. Eng. Sci.* 374:20150286. doi: 10.1098/rsta.2015.0286

John, S. G., Park, J. G., Zhang, Z., and Boyle, E. A. (2007). The isotopic composition of some common forms of anthropogenic zinc. *Chem. Geol.* 245, 61–69. doi: 10.1016/j.chemgeo.2007.07.024

Karayakar, F., Erdem, C., and Cicik, B. (2007). Seasonal variation in copper, zinc, chromium, lead and cadmium levels in hepatopancreas, gill and muscle tissues of the mussel Brachidontes pharaonis Fischer, collected along the Mersin coast, Turkey. *Bull. Environ. Contam. Toxicol.* 79, 350–355. doi: 10.1007/s00128-007-9246-z

Katz, T., Ginat, H., Eyal, G., Steiner, Z., Braun, Y., Shalev, S., et al. (2015). Desert flash floods form hyperpycnal flows in the coral-rich Gulf of Aqaba, Red Sea. *Earth Planet. Sci. Lett.* 417, 87–98. doi: 10.1016/j.epsl.2015.02.025

Komárek, M., Ettler, V., Chrastný, V., and Mihaljevič, M. (2008). Lead isotopes in environmental sciences: a review. *Environ. Int.* 34, 562–577. doi: 10.1016/j.envint.2007.10.005

Kümmerer, K., and Helmers, E. (2000). Hospital effluents as a source of gadolinium in the aquatic environment. *Environ. Sci. Technol.* 34, 573–577. doi: 10.1021/es990633h

Labonne, M., Ben Othman, D., and Luck, J. M. (1998). Recent and past anthropogenic impact on a mediterranean lagoon: lead isotope constraints from mussel shells. *Appl. Geochem.* 13, 885–892. doi: 10.1016/S0883-2927(98)00016-X

Labonne, M., Ben Othman, D., and Luck, J. M. (2001). Pb isotopes in mussels as tracers of metal sources and water movements in a lagoon (Thau Basin, S. France). *Chem. Geol.* 181, 181–191. doi: 10.1016/S0009-2541(01)00281-9

Lazar, B., Erez, J., Silverman, J., Rivlin, T., Rivlin, A., Dray, M., et al. (2008). "Recent environmental changes in the chemical-biological oceanography of the Gulf of Aqaba (Eilat)," in *Aqaba-Eilat, Improbable Gulf. Environment, Biodiversity and Preservation*, ed. F. D. Por (Jerusalem: Magnes Press), 49–61.

Lee, J. M., Boyle, E. A., Gamo, T., Obata, H., Norisuye, K., and Echegoyen, Y. (2015). Impact of anthropogenic Pb and ocean circulation on the recent distribution of Pb isotopes in the Indian Ocean. *Geochim. Cosmochim. Acta* 170, 126–144. doi: 10.1016/j.gca.2015.08.013

Li, J. X., Zheng, L., Sun, C. J., Jiang, F. H., Yin, X. F., Chen, J. H., et al. (2016). Study on ecological and chemical properties of rare earth elements in tropical marine organisms. *Chin. J. Anal. Chem.* 44, 1539–1546. doi: 10.1016/S1872-2040(16)60963-5

Liu, X., and Wang, W.-X. (2016). Time changes in biomarker responses in two species of oyster transplanted into a metal contaminated estuary. *Sci. Total Environ.* 544, 281–290. doi: 10.1016/j.scitotenv.2015.11.120

Lorenzo, J. I., Aierbe, E., Mubiana, V. K., Blust, R., and Beiras, R. (2003). "Indications of regulation on copper accumulation in the blue mussel *Mytilus edulis*," in *Molluscan Shellfish Safety*, eds A. Villalba, B. Reguera, J. L. Romalde, and R. Beiras (London: UNESCO), 533–544.

Ma, L., Dang, D. H., Wang, W., Evans, R. D., and Wang, W.-X. (2019). Rare earth elements in the Pearl River Delta of China: potential impacts of the REE industry on water, suspended particles and oysters. *Environ. Pollut.* 244, 190–201. doi: 10.1016/j.envpol.2018.10.015

Mahowald, N. M., Engelstaedter, S., Luo, C., Sealy, A., Artaxo, P., Benitez-Nelson, C., et al. (2009). Atmospheric iron deposition: global distribution, variability, and human perturbations. *Ann. Rev. Mar. Sci.* 1, 245–278. doi: 10.1146/annurev.marine.010908.163727

Mclennan, S. M. (1989). Rare earth elements in sedimentary rocks: influence of provenance and sedimentary processes. *Geochem. Mineral. Rare Earth Elem. Rev. Mineral.* 21, 169–200. doi: 10.1515/9781501509032-010

Moloukhia, H., and Sleem, S. (2011). Bioaccumulation, fate and toxicity of two heavy metals common in industrial wastes in two aquatic molluscs. *J. Am. Sci.* 7, 459–464.

Morton, B. (1988). The population dynamics and reproductive cycle of *Brachidontes* variabilis (*Bivalvia*: *Mytilidae*) in a Hong Kong mangrove. *Malacol. Rev.* 21, 109–117.

Mubiana, V. K., and Blust, R. (2007). Effects of temperature on scope for growth and accumulation of Cd, Co, Cu and Pb by the marine bivalve *Mytilus edulis*. *Mar. Environ. Res.* 63, 219–235. doi: 10.1016/j.marenvres.2006.08.005

Naimo, T. J. (1995). A review of the effects of heavy metals on freshwater mussels. *Ecotoxicology* 4, 341–362. doi: 10.1007/BF00118870

Nozaki, Y., Lerche, D., Alibo, D. S., and Tsutsumi, M. (2000). Dissolved indium and rare earth elements in three Japanese rivers and Tokyo Bay: evidence for anthropogenic Gd and In. *Geochim. Cosmochim. Acta* 64, 3975–3982. doi: 10.1016/S0016-7037(00)00472-5

Nriagu, J. O., and Pacyna, J. M. (1988). Quantitative assessment of worldwide contamination of air, water and soils by trace metals. *Nature* 333, 134–139. doi: 10.1038/333134a0

Pattan, J. N., Pearce, N. J. G., and Mislankar, P. G. (2005). Constraints in using Cerium-anomaly of bulk sediments as an indicator of paleo bottom water redox environment: a case study from the Central Indian Ocean Basin. *Chem. Geol.* 221, 260–278. doi: 10.1016/j.chemgeo.2005.06.009

Phillips, D. J. H. (1976). The common mussel *Mytilus edulis* as an indicator of pollution by zinc, cadmium, lead and copper. II. Relationship of metals in the mussel to those discharged by industry. *Mar. Biol.* 38, 71–80. doi: 10.1007/BF00391487

Phillips, D. J. H. (1980). *Quantitative Aquatic Biological Indicators: Their Use to Monitor Trace metal and Organochlorine Pollution*. London: Applied Science Publishers.

Rainbow, P. S. (2002). Trace metal concentrations in aquatic invertebrates: why and so what? *Environ. Pollut.* 120, 497–507. doi: 10.1016/S0269-7491(02)00238-5

Raisuddin, S., Kwok, K. W. H., Leung, K. M. Y., Schlenk, D., and Lee, J. S. (2007). The copepod *Tigriopus*: a promising marine model organism for ecotoxicology and environmental genomics. *Aquat. Toxicol.* 83, 161–173. doi: 10.1016/j.aquatox.2007.04.005

Richardson, C., Chenery, S., and Cook, J. (2001). Assessing the history of trace metal (Cu, Zn, Pb) contamination in the North Sea through laser ablation-ICP-MS of horse mussel *Modiolus modiolus* shells. *Mar. Ecol. Prog. Ser.* 211, 157–167. doi: 10.3354/meps211157

Roditi, H. A., Fisher, N. S., and Sañudo-Wilhelmy, S. A. (2000). Field testing a metal bioaccumulation model for zebra mussels. *Environ. Sci. Technol.* 34, 2817–2825. doi: 10.1021/es991442h

Russell Flegal, A., and Stukas, V. J. (1987). Accuracy and precision of lead isotopic composition measurements in seawater. *Mar. Chem.* 22, 163–177. doi: 10.1016/0304-4203(87)90006-5

Sasekumar, A. (1974). Distribution of macrofauna on a Malayan mangrove shore. *J. Anim. Ecol.* 43, 51–69. doi: 10.2307/3157

Shelley, R. U., Morton, P. L., and Landing, W. M. (2015). Elemental ratios and enrichment factors in aerosols from the US-GEOTRACES North Atlantic transects. *Deep. Res. 2 Top. Stud. Oceanogr.* 116, 262–272. doi: 10.1016/j.dsr2.2014.12.005

Squadrone, S., Brizio, P., Stella, C., Mantia, M., Battuello, M., Nurra, N., et al. (2019). Rare earth elements in marine and terrestrial matrices of Northwestern Italy: implications for food safety and human health. *Sci. Total Environ.* 660, 1383–1391. doi: 10.1016/j.scitotenv.2019.01.112

Steding, D. J., Dunlap, C. E., and Flegal, A. R. (2000). New isotopic evidence for chronic lead contamination in the San Francisco Bay estuary system: implications for the persistence of past industrial lead emissions in the biosphere. *Proc. Natl. Acad. Sci. U.S.A.* 97, 11181–11186. doi: 10.1073/pnas.180125697

Taylor, J. D. (1971). Reef associated molluscan assemblages in the western Indian Ocean. *Symp. Zool. Soc. Lond.* 28, 501–534.

Taylor, S. R., and McLennan, S. M. (1985). *The Continental Crust: Its Composition and Evolution*. Oxford: Blackwell Scientific Publications.

Ternon, E., Guieu, C., Löye-Pilot, M. D., Leblond, N., Bosc, E., Gasser, B., et al. (2010). The impact of Saharan dust on the particulate export in the water column of the North Western Mediterranean Sea. *Biogeosciences* 7, 809–826. doi: 10.5194/bg-7-809-2010

Torfstein, A., Goldstein, S. L., and Stein, M. (2018). Enhanced Saharan dust input to the levant during Heinrich stadials. *Quat. Sci. Rev.* 186, 142–155. doi: 10.1016/j.quascirev.2018.01.018

Torfstein, A., Kienast, S. S., Yarden, B., Rivlin, A., Isaacs, S., and Shaked, Y. (2020). Bulk and export production fluxes in the Gulf of Aqaba, Northern Red Sea. *ACS Earth Space. Chem.* 4, 1461–1479. doi: 10.1021/acsearthspacechem.0c00079

Torfstein, A., Teutsch, N., Tirosh, O., Shaked, Y., Rivlin, T., Zipori, A., et al. (2017). Chemical characterization of atmospheric dust from a weekly time series in the north Red Sea between 2006 and 2010. *Geochim. Cosmochim. Acta* 211, 373–393. doi: 10.1016/j.gca.2017.06.007

Toyoda, K., Nakamura, Y., and Masuda, A. (1990). Rare earth elements of Pacific pelagic sediments. *Geochim. Cosmochim. Acta* 54, 1093–1103. doi: 10.1016/0016-7037(90)90441-M

Turekian, K. K. (1977). The fate of metals in the oceans. *Geochim. Cosmochim. Acta* 41, 1139–1144. doi: 10.1016/0016-7037(77)90109-0

Tzafriri-Milo, R., Benaltabet, T., Torfstein, A., and Shenkar, N. (2019). The potential use of invasive ascidians for biomonitoring heavy metal pollution. *Front. Mar. Sci.* 6:611. doi: 10.3389/fmars.2019.00611

Van der Oost, R., Beyer, J., and Vermeulen, N. P. E. (2003). Fish bioaccumulation and biomarkers in environmental risk assessment: a review. *Environ. Toxicol. Pharmacol.* 13, 57–149. doi: 10.1016/S1382-6689(02)00126-6

Van Geen, A., Adkins, J. F., Boyle, E. A., Nelson, C. H., and Palanques, A. (1997). A120 yr record of widespread contamination from mining of the Iberian pyrite belt. *Geology* 25, 291–294. doi: 10.1130/0091-76131997025<0291:AYROWC<2.3.CO;2

Wang, Z., Yin, L., Xiang, H., Qin, X., and Wang, S. (2019). Accumulation patterns and species-specific characteristics of yttrium and rare earth elements (YREEs) in biological matrices from Maluan Bay, China: implications for biomonitoring. *Environ. Res.* 179:108804. doi: 10.1016/j.envres.2019.108804

White, S. L., and Rainbow, P. S. (1982). Regulation and accumulation of copper, zinc and cadmium by the shrimp Palaemon elegans. *Mar. Ecol. Prog. Ser.* 8, 95–101. doi: 10.3354/meps008095

Wielgus, J., Chadwick-Furman, N. E., and Dubinsky, Z. (2004). Coral cover and partial mortality on anthropogenically impacted coral reefs at Eilat, northern Red Sea. *Mar. Pollut. Bull.* 48, 248–253. doi: 10.1016/j.marpolbul.2003.08.008

Xu, Y., Sun, Q., Yi, L., Yin, X., Wang, A., Li, Y., et al. (2014). The source of natural and anthropogenic heavy metals in the sediments of the Minjiang River Estuary (SE China): implications for historical pollution. *Sci. Total Environ.* 493, 729–736. doi: 10.1016/j.scitotenv.2014.06.046

Yap, C. K., Ismail, A., Tan, S. G., and Omar, H. (2003). Accumulation, depuration and distribution of cadmium and zinc in the green- lipped mussel *Perna viridis* (Linnaeus) under laboratory conditions. *Hydrobiologia* 498, 151–160.

Yin, Y., Huang, J., Paine, M. L., Reinhold, V. N., and Chasteen, N. D. (2005). Structural characterization of the major extrapallial fluid protein of the mollusc *Mytilus edulis*: implications for function. *Biochemistry* 44, 10720–10731. doi: 10.1021/bi0505565

Zega, G., Pennati, R., Candiani, S., Pestarino, M., and De Bernardi, F. (2009). Solitary ascidians embryos (*Chordata*, *Tunicata*) as model organisms for testing coastal pollutant toxicity. *Isj* 6, 29–34.

Zhou, Q., Zhang, J., Fu, J., Shi, J., and Jiang, G. (2008). Biomonitoring: an appealing tool for assessment of metal pollution in the aquatic ecosystem. *Anal. Chim. Acta* 606, 135–150. doi: 10.1016/j.aca.2007.11.018

Zuykov, M., Pelletier, E., and Harper, D. A. T. (2013). Bivalve mollusks in metal pollution studies: from bioaccumulation to biomonitoring. *Chemosphere* 93, 201–208. doi: 10.1016/j.chemosphere.2013.05.001

Conflict of Interest: The authors declare that the research was conducted in the absence of any commercial or financial relationships that could be construed as a potential conflict of interest.

frontiers in Marine Science

ORIGINAL RESEARCH
published: 05 July 2021
doi: 10.3389/fmars.2021.708716

16S and 18S rRNA Gene Metabarcoding Provide Congruent Information on the Responses of Sediment Communities to Eutrophication

Jesse P. Harrison[1,2], Panagiota-Myrsini Chronopoulou[1,3], Iines S. Salonen[1,4], Tom Jilbert[1,5] and Karoliina A. Koho[1]*

[1] Aquatic Biogeochemistry Research Unit, Ecosystems and Environment Research Programme, Faculty of Biological and Environmental Sciences, University of Helsinki, Helsinki, Finland, [2] CSC–IT Center for Science Ltd., Espoo, Finland, [3] Conidia Bioscience Ltd., Surrey, United Kingdom, [4] SUGAR, X-star, Japan Agency of Marine-Earth Science and Technology (JAMSTEC), Yokosuka, Japan, [5] Tvärminne Zoological Station, University of Helsinki, Hanko, Finland

OPEN ACCESS

Edited by:
Allyson O'Brien, The University of Melbourne, Australia

Reviewed by:
Terry Whitledge, University of Alaska Fairbanks, United States
Thadickal V. Joydas, King Fahd University of Petroleum and Minerals, Saudi Arabia

***Correspondence:**
Iines S. Salonen
iines.salonen@helsinki.fi

Specialty section:
This article was submitted to Marine Pollution, a section of the journal Frontiers in Marine Science

Received: *12 May 2021*
Accepted: *15 June 2021*
Published: *05 July 2021*

Citation:
Harrison JP, Chronopoulou P-M, Salonen IS, Jilbert T and Koho KA (2021) 16S and 18S rRNA Gene Metabarcoding Provide Congruent Information on the Responses of Sediment Communities to Eutrophication. Front. Mar. Sci. 8:708716. doi: 10.3389/fmars.2021.708716

Metabarcoding analyses of bacterial and eukaryotic communities have been proposed as efficient tools for environmental impact assessment. It has been unclear, however, to which extent these analyses can provide similar or differing information on the ecological status of the environment. Here, we used 16S and 18S rRNA gene metabarcoding to compare eutrophication-induced shifts in sediment bacterial and eukaryotic community structure in relation to a range of porewater, sediment and bottom-water geochemical variables, using data obtained from six stations near a former rainbow trout farm in the Archipelago Sea (Baltic Sea). Shifts in the structure of both community types were correlated with a shared set of variables, including porewater ammonium concentrations and the sediment depth-integrated oxygen consumption rate. Distance-based redundancy analyses showed that variables typically employed in impact assessments, such as bottom water nutrient concentrations, explained less of the variance in community structure than alternative variables (e.g., porewater NH_4^+ inventories and sediment depth-integrated O_2 consumption rates) selected due to their low collinearity (up to 40 vs. 58% of the variance explained, respectively). In monitoring surveys where analyses of both bacterial and eukaryotic communities may be impossible, either 16S or 18S rRNA gene metabarcoding can serve as reliable indicators of wider ecological impacts of eutrophication.

Keywords: aquaculture, bacteria, eDNA, eukaryotes, eutrophication, metabarcoding, sediment

INTRODUCTION

Assessing the ecological integrity of benthic habitats is crucial to marine ecosystem management (Fernandes et al., 2001), with seafloor monitoring efforts having traditionally relied on morphological inventories of macrofauna (≥0.5 mm size fraction) and associated indices (Lejzerowicz et al., 2015; Pawlowski et al., 2016). While producing such inventories requires considerable time, taxonomic expertise and finances, environmental DNA (eDNA) metabarcoding

has emerged as a high-throughput and low-cost option for characterizing the structure and composition of sediment communities (Pawlowski et al., 2018). Comparisons of morphology-based and metabarcoding approaches for the characterization of sediment macrobenthos have demonstrated that the latter can function as a promising complement to traditional surveying methods (Aylagas et al., 2014, 2016; Cordier et al., 2017; Lobo et al., 2017; Cahill et al., 2018; Stoeck et al., 2018; Clark et al., 2020; Frontalini et al., 2020). By relying on total DNA extraction from samples, eDNA metabarcoding also enables investigations of microbial and meiofaunal ($\leq$0.5 mm) communities that are extremely challenging to study by traditional means, providing a more comprehensive snapshot of ecosystem health than macrofaunal surveys alone (Chariton et al., 2015; Pawlowski et al., 2016; Stoeck et al., 2018; Frontalini et al., 2020).

Efforts to explore the use of metabarcoding in benthic ecosystem monitoring have involved analyses of both sediment eukaryotic (18S rRNA gene) and bacterial (16S rRNA gene) communities (reviewed in Pawlowski et al., 2018). In the context of aquaculture-induced organic enrichment, this work has focused on foraminifera (Pawlowski et al., 2014, 2016; He et al., 2019) and ciliates (Forster et al., 2018), as well as general analyses of eukaryotic (Chariton et al., 2015) and bacterial communities (Dowle et al., 2015; Fodelianakis et al., 2015; Stoeck et al., 2018; Verhoeven et al., 2018; Moncada et al., 2019). The use of metabarcoding as a monitoring tool has also been explored with reference to localized disturbances caused by dredging (Zhang et al., 2017) and off-shore drilling (Lanzén et al., 2016; Laroche et al., 2017; Frontalini et al., 2020). These studies have shown that bacterial and eukaryotic metabarcoding analyses can serve as sensitive methods to detect anthropogenic impacts on sediment habitats, including both short-term responses and long-term effects on community resilience and stability. A recent cross-laboratory comparison of eDNA metabarcoding results produced using a standardized protocol has also demonstrated a high degree of reproducibility between individual metabarcoding data sets, which is essential to the successful deployment of eDNA-based monitoring methods (Dully et al., 2021).

Despite the promising results reported in previous studies and the increasing affordability of large-scale sequencing surveys, neither 16S nor 18S rRNA gene metabarcoding have yet been adopted as a routine component of monitoring programs (but see Lefrançois et al., 2018). While using both techniques in tandem would provide particularly comprehensive data on the status of sediment communities, this is likely to be unfeasible due to monitoring programs being subject to strict time and financial limitations (Borja and Elliott, 2013; Borja et al., 2016). It also remains unclear to what extent these methods can offer similar or contrasting information on the status of seafloor habitats, particularly with reference to identifying physical and chemical variables that are likely to drive community shifts at multiple trophic levels. Although several studies have correlated water column and/or sediment geochemical variables with metabarcoding data (Pawlowski et al., 2014; Chariton et al., 2015; Dowle et al., 2015; Fodelianakis et al., 2015; Lanzén et al., 2016; Forster et al., 2018; He et al., 2019; Moncada et al., 2019), there is a lack of research on this topic involving cross-comparisons of prokaryotic and eukaryotic communities. In cases where both types of metabarcoding analyses have been employed, shifts in community structure have either not been correlated with geochemical data or only a limited set of measurements has been used (La Rosa et al., 2001; Zhang et al., 2017; Keeley et al., 2018; Stoeck et al., 2018). Addressing this absence of information, therefore, is essential to establishing a full understanding of how metabarcoding can be best employed as a tool for marine ecosystem monitoring.

Here we used a field transect approach to compare 16S and 18S rRNA gene metabarcoding as tools to obtain insights into the impacts of aquaculture-induced eutrophication on the structure and composition of sediment communities in the coastal Archipelago Sea (Baltic Sea, Finland). In addition, we determined whether shifts in the structure of these communities were correlated with a shared or divergent set of environmental variables, and whether variables routinely included in benthic monitoring programs could reliably predict community responses to eutrophication. The data show that eutrophication-associated shifts in bacterial and eukaryote community structure are to a large extent linked to a common set of variables, suggesting that community changes detected by 16S or 18S rRNA gene metabarcoding are likely to reflect wider ecological responses to increased organic loading. Our findings additionally demonstrate that the sensitivity of monitoring approaches could be improved through more carefully designed protocols for the collection of environmental metadata, especially with reference to understanding the impacts of eutrophication at multiple levels of biological organization.

MATERIALS AND METHODS

Study Location and Sampling Strategy

Six stations (S1–S6) were sampled in the vicinity of a former rainbow trout farm adjacent to Haverö Island, Archipelago Sea, Baltic Sea (**Figure 1** and **Supplementary Table 1**). The farm was operational between 1987 and 2008 (Jokinen et al., 2018), after which it has been intermittently used for storing live fish. Sites S1–S3 were situated within a basin where the farm was located, S4 on a sill, S5 on the seaward side of the sill and S6 was included as a reference site outside the direct influence of the farm (**Figure 1**). At each site, water column variables were measured with a conductivity-temperature-depth (CTD) profiler (SBE 19 SEACAT, Sea-Bird Electronics Inc., Washington, United States), and sediment cores were collected with a GEMAX twin corer (internal ∅ 9 cm) in September 2017. Separate cores were collected for geochemical analyses (of porewater and bulk sediment), and for microbiological analyses.

Porewater Sampling and Analysis

Porewater samples for geochemical analyses were taken immediately upon retrieval of sediment cores at 2-cm depth intervals from 0 to 20 cm depth, using Rhizon samplers (Rhizosphere Research Products, Wageningen, Netherlands) (Seeberg-Elverfeldt et al., 2005). Two cores were taken for Rhizon

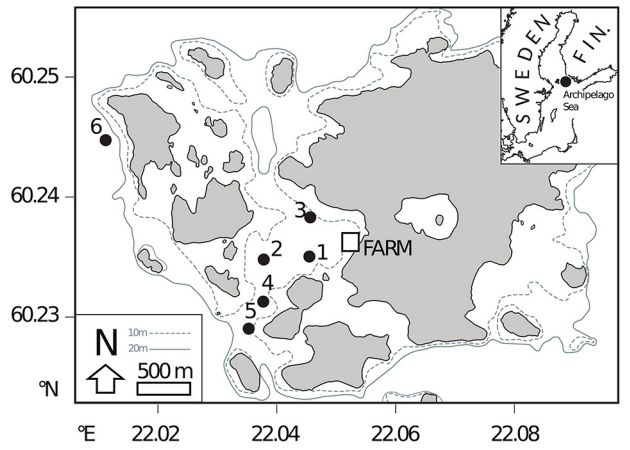

FIGURE 1 | Locations of field sites used for sediment sampling near a former rainbow trout farming site in the Archipelago Sea (Baltic Sea, Finland).

samples, one for nutrient analysis and the other for analysis of hydrogen sulfide (H_2S). From the first core, subsamples for analysis of dissolved nitrogen species were stored at –20°C, while subsamples for inductively coupled plasma mass spectrometry (ICP-MS) analysis of phosphorus were immediately acidified with 1M nitric acid (HNO_3) and stored at 4°C. Samples for H_2S (from the second column) were prepared as described in Jilbert et al. (2018) with pre-addition of 1 ml of 2 M zinc acetate to the sampling syringe. A third core was subsampled with mini-cores (internal ∅ 2.3 cm; n = 1 for site S1 and n = 3 for S2–S6) for determination of the porewater oxygen profile.

Porewater nitrate (NO_3^-), nitrite (NO_2^-), and ammonium (NH_4^+), concentrations were measured at Tvärminne Zoological Station, Hanko, Finland. NO_3^- and NO_2^- concentrations were measured using an autoanalyser equipped with a cadmium reduction column (Aquakem^{TM} 250, Thermo Fisher Scientific^{TM}, Waltham, MA, United States; detection limit of 0.2 μM), according to standard methods (Finnish Standards Association methods SFS 3030 and 3032). NH_4^+ concentrations were measured manually with a detection limit of 0.14 μM, according to methods described in Koistinen et al. (2018). Total porewater phosphorus (P) concentrations were determined at Geo Lab, Utrecht University, the Netherlands, using a Thermo Scientific^{TM} Element 2^{TM} ICP-MS (P determined as ^{31}P). Replicate analyses with reference to in-house standards indicated that the relative error for analyses of porewater nutrient concentrations was <5% in all cases.

Porewater H_2S concentrations were determined by spectrophotometry as described in Jilbert et al. (2018). An acidic solution of ferric chloride ($FeCl_3$) and *N*,*N*-dimethyl-*p*-phenylenediamine was added directly to sample vials. The zinc sulfide (ZnS) precipitate formed during sampling complexes S as methylene blue, allowing spectrophotometric analysis at 670 nm (Cline, 1969; Reese et al., 2011). H_2S concentrations were calibrated against a series of standard solutions of sodium sulfide ($Na_2S{\cdot}3H_2O$), whose S concentrations were determined by iodometric titration.

Inventories of porewater NH_4^+, dissolved P and H_2S were calculated for the uppermost 20 cm of the sediment column, including bottom water concentrations. Depth-integrated concentrations are likely to provide more detailed information on biogeochemical processes taking place in the sediment than spot measurements of bottom water or surface sediment concentrations. The concentrations (μmol cm^{-2}) are expressed as depth-integrated values (Inv_x):

$$\mathrm{Inv}_x = \Phi \int_{-1}^{20} \mathrm{Conc}(x) d_x,$$

Where Φ is the sediment porosity and Conc. (x) is the porewater concentration of NH_4^+, P, or H_2S at each sediment depth interval or in bottom water (represented by a value of –1 in the above equation). The equation is modified from Canfield (1989).

Porewater oxygen profiles were measured with an oxygen microsensor (OX-100; Unisense A/S, Aarhus, Denmark). The microsensor was two-point calibrated in 100% air-saturated filtered seawater, collected from the study site, and in anoxic solution containing sodium ascorbate and NaOH (both at 0.1M). Measurements were carried out at depth intervals of 100 μm. Depth-integrated sediment pore water oxygen consumption rates were calculated from oxygen microprofile data using a least squares fitting routine in the PROFILE software package[1] (Berg et al., 1998).

DNA Isolation, PCR and Sequencing of 16S and 18S rRNA Genes

DNA was isolated from 0.25 g of surface sediment (top 1 cm; five biological replicates for each sampling site, each from a separate core) using a Powersoil® DNA isolation kit (MO BIO, Carlsbad, CA, United States) according to the manufacturer's instructions. A kit control (n = 1) with no added sediment was prepared. PCR was used to amplify 16S rRNA gene (V1–V3 regions) and 18S rRNA (V4 region) gene sequences (**Table 1**). Each PCR contained 0.5 μl of template DNA, 1× Phusion^{TM} Flash High-Fidelity PCR Master Mix (Thermo Fisher Scientific, Waltham, MA, United States), and 0.5 μM of forward and reverse primer mixes, made up to a total volume of 25 μl with sterile ultrapure water. Technical duplicates and no-template controls were included in each PCR run. Cycling conditions were 98°C for 10 s, followed by 20–22 or 28–32 cycles (16S and 18S rRNA gene, respectively) of 98°C for 10 s and 72°C for 15 s, and a final extension step at 72°C for 1 min. PCR products were visualized following electrophoresis on 1% (w/v) agarose gels, after which the duplicates were pooled. Further sample processing was carried out by the DNA Sequencing and Genomics Laboratory, Institute of Biotechnology, University of Helsinki[2]. Custom barcodes for sample demultiplexing (Somervuo et al., 2018) were attached in a second PCR step and the obtained PCR products were purified using Agencourt® AMPure® XP magnetic beads (Beckman Coulter, CA, United States), quantified and pooled in iso-molecular quantities (Salava et al., 2017), followed by sequencing on the Illumina MiSeq platform.

[1]https://berg.evsc.virginia.edu/modeling-and-profile/

[2]http://www.biocenter.helsinki.fi/bi/dnagen/

TABLE 1 | Primers and primer mixes used for the PCR amplification of 16S rRNA and 18S rRNA genes from DNA extracted from sediments collected from the Archipelago Sea (Baltic Sea).

Primer	Nucleotide sequence including overhang (5′–3′)*	Primer mix	References
27F1	*ATCTACACTCTTTCCCTACACGACGCTCTTCCGATCT* **AGAGTTTGATCMTGGCTCAG**	PCR targeting 16S rRNA gene V1–V3 regions: 27F1–3 and 518R1–3 mixed in 1:1:1 ratio	Lane (1991); Muyzer et al. (1993) and Salava et al. (2017)
27F2	*ATCTACACTCTTTCCCTACACGACGCTCTTCCGATCT* **TAGAGAGTTTGATCMTGGCTCAG**		
27F3	*ATCTACACTCTTTCCCTACACGACGCTCTTCCGATCT* **CTCTAGAGTTTGATCMTGGCTCAG**		
518R1	*GTGACTGGAGTTCAGACGTGTGCTCTTCCGATCT* **GTATTACCGCGGCTGCTG**		
518R2	*GTGACTGGAGTTCAGACGTGTGCTCTTCCGATCT* **CGTATTACCGCGGCTGCTG**		
518R3	*GTGACTGGAGTTCAGACGTGTGCTCTTCCGATCT* **TAGTATTACCGCGGCTGCTG**		
E572F1	*ACACTCTTTCCCTACACGACGCTCTTCCGATCT* **CYGCGGTAATTCCAGCTC**	PCR targeting 18S rRNA gene V4 region: E572F1–4 and 897R1–4 mixed in 1:1:1:1 ratio	Comeau et al. (2011) and Hugerth et al. (2014)
E572F2	*ACACTCTTTCCCTACACGACGCTCTTCCGATCT* **GCYGCGGTAATTCCAGCTC**		
E572F3	*ACACTCTTTCCCTACACGACGCTCTTCCGATCT* **TGMCYGCGGTAATTCCAGCTC**		
E572F4	*ACACTCTTTCCCTACACGACGCTCTTCCGATCT* **ARTTACYGCGGTAATTCCAGCTC**		
897R1	*GTGACTGGAGTTCAGACGTGTGCTCTTCCGATCT* **TCYDAGAATTYCACCTCT**		
897R2	*GTGACTGGAGTTCAGACGTGTGCTCTTCCGATCT* **AGTCYDAGAATTYCACCTCT**		
897R3	*GTGACTGGAGTTCAGACGTGTGCTCTTCCGATCT* **CAATTCYDAGAATTYCACCTCT**		
897R4	*GTGACTGGAGTTCAGACGTGTGCTCTTCCGATCT* **GTRAGTTTCYDAGAATTYCACCTCT**		

**Overhang indicated with italics and primer sequence indicated in bold.*

Sequence Processing and Bioinformatics

Following the removal of MiSeq adapter and barcode sequences, further sequence processing was carried out using micca v. 1.6.2[3] (Albanese et al., 2015). Paired-end reads were merged using "micca mergepairs" (**Table 2**; Rognes et al., 2016) and primer sequences were trimmed using "micca trim" (Martin, 2011). Quality filtering was performed using "micca filter" (filtering parameters in **Table 2**; Rognes et al., 2016). The command "micca otu" was used for chimera filtering and OTU clustering, with the clustering step employing a *de novo* greedy clustering algorithm with a 97% similarity threshold (parameters -d 0.97 -c) (Westcott and Schloss, 2015; Rognes et al., 2016). Taxonomic assignments were carried out using "micca classify" and RDP Classifier v. 2.11 (16S rRNA gene sequences; Wang et al., 2007) or the SILVA 132 database (18S rRNA gene sequences, majority taxonomy mapping file with seven taxonomic levels; Quast et al., 2013).

Additional data processing was carried out using R v. 4.0.2 (R Core Team, 2020). To improve between-sample comparability, two replicates that markedly deviated from other replicates in terms of sequencing depth or observed OTU counts were omitted from the 18S rRNA gene sequence data set. Further replicates were randomly discarded to obtain a balanced design for statistical analysis, with the final 18S rRNA gene sequence data set retaining four replicates for each site. For the 16S rRNA gene sequence data set, five replicates were retained for each site. Rarefaction curves for the resulting data sets are provided in **Supplementary Figure 1**. Unclassified phyla and 16S rRNA gene sequences annotated as Chloroplast (class level) or Mitochondria (family level) were removed. Within-station relative abundances of sequences unclassified at the domain level were <0.001% for the 16S rRNA gene sequence data set and <0.01% for the 18S rRNA gene sequence data set, respectively, with similar values observed for each sampling station. Removing unclassified, chloroplast and/or mitochondrial sequences had no major influence on sample clustering, as indicated by comparisons of non-metric multidimensional scaling (nMDS) ordinations

TABLE 2 | Data processing parameters for 16S rRNA and 18S rRNA gene sequences (implemented in micca v. 1.6.2; https://compmetagen.github.io/micca/).

Command	16S rRNA gene sequences	18S rRNA gene sequences
micca mergepairs	-l 50 -d 15	-l 250 -d 85
micca filter	-e 0.25 -m 465 (71.3% of reads retained)	-e 0.25 -m 315 (92% of reads retained)

[3]https://compmetagen.github.io/micca/

(**Supplementary Figure 2**). Prior to statistical analysis, both data sets were subjected to a denoising step using a 5% prevalence threshold (Callahan et al., 2016; **Supplementary Figure 3**). Prevalence is defined as the number of samples in which a taxon appears at least once (Callahan et al., 2016).

Statistical Analysis

Statistical analyses were performed using R v. 4.0.2 (R Core Team, 2020). Diversity values (observed OTU frequencies, Chao1 indices and Shannon's diversity) (Shannon, 1948; Chao, 1984) were calculated for untrimmed sequence data using phyloseq v. 1.34.0 (McMurdie and Holmes, 2013). Shannon's diversity values for Metazoa were compared between sites S1–S3 vs. S4–S6 using a two-sample Wilcoxon rank sum test. Bacterial and eukaryotic OTU counts were subjected to a centered log-ratio (CLR) transformation with a pseudocount of 1 using microbiome v. 1.12.0[4], with nMDS ordinations derived using Aitchison distance matrices (Gloor et al., 2017) calculated using phyloseq (McMurdie and Holmes, 2013). Aitchison distances were used to account for the compositional nature of sequencing data (Gloor et al., 2017). As a complementary approach, OTU counts were converted to relative abundances (%) for qualitative comparisons of inter-site taxon composition.

The Aitchison distance matrices were used to conduct one-way permutational analyses of variance (PERMANOVA) with "sampling site" as the factor, using vegan v. 2.5-7 (999 permutations; Oksanen et al., 2020). *Post hoc* pairwise comparisons (999 permutations) including a Benjamini-Hochberg correction (Benjamini and Hochberg, 1995) were performed using RVAideMemoire v. 0.9–78 (Hervé, 2020). Tests for the homogeneity of multivariate dispersions (PERMDISP; Anderson, 2006) were performed with vegan (999 permutations; Oksanen et al., 2020).

To explore correlations between community structure and sediment, sediment porewater and water column geochemical variables (**Table 3**), linear dependencies between variables were first identified by a principal component analysis (PCA) using centered and scaled data (**Figure 2**), and by inspecting variance inflation factors (VIFs). Two sets of up to five explanatory variables (**Table 4**) were then selected for distance-based redundancy analyses (db-RDA; Legendre and Anderson, 1999; Ramette, 2007) performed with vegan (Oksanen et al., 2020). Distance-based redundancy analyses were selected as the ordination method based on the inspection of primary axis lengths using detrended correspondence analyses (Lepš and Šmilauer, 2003). Variables in the first model (Model 1) were selected due to their minimal multicollinearity (VIFs of $\leq$6), while the second model (Model 2) was limited to variables similar to those often measured during environmental monitoring surveys (see e.g., the HELCOM Monitoring Manual[5]) and had VIFs of $\leq$13.7 (**Table 4**). Both models were run using CLR-transformed 16S or 18S rRNA gene sequence data, resulting in a total of four model runs. Environmental variables were projected onto the ordination space using the envfit() function in vegan (Oksanen et al., 2020), with fitting performed on linear scores of the ordination axes. Following global significance tests for the ordinations, the variance explained by each variable was compared using permutation tests with the remaining variables included as covariates, using the anova() function in vegan (999 permutations; Oksanen et al., 2020).

TABLE 3 | Environmental properties corresponding to six sampling stations in Haverö, Archipelago Sea (Baltic Sea, Finland).

	Sampling station					
Variable	**S1**	**S2**	**S3**	**S4**	**S5**	**S6**
Distance to farm (km)	0.38	0.79	0.47	0.94	1.2	2.48
Water column temperature (°C)	10.1	14.4	14.4	15.2	14.7	13
Water column depth (m)	23	16.2	17.5	12.1	18.9	24.2
Water column salinity (no unit)	5.87	6.07	6.05	6.03	6.09	6.18
Bottom water O_2 concentration (μmol L^{-1})	80.1	163.3	133.2	173.1	184.2	151.9
Bottom water NO_x* concentration (μmol L^{-1})	14.3	6.4	6.8	10.1	3.4	6.2
Bottom water P concentration (μmol L^{-1})	42.3	6.3	4.1	3.2	2.3	3.7
Sediment O_2 penetration depth (mm)	1.5	2.1	1.4	3.9	3.5	4
Sediment depth-integrated O_2 consumption rate (μmol^{-1} cm^{-2} s^{-1})	0.0119	0.0119	0.0156	0.003	0.006	0.005
Sediment median grain size (μm)	3.1	3.4	3.1	93.6	13.1	3.6
Sediment C_{org} content, top 1 cm (% dry mass)	4.9	4.1	4.1	1.2	2.9	3.2
Sediment $\delta^{13}C_{org}$, top 1 cm (Δ PDB)	–24	–22.8	–23.6	–24.6	–23.7	–23.8
Sediment C_{org}:N_{tot} ratio, top 1 cm (mol:mol)	8.36	8.65	8.37	8.14	8.34	8.33
Porewater H_2S inventory (μmol cm^{-2})	6.7	0.5	0.8	0	0.5	0.7
Porewater P inventory (μmol cm^{-2})	4.45	2.47	1.59	0.76	0.73	0.98
Porewater NH_4^+ inventory (μmol cm^{-2})	18.65	5.33	4.48	1.3	1.86	1.79
Porewater NO_x inventory (μmol cm^{-2})	0.2	0.34	0.16	0.07	0.03	0.03
Porewater NO_2^- inventory (μmol cm^{-2})	0.001	0.002	0.001	0.003	0.003	0.003

NO_2^- and NO_3^-.
Inventory calculations were performed for the top 20 cm of sediment cores ("Materials and Methods" section).

RESULTS

Bacterial Community Structure and Composition

Good's coverage estimates of 96.13–98.70% were obtained for the raw 16S rRNA gene sequence data set (see **Supplementary Figure 1A** for rarefaction curves). Following quality filtering and denoising, a total of 1,089,217 reads (clustered into 4,499 OTUs) were retained in the data set. Sediment bacterial community structure differed between sampling stations, as demonstrated by

[4]http://microbiome.github.io/

[5]http://www.helcom.fi/action-areas/monitoring-and-assessment/monitoring-manual/

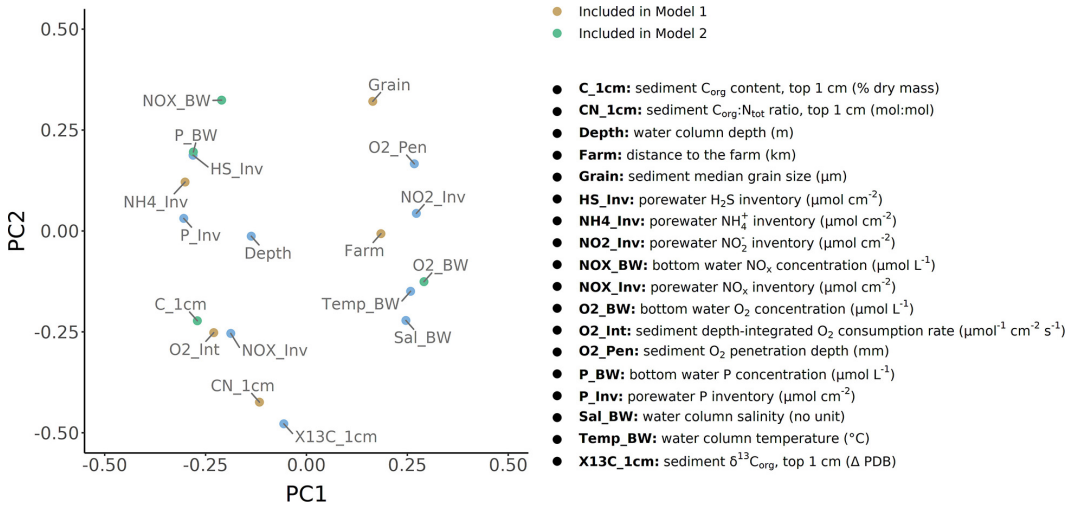

FIGURE 2 | Principal component analysis showing linear dependencies between a total of 18 sediment, sediment porewater, and water column variables (centered and scaled data). The data correspond to measurements determined for a total of six field sampling sites in the Archipelago Sea (Baltic Sea, Finland).

metabarcoding analysis of a total of 30 microbial communities (1-way global PERMANOVA using Aitchison distances: pseudo-$F_{5,24}$ = 6.559, p < 0.001) (**Figure 3A**). *Post hoc* pairwise comparisons showed that all six stations were distinct in terms of bacterial community structure (PERMANOVA with Benjamini-Hochberg correction: p = 0.014 for all tests). A comparison of inter-site variation in multivariate dispersions showed these differences to be due to a location effect rather than a dispersion effect (PERMDISP: pseudo-$F_{5,24}$ = 1.628, p = 0.203).

Comparing OTU relative abundances showed sediments from all sites to be dominated by 16S rRNA gene sequences from the phylum *Proteobacteria,* followed by *Bacteroidetes* (**Figure 4A**; for class-level relative abundances, see **Supplementary Figure 4**). The relative abundances of *Proteobacteria* were comparatively stable along the transect (S1–S5; values of 34–47%), with slightly lower values (30–32%) within the reference site (S6) (**Figure 4A**). However, there were up to three-fold differences in the relative abundances of the four next most dominant phyla, including members of the *Bacteroidetes*, *Acidobacteria*, *Chloroflexi*, and *Ignavibacteriae* (**Figure 5A**). For example, sediments within the site nearest to the fish farm (S1) showed a high relative abundance (>25%) of sequences from the phylum *Bacteroidetes* (classes *Flavobacteriia* and *Bacteroidia*; **Supplementary Figure 4**) with low relative abundances of *Acidobacteria* and *Chloroflexi* in comparison with sites farther from the farm (S4–S6) (**Figure 5A**). The relative abundances of *Ignavibacteriae* were lower in S1 in comparison with other sites while in stations within the basin in the vicinity of the fish farm (i.e., S2 and S3), relative abundances of *Acidobacteria* were also lower than in S4–S6 (**Figure 5A**). In contrast with this variation in relative abundances, no clear inter-site variation in bacterial diversity was observed along the study transect (S1–S5) or when comparing sites to reference station S6, with mean Shannon's diversity ranging from 6.25 (S6) to 7.13 (S4) (**Table 5**).

TABLE 4 | Physical and chemical variables used for db-RDA model construction.

Model	Variable	Variance inflation factor
Model 1	Porewater NH_4^+ inventory (µmol cm^{-2})	2.08
	Distance to farm (km)	5.35
	Sediment depth-integrated O_2 consumption rate (µmol^{-1} cm^{-2} s^{-1})	6.04
	Sediment median grain size (µm)	5.48
	Sediment C_{org}:N_{tot} ratio, top 1 cm (mol:mol)	2.31
Model 2	Sediment C_{org} content, top 1 cm (% dry mass)	7.33
	Bottom water NO_x* concentration (µmol L^{-1})	11.54
	Bottom water P concentration (µmol L^{-1})	8.49
	Bottom water O_2 concentration (mg L^{-1})	13.71

*NO_2^- and NO_3^-.

Eukaryotic Community Structure and Composition

Good's coverage estimates of 99.98–100% were obtained for the raw 18S rRNA gene sequence data set (see **Supplementary Figure 1B** for rarefaction curves). A total of 6,902,650 reads (clustered into 548 OTUs) were retained in the data set following quality filtering. Similar to the bacterial data, metabarcoding analysis of 24 sediment eukaryote communities demonstrated significant differences between stations (1-way global PERMANOVA: pseudo-$F_{5,18}$ = 2.415, p < 0.001; **Figure 3B**). Each station had a distinct eukaryote community structure (*post hoc* pairwise PERMANOVA with Benjamini-Hochberg correction: p = 0.036 for all tests). In contrast with the bacterial data, significant inter-site variation in multivariate dispersion was observed (PERMDISP: pseudo-$F_{5,18}$ = 9.260, p < 0.001). Sediment eukaryote communities at site S4 exhibited a higher degree of multivariate dispersion than communities at S1, S3, and S5, as shown by a *post hoc* Tukey's HSD test (**Figure 6**). However, no significant differences in multivariate dispersion

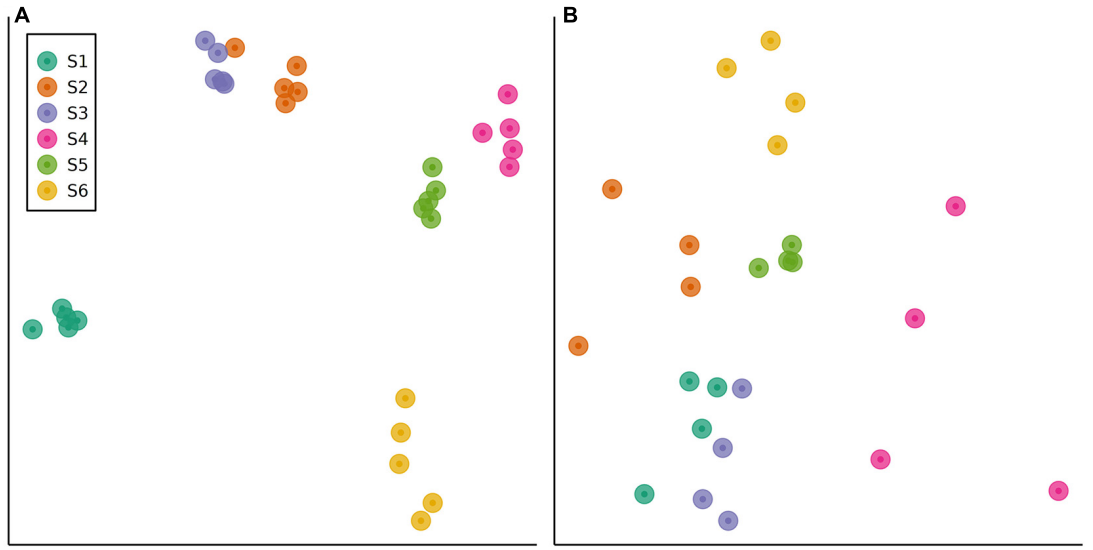

FIGURE 3 | Non-metric multidimensional scaling (nMDS) ordinations of sediment communities in field sites sampled along a eutrophication gradient in the Archipelago Sea (Baltic Sea, Finland). The ordinations were derived from Aitchison resemblance matrices calculated from Illumina MiSeq OTU abundance data. Data are shown for **(A)** bacterial communities (stress = 0.04) and **(B)** eukaryotic communities (stress = 0.16).

($p > 0.05$) were detected between site S6 and sites along the study transect (S1–S5; see **Figure 6**).

Comparing OTU relative abundances showed sediments from all sampling stations to be dominated by unicellular eukaryotic taxa (*Dinoflagellata* followed by *Protalveolata* and *Ochrophyta*) (**Figure 4B**). While the relative abundances of *Dinoflagellata* appeared comparable between stations, nearly two-fold differences in overall eukaryotic diversity (Shannon's diversity) were observed between sites (site-specific means of 1.00–1.88; **Table 5**). For example, Metazoa (**Figure 5B**) exhibited a significant decline in Shannon's diversity in sites near the fish farm (S1–S3; $\bar{x} = 1.17 \pm 0.08$) compared to sites farther from the farm (S4–S6; $\bar{x} = 1.89 \pm 0.11$) (two-sample Wilcoxon rank sum test, $W = 11$, $p < 0.001$). Metazoa detected in sediments from site S1 included copepods (*Calanoida*) and nematodes (*Monhysterida*), with these taxa also detected in other sites (**Figure 5B**). Examples of taxa encountered in sites S4–S6 but either absent or present at low relative abundances (<0.2%) from S1–S3 included *Enoplida* (nematodes), *Haplotaxida* (annelids), *Homalorhagida* (kinorhynchs), and *Macrostomida* (flatworms) (**Figure 5B**).

Correlations Between Community Structure and Environmental Variables

Sediment depth-integrated O_2 consumption rates were two orders of magnitude higher in the basin (sites S1–S3; rates up to 0.016 $\mu mol^{-1}\ cm^{-2}\ s^{-1}$) than within other sites (rates up to 0.006 $\mu mol^{-1}\ cm^{-2}\ s^{-1}$) (**Table 3**). Oxygen concentrations in the bottom water were also up to two times lower in sites near the farm than in other sites (minimum of 80.1 $\mu mol\ L^{-1}$ in S1). Concentrations of porewater nutrients (NH_4^+, NO_x, and P) and sediment organic carbon (C_{org}) were high in S1–S3, with the NH_4^+ inventory in S1 (18.7 $\mu mol\ cm^{-2}$) being approximately an order of magnitude higher than those in S4–S6. Differences in bottom water nutrient concentrations were also observed. Bottom water P concentrations were relatively low in sites S2–S6 (2.3–6.3 $\mu mol\ L^{-1}$), with a high concentration detected at S1 (42.3 $\mu mol\ L^{-1}$). Variation in bottom water NO_x concentrations was less pronounced, with the highest concentration (14.3 $\mu mol\ L^{-1}$) observed at S1. While the sediment within site S4 consisted of fine sand (median grain size of 93.6 μm), all other sites were muddy (median grain sizes of 3.1–13.1 μm). Further information on the environmental conditions within each sampling station is given in **Table 3**.

Correlations between site-specific environmental conditions and sediment bacterial or eukaryotic community structure were explored using distance-based redundancy analyses (db-RDA; see **Table 6**) performed using two separate sets of up to five environmental variables (Models 1 and 2; details on model construction in *Statistical Analysis* and **Table 4**). The first db-RDA model (Model 1) explained 58% (global permutation test: pseudo-$F_{5,24} = 6.559$, $p < 0.001$) and 40% (global permutation test: pseudo-$F_{5,18} = 2.415$, $p < 0.001$) of the variance in sediment bacterial and eukaryotic community structure, respectively (**Figures 7A,B**). As shown by permutation tests for individual db-RDA explanatory variables (with the remaining variables used as covariates), in Model 1 the observed variation in bacterial community structure was strongly correlated with porewater NH_4^+ concentrations (pseudo-$F = 7.230$, $p_{B-H} = 0.005$), followed by sediment depth-integrated O_2 consumption rates and distance to the farm (**Table 6**). A near-significant correlation between bacterial community structure and the sediment C_{org}:N_{tot} ratio was observed (pseudo-$F = 1.924$, $p_{B-H} = 0.065$), while the weakest correlation (pseudo-$F = 1.685$, $p_{B-H} = 0.09$) corresponded to sediment grain size (**Table 6**). In contrast with bacterial communities, all variables included in Model 1 were significantly correlated with variation in eukaryotic community

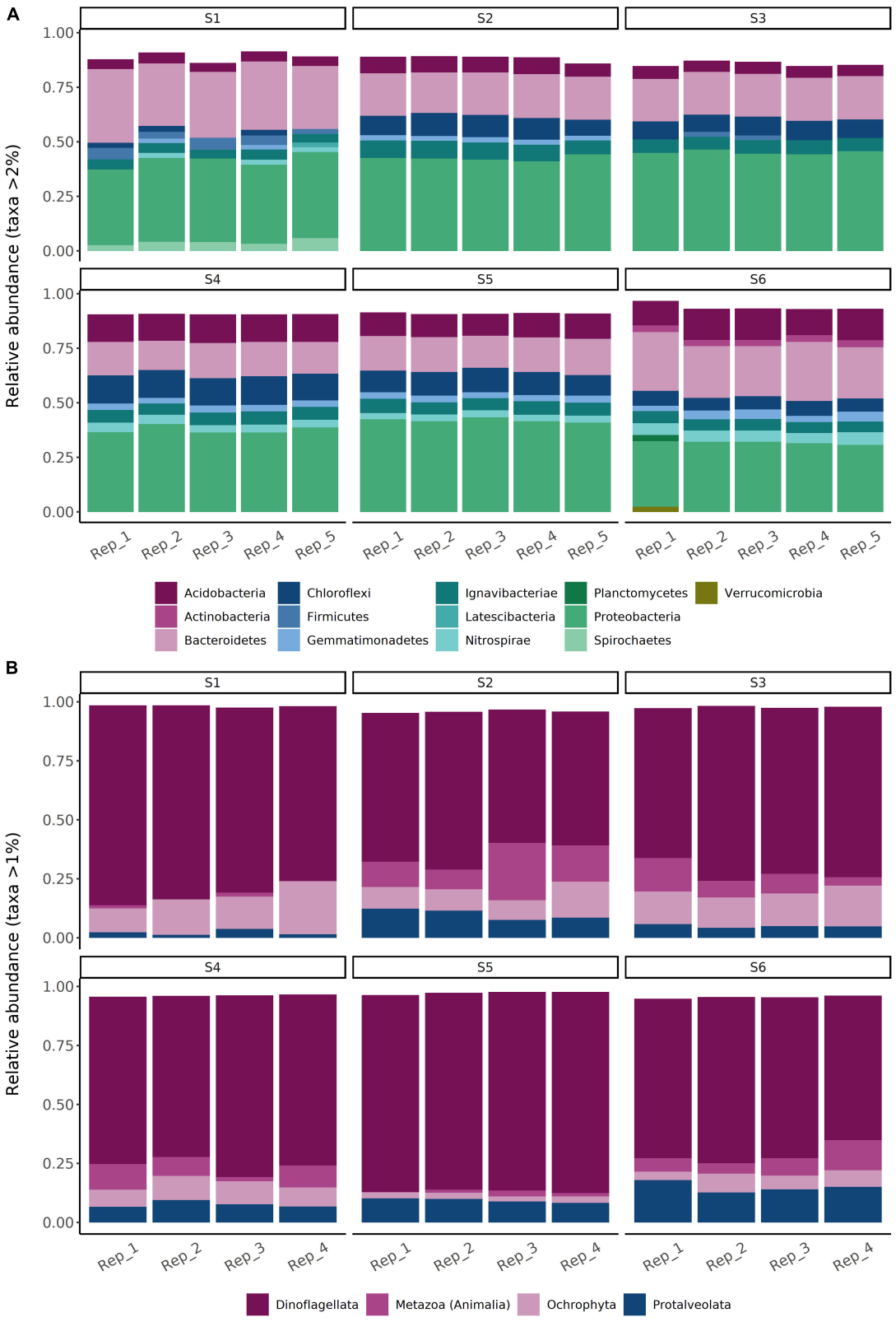

FIGURE 4 | Overall relative abundances (%) of **(A)** bacterial and **(B)** eukaryotic operational taxonomic units (OTUs) within sediment samples collected from a total of six sampling sites in the Archipelago Sea (Baltic Sea). Bacterial data are shown at the phylum level. Eukaryotic data are shown at the Rank 4 level of the SILVA 132 majority taxonomy mapping file with seven taxonomic levels (comprising multiple levels of taxonomic classification).

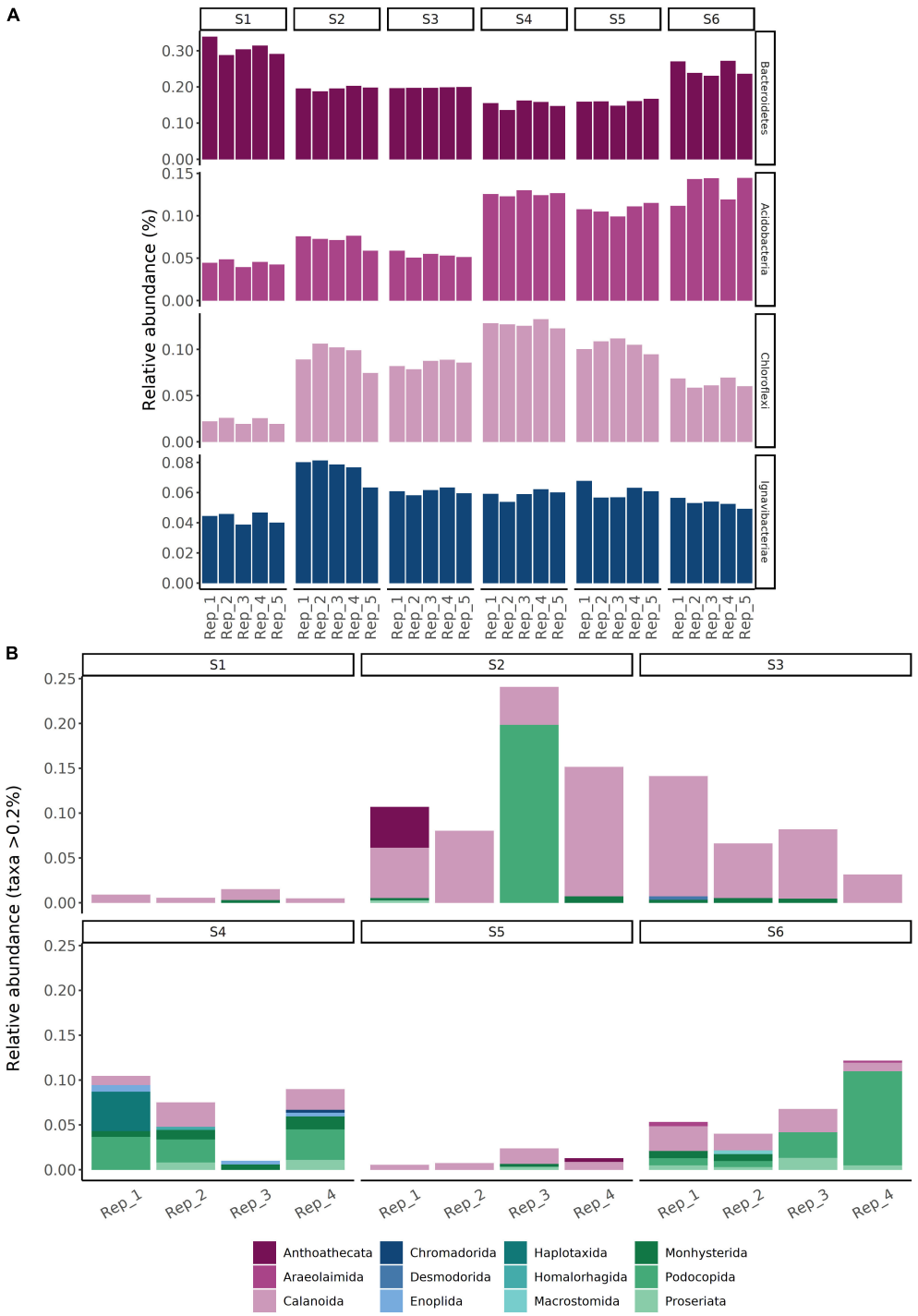

FIGURE 5 | Operational taxonomic unit relative abundances (%) corresponding to subsets of **(A)** bacterial and **(B)** eukaryotic communities within sediments collected from a total of six sampling sites in the Archipelago Sea (Baltic Sea, Finland). The bacterial community subset corresponds to the top four most abundant phyla, aside from members of the *Proteobacteria*. The eukaryotic community subset corresponds to metazoa.

structure (**Table 6**). The environmental variables most strongly correlated with variation in eukaryotic community structure corresponded to the sediment C_{org}:N_{tot} ratio, porewater NH_4^+ concentrations and sediment depth-integrated O_2 consumption rates, followed by distance to the farm (**Table 6**).

The second db-RDA (Model 2) had less explanatory power compared with Model 1, explaining 48% (global permutation test: pseudo-$F_{4,25}$ = 5.679, $p < 0.001$) and 32% (global permutation test: pseudo-$F_{4,19}$ = 2.276, $p < 0.001$) of the variance in sediment bacterial and eukaryotic community structure, respectively

TABLE 5 | Observed bacterial and eukaryotic OTU frequencies and diversity indices (Chao1 and Shannon's diversity) for sediment samples collected from six sampling stations in Haverö, Archipelago Sea (Baltic Sea, Finland).

	Bacterial OTUs			Eukaryotic OTUs		
Site	**Observed**	**Chao1**	**Shannon's diversity**	**Observed**	**Chao1**	**Shannon's diversity**
S1	5,310 ± 162	7,341 ± 176	6.60 ± 0.14	232 ± 13	260 ± 15	1.00 ± 0.09
S2	6,634 ± 239	9,113 ± 221	7.03 ± 0.05	241 ± 14	267 ± 13	1.88 ± 0.07
S3	6,919 ± 114	9,465 ± 94	7.08 ± 0.03	257 ± 7	286 ± 8	1.49 ± 0.08
S4	6,528 ± 167	8,440 ± 146	7.13 ± 0.02	217 ± 7	238 ± 7	1.69 ± 0.09
S5	6,030 ± 138	8,493 ± 112	6.87 ± 0.02	269 ± 5	296 ± 11	1.05 ± 0.01
S6	4,071 ± 290	5,538 ± 487	6.25 ± 0.04	252 ± 4	296 ± 12	1.74 ± 0.03

The values are given as means ± standard error (n = 5 for bacteria, n = 4 for eukaryotes).

(**Figures 7C,D**). Significance values of all tested variables for both models and effect sizes (pseudo-*F* values) are shown in **Table 6**. In contrast to C_{org}:N_{tot} (in Model 1), significant correlations ($p_{B-H} < 0.05$) were observed between the sediment C_{org} content and both bacterial and eukaryotic community structure. Shifts in the structure of both community types were also correlated with bottom water NO_x, P, and O_2 concentrations. Effect sizes within the bacterial data set often exceeded those in the eukaryotic data set. For example, an over fourfold difference in effect sizes was observed in relation to sediment porewater NH_4^+ inventories (see **Table 6**).

DISCUSSION

16S and 18S rRNA gene metabarcoding have been proposed as alternatives to morphology-based macrofaunal inventories that have been traditionally used in benthic monitoring surveys (reviewed by Pawlowski et al., 2018). To date, little information has been available concerning the ability of these methods to provide similar versus contrasting information on ecosystem health. Here, we employed a field transect study to compare shifts in bacterial and eukaryotic community structure in relation to 18 sediment and water column variables along an aquaculture-induced eutrophication gradient near a former rainbow trout farm (active during 1987–2008; Jokinen et al., 2018) in the Archipelago Sea (Baltic Sea, Finland). Correlations between community structure and environmental variables were explored using two separate models including environmental variables selected either on account of their low multicollinearity or because they are often measured during monitoring surveys.

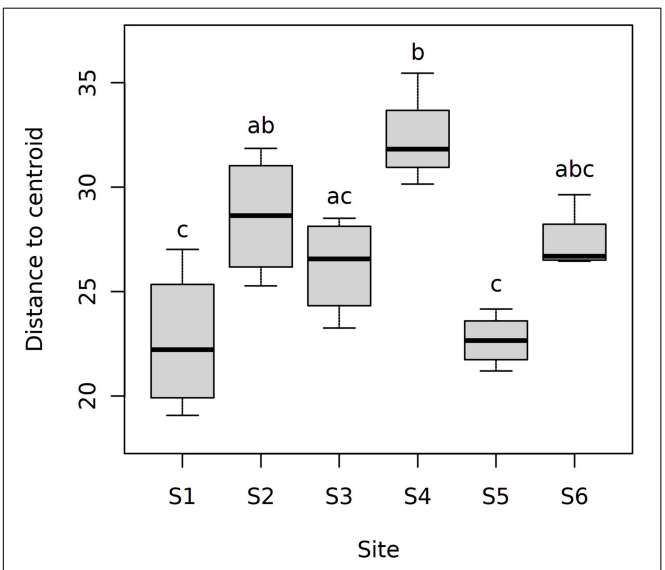

FIGURE 6 | Distances to the group centroid for CLR-transformed eukaryotic OTU abundance data. Data are shown for a total of six sampling sites in the Archipelago Sea (Baltic Sea, Finland). Different letters above the boxes indicate significant differences between sampling sites (Tukey's HSD test, $p < 0.05$).

A key feature of the data was that the site nearest to the farm (S1) showed high relative abundances of taxa belonging to the phylum *Bacteroidetes* in parallel with a reduction in the abundance of other bacterial taxa (members of the phyla *Acidobacteria* and *Chloroflexi*), compared with other stations. Relative abundances of *Ignavibacteriae* were also low in site S1 compared to other sites. Moreover, *Acidobacteria* in sediments from sites S2 and S3 exhibited low abundances in comparison with sites farther from the farm (S4–S6). These shifts in bacterial community structure are in agreement with findings reported by Quero et al. (2020), who conducted a 10-months study into the effects of on-going sea bass and sea bream farming on the structure of sediment bacterial communities in Southern Sicily. Similar to our study, the authors reported increased relative abundances of *Bacteroidetes* in fish farming-impacted sediments, while the relative abundances of *Acidobacteria* and *Chloroflexi* were higher in non-impacted sediment. High relative abundances of *Bacteroidetes* (class *Bacteroidia*) have been found to occur in flocculent matter and microbial mat samples within a hard-bottom salmonid farm in the Hermitage Bay area (Newfoundland, Canada), which at the time of sampling had been inactive for 3 months (Verhoeven et al., 2016). Flocculates sampled near salmonid farming cages exhibited higher abundances of *Bacteroidetes* than samples collected from less disturbed sites (Verhoeven et al., 2018). Since our community analyses focused on the surficial centimeter of the sediment and the samples typically consisted of fine mud, they likely included materials that had originally remained suspended in

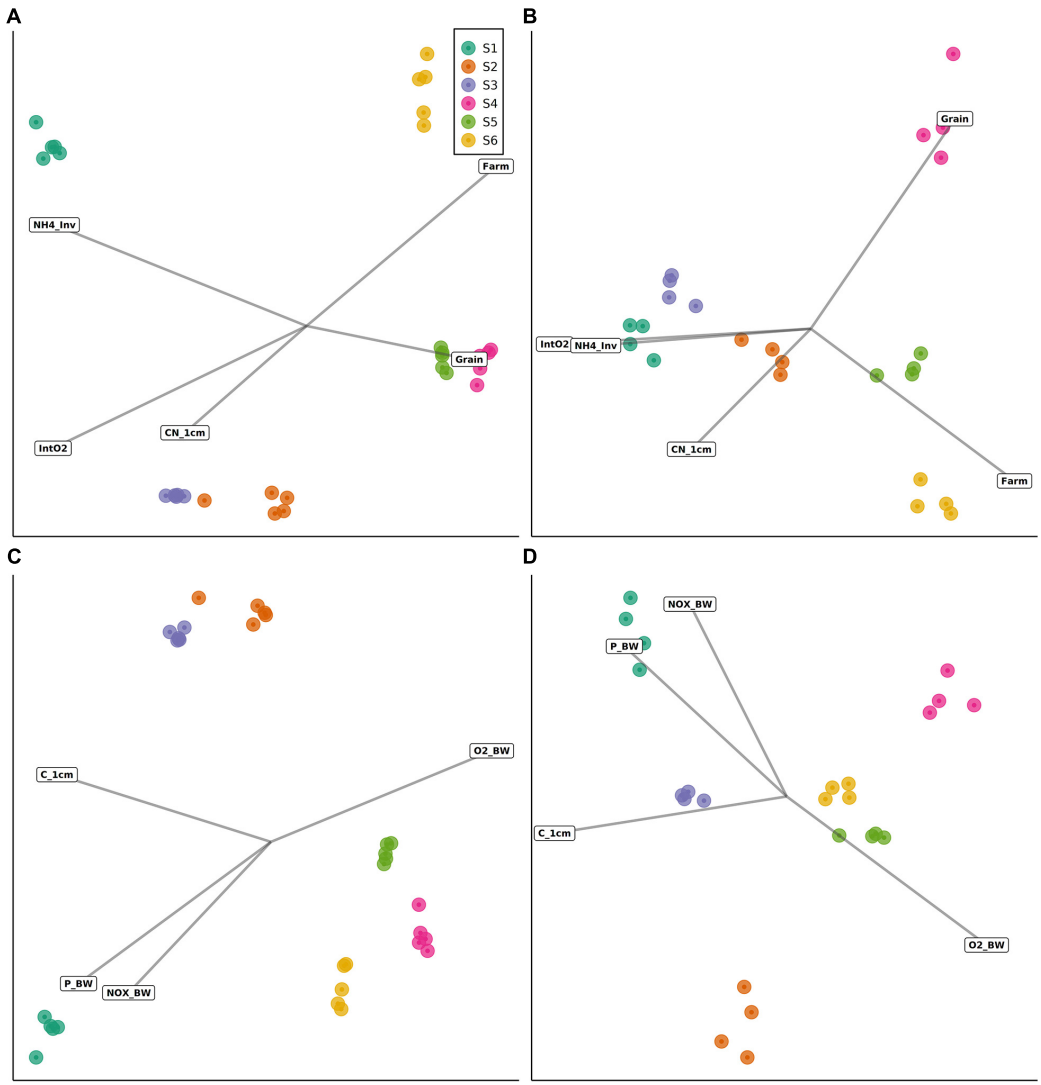

FIGURE 7 | Distance-based redundancy analyses (db-RDA) of sediment bacterial and eukaryotic communities, based on two types of models (see **Table 4** for details). Data are shown for **(A)** bacterial communities (Model 1), **(B)** eukaryotic communities (Model 1), **(C)** bacterial communities (Model 2) and **(D)** eukaryotic communities (Model 2). Environmental variables were projected onto the ordination space using the R function envfit() fitted on linear scores of the ordination axes.

the water column (Milligan and Law, 2005). With the shifts in bacterial taxon composition detected in our study bearing many similarities to those reported in relation to active fish farming activities (despite our study site not being actively used for farming since 2008), the results point toward the possibility of a legacy impact of aquaculture-associated organic loading on the structure and composition of sediment bacterial communities.

In contrast with our results and those reported in Quero et al. (2020), Moncada et al. (2019) reported an increased abundance of *Chloroflexi* near fish farming cages. While we did not find evidence for a similar increase in the relative abundance of *Chloroflexi*, this could be due to site-specific factors. The decline we observed in the diversity of sediment metazoa near the farm was, however, in agreement with general evidence for a shift toward a microbially-dominated state within areas impacted by aquaculture (La Rosa et al., 2001; Mirto et al., 2012). Interestingly, members of the class *Flavobacteriia* were detected even in sites with comparatively high sediment depth-integrated O_2 consumption rates and low bottom water O_2 concentrations (**Table 3**), despite this class often being regarded as aerobic (Kirchman, 2002; Kumagai et al., 2018). The physiological mechanisms enabling this class to persist in low-oxygen environments have been extensively characterized by Kumagai et al. (2018).

Our data showed distinct correlations between bacterial and eukaryotic community structure in relation to the sedimentological and water column variables that were examined (**Tables 3**, **6**). The results further indicated that shifts in the structure of both community types were correlated to a shared subset of environmental variables, including sediment porewater

TABLE 6 | Permutation test results for db-RDA explanatory variables (999 permutations).

Model	Variable	16S rRNA gene metabarcoding		18S rRNA gene metabarcoding	
		Pseudo-*F*	p_{B-H}	Pseudo-*F*	p_{B-H}
Model 1	Porewater NH_4^+ inventory (μmol cm^{-2})	7.230	0.005	1.691	0.012
	Sediment depth-integrated O_2 consumption rate (μmol^{-1} cm^{-2} s^{-1})	3.226	0.013	1.715	0.012
	Distance to farm (km)	3.014	0.018	1.470	0.025
	Sediment C_{org}:N_{tot} ratio, top 1 cm (mol:mol)	1.924	0.065	1.887	0.005
	Sediment median grain size (μm)	1.685	0.090	1.597	0.016
Model 2	Sediment C_{org} content, top 1 cm (% dry mass)	4.912	0.004	2.263	0.004
	Bottom water NO_x* concentration (μmol L^{-1})	3.323	0.010	1.832	0.004
	Bottom water P concentration (μmol L^{-1})	3.070	0.010	1.715	0.007
	Bottom water O_2 concentration (mg L^{-1})	2.605	0.010	1.832	0.004

*NO_2^- and NO_3^-.

The variance explained by each environmental property was tested using the remaining variables as covariates. For details on model construction, see section "Materials and Methods".

NH_4^+ concentrations and the sediment depth-integrated oxygen consumption rate. While these and other variables have been previously related to variation in either prokaryotic (bacterial and archaeal) or eukaryotic community structure within eutrophic sediments (Edlund et al., 2006; Chariton et al., 2015; Dowle et al., 2015; Fodelianakis et al., 2015), our cross-comparison of 16S and 18S rRNA metabarcoding data provides simultaneous information about both domains. The net intensity of organic matter remineralization, as recorded by the porewater NH_4^+ inventory and rate of O_2 consumption, appears to be a key predictor of both bacterial and eukaryotic community structure in the studied locations. Intensity of remineralization is strongly coupled to microbial activity and hence the measured environmental variables.

Considered together, our data support the use of both 16S and 18S rRNA gene metabarcoding analyses as efficient tools to detect anthropogenic impacts such as eutrophication on marine ecosystems (Pawlowski et al., 2018; Stoeck et al., 2018). The overlap in bacterial and eukaryotic community responses to nutrient enrichment and oxygen depletion suggests that either method can provide useful insights into the overall impacts of eutrophication on ecosystem health. Where the variable of interest is known to be associated with shifts in the structure of both bacterial and eukaryotic communities (such as in the case of NH_4^+), 16S rRNA metabarcoding can provide a highly sensitive measure of ecosystem-level responses to eutrophication. The bacterial community data also exhibited less within-station variation than the eukaryote community data (with significant variation in multivariate dispersions only observed for the eukaryote data set; **Figure 6**). While it remains possible that such differences are partially influenced by the use of small sediment volumes (per-replicate mass of 0.25 g; "Materials and Methods" section) (Nascimento et al., 2018), rarefaction analysis and Good's coverage estimates for OTUs were indicative of sufficient sampling depth in both the 16S and 18S rRNA gene data sets in our study (**Supplementary Figure 1** and Results). Ultimately the choice of which metabarcoding approach to use will depend on the overall goals of the monitoring survey, as well as the available resources. Sediment grain size, for example, was found to have a stronger influence on eukaryotic community structure than on bacterial community structure (**Table 6**), which could be of relevance to interpreting the ecological impacts of activities that can disturb the surrounding sediment grain size composition, such as drilling and dredging (Smit et al., 2008) as well as offshore wind farms (Floeter et al., 2017). The sediment C_{org}:N_{tot} ratio was also more strongly associated with eukaryotic than bacterial community shifts, while variation in bacterial community structure was particularly tightly coupled to sediment porewater NH_4^+ concentrations.

The results of this study further suggest that the selection of environmental metadata variables to measure can have wide-ranging consequences for interpreting the results of marine impact assessments. For both the bacterial and eukaryotic data sets, db-RDAs using variables based on their low collinearity explained a greater proportion of the variance in community structure than the second set of db-RDAs employing alternative variables (**Tables 4**, **6**). This implies that, although measurements performed using bottom water samples did correlate with the structure of sediment bacterial and eukaryotic communities, the sensitivity of environmental monitoring protocols could be improved by substituting these variables with appropriate sedimentological data (such as sediment porewater nutrient inventories and/or depth-integrated O_2 consumption rates). The practical feasibility of such modifications is expected to depend on the availability of field equipment, including sediment coring devices and oxygen microelectrodes, and the depth resolution of porewater sampling, which impacts on overall sample processing time. Analytical approaches for porewater nutrient determinations are comparable to those of bottom water samples and hence do not introduce new technical requirements in the laboratory.

The current study focused on a single field transect with samples collected during a single month (see "Materials and Methods" section). Therefore, to ascertain the generality of our

findings and to identify sets of low-collinearity variables that could be efficiently used for monitoring purposes across a broad range of settings (including several types of habitat and different seasons), the conceptual approach presented herein could be extended to alternative locations and studies conducted over longer timescales. To further improve our ability to devise the best possible tools and strategies for benthic marine impact assessments, the types of comparisons performed in our study could also be applied to functional gene expression data. Moncada et al. (2019) showed a reduction in the abundance of dissimilatory sulfate reductase and nitrite reductase genes in mariculture-impacted sediments. While the authors were able to establish correlations between gene expression data and the abundances of selected microbial taxa, they noted that in certain instances this was impossible, likely because we only have a limited understanding of the ecological functions performed by many of the OTUs within sequencing data sets (Moncada et al., 2019). While rRNA gene metabarcoding analyses do not yield direct information on functional gene expression, the choice of which metabarcoding approach to use (and what environmental variables to measure) could nevertheless be greatly aided by the availability of such data.

In summary, our results show that rRNA gene metabarcoding analyses targeting bacterial or eukaryotic communities provide congruent information on the impacts of aquaculture-associated eutrophication on sediment communities, with shifts in the structure of both community types being correlated with a common set of sedimentological and water column variables. Ultimately the choice between 16S and 18S rRNA gene metabarcoding as a tool for monitoring the health of natural ecosystems should be guided by the aims of the study in question and the environmental variable(s) of interest. In this context, our findings clearly demonstrate how the usefulness of both metabarcoding methods is directly dependent on the types of environmental metadata that have been collected. To facilitate the adoption of eDNA metabarcoding as a tool for marine impact assessment, a major challenge will be to determine how diverse physical and chemical variables correlate with microbial versus macrobial community shifts not only locally, but regionally, seasonally and with reference to multiple habitats.

DATA AVAILABILITY STATEMENT

Raw 16S rRNA and 18S rRNA gene sequences supporting the results of this article are available in the NCBI Sequence Read Archive (https://www.ncbi.nlm.nih.gov/sra/docs/) under BioProject accession number PRJNA725053. R scripts used for data analysis, phyloseq objects including data processed in micca and environmental metadata (Materials and Methods) are available on GitHub (https://github.com/jessepharrison/seili-metabarcoding). A Singularity container (https://sylabs.io/singularity/; Kurtzer et al., 2017) definition file and package installation script for reproducing the R environment and package versions used for data analysis are provided in the repository.

AUTHOR CONTRIBUTIONS

JH performed DNA isolations and initial PCRs for sequencing analyses, bioinformatics and data analyses, and wrote the manuscript. KK was responsible for the study design. KK, IS, and P-MC carried out the fieldwork and sampling. KK and TJ performed sample preparations for geochemical analyses and performed the HS measurements. All authors contributed to data interpretation, reviewed the manuscript and approved of its publication.

FUNDING

This work was funded by the Academy of Finland (Grant Nos. 278827 and 304006 awarded to KK).

ACKNOWLEDGMENTS

We thank the R/V Aurelia crew, Markus Weckström, and Anni Jylhä-Vuorio for help with sample collection, and the staff of the Archipelago Research Institute (University of Turku, Finland) for access to sample processing facilities. We acknowledge Lars Paulin and the staff of the DNA Sequencing and Genomics Laboratory (Institute of Biotechnology, University of Helsinki, Finland) for their guidance and carrying out the Illumina MiSeq sequencing analyses. Helen de Waard from Utrecht Geolab (NL) is acknowledged for elemental analyses of the porewater samples and Tvärminne Zoological station for nutrient analyses of porewater samples.

SUPPLEMENTARY MATERIAL

The Supplementary Material for this article can be found online at: https://www.frontiersin.org/articles/10.3389/fmars.2021.708716/full#supplementary-material

Supplementary Figure 1 | Rarefaction curves for **(A)** bacterial and **(B)** eukaryotic Illumina MiSeq metabarcoding data. The data were generated following PCR amplification of bacterial 16S rRNA genes and eukaryotic 18S rRNA genes amplified from eDNA isolated from sediments from six sampling sites in the Archipelago Sea (Baltic Sea, Finland). Curves are shown for OTUs based on a similarity cut-off threshold of 97%, following removal of chimeric sequences.

Supplementary Figure 2 | Non-metric multidimensional scaling (nMDS) ordinations of sediment communities in field sites sampled along a eutrophication gradient in the Archipelago Sea (Baltic Sea, Finland). The ordinations were derived from Aitchison resemblance matrices calculated from Illumina MiSeq OTU abundance data. Data for bacterial communities are shown **(A)** prior to filtering out sequences assigned as NA, Chloroplast (class level) or Mitochondria (family level), **(B)** after filtering out NA sequences, and **(C)** after filtering out NA, chloroplast and mitochondrial sequences. Data for eukaryotic communities are shown **(D)** prior to filtering out NA sequences and **(E)** after filtering out NA sequences.

Supplementary Figure 3 | Phylum-level prevalences (given as fractions) versus total read counts for a) bacterial and b) eukaryotic community Illumina MiSeq data.

Supplementary Figure 4 | Relative abundances (%) of bacterial classes within sediment samples collected from a total of six sampling sites in the Archipelago Sea (Baltic Sea).

REFERENCES

Albanese, D., Fontana, P., De Filippo, C., Cavalieri, D., and Donati, C. (2015). MICCA: a complete and accurate software for taxonomic profiling of metagenomic data. *Sci. Rep.* 5:9743.

Anderson, M. J. (2006). Distance-based tests for homogeneity of multivariate dispersions. *Biometrics* 62, 245–253. doi: 10.1111/j.1541-0420.2005.00440.x

Aylagas, E., Borja, Á, Irigoien, X., and Rodríguez-Ezpeleta, N. (2016). Benchmarking DNA metabarcoding for biodiversity-based monitoring and assessment. *Front. Mar. Sci.* 3:96. doi: 10.3389/fmars.2016.00096

Aylagas, E., Borja, Á, and Rodríguez-Ezpeleta, N. (2014). Environmental status assessment using DNA metabarcoding: towards a genetics based Marine Biotic Index (gAMBI). *PLoS One* 9:e90529. doi: 10.1371/journal.pone.0090529

Benjamini, Y., and Hochberg, Y. (1995). Controlling the false discovery rate: a practical and powerful approach to multiple testing. *J. R. Stat. Soc. Ser. B Stat. Methodol.* 57, 289–300. doi: 10.1111/j.2517-6161.1995.tb02031.x

Berg, P., Risgaard-Petersen, N., and Rysgaard, S. (1998). Interpretation of measured concentration profiles in sediment pore water. *Limnol. Oceanogr.* 43, 1500–1510. doi: 10.4319/lo.1998.43.7.1500

Borja, Á, and Elliott, M. (2013). Marine monitoring during an economic crisis: the cure is worse than the disease. *Mar. Pollut. Bull.* 68, 1–3. doi: 10.1016/j.marpolbul.2013.01.041

Borja, Á, Elliott, M., Snelgrove, P. V. R., Austen, M. C., Berg, T., Cochrane, S., et al. (2016). Bridging the gap between policy and science in assessing the health status of marine ecosystems. *Front. Mar. Sci.* 3:175. doi: 10.3389/fmars.2016.00175

Cahill, A. E., Pearman, J. K., Borja, A., Carugati, L., Carvalho, S., Danovaro, R., et al. (2018). A comparative analysis of metabarcoding and morphology-based identification of benthic communities across different regional seas. *Ecol. Evol.* 8, 8908–8920. doi: 10.1002/ece3.4283

Callahan, B. J., Sankaran, K., Fukuyama, J. A., McMurdie, P. J., and Holmes, S. P. (2016). Bioconductor workflow for microbiome data analysis: from raw reads to community analyses. *F1000Research* 5:1492. doi: 10.12688/f1000research.8986.2

Canfield, D. E. (1989). Sulfate reduction and oxic respiration in marine sediments: implications for organic carbon preservation in euxinic environments. *Deep Sea Res.* 36, 121–138. doi: 10.1016/0198-0149(89)90022-8

Chao, A. (1984). Non-parametric estimation of the number of classes in a population. *Scand. J. Stat.* 11, 265–270.

Chariton, A. A., Stephenson, S., Morgan, M. J., Steven, A. D. L., Colloff, M. J., Court, L. N., et al. (2015). Metabarcoding of benthic eukaryote communities predicts the ecological condition of estuaries. *Environ. Pollut.* 203, 165–174. doi: 10.1016/j.envpol.2015.03.047

Clark, D. E., Pilditch, C. A., Pearman, J. K., Ellis, J. I., and Zaiko, A. (2020). Environmental DNA metabarcoding reveals estuarine benthic community response to nutrient enrichment - evidence from an in-situ experiment. *Environ. Pollut.* 267:115472. doi: 10.1016/j.envpol.2020.115472

Cline, J. (1969). Spectrophotometric determination of hydrogen sulfide in natural waters. *Limnol. Oceanogr.* 14, 454–458. doi: 10.4319/lo.1969.14.3.0454

Comeau, A. M., Li, W. K. W., Tremblay, J. -É, Carmack, E. C., and Lovejoy, C. (2011). Arctic Ocean microbial community structure before and after the 2007 record sea ice minimum. *PLoS One* 6:e27492. doi: 10.1371/journal.pone.0027492

Cordier, T., Esling, P., Lejzerowicz, F., Visco, J., Ouadahi, A., Martin, C., et al. (2017). Predicting the ecological quality status of marine environments from eDNA metabarcoding data using supervised machine learning. *Environ. Sci. Technol.* 51, 9118–9126. doi: 10.1021/acs.est.7b01518

Dowle, E., Pochon, X., Keeley, N., and Wood, S. A. (2015). Assessing the effects of salmon farming seabed enrichment using bacterial community diversity and high-throughput sequencing. *FEMS Microbiol. Ecol.* 91:fiv089. doi: 10.1093/femsec/fiv089

Dully, V., Balliet, H., Frühe, L., Däumer, M., Thielen, A., Gallie, S., et al. (2021). Robustness, sensitivity and reproducibility of eDNA metabarcoding as an environmental biomonitoring tool in coastal salmon aquaculture - An inter-laboratory study. *Ecol. Indic.* 121:107049. doi: 10.1016/j.ecolind.2020.107049

Edlund, A., Soule, T., Sjöling, S., and Jansson, J. K. (2006). Microbial community structure in polluted Baltic Sea sediments. *Environ. Microbiol.* 8, 223–232. doi: 10.1111/j.1462-2920.2005.00887.x

Fernandes, T. F., Eleftheriou, A., Ackefors, H., Eleftheriou, M., Ervik, A., Sanchez-Mata, Y., et al. (2001). The scientific principles underlying the monitoring of the environmental impacts of aquaculture. *J. Appl. Ichthyol.* 17, 181–193. doi: 10.1046/j.1439-0426.2001.00315.x

Floeter, J., van Beusekom, J. E. E., Auch, D., Callies, U., Carpenter, J., Dudeck, T., et al. (2017). Pelagic effects of offshore wind farm foundations in the stratified North Sea. *Prog. Oceanogr.* 156, 154–173. doi: 10.1016/j.pocean.2017.07.003

Fodelianakis, S., Papageorgiou, N., Karakassis, I., and Ladoukakis, E. D. (2015). Community structure changes in sediment bacterial communities along an organic enrichment gradient associated with fish farming. *Ann. Microbiol.* 65, 331–338. doi: 10.1007/s13213-014-0865-4

Forster, D., Filker, S., Kochems, R., Breiner, H.-W., Cordier, T., Pawlowski, J., et al. (2018). A comparison of different ciliate metabarcode genes as bioindicators for environmental impact assessments of salmon aquaculture. *J. Eukaryot. Microbiol.* 66, 294–308. doi: 10.1111/jeu.12670

Frontalini, F., Cordier, T., Balassi, E., Armynot du Chatelet, E., Cermakova, K., Apothéloz-Perret-Gentil, L., et al. (2020). Benthic foraminiferal metabarcoding and morphology-based assessment around three offshore gas platforms: congruence and complementarity. *Environ. Int.* 144:106049. doi: 10.1016/j.envint.2020.106049

Gloor, G. B., Macklaim, J. M., Pawlowsky-Glahn, V., and Egozcue, J. J. (2017). Microbiome datasets are compositional: and this is not optional. *Front. Microbiol.* 8:2224. doi: 10.3389/fmicb.2017.02224

He, X., Sutherland, T. F., Pawlowski, J., and Abbott, C. L. (2019). Responses of foraminifera communities to aquaculture-derived organic enrichment as revealed by environmental DNA metabarcoding. *Mol. Ecol.* 28, 1138–1153. doi: 10.1111/mec.15007

Hervé, M. (2020). *RVAideMemoire: Testing and Plotting Procedures for Biostatistics. R Package Version 0.9-78*. Available online at: https://CRAN.R-project.org/package=RVAideMemoire (accessed November 29, 2020).

Hugerth, L. W., Muller, E. E. L., Hu, Y. O. O., Lebrun, L. A. M., Roume, H., Lundin, D., et al. (2014). Systematic design of 18S rRNA gene primers for determining eukaryotic diversity in microbial consortia. *PLoS One* 9:e95567. doi: 10.1371/journal.pone.0095567

Jilbert, T., Asmala, E., Schröder, C., Tiihonen, R., Myllykangas, J.-P., Virtasalo, J., et al. (2018). Impacts of flocculation on the distribution and diagenesis of iron in boreal estuarine sediments. *Biogeosciences* 15, 1243–1271. doi: 10.5194/bg-15-1243-2018

Jokinen, S. A., Virtasalo, J. J., Jilbert, T., Kaiser, J., Dellwig, O., Arz, H. W., et al. (2018). A 1500-year multiproxy record of coastal hypoxia from the northern Baltic Sea indicates unprecedented deoxygenation over the 20th century. *Biogeosciences* 15, 3975–4001. doi: 10.5194/bg-15-3975-2018

Keeley, N., Wood, S. A., and Pochon, X. (2018). Development and preliminary validation of a multi-trophic metabarcoding biotic index for monitoring benthic organic enrichment. *Ecol. Indicat.* 85, 1044–1057. doi: 10.1016/j.ecolind.2017.11.014

Kirchman, D. L. (2002). The ecology of *Cytophaga-Flavobacteria* in aquatic environments. *FEMS Microbiol. Ecol.* 39, 91–100. doi: 10.1016/s0168-6496(01)00206-9

Koistinen, J., Sjöblom, M., and Spilling, K. (2018). "Determining inorganic and organic nitrogen," in *Biofuels from Algae. Methods in Molecular Biology*, Vol. 1980, ed. K. Spilling (New York, NY: Humana), doi: 10.1007/7651_2018_128

Kumagai, Y., Yoshizawa, S., Nakajima, Y., Watanabe, M., Fukunaga, T., Ogura, Y., et al. (2018). Solar-panel and parasol strategies shape the proteorhodopsin distribution pattern in marine *Flavobacteriia*. *ISME J.* 12, 1329–1343. doi: 10.1038/s41396-018-0058-4

Kurtzer, G. M., Sochat, V., and Bauer, M. W. (2017). Singularity: scientific containers for mobility of compute. *PLoS One* 12:e0177459. doi: 10.1371/journal.pone.0177459

La Rosa, T., Mirto, S., Mazzola, A., and Danovaro, R. (2001). Differential responses of benthic microbes and meiofauna to fish-farm disturbance in coastal sediment. *Environ. Pollut.* 112, 427–434. doi: 10.1016/s0269-7491(00)00141-x

Lane, D. J. (1991). "16S/23S rRNA sequencing," in *Nucleic Acid Techniques in Bacterial Systematics*, eds E. Stackebrandt and M. Goodfellow (New York, NY: John Wiley and Sons), 115–175.

Lanzén, A., Lekang, K., Jonassen, I., Thompson, E. M., and Troedsson, C. (2016). High-throughput metabarcoding of eukaryotic diversity for environmental

monitoring of offshore oil-drilling activities. *Mol. Ecol.* 25, 4392–4406. doi: 10.1111/mec.13761

Laroche, O., Wood, S. A., Tremblay, L. A., Lear, G., Ellis, J. I., and Pochon, X. (2017). Metabarcoding monitoring analysis: the pros and cons of using co-extracted environmental DNA and RNA data to assess offshore oil production impacts on benthic communities. *PeerJ* 5:e3347. doi: 10.7717/peerj.3347

Lefrançois, E., Apothéloz-Perret-Gentil, L., Blancher, P., Botreau, S., Chardon, C., Domaizon, I., et al. (2018). Development and implementation of eco-genomic tools for aquatic ecosystem biomonitoring: the SYNAQUA French-Swiss program. *Environ. Sci. Pollut. Res.* 25, 33858–33866. doi: 10.1007/s11356-018-2172-2

Legendre, P., and Anderson, M. J. (1999). Distance-based redundancy analysis: testing multispecies responses in multifactorial ecological experiments. *Ecol. Monogr.* 69, 1–24. doi: 10.1890/0012-9615(1999)069[0001:dbratm]2.0.co;2

Lejzerowicz, F., Esling, P., Pillet, L., Wilding, T. A., Black, K. D., and Pawlowski, J. (2015). High-throughput sequencing and morphology perform equally well for benthic monitoring of marine ecosystems. *Sci. Rep.* 5:13932.

Lepš, J., and Šmilauer, P. (2003). *Multivariate Analysis of Ecological Data using CANOCO*. Cambridge: Cambridge University Press.

Lobo, J., Shokralla, S., Costa, M. H., Hajibabaei, M., and Costa, F. O. (2017). DNA metabarcoding for high-throughput monitoring of estuarine macrobenthic communities. *Sci. Rep.* 7:15618.

Martin, M. (2011). Cutadapt removes adapter sequences from high-throughput sequencing reads. *EMBnet J.* 17, 10–12. doi: 10.14806/ej.17.1.200

McMurdie, P. J., and Holmes, S. P. (2013). phyloseq: an R package for reproducible interactive analysis and graphics of microbiome census data. *PLoS One* 8:e61217. doi: 10.1371/journal.pone.0061217

Milligan, T. G., and Law, B. A. (2005). "The effect of marine aquaculture on fine sediment dynamics in coastal inlets," in *Environmental Effects of Marine Finfish Aquaculture. Handbook of Environmental Chemistry*, Vol. 5M, ed. B. T. Hargrave (Berlin: Springer), 239–251. doi: 10.1007/b136013

Mirto, S., Gristina, M., Sinopoli, M., Maricchiolo, G., Genovese, L., Vizzini, S., et al. (2012). Meiofauna as an indicator for assessing the impact of fish farming at an exposed marine site. *Ecol. Indicat.* 18, 468–476. doi: 10.1016/j.ecolind.2011.12.015

Moncada, C., Hassenrück, C., Gärdes, A., and Conaco, C. (2019). Microbial community composition of sediments influenced by intensive mariculture activity. *FEMS Microbiol. Ecol.* 95:fiz006.

Muyzer, G., de Waal, E. C., and Uitterlinden, A. G. (1993). Profiling of complex microbial populations by denaturing gradient gel electrophoresis analysis of polymerase chain reaction-amplified genes coding for 16S ribosomal RNA. *Appl. Environ. Microbiol.* 59, 695–700. doi: 10.1128/aem.59.3.695-700.1993

Nascimento, F. J. A., Lallias, D., Bik, H. M., and Creer, S. (2018). Sample size effects on the assessment of eukaryotic diversity and community strucgture in aquatic sediments using high-throughput sequencing. *Sci. Rep.* 8:11737.

Oksanen, J., Blanchet, F. G., Friendly, M., Kindt, R., Legendre, P., et al. (2020). *vegan: Community Ecology Package. R Package Version 2.5-7*. Available online at: https://CRAN.R-project.org/package=vegan (accessed November 29, 2020).

Pawlowski, J., Esling, P., Lejzerowicz, F., Cedhagen, T., and Wilding, T. A. (2014). Environmental monitoring through protist next-generation sequencing metabarcoding: assessing the impact of fish farming on benthic foraminifera communities. *Mol. Ecol. Res.* 14, 1129–1140. doi: 10.1111/1755-0998.12261

Pawlowski, J., Esling, P., Lejzerowicz, F., Cordier, T., Visco, J. A., Martins, C. I. M., et al. (2016). Benthic monitoring of salmon farms in Norway using foraminiferal metabarcoding. *Aquacult. Environ. Interact.* 8, 371–386. doi: 10.3354/aei00182

Pawlowski, J., Kelly-Quinn, M., Altermatt, F., Apothéloz-Perret-Gentil, L., Beja, P., Boggero, P., et al. (2018). The future of biotic indices in the ecogenomic era: integrating (e)DNA metabarcoding in biological assessment of aquatic ecosystems. *Sci. Tot. Environ.* 637–638, 1295–1310. doi: 10.1016/j.scitotenv.2018.05.002

Quast, C., Pruesse, E., Yilmaz, P., Gerken, J., Schweer, T., Yarza, P., et al. (2013). The SILVA ribosomal RNA gene database project: improved data processing and web-based tools. *Nucleic Acids Res.* 41, D590–D596.

Quero, G. M., Ape, F., Manini, E., Mirto, S., and Luna, G. M. (2020). Temporal changes in microbial communities beneath fish farm sediments are related to organic enrichment and fish biomass over a production cycle. *Front. Mar. Sci.* 7:524. doi: 10.3389/fmars.2020.00524

R Core Team (2020). *R: A Language and Environment for Statistical Computing*. Vienna: R Foundation for Statistical Computing.

Ramette, A. (2007). Multivariate analyses in microbial ecology. *FEMS Microbiol. Ecol.* 62, 142–160. doi: 10.1111/j.1574-6941.2007.00375.x

Reese, B. K., Finneran, D. W., Mills, H. J., Zhu, M., and Morse, J. W. (2011). Examination and refinement of the determination of aqueous hydrogen sulfide by the methylene blue method. *Aquat. Geochem.* 17, 567–582. doi: 10.1007/s10498-011-9128-1

Rognes, T., Flouri, T., Nichols, B., Quince, C., and Mahé, F. (2016). VSEARCH: a versatile open source tool for metagenomics. *PeerJ* 4:e2409v1.

Salava, A., Aho, V., Lybeck, E., Pereira, P., Paulin, L., Nupponen, I., et al. (2017). Loss of cutaneous microbial diversity during first 3 weeks of life in very low birthweight infants. *Exp. Dermatol.* 26, 861–867. doi: 10.1111/exd.13312

Seeberg-Elverfeldt, J., Schlüter, M., Feseker, T., and Kölling, M. (2005). Rhizon sampling of porewaters near the sediment-water interface of aquatic systems. *Limnol. Oceanogr. Methods* 3, 361–371. doi: 10.4319/lom.2005.3.361

Shannon, C. E. (1948). A mathematical theory of communication. *Bell Syst. Tech. J.* 27, 379–423.

Smit, M. G. D., Holthaus, K. I. E., Trannum, H. C., Neff, J. M., Kjeilen-Eilertsen, G., Jak, R. G., et al. (2008). Species sensitivity distributions for suspended clays, sediment burial, and grain size change in the marine environment. *Environ. Toxicol. Chem.* 27, 1006–1012. doi: 10.1897/07-339.1

Somervuo, P., Koskinen, P., Mei, P., Holm, L., Auvinen, P., Paulin, L., et al. (2018). BARCOSEL: a tool for selecting an optimal barcode set for high-throughput sequencing. *BMC Bioinform.* 19:257. doi: 10.1186/s12859-018-2262-7

Stoeck, T., Frühe, L., Forster, D., Cordier, T., Martins, C. I. M., and Pawlowski, J. (2018). Environmental DNA metabarcoding of benthic bacterial communities indicates the benthic footprint of salmon aquaculture. *Mar. Pollut. Bull.* 127, 139–149. doi: 10.1016/j.marpolbul.2017.11.065

Verhoeven, J. T. P., Salvo, F., Hamoutene, D., and Dufour, S. C. (2016). Bacterial community composition of flocculent matter under a salmonid aquaculture site in Newfoundland, Canada. *Aquacult. Environ. Interact.* 8, 637–646. doi: 10.3354/aei00204

Verhoeven, J. T. P., Salvo, F., Knight, R., Hamoutene, D., and Dufour, S. C. (2018). Temporal bacterial surveillance of salmon aquaculture sites indicates a long lasting benthic impact with minimal recovery. *Front. Microbiol.* 9:3054. doi: 10.3389/fmicb.2018.03054

Wang, Q., Garrity, G. M., Tiedje, J. M., and Cole, J. R. (2007). Naïve Bayesian classifier for rapid assignment of rRNA sequences into the new bacterial taxonomy. *Appl. Environ. Microbiol.* 73, 5261–5267. doi: 10.1128/aem.00062-07

Westcott, S. L., and Schloss, P. D. (2015). *De novo* clustering methods outperform reference-based methods for assigning 16S rRNA gene sequences to operational taxonomic units. *PeerJ* 3:e1487. doi: 10.7717/peerj.1487

Zhang, N., Xiao, X., Pei, M., Liu, X., and Liang, Y. (2017). Discordant temporal turnovers of sediment bacterial and eukaryotic communities in response to dredging: nonresilience and functional changes. *Appl. Environ. Microbiol.* 83:e02526-16.

Conflict of Interest: JH is employed by CSC–IT Center for Science Ltd., Espoo, Finland. P-MC is employed by Conidia Bioscience Ltd., Surrey, United Kingdom.

The remaining authors declare that the research was conducted in the absence of any commercial or financial relationships that could be construed as a potential conflict of interest.

frontiers in Marine Science

REVIEW
published: 29 July 2021
doi: 10.3389/fmars.2021.711151

Decommissioning Research Needs for Offshore Oil and Gas Infrastructure in Australia

Jess Melbourne-Thomas[1,2], Keith R. Hayes[3], Alistair J. Hobday[1,2], L. Richard Little[1], Joanna Strzelecki[4], Damian P. Thomson[4], Ingrid van Putten[1,2] and Sharon E. Hook[1]*

[1] CSIRO Oceans and Atmosphere, Hobart, TAS, Australia, [2] Centre for Marine Socioecology, University of Tasmania, Hobart, TAS, Australia, [3] CSIRO Data61, Hobart, TAS, Australia, [4] CSIRO Oceans and Atmosphere, Indian Ocean Marine Research Centre, Crawley, WA, Australia

When offshore oil and gas infrastructure is no longer needed, it is either removed, partially removed, left in place, or left in place but repurposed. These processes are collectively referred to as decommissioning. Australian legislation requires oil and gas companies to develop acceptable plans for the safe removal of all offshore infrastructure at the end of a project's life. Over the next 50 years, the liability for this decommissioning in Australia is expected to exceed US$45 billion. Unlike countries such as Norway, the United Kingdom and the Netherlands, Australian decommissioning activities are in their infancy, with only three cases (to date) in Commonwealth waters where infrastructure has been left in place or partially removed as part of decommissioning. Differences between the Australian marine environment and that of other regions around the world where decommissioning-related research is better progressed include very low sedimentation rates, both tropical and temperate habitats, different species composition, low primary production, and frequent tropical cyclones, as well as unique sociodemographic and cultural characteristics. Accordingly, the outcomes of the decision support tools used in other regions to identify preferred decommissioning options may not be equally applicable in Australia. Here we describe research to support risk and impact assessment for offshore decommissioning in Australia, where full removal of infrastructure is the "base case" regulatory default, but other options including partial removal and/or repurposing might provide similar or better outcomes when environmental, social, economic and seafood safety aspects are considered. Based on our review we propose an integrated framework for research needs to meet legislative requirements for decommissioning and identify research gaps that need to be addressed to inform decision-making for decommissioning in the Australian context.

Keywords: oil and gas decommissioning, Australia, decision-making, productivity, connectivity, contaminants, social license

OPEN ACCESS

Edited by:
Allyson O'Brien,
The University of Melbourne, Australia

Reviewed by:
Erin L. Meyer-Gutbrod,
University of South Carolina, United States
Terry Whitledge,
University of Alaska Fairbanks, United States

****Correspondence:***
Jess Melbourne-Thomas
jess.melbourne-thomas@csiro.au

Specialty section:
This article was submitted to Marine Pollution, a section of the journal Frontiers in Marine Science

Received: *18 May 2021*
Accepted: *05 July 2021*
Published: *29 July 2021*

Citation:
Melbourne-Thomas J, Hayes KR, Hobday AJ, Little LR, Strzelecki J, Thomson DP, van Putten I and Hook SE (2021) Decommissioning Research Needs for Offshore Oil and Gas Infrastructure in Australia. Front. Mar. Sci. 8:711151. doi: 10.3389/fmars.2021.711151

INTRODUCTION

Decommissioning is the process of plugging and abandoning oil and gas wells then removing or repurposing infrastructure at the end of its useful life. Decommissioning, as mandated in a range of national policies, should happen in a safe and environmentally and socially responsible manner. There has been very limited decommissioning in Australian Commonwealth waters

(i.e., those that are more than 3 nautical miles offshore) to date, and almost no associated monitoring (Raitt et al., 2019). Australia has in the order of 3,500 km of pipeline, 57 platforms, and 11 floating facilities currently operating in Commonwealth waters (National Offshore Petroleum Safety and Environmental Management Authority [NOPSEMA], 2019a; Advisian, 2020), with additional pipelines and platforms in Western Australian and Victorian state waters. Australia's National Offshore Petroleum Information Management System lists 1,648 wells drilled offshore since January 2001, with most activity concentrated in Australia's north-west and the south-east regions (**Figure 1**). Few of Australia's oil fields have been depleted to the point where decommissioning is required but more than half of Australia's offshore petroleum assets are older than 20 years, with some exceeding 50 years, and as a consequence, would be expected to be approaching end of life soon. Estimates of Australia's decommissioning liability over the next 50 years are between US$30 and 50 billion (National Energy Resources Australia [NERA], 2019; Advisian, 2020; Wood Mackenzie, 2020).

The benefits and costs (particularly the environmental ones) associated with the operational phase of oil and gas infrastructure have been well established internationally (e.g., Schroeder and Love, 2004; Bernstein, 2015; Claisse et al., 2015; Cordes et al., 2016; Fowler et al., 2018; Bull and Love, 2019; Sommer et al., 2019; Beyer et al., 2020; Meyer-Gutbrod et al., 2020) and in Australia (e.g., Macreadie et al., 2011; McLean et al., 2017, 2018, 2021; Schramm et al., 2021). However, the environmental costs and benefits associated with decommissioning are less well studied, particularly in Australia because there is little precedent for the regulatory requirements for building an environmental case that justifies choosing a leave-in-place decommissioning option here. Moreover, the interdependence of the costs and benefits between the operational and decommissioning phases is relatively understudied. For example, during the operational phase, discharging produced water (PW; see **Box 1** for acronyms and definitions of terms used in this paper) containing high concentrations of organic carbon and nutrients such as ammonia affects the productivity of the surrounding ecosystem. It is not certain how comparable the productivity will be once that discharge stops. There are also likely to be social consequences—or costs—to decommissioning decisions (discussed below).

Generalisations about the ecological value of decommissioned oil and gas infrastructure from other well studied regions may manifest differently in Australian waters because: (1) Australia's large marine estate contains a large number of different temperate and tropical marine habitats at the continental scale (**Figure 1**); (2) species assemblages in Australia are distinct from northern hemisphere regions which have been the focus of decommissioning research to date (notably the Gulf of Mexico, California, the North Sea, and the Adriatic Sea; see section "Status of Decommissioning Research Internationally and in Australia"); (3) the low rate of sedimentation in the Australian marine environment (e.g., Blom and Alsop, 1988; Baker et al., 2008), a consequence of comparatively low primary production and low riverine discharge, may affect the persistence of environmental contaminants around offshore infrastructure; and (4) finally, Australia has unique circumstances for social acceptability/social license in the context of decommissioning (see section "Socioeconomic Considerations").

BOX 1 | Glossary and acronyms.
BPEO – Best Practicable Environmental Option Analysis; a type of decision support tool used in decommissioning
CA – Comparative Analysis; a type of decision support tool used in decommissioning
Commonwealth Waters – located more than three nautical miles offshore
Drill cuttings – the waste material, containing drilling muds, from drilling wellheads. Drill cuttings may have been in contact with the formation.
Drilling muds – fluids containing lubricants used when drilling wellheads
EP – Environment plans; documents required by NOPSEMA that describe the potential risks of an activity to the environment and how those risks will be mitigated.
Formation – in this case, the geological layer in the subsurface in which the petroleum formed and from which it was extracted
MCA – Multi Criteria Assessment; a type of decision support tool
Mattresses – subsea infrastructure supporting pipelines
NEBA – Net Environmental Benefit Analysis; a type of decision support tool
NOPSEMA – National Offshore Petroleum Safety and Environmental Management Authority; the Commonwealth agency with regulatory authority for the offshore oil and gas industry.
QRA – Quantitative Risk Assessment; a type of decision support tool
PAH – Polycyclic Aromatic Hydrocarbons; components within oil that confer toxicity
PRA – Probabilistic Risk Assessment; a type of decision support tool
PW – Produced water; water from the formation that is brought to the surface during the oil production process
Sediment infauna – animals that live in sediments
Topsides – the upper portion of an oil and gas platform (above the water line).

Here we provide an outline of research areas/needs that will help to ensure decommissioning in Australia builds on extant knowledge from other locations while recognising Australia's specific and unique characteristics. The aims of this paper are to:

(i) consider research needs for evaluating environmental risk and impacts for decommissioning options in Australia, relative to the unique aspects of its biodiversity, marine environment and sociodemographic and cultural characteristics
(ii) develop a general framework that identifies the information needed to make environmentally sound decisions about decommissioning options (and that considers linkages between these aspects)

THE REGULATORY CONTEXT IN AUSTRALIA

The National Offshore Petroleum Safety and Environmental Management Authority (NOPSEMA) is Australia's independent regulator for health and safety, structural (well) integrity and environmental management for oil and gas operations and greenhouse gas storage activities in Commonwealth waters, and in coastal waters where regulatory powers and functions have been conferred (National Offshore Petroleum Safety and Environmental Management Authority [NOPSEMA], 2019c). Current decommissioning legislation defines a "base case"

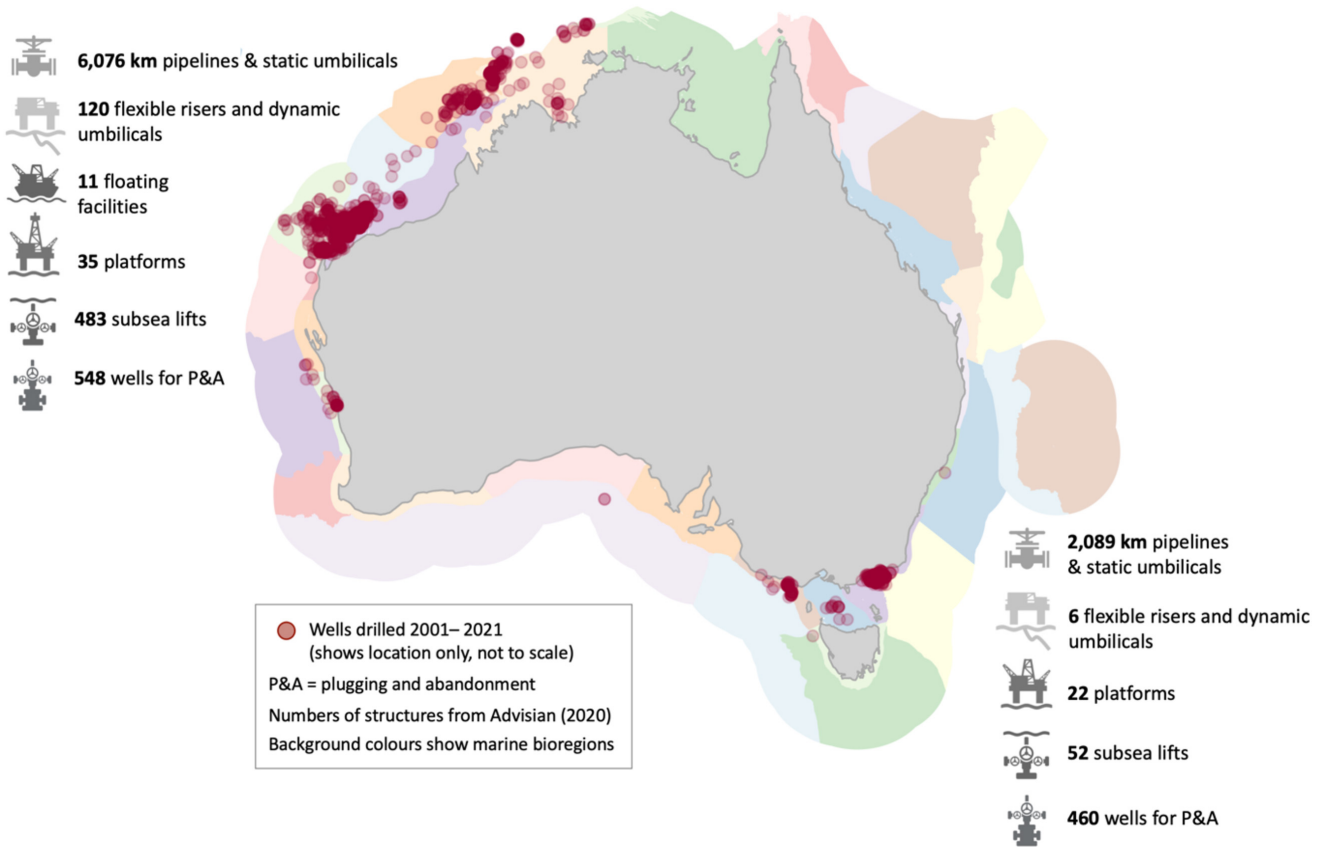

FIGURE 1 | Locations of offshore oil and gas activity in Australia. Red circles show wells drilled by the oil and gas industry in the Australian marine environment between January 2001 and January 2021 (not to scale; data from https://nopims.dmp.wa.gov.au/Nopims/). Numbers of structures are indicative based on publicly available information and are derived from Advisian (2020). The diversity of marine environments in which these operations have occurred is shown by IMCRA v4.0 bioregions (pastel colours; Commonwealth of Australia, 2006). Commonwealth waters are those that are more than three nautical miles offshore.

expectation that oil and gas producers will remove all infrastructure prior to surrender of the petroleum title. While full removal of infrastructure is the default decommissioning option, other options include: (1) partial removal (this may range from almost complete removal where infrastructure is removed near to the sea-floor, but foundations are left in place, through to minimal removal where topsides are removed and any navigational risks addressed); (2) remain *in situ* (infrastructure is left in place, or toppled, after some level of removal); or (3) reefing (the process of using decommissioned infrastructure to form an artificial reef in the expectation of some environmental, social or economic value—infrastructure may be positioned *in situ* or placed elsewhere) (Shaw et al., 2018; see also **Table 1**). NOPSEMA's view is that the option selected needs to provide equal or better environmental outcomes than the base case, and demonstrate that environmental risks can be managed to be at an ALARP (As Low As Reasonable Practicable) and acceptable level (see section "Assessing the Impacts and Risk of Different Decommissioning Options"). The mechanism for demonstrating that the environmental risks associated with a preferred decommissioning option are ALARP is via submission of an Environmental Plan. An Environment Plan will be rejected if it does not predict at least equal or better environmental outcomes for decommissioning *in situ* rather than the default base case. NOPSEMA recently released a new compliance strategy comprising objectives, action and targets to achieve the overarching goal that decommissioning is completed by titleholders in a timely, safe, and environmentally responsible manner (National Offshore Petroleum Safety and Environmental Management Authority [NOPSEMA], 2021). These updates identify triggers for decommissioning which include a pending sale, the time a facility has been in a non-production state, and/or an apparent lack of planning for decommissioning. Notably, current proposed changes to legislation also include so-called "trailing liability," which would mean that under certain circumstances a company could remain liable to remediate an offshore petroleum asset and the immediate environment surrounding the infrastructure even after the title has been sold (Commonwealth of Australia, 2020).

Australian State- and Territory-level legislation that applies to offshore petroleum facilities in their jurisdictional waters (nearer than three nautical miles to shore) generally mirrors Commonwealth legislation. The Commonwealth Environment Protection and Biodiversity Conservation Act 1999 (EPBC Act)

TABLE 1 | Decommissioning options for oil and gas infrastructure.

Platform infrastructure	Decommissioning options
Topsides	Leave in place (repurpose)
	Remove
Platform jackets	Leave in place
	Relocate for artificial reefing
	Partial removal
	Complete removal
Floating Storage Production and Offtake facilities (FPSO) and Risers	Remove
Concrete Gravity Structures	Leave in place
	Remove
Sea bed Wellheads, Manifolds and Valves	Remove
Wells	Plug and abandon
Mattresses	Leave in place
	Remove
Pipelines	Cut ends and leave in place
	Trench and bury
	Remove

Adapted from Advisian (2017).

also applies in State or Northern Territory waters to activities that may affect a matter of national environmental significance. In these circumstances, there may be a bilateral agreement in place to allow the State assessment process to be relied upon by the Commonwealth.

STATUS OF DECOMMISSIONING RESEARCH INTERNATIONALLY AND IN AUSTRALIA

There have been a number of studies that show clear benefits of leaving oil and gas infrastructure *in situ,* and others that demonstrate how these structures pose a risk to the environment. Generally, the factors that influence these costs and benefits are considered to be: (i) the creation of habitat for managed or valued species, as well as the potential risk of oil and gas infrastructure aiding the spread of invasive species; (ii) the potential for impacts of legacy contaminants associated with either drilling or oil and gas production; and (iii) potential socioeconomic concerns relevant to stakeholders needs (including social acceptability of different decommissioning options). These factors are likely to influence each other (**Figure 2**; Schläppy et al., 2021) and should not be considered in isolation. In the sections below, we describe the lessons learned from the international literature for each of these factors, and also describe the circumstances that are unique to the Australian context.

Ecological Considerations for Decommissioning

Habitats and Biodiversity

The positive effects of oil and gas structures on biodiversity and/or productivity are frequently cited to support a leave-in-place decommissioning decision. Biodiversity on and around infrastructure may increase due to the presence of hard, complex substrate, as well as enhanced recruitment and/or due to the ongoing attraction of fish and invertebrates (Macreadie et al., 2011; Love et al., 2012; McLean et al., 2017; Bull and Love, 2019; Claisse et al., 2019). Approval to leave-in-place requires operators to provide evidence that the infrastructure is of high conservation value with respect to habitats and biodiversity. Specifically, the biomass, community composition, productivity and health of the organisms inhabiting the oil and gas structures must be quantified to determine the conservation value of the habitat.

It is well documented that oil and gas infrastructure is used as habitat by a variety of marine species (Love et al., 2000, 2012, 2019a; Bull and Love, 2019). For example, oil and gas platforms offshore of Santa Barbara, California, host abundant, and productive fish communities (Love et al., 2012; Claisse et al., 2014; Pondella et al., 2015), with differences in the composition of invertebrate communities relative to nearby reefs (Love et al., 2019b), including a large number of introduced species at the oil platforms (Page et al., 2006). Studies in the Gulf of Mexico also found a higher diversity of target fish species (i.e., *Lutjanus campechanus*, Red Snapper) and deep sea coral communities associated with platforms than with comparable sites 2–3 km away (Ajemian et al., 2015; Benfield et al., 2019). These structures may also offer feeding benefits for apex predators such as seals (Russell et al., 2014).

Artificial hard structures are known to have different species assemblages than natural reefs (Carvalho et al., 2013). The (comparatively) smooth surfaces of oil and gas infrastructure may alter the species composition. Increased habitat complexity (3-D relief of a surface) generally increases the biodiversity and abundance of marine fouling communities (Strain et al., 2021), with platform complexity linked to enhanced diversity and abundance of fishes (e.g., Meyer-Gutbrod et al., 2019a). The smooth surfaces of oil and gas infrastructure may also alter the species composition of invertebrate communities, especially when they are "new" and the ecological succession process is just commencing (Sommer et al., 2019). Artificial structures are also frequently coated with antifoulants, which can favour the survival of weedy, generalist species (Piola et al., 2009). However, the longer infrastructure is immersed, the more similar species assemblages become with surrounding natural habitat (Sommer et al., 2019).

Communities with different composition than nearby hard substrate may still have conservation value. For instance, in the North Sea it was shown that oil and gas structures increased connectivity for threatened and endangered cold-water corals (Fowler et al., 2014). Similarly, widespread bottom trawling on Australia's Northwest shelf in the 1970s and 1980s caused a change in the associated fish community, and it is possible that oil and gas infrastructure provided refuge for some species. In Australia, numerous studies have demonstrated that fish utilise oil and gas infrastructure as habitat (Macreadie et al., 2011, 2012; Pradella et al., 2014; McLean et al., 2017, 2018) and often support higher biomass and abundances of large, commercially important species than adjacent sandy habitats (Bond et al., 2020). However, the composition of communities at oil platforms and pipelines

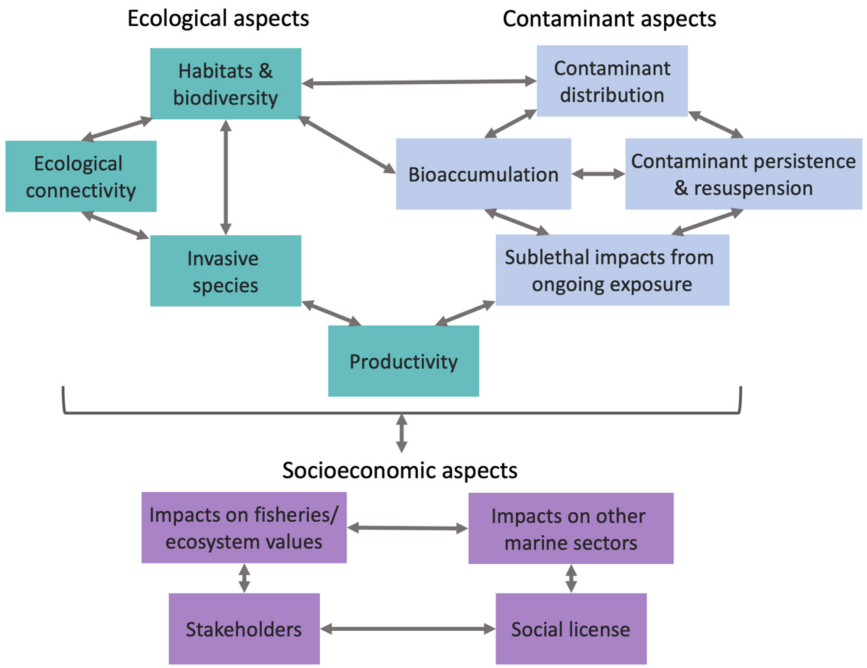

FIGURE 2 | Summary of connections between different research elements needed to consider risk and impacts for decommissioning options. Boxes and arrows are colour coded as: ecological aspects (green), contaminant aspects (blue) and socioeconomic aspects (purple).

has generally not been compared to natural areas in Australia (e.g., Macreadie et al., 2011, 2012; Pradella et al., 2014).

There may be seasonal differences in the habitat value of oil and gas infrastructure. Geographical and seasonal variation in large-scale oceanographic currents and water temperatures present unique considerations when assessing habitat quality of infrastructure. For example, on Australia's Northwest shelf, where there is considerable co-located infrastructure (**Figure 1**), environmental conditions are strongly influenced by large-scale oceanographic currents, including the south-westerly-flowing Indonesian Throughflow and Leeuwin currents. These currents transport warm, clear, oligotrophic waters to the outermost Northwest shelf between March and August (Cresswell and Peterson, 1993), resulting in strong seasonal variation in environmental conditions and larval connectivity across the shelf (Young et al., 1986; Beckley et al., 2009). Abundances of fish and invertebrate larvae in the water column have been shown to be highly variable across seasons (Young et al., 1986), being generally highest in August when the Leeuwin current is nearing the end of its seasonal peak (Beckley et al., 2009; Ridgway and Godfrey, 2015). Video-based observations of fish larvae on pipeline infrastructure across the Northwest shelf also supports the notion that larval distribution and connectivity is strongly influenced by large-scale oceanographic currents, with highest abundances and diversity of fish larvae also occurring in August when the Leeuwin current is nearing the end of its seasonal peak (McLean et al., 2017). Variation in large-scale oceanographic currents may therefore be an important consideration in assessing the quality of habitat of co-located infrastructure on Australia's Northwest shelf. We recommend that in Australia, biological surveys be conducted in multiple seasons to account for these differences.

Productivity

Biological productivity at oil and gas infrastructure may justify leaving (partial) structures *in situ*. The wide depth range of oil and gas platforms can provide predator refuges at midwater depths, allowing for vertical separation between juvenile and larger fishes (Love et al., 2000; Pondella et al., 2015). Recent literature shows Californian oil platforms have amongst the highest production for fish of any system measured worldwide (Claisse et al., 2014), yet habitat values vary greatly among platforms, even among those located in similar ecological settings (Fowler et al., 2015). Productivity at one platform therefore cannot be used to infer the productivity of other platforms, especially across great distances (Fowler et al., 2015).

High fishery productivity on Californian oil platforms is strongly linked to high biomasses of structural epifauna ("biofouling communities") and high nutrients. Abundant biofouling communities, including barnacles and blue mussels, are fuelled by the primary production that occurs in the nutrient rich environments of the Southern California coast and also in the North Sea. These abundant biofouling communities can contribute to fish production via three mechanisms. First, increased physical complexity greatly increases surface area of hard substrate available to larval fish (Love et al., 2019a), promoting enhanced larval recruitment (Emery et al., 2006). Second, the larvae produced by fouling communities provides food for juvenile fish that recruit as larvae and utilise the structures as a predator refuge (Bull and Love, 2019). Third,

organisms (e.g., blue mussels) grow on platforms until their body weight exceeds their capacity to remain attached, at which point they fall to the base of the platform, creating shell mounds at rates of up to 70 kg of shell per day (Love et al., 1999; see **Figure 3**). These shell mounds host a rich and diverse community of invertebrates and fishes, which provide food for large, predatory fishes at the base of the platform (Love et al., 1999; Page et al., 2005; Meyer-Gutbrod et al., 2019b). In the Gulf of Mexico, by contrast, where shell mounds are comparatively rare, there is not a comparable invertebrate community and, as a consequence, there are fewer large predatory fish (reviewed in Goddard and Love, 2010). In Australian waters, primary productivity is relatively low, and Australian oil and gas infrastructure is not typically associated with shell mounds (**Figure 3**). The fish productivity at Australian platforms needs to be determined for productivity to be used as a justification for decommissioning infrastructure *in situ*.

The options chosen for decommissioning may affect the productivity and conservation value of the system. For instance, the fisheries productivity at a platform may change with depth (Love et al., 2000; Pondella et al., 2015). Partial removal would likely result in the loss of fish biomass and production for species typically occupying the shallow portions of the platform structure. In California, it has been estimated that complete removal of a platform would result in 95% or more reduction in the average fish biomass and production, while losses due to partial removal would average 10% or less (Meyer-Gutbrod et al., 2020). We are unaware of similar studies having been conducted in Australia. If the value of oil and gas infrastructure as habitat is used to justify leaving the platforms partially in place, we recommend determining how the removal of the upper portions of the structure will change the habitat value.

Invasive Species

Subsea infrastructure may act as a conduit to facilitate the spread of invasive marine species by providing suitable habitat in areas where it does not exist naturally. The pipelines that interconnect oil platforms could provide a connecting pathway for dispersal of mobile non-indigenous species. The organisms that encrust oil platforms are generally distinct from those in surrounding communities and the densities of fish and invertebrates on pipelines generally higher than surrounding areas (Love and York, 2005). In Brazil, the servicing of platforms by industry vessels is thought to be a major source of invasive (exotic) species introductions, potentially endangering nearby natural environments (Braga et al., 2021).

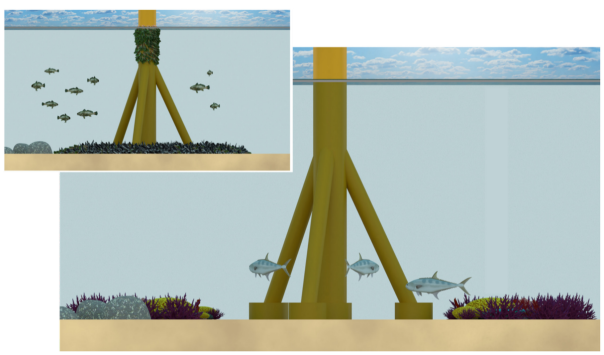

FIGURE 3 | Shell mounds in California (inset) compared with the Australian context (no shell mounds). For structures in Californian environments there is a high level of growth of mussels on infrastructure, which deposits shell mounds to the seafloor (and then provides habitat and a food source for fish and invertebrates). By contrast, Australian oil and gas infrastructure is not typically associated with shell mounds, and as a consequence, may not support similar levels of fish productivity to California.

In general, a high abundance of exotic species (some of which are cryptic) has been found on platforms off the Santa Barbara coast (Page et al., 2006). The exotic species can reach densities of up to 40% cover and may have very different compositions between different structures. The exotic species are absent or rare on natural reefs in the area. Platforms can enhance connectivity (see also the section "Ecological Connectivity and Ocean Environment") and so contribute to the spread of invasive species (e.g., *Watersipora*, an invasive bryozoan; Page, 2019). These differences in species composition are not limited to invertebrates—in the Gulf of Mexico, fish species composition around platforms differs from the surrounding area, and it has been suggested that fish "followed" the platforms as they were towed in from South America (reviewed in Bull and Love, 2019). Although invasive species are comparatively rare in tropical marine waters of the Indo-Pacific (Wells, 2018; Wells et al., 2019) for unknown reasons, the one documented invasive species in Australia's north-west (the ascidian *Didemnum perlucidum*) was recorded on artificial structures associated with oil and gas activity (Wells, 2018).

Nuisance species (e.g., those that can grow to unwanted abundance) in the pelagic environment may increase because of oil and gas infrastructure. Oil and gas infrastructure can also contribute to jellyfish and Harmful Algal Blooms (Duarte et al., 2013; Schulze et al., 2020). The surge in numbers of moon jellyfish in Adriatic Sea was positively correlated with propagation of offshore marine constructions including oil and gas platforms (Vodopivec et al., 2017) as artificial substrates are preferred settling surfaces for polyps—the juvenile life stage (Holst and Jarms, 2007). Encrusting communities represent a potential habitat for the dinoflagellate *Gambierdiscus toxicus* that causes ciguatera fish poisoning. This dinoflagellate was found in all the platforms (n = 6) surveyed in Gulf of Mexico (Villareal et al., 2007). Availability of substrate in combination with climate change that has been linked to expansion in the range of *Gambierdiscus* spp. (Villareal et al., 2007) and jellyfish (Purcell, 2005) makes the risk likely to increase in future.

We are not aware of studies which quantify the proportion of exotic sessile epifauna on and around Australian oil and gas infrastructure. The relative contribution of exotic species, and the consequences both for indigenous organisms and biological communities, needs to be assessed in determining the value of oil and gas infrastructure as habitat for conservation purposes in Australia. The biofouling communities on oil and gas infrastructure should be characterised to determine whether the species they contain have conservation value, or alternatively,

include invasive pests. Depending on local concerns, these surveys could be extended to the pelagic environment.

Ecological Connectivity and Ocean Environment

Most prior ecological studies have examined platforms in isolation (e.g., Love et al., 2005; Benfield et al., 2019) and have not measured the ecological connectivity among structures. Determining this conservation value is especially important as oil platforms, which are grouped around petroleum deposits (e.g., **Figures 1**, **4**), are unlikely to be ecologically isolated. Similar to reefs, oil and gas structures represent interconnected networks of hard structures which larvae can pass between. Connectivity of oil and gas infrastructure may allow for associated fish to "seed" natural areas elsewhere, or for introduced species and other marine pests to proliferate (Nishimoto et al., 2019). Local hydrodynamic conditions may affect the connectivity of infrastructure with nearby reefs or fishing areas, also altering the value of the area as habitat. Decommissioning research should therefore consider how well these structures are connected, and what the implications of removing one or more structures from the network would be. In addition, the value of structures may change over time. As described above (see section "Habitats and Biodiversity"), platforms which have been in place for a long time could have undergone colonisation and succession, leading to the formation of diverse and stable communities. As a consequence, these older platforms may be disproportionally valuable as sources of larvae/juveniles to neighbouring areas, so therefore provide higher preservation value, i.e., "the spillover effect" (e.g., Palumbi, 2003).

Large-scale oceanographic currents will not only affect larval abundance, composition, and levels of connectivity, but may affect rates of infrastructure decay as well, such that the life span of structures in tropical Australian waters is shorter than in temperate systems, and posing the potential for increased contaminant exposure. Corrosion of steel in the marine environment is influenced by many environmental factors, including water velocity and temperature, with accelerated rates of corrosion associated with warmer, faster moving water (Melchers, 2006). As a result, the warm water transported onto Australia's Northwest shelf by the Leeuwin current may accelerate rates of corrosion and decomposition of infrastructure. At the same time, cyclones are common on the Northwest shelf (1–2 cyclones per year: Drost et al., 2017), producing significant wave heights of greater than 5 m (Cuttler et al., 2018) and maximum wave heights in excess of 17 m (CSIRO-BHP unpublished wave buoy data during cyclone Olwyn, March 12, 2015). Rates of infrastructure decay are therefore unlikely to be linear and may be strongly influenced by the prevailing environmental conditions within the region.

Climate change is modifying the distribution of marine species (e.g., Pecl et al., 2017; Melbourne-Thomas et al., 2021) and decommissioning decisions need to consider the effect of climate change on biodiversity, biomass and recruitment so that changes in the ecosystem due to climate change (such as poleward migration of a species) can be differentiated from those changes brought about by the presence of oil and gas infrastructure. Warming-induced changes in spawning phenology that impacted larval transport and consequently ranges shifts of marine invertebrates were observed in Northwest Atlantic continental shelf areas (Fuchs et al., 2020).

Future decommissioning research in Australia assessing ecological aspects will need to holistically consider habitat value, ecological connectivity of the system, the importance of invasive species, productivity, and the changing environment. Hence, research needs to include modelling based on scenarios and projections for changing conditions into the future.

Contaminant Aspects: Distribution of Contaminants and Decommissioning

There is the potential for contaminants associated with oil and gas infrastructure to influence the value of infrastructure as habitat either by reducing the productivity of fish communities, altering the species composition found at the sites or by reducing the perceived or actual safety of the area for collecting fish or other types of seafood for human consumption. Removing oil and gas infrastructure may resuspend buried contaminants, making them bioavailable to filter feeding organisms and the fish that prey on them. Ongoing exposure to petroleum hydrocarbons and other toxic compounds may alter the health (e.g., diminish reproductive capacity) of fishes that inhabit the area (Codi King et al., 2011; **Box 2**). It is also possible that the contaminants that were once associated with drill cuttings and PW discharge have either been degraded or dispersed by sediment movement over time. The sources of these contaminants, their fate and transport in the marine environment, and examples from the international literature of how they can be transformed are highlighted in the sections below.

Contaminant Distribution

The primary sources of contaminants associated with offshore oil and gas infrastructure include: drilling muds, drill cuttings, PW, and occasionally incidental oil spills or pipeline leaks (Cordes et al., 2016; Lelchat et al., 2020). The impacts of oil spills have been reviewed recently (Barron et al., 2020; Hook, 2020), and would be infrequent, so the remainder of the text focusses on PW, drill cuttings and drilling muds. PW is the water in the formation that is brought to the surface during the production process (Neff et al., 2011). Frequently, this water is discharged into the marine environment (Parkerton et al., 2018). PW contains environmental contaminants at concentrations sufficient to cause toxic impacts in standardised ecotoxicological bioassays (Parkerton et al., 2018), and causes adverse outcomes in fish continuously exposed in the laboratory (reviewed in Bakke et al., 2013; Beyer et al., 2020). However, few impacts from exposure to PW have been measured in the field because of the rapid dilution that occurs in turbulent marine environments (reviewed in Bakke et al., 2013; Beyer et al., 2020). None the less, over the life of an oil platform, it is possible that some of the metals and hydrophobic PAHs could precipitate out and concentrate in the sediment, leading to the accumulation of potential toxic concentrations over time.

Drilling muds are injected into the borehole during drilling, and include lubricants, as well barium and other materials used to decrease the buoyancy of the material and prevent blowouts

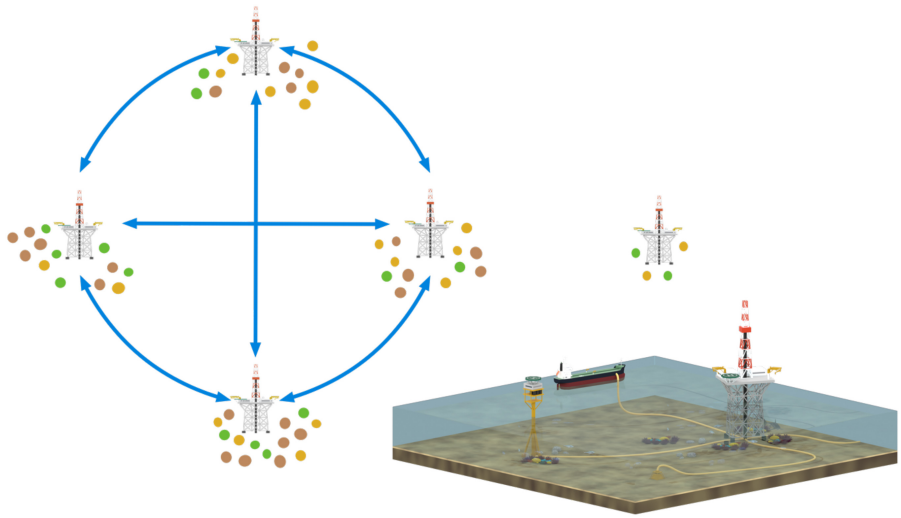

FIGURE 4 | Connectivity of biological particles (e.g., larvae) between oil and gas infrastructure in offshore environments depends on the proximity of structures to each other, pathways for connections (such as pipelines), pelagic larval duration (and behaviour), as well as patterns of oceanographic currents. Inset image shows a visual rendering of different types of co-located structures.

(Lelchat et al., 2020). Drill cuttings are the materials produced during drilling process, and include drilling muds, as well as the material removed from the borehole. This material may have been in contact with the oil in the formation (Lelchat et al., 2020). For the oldest offshore platforms, an oil based lubricant was used in drilling muds, but these have been phased out since the early 1990s in favour of less toxic synthetic based muds and water based muds (Gagnon and Bakhtyar, 2013).

Contaminant Persistence and Resuspension

Once released into the environment, cuttings piles are resistant to chemical change, as they are frequently anaerobic, slowing the rates of petroleum degradation (Nguyen et al., 2018). Resuspension and dispersion are the primary means of contaminant dispersal (reviewed in Bakke et al., 2013). Drill cuttings can have physical impacts on benthic communities, such as the smothering of marine organisms (Henry et al., 2017). Toxicity from those cuttings piles is primarily driven by the hydrocarbons and depends on the type of lubricant used during drilling (reviewed in Bakke et al., 2013). In the North Sea, when oil-based muds were initially discharged, impacts could be seen at distances greater than 5 km (reviewed in Bakke et al., 2013). Now, the contaminants in oil-based muds have dissipated and been buried, and are impacts rarely seen at distances greater than 500 m (reviewed in Bakke et al., 2013). Physical stressors (such as burial from sedimentation and sediment oxygen levels) may pose a greater risk to organisms than chemical stressors when the less toxic synthetic based muds are used (reviewed in Bakke et al., 2013). Impacts from water-based muds are primarily physical and would be expected to be short-term (Bakke et al., 2013). Even exploratory drilling (which does not result in oil production) can have environmental impacts (Junttila et al., 2018), with altered barite and metal concentrations and changes in sediment grain size measured near exploratory well heads. Some of the metals associated with exploratory drilling were elevated sufficiently to cause toxicity in sediments collected from areas near exploratory drilling (Junttila et al., 2018).

Drill cuttings piles can be dispersed in areas of high current flows (Henry et al., 2017), diluting the contaminants contained within them until they no longer cause adverse impacts. Burial of contaminants via sedimentation also reduces the persistence of their impacts on the marine ecosystem, as they effectively become "out of reach" for biological systems (Henry et al., 2017). How these processes can alter the toxic impact of contaminants contained within drilling muds and cuttings piles is demonstrated in the international literature. Large cuttings piles are present in the northern North Sea, whereas in the south, cuttings piles have been dispersed by storms, currents and tides (Bakke et al., 2013). In the northern regions, impacts were typically measured within 1 km of platforms and persisted for 6–8 years, with longer recovery times for oil based muds (Henry et al., 2017). This recovery is based on the amount of time required for the drill cuttings to be covered by clean sediment. In the southern North Sea, where drill cutting did not accumulate, no impacts are typically measured (Henry et al., 2017). In the Gulf of Mexico, which has a high sedimentation rate, metals from PW were the primary contaminant, not petroleum hydrocarbons from the drilling muds and drill cuttings (Kennicutt et al., 1996b). Detoxification mechanisms for oil related compounds were not elevated in fish collected from platforms in the Gulf of Mexico (McDonald et al., 1996).

In Australia, sedimentation rates are known to be very low. For example, in the Bass Strait, separating Tasmania from the rest of Australia, sediments accumulate at less than 6–12 cm/1,000 years (Blom and Alsop, 1988). By comparison, rates of sedimentation in the Gulf of Mexico are 0.2 cm per year (Rohal et al., 2020). Sediment deposition on the Northwest shelf of Australia is also expected to be slow (Baker et al., 2008), especially

BOX 2 | Contaminants from oil and gas infrastructure.

The contaminants that have the highest concern for entering the seafood supply are methylmecury and naturally occurring radiological material (NORM).

Methylmercury bioaccumulation

Methylmercury is a potent developmental neurotoxin and has been associated with cardiovascular disease in adults (Mason et al., 2012; Beckers and Rinklebe, 2017). Seafood consumption, particularly of long lived high trophic level fish or demersal species with strong site-attachment, is the primary route of exposure to methylmercury (Mason et al., 2012). PW can be high in mercury (Neff et al., 2011). As mercury has a high affinity for particles, discharged mercury would be expected to precipitate out of the water column once discharged (Mason et al., 2012). Mercury is methylated by bacteria in low oxygen environments, including marine sediments (Kim et al., 2013). Once formed, methylmercury readily biomagnifies in aquatic food chains, such that its concentrations in upper trophic levels are approximately 10,000 fold higher than in primary producers (Beckers and Rinklebe, 2017). The geochemical processes governing the formation of methylmercury are complex, but the rates of formation are comparatively high in low oxygen environments with abundant sulphides and labile organic material (Bravo et al., 2017), such as would occur in drill cuttings and areas. Indeed, oil contaminated ground water, sediments collected near oil seeps, and sediments collected from oil polluted areas were among those with the highest proportions of mercury methylating bacteria in genomic databases (Podar et al., 2015). Bacteria capable of methylating mercury were also collected from the guts of oligochaete worms (Podar et al., 2015), which are often abundant in oil contaminated sediments. There is also evidence that methylated mercury associated with oil and gas production is entering the food chain. Dab (*Limanda limanda*), a demersal flatfish, collected from the Ekofisk oil field in the North Sea had the highest concentrations of methylmercury of any fish surveyed in the region, including those from the Baltic Sea (Lang et al., 2017). Studies have not explicitly linked high organic matter input and mercury from PW to rates of mercury methylation in sediments and bioaccumulation in associated seafood resources, however, because of the implications for human health (Sevillano-Morales et al., 2015), this risk should be considered before a decommissioned area is opened to recreational fishing.

Naturally occurring radioactive materials (NORMs)

Petroleum formations contain radionuclides, which may be discharged as a constituent of PW (Neff et al., 2011). Radioactivity of PW depends on the geology—in particular, the distribution of U and Th, the chlorinity and total dissolved solids—in the reservoir (Fisher, 1998). Radium in PW is expected to precipitate with sulphate once it mixes with seawater (Olsvik et al., 2012). The ecotoxicity of these compounds at it relates to the decommissioning context has been recently reviewed, with attention drawn to the paucity of data (Amy et al., 2021). Potentially, radioactive material maybe accumulated by worms, then fish that prey on benthic invertebrates (Olsvik et al., 2012). Modelling studies in the Gulf of Mexico have suggested that discharge of radionuclides do not pose a threat to marine organisms. Some authors have hypothesised that since radioactivity is higher in the Gulf of Mexico than elsewhere, risks to organisms are also low (reviewed in Hosseini et al., 2012). Low risk was also predicted for shrimp and mussels in the North Sea (reviewed in Hosseini et al., 2012). While most studies have found that the risk from exposure to NORMs is negligible, because of the lack of research, the uncertainty around this prediction is high (Hosseini et al., 2012).

Radionuclides can be precipitated as NORM scale on pipelines as the minerals mix with sea water (Hosseini et al., 2012). There is concern that if the pipelines are discarded *in situ*, that over time, as the pipelines break down, this material would enter marine food chains as discussed above, potentially causing ecological impacts as well as potentially entering the seafood supply. Recent modelling performed on behalf of the Australian Petroleum Production and Exploration Association (APPEA) suggests that while this is a risk, the process would be slow, and material would be diluted into surrounding marine sediments (Advisian, 2017). However, the concentrations of NORMs should be monitored as part of the decommissioning process, so that adverse outcomes can be predicted and mitigated.

when compared to oil producing regions that have higher biological productivity and higher inputs of riverine sediments. It is plausible that contaminants may be more persistent in Australia, as they are not diluted or buried by sedimentation, and as a consequence, have greater opportunity to exert toxic effects. However, sediments containing drilling muds, and their associated contaminants, may be redistributed by the frequent cyclones that occur offshore of the Northwest shelf (e.g., Dufois et al., 2017) or by the strong currents in the Bass Strait. Contaminant persistence should be quantified on a site specific basis. High contaminant levels may compromise the value of the oil and gas structures as habitat—even if contaminants are buried—since resuspension of sediment "resets" recovery, both by smothering organisms and by making buried contaminants bioavailable (Henry et al., 2017). To minimise impacts on benthic communities, decommissioning options should aim to minimise the resuspension of contaminated sediments if structures and pipelines are removed (Henry et al., 2017), and the potential for contaminant exposure should be estimated.

Bioaccumulation

Contaminants that are associated with sediments can bioaccumulate (Simpson and Batley, 2016). The possible routes of exposure include passive uptake through gills and epidermal layers of burrowing organisms and ingestion of particles by deposit and suspension feeders. Animals that prey on benthic organisms can ingest their contaminant load (Simpson and Batley, 2016). As discussed in **Box 2**, there is the potential for some contaminants, methylmercury in particular, to be bioaccumulated in filter feedings organisms to an extent that the area around infrastructure is not safe for collection of seafood. This possibility, with consideration of Australia's cultural diversity, should be excluded before areas are reopened for fishing or repurposed for aquaculture.

Impacts From Continuous Exposure to Compounds in Drilling Muds and PW

Prolonged exposure to compounds in PW and drilling muds disrupts normal endocrine processes in fish and other resident marine organisms, decreasing the value of platforms as habitats. Xenobiotic metabolising enzymes, including CYP1A, are induced by high molecular weight fraction of oil (reviewed in Whyte et al., 2000; Schlenk et al., 2008). These enzymes break down many aromatic compounds, including steroid hormones (reviewed by Whyte et al., 2000) and may interrupt the normal action of steroid receptors (Arukwe et al., 2008). Crude oil and PAH exposure has been shown to interrupt steroidogenic pathways following laboratory exposures (Arukwe et al., 2008; Kennedy and Smyth, 2015), and reduced reproductive output has been noted in fish from chronically oil contaminated areas (Sol et al., 2000; Johnson et al., 2008). Studies of the chronic impacts from PW and drilling muds (in this case defined as adverse outcomes that arise from long term, ongoing exposure to contamination; Kennicutt et al., 1996a), have found that the PAH, alkylphenols, and napthenic acids associated with PW and drilling muds/cuttings are bioaccumulated by marine organisms,

and may cause biochemical and reproductive changes (Balk et al., 2011; Bakke et al., 2013).

Surveys of some oil and gas producing areas have shown indications of ongoing exposure of fish to PAH. In the North Sea, elevated PAH metabolites are measured in bile and elevated levels of DNA adducts in haddock (fish which forage in the sediment) collected in areas from around platforms (Balk et al., 2011 reviewed in Beyer et al., 2020). These changes were not measured in fish collected from platforms in the Gulf of Mexico (McDonald et al., 1996), which is unsurprising given that there was little PAH gradient measured in the sediment around the platforms surveyed. Bioindicators of exposure to oil were also not changed in fish collected around platforms offshore of the maritime provinces in Canada, where synthetic drilling muds were utilised (Mathieu et al., 2011). In the Adriatic Sea, published studies have also focussed on the association of fish with oil and gas infrastructure and contaminants impacts. As Italian wells were drilled with synthetic drilling muds, and regulations prohibit the discharge of PW at sea, there have been minimal toxic impacts associated with oil and gas infrastructure (Regoli et al., 2019). While changes in meiofaunal composition in sediment have been observed, the links to toxicity have not been established, and may instead been attributed to alterations in sediment grain size and organic enrichment (Terlizzi et al., 2008; Fraschetti et al., 2016).

As a consequence of the potential for prolonged exposure to PAH and other oil constituents to impact fish reproduction, at platforms where contamination is found to persist, the health of the resident fishes should be determined before concluding that the area is good fish habitat. Uptake and detoxification rates differ between environments and species, and so generalisation between regions is difficult, meaning that research will need to be conducted at a range of Australian sites. Biochemical changes that indicate exposure to oil have been measured in fish collected near platforms on Australia's Northwest shelf (King et al., 2005; Codi King et al., 2011). If future surveys indicate elevations in the concentrations of oil and other environmental contaminants around platforms, implications for the health of fisheries species and other species of conservation concern may then need to be determined.

Biological Feedbacks: Contaminant-Influenced Changes in Community Structure

Prolonged exposure to contaminants, especially if coupled with enrichment of organic material, may also accelerate the spread of invasive species around infrastructure in the Australian environment. Toxic responses may cause change in benthic species composition, either through outright mortality, or changes to reproduction, feeding, or other physiological parameters that impact an organism's fitness (Hook et al., 2014). Higher concentrations of environmental contaminants have been associated with increased proportions of invasive species, which frequently have higher tolerance of environmental contaminants (reviewed in Strain et al., 2021). The presence of offshore oil platforms has been shown to change benthic communities in the North Sea and the Gulf of Mexico, both as a result of increased production and enrichment of organic matter, as well as the elevations in environmental contaminants and changes in sediment size around oil platforms (Montagna and Harper, 1996; Henry et al., 2017). In addition, contaminated sediments were found to have decreased larval settlement relative to uncontaminated sediment (Hill et al., 2013). Notably, the abundance of benthic meio/macrofauna can be driven by "top down" processes (such as predation) or "bottom up" processes (increased primary production), and may not reflect contamination at all (Montagna and Harper, 1996). Some of the changes in species composition around oil and gas infrastructure may be associated with the loss of species (suspension feeders, in particular) due to the impacts associated with drilling waste (Lelchat et al., 2020).

In the Gulf of Mexico, a survey of platforms away from the Mississippi River plume found that the concentration of metals, organic matter, and sand (associated with drilling muds) were all increased in abundance near oil and gas platforms (Kennicutt et al., 1996b). Changes in meiofaunal abundance were seen along a metals contamination gradient within 100 m of some platforms (Montagna and Harper, 1996). An increase in the abundance of nematodes and polychaete worms was attributed to increased organic enrichment, while a decrease in harpatacoid copepod and amphipod abundance was associated with toxicity (Montagna and Harper, 1996). When the changes in community structure were examined on the basis of traits, non-selective deposit feeders and organisms that fed on the epifauna increased in abundance near the platforms, but selective feeders decreased in this area (Montagna and Harper, 1996). Studies in the North Sea have also found changes in community structure along a contamination gradient—including an increased abundance of opportunistic or pollution tolerant species (Henry et al., 2017). The potential for contaminant related changes in community structure to influence habitat quality and the potential values of oil and gas infrastructure as either conservation area or for fisheries production should also be evaluated as part of the decision making process around decommissioning in Australia, or any other novel region.

Socioeconomic Considerations

The social and economic values that oil and gas infrastructure contributes to, or alternatively detracts from, need to be determined as part of any assessment of decommissioning options. This includes examining the contribution of the infrastructure, and chosen decommissioning option, to fisheries and other marine sectors, and determining the acceptability of the selected option to stakeholders (**Figure 2**). Although issues around social acceptability are not new, and industry understanding around gaining social license for their operations has grown, Australia is in the unique position that it has a relatively long history of exploring social license concepts (i.e., how to gain and keep social license). Much of the global literature around the concept of social license arose around the mining industry in Australia (Moffat and Zhang, 2014; Bice et al., 2017). Processes regarding Indigenous rights and perspectives in the context of social license have evolved in recent years (Uffman-Kirsch et al., 2020), and also provide insight for the decommissioning context.

Impacts on Fisheries and Ecosystem Values

Oil and gas infrastructure has the potential to add to fisheries production, meaning a "leave-in-place" decommissioning option has prospective fishery value. In the Gulf of Mexico, numerous platforms have been repurposed as fish habitats through "rigs to reefs" programmes, whereby a platform is deployed as an artificial reef following the end of oil and gas production (Bull and Love, 2019). Since the coastal residents in Louisiana and Texas (US states that border the Gulf of Mexico) include a high proportion of recreational fishers (Bull and Love, 2019), and up to 70% of these fishers utilise these platforms as fishing destinations (Reggio, 1987), these programs have been very popular (reviewed in Bull and Love, 2019).

Video evidence demonstrates that Australian demersal fishes utilise oil platforms as habitat (Pradella et al., 2014; Thomson et al., 2018) as elsewhere in the world (Ajemian et al., 2015; Benfield et al., 2019). This utilisation does not necessarily equate to increased production of fisheries species, in terms of either somatic growth, recruitment to the population, or decreased mortality (Bohnsack, 1989). Increased fishery production would result from platforms if habitat was the limiting factor. Otherwise, artificial habitat from platforms might only serve to attract and aggregate fishes, making them more easily caught, potentially resulting in further declines in overexploited fisheries (but see Smith et al., 2015). As discussed in the section "Ecological Considerations for Decommissioning," the effect of platforms on fish population dynamics in Australia are likely different from other reported regions such as California and the Gulf of Mexico (Australian waters are more oligotrophic, have different biofouling organisms, and do not have a shell mound; **Figure 3**). A range of pelagic species are associated with structures in the ocean (Hobday and Campbell, 2009; Champion and Coleman, 2021). While pelagic fisheries world-wide exploit this association via use of fish aggregating devices (FADs), platforms are only likely to enhance catchability and not production of these species.

In Australia there is a large recreational fishing sector—which in some places is larger than the commercial sector in terms of volumes of fish caught (Henry and Lyle, 2003; Lyle et al., 2014; Giri and Hall, 2015; West et al., 2015). There is also high participation in this sector – although this varies by state (Productivity Commission, 2016). It is currently not known how much or intensely the recreational sector might fish around platforms. But with better navigation equipment and larger boats recreational fishers can travel further out and potentially access new areas (including platforms). The above-mentioned contaminant issues should therefore also be considered from a human health and food safety perspective given the active and mobile recreational sector, and the fact that catch is often taken home for consumption (with catch and release being less prevalent than in other parts of the world).

Rigs to reefs where platforms are recycled as artificial reefs may reduce pressure on natural reefs by providing alternative diving and fishing sites and opportunity for tourism. Ningaloo Reef in Western Australia is one of the sites that potentially could benefit from nearby oil and gas infrastructure to relieve growing tourism putting pressure on natural environment (Advisian, 2017). Increased activity on newly constructed reefs can have adverse effect on surrounding habitat and result in overfishing. Therefore, location of the reef needs to be carefully considered and long term monitoring and management plans need to be put in place (Bull and Love, 2019).

If the potential contribution to fisheries is to be used to justify leaving infrastructure *in situ*, the role of the infrastructure in contributing to fisheries production, rather than just aggregating fishes, need to be determined. The potential for platforms to relieve pressure on natural reefs should also be considered, together with information about local-scale fishing activity, and the implications of different decommissioning options for these activities (and associated stocks). These questions will need to be addressed in a location-specific manner in Australia, given the spatial differences that occur in target species, the nature of both commercial and recreational fisheries and the relative importance of other sectors such as tourism.

Social License and Stakeholders

Social license and social acceptance are slightly different concepts (Moffat et al., 2016) but for decommissioning imply that the activity (and the result) meets the expectations of a range of different groups in society and has their ongoing support and/or acceptance. Gaining and keeping social license is not straightforward because it involves approval from different stakeholder groups, including direct users (e.g., fishers, Traditional Owners), groups with indirect interests (e.g., tourists, media) together with political, regulatory and market-based entities (Bice et al., 2017). These stakeholder groups will have different interests and values in offshore infrastructure, the environments in which they occur, and in the decommissioning process itself, which might range from employment, recreational, cultural or environmental values through to the potential for visual disturbance associated with decommissioning activities. Understanding these values can give insight into where social license may be impacted and into processes that may contribute to social acceptance.

The importance of social license in the context of decommissioning is highlighted by the fact that "improved transparency and public engagement in relation to petroleum activities" is a key element of the Australian Government's enhanced framework for decommissioning (Commonwealth of Australia, 2020). Transparency and knowledge transfer have been key in other locations where oil and gas decommissioning has taken place, such as in the North Sea where Nexstep (National Platform for Re-use & Decommissioning)[1] was established to stimulate and facilitate collaboration amongst key stakeholders. Even though it has been 5 years since the establishment of Nextstep, policy renewal is hampered by a divergence between stakeholder alignment and the risk of reputational damage (i.e., social license) (Roos, 2019).

An example of the pertinence of social license in the Australian context is highlighted by Shaw et al. (2018) who indicate that in the case of decommissioning, industry license conditions may stipulate that full removal is required (which may have been supported by stakeholders through consultation), however

[1] https://www.nexstep.nl/

if industry later considers leaving some infrastructure behind this may not meet the expectation of the stakeholders and could compromise social license for the activity. An improved evidence base regarding social license for efficient policy and practice is required (Shaw et al., 2018). Creating reliable data sources to measure social license competitiveness is (globally) important (National Energy Resources Australia [NERA], 2017) and Australia can be a first mover is this regard. This could also include the consideration that social license is important not only for current industry responsible for paying for the decommissioning, but also for new industry "around" the decommissioning to develop. Further to this, it is not just industry's social license that needs to be considered, but also that of the relevant regulator (NOPSEMA in the Australian case). Community stakeholders must have confidence that their concerns can be heard, understood and respected, and that the regulator will enforce compliance with regulations (Van Putten et al., 2018). Maintaining that license will require the regulator to consistently demonstrate that it takes community priorities, concerns and issues into account when making decisions and enforcing industry compliance with regulations (noting that government and community expectations of regulators may evolve and mature over time).

An important aspect of social license is comprehensive and transparent approaches to stakeholder engagement and consultation. The introduction of a public comment period for submitted decommissioning environment plans and public reporting of petroleum activities have been suggested as part of a Government initiative to improve accountability for decommissioning activities (Commonwealth of Australia, 2020). But broader than these two suggestions, research into a standardised consultation process that attempts to gain social license should benefit the decommissioning process. For instance, the Free Prior and Informed Consent (FPIC) approach and associated philosophy—currently only required in cases of Indigenous stakeholder consultation—may be applicable in all communities. To undertake good stakeholder identification and consultation that incorporates the FPIC philosophy several approaches can be taken, including systematic stakeholder mapping (Raum, 2018), participatory processes, co-design and knowledge co-production (Newton and Elliott, 2016; Norström et al., 2020). Such approaches are underpinned by transparency and open consultation, together with respect for appropriate cultural protocols. Importantly, risk perspectives of Traditional Owners in the context of offshore activities and connections to sea country are often not well considered but should be incorporated in decommissioning research activities through ethical and culturally appropriate engagement (e.g., see Hedge et al., 2020). For the Australian context, this process will also need to recognise that the connections of Indigenous Peoples in Australia to land and sea Country are spatially complex (e.g., see Horton, 1996), and that multiple Traditional Owner groups may need to be engaged in consultation processes depending on the location of decommissioning activities.

In summary, factors such as the history and context of social license, spatially complex connections to Sea Country for Traditional Owners, and a large recreational fishing sector mean that engagement of stakeholders and consideration of the consequences of different decommissioning scenarios on their interests and values in offshore infrastructure will need to be carefully considered in the Australian context. More generally, to determine whether oil and gas infrastructure has value as habitat for fisheries or other species with conservation value, or conversely, to determine whether undue risk is posed by (for example) resuspending contaminated sediments, site specific assessments of the conditions around the infrastructure will need to be made. This should include an assessment of the species compositions at the infrastructure relative to nearby, natural hard and soft substrate areas, including quantifying the abundance and diversity of introduced species, and how these contribute to the inevitable compositional differences. Since many decommissioning options involve removing the upper portions of platforms (i.e., "topsides"), estimates should be made of how this removal will affect the value and productivity of the system as a whole. The oceanographic connectivity between structures and between structures and other habitats should be determined, to evaluate the potential for oil and gas infrastructure to "seed" larvae for fisheries production and/or to act as a source of introduced pests. Connectivity should also be modelled to determine whether the different pieces of infrastructure (e.g., individual platforms; sections of pipeline) in the area are acting as an interconnected ecosystem or as isolated habitat. The influence of contaminants associated with oil and gas production on the habitat value and the potential for contaminants to enter the food chain needs to be determined, especially if the area could be used for recreational or commercial fishing.

ASSESSING THE IMPACTS AND RISK OF DIFFERENT DECOMMISSIONING OPTIONS

Decommissioning presents all the hallmarks of a difficult decision-making problem. First, a choice must be made from among several options of what to do with infrastructure at the end of its useful life (as highlighted in **Table 1**). Each option has different consequences when viewed from the perspective of the various criteria—such as safety, environment, technical, economic, and societal—that influence decision makers and the stakeholders that they are accountable to. The choice of a preferred option therefore entails a trade-off between consequences measured on different scales. These consequences, however, are also shrouded in various degrees of uncertainty, which complicates the trade-off and makes the final decision vulnerable to heuristics and bias (Kahneman, 2011).

Problems of this type are common (e.g., Esmail and Geneletti, 2018) but hard to resolve with unstructured dialogue in committee settings. Consequently, a large variety of decision support tools have been developed to assist. **Table 2** summarises six tools that have been used to help identify a preferred decommissioning option and how the methods vary with the scope of the assessment.

One common approach is Multi-Criteria Decision Analysis (MCDA; **Table 2**)—a term used to describe an array of techniques

sharing three common steps: (i) specify the decision context by: (a) identifying a set of alternative choices; and (b) defining the criteria against which these alternatives will judged; (ii) conduct the analysis through some form of (usually weighted) evaluation and scoring of options against criteria; and (iii) identify the preferred option by ranking the aggregated score from highest to lowest (Esmail and Geneletti, 2018). Examples of MCDA include Net Environmental Benefit Analysis, Best Practicable Environmental Option, Multi Criteria Approval and Comparative Assessment (**Table 2**). MCDA approaches provide an opportunity to bring diverse groups of stakeholders together, increase understanding and empathy by asking them to define their values and formulate decision criteria, and encourages consensus on acceptable outcomes by explicitly incorporating these values into the decision-making process. If carefully planned and conducted, the value of MCDA lies in the shared process as well as the outcome.

Risk assessment is the second major class of tools with a large array of qualitative, semi-quantitative and quantitative techniques that are typically applied within environmental, financial and safety domains (e.g., see **Table 2**). Methods for merging risk estimates across domains, for example by converting deaths, illnesses, and environmental outcomes into monetary units or utility units, are available. National Research Council (1996) discusses the strengths and weakness of such an approach in a risk-based decision-making processes, but caution against it in favour of a less technical "deliberative analytical" process that involves analytical experts, public officials and interested and affected parties. Both qualitative and quantitative approaches have been used for decommissioning around the world (**Table 2**) and for fisheries in Australia (e.g., Hobday et al., 2011), however, techniques for merging risk estimates across different domains are rarely employed by Australia's state and federal environmental agencies.

Current Australian Government policy states that any proposed deviation from complete removal of offshore oil and gas infrastructure must deliver equal or better environmental, safety and well integrity outcomes, compared to complete removal (Australian Government Department of Industry, Science, Energy and Resources [DISER], 2018). The Environmental Plan (EP) for any such proposal must also evaluate the environmental impacts and risks of all feasible options, including partial and complete removal (National Offshore Petroleum Safety and Environmental Management Authority [NOPSEMA], 2020b). NOPSEMA warns, however, that while MCDA tools can support consultations with stakeholders on alternative decommissioning options, they do not directly relate to the acceptance criteria for an EP (as described in section 10(A) of the Offshore Petroleum and Greenhouse Gas Storage (Environment) Regulations 2009) which must demonstrate that the proposed option can be undertaken in such a way that the environmental impacts and risks, including potentially cumulative risks, can be managed to a level that is acceptable and ALARP (National Offshore Petroleum Safety and Environmental Management Authority [NOPSEMA], 2020a; **Box 3**).

In Australian waters, any proposed deviation from the decommissioning base case of complete infrastructure removal must address several information requirements and risk-related challenges:

- Sufficient understanding of the distribution and sensitivity of environmental values to decommission-related threats to distinguish low -order from high order environmental risks.

TABLE 2 | Summary of decision support tools that have been used in a decommissioning option evaluation.

Decision support tool	Summary	Reference
Net Environmental Benefit Analysis (NEBA)	Compares human and ecological risk profile of decommissioning options along with ecosystem services, and human use economic and social values. Methods based on ORNL framework but application unclear	Nicolette et al., 2014
Best Practicable Environmental Option (BPEO)	Qualitative (environmental) and quantitative (safety, cost) assessment of nine decommission options that satisfy decommissioning programming constraints (such as reduction of personnel risk wherever possible and removal of any items that could generate debris) used to identify "best" option	Hustoft and Gamblin, 1995
Multi Criteria Approval (MA)	Experts rank the order of importance of 14 environmental criteria. The median value of the standardised rank scores used to identify criteria weights. Ten options then ranked against each criterion. Option scored as "Approved" if option rank against criteria is higher than the median rank, and "Disapproved" otherwise. Options with highest number of Approvals for most important criteria identified as best	Fowler et al., 2014
Comparative Assessment (CA)	Qualitatively compares three decommissioning options (horizontal reefing in place, reefing elsewhere and removal to shore) against five criteria (safety, environment, other users of the sea, execution, and costs/schedule)	Palandro and Azivy, 2018
Probabilistic Risk Assessment (PRA)	Bayes Nets (BNs) are used to assess environmental and economic risk of options that fulfil requirements of a safety assessment. Faber et al. (2002) demonstrates this method by developing BNs to calculate probability of mission failure and expected costs for 12 sequential steps (e.g., removal of topside, cut loose and secure seabed connection, establish ballast and retraction system, etc.) in the onshore disposal of a Gravity Based Structure (GBS)	Faber et al., 2002
Quantitative Risk Assessment (QRA)	QRA has been used for accident statistics from United Kingdom and Europe between 1990 and 2002 to fit triangular density function to Serious Injury Rate (SIR) (serious injuries per 10^6 h exposure) and Fatal Accident Rate (fatalities per 10^8 h exposure) to four categories of decommission activities (onshore, offshore above water, air diving, saturation diving). Estimates of task hours in each category for different decommissioning options used to calculate relative safety risk and hence safest option	Twatchman Snyder Byrd Inc, 2003

BOX 3 | Environmental risk assessment for Australian decommissioning.

There is no single-accepted framework for environmental risk assessment but it is often characterised as a three-phase process that begins with problem formulation, followed by risk calculations, and culminating in a risk management or evaluation phase (National Research Council, 1996; United States Environmental Protection Agency [USEPA], 1998; Renn, 2008). These phases align quite well with the describe, detail and evaluate content requirements of an EP.

The problem formulation phase includes a description of the environmental values that are potentially threatened by a substance or activity (the assessment endpoints) and a hazard analysis. The hazard analysis tries to identify all the ways that the assessment endpoints interact with, and might be harmed by, a substance or activity—i.e., identify the pathways to harm or equivalently the adverse outcome pathways (Ankley et al., 2010).

In this initial stage the EP needs to demonstrate a suitable understanding of the environment(s) in which the proposed option will take place (National Offshore Petroleum Safety and Environmental Management Authority [NOPSEMA], 2019b). This understanding should address ecological, socio-economic and cultural features to ensure that the assessment endpoints adequately capture the diversity of environmental values that may be impacted, but also to allow the hazard analysis to expose the possibility of cumulative impacts through pathways that involve interactions with other industries and users.

Risk calculations usually distinguish between the likelihood of an adverse effect and the magnitude or consequence of that effects (although the nomenclature varies widely between disciplines). Methods for calculating likelihood and consequence can be broadly classified into qualitative or quantitative according to whether likelihood and consequence are expressed in a relative way using an ordinal scale (e.g., high, medium, low), or probability is used to express likelihood and a ratio scale is used to describe consequences (e.g., fish biomass, sediment concentration of a contaminant).

NOPSEMA guidance is agnostic as to which risk calculation method should be used, although any emphasis on cumulative risks effectively precludes qualitative techniques. The guidance does, however, distinguish between "higher order" and "lower order" environmental risks and impacts. The latter is defined as situations wherein the environmental value is not formally managed, is less vulnerable to the impact or risk, is widely distributed, is not protected and/or threatened, and there is confidence in the effectiveness of control measures (National Offshore Petroleum Safety and Environmental Management Authority [NOPSEMA], 2019b).

For higher order risks the EP needs to be more comprehensive which suggests that the environmental risk assessment could adopt a staged-approach, whereby an initial, relatively rapid calculation technique is used to separate and screen out low order risks from higher order ones, and then a more detailed resource intensive approach is applied to any environmental values that are identified as high order. This type of approach would be consistent with other environmental risk assessments (for example Hobday et al., 2011) and is useful when the number of potentially affected environmental values is large.

A large proportion of NOPSEMA guidance is directed towards the risk evaluation phase, perhaps because this phase can be contentious as it entails judgement about the acceptability of risks. Here the EP must demonstrate that all risks have been reduced to ALARP, and for higher-order risks must show separately that the risks are acceptable. For low-order risks, adherence to control methods specified by industry standards would be considered ALARP and thereby acceptable, but this presumes that standards for low-order interactions identified in the problem formulation or risk calculation phase exist and are relevant to Australian conditions.

For higher-order risks and impacts, the ALARP commitment requires the titleholder to implement all control measures where the cost is not grossly disproportionate to the environmental benefit, and subsequently demonstrate that any residual (or unmanaged) risks or impacts are acceptable. In practise this requires environmental standards and measurable acceptance criteria to be specified for any higher-order risks or impacts identified in the problem formulation and/or risk calculation phases, and precludes qualitative risk calculations because ordinal risk or impact estimates cannot be used to measure the magnitude of the deviation between a prediction, an observation or a measurable standard.

- Sufficient understanding of the distribution and magnitude of other socioeconomic activities in the vicinity of decommissioned infrastructure to identify the possibility of cumulative impacts.
- A risk assessment methodology that can screen-out low order risks in a relatively rapid but defensible fashion.
- Industry standards for low order impact control/risk mitigation methods and measurable acceptance criteria for any high-order environmental values.
- A quantitative risk assessment methodology that can be used to predict (possibly cumulative) risks to any high order environmental values, and demonstrate ALARP and acceptable levels of impact on these values.

RECOMMENDATIONS FOR DECOMMISSIONING RESEARCH IN AUSTRALIA

Repurposing Australian offshore oil and gas infrastructure, either as habitat for commercially or ecologically important species, for carbon capture and storage (e.g., see Hastings and Smith, 2020), or for other purposes, may, provide environmental benefit with minimal environmental risk. These risks may differ from those identified in research elsewhere in the world because of differences in biodiversity, biological productivity, ocean/climate effects (e.g., low sedimentation rates, rising temperatures, cyclonic activity, and shallow water depth), as well as sociodemographic and cultural characteristics. A thorough assessment of the ecological value of the infrastructure as habitat in the location of interest, and an environmental risk assessment, must therefore be performed, perhaps quantitatively for high order environmental values and/or cumulative risks (**Box 3**). The risk assessment should characterise the biological production at infrastructure, including relative to nearby natural habitat (such as natural reefs); the risk to both seafood contamination and ecological health posed by legacy contamination at the site (**Box 2**); and the prospective environmental risks posed by introduced species and other marine pests.

Knowledge gaps that currently preclude a comprehensive risk assessment for decommissioning in Australia, as well as other understudied regions of the world, include uncertainty about the impacts of long-term exposure to Naturally Occurring Radioactive Material (NORMs) and the unresolved potential for oil and gas infrastructure to be active areas for mercury methylation (**Box 3**). Questions about socioeconomic impacts may also be a potential obstacle to successful decommissioning. Values that are held by Australia's diverse Aboriginal and Torres Straight Island communities, must be incorporated into the decision-making process and seafood safety assessments must be culturally appropriate (Wilson et al., 2015).

We suggest that decommissioning research activities in Australia should address three key elements and interdependencies—ecological considerations, contaminants and socioeconomics (section on "Status of Decommissioning Research Internationally and in Australia," **Figure 5**), in a manner

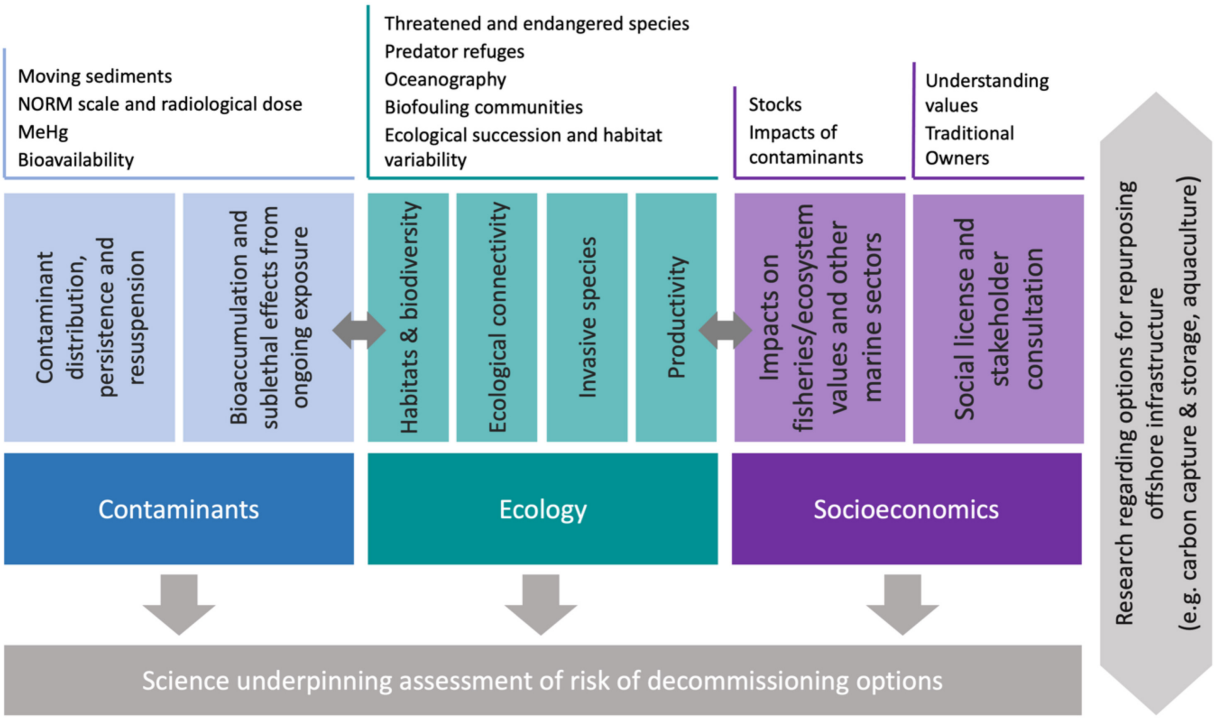

FIGURE 5 | A general framework for integrated research to assess the risk of decommissioning options for oil and gas infrastructure in Australia.

that integrates decision support tools (section on "Assessing the Impacts and Risk of Different Decommissioning Options"). The particular science questions relating to these elements are likely to be location specific, given the variability of marine environments in Australia (**Figure 1**), the different ages and types of offshore infrastructure, and potential differences related to social acceptance and consultation between different regions of Australia. Science underpinning the assessment of environmental risk of decommissioning options should be connected to research relating to options for repurposing offshore infrastructure, such as carbon capture and storage or offshore aquaculture (Sommer et al., 2019). For each decommissioning region, reviewing what is known about each of the elements in **Figure 5**, and then investing in research to address gaps, is one way to demonstrate awareness of the range of issues, and can also underpin the selection of decommissioning options for assets.

Experience in the Gulf of Mexico illustrates how an integrated research framework (**Figure 5**) can succeed. Repurposing offshore oil and gas infrastructure in a "rigs to reefs" program in this region was ultimately successful because: (i) the operators' stakeholder engagement and consultation process identified recreational fishing as a community value (reviewed in Bull and Love, 2019); (ii) surveys of contaminant levels showed that they were below thresholds of concern (Kennicutt et al., 1996a), and unlikely to be affecting benthic biodiversity (Montagna et al., 2002) or fisheries productivity (McDonald et al., 1996); and (iii) the platforms were known to provide habitat for Red Snapper, a commercially important species (Ajemian et al., 2015). These studies, when integrated, provided the scientific underpinning to maintain the social license required to support the "leave in place" decommissioning option. While there are multiple factors that distinguish the Australian decommissioning context from the Gulf of Mexico and elsewhere, the framework in **Figure 5** can be used by operators to help identify similar science needs to underpin decommissioning decisions in Australian waters. Armed with this knowledge, operators, regulators, marine stakeholders and the general public can be confident that sound decisions are being made to manage the transition of oil and gas infrastructure in an environmentally and socially acceptable way.

AUTHOR CONTRIBUTIONS

JM-T and SH conceived the study. All authors contributed to the writing of the manuscript.

ACKNOWLEDGMENTS

We thank John Keesing and Ken Fitzpatrick for valuable discussion and suggestions, and Rowan Trebilco and Derek Fulton for assistance with the figures. Thank you to Christine Lamont and David Christensen from NOPSEMA for assistance with data. Thank you to Andrew Taylor and NERA for advice on **Figure 1**. We also thank Alan Williams, Andrew Ross, and the two reviewers for constructive comments that improved previous versions of this paper.

REFERENCES

Advisian (2017). *Scientific Literature Review Environmental Impacts of Decommissioning Options*. North Sydney, NSW: Advisian.

Advisian (2020). *Offshore Oil and Gas Decommissioning Liability (Australia): Executive Summary*. Australia: NERA.

Ajemian, M. J., Wetz, J. J., Shipley-Lozano, B., Shively, J. D., and Stunz, G. W. (2015). An analysis of artificial reef fish community structure along the northwestern gulf of mexico shelf: potential impacts of "Rigs-to-Reefs" Programs. *PLoS One* 10:e0126354. doi: 10.1371/journal.pone.0126354

Amy, M., Dafforn, K., Penrose, B., Chariton, A., and Cresswell, T. (2021). Ecotoxicological effects of decommissioning offshore petroleum infrastructure: a systematic review. *Crit. Rev. Environ. Sci. Technol.* doi: 10.1080/10643389.2021.1917949

Ankley, G. T., Bennett, R. S., Erickson, R. J., Hoff, D. J., Hornung, M. W., Johnson, R. D., et al. (2010). Adverse outcome pathways: a conceptual framework to support ecotoxicology research and risk assessment. *Environ. Toxicol. Chem.* 29, 730–741. doi: 10.1002/etc.34

Arukwe, A., Nordtug, T., Kortner, T. M., Mortensen, A. S., and Brakstad, O. G. (2008). Modulation of steroidogenesis and xenobiotic biotransformation responses in zebrafish (Danio rerio) exposed to water-soluble fraction of crude oil. *Environ. Res.* 107, 362–370. doi: 10.1016/j.envres.2008.02.009

Australian Government Department of Industry, Science, Energy and Resources [DISER] (2018). *Offshore Petroleum Decommissioning Guideline*. Canberra: DISER.

Baker, C., Potter, A., Tran, M., and Heap, A. D. (2008). *Geomorphology and Sedimentology of the Northwest Marine Region of Australia. Geoscience Australia, Record 2008/07*. Canberra: Geoscience Australia, 220.

Bakke, T., Klungsoyr, J., and Sanni, S. (2013). Environmental impacts of produced water and drilling waste discharges from the Norwegian offshore petroleum industry. *Mar. Environ. Res.* 92, 154–169. doi: 10.1016/j.marenvres.2013.09.012

Balk, L., Hylland, K., Hansson, T., Berntssen, M. H. G., Beyer, J., Jonsson, G., et al. (2011). Biomarkers in natural fish populations indicate adverse biological effects of offshore oil production. *PLoS One* 6:e19735. doi: 10.1371/journal.pone.0019735

Barron, M. G., Vivian, D. N., Heintz, R. A., and Yim, U. H. (2020). Long-Term ecological impacts from oil spills: comparison of exxon valdez, hebei spirit, and deepwater horizon. *Environ. Sci. Technol.* 54, 6456–6467. doi: 10.1021/acs.est.9b05020

Beckers, F., and Rinklebe, J. (2017). Cycling of mercury in the environment: sources, fate, and human health implications: a review. *Crit. Rev. Environ. Sci. Technol.* 47, 693–794. doi: 10.1080/10643389.2017.1326277

Beckley, L. E., Muhling, B. A., and Gaughan, D. J. (2009). Larval fishes off Western Australia: influence of the Leeuwin current North-West shelf. *J. R. Soc. West. Aust.* 92, 101–109.

Benfield, M. C., Kupchik, M. J., Palandro, D. A., Dupont, J. M., Blake, J. A., and Winchell, P. (2019). Documenting deepwater habitat utilization by fishes and invertebrates associated with *Lophelia pertusa* on a petroleum platform on the outer continental shelf of the Gulf of Mexico using a remotely operated vehicle. *Deep Sea Res. I Oceanogr. Res. Pap.* 149:103045. doi: 10.1016/j.dsr.2019.05.005

Bernstein, B. B. (2015). Evaluating alternatives for decommissioning California's offshore oil and gas platforms. *Integr. Environ. Assess. Manag.* 11, 537–541. doi: 10.1002/ieam.1657

Beyer, J., Goksoyr, A., Hjermann, D. O., and Klungsoyr, J. (2020). Environmental effects of offshore produced water discharges: a review focused on the Norwegian continental shelf. *Mar. Environ. Res.* 162:105155. doi: 10.1016/j.marenvres.2020.105155

Bice, S., Brueckner, M., and Pforr, C. (2017). Putting social licence to operate on the map: a social, actuarial and political risk and licensing model (SAP Model). *Resourc. Policy* 53, 46–55. doi: 10.1016/j.resourpol.2017.05.011

Blom, W. M., and Alsop, D. B. (1988). Carbonate mud sedimentation on a temperate shelf: bass basin, southeastern Australia. *Sediment. Geol.* 60, 269–280. doi: 10.1016/0037-0738(88)90124-8

Bohnsack, J. A. (1989). Are high densities of fishes at artificial reefs the result of habitat limitation or behavioral preference? *Bull. Mar. Sci.* 44, 631–645.

Bond, T., Prince, J., McLean, D. L., and Partridge, J. C. (2020). Comparing the utility of industry ROV and hybrid-AUV imagery for surveys of fish along a subsea pipeline. *Mar. Technol. Soc. J.* 54, 33–42. doi: 10.4031/mtsj.54.3.5

Braga, M. D. A., Pavia, S. V., de Gurjao, L. M., Teixeira, C. E. P., Gurgel, A. L. A. R., Periera, P. H. C., et al. (2021). Retirement risks: invasive coral on old oil platform on the Brazilian equatorial continental shelf. *Mar. Pollut. Bull.* 165:112156. doi: 10.1016/j.marpolbul.2021.112156

Bravo, A. G., Bouchet, S., Tolu, J., Bjorn, E., Mateos-Rivera, A., and Bertilsson, S. (2017). Molecular composition of organic matter controls methylmercury formation in boreal lakes. *Nat. Commun.* 8:14255.

Bull, A. S., and Love, M. S. (2019). Worldwide oil and gas platform decommissioning: a review of practices and reefing options. *Ocean Coast. Manag.* 168, 274–306. doi: 10.1016/j.ocecoaman.2018.10.024

Carvalho, S., Moura, A., Curdia, J., da Fonseca, L. C., and Santos, M. N. (2013). How complementary are epibenthic assemblages in artificial and nearby natural rocky reefs? *Mar. Environ. Res.* 92, 170–177.

Champion, C., and Coleman, M. A. (2021). Seascape topography slows predicted range shifts in fish under climate change. *Limnol. Oceanogr.* 6, 143–153. doi: 10.1002/lol2.10185

Claisse, J. T., Love, M. S., Meyer-Gutbrod, E. L., Williams, C. M., and Pondella, D. J. II (2019). Fishes with high reproductive output potential on California offshore oil and gas platforms. *Bull. Mar. Sci.* 95, 515–534. doi: 10.5343/bms.2019.0016

Claisse, J. T., Pondella, D. J., Love, M., Zahn, L. A., Williams, C. M., Williams, J. P., et al. (2014). Oil platforms off California are among the most productive marine fish habitats globallyle. *Proc. Natl. Acad. Sci. U.S.A.* 111, 15462–15467. doi: 10.1073/pnas.1411477111

Claisse, J. T., Pondella, D. J., Love, M., Zahn, L. A., Williams, C. M., and Bull, A. S. (2015). Impacts from partial removal of decommissioned oil and gas platforms on fish biomass and production on the remaining platform structure and surrounding shell mounds. *PLoS One* 10:e0135812. doi: 10.1371/journal.pone.0135812

Codi King, S., Conwell, C., Haasch, M., Mondon, J., Mueller, J., Zhu, S., et al. (2011). "Field evaluation of a suite of biomarkers in an australian tropical reef species, stripey seaperch (*Lutjanus carponotatus*): assessment of produced water from the harriet a platform," in *Produced Water*, eds K. Lee and J. Neff (New York, NY: Springer), 608.

Commonwealth of Australia (2006). *A Guide to the Integrated Marine and Coastal Regionalisation of Australia Version 4.0*. Canberra: Department of the Environment and Heritage.

Commonwealth of Australia (2020). *Enhancing Australia's Decommissioning Framework for Oil and Gas Activities, Consultation Paper, Australian Government Department of Industry, Science, Energy and Resources*. Canberra: Australian Government.

Cordes, E. E., Jones, D. O. B., Schlacher, T. A., Amon, D. J., Bernardino, A. F., Brooke, S., et al. (2016). Environmental impacts of the deep-water oil and gas industry: a review to guide management strategies. *Front. Environ. Sci.* 4:58. doi: 10.3389/fenvs.2016.00058

Cresswell, G., and Peterson, J. (1993). The leeuwin current south of Western Australia. *Mar. Freshw. Res.* 44, 285–303. doi: 10.1071/mf9930285c

Cuttler, M., Hansen, J., Lowe, R., and Drost, E. J. F. (2018). Response of a fringing reef coastline to the direct impact of a tropical cyclone. *Limnol. Oceanogr. Lett.* 3, 31–38. doi: 10.1002/lol2.10067

Drost, E. J. F., Lowe, R. J., Ivey, G. N., Jones, N. L., and Pequignet, C. A. (2017). The effects of tropical cyclone characteristics on the surface wave fields in Australia's North West region. *Cont. Shelf Res.* 139, 35–53. doi: 10.1016/j.csr.2017.03.006

Dufois, F., Lowe, R. J., Branson, P., and Fearns, P. (2017). Tropical cyclone-driven sediment dynamics over the australian north west shelf. *J. Geophys. Res.* 122, 10225–10244. doi: 10.1002/2017jc013518

Duarte, C. M., Pitt, K. A., Lucas, C. H., Purcell, J. E., Uye, S.-i., Robinson, K., et al. (2013). Is global ocean sprawl a cause of jellyfish blooms? *Front. Ecol. Environ.* 11:91–97. doi: 10.1890/110246

Emery, B. M., Washburn, L., Love, M. S., Hishimoto, M. M., and Ohlmann, J. C. (2006). Do oil and gas platforms off California reduce recruitment of bocaccio (Sebastes paucispinis) to natural habitat? An analysis based on trajectories derived from high-frequency radar. *Fish. Bull.* 104, 391–400. doi: 10.1093/jhered/ess002

Esmail, B. A., and Geneletti, D. (2018). Multi-criteria decision analysis for nature conservation: a review of 20 years of applications. *Methods Ecol. Evol.* 9, 42–53. doi: 10.1111/2041-210X.12899

Faber, M. H., Kroon, I. B., Kragh, E., and Decosemaeker, D. B. P. (2002). Risk assessment of decommissioning options using bayesian networks. *J. Offshore Mechanics Arctic Eng.* 124, 231–238. doi: 10.1115/1.1491974

Fisher, R. S. (1998). Geologic and geochemical controls on Naturally Occurring Radioactive Materials (NORM) in produced water from oil, gas, and geothermal operations. *Environ. Geosci.* 5, 139–150. doi: 10.1046/j.1526-0984.1998.08018.x

Fowler, A. M., Jørgensen, A. M., Svendsen, J. C., Macreadie, P. I., Jones, D. O., Boon, A. R., et al. (2018). Environmental benefits of leaving offshore infrastructure in the ocean. *Front. Ecol. Environ.* 16:571–578. doi: 10.1002/fee.1827

Fowler, A. M., Macreadie, P. I., and Booth, D. J. (2015). Should we "reef" obsolete oil platforms? *Proc. Natl. Acad. Sci. U.S.A.* 112:E102. doi: 10.1073/pnas.1422274112

Fowler, A. M., Macreadie, P. I., Jones, D. O. B., and Booth, D. J. (2014). A multi-criteria decision approach to decommissioning of offshore oil and gas infrastructure. *Ocean Coast. Manag.* 87, 20–29. doi: 10.1016/j.ocecoaman.2013.10.019

Fraschetti, S., Guarnieri, G., Gambi, C., Bevilacqua, S., Terlizzi, A., and Danovaro, R. (2016). Impact of offshore gas platforms on the structural and functional biodiversity of nematodes. *Mar. Environ. Res.* 115, 56–64. doi: 10.1016/j.marenvres.2016.02.001

Fuchs, H. L., Chant, R. J., Hunter, E. J., Curchitser, E. N., Gerbi, G. P., and Chen, E. Y. (2020). Wrong-way migrations of benthic species driven by ocean warming and larval transport. *Nat. Clim. Chang.* 10, 1052–1056. doi: 10.1038/s41558-020-0894-x

Gagnon, M. M., and Bakhtyar, S. (2013). Induction of fish biomarkers by synthetic-based drilling muds. *PLoS One* 8:e69489. doi: 10.1371/journal.pone.0069489

Giri, K., and Hall, K. (2015). *South Australian Recreational Fishing Survey 2013/14, Fisheries Victoria Internal Report Series No. 62*. Queenscliff, VIC: Fisheries Victoria.

Goddard, J. H. R., and Love, M. S. (2010). Megabenthic invertebrates on shell mounds associated with oil and gas platforms off California. *Bull. Mar. Sci.* 86, 533–554.

Hastings, A., and Smith, P. (2020). Achieving net zero emissions requires the knowledge and skills of the oil and gas industry. *Front. Clim.* 2:601778. doi: 10.3389/fclim.2020.601778

Hedge, P., van Putten, E. I., Hunter, C., and Fischer, M. (2020). Perceptions, motivations and practices for indigenous engagement in marine science in Australia. *Front. Mar. Sci.* 7:522. doi: 10.3389/fmars.2020.00522

Henry, G. W., and Lyle, J. M. (2003). *The National Recreational and Indigenous Fishing Survey July 2003. FRDC Project No. 99/158*. Canberra, ACT: Australian Government Department of Agriculture.

Henry, L. A., Harries, D., Kingston, P., and Roberts, J. M. (2017). Historic scale and persistence of drill cuttings impacts on North Sea benthos. *Mar. Environ. Res.* 129, 219–228. doi: 10.1016/j.marenvres.2017.05.008

Hill, N. A., Simpson, S. L., and Johnston, E. L. (2013). Beyond the bed: effects of metal contamination on recruitment to bedded sediments and overlying substrata. *Environ. Pollut.* 173, 182–191. doi: 10.1016/j.envpol.2012.09.029

Hobday, A. J., and Campbell, G. W. (2009). Topographic preferences and habitat partitioning by pelagic fishes off southern Western Australia. *Fish. Res.* 95, 332–340. doi: 10.1016/j.fishres.2008.10.004

Hobday, A. J., Smith, A. D. M., Stobutzki, I. C., Bulman, C., Daley, R., Dambacher, J. M., et al. (2011). Ecological risk assessment for the effects of fishing. *Fish. Res.* 108, 372–384.

Holst, S., and Jarms, G. (2007). Substrate choice ad settlement preferences of planula larvae of five Scyphozoa (Cnidaria) from German Bight, North Sea. *Mar. Biol.* 151, 863–871. doi: 10.1007/s00227-006-0530-y

Hook, S. E. (2020). Beyond thresholds: a holistic approach to impact assessment is needed to enable accurate predictions of environmental risk from oil spills. *Integr. Environ. Assess. Manag.* 16, 813–830. doi: 10.1002/ieam.4321

Hook, S. E., Gallagher, E. P., and Batley, G. E. (2014). The role of biomarkers in the assessment of aquatic ecosystem health. *Integr. Environ. Assess. Manag.* 10, 327–341. doi: 10.1002/ieam.1530

Horton, D. R. (1996). *The AIATSIS Map of Indigenous Australia. Australian Institute of Aborigi- nal and Torres Strait Island Studies*. Available online at: https://aiatsis.gov.au/explore/map-indigenous-australia (Accessed April 14, 2021).

Hosseini, A., Brown, J. E., Gwynn, J. P., and Dowdall, M. (2012). Review of research on impacts to biota of discharges of naturally occurring radionuclides in produced water to the marine environment. *Sci. Total Environ.* 438, 325–333. doi: 10.1016/j.scitotenv.2012.08.047

Hustoft, R., and Gamblin, R. (1995). "Preparing for the decommissioning of the Heather Field," in *Proceedings of the Offshore Europe Conference, September 1995. Society of Petroleum Engineers 30372*, (Aberdeen).

Johnson, L. L., Arkoosh, M. R., Bravo, C. F., Collier, T. K., Krahn, M. M., Meador, J. P., et al. (2008). "The effects of polycyclic aromatic hydrocarbons in fish from Puget Sound, Washington," in *The Toxicology of Fishes*, eds R. T. Di Giulio and D. E. Hinton (Boca Raton, FL: CRC Press).

Junttila, J., Dijkstra, N., and Aagaard-Sorensen, S. (2018). Spreading of drill cuttings and sediment recovery of three exploration wells of different ages, SW Barents Sea, Norway. *Mar. Pollut. Bull.* 135, 224–238. doi: 10.1016/j.marpolbul.2018.06.064

Kahneman, D. (2011). *Thinking, Fast and Slow*. New York, NY: Farrar, Straus and Giroux, 499.

Kennedy, C. J., and Smyth, K. R. (2015). Disruption of the rainbow trout reproductive endocrine axis by the polycyclic aromatic hydrocarbon benzo a pyrene. *Gen. Comp. Endocrinol.* 219, 102–111. doi: 10.1016/j.ygcen.2015.03.013

Kennicutt, M. C., Boothe, P. N., Wade, T. L., Sweet, S. T., Rezak, R., Kelly, F. J., et al. (1996a). Geochemical patterns in sediments near offshore production platforms. *Can. J. Fish. Aquat. Sci.* 53, 2554–2566. doi: 10.1139/f96-214

Kennicutt, M. C., Green, R. H., Montagna, P., and Roscigno, P. F. (1996b). Gulf of Mexico offshore operations monitoring experiment (GOOMEX), phase I: sublethal responses to contaminant exposure - introduction and overview. *Can. J. Fish. Aquat. Sci.* 53, 2540–2553. doi: 10.1139/f96-213

Kim, H. H., Kucharzyk, K. H., Zhang, T., and Deshusses, M. A. (2013). Mechanisms regulating mercury bioavailability for methylating microorganisms in the aquatic environment: a critical review. *Environ. Sci. Technol.* 47, 2441–2456. doi: 10.1021/es304370g

King, S. C., Johnson, J. E., Haasch, M. L., Ryan, D. A. J., Ahokas, J. T., and Burns, K. A. (2005). Summary results from a pilot study conducted around an oil production platform on the Northwest Shelf of Australia. *Mar. Pollut. Bull.* 50, 1163–1172. doi: 10.1016/j.marpolbul.2005.04.027

Lang, T., Kruse, R., Haarich, M., and Wosniok, W. (2017). Mercury species in dab (*Limanda limanda*) from the North Sea, Baltic Sea and Icelandic waters in relation to host-specific variables. *Mar. Environ. Res.* 124, 32–40. doi: 10.1016/j.marenvres.2016.03.001

Lelchat, F., Dussauze, M., Lemaire, P., Theron, M., Toffin, L., and Le Floch, S. (2020). Measuring the biological impact of drilling waste on the deep seafloor: an experimental challenge. *J. Hazard. Mater.* 389:122132. doi: 10.1016/j.jhazmat.2020.122132

Love, M. S., and York, A. (2005). A comparison of the fish assemblages associated with an oil/gas pipeline and adjacent seafloor in the Santa Barbara Channel, southern California bight. *Bull. Mar. Sci.* 77, 101–117.

Love, M. S., Caselle, J. E., and Snook, L. (2000). Fish assemblages around seven oil platforms in the Santa Barbara Channel area. *Fish. Bull.* 98, 96–117.

Love, M. S., Schroeder, D. M., and Lenarz, W. H. (2005). Distribution of bocaccio (*Sebastes paucispinis*) and cowcod (*Sebastes levis*) around oil platforms and natural outcrops off California with implications for larval production. *Bull. Mar. Sci.* 77, 397–408.

Love, M. S., Caselle, J., and Snook, L. (1999). Fish assemblages on mussel mounds surrounding seven oil platforms in the Santa Barbara Channel and Santa Maria Basin. *Bull. Mar. Sci.* 65, 497–513.

Love, M. S., Kui, L., and Claisse, J. T. (2019a). The role of jacket complexity in structuring fish assemblages in the midwaters of two California oil and gas platforms. *Bull. Mar. Sci.* 95, 597–615. doi: 10.5343/bms.2017.1131

Love, M. S., Nishimoto, M. M., Snook, L., and Kui, L. (2019b). An analysis of the sessile, structure-forming invertebrates living on California oil and gas platforms. *Bull. Mar. Sci.* 95, 583–596. doi: 10.5343/bms.2017.1042

Love, M. S., Nishimoto, M., Clark, S., and Schroeder, D. M. (2012). Recruitment of young-of-the-year fishes to natural and artificial offshore structures within central and southern California waters, 2008-2010. *Bull. Mar. Sci.* 88, 863–882. doi: 10.5343/bms.2011.1101

Lyle, J. M., Stark, K. E., and Tracey, S. R. (2014). *2012-13 Survey of Recreational Fishing in Tasmania*. Hobart, TAS: The Institute for Marine and Antarctic Studies.

Macreadie, P. I., Fowler, A. M., and Booth, D. J. (2011). Rigs-to-reefs: will the deep sea benefit from artificial habitat? *Front. Ecol. Environ.* 9:455–461. doi: 10.1890/100112

Macreadie, P. I., Fowler, A. M., and Booth, D. J. (2012). Rigs-to-reefs policy: can science trump public sentiment? *Front. Ecol. Environ.* 10:179–180. doi: 10.1890/12.WB.013

Mason, R. P., Choi, A. L., Fitzgerald, W. F., Hammerschmidt, C. R., Lamborg, C. H., Soerensen, A. L., et al. (2012). Mercury biogeochemical cycling in the ocean and policy implications. *Environ. Res.* 119, 101–117. doi: 10.1016/j.envres.2012.03.013

Mathieu, A., Hanlon, J., Myers, M., Melvin, W., French, B., DeBlois, E., et al. (2011). "Studies on fish health around the Terra Nova oil development site on the Grand Banks before and after release of produced water," in *Produced Water: Environmental Risks and Advances in Mitigation Technologies*, eds K. Lee and J. Neff (New York, NY: Springer), 375–399. doi: 10.1007/978-1-4614-0046-2_20

McDonald, S. J., Willett, K. L., Thomsen, J., Beatty, K. B., Connor, K., Narasimhan, T. R., et al. (1996). Sublethal detoxification responses to contaminant exposure associated with offshore production platforms. *Can. J. Fish. Aquat. Sci.* 53, 2606–2617. doi: 10.1139/f96-217

McLean, D. L., Partridge, J. C., Bond, T., Birt, M. J., Bornt, K. R., and Langlois, T. J. (2017). Using industry ROV videos to assess fish associations with subsea pipelines. *Cont. Shelf Res.* 141, 76–97. doi: 10.1016/j.csr.2017.05.006

McLean, D. L., Taylor, M. D., Partridge, J. C., Gibbons, B., Langlois, T. J., Malseed, B. E., et al. (2018). Fish and habitats on wellhead infrastructure on the north west shelf of Western Australia. *Cont. Shelf Res.* 164, 10–27. doi: 10.1016/j.csr.2018.05.007

McLean, D., Cure, K., Abdul Wahab, M. A., Galaiduk, R., Birt, M., Vaughan, B., et al. (2021). A comparison of marine communities along a subsea pipeline with those in surrounding seabed areas. *Cont. Shelf Res.* 219:104394. doi: 10.1016/j.csr.2021.104394

Melbourne-Thomas, J., Audzijonyte, A., Brasier, M. J., Cresswell, K. A., Fogarty, H. E., Haward, M., et al. (2021). Poleward bound: adapting to climate-driven species redistribution. *Rev. Fish Biol. Fish.* doi: 10.1007/s11160-021-09641-3 Online ahead of print,

Melchers, R. E. (2006). Examples of mathematical modelling of long term general corrosion of structural steels in sea water. *Corros. Eng. Sci. Technol.* 41, 38–44. doi: 10.1179/174327806x93992

Meyer-Gutbrod, E. L., Kui, L., Nishimoto, M. M., Love, M. S., Schroeder, D. M., and Miller, R. J. (2019a). Fish densities associated with structural elements of oil and gas platforms in southern California. *Bull. Mar. Sci.* 95, 639–656. doi: 10.5343/bms.2018.0078

Meyer-Gutbrod, E. L., Love, M. S., Claisse, J. T., Page, H. M., Schroeder, D. M., and Miller, R. J. (2019b). Decommissioning impacts on biotic assemblages associated with shell mounds beneath southern California offshore oil and gas platforms. *Bull. Mar. Sci.* 95, 683–701. doi: 10.5343/bms.2018.0077

Meyer-Gutbrod, E. L., Love, M. S., Schroeder, D. M., Claisse, J. T., Kui, L., and Miller, R. J. (2020). Forecasting the legacy of offshore oil and gas platforms on fish community structure and productivity. *Ecol. Appl.* 30:e02185.

Moffat, K., and Zhang, A. (2014). The paths to social licence to operate: an integrative model explaining community acceptance of mining. *Resour. Policy* 39, 61–70. doi: 10.1016/j.resourpol.2013.11.003

Moffat, K., Lacey, J., Zhang, A., and Leipold, S. (2016). The social licence to operate: a critical review. *Forestry* 89, 477–488. doi: 10.1093/forestry/cpv044

Montagna, P. A., and Harper, D. E. (1996). Benthic infaunal long term response to offshore production platforms in the Gulf of Mexico. *Can. J. Fish. Aquat. Sci.* 53, 2567–2588. doi: 10.1139/f96-215

Montagna, P., Jarvis, S. C., and Kennicutt, M. C. (2002). Distinguishing between contaminant and reef effects on meiofauna near offshore hydrocarbon platforms in the Gulf of Mexico. *Can. J. Fish. Aquat. Sci.* 59, 1584–1592. doi: 10.1139/f02-131

National Energy Resources Australia [NERA] (2017). *Sector Competitiveness Plan 2017*. Australia: NERA.

National Energy Resources Australia [NERA] (2019). *National Decommissioning Research Initiative (NDRI) Background*. Australia: NERA.

National Offshore Petroleum Safety and Environmental Management Authority [NOPSEMA] (2019a). *Annual Report 2018-19*. Perth, WA: NOPSEMA.

National Offshore Petroleum Safety and Environmental Management Authority [NOPSEMA] (2019b). *Environmental Plan Decision Making. Document Number N-04750-GL1721 Revision 6*. Perth, WA: NOPSEMA.

National Offshore Petroleum Safety and Environmental Management Authority [NOPSEMA] (2019c). *Introducing NOPSEMA*. Perth, WA: NOPSEMA.

National Offshore Petroleum Safety and Environmental Management Authority [NOPSEMA] (2020a). *Environmental Plan Content Requirement. Document Number N-04750-GN1344 A339814*. Perth, WA: NOPSEMA.

National Offshore Petroleum Safety and Environmental Management Authority [NOPSEMA] (2020b). *Section 572 Maintenance and Removal of Property. Document Number: N-00500-PL1903 A720369*. Perth, WA: NOPSEMA.

National Offshore Petroleum Safety and Environmental Management Authority [NOPSEMA] (2021). *Decommissioning Compliance Strategy 2021-2025*. Perth, WA: NOPSEMA.

National Research Council (1996). *Understanding Risk: Informing Decisions in a Democratic Society*. Washington, DC: The National Academies Press. doi: 10.17226/5138

Neff, J., Lee, K., and DeBlois, E. M. (2011). "Produced water: overview of composition, fates, and effects," in *Produced Water: Environmental Risks and Advances in Mitigation Technologies*, eds K. Lee and J. Neff (New York, NY: Springer), 3–54. doi: 10.1007/978-1-4614-0046-2_1

Newton, A., and Elliott, M. (2016). A Typology of stakeholders and guidelines for engagement in transdisciplinary, participatory processes. *Front. Mar. Sci.* 3:230. doi: 10.3389/fmars.2016.00230

Nguyen, T. T., Cochrane, S. K. J., and Landfald, B. (2018). Perturbation of seafloor bacterial community structure by drilling waste discharge. *Mar. Pollut. Bull.* 129, 615–622. doi: 10.1016/j.marpolbul.2017.10.039

Nicolette, J., Travers, M., and Price, D. (2014). "Utilizing a net environmental benefit analysis approach to support the selection of offshore decommissioning alternatives," in *Proceedings of the 21st International Petroleum Environmental Conference*, (Houston, TX).

Nishimoto, M. M., Simons, R. D., and Love, M. S. (2019). Offshore oil production platforms as potential sources of larvae to coastal shelf regions off southern California. *Bull. Mar. Sci.* 95, 535–558. doi: 10.5343/bms.2019.0033

Norström, A. V., Cvitanovic, C., Löf, M. F., West, S., Wyborn, C., Balvanera, P., et al. (2020). Principles for knowledge co-production in sustainability research. *Nat. Sustain.* 3, 182–190.

Olsvik, P. A., Berntssen, M. H. G., Hylland, K., Eriksen, D. O., and Nolen, E. (2012). Low impact of exposure to environmentally relevant doses of Ra-226 in Atlantic cod (*Gadus morhua*) embryonic cells. *J. Environ. Radioact.* 109, 84–93. doi: 10.1016/j.jenvrad.2012.02.003

Page, H. (2019). Distribution and potential larval connectivity of the non-native *Watersipora* (Bryozoa) among harbors, offshore oil platforms, and natural reefs. *Aquat. Invasions* 14, 615–637. doi: 10.3391/ai.2019.14.4.04

Page, H. M., Dugan, J. E., Culver, C. S., and Hoesterey, J. C. (2006). Exotic invertebrate species on offshore oil platforms. *Mar. Ecol. Prog. Ser.* 325, 101–107. doi: 10.3354/meps325101

Page, H. M., Dugan, J., and Childress, J. (2005). *Role of Food Subsidies and Habitat Structure in Influencing Benthic Communities of Shell Mounds at Sites of Existing and Former Offshore oil Platforms. US Department of the Interior, Minerals Management Service, Pacific OCS Study 2005- 001. Coastal Research Center, Marine Science Institute, University of California, Santa Barbara, California. MMS Cooperative Agreement Number 14-35-0001-31063*. Santa Barbara, CA: Marine Science Institute, 32.

Palandro, D., and Azivy, A. (2018). Overview of decommissioning option assessment: a case for comparative assessment. *Paper Presented at the SPE Symposium: Decommissioning and Abandonment, Kuala Lumpur, Malaysia, December 2018*, Kuala Lumpur. doi: 10.2118/193991-MS

Palumbi, S. R. (2003). Population genetics, demographic connectivity, and the design of marine reserves. *Ecol. Appl.* 13, S146–S158.

Parkerton, T. F., Bok, M., Ireland, A. W., and Prosser, C. M. (2018). An evaluation of cumulative risks from offshore produced water discharges in the Bass Strait. *Mar. Pollut. Bull.* 126, 610–621. doi: 10.1016/j.marpolbul.2017.10.003

Pecl, G. T., Araújo, M. B., Bell, J. D., Blanchard, J., Bonebrake, T. C., Chen, I.-C., et al. (2017). The universal impacts of species on the move. *Science* 355:eaa19214.

Piola, R. F., Dafforn, K. A., and Johnston, E. L. (2009). The influence of antifouling practices on marine invasions. *Biofouling* 25, 633–644. doi: 10.1080/08927010903063065

Podar, M., Gilmour, C. C., Brandt, C. C., Soren, A., Brown, S. D., Crable, B. R., et al. (2015). Global prevalence and distribution of genes and microorganisms involved in mercury methylation. *Sci. Adv.* 1:e1500675. doi: 10.1126/sciadv.1500675

Pondella, D. J., Zahn, L. A., Love, M. S., Siegel, D., and Bernstein, B. B. (2015). Modeling fish production for Southern California's petroleum platforms. *Integr. Environ. Assess. Manag.* 11, 584–593. doi: 10.1002/ieam.1689

Pradella, N., Fowler, A. M., Booth, D. J., and Macreadie, P. I. (2014). Fish assemblages associated with oil industry structures on the continental shelf of north-western Australia. *J. Fish Biol.* 84, 247–255. doi: 10.1111/jfb.12274

Productivity Commission (2016). *Marine Fisheries and Aquaculture, Final Report*. Canberra: Productivity Commission.

Purcell, J. E. (2005). Climate effects on formation of jellyfish and ctenophore blooms: a review. *J. Mar. Biol. Ass. U.K.* 85, 461–476. doi: 10.1017/s0025315405011409

Raitt, P., Selman, A., and Lanoëlle, C. (2019). Engineering and environmental studies for decommissioning of subsea infrastructure. *APPEA J.* 59, 277–288.

Raum, S. (2018). A framework for integrating systematic stakeholder analysis in ecosystem services research: stakeholder mapping for forest ecosystem services in the UK. *Ecosyst. Serv.* 29, 170–184. doi: 10.1016/j.ecoser.2018.01.001

Reggio, V. C. Jr. (1987). *Rigs to Reefs: The Use of Obsolete Petroleum Structures as Artificial Reefs. OCSReport/MMS 87-0015*. Metairie, LA: Minerals Management Service, 17.

Regoli, F., d'Errico, G., Nardi, A., Mezzelani, M., Fattorini, D., Benedetti, M., et al. (2019). Application of a weight of evidence approach for monitoring complex environmental scenarios: the case-study of off-shore platforms. *Front. Mar. Sci.* 6:377. doi: 10.3389/fmars.2019.00377

Renn, O. (2008). *Risk Governance: Coping with Uncertainty in a Complex World*. London: Routledge, 368.

Ridgway, K. R., and Godfrey, J. S. (2015). The source of the leeuwin current seasonality. *J. Geophys. Res.* 120, 6843–6864.

Rohal, M., Barrera, N., Escobar-Briones, E., Brooks, G., Hollander, D., Larson, R., et al. (2020). How quickly will the offshore ecosystem recover from the 2010 Deepwater Horizon oil spill? Lessons learned from the 1979 Ixtoc-1 oil well blowout. *Ecol. Indic.* 117:106593. doi: 10.1016/j.ecolind.2020.106593

Roos, P. (2019). *Policy Change in Offshore Decommissioning Governance: Dealing with Environmental Politics and Coping with Ecological Uncertainty*. Masters Thesis. Wageningen: Wageningen University.

Russell, D. J. F., Brasseur, S. M. J. M., Thompson, D., Hastie, G. D., Janik, V. M., Aarts, G., et al. (2014). Marie mammals trace anthropogenic structures at sea. *Curr. Biol.* 24, R638–R639.

Schläppy, M.-L., Robinson, L., Camilieri-Asc, V., and Miller, K. (2021). Trash or treasure? Considerations for future research on oil and gas decommissioning research. *Front. Mar. Sci.* 8:642539. doi: 10.3389/fmars.2021.642539

Schlenk, D., Celander, M., Gallagher, E. P., George, S., James, M., Kullman, S. W., et al. (2008). "Biotransformation in fishes," in *The Toxicology of Fishes*, eds R. T. Di Giulio and D. E. Hinton (Boca Raton, FL: CRC Press).

Schramm, K. D., Marne, M. J., Elsdon, T. S., Jones, C. M., Saunders, B. J., Newman, S. J., et al. (2021). Fish associations with shallow water subsea pipelines compared to surrounding reefs and soft sediment habitats. *Sci. Rep.* 11:6238. doi: 10.1038/s41598-021-85396-y

Schroeder, D. M., and Love, M. S. (2004). Ecological and political issues surrounding decommissioning of offshore oil facilities in the Southern California Bight. *Ocean Coastal Manag.* 47, 21–48. doi: 10.1016/j.ocecoaman.2004.03.002

Schulze, A., Erdner, D. L., Grimes, C. J., Holstein, D. M., and Miglietta, M. P. (2020). Artificial reefs in the Northern Gulf of Mexico: community ecology amid the "Ocean Sprawl". *Front. Mar. Sci.* 7:447. doi: 10.3389/fmars.2020.00447

Sevillano-Morales, J. S., Cejudo-Gomez, M., Ramirez-Ojeda, A. M., Martos, F. C., and Moreno-Rojas, R. (2015). Risk profile of methylmercury in seafood. *Curr. Opin. Food Sci.* 6, 53–60. doi: 10.1016/j.cofs.2016.01.003

Shaw, J. L., Seares, P., and Newman, S. J. (2018). *Decommissioning Offshore Infrastructure: A Review of Stakeholder Views and Science Priorities*. Perth, WA: WAMSI, 74.

Simpson, S. L., and Batley, G. E. (2016). *Sediment Quality Assessment: A Practical Guide*. Melbourne: CSIRO Publishing, 359.

Smith, J. A., Lowry, M. B., and Suthers, I. M. (2015). Fish attraction to artificial reefs not always harmful: a simulation study. *Ecol. Evol.* 5, 4590–4602. doi: 10.1002/ece3.1730

Sol, S. Y., Johnson, L. L., Horness, B. H., and Collier, T. K. (2000). Relationship between oil exposure and reproductive parameters in fish collected following the Exxon Valdez oil spill. *Mar. Pollut. Bull.* 40, 1139–1147. doi: 10.1016/s0025-326x(00)00074-6

Sommer, B., Fowler, A. M., Macreadie, P. I., Palandro, D. A., Aziz, A. C., and Booth, D. J. (2019). Decommissioning of offshore oil and gas structures - environmental opportunities and challenges. *Sci. Total Environ.* 658, 973–981. doi: 10.1016/j.scitotenv.2018.12.193

Strain, E. M. A., Steinberg, P. D., Vozzo, M., Johnston, E. L., Abbiati, M., Aguilera, M. A., et al. (2021). A global analysis of complexity-biodiversity relationships on marine artificial structures. *Glob. Ecol. Biogeogr.* 30, 140–153.

Terlizzi, A., Bevilacqua, S., Scuderi, D., Fiorentino, D., Guarnieri, G., Giangrande, A., et al. (2008). Effects of offshore platforms on soft-bottom macro-benthic assemblages: a case study in a Mediterranean gas field. *Mar. Pollut. Bull.* 56, 1303–1309. doi: 10.1016/j.marpolbul.2008.04.024

Thomson, P. G., Fowler, A. M., Davis, A. R., Pattiaratchi, C., and Booth, D. J. (2018). Some old movies become classics - a case study determining the scientific value of ROV inspection footage on a platform on Australia's North West Shelf. *Front. Mar. Sci.* 5:471.

Twatchman Snyder Byrd Inc (2003). *Comparative Health and Safety Risk Assessment of Decommissioning Large Offshore Platforms. Study for the US Department of Interior, Minerals Management Service. TSB Project 23021*. Houston, TX: Twatchman Snyder and Byrd Inc.

Uffman-Kirsch, L. B., Richardson, B. J., and van Putten, E. I. (2020). A New paradigm for social licence as a path to marine sustainability. *Front. Mar. Sci.* 7:571373. doi: 10.3389/fmars.2020.571373

United States Environmental Protection Agency [USEPA] (1998). *Guidelines for Environmental Risk Assessment. EPA/630/R-95/002F*. Washington, DC: USEPA, 188.

Van Putten, I. E., Cvitanovic, C., Fulton, E., Lacey, J., and Kelly, R. (2018). The emergence of social licence necessitates reforms in environmental regulation. *Ecol. Soc.* 23:24. doi: 10.5751/ES-10397-230324

Villareal, T. A., Hanson, S., Qualia, S., Jester, E. L. E., Granade, H. R., and Dickey, R. W. (2007). Petroleum prouction platforms as sites for expansion of ciguatera in the northwestern Gulf of Mexico. *Harmful Algae* 6, 253–259. doi: 10.1016/j.hal.2006.08.008

Vodopivec, M., Peliz, ÁJ., and Malej, A. (2017). Offshore marine constructions as propagators of moon jellyfish dispersal. *Environ. Res. Lett.* 12:084003. doi: 10.1088/1748-9326/aa75d9

Wells, F. E. (2018). A low number of invasive marine species in the tropics: a case study from Pilbara (Western Australia). *Manag. Biol. Invasions* 9, 227–237. doi: 10.3391/mbi.2018.9.3.05

Wells, F. E., Tan, K. S., Todd, P. A., Jaafar, Z., and Yeo, D. C. J. (2019). A low number of introduced marine species in the tropics: a case study from Singapore. *Manag. Biol. Invasions* 10, 23–45. doi: 10.3391/mbi.2019.10.1.03

West, L. D., Stark, K. E., Murphy, J. J., Lyle, J. M., and Ochwada-Doyle, F. A. (2015). *Survey of Recreational Fishing in New South Wales and the ACT 2013/14, Fisheries Final Report Series No. 149*. Wollongong, NSW: NSW Department of Primary Industries.

Whyte, J. J., Jung, R. E., Schmitt, C. J., and Tillitt, D. E. (2000). Ethoxyresorufin-O-deethylase (EROD) activity in fish as a biomarker of chemical exposure. *Crit. Rev. Toxicol.* 30, 347–570. doi: 10.1080/10408440091159239

Wilson, M. J., Frickel, S., Nguyen, D., Bui, T., Echsner, S., Simon, B. R., et al. (2015). A targeted health risk assessment following the Deepwater Horizon Oil Spill: polycyclic aromatic hydrocarbon exposure in Vietnamese-American shrimp consumers. *Environ. Health Perspect.* 123, 152–159. doi: 10.1289/ehp.1408684

Wood Mackenzie (2020). *Australia Oil & Gas Industry Outlook Report*. Edinburgh: Wood Mackenzie.

Young, P., Leis, J., and Hausfeld, H. (1986). Seasonal and spatial distribution of fish larvae in waters over the North West Continental Shelf of Western Australia. *Mar. Ecol. Prog. Ser.* 31, 209–222. doi: 10.3354/meps031209

Conflict of Interest: The authors declare that the research was conducted in the absence of any commercial or financial relationships that could be construed as a potential conflict of interest.

frontiers in Marine Science

ORIGINAL RESEARCH
published: 16 September 2021
doi: 10.3389/fmars.2021.713907

Nutrient Pollution and Its Dynamic Source-Sink Pattern in the Pearl River Estuary (South China)

Wei Tao[1], *Lixia Niu*[2,3]*, *Yanhong Dong*[1], *Tao Fu*[2,3] *and Quansheng Lou*[1]

[1] South China Sea Environmental Monitoring Center of State Oceanic Administration, Guangzhou, China, [2] School of Marine Engineering and Technology, Sun Yat-sen University, Guangzhou, China, [3] Southern Laboratory of Ocean Science and Engineering, Zhuhai, China

Nutrient enrichment and its quantitative cause-effect chains of the biogeochemical processes have scarcely been documented in the Pearl River Estuary (South China). Field investigations of nutrient samples taken between 1996 and 2018 showed significant differences in nitrogen and phosphorus with times and sites. The concentrations of DIN and DIP gradually increased over the past two decades, with good fitted linear curves ($R^2 = 0.31$ for DIN, $R^2 = 0.92$ for DIP); while the temporal variation in DSi was non-significant. Higher levels of nitrogen and silicate mainly appeared in the upper estuary because of the riverine influence. The phosphorus pollution was accumulated in the northeast (e.g., Shenzhen bay). The aquatic environment was highly sensitive to nutrient pollution and eutrophication risk, which accordingly corresponded to high phytoplankton production and biodiversity. Phosphorus was the limiting factor of phytoplankton growth in this estuary, and more frequently caused the eutrophication risks and blooms. The nutrient pollution was largely influenced by riverine inputs, quantified by PCA-generation, and the contributions of coastal emission and atmospheric deposition were followed. The two-end member mixing model differentiated the physical alterations from the biological activity and identified the dynamic source-sink patterns of nutrient species. Nitrogen and silicate had relatively conservative behaviors in the estuary and phosphate showed an active pattern.

Keywords: nutrient enrichment, source and sink, environmental fate, eutrophication risk, estuary

OPEN ACCESS

Edited by:
Kenneth Mei Yee Leung, City University of Hong Kong, Hong Kong, SAR China

Reviewed by:
Rajdeep Roy, Indian Space Research Organisation, India
Richard Brum, Australian Institute of Marine Science (AIMS), Australia

***Correspondence:**
Lixia Niu
niulixia@mail.sysu.edu.cn

Specialty section:
This article was submitted to Marine Pollution, a section of the journal Frontiers in Marine Science

Received: *24 May 2021*
Accepted: *24 August 2021*
Published: *16 September 2021*

Citation:
Tao W, Niu L, Dong Y, Fu T and Lou Q (2021) Nutrient Pollution and Its Dynamic Source-Sink Pattern in the Pearl River Estuary (South China). Front. Mar. Sci. 8:713907. doi: 10.3389/fmars.2021.713907

1. INTRODUCTION

The aquatic environment in the estuary has been negatively affected by eutrophication risks and phytoplankton blooms, and the fundamental forcing is the accumulation of nutrient pollution (especially N and P) in the water column from the river to the sea (Bianchi et al., 2010; Guo et al., 2020; Potter et al., 2021). The biogeochemical properties of various nutrients vary spatially and temporally, related to the estuarine processes (Gan et al., 2014; Borges et al., 2020; Wang et al., 2021). These environmental factors and estuarine processes that influence the nutrient fluxes distribute over a large time-and-space scale. Understanding the nutrient status and their influencing factors is essential for managing the nutrient input into the estuarine coastal systems (Jiang et al., 2014; Geng et al., 2021).

Nutrients are important regulators of carbon cycling and primary production in an estuarine environment (Wang et al., 2021). Drastic increases in nutrients have posed a big threat to the

ecological stability of the marine environment (Kim et al., 2014; Yuan et al., 2021), for instance, eutrophication, red tides, and dead fishes caused by hypoxia. These environmental pressures are closely correlated with the biogeochemical characteristics of nutrient source-sink patterns (Han et al., 2012; Li et al., 2017). Correspondingly, the roles of nutrient enrichment and estuarine processes have raised the necessity to understand the biological responses (Farrow et al., 2019; Mathew et al., 2021).

This study investigates nutrient enrichment and related environmental impacts in the Pearl River Estuary (PRE; **Figure 1**), located in the Guangdong province, south China. Nutrients in the PRE are different from those in the South China

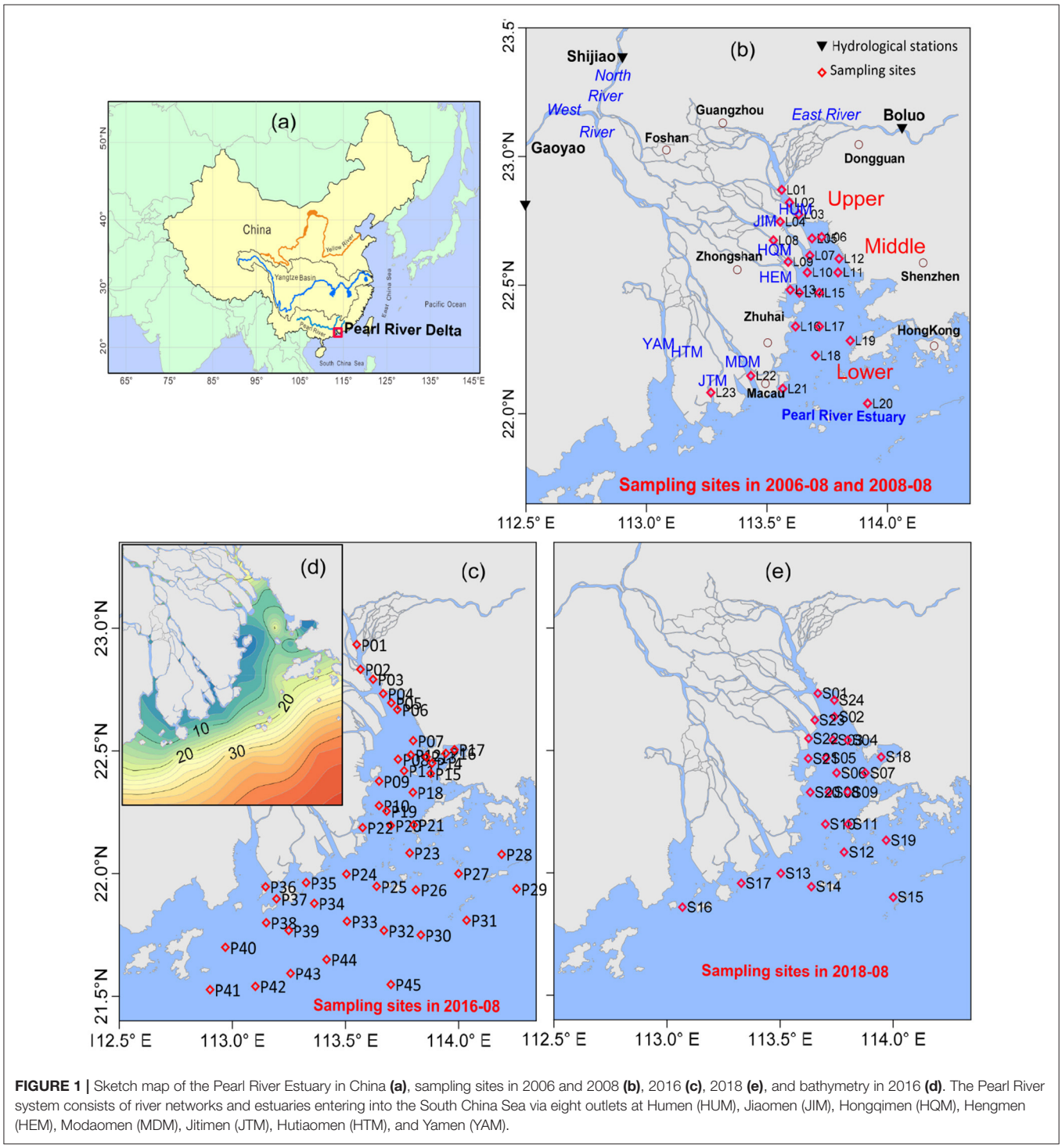

FIGURE 1 | Sketch map of the Pearl River Estuary in China **(a)**, sampling sites in 2006 and 2008 **(b)**, 2016 **(c)**, 2018 **(e)**, and bathymetry in 2016 **(d)**. The Pearl River system consists of river networks and estuaries entering into the South China Sea via eight outlets at Humen (HUM), Jiaomen (JIM), Hongqimen (HQM), Hengmen (HEM), Modaomen (MDM), Jitimen (JTM), Hutiaomen (HTM), and Yamen (YAM).

Sea and the Pearl River channels (Dai et al., 2008; Shi et al., 2019; Zeng et al., 2020). The Pearl River drainage basin discharges a large number of continuous pollutants (i.e., nutrients, PAHs, heavy metals) into the estuarine mixing zone. This estuary thus acts as a dynamic zone of source-sink exchange (Geeraert et al., 2021; Jia et al., 2021; Niu et al., 2021). The principal mechanisms of nutrient transportation in this estuary are complicated because of the strong mixing of freshwater and saline water (Cai et al., 2018; Tao et al., 2020). However, there are still few studies addressing the interacting effects of river discharge and marine current on nutrient status in the PRE.

This field investigation, conducted between 1996 and 2018, considers the interplay between river discharge, nutrients, and biological response. It is critically important that we understand the quantitative cause-effect chains of biogeochemical properties of nutrient enrichment in the 1990s (as 1996, 1999), 2000s (as 2006, 2008), and 2010s (as 2016, 2018). Moreover, the period of 1990-2000 corresponded to the high intensity of human activity (e.g., land reclamation, channel dredging) in the Pearl River Delta (Niu et al., 2020). For this purpose, the objectives of this field investigation are designed to: (1) characterize the nutrient status and related ecosystem response over the past two decades in the PRE, spatially and temporally; (2) determine the driving factors (e.g., salinity, suspended sediment, DO, and COD) that influence nutrient accumulation; (3) differentiate the source-sink exchange of nutrients; and (4) evaluate the ecological significance for estuary management.

2. MATERIALS AND METHODS

2.1. Description of the Study Area

This study is carried out in the PRE (112.9014°–114.2574° E, 21.5279°–22.9333° N). The PRE is a large-scale estuarine system in China. The Pearl River system consists of river networks (approximately a total of 322) and estuaries. The freshwater flows into the South China Sea via eight outlets (at Humen, Jiaomen, Hongqimen, Hengmen, Modaomen, Jitimen, Hutiaomen, and Yamen). Water masses are mainly influenced by the Pearl River Diluted Water, coastal current, and oceanic upwelling. The PRE receives the nutrient resources from the East and West rivers via the east four outlets. The Pearl River ranks at the second level in China regarding its freshwater discharge ($3{,}338 \times 10^8$ m^3/yr). It has a watershed area of 45.37×10^4 km^2 and a mean annual runoff discharge of 336 billion m^3/yr. The freshwater in the wet season (April-September, 80% of the total amount) is four times in the dry season (October-December, January-March, 20%) (Zhao, 1990).

The variation in the hydrology (freshwater, sediment) of the Pearl River is depicted in **Supplementary Figure 1**. Their values are the sum of Gaoyao (West River), Shijiao (North River), and Boluo (East River) hydrological stations. The annual water discharge and sediment over the past two decades (1996–2018) were 28.34×10^9 m^3 and 0.35×10^6 t, respectively. Compared with that in 1996, the water discharge changed +17% in 1999, +9% in 2006, −16% in 2008, −11% in 2016, and +22% in 2018, with the changes of sediment load at −43% in 1999, −40% in 2006, −43% in 2008, −62% in 2016, and −86% in 2018. The long term variation in freshwater was non-significant; a significant decline in sediment load was detected because of the intense human activities such as dam constructions.

2.2. Sample Collection and Analysis

Four cruise surveys were conducted in the PRE in 2006-08 (as L01–23), 2008-08 (as L01–23), 2016-08 (as P01–45), and 2018-08 (as S01–S24). Data in 1996-08 were redrawn from Zhang et al. (1999), and in 1999-07 were extracted from Zhang and Li (2010) and Lin and Li (2002). Sampling sites in this estuary, presented in **Figure 1**, were designed based on their geographic importance and estuarine characteristics. These surveys aimed to explain the nutrient pollution in the 1990s, 2000s, and 2010s, and to identify their source-sink patterns under both the natural and anthropogenic influences. Environmental properties included suspended sediment (SS), salinity, chemical oxygen demand (COD), dissolved oxygen (DO), phosphorus (PO_4), nitrite (NO_2), nitrate (NO_3), ammonium (NH_4), and silicate (SiO_4). Phytoplankton chlorophyll-*a* (Chl*a*) was also measured. DIN is the sum of NO_2, NO_3, and NH_4.

Water samples at different water layers (surface, middle, and bottom) were collected in the Niskin bottles. Here, we focused mostly on surface water samples. Salinity and water depth were measured *in situ* with a Conductivity-Temperature-Depth/Pressure Profiler (CTD, Sea-bird Electronics, USA). The concentrations of SS were weighed in the laboratory. Samples for various nutrients and chlorophyll-*a* were filtered in the field using a 0.45 μm cellulose acetate filter. These treated filtrates were stored at cool and were shipped back to the lab for further analysis. The concentrations of nutrients, DO, COD, and chlorophyll-*a* were determined according to the specification of marine monitoring (GB 17378-2007). The concentrations of dissolved nutrients were determined by colorimetry. The COD concentration was determined by the alkaline permanganate method. The DO concentration was determined by the iodometry method. The concentrations of chlorophyll-*a* were determined by UV spectrophotometry. **Table 1** displays the summary of water quality variables and their ranges in the PRE.

2.3. Statistical Analysis

The case area is approximately divided into three zones according to the estuarine dynamics: upper-PRE (salinity <10; near the mouth), middle-PRE (10 <salinity <20; and lower-PRE (salinity >20). Spatial distributions of variables are plotted with Golden Software Surfer 13. The linkages between environmental factors (salinity, suspended sediment, DO, COD) and nutrients are discussed using the Pearson correlation analysis and regression analysis. The level of significance level less than 0.05 (p <0.05) is defined as statistically significant. A principal component analysis (PCA) is applied to explore the associations between phytoplankton chlorophyll and environmental factors (Niu et al., 2015; Chai et al., 2016). Each variable is standardized to unit prior to PCA. The data preparations for Pearson correlation, linear regression, and PCA are conducted using the statistical package IBM SPSS Statistics 20 for Windows.

TABLE 1 | Summary of water quality parameters and their ranges in the Pearl River Estuary.

Variable	Unit	2006	2008	2016	2018	Sample analysis
Dissolved oxygen (DO)	mg L^{-1}	0.83–6.73	3.41–7.24	1.9–10.48	3.69-6.68	Iodometry
Chemical oxygen demand (COD)	mg L^{-1}	–	0.5–2.95	0.19–3.36	0.32-2.94	Alkaline permanganate method
Salinity	‰	0.22–33.51	0.17–32.09	0.95–33.68	0.98–32.55	CTD
Suspended sediment (SS)	mg L^{-1}	2.9–105.5	1.5–91.3	–	2.1–46.7	Gravimetric analysis
Dissolved phosphorus (DIP)	mg L^{-1}	0.002–0.119	0.016–0.051	0.003–0.232	0.002–0.096	Colorimetry
Dissolved inorganic nitrogen (DIN)	mg L^{-1}	0.044–1.819	0.239–1.797	0.024–2.487	0.085–2.35	Colorimetry
Dissolved silicate (DSi)	mg L^{-1}	0.6–5.86	0.59–3.89	0.034–4.89	–	Colorimetry
Chlorophyll-*a* (Chla)	μg L^{-1}	0.49–13.62	0.8–7	0.15–21.11	0.42–10.15	UV spectrophotometry

The two end-member mixing model is introduced to differentiate biological processes from the effects of physical mixing, as used in the earlier studies of Han et al. (2012), Wu et al. (2016), Li et al. (2017), and Niu et al. (2020). These two end members have different nutrient conditions. The freshwater end-member is dominated by physical forcing with high nutrient concentrations, and the sea end-member correlates with marine currents. The mixing model is based on nutrient-salinity relationships (Rowe and Chapman, 2002; Kim et al., 2020), described as:

$$F_1 + F_2 = 1 \tag{1}$$

$$S_1F_1 + S_2F_2 = S_{in-situ} \tag{2}$$

where $S_{in-situ}$ is the measured salinity; F_1 is the freshwater fraction, and F_2 is the seawater fraction; S_1 and S_2 denote the salinity levels of the two end-members.

The conservative nutrient concentrations of DIN (N*), DIP (P*), and DSi (Si*) calculated by the mixing model are given as:

$$N^* = DIN_1F_1 + DIN_2F_2 \tag{3}$$

$$P^* = DIP_1F_1 + DIP_2F_2 \tag{4}$$

$$Si^* = DSi_1F_1 + DSi_2F_2 \tag{5}$$

where DIN_1, DIN_2, DIP_1, DIP_2, DSi_1, and DSi_2 are the corresponding concentrations of the two end-members for DIN, DIP, and DSi.

The difference/deviation between the model predictions and measurements is defined as Δ, which reflects the status of nutrient production (Δ <0) or uptake (Δ >0) associated with the biological response.

$$\Delta DIN = N^* - DIN_{in-situ} \tag{6}$$

$$\Delta DIP = P^* - DIP_{in-situ} \tag{7}$$

$$\Delta DSi = Si^* - DSi_{in-situ} \tag{8}$$

To evaluate water quality pollution in this estuary, classification of environmental quality assessment (EQA) based on the improved NCCR (EPA, 2008) and eutrophication risk assessment (Karydis et al., 1983; Zhang et al., 2009; Tao et al., 2020) are introduced to quantify the nutrient pollution in the PRE over the past two decades. The water bodies are classified as eutrophic when the eutrophication level is larger than 1. High eutrophication (>5) indicates a more severe environment.

3. RESULTS AND DISCUSSION

3.1. Characteristics of Environmental Variables in the Estuary

The temporal distributions of DO, COD, suspended sediment (SS), and salinity in the PRE between 1996 and 2018 are presented in **Supplementary Figure 2**. DO showed a relatively declined trend between 1999 and 2018. The summer DO ranged from 5.57–7.51 mg L^{-1} in 1999, 0.83–6.73 mg L^{-1} in 2006, 3.41–7.24 mg L^{-1} in 2008, 1.90–10.84 mg L^{-1} in 2016, and 3.69–6.68 mg L^{-1} in 2018. Partial hypoxia (DO <3 mg L^{-1}) occurred occasionally in the waters (as stations L01, L03, L05, L06, L10, L14, and L22 in 2006; and stations P01-P06 in 2016), thereby increasing the ecological risks to the aquatic microorganisms (Braga et al., 2000). Partial hypoxia closely correlated with the anthropogenic nutrient inputs to the estuary. The difference in annual COD was non-significant. The mean COD concentration in the entire estuary was 1.36 mg L^{-1} in 1999, 1.41 mg L^{-1} in 2008, 1.53 mg L^{-1} in 2016, and 1.12 mg L^{-1} in 2018.

The spatial distribution of salinity was displayed in **Supplementary Figure 3**. The mean salinity was 6.95 in 1996, 6.64 in 1999, 17.4 in 2006, 12.99 in 2008, 14.11 in 2016, and 13.13 in 2018. The average salinity in the entire estuary was less than 10 before 2000, while the level increased after 2000. These salinity results suggested that the saline water intruded into the upper estuary due to intense anthropogenic pressures (e.g., land reclamation, sand mining, channel dredging) after 2000. Horizontally, salinity increased southward, and also was relatively high in the eastern zone. The SS trend was inversely distributed in the estuary with the salinity. Temporally, the mean SS concentration was 17.42 mg L^{-1} in 1996, 23.07 mg L^{-1} in 1999, 32.55 mg L^{-1} in 2006, 16.98 mg L^{-1} in 2008, and 30.1 mg L^{-1} in 2018. The SS concentrations were relatively high in the western and northern PRE and decreased from the southwest to the southeast estuary (Zhang et al., 2019). Heavy rainfall during summer raised the water level, and large

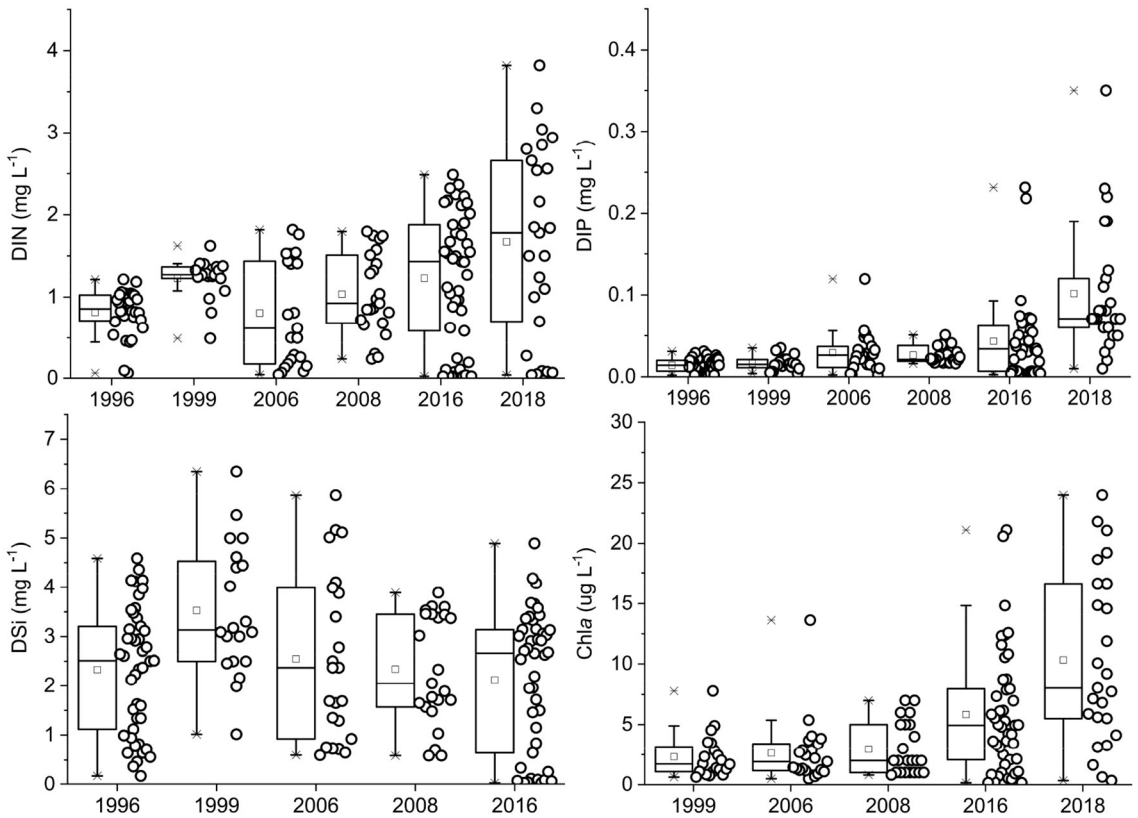

FIGURE 2 | Boxplot graphics of DIN, DIP, DSi, and phytoplankton chlorophyll between 1996 and 2018 in the Pearl River Estuary.

volumes of runoff then discharged more terrigenous sediments into the PRE, which also increased the SS concentrations in that area. Moreover, freshwater forcings in summer were strong and bottom sediments were potentially carried to the surface, resulting in additional re-suspended sediment in the water column (Zhang and Li, 2010).

3.2. Nutrient Enrichment in an Estuarine Environment

The nutrient levels (DIN, DIP, DSi) showed significant variability (p <0.05) in the PRE, temporally and spatially. The concentrations of dissolved nutrients exhibited a clear decreasing trend from the river to the sea (**Figures 2**, **3**). DIN in the entire estuary ranged from 0.07 mg L^{-1} to 1.21 mg L^{-1} (mean 0.81 mg L^{-1}) in 1996, 0.49–1.62 mg L^{-1} (1.22 mg L^{-1}) in 1999, 0.04–1.82 mg L^{-1} (0.80 mg L^{-1}) in 2006, 0.24–1.80 mg L^{-1} (1.04 mg L^{-1}) in 2008, 0.02–2.49 mg L^{-1} (1.23 mg L^{-1}) in 2016, and 0.04–3.82 mg L^{-1} (1.67 mg L^{-1}) in 2018. DIN levels in the surface waters were higher than that in the bottom layers, which was consistent with the previous studies (Yin et al., 2001; Li et al., 2017). Higher DIN values appeared in the upper-PRE, with the mean value of 1.33 mg L^{-1} in 1999, 1.54 mg L^{-1} in 2006, and 2.29 mg L^{-1} in 2016; the west zone of the estuary was more enriched in DIN than the east, implying the contributions of the river channels (i.e., Humen, Hengmen, Jiaomen, Hongqimen). These findings suggested that riverine input was one of the important DIN sources. Over time, DIN gradually increased from 1996 to 2018, with a fitted linear curve (R^2= 0.31, N=6). Among the DIN compositions, NO_3 was the most abundant form (**Supplementary Figure 4**), as reported from other studies in this estuary (Huang et al., 2003; Zhang et al., 2016; Niu et al., 2020; Tao et al., 2020). The proportions of NO_2 and NH_4 were followed. The mean value of NO_3 was 0.63 mg/L in 2006, 0.89 mg/L in 2008, 0.99 mg/L in 2016, and 1.03 mg/L in 2018, accounting for 75, 83, 72, and 81% of DIN, accordingly. NO_3 was mainly detected from the atmospheric deposition and agricultural applications (e.g., fertilizers, pesticides) in the Pearl River basin (Niu et al., 2020). The runoff transported the NO_3 from the upper channel to the estuary.

The DIP concentration in this estuary was relatively low. DIP significantly increased during the sampling periods, with a good fitted linear curve (R^2 = 0.85, N = 6). The DIP concentrations in the total area varied from 0.002–0.029 mg L^{-1} in 1996, 0.004–0.035 mg L^{-1} in 1999, 0.002–0.119 mg L^{-1} in 2006, 0.016–0.051 mg L^{-1} in 2008, 0.003–0.231 mg L^{-1} in 2016, and 0.010–0.350 mg L^{-1} in 2018. The heavy contamination of DIP (>0.03 mg L^{-1}; threshold value of severe pollution) mainly occurred in the northeast zone of the PRE (e.g., Shenzhen coast, Shenzhen Bay), declining to the southwest estuary. The DIP pattern in the entire estuary was different when compared with the spatial trend of

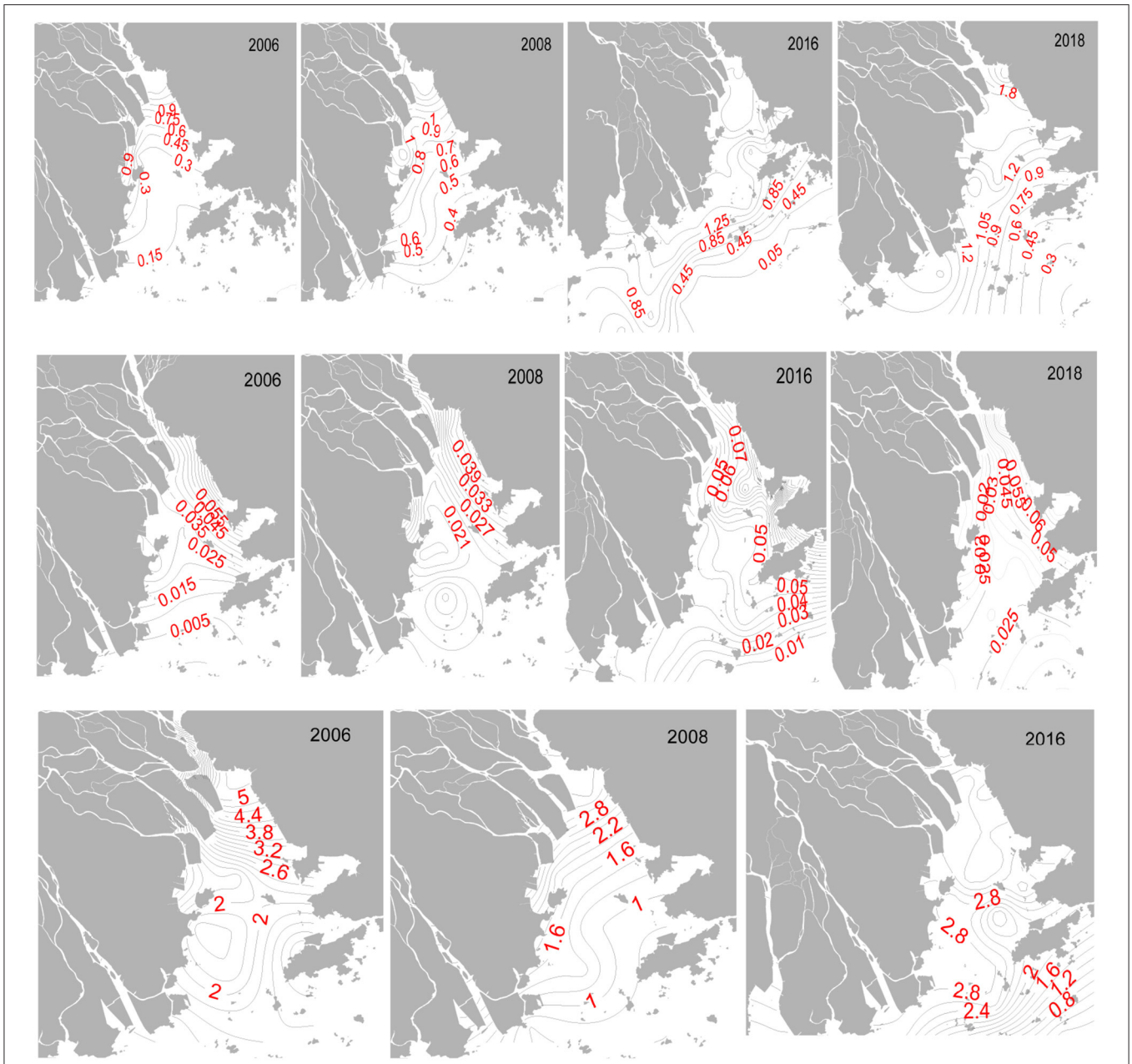

FIGURE 3 | Spatial variations of DIN, DIP, and DSi (unit: mg L^{-1}) in surface water of the Pearl River Estuary.

DIN. These results of DIN and DIP implied that land-based pollutants from the cities of Shenzhen and Dongguan greatly contributed to the DIP levels, and riverine inputs were the main contributor of DIN.

The horizontal distribution of DSi (SiO_4) was similar with DIN (**Figures 3**, **5**). The DSi levels ranged from 0.183–4.59 mg L^{-1} in 1996, 1.023–6.35 mg L^{-1} in 1999, 0.603–5.86 mg L^{-1} in 2006, 0.593–3.89 mg L^{-1} in 2008, and 0.033–4.89 mg L^{-1} in 2016. DSi in the PRE exhibited a significant spatial variation and a non-significant temporal difference over the past two decades.

Compared with many estuarine systems in the world, as listed in **Supplementary Table 1**, the nutrient pollution in the PRE was classified at a severe level. The DIN level in this area was lower than that in the Tweed estuary (Uncles et al., 2003). However, the nutrient concentration in the PRE was still much higher than that in the Yellow River estuary (Wang et al., 2017), the Cochin estuary (Vipindas et al., 2018; Jabir et al., 2020), the Tagus River estuary (Borges et al., 2020), the Caete estuary (Monteiro et al., 2016), and the Razdolnaya River estuary (Shulkin et al., 2018). The DIP was at a comparable level. The DSi concentration in

this estuary was lower than that in the Yangtze River estuary (Chai et al., 2006), but higher than that in the Yellow River estuary (Wang et al., 2017), the Tagus River estuary (Borges et al., 2020), the Razdolnaya River estuary (Shulkin et al., 2018), and the Tweed estuary (Uncles et al., 2003). Therefore, the water quality pollution caused by nitrogen and phosphorus species should be primarily concerned with avoiding more deterioration in the PRE ecosystems.

3.3. Phytoplankton Chlorophyll and Eutrophication Risk

A large amount of nutrients in summer were discharged from rivers into the PRE, which would potentially favor the phytoplankton growth. Chlorophyll-*a* levels in the entire estuary varied widely overtime periods (**Supplementary Figure 5**), ranging from 0.63–7.79 μg L^{-1} in 1999, 0.49–13.62 μg L^{-1} in 2006, 0.50–7.0 μg L^{-1} in 2008, 0.15–21.11 μg L^{-1} in 2016, and 0.42–10.15 μg L^{-1} in 2018. Spatial difference in chlorophyll was significant (p <0.05). The high chlorophyll-*a* levels in 1999, 2006, and 2008 were mainly distributed in the middle and lower estuary, while the high values in 2016 and 2018 were near the river mouths and coasts (Dai et al., 2008; Wei and Huang, 2010; Li et al., 2014). The East River discharged the most pollutants from a major city group (i.e., Guangzhou, Dongguan, and Foshan) through the Humen mouth. Several channels of the West River and North River transported the riverine pollutants through Jiaomen, Hongqimen, and Hengmen. Vertically, chlorophyll-*a* levels decreased with the water depth because of the enrichment of nutrient resources in the surface layer.

The nutrient enrichment would induce the rapid growth of phytoplankton and high eutrophication risk. The eutrophication level in the PRE varied from 0.58 to 30.49 (mean 9.86) in 2008 and 0.003 to 184.71 (31.53) in 2016 (**Supplementary Figure 6**). The aquatic environment of the PRE in 2016 was more polluted than that in 2008, be related to the nutrient characteristics in that period. The total trend of eutrophication level in the estuary was similar to nitrogen and phosphorus, declining from the mouth to the sea. Most of the estuary was classified as eutrophic (E >1). The eutrophication level in the northeast PRE (E >5; e.g., Shenzhen and Dongguan coasts) was higher than that in the southwest. The pollution of eutrophication was negatively and significantly correlated with salinity (Niu et al., 2020; Zeng et al., 2020), demonstrated that the dilution-mixing process of marine waters strongly influenced the eutrophication risk. Based on the EQA, the overall water environment in the PRE was poor-general in 2006, general in 2008, general-poor in 2016, and poor in 2018 (**Table 2**). The aquatic environment in most zones of the PRE was classified as sub-healthy, mainly caused by DIN and DIP during these sampling periods.

3.4. Nutrient Distribution Shaping Phytoplankton Chlorophyll

3.4.1. Nutrient Limitation of Phytoplankton Growth

The stoichiometric requirement for phytoplankton growth suggested that the molar ratio of N:P ranged at 12–22 (mean 16) and Si: N was 1 (Redfield, 1958; Justic et al., 1995). Potential nutrient limitations were identified as follows (Justic et al., 1995): P was limiting if Si:P >22 and N:P >22, N was limiting if N:P <12 and Si: N >1, and Si was limiting if Si:P <12 and Si: N <1. **Figure 4** plots the nutrient ratios (N:P, Si: N, and Si:P) for distinguishing the nutrient limitation of the phytoplankton growth. The average N:P ratio in the total estuary was 212 in 1999, 71 in 2006, 97 in 2008, and 79 in 2016. The average Si:N was 1.42 in 1999, 3.23 in 2006, 1.15 in 2008, and 0.89 in 2016. In 1999 and 2006, only P-limitation was predominantly detected in the whole estuary. Si-and N-limitation occurred occasionally in 2016. Low PO_4 levels, relative to nitrogen and silicate, limited the phytoplankton production in most zones of the PRE. Similar results were also reported by the previous studies (Yin et al., 2004; Zhang et al., 2013; Gan et al., 2014; Li et al., 2017; Niu et al., 2020).

3.4.2. Correlation Between Chlorophyll-*a* and Environmental Factors

The source/sink exchange made the PRE more complex and played an important role in the estuarine ecosystems. Changes in the hydrological cycles affected the distribution of nutrient resources; these forces were the fundamental demand for phytoplankton growth. Principal component analysis (PCA) identified the impact-effect paths of phytoplankton chlorophyll and environmental factors and distinguished the major factors in each path. The first three components were extracted to represent most of the information (eigenvalue >1), shown in **Table 3**, with the cumulative proportion of 77% in 1999, 81% in 2006, and 83% in 2018. **Figure 5** presents the first two-component loading.

In 1999, PC1 with an eigenvalue of 3.95, accounting for 43.89% of the total variance, was heavily weighed by nutrients and salinity. In PC2 (19.86%), chlorophyll and suspended sediment were dominant. In which, nutrients positively contributed to phytoplankton chlorophyll, characterized by the uptake process; salinity and suspended sediment negatively influenced the chlorophyll level, characterized by the external driving force. In 2006, PC1 (46%) was dominated by salinity, suspended sediment, nitrogen, and silicate; PC2 (22%) was mainly represented by DO; chlorophyll-*a* and phosphorus were the main contributors in PC3 (13%). In 2018, salinity and nitrogen were the main contributors in PC1, phosphorus and DO in PC2, and suspended sediment and chlorophyll-*a* in PC3.

In summary, these PCA findings demonstrated the underlying mechanisms of nutrient enrichment, involved with the environmental stresses. Salinity, nitrogen, and silicate showed similar contributions to the chlorophyll-*a* during the time periods. In particular, salinity negatively correlated with phytoplankton chlorophyll, and the influence was transferred through the role of salinity on the nutrients. However, phosphorus and suspended sediment behaved differently. Phosphorus species were closely linked to NO_3 and silicate in 1999, and to NH_4 in 2006 and 2016. The suspended sediment displayed a negative role in 1999 and a positive effect in 2006 and 2016. The direct effects of salinity and suspended sediment on phytoplankton were less than that on the nutrient distributions, although riverine discharge would directly affect the phytoplankton production (Chou et al., 2012). Specifically,

TABLE 2 | Classification of environmental quality assessment in the Pearl River estuary.

Site	1999				Site	2006				Site	2016			
	Chla	DO	DIP	DIN		Chla	DO	DIP	DIN		Chla	DO	DIP	DIN
1	Good	Good	Good	Poor	L01	General	Poor	Good	Poor	P01	General	Poor	Poor	Poor
2	Good	Good	Good	Poor	L02	Good	General	Poor	Poor	P02	General	Poor	Poor	Poor
3	Good	Good	Good	Poor	L03	Good	Poor	Poor	Poor	P03	General	Poor	Poor	Poor
4	Good	Good	Good	Poor	L04	Good	Good	Good	Poor	P04	General	Poor	Poor	Poor
7	Good	Good	Good	Poor	L05	Good	Poor	Good	Poor	P05	General	General	Poor	Poor
9	Good	Good	Poor	Poor	L06	Good	Poor	Poor	Poor	P06	General	Poor	Poor	Poor
10	Good	Good	Good	Poor	L07	Good	Poor	Poor	Poor	P07	Good	Good	Poor	Poor
18	Good	Good	Good	Poor	L08	Good	Good	Good	Poor	P08	Good	General	Poor	Poor
13	Good	Good	Good	Poor	L09	Good	Good	Good	Poor	P09	General	Good	Poor	Poor
14	Good	Good	Good	Poor	L10	Good	Poor	Poor	Poor	P10	General	Good	Poor	Poor
15	Good	Good	Good	Poor	L11	Good	Poor	Poor	Poor	P11	Good	General	Poor	Poor
16	General	Good	Poor	Poor	L12	Good	General	Poor	Poor	P12	Good	Poor	Poor	Poor
17	Good	Good	Good	Poor	L13	Good	Good	Good	Poor	P13	Good	General	Poor	Poor
19	Good	Good	Good	Poor	L14	Good	Poor	Good	Good	P14	General	Good	Poor	Poor
20	Good	Good	Good	Poor	L15	Good	Poor	Good	Good	P15	Good	Good	Poor	Poor
21	Good	Good	Good	Poor	L16	Good	Poor	Poor	Poor	P16	General	Poor	Good	Poor
22	Good	Good	Good	Poor	L17	Good	Poor	Good	Good	P17	General	General	Good	Poor
23	Good	Good	Good	Poor	L18	General	Poor	Good	Good	P18	Good	Good	Poor	Poor
24	Good	Good	Good	Poor	L19	Good	General	Good	Good	P19	Good	Good	Poor	Poor
25	Good	Good	Good	Poor	L20	Good	Good	Good	Good	P20	General	Good	Poor	Poor
Overall evaluation: General					L21	Good	Good	Good	Good	P21	Good	Good	Poor	Poor
					L22	Good	Poor	Good	Good	P22	General	Good	Poor	Poor
					L23	Good	Good	Good	Good	P23	Good	Good	Poor	Poor
					Overall evaluation: Poor-General					P24	General	Good	Good	Poor
										P25	General	Good	Good	Poor
										P26	Good	Good	Good	Good
										P27	Good	Good	Good	Good
										P28	Good	Good	Good	Good
										P29	Good	Good	Good	Good
										P30	Good	Good	Good	Good
										P31	Good	Good	Good	Good
										P32	Good	Good	Good	General
										P33	Good	Good	Good	Good
										P34	Good	Good	Poor	Poor
										P35	General	Good	Poor	Poor
										P36	Good	Good	Poor	Poor
										P37	Good	Good	Poor	Poor
										P38	Good	Good	Good	Poor
										P39	Good	Good	Poor	Poor
										P40	Poor	Good	Good	Poor
										P41	Poor	Good	Good	Poor
										P42	General	Good	Good	Good
										P43	General	Good	Good	Poor
										P44	Good	Good	Good	Good
										P45	Good	Good	Good	Good
										Overall evaluation: General-Poor				

suspended sediment adsorbed the particulate phosphorus via humic acid and iron oxyhydroxide ($Fe(OH)_2$), which would impact the P transformation (Lin et al., 2004).

The above findings also implied different sources for nitrogen-silicate and phosphorus. The human activities induced in the 1990s of the PRE were land reclamation and channel dredging,

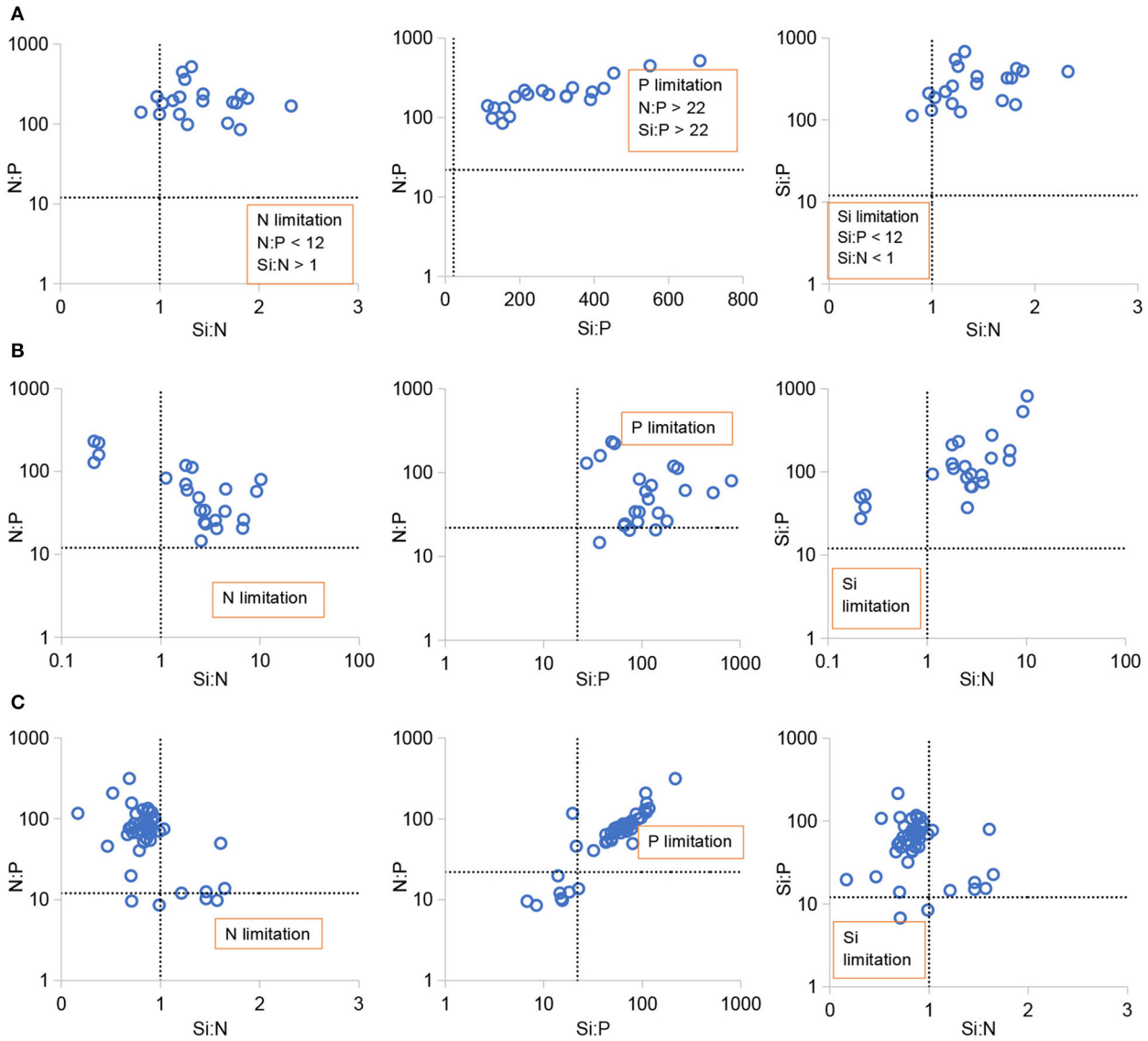

FIGURE 4 | Scatter diagrams of atomic nutrient ratios (N:P, Si:N, and Si:P) during summer in the Pearl River estuary in 1999 **(A)**, 2006 **(B)**, and 2016 **(C)**.

resulting in a declined water area. The estuary then became narrower and deeper, preventing the diffusion and transport of the pollutants (Li et al., 2014; Wu et al., 2016; Niu et al., 2020). Therefore, the nutrient pollution caused by nitrogen and silicate was detected in the upper estuary because of the riverine influence. The phosphorus pollution mainly appeared in the northeast (e.g., Shenzhen bay) and was transported with the salinity front to the sea. It was the reason why the high phytoplankton production appeared in the middle/lower estuary.

3.5. Factors Influencing Nutrient Source-Sink Patterns

3.5.1. Nutrient-Salinity Relationships

Hydrological factors controlled the distributions of nutrients and influenced the riverine inputs (Castillo, 2020; Geng et al., 2021; Zhang et al., 2021). Our study regions were within the contour 30 m, and the salinities were <34 (**Supplementary Figure 3**). The mixing process of freshwater and saline water in that area would influence the spatiotemporal distributions of dissolved nutrients. **Figure 6** plots the nutrient-salinity correlations over the past two decades. The correlation coefficient (R^2) between salinity and DIN was 0.86 in 1999 ($N = 27$, $p < 0.01$), 0.98 in 2006 ($N = 23$, $p < 0.01$), 0.90 in 2008 ($N = 23$, $p < 0.01$), 0.92 in 2016 ($N = 45$, $p < 0.01$), and 0.83 in 2018 ($N = 25$, $p < 0.01$); the coefficient for DIP was 0.44 in 1999 ($p < 0.01$), 0.22 in 2006 and 0.67 in 2016 ($p < 0.01$); for DSi was 0.39 in 1999 ($p < 0.01$), 0.89 in 2006 ($p < 0.01$), 0.97 in 2008 ($p < 0.01$), and 0.89 in 2016 ($p < 0.01$). The slopes of DIN-salinity and DSi-salinity were similar during the sampling times. Off the river mouth, DIN and DSi concentrations continued to decrease as the salinity increased, while DIP concentrations were

TABLE 3 | PCA-generated identification between phytoplankton chlorophyll and environmental factors.

		Extraction sums of squared loading			Component loading in 1999				Component loading in 2006				Component loading in 2018			
		Eigenvalue	Proportion (%)	Cumulative (%)		PC 1	PC 2	PC 3		PC 1	PC 2	PC 3		PC 1	PC 2	PC 3
1999	PC1	3.95	43.89	43.89	Salinity	**−0.87**	0.31	0.24	Salinity	**−0.9**	0.4	0.06	Salinity	**−0.91**	−0.04	−0.35
	PC2	1.79	19.86	63.75	NO_3	**0.95**	0.11	−0.12	NO_3	**0.8**	−0.54	−0.13	NO_3	**0.98**	0.08	0.11
	PC3	1.21	13.46	**77.21**	NH_4	0.46	−0.06	**0.70**	NH_4	0.49	−0.21	**0.62**	NH_4	0.08	**0.93**	0.1
2006	PC1	4.57	45.66	45.66	DIP	**0.7**	0.4	0.07	DIP	0.53	0.35	0.56	DIP	0.34	**0.86**	−0.21
	PC2	2.16	21.56	67.21	DSi	**0.7**	0.43	0.05	DSi	**0.70**	0.66	0.05	DO	−0.02	−0.65	−0.18
	PC3	1.34	13.42	**80.63**	DO	0.12	−0.37	**0.73**	DO	−0.27	**-0.86**	0.2	DIN	**0.93**	0.31	0.14
2018	PC1	5.02	50.21	50.21	DIN	**0.96**	0.11	−0.1	DIN	**0.90**	−0.41	0.01	*Chla*	0.37	0.25	**0.78**
	PC2	2.1	21	71.22	*Chla*	−0.34	**0.81**	0	*Chla*	0.27	0.04	0.61	SS	0.09	−0.04	**0.86**
	PC3	1.22	12.19	**83.4**	SS	0.25	**−0.72**	−0.29	SS	0.66	0.02	−0.46	COD	0.58	0.39	0.59
									NO_2	**0.84**	0.44	0.05	NO_2	0.17	**0.86**	0.15

The bold value indicates a high loading.

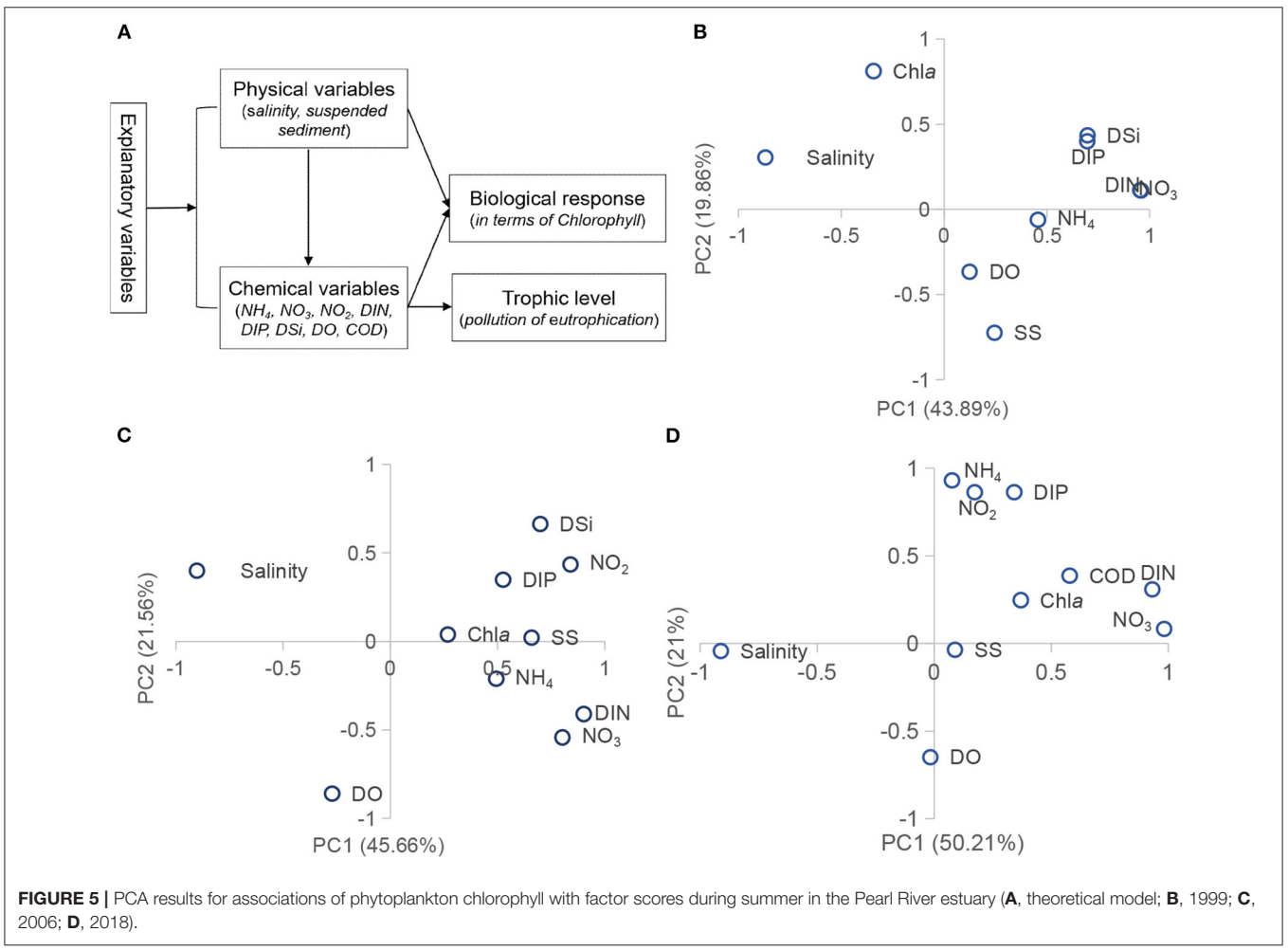

FIGURE 5 | PCA results for associations of phytoplankton chlorophyll with factor scores during summer in the Pearl River estuary (**A**, theoretical model; **B**, 1999; **C**, 2006; **D**, 2018).

more variable, probably because of the external P sources such as P cycling and regeneration, biodegradation, emissions of coastal cities, and adsorption of sediment.

Dissolved nutrients were negatively significantly correlated with salinity, corresponding well with the previous studies in this estuary (Zhang and Li, 2010; Shen et al., 2012; Shi et al., 2017; Niu et al., 2020; Tao et al., 2020). High-salinity marine currents, having fewer nutrients, mixed with the freshwater and diluted the estuarine nutrient concentrations. River inflows, carrying abundant nutrients, increased the nutrient levels in

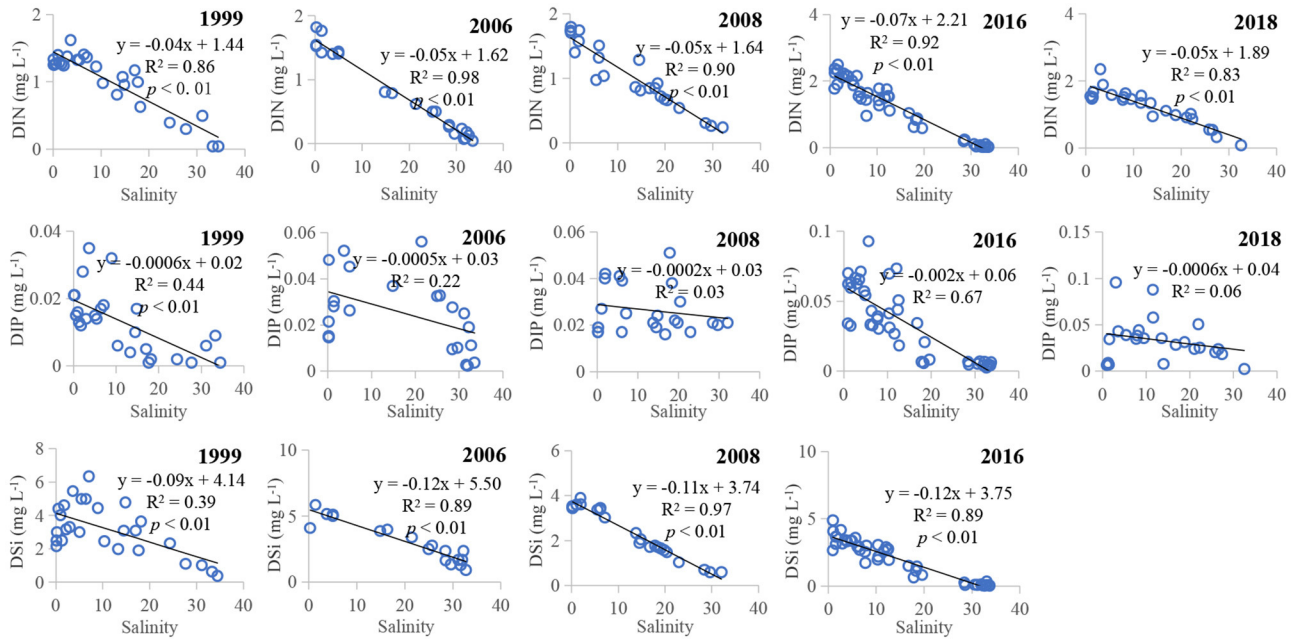

FIGURE 6 | Plots showing the nutrient-salinity relationships during summer between 1999 and 2018 in the Pearl River Estuary.

the estuarine mixing zone. These correlations results indicated that changes in nutrient concentrations were strongly associated with the tide-river mixing processes. The weak tidal forcing in summer resulted in a movement of salinity front to the sea. The nutrients were then transported farther and have provided the nutrient sources for the marine organisms. Therefore, the high phytoplankton production appeared around the salinity front (**Supplementary Figure 5**).

3.5.2. Effect of the Pearl River Discharge

The riverine inputs have provided enriched nutrient resources for the marine microorganisms. Considering the mixing degree of freshwater and seawater, the nutrient-salinity relationships also reflected the source and sink patterns besides the dilution process (Shulkin et al., 2018; Kim et al., 2020). Changes in nutrient concentrations were then considerably modulated by biological uptake processes associated with the physical mixing. We estimated the nutrient activities based on the nutrient-salinity relationships. The freshwater end-member was about 1.5–2.0 mg L^{-1} for DIN and 4–5 mg L^{-1} for DSi during our sampling times. The freshwater end-member for DIP was variable in this estuary because of the complexity of P-input. There was no difference in nutrient concentrations when salinities were >33 (as in 2016), thus the seawater end-member was 0.024 mg L^{-1} for DIN, 0.004 mg L^{-1} for DIP, and 0.07 mg L^{-1} for DSi. **Figure 7** plots the nutrient deviation against salinity in the PRE in 1999, 2006, and 2016, identifying the effects of physical mixing and biological response. The dashed line in the figure represented no deviation ($\Delta = 0$); the negative deviation ($\Delta < 0$) indicated a nutrient addition (e.g., emissions of coastal cities, decomposition of organic matter, regeneration, atmospheric deposition); and the positive deviation ($\Delta > 0$) represented the nutrient removal (e.g., biological uptake, transformation).

In 1999, most of the deviations of nitrogen and silicate in the upper estuary (salinity <10) were less than 0, suggesting that N and Si in that area were mainly characterized by their productions. The likely cause of the riverine input (e.g., Humen, Jiaomen, Hongqimen, and Hengmen) contributed much to the addition of nitrogen and silicate. However, P activity in that area was controlled both by biological uptake and production. In the middle estuary, N, P, and Si activities were mostly characterized by biological uptake. The corresponding higher chlorophyll levels (mean 2.76 μg L^{-1}) could also support the above discussion (Zhang and Li, 2010). Another possible reason was intended to the phosphorus concentrations because of its limiting role for phytoplankton growth. In the lower estuary (particulate at salinities > 33), the low nutrient concentrations could not favor the biological activities.

In 2006, the N activity was dominated by both biological consumption and production in the estuary. The degree of biological uptake of nitrogen was stronger than the addition. The possible N sources were from the river basin (upper estuary) and decomposition of organic matter and coastal zones near Zhuhai-Macau (lower estuary). The main P addition was mainly discovered on the Shenzhen coast (northeast estuary; **Figure 3**). The degrees of P and Si productions were stronger than their consumption processes.

In 2016, the biological uptake and production equally contributed to the nutrient activities. Moreover, the degree of biological uptake was stronger than the nutrient addition in the estuary, with the mean chlorophyll-*a* of 5.84 μg L^{-1} in 2016. In the lower estuary, the nutrient input was dominant. The main N

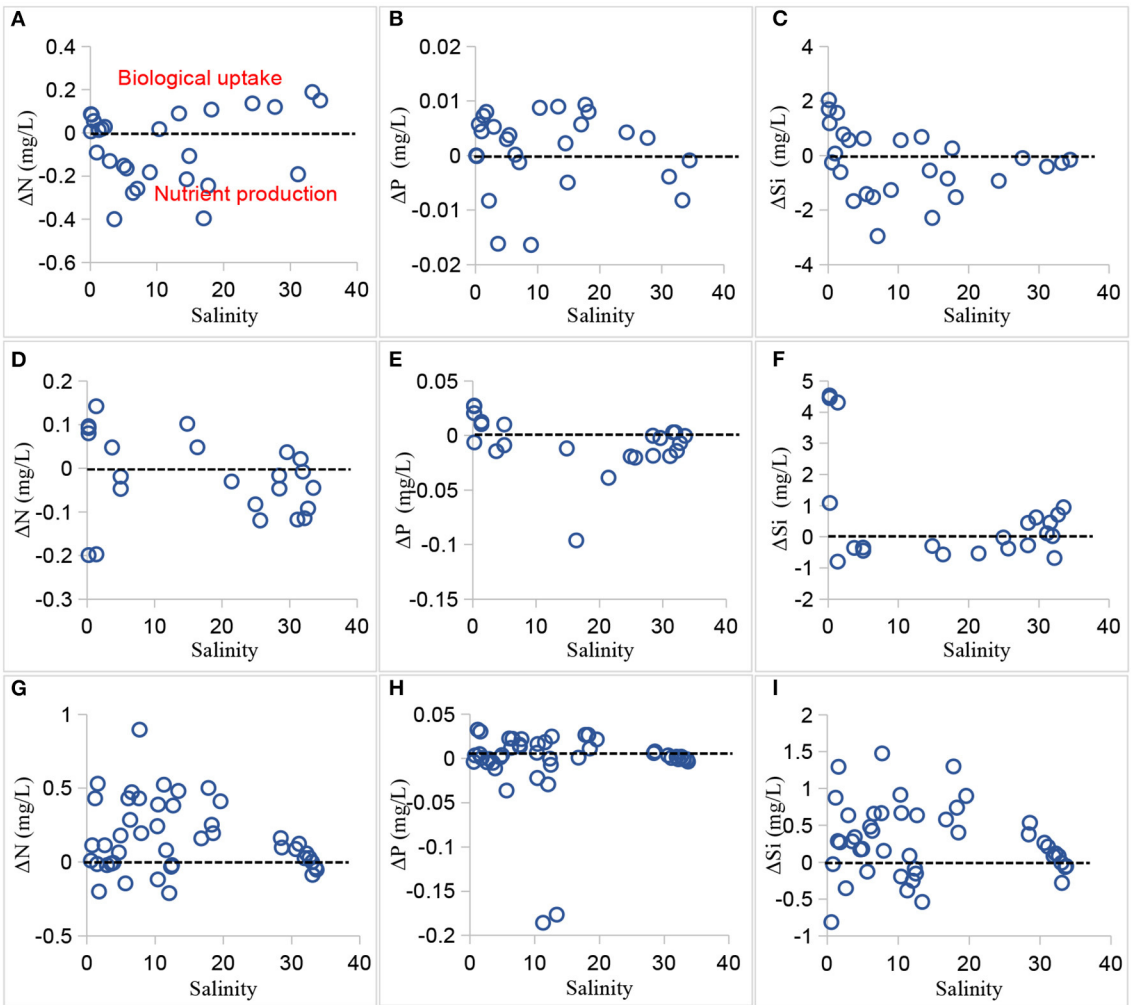

FIGURE 7 | Nutrient deviation vs. salinity during summer in 1999 **(A–C)**, 2006 **(D–F)**, and 2016 **(G–I)**, denoting the difference between observations and predictions based on the linear nutrient-salinity relationships. The dashed line represents no deviation ($\Delta = 0$); the negative deviation ($\Delta < 0$) indicates a nutrient addition (e.g., emissions of coastal cities, cycling and regeneration, atmospheric deposition); the positive deviation ($\Delta > 0$) represents the nutrient removal (e.g., biological uptake, transformation).

and Si activities in the upper and middle estuary showed removal, probably caused by the biological uptake and sedimentation of phytoplankton debris (Han et al., 2012); these N and Si external sources were mainly detected in the upper and lower estuary, likely caused by the river discharge and land-based sources. Observed DIN had higher concentrations in the western estuary. These nitrogen deviations in the east and west PRE suggested different degrees of active internal N cycling, as discussed in other studies (Chai et al., 2006, 2009; Wu et al., 2016). The DIP removal was mainly induced by the biological response and adsorption on the suspended particles, while the P sink was likely due to the P replenishment (as in the middle estuary) and fertilizers in the agricultural applications (Li et al., 2017; Wang, 2018).

In summary, the two end-member mixing model has provided a useful tool to discern the dynamic source-sink patterns of the nutrient activities in the estuary. The DIN deviation results showed that the degree of N removal gradually increased between 1999 and 2016, corresponding to the increased nutrient and chlorophyll-*a* levels. The external N source was mainly detected in the middle and lower estuary, probably caused by the decay of organisms, transformation, atmospheric deposition, and wastewater of urban areas. The source-sink patterns of DSi activities were similar to DIN. Overall, the Si activity during the time periods was significantly changed from the dominated source addition to removal over the period. The degree of P removal gradually increased, and the P source input was mainly detected in the middle and lower estuary except that in 1999. Moreover, DIN was less particle active but may be removed by biological activities such as denitrification; DIP was strongly particle active and could be removed by suspended particulate matter. Additionally, factors of topography, residence time, and other environmental factors have also influenced the dynamic source-sink patterns of nutrient behaviors in the estuary.

3.5.3. Atmospheric Deposition

The atmospheric deposition is one of the potential nutrient sources and is important in regulating the phytoplankton biomass in an estuary (Yadav et al., 2016). Atmospheric deposition of TN and TP display annual cycles (Miyazako et al., 2015). Compared with other source paths of nutrients into the PRE, the contribution of atmospheric dry and wet deposition was relatively low (**Supplementary Table 2**; Li et al., 2011), accounting for 12.64% of TN and 1.14% of TP. The atmospheric deposition of TN in Guangzhou, Shenzhen, Zhuhai-Macau, Dongguan, Zhongshan, and Hongkong was 420, 5,600, 22,086, 930, 1,056, and 6789.6 t/a, respectively, with the corresponding values of 4.2, 63, 245.4, 9.15, and 12.32, and 74.52 t/a for TP.

Over the past two decades, estuarine coastal ecosystems have suffered a number of environmental problems that attributed to nutrient over-enrichment. For instance, surface runoff from agricultural land, atmospheric deposition, waste-water discharge from urban areas, and fuel combustion all added nutrients to the river inflow. Riverine input has provided a large number of nutrients and has contributed much to the dynamic source-sink pattern. In addition, the nutrient levels in summer were higher than other seasons because of the high inflows.

3.6. Ecological Significance in the PRE Ecosystem

Nutrient enrichment in the estuary has become a societal issue, as the excess anthropogenic nutrient input into the waters would trigger eutrophication and phytoplankton blooms (Howarth and Marino, 2006; Boyer et al., 2009; Srichandan et al., 2019). Nutrient input to an estuary can vary widely regarding its forms and sources, strongly correlated with population density and land use (Nedwell et al., 2002; Maier et al., 2009). High nutrient loads have induced disturbances in the phytoplankton species in the PRE. The phytoplankton community structure was changed over the past two decades, associated with the variation in the aquatic environment. The dominant species in the summer of 1999 were *Skeletonema costatum*, *Nitzschia pongens*, *Nitzschia delicatissima*, *Asterionella japonica*, and *Leptocylindrus danicus* (Huang et al., 2004). *Skeletonema costatum*, *Nitzschia delicatissima*, *Chaetoceros curvisetus*, *Chaetoceros debilis*, and *Melosira granulata* were the dominated phytoplankton species in 2006 (Li et al., 2011). In 2016, *Skeletonema costatum*, *Nitzschia delicatissima*, *Chaetoceros decipiens*, *Coscinodiscus jonesianus*, *Chaetoceros affinis*, *Skeletonema tropicum*, and *Thalassiothrix frauenfeldii* were dominant (our unpublished data).

The nutrient pollution in the PRE was classified as severely eutrophic due to the rapid economic development in the Pearl River Delta (e.g., industrialization). Excessive nutrient input related to human pressures has usually led to water quality problems and oxygen depletion for the majority of PRE ecosystems. Nitrogen and phosphorus have beneficial uses as fertilizer but excess applications of nutrients in agriculture (beyond crop needs) can lead to eutrophication in downstream estuaries, even the dead fishes. Once nutrient pollution issues have been identified, coastal managers need to understand the dynamic source-sink patterns in order to better control the nutrient enrichment.

4. CONCLUSIONS

The Pearl River Estuary was enriched in nutrients during the high inflows. The observed DIN and DIP during summer showed a gradual increase between 1996 and 2018, while the annual trend of DSi was non-significant during that period. Phosphorus limitation was detected in most of the PRE; it was also indicative of the relevance of anthropogenic pressures and potential contributions to eutrophication. The degrees of DIN and DIP removal/uptake gradually increased over the past decades, corresponding to the increased phytoplankton chlorophyll-*a*. DIN was less particle active but may be removed by biological activities. However, DIP was strongly particle active and might be removed by suspended matter and biological response. Overall, the dynamic source-sink patterns of nutrients were largely influenced by the biogeochemical characteristics of the estuary; these patterns would regulate the phytoplankton structure. This field investigation discussed how nutrient dynamics were involved with salinity regimes, biological uptake, riverine input, and atmospheric deposition. However, more studies related to nutrient forms and other influencing factors should be explored for a better understanding of the dynamic source-sink patterns of nutrients in the estuary in future.

DATA AVAILABILITY STATEMENT

The original contributions presented in the study are included in the article/**Supplementary Material**, further inquiries can be directed to the corresponding author/s.

AUTHOR CONTRIBUTIONS

WT: data curation and writing—original draft. LN: conceptualization, formal analysis, and writing—original draft. YD: investigation. TF: formal analysis. QL: supervision and project administration. All authors contributed to the article and approved the submitted version.

FUNDING

This research was financially supported by the National Key R&D Program of China (No. 2016YFC0402600) and National Natural Science Foundation of China (No. 51709289).

ACKNOWLEDGMENTS

The authors would like to thank the editors and the reviewers for their valuable comments and suggestions on this paper.

SUPPLEMENTARY MATERIAL

The Supplementary Material for this article can be found online at: https://www.frontiersin.org/articles/10.3389/fmars.2021.713907/full#supplementary-material

REFERENCES

Bianchi, T., DiMarco, S., Cowan, J., Hetland, R., Chapman, P., Day, J., et al. (2010). The science of hypoxia in the northern Gulf of Mexico: a review. *Sci. Tot. Environ*. 408, 1471–1484. doi: 10.1016/j.scitotenv.2009.11.047

Borges, C., Bettencourt, D. S. R., and Palma, C. (2020). Determination of river water composition trends with uncertainty: seasonal variation of nutrients concentration in Tagus river estuary in the dry 2017 year. *Mar. Pollut. Bull*. 158:111371. doi: 10.1016/j.marpolbul.2020.111371

Boyer, J., Kelble, C., Ortner, P., and Rudnick, D. (2009). Phytoplankton bloom status: chlorophyll a biomass as an indicator of water quality condition in the southern estuaries of Florida, USA. *Ecol. Indicat*. 9, s56–s67. doi: 10.1016/j.ecolind.2008.11.013

Braga, E., Bonetti, C., Burone, L., and Bonetti Filho, J. (2000). Eutrophication and bacterial pollution caused by industrial and domestic wastes at Baixada Santista estuarine system, Brazil. *Mar. Pollut. Bull*. 40, 165–173. doi: 10.1016/S0025-326X(99)00199-X

Cai, H., Huang, J., Niu, L., Ren, L., Liu, F., Ou, S., et al. (2018). Decadal variability of tidal dynamics in the Pearl river delta: spatial patterns, causes, and implications for estuarine water management. *Hydrol. Process*. 32, 3805–3819. doi: 10.1002/hyp.13291

Castillo, M. (2020). Suspended sediment, nutrients, and chlorophyll in tropical floodplain lakes with different patterns of hydrological connectivity. *Limnologica* 82:125767. doi: 10.1016/j.limno.2020.125767

Chai, C., Jiang, T., Cen, J., Ge, W., and Lu, S. (2016). Phytoplankton pigments and functional community structure in relation to environmental factors in the Pearl River Estuary. *Oceanologia* 58, 201–211. doi: 10.1016/j.oceano.2016.03.001

Chai, C., Yu, Z., Shen, Z., Song, X., Cao, X., and Yao, Y. (2009). Nutrient characteristics in the Yangtze river estuary and the adjacent east China sea before and after impoundment of the three Gorges Dam. *Sci. Tot. Environ*. 407, 4687–4695. doi: 10.1016/j.scitotenv.2009.05.011

Chai, C., Yu, Z., Song, X., and Cao, X. (2006). The status and characteristics of eutrophication in the Yangtze river (Changjiang) estuary and the adjacent east China Sea, China. *Hydrobiologia* 563, 313–328. doi: 10.1007/s10750-006-0021-7

Chou, W., Fang, L., Wang, W., and Tew, K. (2012). Environmental influence on coastal phytoplankton and zooplankton diversity: a multivariate statistical model analysis. *Environ. Monitor. Assess*. 184, 5679–5688. doi: 10.1007/s10661-011-2373-3

Dai, M., Zhai, W., Cai, W., Callahan, J., Huang, B., Shang, S., et al. (2008). Effects of an estuarine plume-associated bloom on the carbonate system in the lower reaches of the Pearl River Estuary and the coastal zone of the northern south China Sea. *Continent. Shelf Res*. 28, 1416–1423. doi: 10.1016/j.csr.2007.04.018

EPA (2008). *National Coastal Condition Report III (EPA842-R-08-002)*. Environmental Protection Agency, Office of Water and Office of Research and Development, Washington, DC.

Farrow, C., Ackerman, J., Smith, R. H., and Snider, D. (2019). Riverine transport and nutrient inputs affect phytoplankton communities in a coastal embayment. *Freshw. Biol*. 65, 289–303. doi: 10.1111/fwb.13421

Gan, J., Lu, Z., Cheung, A., Dai, M., Liang, L., Harrison, P., et al. (2014). Assessing ecosystem response to phosphorus and nitrogen limitation in the Pearl river plume using the regional ocean modelling system (ROMs). *J. Geophys. Res. Oceans* 119, 8858–8877. doi: 10.1002/2014JC009951

Geeraert, N., Archana, A., Xu, M., Kao, S., Baker, D., and Thibodeau, B. (2021). Investigating the link between pearl river-induced eutrophication and hypoxia in Hong Kong shallow coastal waters. *Sci. Tot. Environ*. 772:145007. doi: 10.1016/j.scitotenv.2021.145007

Geng, M., Wang, K., Yang, N., Li, F., Zou, Y., Chen, X., et al. (2021). Spatiotemporal water quality variations and their relationship with hydrological conditions in Dongting lake after the operation of the three Gorges Dam, China. *J. Clean. Product*. 283:124644. doi: 10.1016/j.jclepro.2020.124644

Guo, C., Chen, Y., Xia, W., Qu, X., Yuan, H., Xie, S., et al. (2020). Eutrophication and heavy metal pollution patterns in the water suppling lakes of China's south-to-north water diversion project. *Sci. Tot. Environ*. 711:134543. doi: 10.1016/j.scitotenv.2019.134543

Han, A., Dai, M., Kao, S., Gan, J., Li, Q., Wang, L., et al. (2012). Nutrient dynamics and biological consumption in a large continental shelf system under the influence of both a river plume and coastal upwelling. *Limnol. Oceanogr*. 57, 486–502. doi: 10.4319/lo.2012.57.2.0486

Howarth, R., and Marino, R. (2006). Nitrogen as the limiting nutrient for eutrophication in coastal marine ecosystems: evolving views over three decades. *Limnol. Oceanogr*. 51, 364–376. doi: 10.4319/lo.2006.51.1_part_2.0364

Huang, L., Jian, W., Song, X., Huang, X., Liu, S., Qian, P., et al. (2004). Species diversity and distribution for phytoplankton of the Pearl River Estuary during rainy and dry seasons. *Mar. Pollut. Bull*. 49, 588–596. doi: 10.1016/j.marpolbul.2004.03.015

Huang, X., Huang, L., and Yue, W. (2003). The characteristics of nutrients and eutrophication in the Pearl River Estuary, south China. *Mar. Pollut. Bull*. 47, 30–36. doi: 10.1016/S0025-326X(02)00474-5

Jabir, T., Vipindas, P., Jesmi, Y., Valliyodan, S., Parambath, P., Singh, A., et al. (2020). Nutrient stoichiometry (N:P) controls nitrogen fixation and distribution of diazotrophs in a tropical eutrophic estuary. *Mar. Pollut. Bull*. 151:110799. doi: 10.1016/j.marpolbul.2019.110799

Jia, Z., Li, S., Liu, Q., Jiang, F., and Hu, J. (2021). Distribution and partitioning of heavy metals in water and sediments of a typical estuary (Modaomen, South China): the effect of water density stratification associated with salinity. *Environ. Pollut*. 287:117277. doi: 10.1016/j.envpol.2021.117277

Jiang, Z., Liu, J., Chen, J., Chen, Q., Yan, X., Xuan, J., et al. (2014). Responses of summer phytoplankton community to drastic environmental changes in the Changjiang (Yangtze River) estuary during the past 50 years. *Water Res*. 54, 1–11. doi: 10.1016/j.watres.2014.01.032

Justic, D., Rabalais, N., and Turner, R. (1995). Stoichiometric nutrient balance and origin of coastal eutrophication. *Mar. Pollut. Bull*. 30, 41–46. doi: 10.1016/0025-326X(94)00105-I

Karydis, M., Ignatiades, L., and Moschopoulou, N. (1983). An index associated with nutrient eutrophication in the marine environment. *Estuar. Coast. Shelf Sci*. 16, 339–344. doi: 10.1016/0272-7714(83)90151-8

Kim, J., Chapman, P., Rowe, G., and DiMarco, S. (2020). Categorizing zonal productivity on the continental shelf with nutrient-salinity ratios. *J. Mar. Syst*. 206:103336. doi: 10.1016/j.jmarsys.2020.103336

Kim, T., Lee, K., Duce, R., and Liss, P. (2014). Impact of atmospheric nitrogen deposition on phytoplankton productivity in the south China sea. *Geophys. Res. Lett*. 41, 3156–3162. doi: 10.1002/2014GL059665

Li, G., Lin, Q., Lin, J., Song, X., Tan, Y., and Huang, L. (2014). Environmental gradients regulate the spatial variations of phytoplankton biomass and community structure in surface water of the Pearl River Estuary. *Acta Ecol. Sin*. 34, 129–133. doi: 10.1016/j.chnaes.2014.01.002

Li, K., Chen, Z., and Jiang, G. (2011). *Pollution Characteristics and Their Ecological Responses in the Pearl River Estuary and Adjacent Zones (in Chinese)*. Beijing: China Construction Industry Press.

Li, R., Xu, J., Li, X., Shi, Z., and Harrison, P. (2017). Spatiotemporal variability in phosphorus species in the Pearl River Estuary: influence of the river discharge. *Sci. Rep*. 7:13649. doi: 10.1038/s41598-017-13924-w

Lin, W., and Li, S. (2002). Vertical distribution of cod and do and its affecting factors in the Pearl River Estuary in summer (in Chinese with English abstract). *Acta Sci. Nat. Univers. Sunyatseni* 41, 82–86.

Lin, Y., Su, J., Hu, C., Zhang, M., Li, Y., Guan, W., et al. (2004). N and P in waters of the Zhujiang river estuary in summer (in Chinese with English abstract). *Acta Oceanol. Sin*. 26, 63–73.

Maier, G., Nimmo-Smith, R., Glegg, G., Tappin, A., and Worsfold, P. (2009). Estuarine eutrophication in the UK: current incidence and future trends. *Aquat. Conserv. Mar. Freshw. Ecosyst*. 19, 43–56. doi: 10.1002/aqc.982

Mathew, J., Singh, A., and Gopinath, A. (2021). Nutrient concentrations and distribution of phytoplankton pigments in recently deposited sediments of a positive tropical estuary. *Mar. Pollut. Bull*. 168:112454. doi: 10.1016/j.marpolbul.2021.112454

Miyazako, T., Kamiya, H., Godo, T., Koyama, Y., Nakashima, Y., Sato, S., et al. (2015). Long-term trends in nitrogen and phosphorus concentrations in the Hii river as influenced by atmospheric deposition from east Asia. *Limnol. Oceanogr*. 60, 629–640. doi: 10.1002/lno.10051

Monteiro, M., Jimeinez, J., and Pereira, L. (2016). Natural and human controls of water quality of an Amazon estuary (Caete-Pa, Brazil). *Ocean Coast. Manage*. 124, 42–52. doi: 10.1016/j.ocecoaman.2016.01.014

Nedwell, D., Dong, L., Sage, A., and Underwood, G. (2002). Variations of the nutrients loads to the mainland UK estuaries: correlation with catchment areas, urbanization and coastal eutrophication. *Estuar. Coast. Shelf Sci*. 54, 951–970. doi: 10.1006/ecss.2001.0867

Niu, L., Luo, X., Cai, H., Liu, F., Zhang, T., and Yang, Q. (2021). Seasonal dynamics of polycyclic aromatic hydrocarbons between water and sediment in a tide-dominated estuary and ecological risks for estuary management. *Mar. Pollut. Bull*. 162:111831. doi: 10.1016/j.marpolbul.2020.111831

Niu, L., Luo, X., Hu, S., Liu, F., Cai, H., Ren, L., et al. (2020). Impact of anthropogenic forcing on the environmental controls of phytoplankton dynamics between 1974 and 2017 in the Pearl River Estuary, China. *Ecol. Indicat*. 116:106484. doi: 10.1016/j.ecolind.2020.106484

Niu, L., Van Gelder, P., Zhang, C., Guan, Y., and Vrijling, J. (2015). Statistical analysis of phytoplankton biomass in coastal waters: case study of the Wadden sea near Lauwersoog (the Netherlands) from 2000 through 2009. *Ecol. Informat*. 30, 12–19. doi: 10.1016/j.ecoinf.2015.08.003

Potter, I., Rose, T., Huisman, J., Hall, N., Denham, A., and Tweedley, J. (2021). Large variations in eutrophication among estuaries reflect massive differences in composition and biomass of macroalgal drift. *Mar. Pollut. Bull*. 167:112330. doi: 10.1016/j.marpolbul.2021.112330

Redfield, A. (1958). The biological control of chemical factors in the environment. *Am. Sci*. 46, 205–221.

Rowe, G., and Chapman, P. (2002). Continental shelf hypoxia: some nagging questions. *Gulf Mexico Sci*. 20, 153–160. doi: 10.18785/goms.2002.08

Shen, P., Li, Y., Qi, Y., Zhang, L., Tan, Y., and Huang, L. (2012). Morphology and bloom dynamics of cochlodinium geminatum schutt in the Pearl Pearl River Estuary, south China Sea. *Harmful Algae* 13, 10–19. doi: 10.1016/j.hal.2011.09.009

Shi, Y., Zhao, H., Wang, X., Zhang, J., Sun, X., and Yang, G. (2019). Distribution characteristics of nutritive salts and chlorophyll a in the Pearl River Estuary. *J. Guangdong Ocean Univers*. 39, 56–65. doi: 10.3969/j.issn.1673-9159.2019.01.009

Shi, Z., Xu, J., Huang, X., Zhang, X., Jiang, Z., Ye, F., et al. (2017). Relationship between nutrients and plankton biomass in the turbidity maximum zone of the Pearl River Estuary. *J. Environ. Sci. China* 57, 72–84. doi: 10.1016/j.jes.2016.11.013

Shulkin, V., Tishchenko, P., Semkin, P., and Shvetsova, M. (2018). Influence of river discharge and phytoplankton on the distribution of nutrients and trace metals in Razdolnaya river estuary, Russia. *Estuar. Coast. Shelf Sci*. 211, 166–176. doi: 10.1016/j.ecss.2017.09.024

Srichandan, S., Baliarsingh, S., Prakash,1, S., Lotliker, A., Parida, C., and Sahu, K. (2019). Seasonal dynamics of phytoplankton in response to environmental variables in contrasting coastal ecosystems. *Environ. Sci. Pollut. Res*. 26, 12025–12041. doi: 10.1007/s11356-019-04569-5

Tao, W., Niu, L., Liu, F., Cai, H., Ou, S., Zeng, D., et al. (2020). Influence of river-tide dynamics on phytoplankton variability and their ecological implications in two Chinese tropical estuaries. *Ecol. Indicat*. 115:106458. doi: 10.1016/j.ecolind.2020.106458

Uncles, R., Frickers, P., and Harris, C. (2003). Dissolved nutrients in the Tweed estuary, UK: inputs, distributions and effects of residence time. *Sci. Tot. Environ*. 314–316, 727–736. doi: 10.1016/S0048-9697(03)00080-9

Vipindas, P., Anas, A., Jayalakshmy, K., Lallu, K., Benny, P., and Shanta, N. (2018). Impact of seasonal changes in nutrient loading on distribution and activity of nitrifiers in a tropical estuary. *Continent. Shelf Res*. 154, 37–45. doi: 10.1016/j.csr.2018.01.003

Wang, F., Cheng, P., Chen, N., and Kuo, Y. (2021). Tidal driven nutrient exchange between mangroves and estuary reveals a dynamic source-sink pattern. *Chemosphere* 270:128665. doi: 10.1016/j.chemosphere.2020.128665

Wang, Y. (2018). Actual costs of uneconomic growth of marine fisheries in China's Pearl river delta. *Nat. Resour*. 9, 297–312. doi: 10.4236/nr.2018.97018

Wang, Y., Liu, D., Lee, K., Dong, Z., Di, B., Wang, Y., et al. (2017). Impact of water-sediment regulation scheme on seasonal and spatial variations of biogeochemical factors in the Yellow river estuary. *Estuar. Coast. Shelf Sci*. 198, 92–105. doi: 10.1016/j.ecss.2017.09.005

Wei, P., and Huang, L. (2010). Water quality and eutrophication in the Guangzhou sea zone of the Pearl River Estuary. *Chin. J. Oceanol. Limnol*. 28, 113–121. doi: 10.1007/s00343-010-9032-3

Wu, M., Hong, Y., Yin, J., Dong, J., and Wang, Y. (2016). Evolution of the sink and source of dissolved inorganic nitrogen with salinity as a tracer during summer in the Pearl River Estuary. *Sci. Rep*. 6:36638. doi: 10.1038/srep36638

Yadav, K., Sarma, V., Rao, D., and Kumar, M. (2016). Influence of atmospheric dry deposition of inorganic nutrients on phytoplankton biomass in the coastal Bay of Bengal. *Mar. Chem*. 187, 25–34. doi: 10.1016/j.marchem.2016.10.004

Yin, K., Qian, P., Wu, M., Chen, J., Huang, L., Song, X., et al. (2001). Shift from P to N limitation of phytoplankton growth across the Pearl river estuarine plume during summer. *Mar. Ecol. Prog. Ser*. 221, 17–28. doi: 10.3354/meps221017

Yin, K., Song, S., Sun, J., and Wu, M. (2004). Potential P limitation leads to excess N in the Pearl river estuarine coastal plume. *Continent. Shelf Res*. 24, 1895–1907. doi: 10.1016/j.csr.2004.06.014

Yuan, X., Krom, M., Zhang, M., and Chen, N. (2021). Human disturbance on phosphorus sources, processes and riverine export in a subtropical watershed. *Sci. Tot. Environ*. 769:144658. doi: 10.1016/j.scitotenv.2020.144658

Zeng, D., Niu, L., Tao, W., Fu, L., and Yang, Q. (2020). Nutrient dynamics in Pearl River Estuary and their eutrophication evaluation (in Chinese with English abstract). *J. Guangdong Ocean Univers*. 40, 73–82.

Zhang, D., Qi, Q., Tong, S., Wang, J., Zhang, M., Zhu, G., et al. (2021). Effect of hydrological fluctuation on nutrient stoichiometry and trade-offs of *Carex schmidtii*. *Ecol. Indicat*. 120:106924. doi: 10.1016/j.ecolind.2020.106924

Zhang, G., Cheng, W., Chen, L., Zhang, H., and Gong, W. (2019). Transport of riverine sediment from different outlets in the Pearl River Estuary during the wet season. *Mar. Geol*. 415:105957. doi: 10.1016/j.margeo.2019.06.002

Zhang, H., and Li, S. (2010). Effects of physical and biochemical processes on the dissolved oxygen budget for the Pearl River Estuary during summer. *J. Mar. Syst*. 79, 65–88. doi: 10.1016/j.jmarsys.2009.07.002

Zhang, J., Huang, X., Jiang, Z., and Huang, D. (2009). Seasonal changes of eutrophication level in the Pearl River Estuary from 2006 to 2007 and its relationship with environmental factors (in Chinese with English abstract). *Acta Ecol. Sin*. 31, 113–120.

Zhang, J., Yu, Z., Wang, J., Ren, J., Chen, H., and Xiong, H. (1999). The subtropical Zhujiang (Pearl river) estuary: nutrient, trace species and their relationship to photosynthesis. *Estuar. Coast. Shelf Sci*. 49, 385–400. doi: 10.1006/ecss.1999.0500

Zhang, L., Shi, Z., Zhang, J., Jiang, Z., Huang, L., and Huang, X. (2016). Characteristics of nutrients and phytoplankton productivity in Guangdong coastal regions, south China. *Mar. Pollut. Bull*. 113, 572–578. doi: 10.1016/j.marpolbul.2016.08.081

Zhang, X., Shi, Z., Liu, Q., Ye, F., Tian, L., and Huang, X. (2013). Spatial and temporal variations of picoplankton in three contrasting periods in the Pearl River Estuary, south China. *Continent. Shelf Res*. 56, 1–12. doi: 10.1016/j.csr.2013.01.015

Zhao, H. (1990). *Evolution of the Pearl River Estuary*. Beijing: Ocean Press.

Conflict of Interest: The authors declare that the research was conducted in the absence of any commercial or financial relationships that could be construed as a potential conflict of interest.

frontiers in Marine Science

ORIGINAL RESEARCH
published: 12 October 2021
doi: 10.3389/fmars.2021.729954

Deep Learning for Simulating Harmful Algal Blooms Using Ocean Numerical Model

Sang-Soo Baek[1], JongCheol Pyo[2], Yong Sung Kwon[3], Seong-Jun Chun[4], Seung Ho Baek[5], Chi-Yong Ahn[6], Hee-Mock Oh[6], Young Ok Kim[7] and Kyung Hwa Cho[1]**

[1] School of Urban and Environmental Engineering, Ulsan National Institute of Science and Technology, Ulsan, South Korea, [2] Center for Environmental Data Strategy, Korea Environment Institute, Sejong, South Korea, [3] Environmental Impact Assessment Team, Division of Ecological Assessment Research, National Institute of Ecology, Seocheon, South Korea, [4] LMO Research Team, Bureau of Ecological Research, National Institute of Ecology (NIE), Seocheon, South Korea, [5] Risk Assessment Research Center, Korea Institute of Ocean Science & Technology, Geoje, South Korea, [6] Cell Factory Research Center, Korea Research Institute of Bioscience and Biotechnology (KRIBB), Daejeon, South Korea, [7] Marine Ecosystem Research Center, Korea Institute of Ocean Science and Technology, Busan, South Korea

In several countries, the public health and fishery industries have suffered from harmful algal blooms (HABs) that have escalated to become a global issue. Though computational modeling offers an effective means to understand and mitigate the adverse effects of HABs, it is challenging to design models that adequately reflect the complexity of HAB dynamics. This paper presents a method involving the application of deep learning to an ocean model for simulating blooms of *Alexandrium catenella*. The classification and regression convolutional neural network (CNN) models are used for simulating the blooms. The classification CNN determines the bloom initiation while the regression CNN estimates the bloom density. GoogleNet and Resnet 101 are identified as the best structures for the classification and regression CNNs, respectively. The corresponding accuracy and root means square error values are determined as 96.8% and 1.20 [log(cells L^{-1})], respectively. The results obtained in this study reveal the simulated distribution to follow the *Alexandrium catenella* bloom. Moreover, Grad-CAM identifies that the salinity and temperature contributed to the initiation of the bloom whereas NH_4-N influenced the growth of the bloom.

Keywords: harmful algal blooms, deep learning, convolutional neural network, classification, regression

OPEN ACCESS

Edited by:
Kenneth Mei Yee Leung, City University of Hong Kong, Hong Kong SAR, China

Reviewed by:
Yongquan Yuan, Institute of Oceanology, Chinese Academy of Sciences (CAS), China
Hai Doan-Nhu, Institute of Oceanography in Nhatrang, Vietnam

****Correspondence:***
Kyung Hwa Cho
khcho@unist.ac.kr
Young Ok Kim
yokim@kiost.ac.kr

Specialty section:
This article was submitted to Marine Pollution, a section of the journal Frontiers in Marine Science

Received: *24 June 2021*
Accepted: *15 September 2021*
Published: *12 October 2021*

Citation:
Baek S-S, Pyo J, Kwon YS, Chun S-J, Baek SH, Ahn C-Y, Oh H-M, Kim YO and Cho KH (2021) Deep Learning for Simulating Harmful Algal Blooms Using Ocean Numerical Model. Front. Mar. Sci. 8:729954. doi: 10.3389/fmars.2021.729954

INTRODUCTION

The occurrence, period, and frequency of harmful algal blooms (HABs) have increased in recent years, thereby posing a serious threat to the aquatic ecosystem (Weiher and Sen, 2006; Gobler et al., 2017). The United States spends $22 million annually on public-health damages and suffers an annual loss of $75 million due to HABs (Hoagland et al., 2002; Weiher and Sen, 2006; Anderson et al., 2012). In South Korea, the economic loss incurred due to HAB over the past three decades was $121 million (Park et al., 2013). China and Japan have similarly incurred enormous economic losses in northeast Asia (Wang and Wu, 2009; Itakura and Imai, 2014). These damages can be attributed to the changes in the aquatic environmental conditions due to climate change and/or nutrient enrichment caused by such human activities as agriculture, industrialization, tourism, and urbanization (Heisler et al., 2008; Gobler et al., 2017). Accordingly, HABs have escalated to become a global concern. Anthropogenic global warming is visible in the northward expansion of the warm pool to the northwestern Pacific. The Korean Peninsula, which is closed on the marginal sea of

the northwestern Pacific, has been reported as a vulnerable region in the new normal climate. Accordingly, there exists the threat of HAB expansion into the Korean coastal waters owing to changes in HAB dynamics due to global warming. Outbreaks of PSP in Korean coastal waters have been perceived as spring events since the first record in 1986 (Chang et al., 1987). Recurrent PSP events in the spring of Korea have been linked to the spring blooms of *Alexandrium catenella* (*A. catenella*) (previously reported as *A. tamarense*). The spring blooms of the toxic dinoflagellate population are regular in the coastal waters of marginal sea connected to the northwestern Pacific (Han et al., 1992; Ishikawa et al., 2014).

Prior research concerning HABs has mainly focused on increasing awareness and improving monitoring techniques (Kim et al., 2002; Wang et al., 2008). Since the 1970s, a significant amount of infrastructure, labor, and time has been required for HAB field monitoring. However, the extent of this requirement has differed based on the properties of HAB. Moreover, given the need for HAB monitoring and relevant analyses, computational modeling has been considered to be an alternative approach to understand and mitigate the effects of HABs (Yoshioka and Yaegashi, 2018; Pyo et al., 2019). Pinto et al. (2016) simulated the abundance of HAB species using a particle-tracking model. Likewise, He et al. (2008) developed a mathematical model for simulating *A. catenella* (former *A. fundyense*) bloom in the western Gulf of Maine. Although these efforts have contributed toward the improvement of the simulation performance of algal blooms, overcoming the limitations of these models remains a major challenge owing to the complexity of HAB dynamics that are dependent on the multiple effects from physical, chemical, and biological systems (McGillicuddy, 2010).

A data-driven deep-learning model can push the frontiers of the aforementioned models further. Deep learning has been proposed as a promising technique owing to its big-data handling capabilities (Szegedy et al., 2015). Deep learning has been adopted in several fields, including speech recognition, image analysis, and biological mechanisms (Chen and Manning, 2014; Young et al., 2018). Shen et al. (2019) estimated cyanobacteria blooms in river waters using a support vector machine. Additionally, Pyo et al. (2020) simulated algal blooms in freshwater systems using a convolutional neural network (CNN). However, these studies focused on HABs in inland waters, which further access is necessary to undergo more dynamic and complex hydrological and ecological cycles in seawater. Recently, Baek et al. (2021) suggested a method for identifying factors that influence *A. catenella* bloom using decision tree and hydrodynamic models. They revealed that water temperature and nutrients affected the growth of *A. catenella*. However, this approach is not suitable for continuous *A. catenella* bloom simulation because it can only generate four bloom levels based on cell density.

This study evaluates the applicability of deep learning for HAB simulation with the ocean model to generate the temporal–spatial distribution of physical, chemical, and biological variables. Using these variables and CNNs, we simulated the temporal distribution of *A. catenella*, a notorious dinoflagellate species causing paralytic shellfish poisoning (PSP). Convolutional neural network-based deep learning models can extract the features of multi-dimensional data using convolutional filters (Deng et al., 2009). Additionally, using gradient-weighted class activation mapping (Grad-CAM), we identified the factors that influence the simulation of *A. catenella* (Selvaraju et al., 2017).

MATERIALS AND METHODS

Data Collection

We conducted spatial–temporal monitoring to investigate the occurrence of *A. catenella*. The monitoring site is located on the southeastern coast near Namhae, Geoje Island, and Busan, South Korea (**Figure 1**), opened toward off sea, causing fresh and oceanic water intrusion (Kang et al., 2012). In particular, the eastern coast of Geoje Island has frequently occurring PSP initiation (National Fisheries Research and Development Institute, 2020). PSP outbreaks provoked by *A. catenella* bloom in our study area have been reported (Chang et al., 1987; Kim et al., 2015). Water surface elevation, wind, and wind velocity data were measured by the Korea Ocean Observing and Forecasting System and used to set up the model. Two observations at stations 1 and 2 were used to calibrate the water level, temperature, and salinity. Another three observations at stations 3, 4, and 5 were used to calibrate NH4-N and PO4-P (**Figure 1**).

One-thousand one-hundred and seventy-five samples were collected from the water surface at the sampling sites, which had water depths of 12 to 59 m. The monitoring period was from January 2017 to December 2019. Water samples were acquired with a Van Dorn bottle and fixed with Lugol solution (final conc., 2%) from 9:00 AM to 4:00 PM. The fixed seawater was concentrated to 5–50 mL aliquots by overnight sedimentation. *Alexandrium catenella* cells were enumerated using a Sedgwick–Rafter counting slide at a 200× magnification with a light microscope (Zeiss Axioscope 2). To identify the species based on morphological and molecular analyses, the cells were processed as described by Kim et al. (2020). Cysts of *A. catenella* were isolated from sediment samples collected using a core sampler and incubated at bottom temperatures on the sampling dates. The germination ratio of the cysts was estimated by the percentage of cysts germinating within one month. Growth experiments of *A. catenella* were conducted under several temperature and salinity conditions, reflecting the sampling site environments. The measurements of germination ratio and growth rate were described in detail by Kim et al. (2020).

Preparation of Input Data for Deep Learning

The input data in this study consisted of two parts: (1) ocean physical data (e.g., water velocity, water temperature, water elevation, and retention time) and chemical data (e.g., salinity, PO_4-P, and NH_4-N) and (2) ocean biological data [e.g., germination ratio, growth rate, and operational taxonomic unit (OTU)]. This study applied the environmental fluid dynamics code (EFDC) model, adopted for simulating ocean and coastal waters (Dai et al., 2011; Du and Shen, 2016) to generate the ocean physical and chemical data. The EFDC model is a fluid simulation

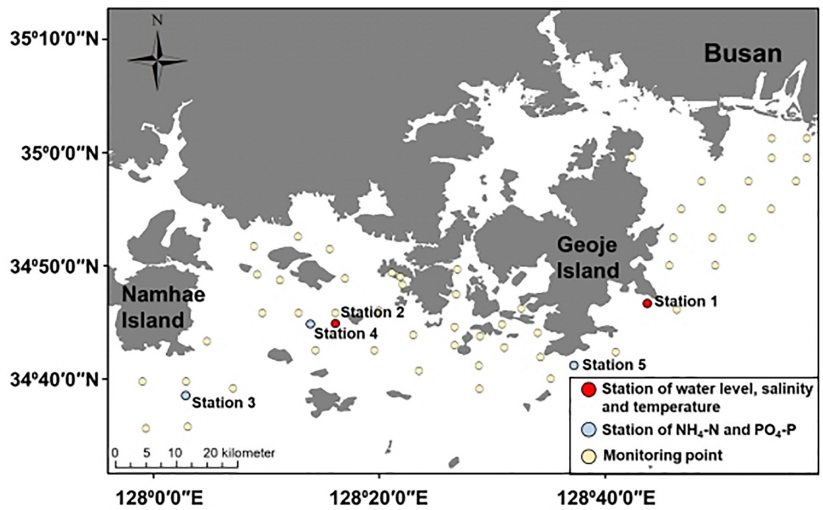

FIGURE 1 | Study site—red dots indicate the observation station for water elevation, salinity, and temperature; blue dots indicate the observation point for NH_4-N and PO_4-P; yellow circles indicates the monitoring point for *A. catenella*.

model that includes three-dimensional flow and biochemical transport in the ocean, estuaries, and lakes. EFDC can solve free surface, vertical hydrostatic, and turbulent equations for fluids with different densities. The governing equation was derived using the vertical hydrostatic boundary with turbulent equations and consists of the momentum [Eq. (S1, S2)], vertical hydrostatic pressure (Eq. S3), and continuity equations [Eq. (S4, S5)] (Jeong et al., 2010). The ocean physical and chemical data included the temporal and spatial distributions of water velocity, water temperature, water elevation, retention time, salinity, PO_4-P, and NH_4-N. These data have been verified as variables that influence the life cycle of *A. catenella* (Itakura and Yamaguchi, 2001; Kim and Yoo, 2007; Armi et al., 2011; Kim et al., 2020). The ocean physical and chemical distributions were calculated by the EFDC model. Ocean biological data included the temporal and spatial distributions of the germination ratio of *A. catenella* cysts, growth rate of vegetative cells of the species, and OTU of bacteria. The cyst germination and growth rates are critical elements in recurrent outbreaks of *A. catenella* blooms *in situ*, although dormant populations are significantly affected by environmental variables. Hence, we adopted these rates as the input data to simulate *A. catenella*. The data pertaining to cyst germination and growth rate were obtained by Kim et al. (2020). The microbial community data in this area, including the OTU data, were extracted from the previous study (Cui et al., 2020). operational taxonomic units were analyzed at a distance of 0.01 using the mothur v1.39.3 pipeline with SILVA database, release 132 (Schloss et al., 2009; Kozich et al., 2013). Three representative OTUs (OTU1, OTU2, and OTU3), which were identified as *A. catenella*-related OTUs based on ecological network analysis in the previous study (Cui et al., 2020), were selected for further analysis in this study. Taxonomically, OTU1, OTU2, and OTU3 were assigned to genera Fluviicola (family Crocinitomicaceae), Ascidiaceihabitans (family Rhodobacteraceae), Candidatus Actinomarina (family Candidatus Actinomarinaceae), respectively. **Supplementary Figure 1** presents the process used to generate the temporal and spatial distribution of biological data. A linear model was adopted to generate the variation of biological data by changing the environmental variables. The linear regressions of the germination ratio and growth rate were calculated using temperature and salinity from *in vivo* experiments (**Supplementary Figure 1A**), whereas that of the OTU distribution was generated using the temperature, salinity, PO_4-P, and NH_4-N values from monitoring (**Supplementary Figure 1B**). A linear regression model explains the relationship between one response variable and multiple explanatory variables (Montgomery et al., 2021); therefore, these linear models used the simulated water temperature, salinity, PO_4-P, and NH_4-N from EFDC to determine the temporal and spatial distribution of biological data (**Supplementary Figure 1C**). The simulation period was from January 2017 to December 2019. These ocean physical, chemical, and biological data were validated using observational data. The EFDC grid was a Cartesian grid with a cell size of 200 m × 400 m. Observations of wind direction, velocity and water surface elevation were used to set up the EFDC model. More details of the experiments on germination ratio, growth rate, and OTU are presented in the **Supplementary Information**.

Figure 2 shows the two-step process of generating input data to apply CNN for simulating the bloom of *A. catenella*: (1) extracting the spatial–temporal distribution of the physical, chemical, and biological information at the study site (**Figures 2A,B**) and (2) converting the input data to two-dimensional data (**Figure 2C**). These physical, chemical, and biological data have three dimensions, $m \times m \times (n + 1)$, and the simulation point of *A. catenella* is located in the center. Here, m is the size (i.e., height × width) of the input window that includes the simulation point, and n is the lookback, which indicates the number of time steps included based on the current simulation time. For example, when $m = 3$ and $n = 5$, the data size

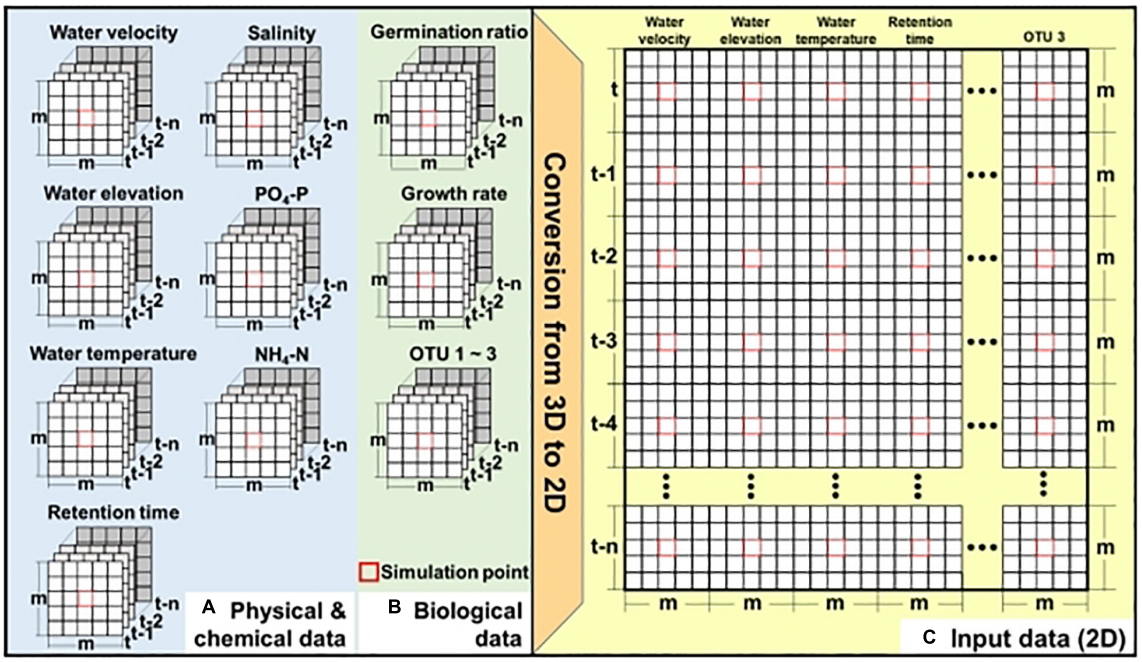

FIGURE 2 | Preparation of input data for CNN—**(A)** physical and chemical data obtained using EFDC, **(B)** biological data obtained using EFDC and linear equation, and **(C)** two-dimensional input data. Here, *m* denotes the input window (i.e., height × width), including the simulation point located at the center of input window while *n* denotes the lookback size. Red boxes indicate the simulation point.

is 3 × 3 × (5 + 1). Because the CNN approach was developed focusing on two-dimensional data (length × height) or RGB data (length × height × 3), we converted these inputs into two-dimensional data before applying the CNN (Shin et al., 2016; Koundinya et al., 2018).

Simulation of *Alexandrium catenella* Based on DL

The simulation layout of *A. catenella* is presented in **Figure 3**. The simulation comprises of the following three steps: (1) optimizing the input and CNN structures, (2) simulating the bloom of *A. catenella* based on the optimal input and CNN structures, and (3) identifying *A. catenella* bloom factors based on Grad-CAM. Because these CNN structures (e.g., Resnet, GoogLeNet, and Inception) were developed using data of size 299 × 299, the input data had to be converted (Szegedy et al., 2016; Akiba et al., 2017). Subsequently, the converted data are fed to the classification and regression CNN models; the classification CNN model decided the initiation of *A. catenella*, while the regression CNN model generated the density after *A. catenella* was initiated. The initiation and the density indicated the occurrence and the number of *A. catenella* cells, respectively. The use of two CNNs with different roles can prevent bias in model training, as most of our monitoring data were zero, indicating that *A. catenella* did not occur. In addition, we optimized the input window (*m*), lookback (*n*), and CNN structures (**Figure 3A**) to generate the spatial–temporal distribution of *A. catenella* (**Figure 3B**). Using the optimal parameter values and CNN structures, we analyzed the performance of *A. catenella* forecasting with increasing forecast lead times (days) of up to seven days. Model training was performed using Intel ® Xeon CPU E-52687W v4 @ 3.00 GHz, 128 GB RAM, and NVIDIA GTX 1080 Ti. CNN was implemented with the machine and deep learning toolboxes in MATLAB. Accuracy was used for evaluating the classification CNN model, while RMSE and R^2 were used for the regression CNN model. Relevant explanations can be found in the **Supplementary Information**.

Convolutional Neural Network

Convolutional Neural Network (CNN) is a popular deep learning model that extracts data features using convolving filters (Deng et al., 2009). A typical CNN architecture consists of convolutional, pooling, ReLU, batch normalization, concatenation, normalized, and fully connected layers (LeCun et al., 2015). Each layer has a specialized role in the architecture: convolutional and pooling layers are used for feature extraction. ReLU and normalization layers are used for a linear and normalization calculation, respectively (LeCun et al., 2015). These layers can be combined to enhance model performance (Szegedy et al., 2016; Khan et al., 2019). Details concerning the CNN layers can be found in the **Supplementary Materials** document. **Supplementary Figure 2** shows the CNN structures employed in this study. GoogleNet and Inception v3 models adopt parallel CNN layers (Szegedy et al., 2016). ResNet 50 and ResNet 101 have skip connections, i.e., the information of the output layer is transferred into the next layer, and into the earlier layer (Szegedy et al., 2016). This structure can increase model performance by reducing overfitting and vanishing gradient

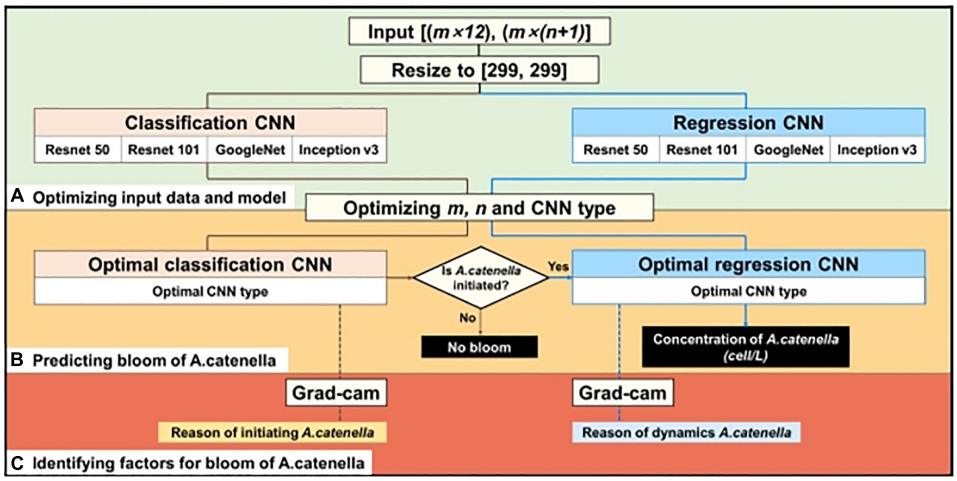

FIGURE 3 | Procedure of simulating *A. catenella* using CNN—**(A)** optimizing input data and CNN structures, **(B)** predicting bloom of *A. catenella* based on optimal input and structures, and **(C)** identifying factors for bloom of *A. catenella* using Grad-CAM. Brown and blue lines indicate the processes of classification and regression CNN models, respectively.

problems (He et al., 2016a). In our study, the softmax and mean squared error (MSE) (see **Supplementary Information** for more details) were used as the loss function for classification and regression CNN, respectively. The loss functions were applied for calculating the error between simulation and observation during model training. For model training, the CNN used hyperparameters, including epoch number, batch size, and learning rate (Loussaief and Abdelkrim, 2018). Epoch is the number of times the learning worked in the entire dataset, whereas batch size is the number of samples used for training (Robert, 2014). The learning rate controls the step size at each iteration to minimize the loss function (Robert, 2014). The CNN comprised 500 epochs with a mini-batch size of 32; the applied learning rates equaled 0.001 and 0.0001 for the first 200 and remaining 300 epochs, respectively. Each epoch generated a corresponding model, and the final model was selected to produce the lowest validation accuracy and MSE. Our study adopted random sampling to divide *A. catenella* observations into training and validation sets. A uniform distribution was used for the random sampling. Previous studies have also used random sampling with a uniform distribution to divide the data into training and validation sets (Brion et al., 2002; Caruana and Niculescu-Mizil, 2006).

Gradient-Weighted Class-Activation Mapping

The deep-learning model used in this study applied Grad-CAM for identifying factors contributing to *A. catenella* bloom (**Figure 3C**). The Grad-CAM localization map describes the simulation results by highlighting the important regions (Selvaraju et al., 2017). The model interpretability technique is proposed as a strategy that enables the input-based understanding of the results obtained because neural networks are incapable of explaining model results (Selvaraju et al., 2017). Several prior studies have verified the use of Grad-CAM in the visualization of model features (Selvaraju et al., 2017; Chen et al., 2020). This method is based on class activation mapping (CAM) that can extract the significant features by emphasizing the input data region. However, the use of CAM is restricted to CNN structures that comprise a global average pooling layer (Selvaraju et al., 2016). Grad-CAM overcomes this limitation using gradient information from the final convolutional layer for visualizing the important input data regions (Selvaraju et al., 2017). A detailed description of Grad-CAM is presented by Selvaraju et al. (2017).

RESULTS

Ocean Modeling Results

We compared the simulated and observed water elevation, salinity, water temperature, NH_4-N, and PO_4-P results. The physical and chemical simulations are illustrated in **Supplementary Figures 3, 4**. The coefficient of determination (R^2) of water temperature and elevation was above 0.90 at stations 1 and 2, while salinity was 0.26 and 0.65 at stations 1 and 2, respectively. The average root-mean-squared errors (RMSEs) of water temperature, elevation, and salinity were 0.82°C, 0.07 m, and 1.12, respectively. Compared to water temperature and elevation simulations, the salinity simulation had a larger error than observation. The average coefficient of determination (R^2) of NH_4-N and PO_4-P were 0.67 and 0.30, and the average RMSE values were 0.09 and 0.01 mg L^{-1}, respectively. Although both NH_4-N and PO_4-P simulations follow the observation trend, their values were underestimated at the peak point. The linear regression equations of growth rate, germination rate, and OTU are presented in **Supplementary Figure 5**. The growth and germination rates were more strongly influenced by temperature and salinity, respectively, whereas the OTUs related to *A. catenella* were affected by salinity and PO_4-P.

Optimal Input Window Design

Figures 4(A.1-4,B.1-4) shows the performance of classification and regression CNN, respectively, with respect to input window size (*m*) and lookback (*n*). Here, *m* denotes the input window size (e.g., height × width), including the simulation point that was located at the center of the input window, and *n* is the number of time steps. For example, if the input window size is three and lookback is five, the model considers a spatial distribution with 3 × 3 grid cells and temporal information from the previous five days to the current simulation time. In the classification model, except GoogleNet, there existed multiple optimal designs (*m*, *n*) in each structure; GoogleNet had an optimal design structure of (3, 30). The model performance of other structures deteriorated when *m* was above five and *n* was below fifteen (days). In the regression model, Resnet 50 and Resnet 101 had a similar optimal design of (1, 29), while GoogleNet and Inception v3 required different (m, n) designs; the optimal design of GoogleNet was (1, 2) and that of Inception v3 was (1, 27).

Simulation of *Alexandrium catenella*

The model performance with optimal input design is summarized in **Table 1**. Among them, GoogleNet and Resnet 101 offer the best classification performance with an accuracy of 96.83% and RMSE of 1.20 [log(cells L^{-1})], respectively. The model performance of Resnet 50 was similar to Resnet 101 with accuracy and RMSE of 96.29% and 1.29 [log(cells L^{-1})], respectively. Inception v3 (accuracy of 95.76%) and GoogleNet [RMSE of 1.66 log(cells L^{-1})] presented the worst performance in classification (with 95.76% accuracy) and regression models, respectively.

The results of the regression CNN model are plotted against observed *A. catenella* in **Figures 4C.1-4**. In Resnet 101, the simulated *A. catenella* showed good agreement with observations. GoogleNet showed that the simulated *A. catenella* was overestimated in the low-density cells and underestimated in the high-density cells. The temporal-spatial distribution of *A. catenella* is presented with observation using GoogleNet and ResNet 101 because these structures showed the best performance in classification and regression CNN (**Figure 5A**). The simulated distribution substantially followed actual *A. catenella* blooms. On December 17, 2016, and May 23, 2017, most areas did not provoke *A. catenella* bloom in both simulated and observed distribution, indicating that our model can simulate this phenomenon. On March 27, 2018, *A. catenella* blooms were observed in the coastal water. During this period, the simulated distribution of blooms can describe the actual spatial features; the eastern coast presented a relatively higher density than the western one. The data on March 28 and April 25 of 2017 shows increasing *A. catenella* spring bloom in the study area. The simulated distribution in both periods was in line with the actual distribution; the model generated high-density cells in the eastern coast and non-bloom near Geoje Island of the west coast. On August 19, 2019, the model determined the non-bloom and substantially low density on the western coast. Mismatched results of the spatial distributions are revealed in three spaces without observed data; the channel connected to the northern enclosed bay on May 23, 2017, the western off sea on March 28, 2017, and the enclosed bay on August 19, 2019. **Figure 5B** shows the performance of *A. catenella* forecasting with various lead times. All forecast results were found to be worse than those of nowcasting. The average accuracy of the classification model was 95.85% for a lead of up to five days, decreasing sharply thereafter. The average RMSE of the regression model was 1.36 [log(cells L^{-1})] until five forecast lead (days) and increased sharply thereafter.

Model Interpretability for Gradient-Weighted Class Activation Mapping

Gradient-weighted class activation mapping (Grad-CAM) shows the feature maps of classification and regression CNN models with GoogleNet and Resnet 101 structures, respectively (**Figure 6**). These maps were generated depending on the outbreak of *A. catenella* blooms (e.g., bloom and non-bloom) and density level (e.g., 5–25th percentile, 25–50th percentile, 50–75th percentile, and 75–95th percentile). The regions with high values are regarded as important features in the map. In the classification model, the important features are affiliated with salinity, temperature, water elevation, latitude-velocity of water, and NH_4-N from 20 to 28 days of lookback when the bloom is not provoked (**Figure 6(A.1)**). Among these variables, temperature and salinity are the most influenced variables, as evident from the high feature map values. In contrast, the important bloom features highlighted the variables from 3 to 12 days (**Figure 6(A.2)**). In the regression CNN model, the 5–25th percentile density show salinity, temperature, water elevation, and NH_4-N from 5 to 30 days of

TABLE 1 | Model performance and optimal inputs (*m* and *n*).

	Classification model				Regression model					
Structure	***m***	***n***	**Accuracy (%)**		***m***	***n***	**RMSE [(log(cells L^{-1})]**		**R^2**	
			Train	**Validation**			**Train**	**Validation**	**Train**	**Validation**
Resnet 50	1*	16	96.87	96.29	1	29	0.93	1.29	0.93	0.84
Resnet 101	1*	19	99.32	96.29	1	29	0.72	1.20	0.92	0.85
GoogleNet	3	30	96.14	96.83	1	2	1.62	1.66	0.62	0.71
Inception v3	1*	25	100	95.76	1	27	0.74	1.27	0.94	0.84

*Yellow indicates the optimum structure; * indicates that existence of multiple optimum designs.*

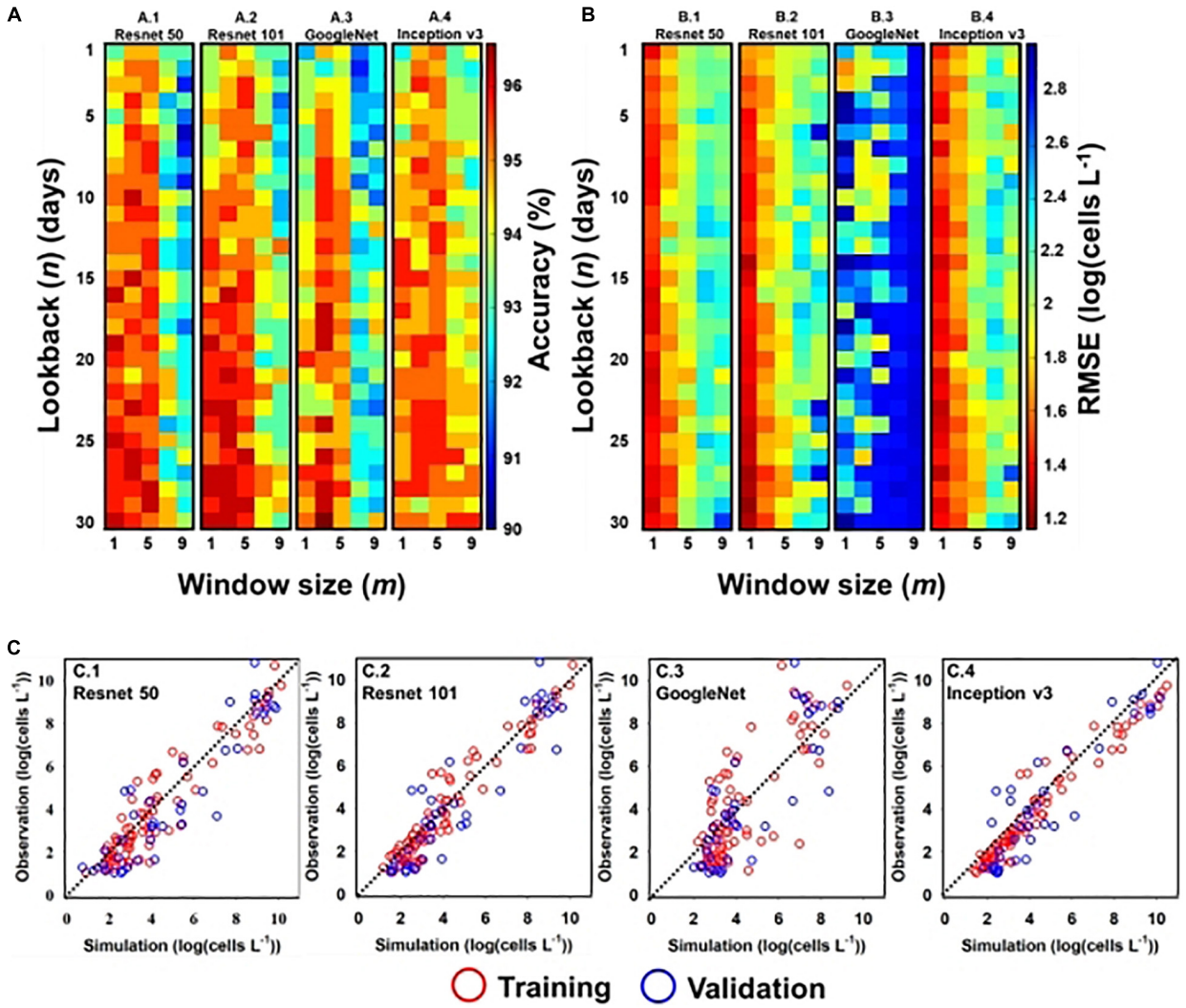

FIGURE 4 | Optimal input and simulation results of *A. catenella*—**(A)** optimal input (*m* and *n*) of classification CNN structures: **(A.1)** Resnet 50, **(A.2)** Resnet 101, **(A.3)** GoogleNet, and **(A.4)** Inception v3; **(B)** optimal input (*m* and *n*) of regression CNN structures: **(B.1)** Resnet 50, **(B.2)** Resnet 101, **(B.3)** GoogleNet, and **(B.4)** Inception v3; **(C)** simulated and observed densities of *A. catenella* with regression CNN structures [e.g., **(C.1)** Resnet 50, **(C.2)** Resnet 101, **(C.3)** GoogleNet, and **(C.4)** Inception v3] with optimal input. In **(A)** and **(B)**, *m* and *n* denote the input window (i.e., height × width) and lookback sizes, respectively, whereas the color range indicates the accuracy from the lowest (blue) to the highest (red) values. In **(C)**, the red and blue circles indicate the training and validation sets, respectively. The observed line has a slope of 1:1.

lookback as important variables (**Figure 6(B.1)**). The important variables in the 25–50th percentile were similar to the 5–25th percentile density (**Figure 6(B.2)**). In the 50–75th percentile, the lookback from 6 to 27 days is highlighted in the model, while that in the 75–95th percentiles ranged from 4 to 22 days (**Figures 6(B.3), (B.4)**) respectively).

DISCUSSION

Ocean Modeling Results

The physical and chemical simulation results showed good agreement with the observation results (**Supplementary Figures 3, 4**, respectively). However, the salinity simulation was worse than that of water temperature and elevation. Previous studies have also shown that salinity cannot improve model accuracy (Hjøllo et al., 2009; Martyr-Koller et al., 2017) because it is vulnerable to external sources (e.g., rainfall and freshwater), increasing simulation uncertainty (Arfib and Charlier, 2016). The simulated water temperature at station 1 was overestimated during winter (December to February), while station 2 provided reliable outcomes in this season. This is because the model was limited to tracking water temperature at two different points if the difference between them was more than 5 °C. Moreover, the NH_4-N simulation followed the observed trends, whereas the PO_4-P simulation was less accurate. Specifically, the simulated NH_4-N was underestimated at the peak point of observation and the simulated PO_4-P was only able to follow the variation

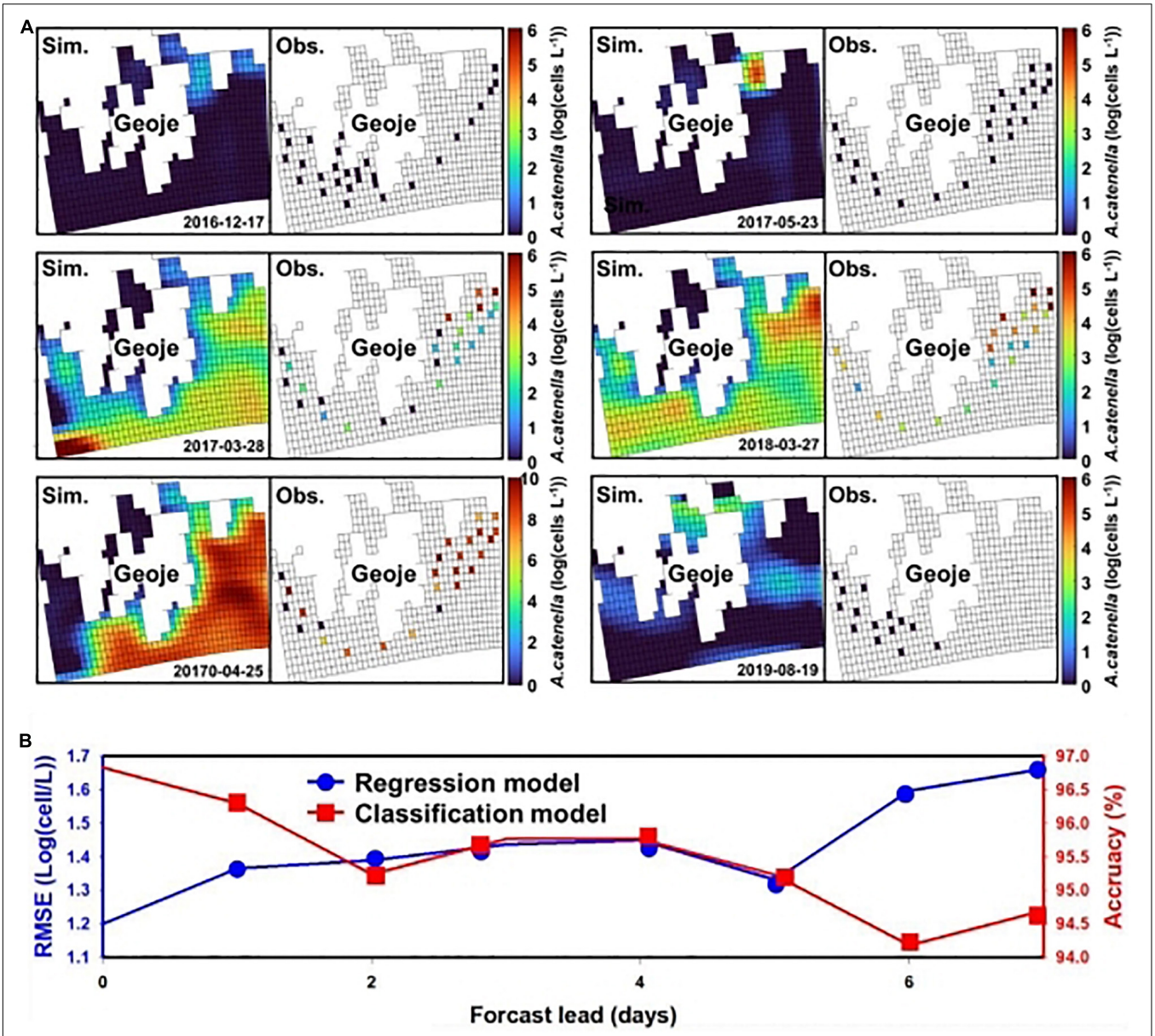

FIGURE 5 | Spatial distribution of *A. catenella* and forecast performance with lead time—**(A)** spatial distribution of *A. catenella* on December 17, 2016, March 28, 2017, April 25, 2017, May 23, 2017, March 27, 2018, and August 19, 2019; **(B)** *A. catenella* forecast performance with lead time. In **(A)**, the left and right figures indicate the simulated and observed distributions of *A. catenella*, respectively. The color range indicates the density variation in *A. catenella* from the lowest (blue) to the highest (red) value. The spatial distributions were generated using GoogleNet and ResNet 101. In **(B)**, the blue and red curves indicate the performance of regression and classification CNN models, respectively. The x and y (left and right) axes denote the forecast lead time (days), root-mean-square error (RMSE) of the regression model, and accuracy of the classification model, respectively. The model with lower RMSE is considered for regression while that with higher accuracy is selected for classification.

in observation. This demonstrated that the simulation of PO_4-P and NH_4-N could not improve model accuracy because these nutrients were observed in low concentrations, making the model sensitive to external sources. Eilola et al. (2009) and Feng et al. (2015) demonstrated that the simulated PO_4-P was underestimated when compared with the observed values, and the simulated nitrogen encountered limitations when following the peak concentration. Additionally, the validation of these simulations is still limited by the lack of observed data. In further research, we will collect more data from additional sites.

Optimal Input Design

In general, the optimal inputs of both the models yielded a small window size below five and long lookback of more than 19 days (**Figures 4A,B**). Therefore, spatial information below 5 5 grids was sufficient for simulating *A. catenella*, and temporal

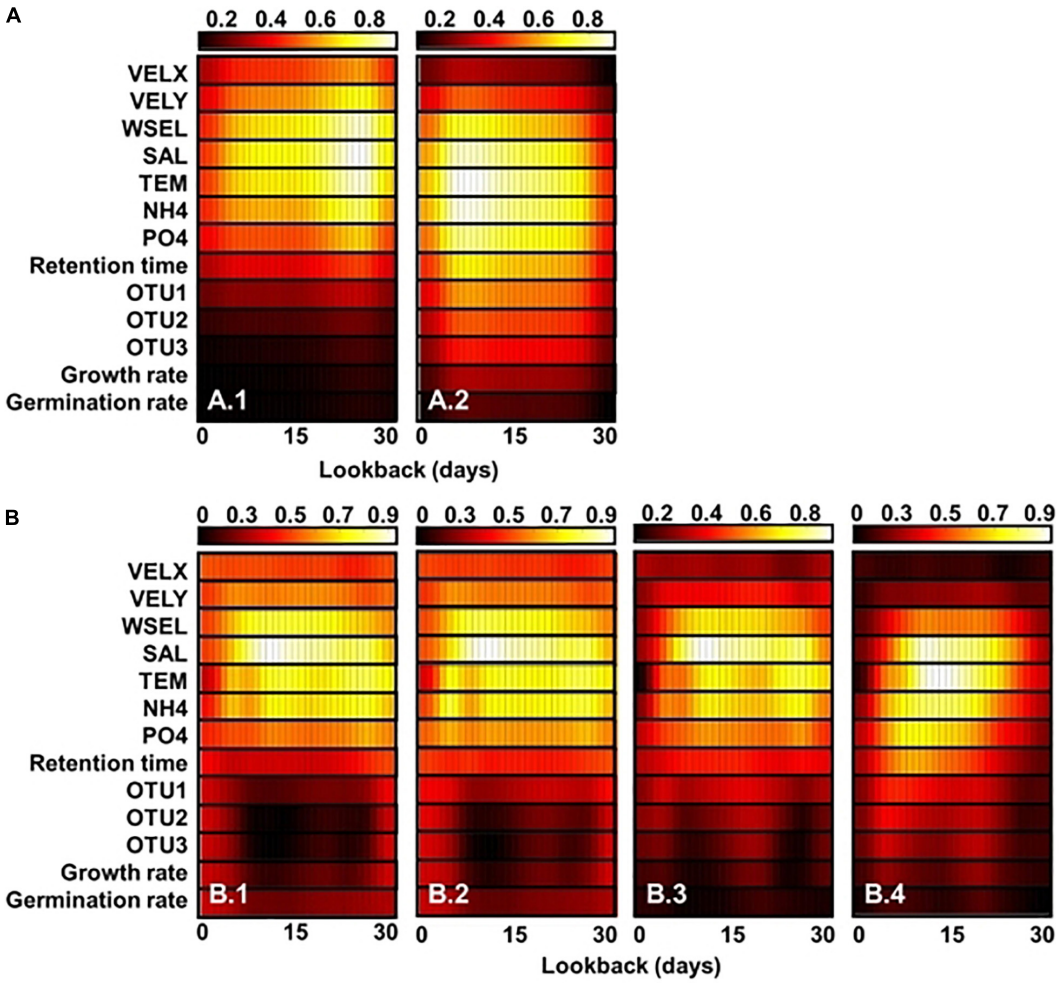

FIGURE 6 | Feature heat maps of classification **(A)** and regression **(B)** CNN models obtained using Grad-CAM for the (A.1) bloom and (A.2) no-bloom conditions as well as cases wherein the *A. catenella* density lies in the (B.1) 5–25, (B.2) 25–50, (B.3) 50–75, and (B.4) 75–90 percentile ranges. The x and y axes represent the lookback and variables values, respectively. The color indicates the degree importance from the lowest (black) to the highest (white). The larger the variable value in a given cell, the greater is its importance. VELX, VELY, WSEL, SAL, TEM, OTU1, OUT2, and OUT3 denote the longitudinal velocity, latitudinal velocity, water-surface elevation, salinity, water temperature, microparticle-associated bacteria, nanoparticle-associated (NP) bacteria, and free-living (FL) bacteria, respectively.

information from past 30 days was adequate for improving the simulation performance. The suitable range of grid sizes for the spatial distribution reflected the behavioral characteristics of the species. For the models with window sizes of seven and nine, the simulation performances decreased sharply, indicating that superfluous information might deteriorate the model accuracy. Previous studies have demonstrated that needless data could restrict the effectiveness of model training (Chulkov et al., 2019; Cova and Pais, 2019; Xu et al., 2019). In contrast, in the classification model, the optimal size (m, n) of the input varied depending on the structure based on whether the CNN structures adopted a skip connection or a parallel CNN layer (He et al., 2016b; Szegedy et al., 2016). This demonstrated that the model performance was affected by the structure and the properties of the input data. In addition, a simpler structure, such as GoogLeNet, was appropriate for classifying both bloom and non-bloom (**Figure 4(A.3)**). In the regression model, Resnet 50 and 101 had similar optimal input properties, whereas GoogleNet and Inception v3 showed lower performances than Resnet. Among the structures, Resnet 101 was the best regression model. This demonstrates that skip connection is appropriate for estimating the density of *A. catenella* as it can directly connect information from a previous layer to the next layer using skipped layers (Khan et al., 2019). On the contrary, GoogleNet and Inception v3 applied parallel CNN layers having 1×1, 3×3, and 5×5 filter sizes. Hence, the optimization process is important to improve how the input data and model structures affect model training.

Simulation of *Alexandrium catenella*

ResNet 101 offered the best performance in terms of simulating the cell density of *A. catenella* that followed the observation distribution, whereas GoogLeNet showed limited performance in simulating *A. catenella* in low and high densities (**Figure 4C**).

Specifically, the simulated *A. catenella* from GoogLeNet was overestimated in the case of low density and underestimated in the case of high density, indicating that this model was trained with a narrower range of cell density than that of the other models. The performance discrepancy between ResNet 101 and GoogLeNet may be attributed to the number of layers; ResNet 101 had more layers than GoogLeNet. This demonstrates that the number of layers could affect a model's performance. According to previous studies concerning CNNs (Khan et al., 2019; Baek et al., 2020), the performance of deep learning models can be influenced by the number of layers. However, a higher number of layers can increase model complexity, leading to the overfitting problem, i.e., the simulated results will correspond too closely to the training data, thereby failing to fit the validation data and predict future simulated results in a reliable manner (Cortes et al., 2017). In contrast, GoogLeNet demonstrated the attainment of a superior validation accuracy (96.83%) as compared to other structures. This confirms that a complex structure is not necessary to identify bloom occurrence and that sufficiently accurate results can be obtained via cell estimation. The simulated distribution substantially followed the feature of actual *A. catenella* blooms (**Figure 5A**). Depending on bloom and non-bloom, the model generated similar spatial patterns of density with observation: on December 17, 2016, May 23, 2017, and August 19, 2019, there were no bloom outbreaks in both simulated and observed distributions; on March 27, 2018, the *A. catenella* blooms were observed in both the distributions; on March 28, 2017, and April 25, 2017, both distributions showed the bloom and non-bloom area in the coast. However, on March 28, 2017, the simulated distribution was determined as blooms in most areas, while there was no bloom of the observed distribution in the western sea. The high uncertainty in population dynamics could be due to *in situ* environmental and biological variables heterogeneously influencing the initiation, development, and ultimate demise of HABs (McGillicuddy et al., 2015; Brandenburg et al., 2017). The model generated a notable density in the specific spaces without observed data; the simulation of May 23, 2017, and August 19, 2019, presented a higher density in the channel connected to the northern enclosed bay and the enclosed bay, respectively. The mismatch results between simulation and observation also increase the model uncertainty by limiting the quantification of the exact spatial distribution of HABs. Remote sensing can solve this by improving model performance with the spatial distribution of physical, chemical, biological, and atmospheric factors (Shen et al., 2020). Forecast simulation showed lower performance than nowcasting. The performance of the classification and regression model decreased with increasing lead time and deteriorated sharply at a specific date (**Figure 5B**). These simulation results showed that the model performance would degrade with increasing forecast lead time (days) because the input data might correspond poorly with the future ocean physical and biological processes affecting *A. catenella*. Prior studies have reported a decline in model performance with increasing lead time. Chattopadhyay et al. (2020) reported a decrease in the model performance from 73 to 47% while predicting a cold-spell class as the lead time changed from 1 to 5 days. Pyo et al. (2020) observed the validation accuracy to decrease with increasing lead time when simulating Microcystis—a causative algal taxon of freshwater HAB. As reported by Miao et al. (2019), an increase in the forecast lead time causes an increase in model uncertainty and imperfect representation of the extracted features. This deteriorated model training and reduced the forecast accuracy. Therefore, this study demonstrated the robust short-term *A. catenella* forecasting ability of the DL model.

Model Interpretability for Gradient-Weighted Class Activation Mapping

Temperature and salinity are factors with the greatest influence on the classification and regression models, as confirmed by the high values observed in the feature map (**Figures 6A,B**). Temperature and salinity affect cyst germination and *A. catenella* growth, thereby causing the proliferation of *A. catenella* cells (Itakura and Yamaguchi, 2001; Nagai et al., 2004). Ichimi et al. (2001) reported that temperature plays a critical role in cyst germination and algal bloom. Parkhill and Cembella (1999) demonstrated that salinity influences *A. catenella* growth. NH_4-N and water elevation were also highlighted. *A. catenella* uses a nitrogen source for growth and prefers ammonium uptake (Siu et al., 1997). Collos et al. (2006) observed that the growth of *A. catenella* is limited by ammonium uptake and accumulation. Moreover, an increase in water elevation tends to weaken and accelerate the advection and dispersion of algal blooms, respectively (Wu and Kong, 2009). Additionally, Giddings et al. (2014) demonstrated that the physical factors of oceans influence HAB development. The regression CNN model identifies fewer important features that increase the density of *A. catenella.* In particular, factors, such as the salinity, temperature, and NH_4-N concentration over a 5–30-day lookback period were highlighted in the 5–25th percentile while higher densities were simulated considering variables over 6–22-day lookback period. The results can be related to the initiation for bloom development of a given inoculum size at a suitable time. The Grad-CAM result reveals that the proposed model generates cell density by changing the highlighted variables. This is because the variables of influence differ depending on the life cycle *A. catenella*. The water temperature and salinity initiate the development of *A. catenella* while the nutrient and retention time accelerate its growth (Itakura and Yamaguchi, 2001; Nagai et al., 2004; Armi et al., 2011). Previous studies have reported the transitions in the highlighted region as change input. Panwar et al. (2020) adopted Grad-CAM to identify important areas of COVID-19 detection and demonstrated the change in the highlighted area as an input image. Cheng et al. (2019) extracted hip-fracture features using Grad-CAM and X-ray images. This study estimates the spatiotemporal distribution of *A. catenella* using CNN and determines the cause of bloom using Grad-CAM. Most previously reported algal simulations have focused on inland water species, such as cyanobacteria, green algae, and diatom. However, only few studies have addressed HAB modeling in seawater and only analyzed limited species (e.g., *A. fundyense*). HAB modeling in marine ecosystems should

consider several environmental factors, such as the temperature, salinity, and velocity of water as well as symbiosis among different species. The paucity of relevant research in this domain could be attributed to the need for the use of complex modeling techniques and availability of limited observations (Ralston and Moore, 2020). This study overcomes this limitation via successful application of deep learning for simulating *A. catenella* HAB using an ocean model. Further research can be performed considering other species (e.g., *Cochlodinium* and *Karenia*) with additional monitoring. The findings of this research are expected to improve the applicability, expendability, and accuracy of HAB modeling using the deep learning models. Therefore, the proposed approach can be considered useful in establishing HAB management in marine environments.

CONCLUSION

This study applied regression and classification using CNN models for simulating spring blooms of *A. catenella*. The classification was used to analyze the initiation of *A. catenella*, while the regression generated the density of the genera. GoogLeNet and Resnet 101 were identified as the best deep learning structures for classification and regression using CNNs, yielding an accuracy and RMSE of 96.8% and 1.20 [log(cells L^{-1})], respectively. Using Grad-CAM, the salinity, temperature, and NH_4-N were found to be significant variables that influence the bloom of *A. catenella*. In particular, factors such as the salinity, temperature, and NH_4-N concentration over a 5–30-day lookback period were highlighted in the 5–25th percentile, while higher densities were simulated considering variables over the 6–22 day lookback period. The results can be related to the initiation for bloom development of a given inoculum size at a suitable time. As per the authors, the study makes a significant contribution to the literature because understanding and mitigating harmful algal blooms (HABs) are important for reducing economic losses and public health damages. In contrast to modeling methods that can only measure simulation performance, the proposed model can simulate the initiation and growth of HABs based on influencing factors. However, to establish an AI-based HAB modeling system, the following challenges remain: (1) additional monitoring that includes environmental variables (NH_4-N and PO_4-P) and target species (*A. catenella*) is required, and (2) models should be trained using observations from various sites to improve model adaptability. Further research can improve the models via continuous data acquisition. Hence, the suggested models could be useful in establishing HAB management systems for aquatic environments.

DATA AVAILABILITY STATEMENT

All data needed to evaluate the conclusions in the paper are present in the paper and/or the **Supplementary Material**. Additional data related to this paper may be requested from the authors.

AUTHOR CONTRIBUTIONS

S-SB, YOK, and KHC conceptualized the proposed research. S-SB was responsible for preparing the methodology, data visualization, and preparing the original draft of the manuscript. YSK and JCP performed the data curation. SHB, C-YA, and H-MO performed the data validation. YOK and KHC handled funding acquisition. All authors reviewed and edited the manuscript, subsequent to the first draft.

FUNDING

This study was supported by the Ministry of Science, ICT & Future Planning (grant NRF-2016M1A5A1027457) and Korean Institute of Ocean Science and Technology (PE99912).

SUPPLEMENTARY MATERIAL

The Supplementary Material for this article can be found online at: https://www.frontiersin.org/articles/10.3389/fmars.2021.729954/full#supplementary-material

REFERENCES

Akiba, T., Suzuki, S., and Fukuda, K. (2017). Extremely large minibatch sgd: training resnet-50 on imagenet in 15 minutes. *arXiv* [Preprint] arXiv:1711.04325,

Anderson, D. M., Cembella, A. D., and Hallegraeff, G. M. (2012). Progress in understanding harmful algal blooms: paradigm shifts and new technologies for research, monitoring, and management. *Annu. Rev. Mar. Sci.* 4, 143–176. doi: 10.1146/annurev-marine-120308-081121

Arfib, B., and Charlier, J.-B. (2016). Insights into saline intrusion and freshwater resources in coastal karstic aquifers using a lumped rainfall–discharge–salinity model (the Port-Miou brackish spring, SE France). *J. Hydrol.* 540, 148–161. doi: 10.1016/j.jhydrol.2016.06.010

Armi, Z., Milandri, A., Turki, S., and Hajjem, B. (2011). *Alexandrium catenella* and *Alexandrium tamarense* in the North Lake of Tunis: bloom characteristics and the occurrence of paralytic shellfish toxin. *Afr. J. Aquat. Sci.* 36, 47–56. doi: 10.2989/16085914.2011.559688

Baek, S. S., Choi, Y., Jeon, J., Pyo, J., Park, J., and Cho, K. H. (2020). Replacing the internal standard to estimate micropollutants using deep and machine learning. *Water Res.* 188:116535. doi: 10.1016/j.watres.2020.116535

Baek, S. S., Kwon, Y. S., Pyo, J., Choi, J., Kim, Y. O., and Cho, K. H. (2021). Identification of influencing factors of A. catenella bloom using machine learning and numerical simulation. *Harmful Algae* 103:102007. doi: 10.1016/j.hal.2021.102007

Brandenburg, K. M., de Senerpont Domis, L. N., Wohlrab, S., Krock, B., John, U., van Scheppingen, Y., et al. (2017). Combined physical, chemical and biological factors shape *Alexandrium ostenfeldii* blooms in the Netherlands. *Harmful Algae* 63, 146–153. doi: 10.1016/j.hal.2017.02.004

Brion, G. M., Neelakantan, T., and Lingireddy, S. (2002). A neural-network-based classification scheme for sorting sources and ages of fecal contamination in water. *Water Res.* 36, 3765–3774. doi: 10.1016/s0043-1354(02)00091-x

Caruana, R., and Niculescu-Mizil, A. (2006). "An empirical comparison of supervised learning algorithms," in *Proceedings of the 23rd International Conference on Machine Learning*, (New York, NY), 161–168.

Chang, D. S., Shin, I. S., Pyeun, J. H., and Park, Y. H. (1987). A study on paralytic shellfish poison of sea mussel, *Mytilus edulis*-food poisoning accident in Gamchun Bay, Pusan, Korea, 1986. *Kor. J. Fish. Aquat. Sci.* 20, 293–299.

Chattopadhyay, A., Nabizadeh, E., and Hassanzadeh, P. (2020). Analog forecasting of extreme-causing weather patterns using deep learning. *J. Adv. Model. Earth Syst.* 12:e2019MS001958.

Chen, D., and Manning, C. D. (2014). "A fast and accurate dependency parser using neural networks," in *Proceedings of the 2014 Conference on Empirical Methods in Natural Language Processing (EMNLP)*, (Doha), 740–750.

Chen, L., Chen, J., Hajimirsadeghi, H., and Mori, G. (2020). "Adapting grad-CAM for embedding networks," in *Proceedings of the IEEE Winter Conference on Applications of Computer Vision*, (Snowmass, CO), 2794–2803.

Cheng, C. T., Ho, T. Y., Lee, T. Y., Chang, C. C., Chou, C. C., Chen, C. C., et al. (2019). Application of a deep learning algorithm for detection and visualization of hip fractures on plain pelvic radiographs. *Eur. Radiol.* 29, 5469–5477. doi: 10.1007/s00330-019-06167-y

Chulkov, A. O., Nesteruk, D. A., Vavilov, V. P., Moskovchenko, A. I., Saeed, N., and Omar, M. (2019). Optimizing input data for training an artificial neural network used for evaluating defect depth in infrared thermographic nondestructive testing. *Infrared Phys. Technol.* 102:103047. doi: 10.1016/j.infrared.2019.103047

Collos, Y., Lespilette, M., Vaquer, A., Laabir, M., and Pastoureaud, A. (2006). Uptake and accumulation of ammonium by *Alexandrium catenella* during nutrient pulses. *Afr. J. Mar. Sci.* 28, 313–318. doi: 10.2989/18142320609504169

Cortes, C., Gonzalvo, X., Kuznetsov, V., Mohri, M., and Yang, S. (2017). "Adanet: adaptive structural learning of artificial neural networks," in *Proceedings of the 34 th International Conference on Machine Learning (PMLR, 2017)*, (Sydney), 874–883.

Cova, T. F., and Pais, A. A. (2019). Deep learning for deep chemistry: optimizing the prediction of chemical patterns. *Front. Chem.* 7:809.

Cui, Y., Chun, S. J., Baek, S. S., Baek, S. H., Kim, P. J., Son, M., et al. (2020). Unique microbial module regulates the harmful algal bloom (*Cochlodinium polykrikoides*) and shifts the microbial community along the Southern Coast of Korea. *Sci. Total Environ.* 721:137725. doi: 10.1016/j.scitotenv.2020.137725

Dai, Z., Chu, A., Stive, M., Zhang, X., and Yan, H. (2011). Unusual salinity conditions in the Yangtze Estuary in 2006: Impacts of an extreme drought or of the Three Gorges Dam? *Ambio* 40, 496–505. doi: 10.1007/s13280-011-0148-2

Deng, J., Dong, W., Socher, R., Li, L. J., Li, K., and Fei-Fei, L. (2009). "Imagenet: a large-scale hierarchical image database," in *Proceedings of the IEEE Conference on Computer Vision and Pattern Recognition*, (Miami, FL), 248–255.

Du, J., and Shen, J. (2016). Water residence time in Chesapeake Bay for 1980–2012. *J. Mar. Syst.* 164, 101–111. doi: 10.1016/j.jmarsys.2016.08.011

Eilola, K., Meier, H. M., and Almroth, E. (2009). On the dynamics of oxygen, phosphorus and cyanobacteria in the Baltic Sea; a model study. *J. Mar. Syst.* 75, 163–184. doi: 10.1016/j.jmarsys.2008.08.009

Feng, Y., Friedrichs, M. A., Wilkin, J., Tian, H., Yang, Q., Hofmann, E. E., et al. (2015). Chesapeake Bay nitrogen fluxes derived from a land-estuarine ocean biogeochemical modeling system: Model description, evaluation, and nitrogen budgets. *J. Geophys. Res. Biogeosci.* 120, 1666–1695. doi: 10.1002/2015jg002931

Giddings, S. N., MacCready, P., Hickey, B. M., Banas, N. S., Davis, K. A., Siedlecki, S. A., et al. (2014). Hindcasts of potential harmful algal bloom transport pathways on the Pacific Northwest coast. *J. Geophys. Res. Oceans* 119, 2439–2461. doi: 10.1002/2013jc009622

Gobler, C. J., Doherty, O. M., Hattenrath-Lehmann, T. K., Griffith, A. W., Kang, Y., and Litaker, R. W. (2017). Ocean warming since 1982 has expanded the niche of toxic algal blooms in the North Atlantic and North Pacific oceans. *Proc. Natl. Acad. Sci. U.S.A.* 114, 4975–4980. doi: 10.1073/pnas.1619575114

Han, M. S., Jeon, J. K., and Kim, Y. O. (1992). Occurrence of dinoflagellate *Alexandrium tamarense*, a causative organism of paralytic shellfish poisoning in Chinhae Bay. *Korea. J. Plankton Res.* 14, 1581–1592. doi: 10.1093/plankt/14.11.1581

He, K., Zhang, X., Ren, S., and Sun, J. (2016a). "Deep residual learning for image recognition," in *Proceedings of the IEEE Conference on Computer Vision and Pattern Recognition*, (Las Vegas, NV), 770–778.

He, K., Zhang, X., Ren, S., and Sun, J. (2016b). "Identity mappings in deep residual networks," in *European Conference on Computer Vision*, eds B. Leibe, J. Matas, N. Sebe, and M. Welling (Cham: Springer), 630–645. doi: 10.1007/978-3-319-46493-0_38

He, R., McGillicuddy, D. J. Jr., Keafer, B. A., and Anderson, D. M. (2008). Historic 2005 toxic bloom of *Alexandrium fundyense* in the western Gulf of Maine: 2. Coupled biophysical numerical modeling. *J. Geophys. Res. Oceans* 113, C07040.

Heisler, J., Glibert, P. M., Burkholder, J. M., Anderson, D. M., Cochlan, W., Dennison, W. C., et al. (2008). Eutrophication and harmful algal blooms: a scientific consensus. *Harmful Algae* 8, 3–13. doi: 10.1016/j.hal.2008.08.006

Hjøllo, S. S., Skogen, M. D., and Svendsen, E. (2009). Exploring currents and heat within the North Sea using a numerical model. *J. Mar. Syst.* 78, 180–192. doi: 10.1016/j.jmarsys.2009.06.001

Hoagland, P. A. D. M., Anderson, D. M., Kaoru, Y., and White, A. W. (2002). The economic effects of harmful algal blooms in the United States: estimates, assessment issues, and information needs. *Estuaries.* 25, 819–837. doi: 10.1007/bf02804908

Ichimi, K., Yamasaki, M., Okumura, Y., and Suzuki, T. (2001). The growth and cyst formation of a toxic dinoflagellate, *Alexandrium tamarense*, at low water temperatures in northeastern Japan. *J. Exp. Mar. Biol. Ecol.* 261, 17–29. doi: 10.1016/s0022-0981(01)00256-8

Ishikawa, A., Hattori, M., Ishii, K. I., Kulis, D. M., Anderson, D. M., and Imai, I. (2014). *In situ* dynamics of cyst and vegetative cell populations of the toxic dinoflagellate *Alexandrium catenella* in Ago Bay, central Japan. *J. Plankton Res.* 36, 1333–1343. doi: 10.1093/plankt/fbu048

Itakura, S., and Imai, I. (2014). Economic impacts of harmful algal blooms on fisheries and aquaculture in western Japan-An overview of interannual variability and interspecies comparison. *PICES Sci. Rep.* 47, 17.

Itakura, S., and Yamaguchi, M. (2001). Germination characteristics of naturally occurring cysts of *Alexandrium tamarense* (Dinophyceae) in Hiroshima Bay, Inland Sea of Japan. *Phycologia* 40, 263–267. doi: 10.2216/i0031-8884-40-3-263.1

Jeong, S., Yeon, K., Hur, Y., and Oh, K. (2010). Salinity intrusion characteristics analysis using EFDC model in the downstream of Geum River. *J. Environ. Sci.* 22, 934–939. doi: 10.1016/s1001-0742(09)60201-1

Kang, E.-J., Yang, H., Lee, H.-H., Kim, K.-S., and Kim, C.-H. (2012). Characteristics of fish fauna collected from near estuaries bank and fish-way on the bank of Naktong river. *Kor. J. Ichthyol.* 24, 201–219.

Khan, R. U., Zhang, X., and Kumar, R. (2019). Analysis of ResNet and GoogleNet models for malware detection. *J. Comp. Virol. Hacking Tech.* 15, 29–37. doi: 10.1007/s11416-018-0324-z

Kim, H.-C., and Yoo, S. (2007). Relationship between phytoplankton bloom and wind stress in the sub-polar frontal area of the Japan/East Sea. *J. Mar. Syst.* 67, 205–216. doi: 10.1016/j.jmarsys.2006.05.016

Kim, Y. O., Choi, J., Baek, S. H., Lee, M., and Oh, H.-M. (2020). Tracking *Alexandrium catenella* from seed-bed to bloom on the southern coast of Korea. *Harmful Algae* 99:101922. doi: 10.1016/j.hal.2020.101922

Kim, Y.-O., Park, M.-H., and Han, M.-S. (2002). Role of cyst germination in the bloom initiation of *Alexandrium tamarense* (Dinophyceae) in Masan Bay, Korea. *Aquat. Microb. Ecol.* 29, 279–286. doi: 10.3354/ame029279

Kim, Y. S., Son, H.-J., and Jeong, S.-Y. (2015). Isolation of an algicide from a marine bacterium and its effects against the toxic dinoflagellate *Alexandrium catenella* and other harmful algal bloom species. *J. Microbiol.* 53, 511–517. doi: 10.1007/s12275-015-5303-1

Koundinya, S., Sharma, H., Sharma, M., Upadhyay, A., Manekar, R., Mukhopadhyay, R., et al. (2018). "2d-3d CNN based architectures for spectral reconstruction from RGB images," in *Proceedings of the IEEE Conference on Computer Vision and Pattern Recognition Workshops*, (Salt Lake City, UT), 844–851.

Kozich, J. J., Westcott, S. L., Baxter, N. T., Highlander, S. K., and Schloss, P. D. (2013). Development of a dual-index sequencing strategy and curation pipeline for analyzing amplicon sequence data on the MiSeq Illumina sequencing platform. *Appl. Environ. Microbiol.* 79, 5112–5120. doi: 10.1128/AEM.01043-13

LeCun, Y., Bengio, Y., and Hinton, G. (2015). Deep learning. *Nature* 521, 436–444.

Loussaief, S., and Abdelkrim, A. (2018). Convolutional neural network hyperparameters optimization based on genetic algorithms. *Int. J. Adv. Comp. Scie. Appl.* 9, 252–266.

Martyr-Koller, R. C., Kernkamp, H. W. J., Van Dam, A., van der Wegen, M., Lucas, L. V., Knowles, N., et al. (2017). Application of an unstructured 3D finite

volume numerical model to flows and salinity dynamics in the San Francisco Bay-Delta. *Estuar. Coast. Shelf Sci.* 192, 86–107. doi: 10.1016/j.ecss.2017.04.024

McGillicuddy, D. J. Jr. (2010). Models of harmful algal blooms: conceptual, empirical, and numerical approaches. *J. Mar. Syst.* 83:105. doi: 10.1016/j.jmarsys.2010.06.008

McGillicuddy, D. J. Jr., Sedwick, P. N., Dinniman, M. S., Arrigo, K. R., Bibby, T. S., Greenan, B. J. W., et al. (2015). Iron supply and demand in an Antarctic shelf ecosystem. *Geophys. Res. Lett.* 42, 8088–8097. doi: 10.1002/2015GL065727

Miao, Q., Pan, B., Wang, H., Hsu, K., and Sorooshian, S. (2019). Improving monsoon precipitation prediction using combined convolutional and long short term memory neural network. *Water* 11:977. doi: 10.3390/w11050977

Montgomery, D. C., Peck, E. A., and Vining, G. G. (2021). *Introduction to Linear Regression Analysis*. Hoboken, NJ: John Wiley & Sons.

Nagai, S., Matsuyama, Y., Oh, S.-J., and Itakura, S. (2004). Effect of nutrients and temperature on encystment of the toxic dinoflagellate *Alexandrium tamarense* (Dinophyceae). *Plankton Biol. Ecol.* 51, 103–109.

National Fisheries Research and Development Institute (NFRDI) (2020). *Paralytic Shellfish Poisoning Report*. Available online at: https://www.nifs.go.kr/page?id=kr_index (accessed June 13, 2021).

Panwar, H., Gupta, P. K., Siddiqui, M. K., Morales-Menendez, R., Bhardwaj, P., and Singh, V. (2020). A deep learning and grad-CAM based color visualization approach for fast detection of COVID-19 cases using chest X-ray and CT-Scan images. *Chaos Solitons Fractals* 140:110190. doi: 10.1016/j.chaos.2020.110190

Park, T. G., Lim, W. A., Park, Y. T., Lee, C. K., and Jeong, H. J. (2013). Economic impact, management and mitigation of red tides in Korea. *Harmful Algae* 30, S131–S143.

Parkhill, J.-P., and Cembella, A. D. (1999). Effects of salinity, light and inorganic nitrogen on growth and toxigenicity of the marine dinoflagellate *Alexandrium Tamarense* from Northeastern Canada. *J. Plankton Res.* 21, 939–955. doi: 10.1093/plankt/21.5.939

Pinto, L., Mateus, M., and Silva, A. (2016). Modeling the transport pathways of harmful algal blooms in the Iberian coast. *Harmful Algae* 53, 8–16. doi: 10.1016/j.hal.2015.12.001

Pyo, J., Duan, H., Baek, S., Kim, M. S., Jeon, T., Kwon, Y. S., et al. (2019). A convolutional neural network regression for quantifying cyanobacteria using hyperspectral imagery. *Remote Sens. Environ.* 233:111350. doi: 10.1016/j.rse.2019.111350

Pyo, J., Park, L. J., Pachepsky, Y., Baek, S. S., Kim, K., and Cho, K. H. (2020). Using convolutional neural network for predicting cyanobacteria concentrations in river water. *Water Res.* 186:116349. doi: 10.1016/j.watres.2020.116349

Ralston, D. K., and Moore, S. K. (2020). Modeling harmful algal blooms in a changing climate. *Harmful Algae* 91:101729. doi: 10.1016/j.hal.2019.101729

Robert, C. (2014). *Machine Learning, a Probabilistic Perspective*. Milton Park: Taylor & Francis.

Schloss, P. D., Westcott, S. L., Ryabin, T., Hall, J. R., Hartmann, M., Hollister, E. B., et al. (2009). Introducing mothur: open-source, platform-independent, community-supported software for describing and comparing microbial communities. *Appl. Environ. Microbiol.* 75, 7537–7541. doi: 10.1128/AEM.01541-09

Selvaraju, R. R., Cogswell, M., Das, A., Vedantam, R., Parikh, D., and Batra, D. (2017). "Grad-cam: visual explanations from deep networks via gradient-based localization," in *Proceedings of the IEEE International Conference on Computer Vision*, (Venice), 618–626.

Selvaraju, R. R., Das, A., Vedantam, R., Cogswell, M., Parikh, D., and Batra, D. (2016). Grad-CAM: Why did you say that? *arXiv* [preprint] arXiv:1611.07450,

Shen, J., Qin, Q., Wang, Y., and Sisson, M. (2019). A data-driven modeling approach for simulating algal blooms in the tidal freshwater of James River in response to riverine nutrient loading. *Ecol. Modell.* 398, 44–54. doi: 10.1016/j.ecolmodel.2019.02.005

Shen, M., Duan, H., Cao, Z., Xue, K., Qi, T., Ma, J., et al. (2020). Sentinel-3 OLCI observations of water clarity in large lakes in eastern China: implications for SDG 6.3. 2 evaluation. *Remote Sens. Environ.* 247:111950. doi: 10.1016/j.rse.2020.111950

Shin, H. C., Roth, H. R., Gao, M., Lu, L., Xu, Z., Nogues, I., et al. (2016). Deep convolutional neural networks for computer-aided detection: CNN architectures, dataset characteristics and transfer learning. *IEEE Trans. Med. Imaging* 35, 1285–1298. doi: 10.1109/tmi.2016.2528162

Siu, G. K., Young, M. L., and Chan, D. (1997). *Asia-Pacific Conference on Science and Management of Coastal Environment*. Cham: Springer, 117–140.

Szegedy, C., Liu, W., Jia, Y., Sermanet, P., Reed, S., Anguelov, D., et al. (2015). "Going deeper with convolutions," in *Proceedings of the IEEE Conference on Computer Vision and Pattern Recognition*, (Boston, MA), 1–9.

Szegedy, C., Vanhoucke, V., Ioffe, S., Shlens, J., and Wojna, Z. (2016). "Rethinking the inception architecture for computer vision," in *Proceedings of the IEEE Conference on Computer Vision and Pattern Recognition*, (Las Vegas, NV), 2818–2826.

Wang, J., and Wu, J. (2009). Occurrence and potential risks of harmful algal blooms in the East China Sea. *Sci. Total Environ.* 407, 4012–4021. doi: 10.1016/j.scitotenv.2009.02.040

Wang, S., Tang, D., He, F., Fukuyo, Y., and Azanza, R. V. (2008). Occurrences of harmful algal blooms (HABs) associated with ocean environments in the South China Sea. *Hydrobiologia* 596, 79–93. doi: 10.1007/s10750-007-9059-4

Weiher, R., and Sen, A. (2006). *Economic Statistics for NOAA*, 4edn Edn. Silver Spring, MD: National Oceanic and Atmospheric Sciences Administration, 1–67.

Wu, X., and Kong, F. (2009). Effects of light and wind speed on the vertical distribution of *Microcystis aeruginosa* colonies of different sizes during a summer bloom. *Int. Rev. Hydrobiol.* 94, 258–266. doi: 10.1002/iroh.200811141

Xu, Y., Lin, K., Wang, S., Wang, L., Cai, C., Song, C., et al. (2019). Deep learning for molecular generation. *Future Med. Chem.* 11, 567–597.

Yoshioka, H., and Yaegashi, Y. (2018). Robust stochastic control modeling of dam discharge to suppress overgrowth of downstream harmful algae. *Appl. Stochastic Model. Bus. Ind.* 34, 338–354. doi: 10.1002/asmb.2301

Young, T., Hazarika, D., Poria, S., and Cambria, E. (2018). Recent trends in deep learning based natural language processing. *IEEE Comput. Intell. Mag.* 13, 55–75. doi: 10.1109/mci.2018.2840738

Conflict of Interest: The authors declare that the research was conducted in the absence of any commercial or financial relationships that could be construed as a potential conflict of interest.

Publisher's Note: All claims expressed in this article are solely those of the authors and do not necessarily represent those of their affiliated organizations, or those of the publisher, the editors and the reviewers. Any product that may be evaluated in this article, or claim that may be made by its manufacturer, is not guaranteed or endorsed by the publisher.

frontiers in Marine Science

ORIGINAL RESEARCH
published: 17 November 2021
doi: 10.3389/fmars.2021.741912

Study of Heavy Metals and Microbial Communities in Contaminated Sediments Along an Urban Estuary

*Jun Yi[1], Linus Shing Him Lo[2], Hongbin Liu[2,3], Pei-Yuan Qian[2,3] and Jinping Cheng[1,2,3]**

[1] State Key Laboratory of Estuarine and Coastal Research, East China Normal University, Shanghai, China, [2] Hong Kong Branch of the Southern Marine Science and Engineering Guangdong Laboratory (Guangzhou), State Key Laboratory of Marine Pollution and Department of Ocean Science, The Hong Kong University of Science and Technology, Hong Kong SAR, China, [3] The Southern Marine Science and Engineering Guangdong Laboratory (Guangzhou), Guangzhou, China

Estuarine sediments are increasingly contaminated by heavy metals as a result of urbanization and human activities. Continuous multi-heavy metal accumulation in the ecosystem can provoke new effects on top of the complex environmental interactions already present in estuarine ecosystems. It is important to study their integrated influence on imperative microbial communities to reflect on the environmental and ecological risks they may impose. Inductively coupled plasma optical emission spectroscopy analysis for five metals Cd, Cr, Cu, Pb, and Zn showed that Cr and Cu concentrations in intertidal sediments of the urbanized Yangtze River estuary in China have consistently exceeded respective threshold effect concentration (TEC) levels. The geo-accumulation and potential ecological risk index results of the five metals showed that all sampling sites were weakly to moderately polluted, and at considerable to high ecological risk, respectively. Redundancy and correlation analyses showed that Zn followed by Cr in the ecosystem were explanatory of the shifts in recorded microbial community structures. However, the spatial variation in metal concentrations did not correspond to the selection of metal resistance genes (MRGs). Unlike many other dominant bacterial taxa, most of the sulfate-reducing bacteria (SRB) and associated sulfate respiration as the dominant microbially contributed ecological function were found to negatively correlate with Zn and total heavy metal pollution. Zn concentration was proposed to be a potent indicator for heavy metal pollution-associated microbial community compositional shifts under urbanized estuarine conditions. The associations between heavy metals and estuarine microbial communities in this study demonstrate the influence of heavy metals on microbial community structure and adaptations that is often overshadowed by environmental factors (i.e., salinity and nutrients).

Keywords: estuarine sediments, microbial communities, heavy metals, metal resistance genes, ecological functions

OPEN ACCESS

Edited by:
Allyson O'Brien,
The University of Melbourne, Australia

Reviewed by:
Lucienne R. D. Human,
Elwandle Coastal Node, South African Environmental Observation Network, South Africa
Prasanta Rath,
Kalinga Institute of Industrial Technology Deemed to Be University, India
Wenguang Sun,
University of Nebraska-Lincoln, United States

***Correspondence:**
Jinping Cheng
jincheng@ust.hk

Specialty section:
This article was submitted to Marine Pollution, a section of the journal Frontiers in Marine Science

Received: *15 July 2021*
Accepted: *27 October 2021*
Published: *17 November 2021*

Citation:
Yi J, Lo LSH, Liu H, Qian P-Y and Cheng J (2021) Study of Heavy Metals and Microbial Communities in Contaminated Sediments Along an Urban Estuary. Front. Mar. Sci. 8:741912. doi: 10.3389/fmars.2021.741912

INTRODUCTION

Estuarine ecosystems are some of the most economically and ecologically important ecosystems on Earth. However, most estuaries face environmental pollution problems resulting from human industrial activities and urbanization, through routes such as urban runoff and industrial waste discharge. As the intersection between terrestrial and marine ecosystems, urbanized estuarine

sediments are often found to be sinks for wide range of pollutants from land (Barletta et al., 2019). Heavy metal pollution in the estuarine environment is an increasing concern as most metals beyond threshold concentrations are capable of exerting toxicity to organisms (Prabhakaran et al., 2016). Metals in the environment can find their ways to enter the food chain. The toxicity and associated risks of individual metals are relatively well studied with established baselines. However, the joint toxicity and risks imposed by multi-heavy metal mixtures that currently co-exist in the environment have proven to be a challenge. Furthermore, estuarine environments are naturally dynamic systems that are often coupled with seawater dilution effects and various anthropogenic input. All environmental variables can then further exert knock-on effects on the interactions between heavy metal pollutants and the aquatic biota. Thus, the integrated impact of heavy metal pollution in estuarine environments cannot be easily understood in full. Currently, most existing assessments and studies cannot fully consider all major contributing factors such as different environmental variables, multi-heavy metal mixtures and their speciation, and aquatic biota as receivers (Gu and Gao, 2021), when attempting to investigate underlying relationships and mechanisms between heavy metals and the biota. Nevertheless, the need for a better understanding remains fundamental to address the joint toxicity and associated risks of multiple heavy metal-pollution issues.

The microbial communities that inhabit estuarine sediments are both highly diverse and susceptible to environmental changes (Wang et al., 2012). Shifts in microbial community structures, in response to changing environmental conditions, can be sensitive indicators to reflect and assess environmental pollution levels and risks. Previous microbial ecology studies have largely focused on investigating the impact of changing environmental factors such as salinity, pH, and nutrient concentration gradients. Yi et al. (2020) showed that sedimentary microbial communities can well reflect changes in important physicochemical properties such as pH and nutrient concentrations along spatiotemporal scale. In contrast, our current understanding of the interactions between microbial communities and other anthropogenic pollutants in the environment, such as heavy metals, is limited in comparison, but the field is rapidly advancing. Previous study by Yin H. et al. (2015) found that increasing heavy metal contamination in sediments can lead to decrease in relative abundance of major bacterial phyla such as *Proteobacteria* and *Actinobacteria*. In wetland sediments, elements Cr, Pb, and Zn were reported to associate negatively with the relative abundance of bacterial phyla *Nitrospirae, Bacteroidetes,* and *Verrucomicrobia* (Li et al., 2020). Variations in bacterial community structures in heavy metal polluted conditions have been partially attributed to the selective enrichment of metal-resistant bacteria and archaea (Sheeba et al., 2017); and metal resistance can be co-selected with antibiotic resistance genes (Zhao et al., 2019). In all cases, shifts in bacterial community structure resulting from either natural or anthropogenically induced environmental changes can have knock-on effects on their associated metabolic functions (Echavarri-Bravo et al., 2015).

Microbes play an important role in regulating almost all redox reactions and hence the biogeochemical processes of the ecosystem (Falkowski et al., 2008). In aquatic environments, the diverse group of sulfate-reducing bacteria (SRB) is a dominant and important component of the sulfur cycle (Niu et al., 2018). A shift in SRB composition due to environmental stress from heavy metals may result in ecological functional consequences. Furthermore, from a geomicrobiology perspective, microbes can facilitate the cycling of heavy metals through means such as biosorption (Jin et al., 2018). This cycling process depends on physiochemical factors including pH, metal concentration present, redox potential and chemistry of metal ions within the system (Shamim, 2018). SRB-generated sulfide can interact with many heavy metals to form low solubility metal sulfides, such as copper sulfide, zinc sulfide, and lead sulfide, which are less bio-available (Bao et al., 2018). This has implications in heavy metal removal and reduces the environmental pressure exerted by heavy metal pollution (Kiran et al., 2018). Thus, investigating the interactions and interconnected relationship between microbial functional groups and heavy metals can have great potential and implication in managing ecological health and functioning of ecosystems.

Previous studies have reported that the Yangtze River estuary in China was heavily and increasingly polluted by different heavy metals including As, Cd, Cr, Cu, Hg, Pb, and Zn (Liu et al., 2015; Fan et al., 2020). This can be largely attributed to the rapid growth in industrial activities and input over the past decades. In the Yangtze River delta, accumulating Cu, Cr, and Zn are primarily contributed by natural sources with added input from industries such as anti-fouling paints in shipping activities, agricultural fertilizers, metal mining and refinery; Cd and Pb are trace metals more commonly derived from atmospheric emission and deposition, and industrial discharges from electroplating plants (Yin S. et al., 2015; Liu et al., 2019; Hu et al., 2021). Together, excessive concentrations of these heavy metals pose a multitude of environmental health risks that destabilize an ecosystem through toxic impact on the biota, which can subsequently lead to human health risks. In Guo et al. (2019) revealed high average concentrations for four of the heavy metals Cr, Cu, Pb, and Zn (41.28, 80.54, 56.82, and 364.08mg/kg, respectively) in the intertidal surface sediments of Yangtze River estuary. The toxicity and risk of exposure to such heavy metal mixtures at increasing concentrations must be constantly examined. While monitoring programs of heavy metal pollution have seen global efforts, relatively few field studies have attempted to disentangle the potential integrated impact of multiple metals and the roles that microbial community may play.

The Yangtze estuary is bifurcated by the Chongming Island into a less disturbed northern branch of salt marshes, and a more anthropogenically disturbed southern branch of mudflats. The two branches receive similar freshwater input but differ in environmental conditions and anticipated heavy metal pollution status. Potential difference in environmental heavy metal compositions and their influence on inhabiting bacterial communities have yet to be explored. The Yangtze River estuary serves as a representative dynamic, heavy metal-contaminated study site with great ecological and economic significance. It is anticipated that the estuarine environment will be increasingly heavy metal-polluted. Comprehensive studies will be required to elucidate potential patterns and responses in estuarine microbial communities. Here in this study, environmental intensity,

contamination status, and ecological risks imposed by heavy metals Cd, Cr, Cu, Pb, and Zn in sediments were first analyzed and assessed. The geo-accumulation index (I_{geo}) was used to evaluate the pollution risk of heavy metals in sediments, accounting for human influence and geological processes on the background value. The potential ecological risk index (*RI*) was then used to assess the heavy metal pollution in sediments with respect to both the toxicity of heavy metals and the response of the environment (Liu et al., 2021). We then used 16S rRNA metabarcoding data from sediment samples to analyze the diversity, relative abundance, and ecological functions of microbial communities, allowing potential influence of heavy metal pollution on estuarine microbial communities to be revealed. The reproducibility of metal-microbial interactions and potential abundance of metal resistance genes (MRGs) in sedimentary bacterial communities were also experimentally investigated. This study can help understand the role of heavy metals and the responses and potential adaptations of microbial communities to various heavy metal-polluted environments. This will improve current knowledge on the ecological risks imposed by multiple heavy metal accumulation in estuarine ecosystems and will be a beneficial reference for future metal-microbial interaction studies.

MATERIALS AND METHODS

Sampling Sites and Sample Collection

Sediment samples were collected from five sampling sites at the Yangtze River estuary in October 2015 and April 2016. Sampling sites include Beibayao (BBY, 31°40′ N, 121°41′ E), Dongwangsha (DWS, 31°23′ N, 121°30′ E), Wusongkou (WSK, 31°24′ N, 121°30′ E), Shidongkou (SDK, 31°28′ N, 121°23′ E) and Liuhekou (LHK, 31°31′ N, 121°17′ E). BBY and DWS sites were salt marshes to the east of Chongming Island. WSK, SDK, and LHK sites were estuarine mudflats along the south branch of the Yangtze River estuary (**Figure 1**). All sediment samples were collected during the low tide period.

At each sampling site, the surface sediments were sampled using a stainless-steel shovel and sealed in separate sterile plastic bags in an icebox. Triplicate samples were collected. Samples were immediately transported back to laboratory on the same day and then stored at 4°C. At the laboratory, samples were separated into two portions. One portion included 100 g of each sediment sample to be used for heavy metal characterization, stored at room temperature in sterile plastic bags. The remaining portion was stored at −80°C for DNA extraction and subsequent sequencing analysis. All samples were prepared and handled within 7 days after collection.

Characterization of Physicochemical Properties and Heavy Metals in Sediments

The physicochemical properties of sediment samples were measured *in situ* or in the laboratory. The salinity and pH of pore water in the sediment samples were measured *in situ* using a portable salinity meter (Model 30, YSI Incorporated, United States) and pH meter (Five-Go, Mettler-Toledo Instruments, Shanghai, China). Triplicate readings were taken to ensure accuracy of measurements. After transporting the samples to the laboratory, the sediments were dried at 50°C for further characterization. The sediment grain size was measured using a laser granulometer (LS13320, Beckman Coulter Corporation, CA, United States).

Five important heavy metals, copper (Cu), zinc (Zn), lead (Pb), chromium (Cr), and cadmium (Cd), were selected for analysis in this study. First, sediment samples were grinded into fine particles and sieved through a 0.15 mm sieve. Then, sediment samples were digested with 10 mL of acid solution containing HNO_3: $HClO_4$: HF at a ratio of 5:3:2 and heated on a hot plate at 120°C for 2 h then at 180°C until fully digested. After digestion, samples were filtered through a 0.45 μm filter membrane. Filtrates were prepared for detection and subjected to inductively coupled plasma optical emission spectroscopy (ICP-OES) using an iCAP 7000 Optical Emission Spectrometer (Thermo Fisher Scientific, United States) to test for Zn and Cr, and atomic absorption spectroscopy (AAS) using an AAnalyst 800 atomic absorption spectrometer (PerkinElmer, United States) to test for Cu, Pb, and Cd. Quality assurance and quality control were implemented through the use of triplicate samples, analytical blanks and standard reference materials (Yangtze River standard stream sediment sample GSD-9), subjected to the same procedure to validate the method and data. The recovery rates for the heavy metals were between 74.8 and 105.7%. The relative standard deviation between replicate samples were generally less than 5%.

Risk Assessment Methods

Geo-Accumulation Index (I_{geo})

The I_{geo} originally defined by Muller (1969) was calculated using the following equation (Zhang et al., 2017):

$$I_{geo} = \log_2 \frac{c_i}{1.5 \times B_i} \quad (1)$$

Where C_i is the measured concentration of heavy metal *i*, and B_i is the geological background concentration of heavy metal *i*. The constant factor of 1.5 is used to account for variation in background values for metals. The geological background concentrations of Zn, Cu, Cr, Pb, and Cd in sediments from Yangtze River intertidal mudflats were 48.79, 17.43, 28.27, 20.14, and 0.09 mg/kg, respectively, according to an earlier study based on intertidal sediments supposedly formed between 70 and 100 years ago, before any impact imposed by human activities (Xu et al., 1997). The China National Environmental Monitoring Center (Wei et al., 1991) have also previously reported similar geological background concentrations of Zn, Cu, Cr, Pb, and Cd in soils from Shanghai to be 81.3, 27.2, 70.2, 25.0, and 0.138 mg/kg, respectively. The I_{geo} values of heavy metals can be classified into seven grades as follows: $I_{geo} < 0$, class 0, unpolluted; $0 < I_{geo} < 1$, class I, weakly polluted; $1 < I_{geo} < 2$, class II, moderately polluted; $2 < I_{geo} < 3$, class III, moderately to heavily polluted; $3 < I_{geo} < 4$, class IV, heavily polluted; $4 < I_{geo} < 5$, class V, heavily to extremely polluted; and $I_{geo} > 5$, class VI, extremely polluted.

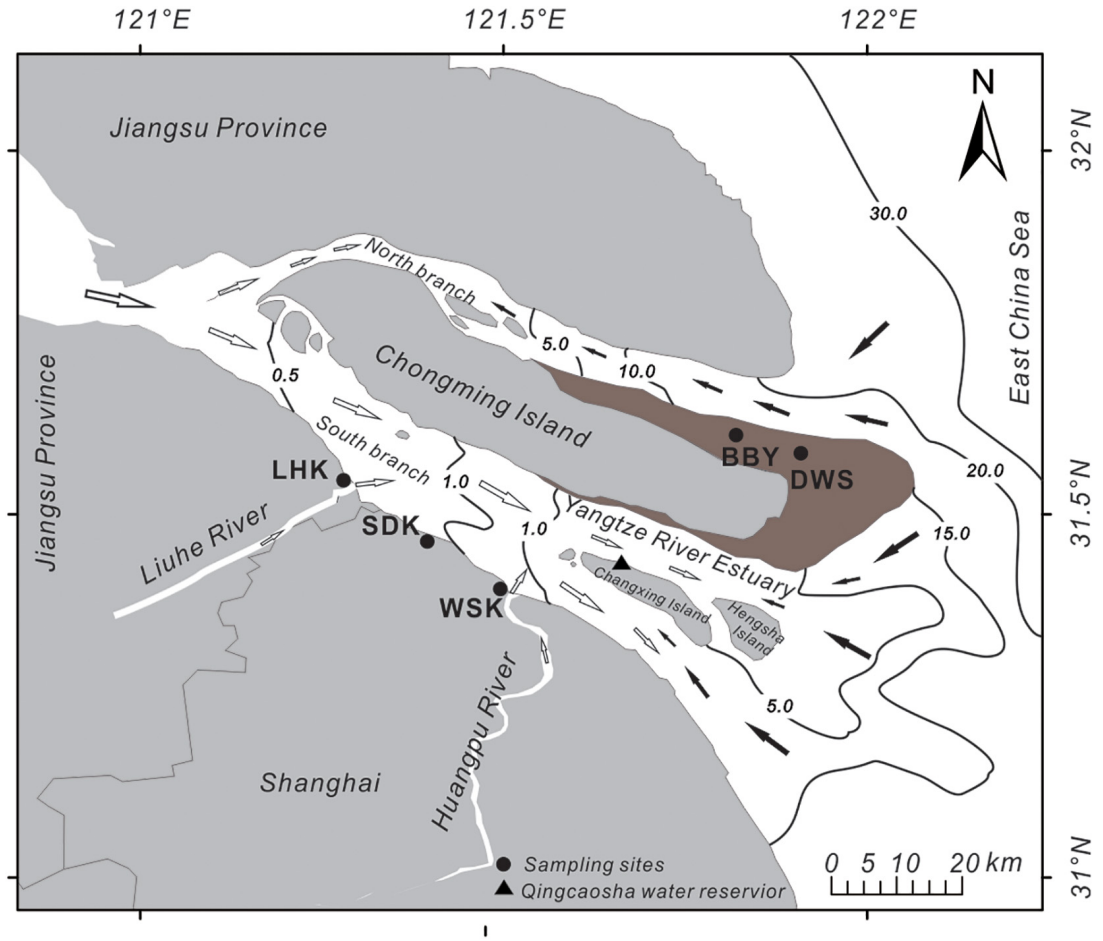

FIGURE 1 | Map of the locations of the five sampling sites at the Yangtze River estuary. LHK, SDK, and WSK sample sites are estuarine mudflats; BBY and DWS sample sites are salt marshes. Black arrows indicate the direction of incoming saltwater; white arrows indicate the direction of downstream freshwater. Numbered black lines indicate salinity gradients.

Potential Ecological Risk Index

The risk index *(RI)* defined by Hakanson (1980) was calculated using the following equations:

$$C_r^i = C_k^i / C_n^i \tag{2}$$

$$E_r^i = T_r^i \times C_r^i \tag{3}$$

$$RI = \sum E_r^i \tag{4}$$

where C_r^i is the contamination factor of heavy metal *i* and C_k^i and C_n^i are the measured concentration and background reference concentration of heavy metal *i*, respectively. E_r^i is the potential ecological risk factor and T_r^i is the toxic response factor of heavy metal *i*. The toxic response factor accounts for the threat to humans and to aquatic ecological system; the values for of Cd, Cr, Cu, Pb, and Zn are 30, 2, 5, 5, and 1, respectively (Hakanson, 1980). The *RI* then represents potential ecological risk considering the overall contamination. The resulting E_r^i and *RI* values are classified into five and four modified grades (Ma and Han, 2019) as shown in **Supplementary Table 1**.

DNA Extraction and 16S rRNA Gene Sequencing

The total DNA was extracted and purified from each sediment sample, using the E.Z.N.A.^{TM} Soil DNA Kit (Omega Bio-Tek, Inc., United States). The bacterial 16S rRNA gene was selected for amplification with primers 341F (5′-CCTACGGGNGGCWGCAG-3′) and 805R (5′GACTACHVGGGTATCTAATCC-3′) targeting the V3–V4 hypervariable regions (Herlemann et al., 2011). PCR was conducted following methods detailed in a previous study (Yi et al., 2020). The PCR products were paired-end sequenced using the Illumina^{TM} MiSeq sequencing platform (Illumina, United States), conducted at Sangon Biotech (Shanghai, China). The sequence reads generated are deposited in the National Center for Biotechnology Information (NCBI) Sequence Read

Archive under the following accession numbers: SRX3855667 (BBY), SRX3855668 (DWS), SRX3855669 (WSK), SRX3855670 (SDK) and SRX3855671 (LHK) for October 2015 samples; SRX12453355 (BBY), SRX12453356 (DWS), SRX12453359 (WSK), SRX12453358 (SDK) and SRX12453357 (LHK) for April 2016 samples.

Data Analysis

Taxonomic Assignment and Functional Annotation

The Quantitative Insights Into Bacterial Ecology 2 (QIIME2; Bolyen et al., 2019) platform was used to process sequencing data and conduct subsequent analysis. In brief, raw sequencing data from samples were imported into QIIME2 and demultiplexed according to the barcode sequences. The bacterial paired-end reads were then merged using the VSEARCH pipeline (Rognes et al., 2016). After filtering chimeric and short sequences, reads were clustered into OTUs with a 97% similarity cutoff (Edgar et al., 2011; Rognes et al., 2016). The Ribosomal Database Project classifier (Wang et al., 2007) was then used to classify OTUs to taxonomy according to the Greengenes database (DeSantis et al., 2006; McDonald et al., 2012). At each taxonomic level (phylum, class, order, family), taxa were considered dominant if their average relative abundance was above 1%. The Functional Annotation of Prokaryotic Taxa (FAPROTAX) tool was then used to annotate the ecological functions of bacterial communities (Louca et al., 2016) through reference to microbial database based on cultured microorganisms and past literature.

Metal Resistance Gene Analysis

Sequencing reads were also aligned against the 16S Ribosomal RNA database at NCBI GenBank using BLAST+ 2.12.0 (Camacho et al., 2009). The taxonomic affiliations according to NCBI taxonomy database were recorded for identical hits. Candidate genomes were compiled and aligned against the BacMet 2.0 reference database of genes with experimentally confirmed metal resistance functions (Pal et al., 2014). The search was conducted using the BLASTx option of DIAMOND sequence aligner 2.0.11 (Buchfink et al., 2015) under the following criteria: *e*-value 10^{-5}, amino acid identity $\geq$ 90%, and alignment length $>$ 25 amino acids (Gupta et al., 2018). The relative abundance of MRGs associated to our studied metals (Cd, Cr, Cu, Pb, Zn, and multimetal-resistant) were then calculated.

Statistical Analysis

Differences in physicochemical properties and heavy metal concentrations between estuarine mudflat (WSK, SDK, and LHK) and salt marsh (BBY and DWS) sediment samples were analyzed using independent-samples *t*-test. Differences in microbial relative abundance were analyzed using Welch's *t*-test (White et al., 2009). Spearman's correlation was used to investigate the relationship between heavy metal concentrations, bacterial community structure and ecological functions. The SPSS Statistics Professional Version 22.0 (IBM Corp., United States) software was used to carry out the statistical analyses unless otherwise specified. Differences were considered significant when $P < 0.05$.

Redundancy analysis (RDA) was used to study bacterial communities in relation to the concentrations and geo-accumulation indices of heavy metals (Zhang et al., 2016), which can help to disclose the overall impact on microbial communities. For RDA, all explanatory variables were log (x + 1) transformed prior to analysis. Permutation test parameters were set to 999 permutations in each test. All RDA were conducted using Canoco5 (ter Braak and Šmilauer, 2002).

RESULTS

Physicochemical Characteristics of Sediments

The major physicochemical characteristics of sediments at studied sampling sites are summarized in **Table 1**. Salinity was significantly higher in the salt marsh sediments (BBY and DWS) compared to the estuarine mudflat sediments (WSK, SDK, and LHK) ($P < 0.05$). The pH values of pore water in both the studied salt marsh and estuarine mudflat sediment samples were mostly slightly alkaline. But in October 2015, the pH value of pore water was significantly lower in estuarine mudflat sediments (pH values at WSK, SDK, and LHK were below 7) compared to that of the salt marsh sediments ($P < 0.05$). Sediment samples from most of the sampling sites were mainly composed of silt and clay (amounted to over 90% of total) with small amounts (below 10%) of sand, with the exception of WSK and SDK sediments sampled in April 2016.

Risk Assessment of Heavy Metal Concentrations in Sediments

Heavy metal concentrations in intertidal sediments sampled during October 2015 and April 2016 across the five sampling sites were examined and summarized in **Supplementary Table 2**. Samples from the salt marshes (BBY and DWS) had slightly lower heavy metal concentrations compared to samples from the estuarine mudflats (WSK, SDK, and LHK). The concentration values were compared with known threshold effect concentration (TEC) values from a previous study (MacDonald et al., 2000), as presented in **Figure 2**. Results showed that Cr and Cu concentrations in intertidal sediments across all sampling sites exceeded respective TEC levels. In contrast, the concentrations of Cd were consistently below the TEC level. A notable difference was observed for Zn concentrations, as it was recorded to be below the TEC level in the salt marsh sampling sites (BBY and DWS), and above the TEC level in estuarine mudflat sampling sites (WSK, SDK, and LHK). Similar pattern was observed but to a lesser extent after 6 months in April 2016. Pb concentrations recorded were consistently, albeit barely, under the TEC level in estuarine mudflat sampling sites, and occasionally above the TEC level in brackish marsh sites.

Geo-Accumulation Indices of Heavy Metals in Sediments

The geo-accumulation indices (I_{geo}) of heavy metals in the sediment samples are summarized in **Figure 3**. In October 2015,

TABLE 1 | Summary of environmental variables of salt marsh and estuarine mudflat sediment samples.

Variable \ Sample	October 2015					April 2016				
	BBY	DWS	WSK	SDK	LHK	BBY	DWS	WSK	SDK	LHK
Salinity*	**8.90**	**7.90**	**0.40**	**0.30**	**0.30**	**7.08**	**8.10**	**0.28**	**0.16**	**0.26**
pH*	**7.21**	**7.45**	**6.79**	**6.83**	**6.94**	7.56	7.36	7.76	7.67	7.52
Sand (%)	2.65	1.15	5.25	3.14	6.69	2.46	0.84	13.27	20.26	3.52
Silt (%)	76.39	65.77	77.88	79.33	72.24	76.00	52.57	73.60	62.86	76.57
Clay (%)	20.95	33.08	16.87	17.54	21.06	21.55	46.59	13.13	16.88	19.92
Monthly rainfall (mm)			78.0					153.6		

**Asterisk represents a significant difference between salt marsh and estuarine mudflat sediments in at least one of the sample sets according to t-test ($P < 0.05$). Corresponding data with significant differences are bolded.*

Zn, Cr and Cd were recorded at moderate levels in estuarine mudflat sediments; in the Chongming salt marsh sediments, only Cd was recorded at a moderate level, with Cr being very close to the moderate level at an I_{geo} of 0.985. In April 2016, I_{geo} values for Zn and Cd were classified as weakly polluted in estuarine mudflats following the decrease in Zn and Cd concentrations measured. In contrast, the I_{geoCr} results for salt marsh sediments showed increase and was classified as moderately polluted. While Cd concentrations recorded were below the established TEC levels for all sites consistently over two periods of time, I_{geoCd} suggested that the studied sediments in estuarine areas could be considered moderately polluted by Cd. Based on the I_{geo} of the five heavy metals studied, the cumulative $I_{geo\ total}$ of heavy metals in the estuarine mudflat and salt marsh sediments was calculated to provide an overview of total heavy metal pollution. In 2015, at an $I_{geo\ total}$ of 5.25 and 3.544 for estuarine mudflat and salt marsh sediments, respectively, the estuarine mudflats can be considered moderately polluted by heavy metals, while the Chongming salt marsh sediments were weakly polluted by heavy metals. In 2016 April, both salt marsh and estuarine mudflat sediments were considered weakly polluted by total heavy metals ($I_{geo\ total}$ of 3.216 and 3.894).

Potential Ecological Risk Indices of Heavy Metals in Sediments

The potential ecological risk indices (*RI*) and risk levels of heavy metals at different sampling sites are summarized in **Figure 4**. As shown in **Table 2**, Cr, Cu, Pb, and Zn had relatively low toxicity coefficients and hence relatively low ecological risk factor contributed toward the corrected *RI*. The observation was consistent across all sampling sites. In contrast, the ecological risk factors for Cd were much higher for its high toxicity, ranging from considerable risk in salt marsh sites (BBY and DWS) to high risk in the estuarine mudflat sites (SDK and LHK). The presence of Cd at high concentrations above background across all sites primarily contributed to the *RI* and risk levels recorded, defined as the total of the potential ecological risk factors of individual heavy metals considered. As a result, almost all studied sample sites could be considered consistently exposed to at least considerable levels of ecological risk from heavy metals from October 2015 to April 2016.

Relative Abundance of Bacterial Taxa in Sediment Communities

The microbial community profiles of the more heavily polluted 2015 sediment samples were first analyzed and compared. The relative abundances of dominant bacterial phyla recorded from representative microbial communities sampled are summarized in **Figure 5A**. Bacterial phyla *Proteobacteria* and *Actinobacteria* had higher relative abundance at salt marsh (BBY) sampling site than at estuarine mudflat (SDK) sampling site, while *Firmicutes, Bacteroidetes,* and *Acidobacteria* showed the opposite. At the class level, *Deltaproteobacteria,* and *Gammaproteobacteria*, which are major subtaxa of *Proteobacteria*, also showed higher relative abundances in salt marsh sediments than in estuarine mudflat sediments, as shown in **Figure 5B**. The opposite was recorded for *Betaproteobacteria. Acidimicrobiia* is a major class of *Actinobacteria* and both the phylum and the class showed similar significant changes in relative abundance with spatial variation. The class *Deltaproteobacteria*, which is largely responsible for regulating the sulfur cycle, was selected to further study the impact of heavy metal pollution on bacterial functional groups. The relative abundance of genera associated with respiration of sulfur compound was examined and *Desulfococcus*, *Desulfosarcina*, and *Desulfomicrobium* were found to significantly differ between estuarine mudflat and salt marsh sediments, as shown in **Figure 5C**.

The Influence of Heavy Metals on Microbial Community Composition

Dominant bacteria at each taxonomic rank (relative abundance > 1%) were subjected to RDA to investigate the relationship between bacterial community structure and heavy metal concentration in the environment. Results first revealed that Cr (Explains = 40.0%, $F = 2.0$, $P = 0.018$) and Zn (Explains = 36.9%, $F = 2.0$, $P = 0.036$) were significant factors influencing microbial community composition and relative abundance at the phylum level. At lower taxonomic levels including class, order, and family, RDA revealed that only Zn remained to be a significant factor (**Supplementary Tables 3–6**). The concentrations of Zn were above TEC in estuarine mudflat sediments and below TEC in salt marsh sediments, supporting the spatial variation in microbial community composition being linked to Zn concentration. Zn concentration should be

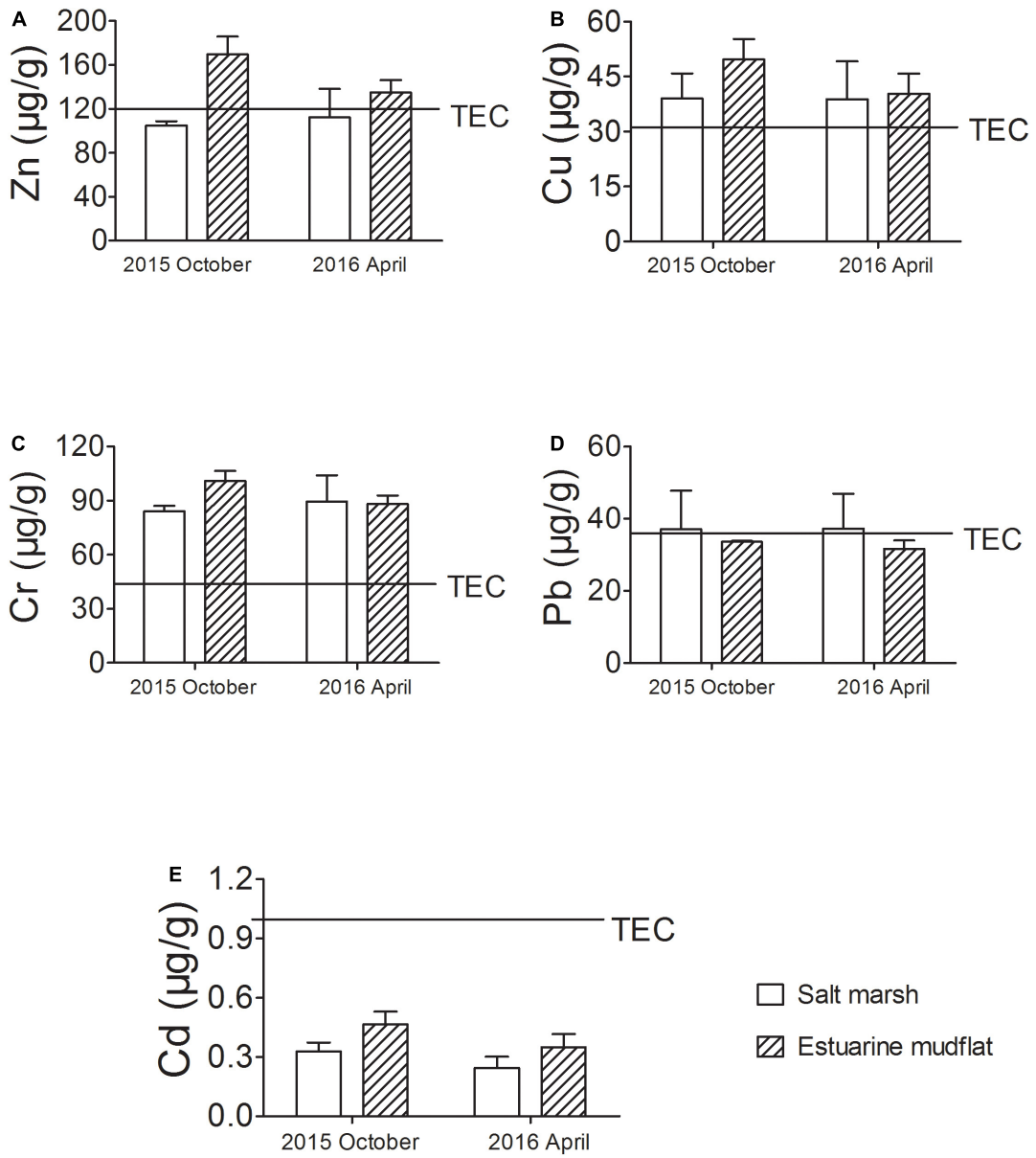

FIGURE 2 | Concentrations of heavy metals **(A)** Zn, **(B)** Cu, **(C)** Cr, **(D)** Pb, and **(E)** Cd in the intertidal sediments from estuarine mudflats (WSK, SDK, and LHK) and Chongming salt marshes (BBY and DWS) collected during October 2015 and April 2016 at the Yangtze River estuary. The threshold effect concentrations (TEC) of respective heavy metals are indicated (MacDonald et al., 2000).

considered a useful indicator to be monitored to identify future community shifts. A similar set of RDA analysis was performed using I_{geo} indices instead of heavy metal concentrations, as summarized in **Figure 6**. The influence on microbial communities were overall similar. Results revealed that the I_{geoCr} had significant impact (Conditional Term Effects) on the dominant bacterial phyla in the communities ($P = 0.022$), while I_{geoZn} had significant impact on the dominant bacterial classes ($P = 0.048$), orders ($P = 0.046$) and families ($P = 0.001$) in the communities. At the genus level, variation in heavy metals had no significant impact on the dominant genera in communities.

Spearman's correlation was used to further investigate how heavy metal pollution may correspond and map with the relative abundance of bacterial taxa. Significant correlations were identified for various bacterial taxa across different taxonomic ranks. Among the 10 recorded dominant phyla (relative abundance > 1%), 4 phyla showed a significant positive correlation with the various heavy metals studied. Similarly, among the 17 dominant classes, 28 dominant orders, 25 dominant families, and 16 dominant genera, results reported 5 classes, 11 orders, 9 families, and 5 genera to show significant correlation with the different heavy metals, as summarized in

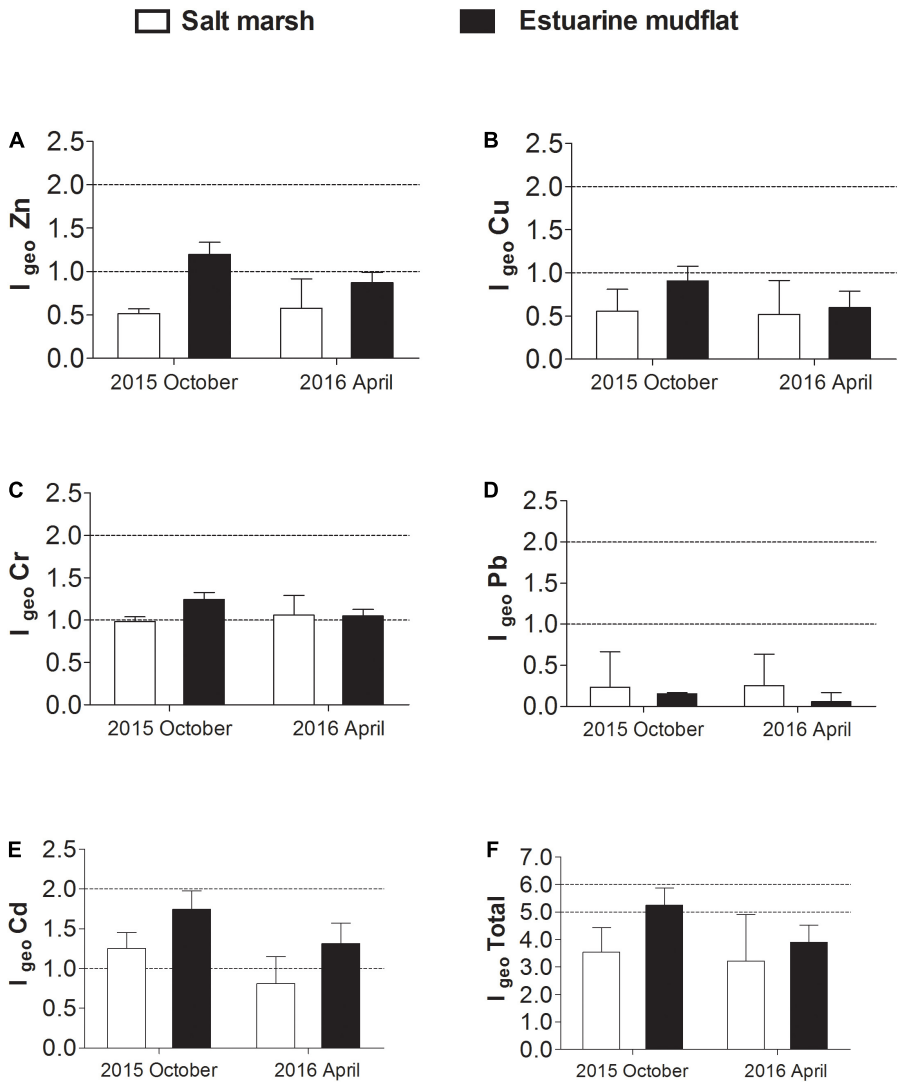

FIGURE 3 | Geo-accumulation indices (I_{geo}) of heavy metals **(A)** Zn, **(B)** Cu, **(C)** Cr, **(D)** Pb, **(E)** Cd and their **(F)** I_{geo} total of measured heavy metals in the estuarine mudflat (WSK, SDK, and LHK) and Chongming salt marsh (BBY and DWS) sediments from the Yangtze River estuary, collected during October 2015 and April 2016. An $I_{geo\ total}$ of less than 5 represents Class I, weakly polluted; an $I_{geo\ total}$ between 5 and 10 represents Class II, moderately polluted.

Figure 7A. To better understand the environmental implications of pollution, a similar analysis was conducted with I_{geo} indices instead, as summarized in **Figure 7B**. Overall, the results of the two analyses complement each other. For most of these dominant taxa, a positive correlation was identified between their relative abundance and either heavy metal concentrations or respective I_{geo} indices. This may be indicative of the tolerance for various heavy metals within bacterial communities if the environmental conditions are otherwise favorable. In contrast, the relative abundances of order *Desulfobacterales* and its subset family *Desulfobulbaceae*, as well as order *Rhodobacterales* and its subset family *Rhodobacteraceae,* showed significant negative correlations with heavy metals and I_{geo} indices. These bacterial groups may be relatively susceptible to heavy metal pollution. Subsequently, only the dominant bacterial phylum *Acidobacteria*, order *Burkholderiales*, *Nitrosomonadales* and family *Comamonadaceae* had positive correlation with combined heavy metal pollution ($I_{geo\ total}$).

The Influence of Heavy Metals on Relative Functional Contributions by Microbial Communities

Bacterial communities were functionally annotated with FAPROTAX; the relationship between heavy metals and the relative contributions to ecological functions by bacterial functional groups were subjected to analysis using Spearman's correlation. A total of 50 annotated ecological functions was contributed by sampled microbial communities, of which 11 showed significant correlations with either Cu, Zn, Cd, and/or Cr,

TABLE 2 | Potential ecological risk factor (E_r^i), risk indices (*RI*), and risk levels of heavy metals in the intertidal sediments at Yangtze River estuary.

Source	T_r^i	Cd	Cr	Cu	Pb	Zn	*RI*	Risk level
		30	2	5	5	1		
2015 October	BBY	93.33	6.16	9.22	6.56	2.06	117.34	Considerable
	DWS	123.33	5.73	13.16	11.86	2.23	156.31	Considerable
	WSK	110.00	6.34	11.13	8.24	2.91	138.62	Considerable
	SDK	176.67	7.52	16.40	8.38	4.07	213.04	High
	LHK	176.67	7.54	15.23	8.44	3.44	211.32	High
2016 April	BBY	63.33	5.31	8.16	6.85	1.77	85.43	Moderate
	DWS	100.00	7.35	14.11	11.65	2.83	135.94	Considerable
	WSK	93.33	6.87	10.26	8.56	2.67	121.69	Considerable
	SDK	96.67	5.75	9.64	6.69	2.42	121.17	Considerable
	LHK	160.00	6.06	14.76	8.30	3.20	192.33	High

as summarized in **Figure 8A**. Among the 11, sulfate respiration was the most dominant function contributed by microbial functional groups. Similarly, the analysis was repeated with I_{geo} indices to indicate the relationship between heavy metal pollution and microbial community ecological functions; there were 6 ecological functions which showed significant correlations with heavy metal pollution, as summarized in **Figure 8B**. The I_{geo} of heavy metals yielded more specific results.

Notably, sulfate respiration and methanol oxidation have significant negative correlations with total heavy metal pollution, while aromatic compound degradation and iron oxidation have significant positive correlations with heavy metal pollution. The order *Desulfobacterales* was largely responsible for the contributions in sulfate respiration. Based on the results from the previous section, for *Desulfobacterales,* both bacterial abundance and its contribution in regulating sulfate respiration showed similar negative correlations with the studied heavy metal (Zn, Cu, Cr, Pb, and Cd) and their respective I_{geo} indices. This consistency suggested a spatial pattern in microbial sulfate respiration processes which is linked to heavy metal pollution. Throughout the analysis, Pb was found to have negligible influence on the ecological functions of microbial communities, which is likely due to Pb having the lowest I_{geo} value among the five heavy metals recorded in the intertidal sediments. Microbial communities may have adapted to the gradual accumulation of Pb.

The Potential Abundance of Metal Resistance Genes in Recovered Microbial Communities

The relative abundance of MRGs corresponding to studied metals (Cd, Cr, Cu, Pb, and Zn) in microbial communities were calculated and summarized in **Figure 9**. Results showed that, out of the five studied heavy metals, Cu and Cr resistance genes were common among most study sites in Yangtze River estuary. Cd resistance genes were rare and only recorded in three samples at 3.69–5.53 $\times$ 10^{-5} copies per 16S rRNA. There are no records of Pb resistance genes. Overall, bacterial communities from the salt marshes sites (DWS and BBY) displayed a higher diversity and relative abundance in MRG types harbored for the October 2015 samples, while the opposite was recorded for April 2016.

The Interactions Between Heavy Metals and Microbial Communities Over Time

A similar data analysis pipeline was applied for sediment samples collected in April 2016 to investigate the identified correlation between metal concentration and estuarine microbial communities. A special focus was placed onto the dominant bacterial taxa (relative abundance > 1%) previously shown to be significantly correlated with heavy metal pollution. The change in relative abundance of identified bacterial is summarized in **Figure 10**. Temporal variation was observed for several bacterial taxa. Notably, at the phylum level, *Verrucomicrobia* and *Acidobacteria* significantly increased in relative abundance among all sites, whereas *Nitrospirae* and its subtaxa showed corresponding decrease in relative abundance (Welch's *t*-test, $P < 0.05$). A redundant analysis was repeated to investigate the impact of heavy metal concentration and associated pollution index (I_{geo}) on microbial community composition at different taxonomic levels from phylum to family. Results showed that no significant impact on community composition can be linked with the minor shifts in heavy metal concentration (**Supplementary Tables 7–10**).

DISCUSSION

Urbanized coastal estuarine ecosystems worldwide have received increasing anthropogenic input over time. Discharged multi-heavy metal pollutants accumulating in aquatic environments are indisputable environmental threats. From the present study, the urbanized Yangtze intertidal sediments were shown to contain various heavy metals at total concentrations that exceeds established individual threshold levels. Among the five studied heavy metals, four (Zn, Cu, Cr, and Pb) are of confirmed concern as they have been found to exceed the TEC by similar if not a greater margin when compared to previous literature (Wang et al., 2014; Xu et al., 2014; Liu et al., 2015). In 2015, Zn, Cu and Cr concentrations were found to be consistently higher in the estuarine mudflat sediment samples. The concentration difference shrunk in April 2016 as the average heavy metal concentrations in estuarine sediments showed uniform reduction, while those of the salt marsh remained similar. This observed fluctuation, however, could be due to seasonal variations. Precipitation may subject surface sediments in the Yangtze River estuary to constant washing effect that is difficult to consider and account for properly. There was a spatial difference in heavy metal distribution, which was anticipated with the difference in environmental conditions and potentially anthropogenic disturbance. While both southern and northern channels of the Yangtze River receive similar upstream freshwater input, the sampling sites on the southern branch may receive more local anthropogenic input such as urban runoff. Sampling sites to the east of Chongming Island are relatively distant from direct human impact and more frequently contacted by seawater and dilution effects. The current results indicated that

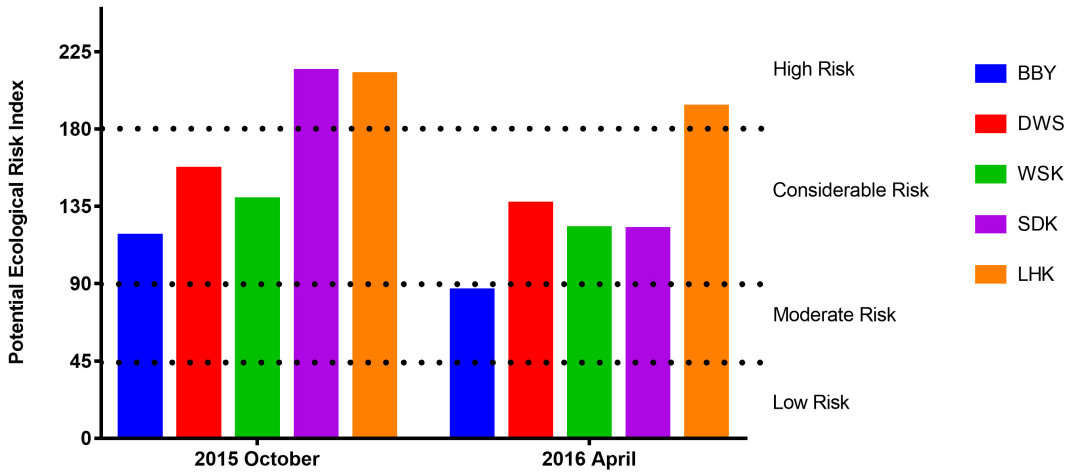

FIGURE 4 | Potential ecological risk indices (*RI*) of heavy metals in intertidal sediments from various sites at the Yangtze River estuary sampled during October 2015 and April 2016. WSK, SDK, and LHK were estuarine mudflats, BBY and DWS were salt marshes. The potential ecological risk levels represented by the *RI* values are indicated by dotted lines.

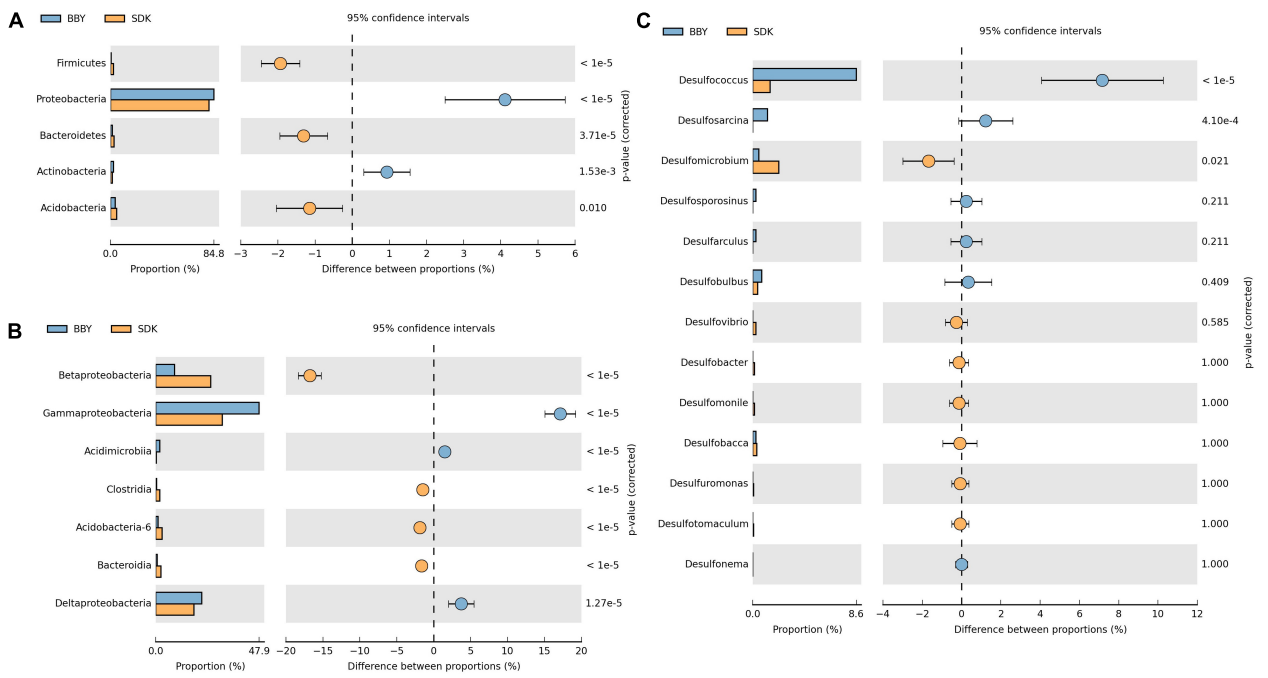

FIGURE 5 | The difference in proportions of recorded bacterial OTUs classified by dominant **(A)** phyla, **(B)** classes, and **(C)** sulfur-reducing bacteria in sediment samples from representative estuarine mudflat (SDK) and the Chongming salt marsh (BBY) sites, collected in October 2015. Significant difference between proportions were analyzed using Welch's *t*-test.

variations in estuarine mudflat heavy metal concentration could be more associated with local impact instead of upstream input. Nevertheless, further pollution source tracking will be required to convincingly determine the nature of heavy metal distribution in the Yangtze River.

According to the I_{geo} and *RI* results, Cd and Zn were major contributors to recorded pollution levels that should be considered an environmental and ecological risk. Despite relatively low Cd concentration, Cd poses considerable to high risks for its high toxic response factor, and the ability for Cd exposure to impact microbial community structure, heavy metal (Salam et al., 2020) and antibiotic resistome (Zhao et al., 2019). Within the Yangtze River estuary, the estuarine mudflat sediments were found to be more polluted (Class II, moderately polluted) and up to high ecological risk compared to the salt marsh sediments. The ability for

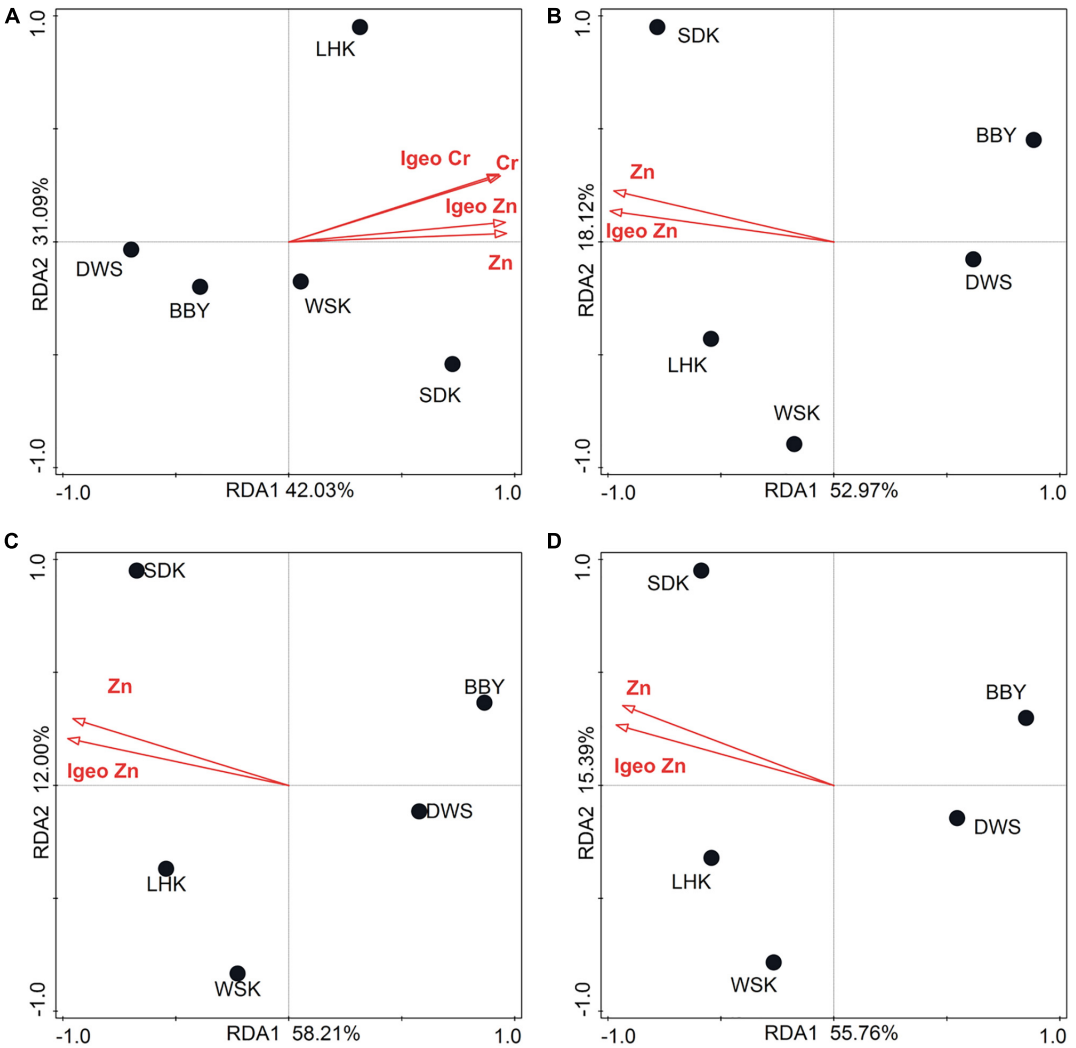

FIGURE 6 | RDA ordination plots of the composition and abundances of dominant bacterial **(A)** phyla, **(B)** classes, **(C)** orders, and **(D)** families from sediment samples collected in October 2015 in relation to heavy metals and their I_{geo} indices.

heavy metal concentration and pollution levels to explain and predict the response of microbial community composition was subsequently tested on the October 2015 samples. This subset was selected for downstream analysis to minimize the impact of unaccountable factors such as rainfall dilution. October samples serve as sediments representative of the dry season with low monthly precipitation and could be considered a better subset to reflect the impact of heavy metal pollution exposure on sedimentary bacterial communities. RDA results revealed Zn to be the only consistent significant factor indicative of shifts in dominant microbial community composition from the class level to the family level. Spearman's correlation analysis further showed that many dominant taxa among all estuarine sediment samples positively correlate with Zn concentration and pollution indices.

Relatively few taxa have shown negative correlations (e.g., Order *Desulfobacterales* and subtaxa) or were seemingly unaffected (e.g., Class *Nitrospira* and subtaxa). For the April 2016 sample subset, similar explanatory effects of heavy metal Zn on microbial compositions cannot be detected. This may have indicated a dilution effect for surface sediments sampled. It is also likely that this seasonal change introduced more complex variations in dominant microbial taxa across the sediment samples. To examine this potential difference, responses of dominant taxa previously reported to significantly correlate with heavy metal concentrations were subsequently investigated. It is anticipated that the relative abundance of this group of bacteria taxa associated with heavy metals could be robust when metal concentrations do not greatly differ. Yet, a significant increase in relative abundance of *Verrucomicrobia* was observed between 2015 and 2016. This is because *Verrucomicrobia* is a key bacterial phylum reported to favor the wet season (Yi et al., 2020) and correlate negatively with heavy metals Cr, Pb, and Zn (Li et al., 2020), which may explain the observation. For most of the other

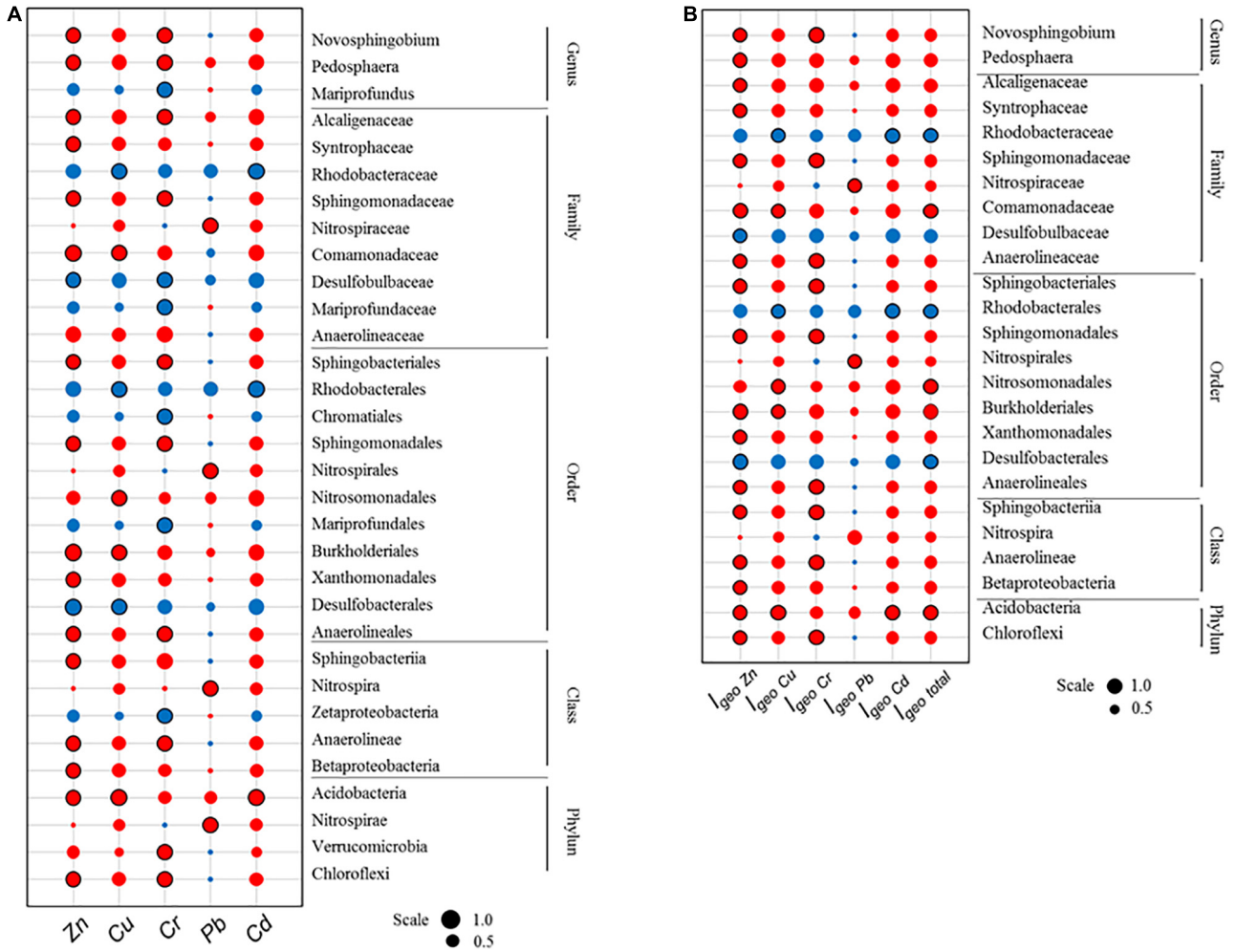

FIGURE 7 | Spearman's correlation between **(A)** heavy metal concentration or **(B)** heavy metal I_{geo} index and relative abundances of dominant bacterial taxa in microbial communities from sediment samples collected in October 2015. Red and blue colors indicate positive and negative correlations, respectively. Scale represents the numeric data of Spearman coefficients. Significant correlations ($P < 0.05$) are indicated by a black circular border.

previous identified heavy metal-associated taxa, it is also revealed that decreasing trends in Zn and heavy metal concentration in estuarine sediments did not significantly impact their relative abundances. Among the multi-metals studied, increased Zn concentrations may serve as an important indicator to quantify influence and stress of heavy metal pollution on microbial communities. Their potential ability to further select tolerant taxa and should be closely monitored.

Heavy metals are one of the many pollutants recorded in the environment. Although the present study has unveiled new associations between heavy metals and estuarine microbial communities, the mechanisms behind their impact, behavior and interactions with the complex ecosystem are still far from clear. A previous study has shown that Zn concentrations can alter microbial community compositions in soil and affect soil enzyme activities (Liu et al., 2020); an excess in Zn may decrease enzyme activity. A similar path of impact may have indirectly caused the recorded shifts in structure of sedimentary microbial communities. Alternatively, the ability for microbes to acquire MRGs as a response to continuous exposure should also be considered. It has been shown that exposure to heavy metals such as Cu for 21 days may induce community-wide tolerance to heavy metals at the cost of a loss in diversity with the sensitive taxa (Ahmed et al., 2020).

For the Yangtze River sedimentary microbial community, presence of Cu resistance genes was widely recorded but at relatively low abundance (between 3.50×10^{-5} and 4.61×10^{-4} copies per 16S rRNA). Cd and Zn resistance genes were rare in both occurrence and abundance, and no convincing associations could be drawn with the spatial difference in heavy metal concentrations. Further, highest diversity and abundance of MRGs were displayed in estuarine mudflat sediments from April 2016. The potential influx of microbes from land may have carried more resistance genes. This could also be a result of sediment conditions influencing the actual bioavailability of heavy metals for

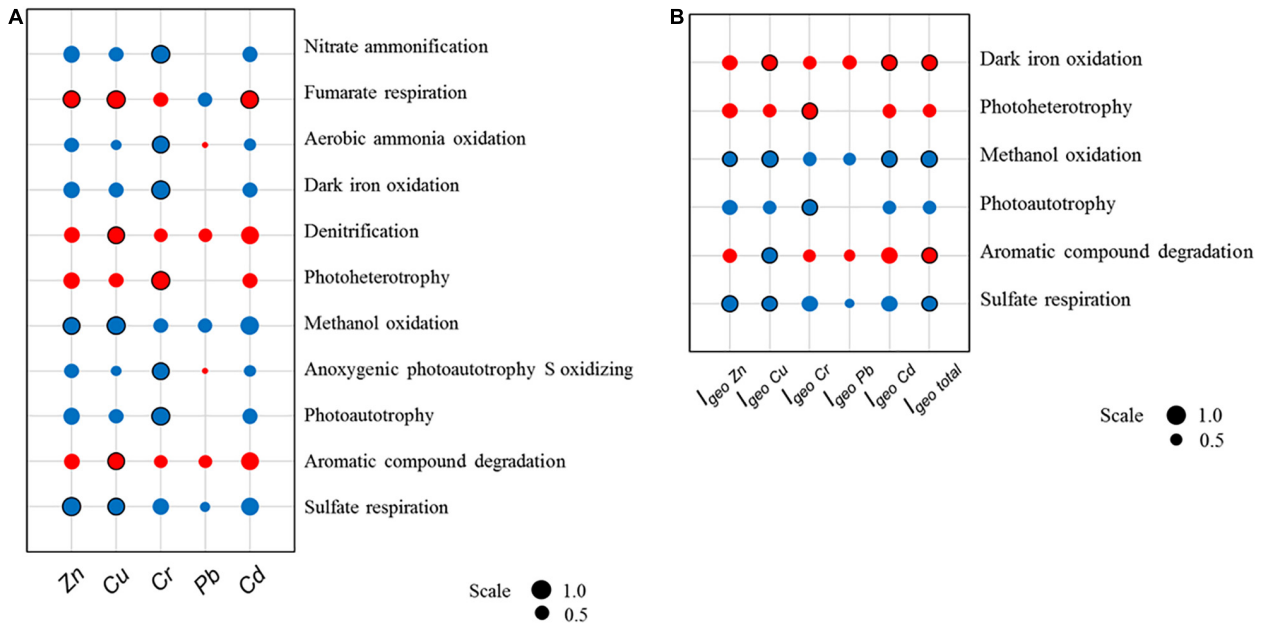

FIGURE 8 | Spearman's correlations between **(A)** heavy metal concentrations or **(B)** heavy metal I_{geo} indices and relative contributions toward ecological functions by microbial communities from sediment samples collected in October 2015. Red and blue colors indicate positive and negative correlations, respectively. Scale represents the numeric data of Spearman's coefficients. Significant correlations ($P < 0.05$) are indicated by a black circular border.

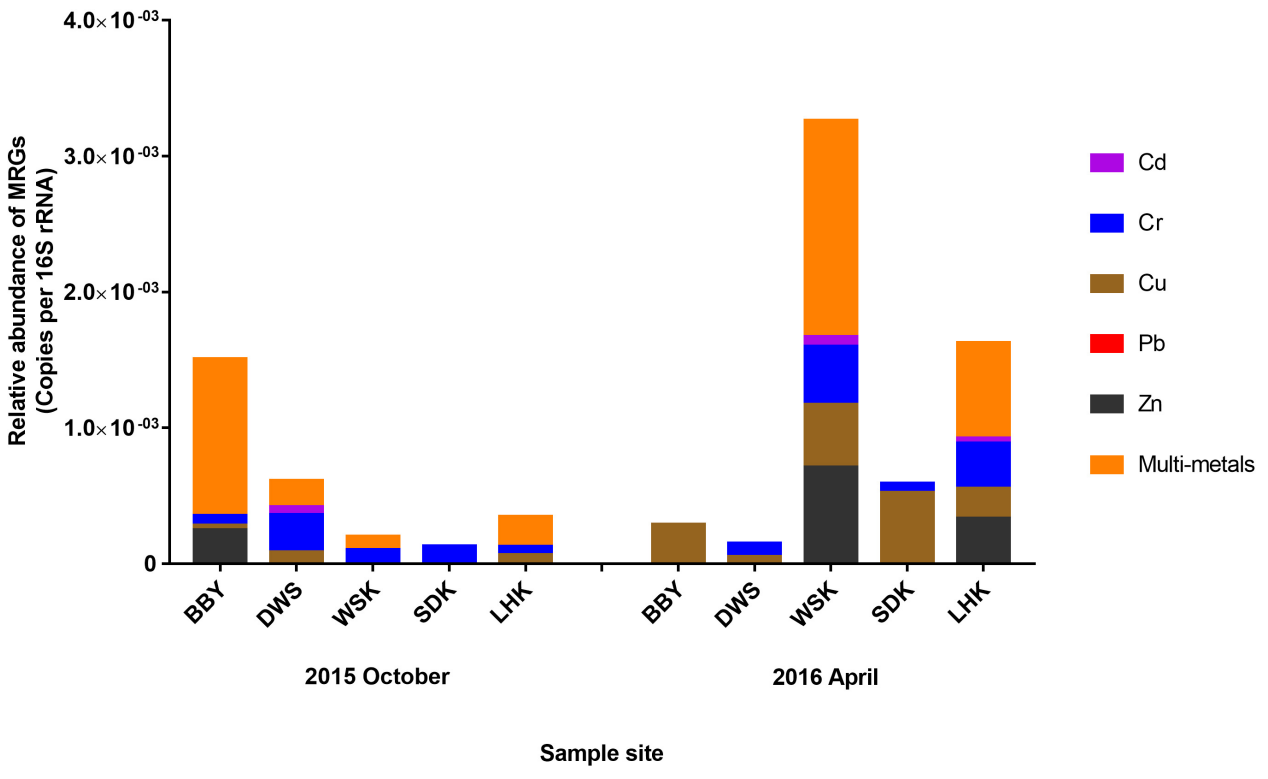

FIGURE 9 | Relative abundance of metal resistance genes (MRGs) in bacterial community at various sites of the Yangtze River estuary sampled during October 2015 and April 2016. WSK, SDK, and LHK were estuarine mudflats; BBY and DWS were salt marshes.

FIGURE 10 | Relative abundances of heavy metal-associated bacterial taxa in sediments from various sites of the Yangtze River estuary (Red = October 2015, Blue = April 2016). Asterisks represent a significant difference between the 2 months according to Welch's *t*-test ($P < 0.05$).

bacterial communities (Miranda et al., 2021). This suggested that habitat niche and microbial community characteristics may have greater influence on MRG distribution over heavy metal concentrations (Song et al., 2019). In this study, heavy metal content was dissolved and measured in total concentration. Chemical metal speciation analyses could help to identify the different chemical metal forms available as potentially better predictors. Specifically, microbial groups such as SRBs and methanotrophs can be responsible for a range of speciation transformation processes for metals (Zhao et al., 2021). Many

studies have attempted to utilize specific microbial groups as a promising heavy metal bioremediation tool. However, predicting metal bioavailability and interactions with microbes at a community-level is still naturally complex. A combination of controlled laboratory exposure and transcriptomic studies will be beneficial to complement existing field results on the integrated impact of heavy metal pollution in an estuarine environment condition.

The relationship between microbial community structure and heavy metal pollution was also investigated. The relative abundance results showed that major bacterial phyla such as *Proteobacteria* and *Actinobacteria* preferred the relatively less polluted salt marsh environment. The opposite was recorded for phyla such as *Firmicutes* and *Acidobacteria*. Results at the class level greatly varied within *Proteobacteria*. *Gammaproteobacteria* and *Deltaproteobacteria* were major taxa found in marine sediments (Di Cesare et al., 2020) and preference was shown for the less polluted sites. In contrast, *Betaproteobacteria* were more abundant in the more polluted southern branch. These class level results have been consistent and are not restricted to estuarine environments as similar trends saw resemblance in microbial communities in Cd-contaminated soils (Li et al., 2017). The spatial variation is believed to stem from the adaptation by bacterial subtaxa utilizing these different biogeographical niches, alongside different sources and concentrations of nutrients such as carbon (Bouskill et al., 2010). Hence, heavy metal concentration should be considered important parameters that interact with, but is often overshadowed by, the distinct impact of environmental parameters such as salinity gradients.

Additionally, potential shifts in microbial functional groups were examined. In particular, the respiration of sulfur compound is a known major ecological function contributed by class *Deltaproteobacteria*. Results indicated that sulfate respiration has significant negative correlations with total heavy metal pollution, while sulfate-oxidizing processes has been found to positively correlate with heavy metals (Lu et al., 2019). This observation is closely associated to the relative abundances of order *Desulfobacterales* and its subset family *Desulfobulbaceae*, as they are major contributors to sulfate respiration. Both these taxa showed significant negative correlations with heavy metals in general. Their subset genus *Desulfococcus* have also been proposed as sentinel bacteria used to detect metal pollution risks (Fernández-Cadena et al., 2020). Thus, SRBs are yet another important bacteria group to investigate its interaction with the environment and potential susceptibility in the context of heavy metal pollution (Niu et al., 2018). Additionally, in the study by Zhao et al. (2018), SRBs were found to facilitate the transformation of mercury to methylmercury in paddy soils with the release of root exudates from rice cultivation. While heavy metal can influence the structure of microbial communities and functional groups, bacterial groups can also take part in converting different forms of metals through means of adsorption and chemical precipitation. SRBs were employed in treatments such as wastewater remediation to remove pollutants such as organic contaminants and heavy metals (Li et al., 2018). A better understanding of microbial interactions with exposure to heavy metals in the field is desired as microbial services can offer many great application opportunities.

CONCLUSION

The present study assessed concentrations, pollution statuses, and ecological risks of heavy metals in sediments of the Yangtze River estuary. Moderate levels of multi-heavy metal pollution were recorded, posing a considerable level of potential ecological risk. The integrated impact of multi-heavy metal pollution on microbial community structure and ecological functions was investigated. We revealed new associations between sedimentary microbial communities and various heavy metals under an estuarine environment condition. Results highlighted the importance of Zn among the studied metals for its potential as a stressor and indicator for heavy metal pollution-associated community shifts. Zn concentration under urbanized estuarine conditions deserves further monitoring attention. Additionally, MRGs were generally found to be present at low relative abundance with no significant associations with heavy metal concentrations. It is suggested that microbial community characteristics and sediment conditions may play more determinant roles in MRG distribution. We conclude by calling attention to the need for future studies and assessments to carefully consider the dynamic influence and interactive mechanisms between multiple heavy metals and microbial communities. This should be done in conjunction with dominant environmental factors especially when attempting to disentangle the complex nature of microbial ecotoxicology. This will benefit both our fundamental understanding of metal-biota-environment interactions and contribute to a better basis for risk assessment and ecosystem management.

DATA AVAILABILITY STATEMENT

The datasets presented in this study can be found in online repositories. The name of the repository and accession numbers can be found in the article and below: National Center for Biotechnology Information (NCBI; https://www.ncbi.nlm.nih.gov); accession numbers SRX3855667-SRX3855671 and SRX12453355-SRX12453359.

AUTHOR CONTRIBUTIONS

JY performed data curation, methodology, investigation, formal analysis, and writing of the manuscript. LL performed investigation and writing of the manuscript. HL and P-YQ provided resources and supervision, and commented on the writing of the manuscript. JC performed conceptualization, resources, supervision, funding acquisition, data curation, formal analysis, and writing of the manuscript. All authors contributed to the article and approved the submitted version.

FUNDING

This work was supported by the Hong Kong Branch of Southern Marine Science and Engineering Guangdong Laboratory (Guangzhou) (SMSEGL20SC01).

SUPPLEMENTARY MATERIAL

The Supplementary Material for this article can be found online at: https://www.frontiersin.org/articles/10.3389/fmars.2021.741912/full#supplementary-material

REFERENCES

Ahmed, A. M., Tardy, V., Bonnineau, C., Billard, P., Pesce, S., and Lyautey, É (2020). Changes in sediment microbial diversity following chronic copper-exposure induce community copper-tolerance without increasing sensitivity to arsenic. *J. Hazard. Mater.* 391:122197. doi: 10.1016/j.jhazmat.2020.122197

Bao, P., Li, G. X., Sun, G. X., Xu, Y. Y., Meharg, A. A., and Zhu, Y. G. (2018). The role of sulfate-reducing prokaryotes in the coupling of element biogeochemical cycling. *Sci. Total Environ.* 613, 398–408. doi: 10.1016/j.scitotenv.2017.09.062

Barletta, M., Lima, A. R., and Costa, M. F. (2019). Distribution, sources and consequences of nutrients, persistent organic pollutants, metals and microplastics in South American estuaries. *Sci. Total Environ.* 651, 1199–1218. doi: 10.1016/j.scitotenv.2018.09.276

Bolyen, E., Rideout, J. R., Dillon, M. R., Bokulich, N. A., Abnet, C. C., Al-Ghalith, G. A., et al. (2019). Reproducible, interactive, scalable and extensible microbiome data science using QIIME 2. *Nat. Biotechnol.* 37, 852–857. doi: 10.1038/s41587-019-0209-9

Bouskill, N. J., Barker-Finkel, J., Galloway, T. S., Handy, R. D., and Ford, T. E. (2010). Temporal bacterial diversity associated with metal-contaminated river sediments. *Ecotoxicology* 19, 317–328. doi: 10.1007/s10646-009-0414-2

Buchfink, B., Xie, C., and Huson, D. H. (2015). Fast and sensitive protein alignment using DIAMOND. *Nat. Methods* 12, 59–60. doi: 10.1038/nmeth.3176

Camacho, C., Coulouris, G., Avagyan, V., Ma, N., Papadopoulos, J., Bealer, K., et al. (2009). BLAST+: architecture and applications. *BMC Bioinformatics* 10:421. doi: 10.1186/1471-2105-10-421

DeSantis, T. Z., Hugenholtz, P., Larsen, N., Rojas, M., Brodie, E. L., Keller, K., et al. (2006). Greengenes, a chimera-checked 16S rRNA gene database and workbench compatible with ARB. *Appl. Environ. Microbiol.* 72, 5069–5072. doi: 10.1128/AEM.03006-05

Di Cesare, A., Petra, P., Ester, M. E., Neven, C., Maritina, M. Š, Gianluca, C., et al. (2020). The role of metal contamination in shaping microbial communities in heavily polluted marine sediments. *Environ. Pollut.* 265:114823. doi: 10.1016/j.envpol.2020.114823

Echavarri-Bravo, V., Paterson, L., Aspray, T. J., Porter, J. S., Winson, M. K., Thornton, B., et al. (2015). Shifts in the metabolic function of a benthic estuarine microbial community following a single pulse exposure to silver nanoparticles. *Environ. Pollut.* 201, 91–99. doi: 10.1016/j.envpol.2015.02.033

Edgar, R. C., Haas, B. J., Clemente, J. C., Quince, C., and Knight, R. (2011). UCHIME improves sensitivity and speed of chimera detection. *Bioinformatics* 27, 2194–2200. doi: 10.1093/bioinformatics/btr381

Falkowski, P. G., Fenchel, T., and Delong, E. F. (2008). The microbial engines that drive Earth's biogeochemical cycles. *Science* 320, 1034–1039. doi: 10.1126/science.1153213

Fan, H., Chen, S., Li, Z., Liu, P., Xu, C., and Yang, X. (2020). Assessment of heavy metals in water, sediment and shellfish organisms in typical areas of the Yangtze River Estuary, China. *Mar. Pollut. Bull.* 151:110864. doi: 10.1016/j.marpolbul.2019.110864

Fernández-Cadena, J. C., Ruíz-Fernández, P. S., Fernández-Ronquillo, T. E., Díez, B., Trefault, N., Andrade, S., et al. (2020). Detection of sentinel bacteria in mangrove sediments contaminated with heavy metals. *Mar. Pollut. Bull.* 150:110701. doi: 10.1016/j.marpolbul.2019.110701

Gu, Y. G., and Gao, Y. P. (2021). A new method for estimating sedimental integrated toxicity of heavy metal mixtures to aquatic biota: a case study. *Ecotoxicology* 30, 373–380. doi: 10.1007/s10646-021-02346-0

Guo, X. P., Yang, Y., Niu, Z. S., Lu, D. P., Zhu, C. H., Feng, J. N., et al. (2019). Characteristics of microbial community indicate anthropogenic impact on the sediments along the Yangtze Estuary and its coastal area, China. *Sci. Total Environ.* 648, 306–314. doi: 10.1016/j.scitotenv.2018.08.162

Gupta, S. K., Shin, H., Han, D., Hur, H. G., and Unno, T. (2018). Metagenomic analysis reveals the prevalence and persistence of antibiotic-and heavy metal-resistance genes in wastewater treatment plant. *J. Microbiol.* 56, 408–415. doi: 10.1007/s12275-018-8195-z

Hakanson, L. (1980). An ecological risk index for aquatic pollution control. A sedimentological approach. *Water Res.* 14, 975–1001. doi: 10.1016/0043-1354(80)90143-8

Herlemann, D. P., Labrenz, M., Jürgens, K., Bertilsson, S., Waniek, J. J., and Andersson, A. F. (2011). Transitions in bacterial communities along the 2000 km salinity gradient of the Baltic Sea. *ISME J.* 5, 1571–1579. doi: 10.1038/ismej.2011.41

Hu, Y., He, N., Wu, M., Wu, P., He, P., Yang, Y., et al. (2021). Sources and ecological risk assessment of the seawater potentially toxic elements in Yangtze River Estuary during 2009–2018. *Environ. Monit. Assess.* 193, 1–14. doi: 10.1007/s10661-020-08795-0

Jin, Y., Luan, Y., Ning, Y., and Wang, L. (2018). Effects and mechanisms of microbial remediation of heavy metals in soil: a critical review. *Appl. Sci.* 8:1336. doi: 10.3390/app8081336

Kiran, M. G., Pakshirajan, K., and Das, G. (2018). Heavy metal removal from aqueous solution using sodium alginate immobilized sulfate reducing bacteria: mechanism and process optimization. *J. Environ. Manage.* 218, 486–496. doi: 10.1016/j.jenvman.2018.03.020

Li, C., Quan, Q., Gan, Y., Dong, J., Fang, J., Wang, L., et al. (2020). Effects of heavy metals on microbial communities in sediments and establishment of bioindicators based on microbial taxa and function for environmental monitoring and management. *Sci. Total Environ.* 749:141555. doi: 10.1016/j.scitotenv.2020.141555

Li, X., Lan, S. M., Zhu, Z. P., Zhang, C., Zeng, G. M., Liu, Y. G., et al. (2018). The bioenergetics mechanisms and applications of sulfate-reducing bacteria in remediation of pollutants in drainage: a review. *Ecotoxicol. Environ. Saf.* 158, 162–170. doi: 10.1016/j.ecoenv.2018.04.025

Li, X., Meng, D., Li, J., Yin, H., Liu, H., Liu, X., et al. (2017). Response of soil microbial communities and microbial interactions to long-term heavy metal contamination. *Environ. Pollut.* 231, 908–917. doi: 10.1016/j.envpol.2017.08.057

Liu, P., Zheng, C., Wen, M., Luo, X., Wu, Z., Liu, Y., et al. (2021). Ecological risk assessment and contamination history of heavy metals in the sediments of Chagan Lake, Northeast China. *Water* 13:894. doi: 10.3390/w13070894

Liu, R., Guo, L., Men, C., Wang, Q., Miao, Y., and Shen, Z. (2019). Spatial-temporal variation of heavy metals' sources in the surface sediments of the Yangtze River Estuary. *Mar. Pollut. Bull.* 138, 526–533. doi: 10.1016/j.marpolbul.2018.12.010

Liu, Y. M., Cao, W. Q., Chen, X. X., Yu, B. G., Lang, M., Chen, X. P., et al. (2020). The responses of soil enzyme activities, microbial biomass and microbial community structure to nine years of varied zinc application rates. *Sci. Total Environ.* 737:140245. doi: 10.1016/j.scitotenv.2020.140245

Liu, Z., Pan, S., Sun, Z., Ma, R., Chen, L., Wang, Y., et al. (2015). Heavy metal spatial variability and historical changes in the Yangtze River estuary and North Jiangsu tidal flat. *Mar. Pollut. Bull.* 98, 115–129. doi: 10.1016/j.marpolbul.2015.07.006

Louca, S., Parfrey, L. W., and Doebeli, M. (2016). Decoupling function and taxonomy in the global ocean microbiome. *Science* 353, 1272–1277. doi: 10.1126/science.aaf4507

Lu, M., Luo, X., Jiao, J. J., Li, H., Wang, X., Gao, J., et al. (2019). Nutrients and heavy metals mediate the distribution of microbial community in the marine sediments of the Bohai Sea, China. *Environ. Pollut.* 255:113069. doi: 10.1016/j.envpol.2019.113069

Ma, L., and Han, C. (2019). "Water quality ecological risk assessment with sedimentological approach," in *Water Quality-Science, Assessments and Policy*, ed. K. Summers (London: IntechOpen). doi: 10.5772/intechopen.88594

MacDonald, D. D., Ingersoll, C. G., and Berger, T. A. (2000). Development and evaluation of consensus-based sediment quality guidelines for freshwater

ecosystems. *Arch. Environ. Contam. Toxicol.* 39, 20–31. doi: 10.1007/s002440010075

McDonald, D., Price, M. N., Goodrich, J., Nawrocki, E. P., DeSantis, T. Z., Probst, A., et al. (2012). An improved Greengenes taxonomy with explicit ranks for ecological and evolutionary analyses of bacteria and archaea. *ISME J.* 6, 610–618. doi: 10.1038/ismej.2011.139

Miranda, L. S., Ayoko, G. A., Egodawatta, P., Hu, W. P., Ghidan, O., and Goonetilleke, A. (2021). Physico-chemical properties of sediments governing the bioavailability of heavy metals in urban waterways. *Sci. Total Environ.* 763:142984. doi: 10.1016/j.scitotenv.2020.142984

Muller, G. (1969). Index of geoaccumulation in sediments of the Rhine River. *Geojournal* 2, 108–118.

Niu, Z. S., Pan, H., Guo, X. P., Lu, D. P., Feng, J. N., Chen, Y. R., et al. (2018). Sulphate-reducing bacteria (SRB) in the Yangtze Estuary sediments: abundance, distribution and implications for the bioavailibility of metals. *Sci. Total Environ.* 634, 296–304. doi: 10.1016/j.scitotenv.2018.03.345

Pal, C., Bengtsson-Palme, J., Rensing, C., Kristiansson, E., and Larsson, D. J. (2014). BacMet: antibacterial biocide and metal resistance genes database. *Nucleic Acids Res.* 42, D737–D743. doi: 10.1093/nar/gkt1252

Prabhakaran, P., Ashraf, M. A., and Aqma, W. S. (2016). Microbial stress response to heavy metals in the environment. *RSC Adv.* 6, 109862–109877. doi: 10.1039/C6RA10966G

Rognes, T., Flouri, T., Nichols, B., Quince, C., and Mahé, F. (2016). VSEARCH: a versatile open source tool for metagenomics. *PeerJ* 4:e2584. doi: 10.7717/peerj.2584

Salam, L. B., Obayori, O. S., Ilori, M. O., and Amund, O. O. (2020). Effects of cadmium perturbation on the microbial community structure and heavy metal resistome of a tropical agricultural soil. *Bioresour. Bioprocess.* 7:25. doi: 10.1186/s40643-020-00314-w

Shamim, S. (2018). Biosorption of heavy metals. *Biosorption* 2, 21–49. doi: 10.5772/intechopen.72099

Sheeba, V. A., Abdulaziz, A., Gireeshkumar, T. R., Ram, A., Rakesh, P. S., Jasmin, C., et al. (2017). Role of heavy metals in structuring the microbial community associated with particulate matter in a tropical estuary. *Environ. Pollut.* 231, 589–600. doi: 10.1016/j.envpol.2017.08.053

Song, W., Qi, R., Zhao, L., Xue, N., Wang, L., and Yang, Y. (2019). Bacterial community rather than metals shaping metal resistance genes in water, sediment and biofilm in lakes from arid northwestern China. *Environ. Pollut.* 254:113041. doi: 10.1016/j.envpol.2019.113041

ter Braak, C. J. F., and Šmilauer, P. (2012). *Canoco Reference Manual and User's Guide: Software for Ordination (Version 5.0)*. Ithaca, NY: Microcomputer Power.

Wang, J., Liu, R., Zhang, P., Yu, W., Shen, Z., and Feng, C. (2014). Spatial variation, environmental assessment and source identification of heavy metals in sediments of the Yangtze River Estuary. *Mar. Pollut. Bull.* 87, 364–373. doi: 10.1016/j.marpolbul.2014.07.048

Wang, Q., Garrity, G. M., Tiedje, J. M., and Cole, J. R. (2007). Naive Bayesian classifier for rapid assignment of rRNA sequences into the new bacterial taxonomy. *Appl. Environ. Microbiol.* 73, 5261–5267. doi: 10.1128/AEM.00062-07

Wang, Y., Sheng, H. F., He, Y., Wu, J. Y., Jiang, Y. X., Tam, N. F. Y., et al. (2012). Comparison of the levels of bacterial diversity in freshwater, intertidal wetland, and marine sediments by using millions of illumina tags. *Appl. Environ. Microbiol.* 78, 8264–8271. doi: 10.1128/AEM.01821-12

Wei, F., Zheng, C., Chen, J., and Wu, Y. (1991). Study of the background contents of 61 elements of soils in China. *Environ. Sci.* 12, 12–19.

White, J. R., Nagarajan, N., and Pop, M. (2009). Statistical methods for detecting differentially abundant features in clinical metagenomic samples. *PLoS Comput. Biol.* 5:e1000352. doi: 10.1371/journal.pcbi.1000352

Xu, S., Tao, J., Chen, Z., Chen, Z., and Lu, Q. (1997). Dynamic accumulation of heavy metals in tidal flat sediments of Shanghai. *Oceanol. Limnol. Sin.* 28, 509–515.

Xu, X., Zhao, Y., Zhao, X., Wang, Y., and Deng, W. (2014). Sources of heavy metal pollution in agricultural soils of a rapidly industrializing area in the Yangtze Delta of China. *Ecotoxicol. Environ. Saf.* 108, 161–167. doi: 10.1016/j.ecoenv.2014.07.001

Yi, J., Lo, L. S. H., and Cheng, J. (2020). Dynamics of microbial community structure and ecological functions in estuarine intertidal sediments. *Front. Mar. Sci.* 7:585970. doi: 10.3389/fmars.2020.585970

Yin, H., Niu, J., Ren, Y., Cong, J., Zhang, X., Fan, F., et al. (2015). An integrated insight into the response of sedimentary microbial communities to heavy metal contamination. *Sci. Rep.* 5:14266. doi: 10.1038/srep14266

Yin, S., Feng, C., Li, Y., Yin, L., and Shen, Z. (2015). Heavy metal pollution in the surface water of the Yangtze Estuary: a 5-year follow-up study. *Chemosphere* 138, 718–725. doi: 10.1016/j.chemosphere.2015.07.060

Zhang, C., Nie, S., Liang, J., Zeng, G., Wu, H., Hua, S., et al. (2016). Effects of heavy metals and soil physicochemical properties on wetland soil microbial biomass and bacterial community structure. *Sci. Total Environ.* 557, 785–790. doi: 10.1016/j.scitotenv.2016.01.170

Zhang, G., Bai, J., Xiao, R., Zhao, Q., Jia, J., Cui, B., et al. (2017). Heavy metal fractions and ecological risk assessment in sediments from urban, rural and reclamation-affected rivers of the Pearl River Estuary, China. *Chemosphere* 184, 278–288. doi: 10.1016/j.chemosphere.2017.05.155

Zhao, J. Y., Ye, Z. H., and Zhong, H. (2018). Rice root exudates affect microbial methylmercury production in paddy soils. *Environ. Pollut.* 242, 1921–1929. doi: 10.1016/j.envpol.2018.07.072

Zhao, Q., Li, X., Xiao, S., Peng, W., and Fan, W. (2021). Integrated remediation of sulfate reducing bacteria and nano zero valent iron on cadmium contaminated sediments. *J. Hazard. Mater.* 406:124680. doi: 10.1016/j.jhazmat.2020.124680

Zhao, Y., Cocerva, T., Cox, S., Tardif, S., Su, J. Q., Zhu, Y. G., et al. (2019). Evidence for co-selection of antibiotic resistance genes and mobile genetic elements in metal polluted urban soils. *Sci. Total Environ.* 656, 512–520. doi: 10.1016/j.scitotenv.2018.11.372

Conflict of Interest: The authors declare that the research was conducted in the absence of any commercial or financial relationships that could be construed as a potential conflict of interest.

Publisher's Note: All claims expressed in this article are solely those of the authors and do not necessarily represent those of their affiliated organizations, or those of the publisher, the editors and the reviewers. Any product that may be evaluated in this article, or claim that may be made by its manufacturer, is not guaranteed or endorsed by the publisher.

frontiers in Marine Science

ORIGINAL RESEARCH
published: 30 November 2021
doi: 10.3389/fmars.2021.778136

Oil Spill Detection Using Fluorometric Sensors: Laboratory Validation and Implementation to a FerryBox and a Moored SmartBuoy

Siim Pärt[1]*, *Harri Kankaanpää*[2], *Jan-Victor Björkqvist*[1,3,4] and *Rivo Uiboupin*[1]

[1] Department of Marine Systems, Tallinn University of Technology, Tallinn, Estonia, [2] Marine Research Centre, Finnish Environment Institute, Helsinki, Finland, [3] Norwegian Meteorological Institute, Bergen, Norway, [4] Finnish Meteorological Institute, Helsinki, Finland

A large part of oil spills happen near busy marine fairways. Presently, oil spill detection and monitoring are mostly done with satellite remote sensing algorithms, or with remote sensors or visual surveillance from aerial vehicles or ships. These techniques have their drawbacks and limitations. We evaluated the feasibility of using fluorometric sensors in flow-through systems for real-time detection of oil spills. The sensors were capable of detecting diesel oil for at least 20 days in laboratory conditions, but the presence of CDOM, turbidity and algae-derived substances substantially affected the detection capabilities. Algae extract was observed to have the strongest effect on the fluorescence signal, enhancing the signal in all combinations of sensors and solutions. The sensors were then integrated to a FerryBox system and a moored SmartBuoy. The field tests support the results of the laboratory experiments, namely that the primary source of the measured variation was the presence of interference compounds. The 2 month experiments data did not reveal peaks indicative of oil spills. Both autonomous systems worked well, providing real-time data. The main uncertainty is how the sensors' calibration and specificity to oil, and the measurement depth, affects oil detection. We recommend exploring mathematical approaches and more advanced sensors to correct for natural interferences.

Keywords: oil spill, flow-trough system, fluorometric sensors, Baltic Sea, natural interferences, sensor selectivity

OPEN ACCESS

Edited by:
Kenneth Mei Yee Leung, City University of Hong Kong, Hong Kong SAR, China

Reviewed by:
Maged Marghany, Syiah Kuala University, Indonesia
Norimitsu Sakagami, Tokai University, Japan

***Correspondence:**
Siim Pärt
siim.part@taltech.ee

Specialty section:
This article was submitted to Marine Pollution, a section of the journal Frontiers in Marine Science

Received: *16 September 2021*
Accepted: *02 November 2021*
Published: *30 November 2021*

Citation:
Pärt S, Kankaanpää H, Björkqvist J-V and Uiboupin R (2021) Oil Spill Detection Using Fluorometric Sensors: Laboratory Validation and Implementation to a FerryBox and a Moored SmartBuoy. Front. Mar. Sci. 8:778136. doi: 10.3389/fmars.2021.778136

1. INTRODUCTION

Oil spills are a major threat to the marine ecosystems, local communities and economy (Samiullah, 1985; Farrington, 2014; Jørgensen et al., 2019; Câmara et al., 2021; Sandifer et al., 2021). The research into the consequences of oil pollution has been long and extensive. The effects to wildlife are broad, ranging from exposure of birds (Jenssen, 1994; Stephenson, 1997; Fox et al., 2016) and mammals (Engelhardt, 1987; Bodkin et al., 2002; Ridoux et al., 2004) to oil to toxic, mutagenic and/or carcinogenic effects of polycyclic aromatic hydrocarbons (PAHs) present in crude oil and products based on fossil oil (Hylland, 2006; Abdel-Shafy and Mansour, 2016; Hayakawa, 2018; Honda and Suzuki, 2020). Besides harming the natural environment, oil spills can impair the economy in the affected region (Cohen, 1993; Taleghani and Tyagi, 2017; Ribeiro et al., 2021) and have adverse effects on human health and psychology (D'Andrea and Reddy, 2014; Shultz et al., 2015; Sandifer et al., 2021).

The Baltic Sea has always been an important route for maritime trade and transport, accounting for up to 15% of the world's maritime traffic (HELCOM, 2003; WWF, 2010). Oil shipments in the Baltic Sea are projected to grow by 64% by 2030, from about 180 million tons to nearly 300 million tons (HELCOM, 2018a) and the overall volume of ship traffic has been estimated to double during the period 2010–2030 (Rytkönen et al., 2002). The immense volume of shipping in the Baltic Sea is accompanied by a high risk of accidents. According to the Helsinki Commission (HELCOM), 1,520 maritime accidents have occurred in the Baltic Sea area during the period 2011–2015, with a fairly stable rate of 300 accidents per year; 4% of these accidents led to loss of life, serious injuries or environmental damages (HELCOM, 2018a).

A considerable contributor to marine oil pollution is oil pollution by ships, which are concentrated to main shipping lanes and other areas of high maritime activity (Serra-Sogas et al., 2008; Ferraro et al., 2009; Liubartseva et al., 2015; Sankaran, 2019; Polinov et al., 2021). It is estimated that in the Baltic Sea 10% of the total amount of oil hydrocarbons comes from illegal discharges by vessels (HELCOM, 2003). These various smaller spills, referred to as operational oil spills, are not the result of ship accidents, but instead result from discharges of small amounts of oil, or more usually unfiltered oily water. Most of this pollution risk is concentrated along major ship routes (HELCOM, 2013). The number and size of these spills has been decreasing (HELCOM, 2018c). For example, in 2015 the number of observed spills was 80 and the total estimated annual volume of oil spills observed in 2009–2015 was in the order of 20 m^3 (HELCOM, 2018a). However, even small amounts of oil can have a negative impact on the marine environment (Brussaard et al., 2016).

Current oil spill remote sensing methods have become more reliable but they still have many drawbacks and limitations (Fingas and Brown, 2018). Nowadays the most dominant and cost-effective means for remote spill detection is the combination of satellite-based synthetic aperture radar (SAR) images and aircraft surveillance flights for verification (Gade et al., 2000; Uiboupin et al., 2008; Solberg, 2012; Fingas and Brown, 2018). SAR sensors give a good coverage and are not limited by cloud cover or weather conditions. Furthermore, there are many studies on algorithms meant for identification of oil spills from SAR data (Marghany, 2016; Krestenitis et al., 2019; Al-Ruzouq et al., 2020; Zeng and Wang, 2020). Besides SAR, optical remote sensing techniques gathering information in different spectral range (ultraviolet, visible, and near-infrared) and can give useful information about oil pollution (Solberg, 2012; Fingas and Brown, 2018; Al-Ruzouq et al., 2020). Ships and aircraft equipped with radar or optical sensor are also widely used for detection and monitoring of oil pollution (Jensen et al., 2008; Xu et al., 2020). Also, sensors like microwave radiometers and laser fluorometers mounted on aircraft can provide additional information about the oil type and amount (Jha et al., 2008; Solberg, 2012).

Oil spills can be difficult to detect even with modern aerial surveillance equipment for numerous reasons. They can be small, and in rough sea the oil is mixed well below the surface, while a visible slick might also disappear because of evaporation. Optical methods of satellite sensing are also limited by resolution, cloud cover and the sea state (Brekke and Solberg, 2005; Jha et al., 2008; Fingas and Brown, 2018). Even the most studied and used remote sensing method of detecting oil from SAR images has problems, such as lookalikes—radar signatures similar to oil pollution but which can actually be for example floating algae, ship wakes, cold upwelling water or natural surface films produced by plankton or fish (Sipelgas and Uiboupin, 2007; Alpers et al., 2017; Al-Ruzouq et al., 2020). Even a comprehensive satellite coverage might therefore not be able to detect all oil spills. Nonetheless, PAHs will remain in the water after the spill is no longer visible on the surface but are still detectable by in-water fluorometers. Thus, the real-time detection of these spills would benefit from additional detection systems. In addition, *in-situ* sensors can be used for validation for remote sensing techniques and vice versa. One possible *in-situ* solution is to use fluorometric sensors installed on a suitable platform.

Ships of Opportunity (SOOPs) fitted with oceanographic instrumentation and automated water sampling systems, so-called FerryBoxes, are commonly used for studies of near surface waters (Petersen et al., 2003, 2011; Hydes et al., 2010; Petersen, 2014). Also, the Baltic Sea is well covered with FerryBox lines (Petersen, 2014; Schneider et al., 2014; Karlson et al., 2016; Kikas and Lips, 2016). FerryBoxes have a great potential for gathering scientific data, especially when installed on ferries and cargo ships cruising the same route on a regular basis. While SOOPs give a good spatial coverage, monitoring buoys give an excellent temporal coverage. Such autonomous monitoring buoy systems are being developed and operated worldwide to measure the physical and biogeochemical properties of coastal surface waters (Mills et al., 2003; Nam et al., 2005). The technological progress has resulted in SmartBuoys with a stable power supply, two-way communication and real-time data acquisition for effective environmental monitoring (Chavez et al., 1997; Mills et al., 2003; Nam et al., 2005; Benson et al., 2008; Papoutsa et al., 2012). Moroni et al. (2016) have developed a sensorized buoy for detecting oil spills from the air-side. Fluorescence-based *in-situ* sensors and systems have been globally used for real-time monitoring of oil spills and determining the levels of the contamination (Lambert et al., 2001, 2003; He et al., 2003; Kim et al., 2010; Malkov and Sievert, 2010; Tedetti et al., 2010). Combining FerryBoxes and SmartBuoys with portable fluorometric sensors could provide an additional method for early notification of oil spills in the sea. Nonetheless, to our knowledge, such an approach has not previously been adopted.

Fluorometric detection (FLD) is essentially about measuring fluorescence at predetermined wavelengths, meaning that FLD can't resolve between different sources of hydrocarbons and fluorescent compounds – for example oil and oil refined products, combustion processes (e.g., power plants, maritime and land-based traffic, forest fires). Compound-specific laboratory methods such as gas chromatography–mass spectrometry can make such distinctions, but field-usability (data continuity), speed and low running costs still make FLD-based field protocols appealing alternatives compared to laboratory-based techniques.

For purposes of the operational detection of oil spills, the accuracy of the sensor is a crucial, but not the sole part. We split

up the operational chain of oil-detection with fluorometers to five steps: 1) the sensors need to accurately and selectively detect oil, 2) the system where the sensors are operating need to function at least semi-autonomously, 3) the system needs to reliably transmit real time data, 4) an automated algorithm detects anomalic events and 5) the data is available to the user in a reliable interface on a short notice. In this study we focus on steps 1–3 and 5. We first present laboratory tests of sensors and then evaluate the real-time oil detection capability of two autonomous *in-situ* remote sensing platforms that are equipped with fluorometers. The two platforms, a FerryBox and a SmartBuoy, covered high-risk areas in the Baltic Sea.

2. MATERIALS AND METHODS

2.1. UviLux, EnviroFlu-HC 500 and Turner Design C3 Fluorometers

Three commercially available fluorometric instruments, designed for *in-situ* and real-time quantification of oil or oil compounds, were chosen for the experiments: UviLux and EnviroFlu-HC 500 for the FerryBox system, and C3 Submersible Fluorometer for the SmartBuoy. All three sensors were also tested in laboratory conditions.

The UviLux UV-fluorometer (Chelsea Technologies Ltd, UK) is an *in-situ* UV fluorometer. Oil detection is based on the measurement of PAH concentrations. The sensitivity of the sensor is 0.005 μg carbazole per liter, the calibrated range is 0.005–2,000 μg carbazole per liter, the excitation wavelength is 255 nm, and the emission wavelength is 360 nm.

The EnviroFlu-HC 500 submersible UV fluorometer (TriOS Optical Sensors, Germany) is an instrument designed for the measurement of PAHs in water. The fluorometer has a minimum detection limit of 0.3 μg phenantrene per liter, a calibrated range of 0–500 μg phenantrene per liter, an excitation wavelength 254 nm, and an emission wavelength of 360 nm.

The Turner Design C3 submersible fluorometer (Turner Design, USA) is manufactured according to users' requirements. C3 fluorometers come with a factory-installed temperature probe and can be configured with up to three optical sensors. Each optical sensor is designed with fixed excitation and emission filters. For the SmartBuoy experiment the C3 fluorometer was equipped with three sensors: a hydrocarbon sensor for crude oil with sensitivity of 0.2 μg pyrenetetrasulfonic acid (PTSA) per liter and linear range 0–1500 μg PTSA per liter, excitation light 325/120 nm and emission light 410–600 nm; a sensor for colored dissolved organic matter (CDOM) with minimum detection limit (MDL) 0.1 μg quinine sulfate per liter, linear range 0–1.5 μg quinine sulfate per liter, excitation wavelength 325–120 nm and emission wavelength 470–60 nm; a turbidity sensor with MDL 0.05 Nephelometric Turbidity Units (NTU) and range 0–1,500 NTU, excitation wavelength 850 nm, and emission wavelength 850 nm.

2.2. Laboratory Tests

In order to examine selectivity and sensitivity of fluorometric sensors to oil, two separate laboratory experiments were performed in 2017. All experiments were performed in a dark climatic room set to a temperature of 16°C.

The first experiment examined the selectivity of the sensors, i.e., interferences to oil detection caused by interfering substances. Baltic Sea water (S; salinity 6.2 PSU) was used as a blank and as a solution for extraction of humic substances (H), cyanobacterial algae (A) and production of clay suspension (C).

Stock solutions (one of each) of clay suspension (from Baltic Sea's clayey sediment), seawater extract of humic substances (originating from decayed plant material) and a seawater extract of cyanobacterial algae (from dried Baltic Sea surface phytoplankton) were produced. Also, two batches of water accommodated fraction (WAF; W) of diesel oil were produced. Each extract was made by combining 100 ml of commercial winter-quality diesel oil with 1,000 ml of seawater under gentle stirring overnight. All solutions were prepared 1 week prior to measurements in the aquarium. Concentrations of PAHs were quantified using gas chromatography—mass spectrometry and aliphatic hydrocarbons (decane-tetracontane) using gas chromatography—flame ionization detection at SYKE laboratory center. No attempt was made to determine chemical composition of each interference solution in detail, instead the solutions mimicked natural constituents in Baltic Sea water.

Altogether six glass beakers (each 2,000 ml) were wrapped with black plastic except for the top section and filled with 1,200 ml of seawater. Aliquots of the clay suspension (50.0 ml), humic extract (50.0 ml), cyanobacteria algae extract (10.0 ml) and diesel WAF (50 ml) were sequentially added so that all combinations of the aforementioned solutions in seawater were achieved. The solutions were kept in slow stirring motion using a magnetic stirrer. In first three sets of measurements no WAF was added. WAF was applied in three last measurement sets. After addition of each solution the responses were measured using one sensor at a time at exactly 50 mm below the upper level of the beakers. The top part of the beakers and the sensor housing were wrapped with black plastic. Fluorescence responses were collected for 3–5 min with each sensor and the average and standard deviation of fluorescence for each period of data collection were calculated.

The logging rates used with fluorometer sensors during the experiment were 1 min (average of values collected at 0.5 Hz), 30 and 1 s for the UviLux, EnviroFlu-HC and Turner C3 sensors, respectively. Data from EnviroFlu-HC were logged into a laptop PC using the TriOS MSDA_XE software and the data from Turner C3 into a PC using Turner C-soft software. Data from UviLux were logged into a portable logger connected to automatic GSM network-based modem and sent via GSM network to Tallinn University of Technology once a minute. Altogether 1.32 million, 79,000 and 30,000 time points of data from Turner C3, Enviroflu-HC and UviLux were generated, respectively. The small dilution effect in WAF solutions, caused by the volume increase by the added interference solutions, was compensated by a corresponding multiplier factor in final calculations thus yielding oil-related fluorescence (ORF) presented. Normalized responses from each fluorometer were calculated by dividing observed responses from different solutions with responses obtained

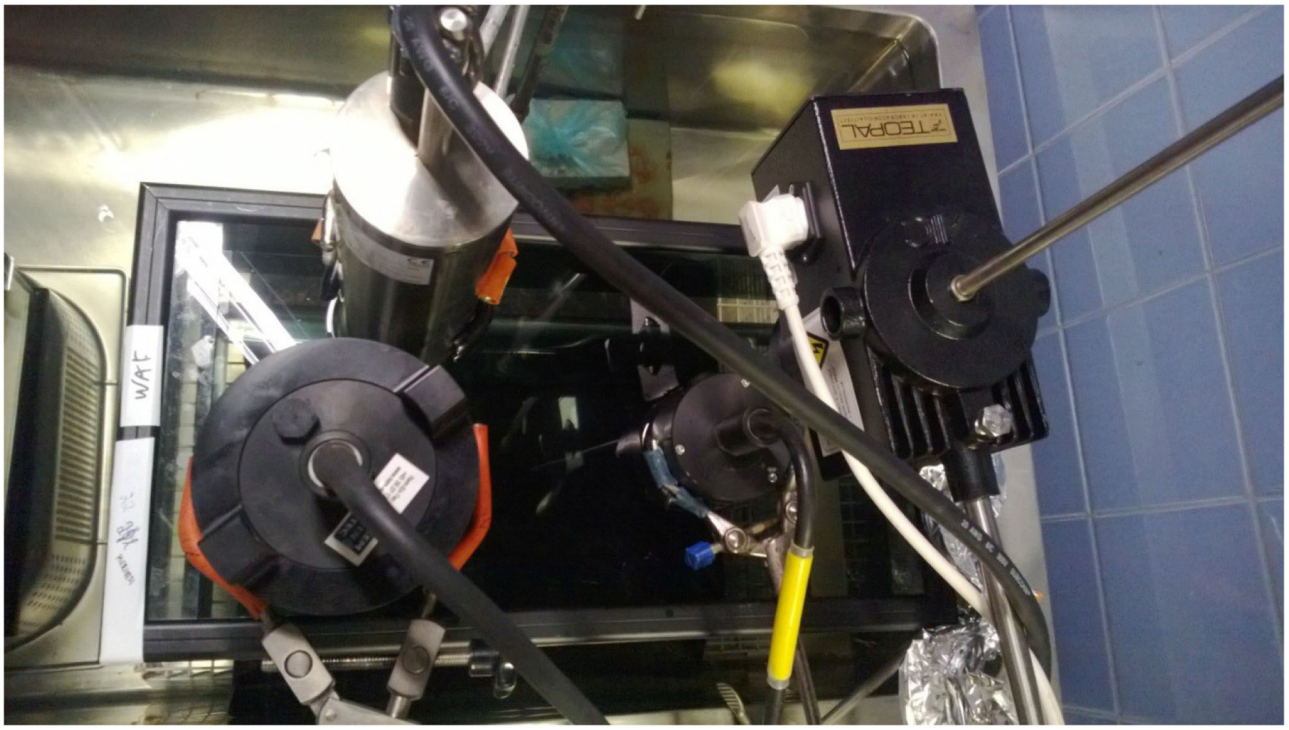

FIGURE 1 | Above view of the experimental set up. Instruments: TriOS EnviroFlu-HC (with metallic cover, upper part), Turner C3 (with black cover, left) and UviLux (black cover, right). The electric motor of the stirrer is at far right. Photograph: Harri Kankaanpää.

from seawater. No compensation was calculated for CDOM or turbidity values.

The second experiment for diesel WAF persistence and for method comparison lasted for 3 weeks. A 25-liter glass aquarium was used and placed over a black plastic sheet in a steel tank and filled with 21.8 liters of filtered seawater (salinity 6.2 PSU). Thermostatted (11°C) tap water was circulated in the exterior tank. The FLD sensors were fixed into laboratory stands so that the optical window of each sensor was at 10 cm below the surface of liquid (**Figure 1**). Gentle mixing was applied using an electricity-powered laboratory stirrer. The aquarium was covered by a black plastic wrapping except during water sampling and maintenance. The UviLux sensor needed to be moved further away from the two other sensors due to interference that was unfortunately not noticed before 7 days into the experiment. The data transmission, storage and sensors' acquisition rates were as described for the first experiment.

The persistence of diesel oil fractions in seawater and comparability between oil detection methods were measured in the second test. The methods were: the three fluorometric sensors, total oil monitoring method used by Finland, gas chromatography flame ionization detection (GC–FID; for aliphatic hydrocarbons) and gas chromatography—mass spectrometry (GC–MS; for PAHs including 1– and 2–methylnapthtalene). At S1–S9, water samples of 100 ml were collected for total oil HELCOM protocol and another 100 ml for the GC–MS and GC–FID analyses.

The Finnish HELCOM monitoring method for total oil analysis can be described briefly as follows: seawater is extracted with 10 ml of n–hexane under stirring. Fluorescence is measured using 310 and 360 nm excitation and emission wavelengths, respectively. Calibration is performed using solutions of Norwegian crude oil (Ekofisk) dissolved in n–hexane. Limit of quantification is 0.05 μg oil/l and analytical error is ±15%.

Aliphatic hydrocarbons (decane-tetracontane) were extracted using n-hexane, cleaned up using adsorbent, concentrated, separated using gas chromatography and quantified by flame ionization detection. The method has a limit of quantification of 100 μg total aliphatics/l and analytical error of 30 %. PAHs were extracted using n-hexane under stirring or solid phase extraction. The n-hexane solution was then concentrated and analyzed using GC–MS. The quantification limits of the method were between 0.005 and 0.01 μg/l, while the analytical errors varied between 20 and 40% depending on compound.

Normalized responses for each detection method were calculated by dividing observed responses with period S1 responses at given water sampling time points (S1–S9).

2.3. FerryBox Operation and Oil Detection Capability

A FerryBox system developed by Marine Systems Institute at Tallinn University of Technology is used on board of the M/S Baltic Queen (Tallink Group, Estonia) (**Figure 2**), which commutes between Tallinn (Estonia), Mariehamn (Åland) and

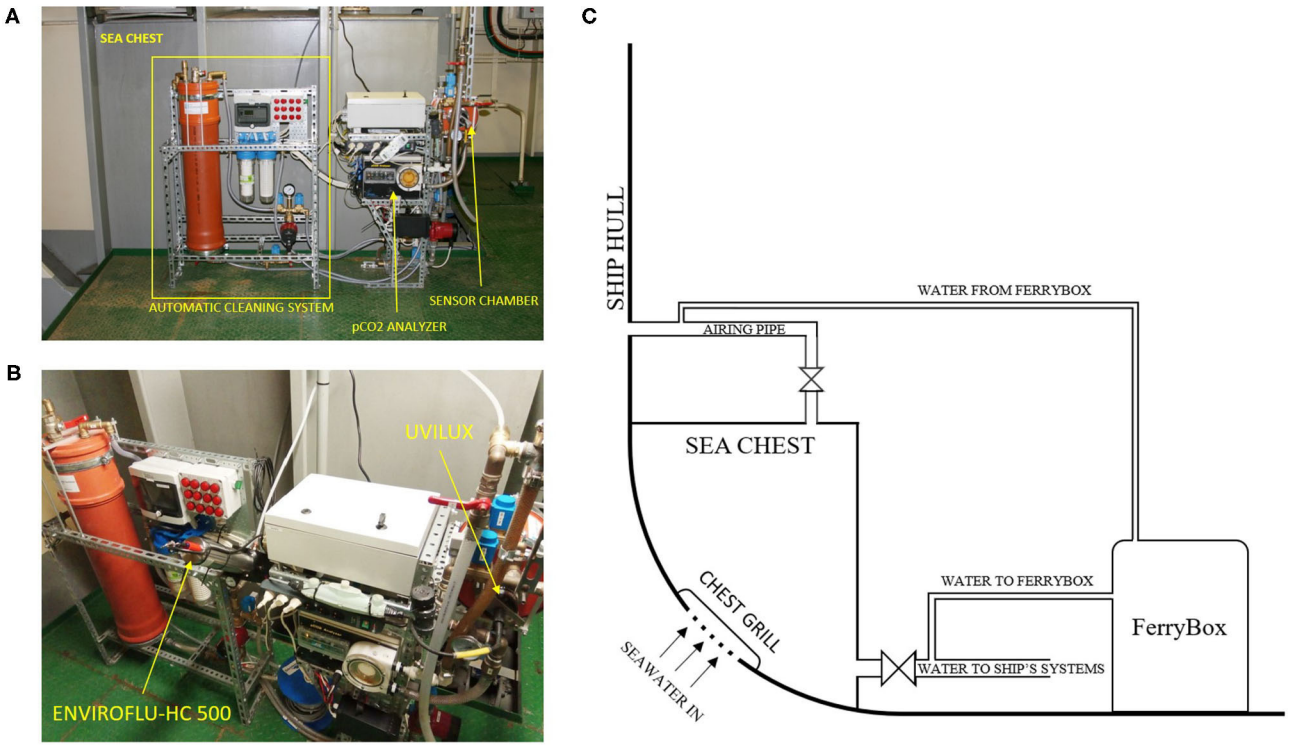

FIGURE 2 | FerryBox system on board M/S Baltic Queen **(A)** and the same system with UviLux and EnviroFlu-HC fluorometers during the experiment **(B)**. General scheme of the FerryBox's placement and water flow on M/S Baltic Queen is shown on figure **(C)**. Photographs: Kaimo Vahter.

Stockholm (Sweden) (**Figure 3**). The ship route covers the western Gulf of Finland, Northern Baltic Proper, Southern Archipelago Sea, and Southern Åland Sea (**Figure 3**). One crossing, including a stop in Mariehamn harbor, is about 425 km long and takes approximately 17 h. The ship then returns after a 7 h stay in the destination harbor.

All FerryBoxes are flow-through systems where the water is taken in from an inlet in a vessel hull and then pumped into a measuring circuit containing sensors (Petersen, 2014). On M/S Baltic Queen the water was taken from the ship's sea chest and pumped continuously through the FerryBox system at a rate of 9 l/min. The opening of the chest is situated about 4 m below the waterline. Parameters were measured with 1-min intervals, giving an approximately 0.5 km spatial resolution along the fairway, depending on the ship's speed. A typical transect contained roughly 1,000 records for each variable.

The UviLux and EnviroFlu-HC fluorometers, were installed in parallel to the FerryBox system (**Figure 2B**), which recorded additional real-time seawater properties. Conductivity (salinity) and temperature was measured with a High-Precision Pressure Level Transmitter Series 36XiW (KELLER AG, Switzerland), turbidity was measured with a Seapoint Turbidity Meter (Seapoint Sensors Inc., USA) and pCO2 was measured with an OceanPack^{TM} pCO2 analyzer (SubCtech, Germany).

We made four maintenance visits to M/S Baltic Queen in order to clean the FerryBox system and the sensors. These visits were made roughly every 2 weeks (March 3, March 20, April 3, April 15) during our 2-month experiment (February 21 to April 21, 2018). The maintenance consisted of washing the system with a solution of oxalic acid and a manual cleaning of the optical sensors. The FerryBox also has a automatic cleaning system, which was not functional during the experiment. Similar automatic acid-washing cleaning method is applied to prevent biofouling on a FerryBox traveling between Tallinn and Helsinki (Lips et al., 2016).

Measurements from the sensors in the FerryBox were collected by a datalogger (RTCU-MX2i pro by Logic IO) on board M/S Baltic Queen. The datalogger includes a modem and a GPS, and adds the position and a time stamp to the measurement before sending the data to an on-shore FTP server of the Marine Systems Institute using the GSM/GPRS protocol. The data were sent in real-time (every minute).

A publicly available, web-based, user interface was built to visualize the data online, where the ship's track, real-time position and gathered FerryBox data was available in real-time (**Figure 4**) (TalTech, 2017). The web-based user interface is also equipped with different options to view historical data: the user can select parameters or time periods, and construct a map view and 2D graphs of multiple parameters. Data are also available in a tabulated form and parameters can be viewed in color-coded view along the ship's track. The data that were provided in real-time during the experiment is still available on the web-page.

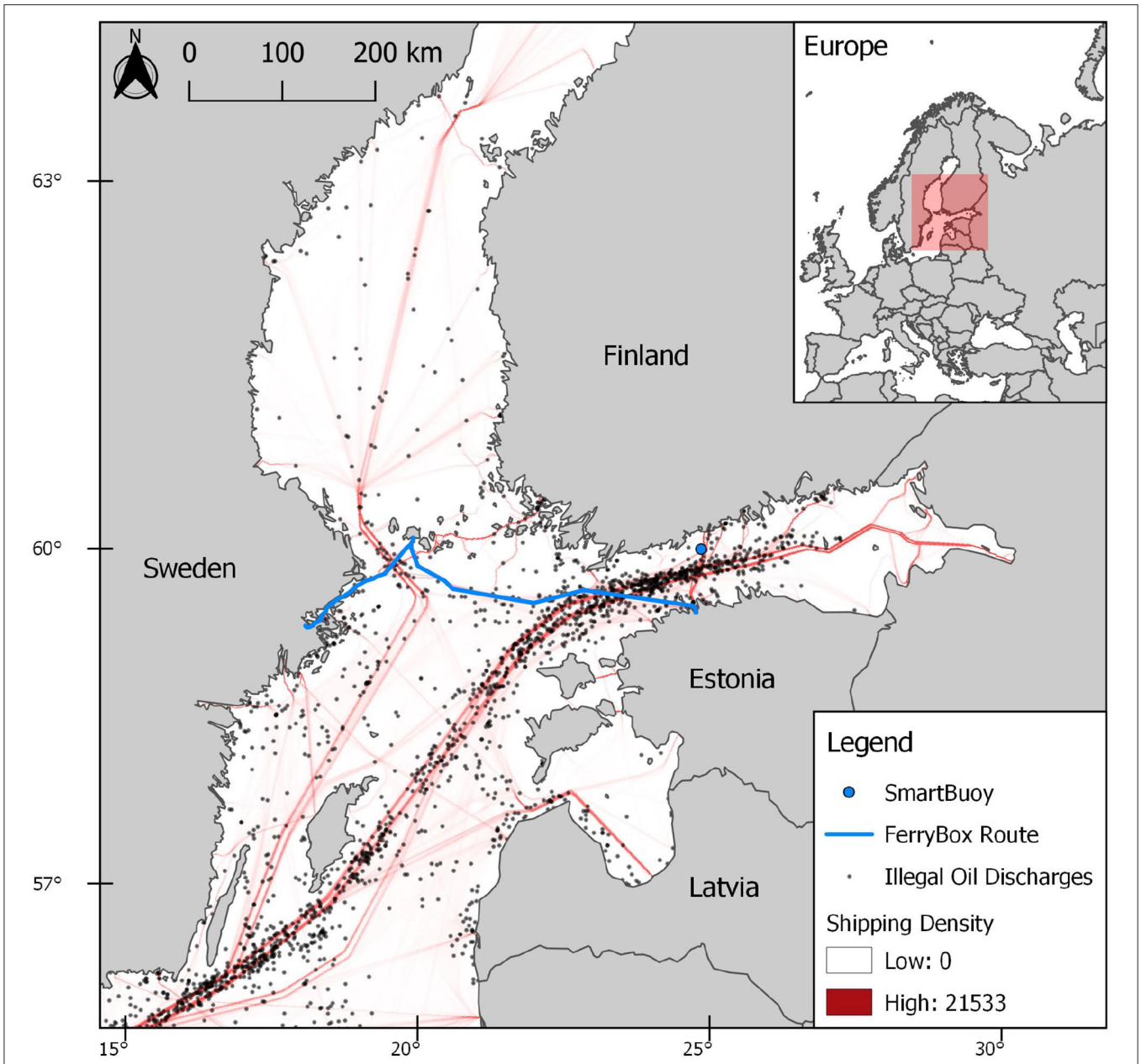

FIGURE 3 | FerryBox line and SmartBuoy mooring location in the Baltic Sea. Points of information describing the location and size of illegal oil discharges observed during aerial surveillance flights by HELCOM Contracting Parties during 1998–2017 (HELCOM, 2018b). Shipping density (defined as the number of ships crossing a 1 × 1 km grid cell) of all IMO (International Maritime Organization) registered ships operating in the Baltic Sea in 2016 (HELCOM, 2017).

2.4. SmartBuoy Setup and Experiment for Oil Spill Detection

The SmartBuoy, developed by Meritaito Ltd (Finland), is a combination of a polyethylene spar buoy with mobile and/or satellite communication technology and a versatile selection of monitoring sensors (**Figure 5**). The Turner Design C3 fluorometer was installed inside of the buoy in a vertical monitoring well with an open flow through a pipe, enabling continuous sea water exchange. The monitoring depth was 2–3 m depending on the sea level. Concentration of CDOM and turbidity values were measured simultaneously with the hydrocarbon measurements. To ensure high data quality, the C3 sensor was equipped with a mechanical wiper cleaning all three optical lenses before taking the measurements. In addition to the water quality monitoring, the SmartBuoy also collected data about current speed and direction at the depth of 7 m to identify spreading direction of potential oil spills. Furthermore, the significant wave height was calculated from roughly 8.5-min time series, measured by a pressure sensor (Aanderaa Wave and Tide Sensor 5218).

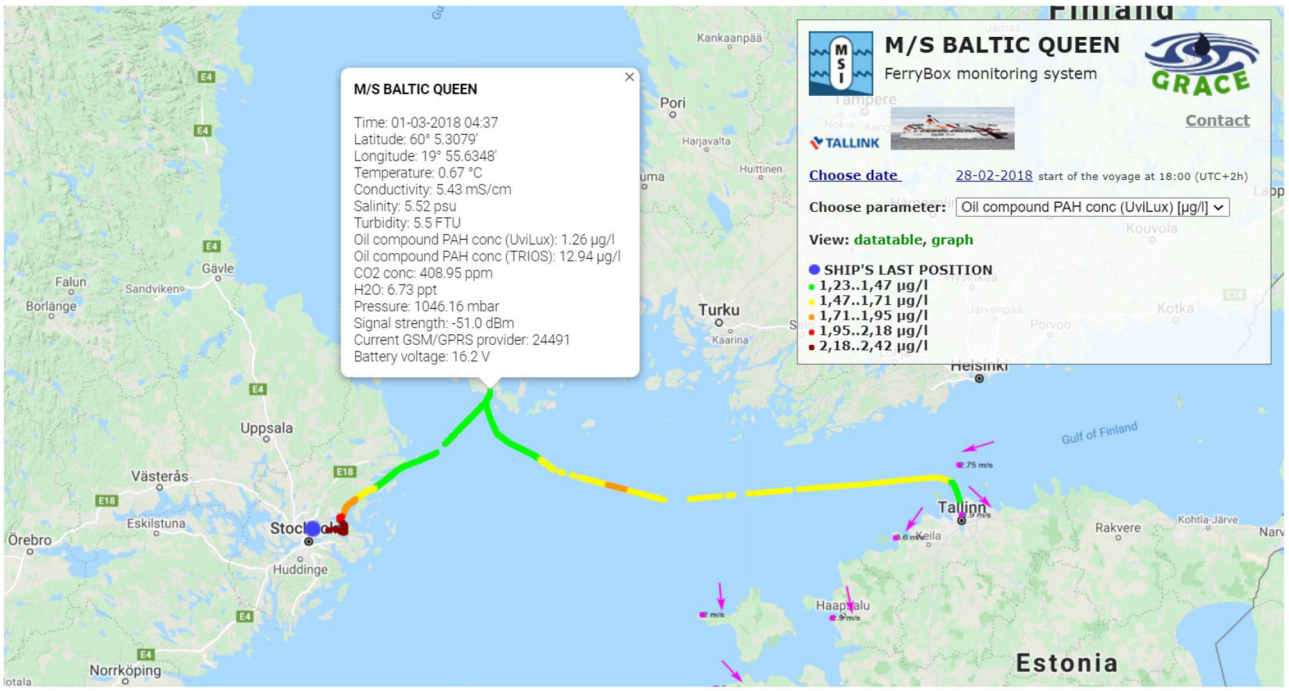

FIGURE 4 | Web-based user interface for viewing the real-time data from the FerryBox system (TalTech, 2017). The gaps in the data were caused by loss of the GSM-network.

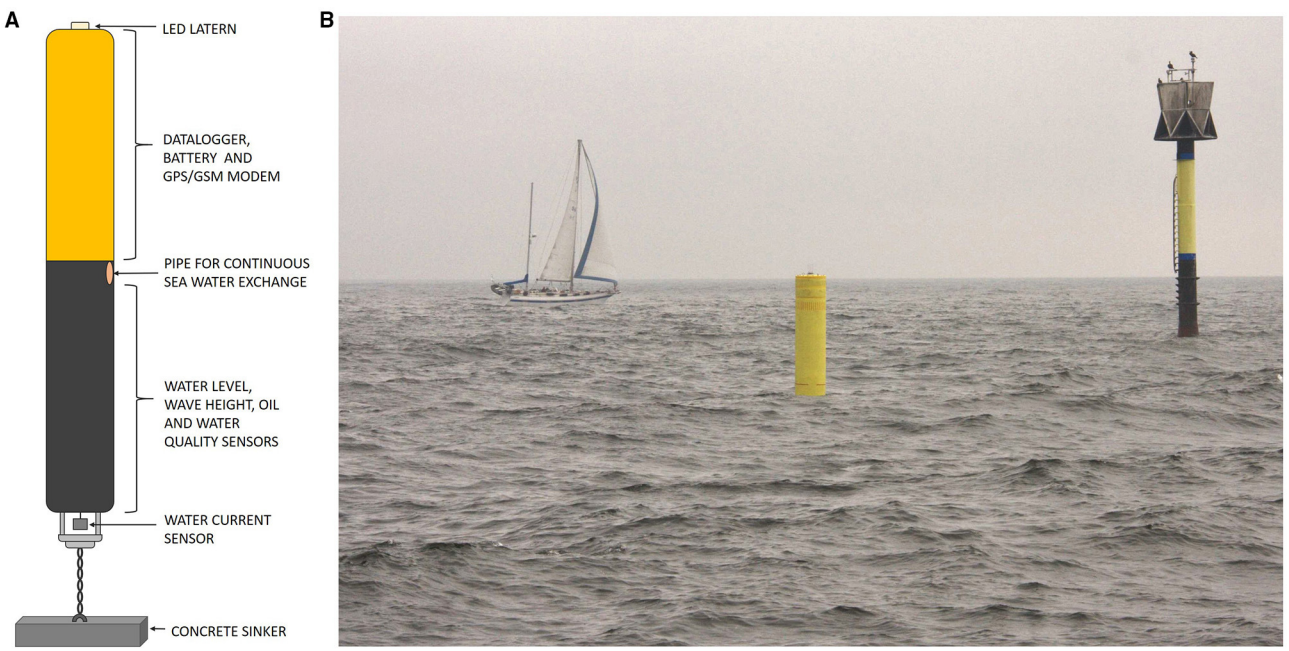

FIGURE 5 | Schematic figure of the SmartBuoy system **(A)** and the SmartBuoy deployed to the off-shore area in the Gulf of Finland for oil spill detection **(B)**. Photograph: Joose Mykkänen.

TABLE 1 | Relative responses (fold compared to average fluorescence in seawater) of sensors to interference solutions, sensitivity to water accommodated fraction (WAF) of diesel oil.

	UviLux	Turner C3	TriOS Enviroflu-HC
Maximum attenuation without diesel WAF	none	0.95 (clay suspension)	0.97 (clay suspension)
Maximum false positive without diesel WAF	7.61 (algae extract)	3.96 (humic extract + algae extract)	2.64 (algae extract)
Sensitivity to WAF (change from S to SW)	4.48	1.1	2.62
Maximum attenuation during presence of diesel WAF	4.41 (humic extract)	none	2.25 (clay suspension + humic extract)
Maximum false enhancement during presence of diesel WAF	10.6 (algae extract)	3.89 (humic extract + algae extract)	4.95 (algae extract)

Water quality and sea state sensors were connected to a datalogger (Aanderaa SmartGuard 5300) that was programmed to operate the sensors with an 1-h measurement and data transmission interval. Real-time data from the SmartBuoy were transmitted over satellite modem to a server, where it were subjected to an automatic data quality control before being visualized online.

The SmartBuoy buoy was moored on a junction of the main merchant shipping lanes in the Gulf of Finland (**Figure 3**) for a 2-month measurement period (October 25 to December 24, 2018). Vessels navigating on the north–south direction shipping lane between Helsinki and Tallinn were passing close to the buoy, and vessels on the east–west direction shipping lane passed the buoy further south. The SmartBuoy was visited once during the monitoring period for datalogger reprogramming and manual maintenance of the sensors.

3. RESULTS OF THE LABORATORY EXPERIMENTS

The produced WAF contained the following main PAH constituents (all μg/l): naphthalene (65), 1-methylnapthtalene (89), 2-methylnapthtalene (31), anthracene (1.6), acenaphthene (2.7), acenaphthylene (1.2), phenanthrene (1.2), fluoranthene (0.20), fluorene (4.4) and pyrene (0.2). Other PAHs fell below the 0.005 μg/l limit of quantification. The concentration of aliphatic compounds was 1,200 μg/l.

3.1. Effect of Interference Solutions

In the first laboratory experiment we investigated how the sensors reacted to the addition of interference solutions. In the absence of interference solutions, Turner C3 showed the largest absolute fluorescence values (primary data), followed by Enviroflu-HC and Uvilux. The data from Turner C3's PAH and CDOM channels had occasional spikes, but overall the data stability from each channel of the detectors were good. When WAF was added to the seawater, the relative change in signal strength (normalized response) was largest for UviLux (4.48-fold), followed by EnviroFlu-HC (2.62-fold) and Turner C3 (1.1-fold) (**Table 1**).

All sensors reacted when interference solutions were added to seawater. The addition of suspended clay to seawater slightly attenuated the PAH channel's fluorescence signal in Turner C3 and Enviroflu-HC, while slightly enhancing it in UviLux (**Figure 6**, left half, S vs. SC). When suspended clay was added to the seawater-WAF solution, the signal was slightly attenuated in Enviroflu-HC and UviLux, and slightly enhanced in Turner C3 (**Figure 6**, right half, SW vs. SWC). In all combinations, the changes were at most 12% (0.88–1.04).

The sensors were more sensitive to the presence of humic substance extracts, with the PAH-signals increasing between 1.05- and 1.8-fold in all sensors (compared to seawater). The enhancement was strongest in Turner C3 and weakest in EnviroFlu-HC (**Figure 6**, left half, S vs. SH). In the seawater-WAF solution the added humic extracts enhanced the PAH signal in Turner C3 (1.67-fold), while slightly attenuating the signal in the other sensors (**Figure 6**, right half, SW vs. SWH).

Clearly the largest effect on the PAH fluorescence signal was observed after adding algae extract. The signal was enhanced in all combinations of sensors and solutions. Importantly, the enhancement caused by the algae extract was stronger than the PAH signal of the WAF-solution without any interference solutions, which means that the presence of algae can interfere strongly with the sensors ability to detect oil compounds in the water. The enhancements when adding the algae extract to the seawater were roughly between 3- and 8-fold, with UviLux showing the largest change and EnviroFlu-HC showing the smallest change (**Figure 6**, right half, SW vs. SWA). When the algae extract was added to the seawater-WAF solution, the PAH signal was enhanced roughly 2- to 3-fold in all sensors, with Turner C3 showing the strongest change in signal strength (**Figure 6**, right half, SW vs. SWA).

3.2. Diesel WAF Persistence and Method Comparison

In the second laboratory experiment we studied how long the sensors can detect oil compounds in seawater, while also comparing detection methods. Lagging software caused several gaps in the Turner C3 data and one gap in the EnviroFlu-HC data. UviLux was relocated after 165 h when we noted that it did not react clearly to the third addition of WAF (WAF3; **Figure 7**), having large subsequent oscillations in the signal. This behavior was caused by optical interference by the two other sensors. Despite that there was substantial suppression in UviLux responses during the suppressed period, the sensor overall did show slight responses even during this period. These small responses occurred simultaneously when adding WAF 1 and WAF 3 (but not when adding WAF 2), and were also simultaneous with HELCOM and Enviroflu-HC responses (**Figure 7**). After UviLux was relocated, it provided data with

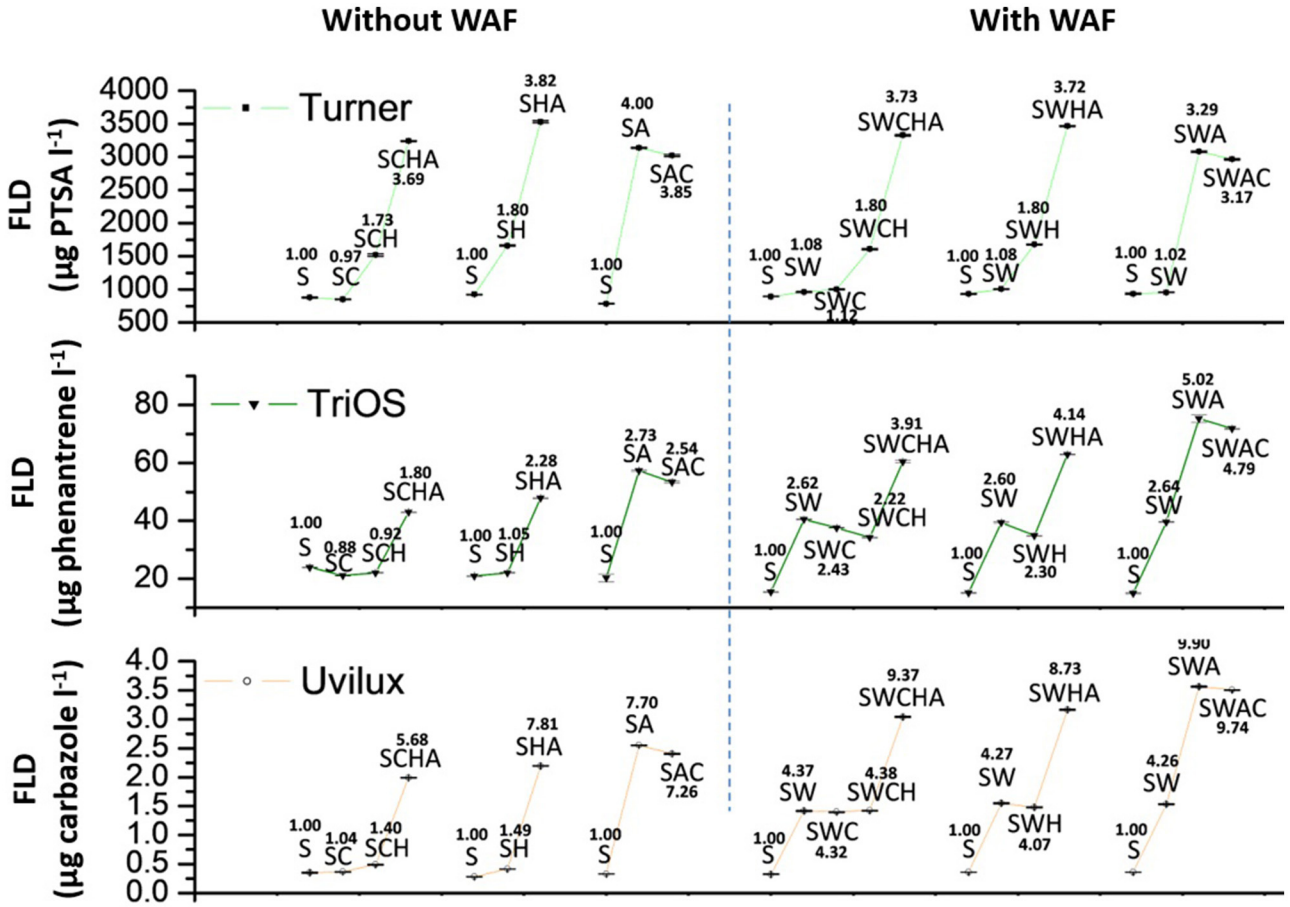

FIGURE 6 | Fluorescence responses from EnviroFlu-HC (TriOS), Turner C3 (Turner) and UviLux sensors in seawater, seawater containing interferences of clay, humic substances, algae substances, and seawater containing diesel WAF with and without the interferences. S = seawater, C = clay suspension, H = humic substance extract, A = cyanobacterial algae extract, and W = water accommodated fraction (diesel fuel extracted in seawater). PTSA = 1,3,6,8-pyrenetetrasulphonic acid tetrasodium salt. The change in FLD response respective to the baseline (S) value in each series (e.g., S–SC–SCH–SCHA) is indicated on top of each treatment.

a considerably higher response and less noise. For response calculations we therefore only used the UviLux data gathered after the relocation.

The responses from all sensors and the standard HELCOM oil monitoring method indicated that fluorescent compounds originating from diesel oil were detectable for at least 20 days since the start of the experiment (**Figure 7**). The temporal evolution in PAH-related responses measured by the EnviroFlu-HC and UviLux sensors were in line with the HELCOM method, especially after the readjustment of the sensors. In contrast, Turner C3 showed slightly increasing fluorescence between 100 and 505 h while the signal from the other two sensors decayed and leveled off.

Table 2 summarizes the responses obtained from sensor-based fluorescence right before water samples (GC methods) were collected at events S5 and S7. Event before sample S7 should serve as the primary point for response comparison since it was taken after the readjustment of sensor locations (R). The relative responses compared to initial state S1 of the fluorescence-based methods, during 165–505 h were (from strongest to weakest): HELCOM, UviLux, EnviroFlu-HC and Turner C3 (**Figure 7** including responses at each S event).

Several PAH molecules were good indicators for diesel-originating contamination (**Table 2**). All napthtalenes provided pronounced responses also at S1 (strongest to weakest): 1-methylnaphtalene (1-MN), naphthalene (NAF) and 2-methylnaphtalene (2-MN) (data not shown). Also, anthracene, acenapthtene and phenantrene were sensitive and showed a similar temporal evolution as the FLD-based responses and the methylated napthtalenes (1/2-MN).

Concentration of fluoranthene did not change over the experimental period, and Dibenz[a.h]anthracene showed a declining trend compared to the initial seawater (**Figure 8**). These substances (in addition to acenapthtylene, fluoranthene, dibenzo[a,h]anthracene and pyrene) were poor proxies for WAF contamination in the seawater (**Figure 8**).

The concentration of aliphatic hydrocarbons followed a similar pattern as those of FLD, methylated napthtalene and

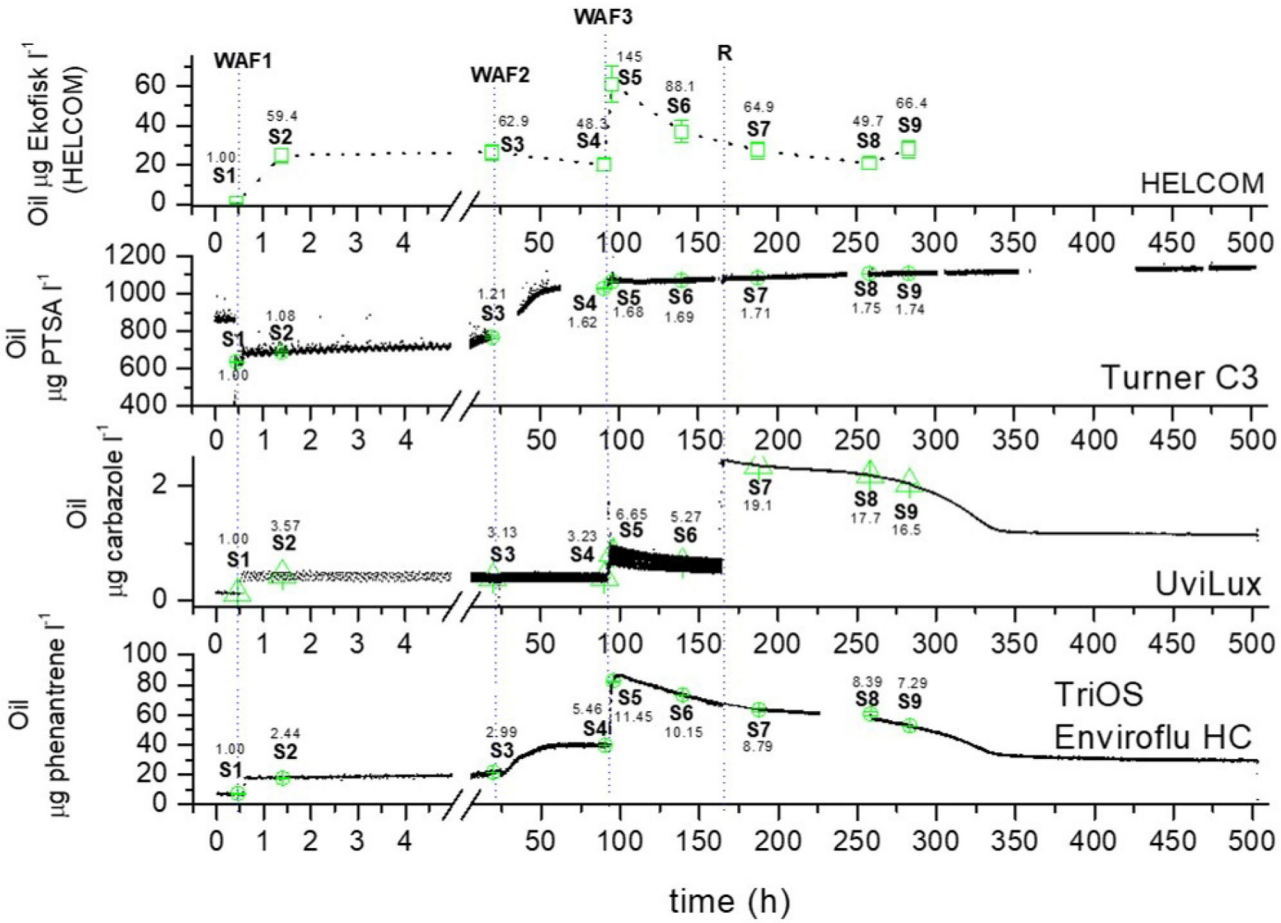

FIGURE 7 | Evolution of responses of fluorescence signals obtained in experiment two over 503.2 h originating from HELCOM reference method (top), Turner C3, UviLux and EnviroFlu-HC (bottom). S1–S9: water sampling events; WAF1–WAF3: events of WAF addition; R: relocation of the sensors. Normalized response values relative to the initial background level (at S1) measured before just before S events are indicated above each S event.

the more sensitive PAHs. The PAH and aliphatic hydrocarbon concentrations also had a similar evolution pattern as the values derived using the HELCOM fluorescence method. Interestingly, the increase in aliphatic hydrocarbon concentrations between S8 and S9 showed a similar increase as the HELCOM method; this change was not visible in any other parameter (**Figures 7**, **8**).

4. RESULTS OF THE FIELD EXPERIMENTS

4.1. FerryBox Experiment

The real-time transmission and online presentation of the FerryBox data worked well, but data gaps occurred systematically in the Baltic Proper due to loss of the GSM network. These gaps typically lasted a maximum of a few hours. An example is presented in **Figure 4**. The complete data was recovered from the datalogger after the fact. Altogether 58 ship voyages were analyzed. The PAH-transects were visually checked for peaks that would have indicated an oil pollution. No such anomalies were found during the 2-month measurement period the UviLux and EnviroFlu-HC fluorometers were installed to the FerryBox system.

The detected PAH values stayed between 1 and 2.6 μg carbazole/l for the UviLux and 12.4–25.5 μg phenantrene/l for the EnviroFlu-HC (**Figures 9A,B**). The detected hydrocarbon values were lowest in the sea areas near Åland and highest in the Stockholm archipelago, where the effect of the natural background of organic carbon from river waters is greater (**Figures 9A,B**). From 20.5°, longitude eastward, the PAH values were quite homogeneous. Some variation can be seen e.g., between 22°, and 23° longitude (trips 19–23), showing up more clearly in the UviLux data (**Figures 9A,B**). We surmise that the detected values do not reflect concentration of carbazole, phenantrene or oil in seawater. This interpretation is supported by the chemical monitoring (HELCOM/EU MSFD) and analysis of the Baltic Sea, which has found concentrations below 1 μg oil hydrocarbons/l rather constantly (Pikkarainen and Lemponen, 2005; FIMR and Olsonen, 2007). These low values are considered to be typical for seawater without significant oil pollution (Bícego et al., 1996; Zanardi et al., 1999).

TABLE 2 | Overview on the response levels generated by the fluorescence-based methods and parameters obtained from GC–FID and GC–MS analyses.

Parameter	Background level $\mu g\ l^{-1}$	Response at S5 $\mu g\ l^{-1}$	Response relative to background level at S5 (-fold)	Response at S7 $\mu g\ l^{-1}$	Response relative to background level at S7 (-fold)
Turner C3 fluorescence (PTSA)	634.7 ± 3.74	1071.7 ± 2.23	1.68	1084.14 ± 2.85	1.71
TriOS Enviroflu-HC fluorescence (phenantrene)	7.22 ± 0.41	82.63 ± 0.56	11.45	63.4 ± 1.27	8.79
UviLux fluorescence (carbazole)	0.123 ± 0.003[a]	0.819 ± 0.003[a]	6.65[a]	2.351 ± 0.002	19.10
HELCOM fluorescence	0.42	61 ± 9.15[b] (± < 0.1)[c]	145.2	27.27 ± 4.09 (±0.06)[c]	64.92
Aliphatics C10–C21[d]	98 ± 29.4	750 ± 225	7.65	120 ± 36	1.22
Aliphatics C22–C40[d]	300 ± 90	970 ± 290	3.23	290 ± 87	0.97
Aliphatics C10–C40[d]	400 ± 120	1700 ± 510	4.25	410 ± 123	1.025
Total PAHs[e]	0.988 ± 0.2964[e]	9.39 ± 2.82	9.50	1.62 ± 0.48	1.63
Napththalene[f]	0.11 ± 0.02	1.7 ± 0.34	15.45	0.2 ± 0.04	1.82
1-methylnapththalene[e]	0.07 ± 0.02	2.9 ± 0.87	41.4	0.25 ± 0.08	3.57
2-methylnapththalene[e]	< 0.005	3.5 ± 1.05	700[g]	0.17 ± 0.05	34[g]
Anthracene[h]	< 0.01	0.10 ± 0.03	9.7	0.11 ± 0.04	11
Acenapththene[f]	0.084 ± 0.017	0.21 ± 0.04	2.5	0.098 ± 0.02	1.17
Acenapththylene[d]	< 0.005	< 0.005	NA	0.087 ± 0.026	5.22
Fluoranthene[d]	0.16 ± 0.05	0.16 ± 0.05	1	0.16 ± 0.05	1
Fluorene[f]	0.14 ± 0.028	0.38 ± 0.08	2.71	0.18 ± 0.04	1.29
Dibenz[a.h]anthracene[d]	0.094 ± 0.028	<0.01	0.11[g]	< 0.01	0.11[g]
Phenanthrene[d]	0.22 ± 0.066	0.32 ± 0.096	1.45	0.24 ± 0.072	1.09
Pyrene[d]	0.11 ± 0.03	0.12 ± 0.04	1.09	0.12 ± 0.04	1.09

[a]*Suppressed signal.* [b]*± 15% error attributed for the method.* [c]*Actual repeatability of parallel samples at S5 and S7.* [d]*Based on ±30% error attributed for the method.* [e]*Based on ±30% error attributed for the method.* [f]*Based on ±20% error attributed for the method.* [g]*Calculation of relative difference is based on the limit of quantification.* [h]*Based on ±35% error attributed for the method. NA = not available.*

The FerryBox and the accompanying sensors were maintained and cleaned frequently. Nevertheless, biofouling still impacted the quality of the measured data as can be seen from the decreasing values between the maintenance visits (**Figures 9A,B**). The field data suggests that EnviroFlu-HC is affected more strongly by the fouling than UviLux.

4.2. SmartBuoy Experiment

The obtained values ranged between 790 and 1,250 during the monitoring period. The variation pattern was nearly identical with the variation of collected colored organic carbon (CDOM) values, varying between 600 and 890 (**Figure 9**). The measured data had systematic gaps. On the 12th of December a maintenance visit to the boy was made to reprogram the datalogger and manually clean the sensors.

The correlation between the collected hydrocarbon dataset and the CDOM data set collected by the C3 sensor on SmartBuoy was very high (**Figure 9D**). No anomalic spikes indicative of oil-contamination were present during the test period. The C3 sensor on SmarBuoy was equipped with a mechanical wiper, which cleaned all three optical lenses prior to measuring. No significant reduction in data quality due to biofouling was detected compared to the FerryBox where the detected values gradually decreased after the cleaning (**Figure 9**). The linear relationship between the two variables changed after the maintenance on 12 December. This change was probably caused by the readjustment of the mechanical wipers (Joose Mykkänen, Personal communication). Nonetheless, the correlation between the variables remained high (**Figure 9D**).

During the experimental period, the buoy tolerated several events with significant wave heights over 2 m. The maximum significant wave height reached almost 3 m, which is estimated to be exceeded at this location roughly 1% of the times (Tuomi et al., 2011; Björkqvist et al., 2018). During the monitoring period the current speed reached 39 cm/s, with the mean value being 12 cm/s. The mean yearly current speed (for depth 0–7.5 m) in the area is expected to be under 10 cm/s (Westerlund et al., 2018).

5. DISCUSSION

Laboratory tests showed that optical interferences strongly affected optical PAH detection. The effect of these interferences was corroborated by the strong correlation between oil-related fluorescence and CDOM fluorescence (**Figure 9D**). CDOM causes interference and false positives whenever it is present sufficiently and not accounted for properly. Similar results arose from the presence of cyanobacteria-derived material. The Baltic Sea contains substantial concentrations of CDOM at any time of year, most prominently close to river outlets. The quenching of

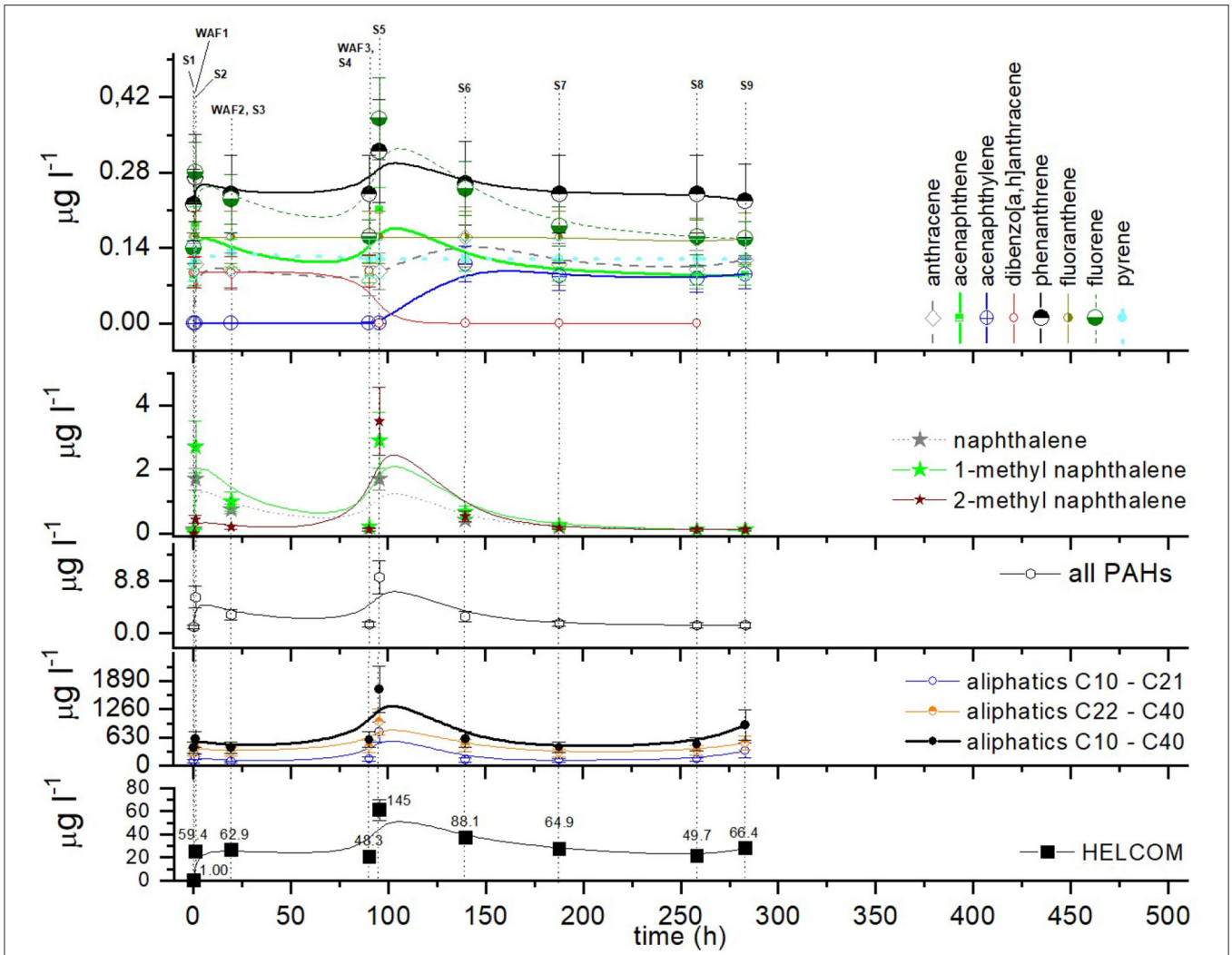

FIGURE 8 | Concentrations of hydrocarbon compounds analyzed using GC–FID (aliphatic hydrocarbons) and GC–MS (PAHs) from samples of experiment two. The values on top of HELCOM data points denote signal relative to baseline. S1–S9 are water sampling events and WAF1–WAF3 events of WAF addition.

oil-related fluorescence caused by clay-derived turbidity further complicates the interpretation of the signal.

Extensive spring and summer blooms of phytoplankton occur regularly in the Baltic sea (Kahru et al., 2007, 2016; Groetsch et al., 2014). We can also suspect greater interference during summer blooms of cyanobacteria and minor contribution throughout the year as there are always small quantities of chlorophylls and phycocyanin of phytoplankton origin in the surface waters. The spring bloom duration in the Baltic Sea is about one and a half months (Groetsch et al., 2016) and the peak of the bloom in 2018 coincided with the end of the FerryBox experiment (Almén and Tamelander, 2020). Nevertheless, we did not see the signal enhancing effect of the phytoplankton during the FerryBox experiment, as the PAH signals should have increased toward the end of the testing period together with the bloom intensity.

There also exist several overall issues when using fluorometers that are related to the information about the presence and relative concentration of oil compounds in water. Fluorometers are generally calibrated using a specific oil or specific compounds; thus, the relevant concentration results are relative to the specific oil or compound and the procedure used to calibrate the instrument (Lambert et al., 2003). The response of the fluorometer to oil depends significantly on the oil composition and its weathering state, complicating the quantification of oil concentration further (Henry et al., 1999). Also other studies have noted that the other fluorescent substances in seawater can significantly interfere with direct fluorescence measurements of petroleum hydrocarbons (Henry et al., 1999; Bugden et al., 2008; Tedetti et al., 2010; Cyr et al., 2019). Lastly, a reliable comparison of different sensors would also require a consensus over the units used to report FLD-based results.

Taking account of the aforementioned issues and the knowledge that most of the oil pollution in the Baltic Sea comes from small operational oil spills, and that most cases requiring

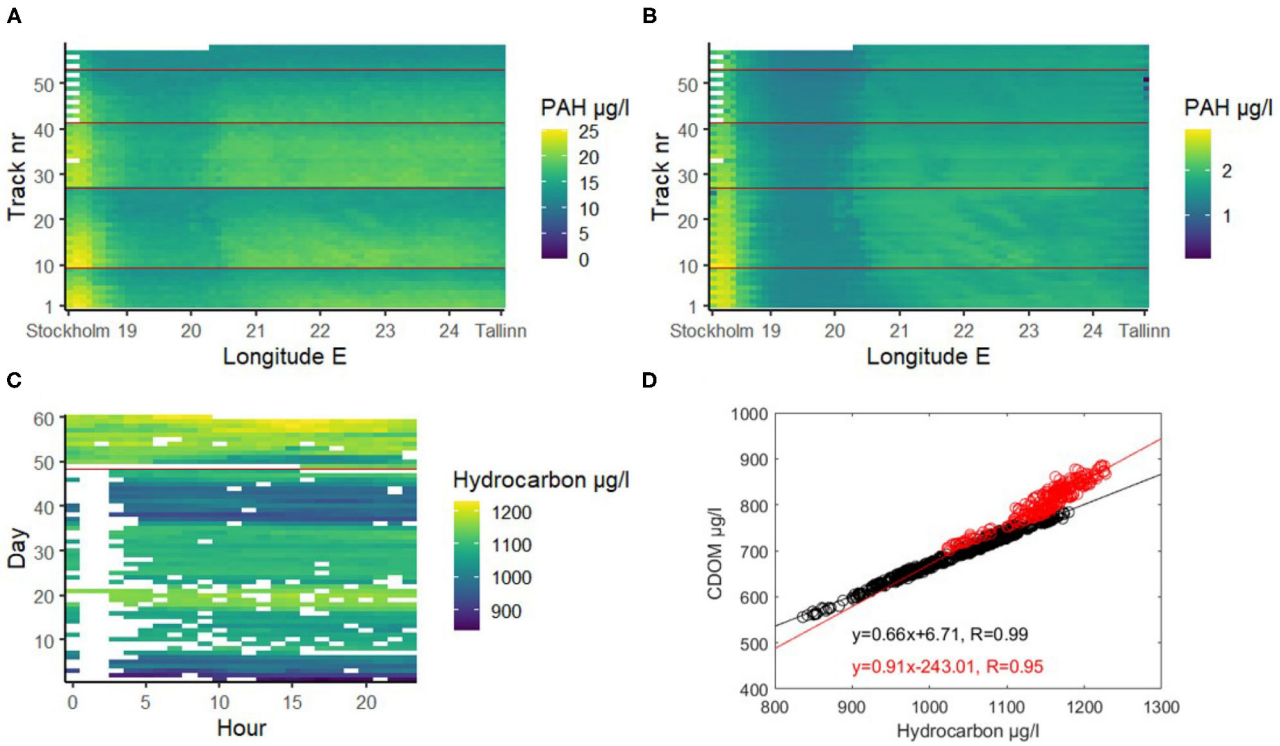

FIGURE 9 | Heatmap plots showing spatiotemporal distributions of PAH concentrations in seawater along the ship track between Stockholm and Tallinn (February 21 to April 21, 2018) measured with the UviLux **(A)** and EnviroFlu-HC **(B)** fluorometric sensors. A temporal heatmap of the SmartBuoy data (October 25 to December 24, 2018) **(C)** and correlation between CDOM and hydrocarbon data before (black) and after (red) the maintenance **(D)**. Red lines on the heatmaps indicate system maintenance visits.

criminal prosecution have involved diesel oil, the latter was selected to mimic the oil pollution in our laboratory experiments. Moreover, based on this background and the results of the laboratory tests, the field trials concentrated only on the detection of oil pollution, which should have appeared as a clear peak, deviating from the background fluorescence in the measured response patterns. The question of capabilities to detect different types of oil in the field is not only a question of the detection capabilities of the actual sensors, since also the weathering process for e.g., crude oil and diesel oil differ. In addition, the calibration of the sensors can reflect the a priori expectations of what type of oil might be encountered. It is therefore impossible to give any general recommendations on this subject, and follow-up studies are needed to test the suitability of the sensors used in this study in case they are planned to be used outside the Baltic Sea.

Due to the interfering substances it is difficult to distinguish water quality variations from the responses from oil spills. To combat that problem, suitable mathematical protocols should be explored. Some newer sensors also include built-in correction methods to discriminate oil from the natural interferences. Examples of sensors with such specification are Vlux OilPro (Chelsea Technologies Ltd), SeaOWL UV-A^{TM} (Sea-Bird Scientific) and HM-900 (Pyxis).

Another aspect that needs careful consideration is the measurement or water intake depth of the oil detection systems. After a spill, wind, waves and currents can break the oil spill into droplets and may propel the oil deeper into the water column; this process is called natural dispersion. Dispersion is a complicated physio–chemical process affected by the characteristics of the oil spill (oil type, density, viscosity, thickness) and other seawater properties such as temperature and salinity (Xiankun et al., 1993; Papadimitrakis et al., 2011). Various other physical, chemical, and biological processes begin to alter the oil as well, altogether referred to as weathering process (Mishra and Kumar, 2015; Tarr et al., 2016).

Using sampling and further laboratory analysis the maximum detection depths of naturally dispersed oils has been between 2.5 and 15 m (Cormack and Nichols, 1977; Lichtenthaler and Daling, 1983, 1985). An experiment by Cormack and Nichols (1977), part of which was monitoring naturally dispersed Ekofisk crude oil in the water column, showed comparatively rapid decrease in oil concentration down to 5 m depth, followed by a slower decrease to background levels at 20 m. A similar experiment in Norwegian waters with 10 m^3 of topped Statfjord crude oil showed that small concentrations of oil were present to at least at a depth of 3 m in the water column under the slick (Lichtenthaler and Daling, 1985). In another experiment done with 2,000 liters of Statfjord

crude oil and of topped Statfjord crude oil the maximum detection depths were 2.5 m (Lichtenthaler and Daling, 1983).

At the Baffin Island Oil Spill experimental site in the Canadian Arctic, flow-through fluorometry was successfully used to monitor a subsurface release of chemically dispersed crude oil cloud over several days, providing real-time and continuous data on oil concentrations in the water column (Green et al., 1983). Nonetheless, during a surface release experiment performed in the same study, petroleum hydrocarbons from the untreated oil were not detected in the water column deeper than 1 m (Humphrey et al., 1987). In a contained oil spill experiment, part of which was 3 liters of crude oil spilled in moored 66 m^3 containers in the ocean, a continuous flow-through fluorescence system was capable of detecting oil concentrations down to 8 m, over a period of 7 days (Green et al., 1982). Lunel (1995), using continuous-flow fluorometry (calibrated using discrete samples) found traces of oil down to 5 m after 20 metric ton of a mixture of medium fuel oil and gas oil (in a 50–50 ratio) were experimentally released in United Kingdom waters. Nevertheless, these experiments made in U.K., the Canadian Arctic and inside the British Colombian archipelago might not be directly transferable to the Baltic Sea because of differences in hydrography, and wind and wave conditions.

The probability of detecting oil pollution clearly depends on the weather conditions, and the size, oil type, source and weathering state of the spill. Most of the FerryBox systems are limited to a fixed depth set by the ship's design, as is the case in this study. For the FerryBox system on M/S Baltic Queen, the water is taken in at a depth of approximately 4 m and the SmartBuoy sensors situate 2–3 m below the surface, depending on the sea level. In light of the results of the aforementioned studies, these depths should be suitable for detecting anomalies in fluorescence. Also, for the FerryBox the water will also be mixed by the moving ship itself. Nonetheless, when devising such systems in the future, measurement depths as close to the surface as possible are recommended to ensure higher chance of spill detection.

Biofouling (marine growth) is likewise a major factor limiting the reliability of optical sensors in aquatic studies, especially during long term measurements. Biofouling is the net result of various physical, chemical and biological factors such as water temperature, conductivity, season, and location—to name a few (Delauney et al., 2010). Several antifoulant approaches for optical systems on autonomous platform have been suggested (Manov et al., 2004; Delauney et al., 2010). In our experiments the automatic mechanical cleaning of the sensor on the SmartBoy was satisfactory but the fouling of the FerryBox sensors after the maintenance visits is clearly there. It is not evident how much biofouling affects the oil detection capabilities of the sensors, but in our experiment is seemed to be of secondary importance compared to the presence of the other interfering substances.

6. CONCLUSIONS

Laboratory experiments indicated that the sensitivity of the sensors to diesel oil is good and they provide useful data on oil in seawater. Fluorescent compounds from the oil were detectable by the fluorometric sensors for at least 20 days. Our laboratory tests were conducted with diesel oil, Baltic Sea water, and local interfering substances and therefore may not be representative of different types of oils or marine areas. The main issue with the sensors we used was their specificity, since the presence of humic substances (CDOM), phytoplankton (phycocyanin and chlorophylls) or high turbidity (suspended/colloidal clay) can cause false positives or signal quenching when detecting oil. In our tests the impact of algal material was clearly the most significant. We suggest exploring mathematical protocols or use of more sophisticated sensors for distinguishing actual oil pollution from co-occurring optical interference.

The three tested portable fluorometers were successfully integrated to the FerryBox and SmartBuoy systems. The systems functioned semi-autonomously well during the 2-month testing periods, as did the real-time data transmissions and user interfaces/data visualization. The signal quenching effect of the biofouling could be seen on the FerryBox fluorometers, but it was a secondary problem compared to the interfering substances in the seawater. Nonetheless, automatic cleaning methods of the systems and sensors are recommended.

In this paper we did not touch upon the automatic detection of the anomalic events in the detected values that would indicate an oil spill, but this kind of an algorithm should be developed if the detection system is to be used operationally. When these systems can reliably detect oil, a comprehensive network of SmartBuoys and FerryBoxes covering the major fairways can greatly complement the aerial surveillance, ship-based and satellite monitoring that are presently used to, among other things, detect oil in seawater.

DATA AVAILABILITY STATEMENT

The raw data supporting the conclusions of this article will be made available by the authors, without undue reservation. The data received from the real-time transmission of the FerryBox system can be viewed on a public web-site (TalTech, 2017).

AUTHOR CONTRIBUTIONS

SP: investigation, validation, formal analysis, writing—original draft, and visualization. HK: methodology, investigation, formal analysis, writing—original draft, and visualization. J-VB: validation, writing—review and editing, and supervision. RU: writing—review and editing and supervision. All authors contributed to the article and approved the submitted version.

FUNDING

This manuscript has been produced within project GRACE, which received funding from the European Union's Horizon 2020 research and innovation programme under Grant agreement no. 679266 and supported by the Estonian Research Council (Grant no. PSG22).

ACKNOWLEDGMENTS

We gratefully acknowledge the contributions of Tarmo Kõuts, who was the head of work package 1 (Oil spill detection, monitoring, fate and distribution) in the GRACE project and did the original conceptualization of the FerryBox experiment. We want to thank AS Tallink Grupp for allowing us to use the FerryBox installation of their vessel for the purposes of this study. Furthermore, we would like to thank Kaimo Vahter for his contribution to the installation and upkeep of the FerryBox system, and for transfer and technical advice on the UviLux. We also appreciate the work done by the employees of Arctia Meritaito Oy and Luode Consulting Oy in carrying out the SmartBuoy experiment, and thank them for providing the consequent data and for lending instrumentation (TriOS HC-500 and Turner C3), especially Joose Mykkänen from Luode Consulting is thanked for providing technical assistance during the campaign. Jari Nuutinen and Helena Kutramoinen are thanked for the GC–MS and GC–FID analyses. Furthermore, we also wish to acknowledge help by Jere Riikonen (SYKE MRC) in laboratory experiments and Kirsten Jørgensen (SYKE MRC) acting as coordinator of GRACE.

REFERENCES

Abdel-Shafy, H. I., and Mansour, M. S. (2016). A review on polycyclic aromatic hydrocarbons: source, environmental impact, effect on human health and remediation. *Egypt. J. Petroleum* 25, 107–123. doi: 10.1016/j.ejpe.2015.03.011

Almén, A. K., and Tamelander, T. (2020). Temperature-related timing of the spring bloom and match between phytoplankton and zooplankton. *Mar. Biol. Res.* 16, 674–682. doi: 10.1080/17451000.2020.1846201

Alpers, W., Holt, B., and Zeng, K. (2017). Oil spill detection by imaging radars: challenges and pitfalls. *Remote Sens. Environ.* 201, 133–147. doi: 10.1016/j.rse.2017.09.002

Al-Ruzouq, R., Gibril, M. B. A., Shanableh, A., Kais, A., Hamed, O., Al-Mansoori, S., et al. (2020). Sensors, features, and machine learning for oil spill detection and monitoring: a review. *Remote Sens.* 12, 1–42. doi: 10.3390/rs12203338

Benson, B., Chang, G., Spada, F., Manov, D., and Kastner, R. (2008). "Real-time telemetry options for ocean observing systems," in *European Telemetry Conference* (Munich), 5.

Bícego, M. C., Weber, R. R., and Ito, R. G. (1996). Aromatic hydrocarbons on surface waters of Admiralty Bay, King George Island, Antarctica. *Mar. Pollut. Bull.* 32, 549–553. doi: 10.1016/0025-326X(96)84574-7

Björkqvist, J.-V., Lukas, I., Alari, V., van Vledder, G. P., Hulst, S., Pettersson, H., et al. (2018). Comparing a 41-year model hindcast with decades of wave measurements from the Baltic Sea. *Ocean Eng.* 152, 57–71. doi: 10.1016/j.oceaneng.2018.01.048

Bodkin, J. L., Ballachey, B. E., Dean, T. A., Fukuyama, A. K., Jewett, S. C., McDonald, L., et al. (2002). Sea otter population status and the process of recovery from the 1989 'Exxon Valdez' oil spill. *Mar. Ecol. Prog. Ser.* 241, 237–253. doi: 10.3354/meps241237

Brekke, C., and Solberg, A. H. (2005). Oil spill detection by satellite remote sensing. *Remote Sens. Environ.* 95, 1–13. doi: 10.1016/j.rse.2004.11.015

Brussaard, C. P., Peperzak, L., Beggah, S., Wick, L. Y., Wuerz, B., Weber, J., et al. (2016). Immediate ecotoxicological effects of short-lived oil spills on marine biota. *Nat. Commun.* 7:11206. doi: 10.1038/ncomms11206

Bugden, J. B. C., Yeung, C. W., Kepkay, P. E., and Lee, K. (2008). Application of ultraviolet fluorometry and excitation–emission matrix spectroscopy (EEMS) to fingerprint oil and chemically dispersed oil in seawater. *Mar. Pollut. Bull.* 56, 677–685. doi: 10.1016/j.marpolbul.2007.12.022

Câmara, S. F., Pinto, F. R., da Silva, F. R., Soares, M. D. O., and De Paula, T. M. (2021). Socioeconomic vulnerability of communities on the Brazilian coast to the largest oil spill (2019–2020) in tropical oceans. *Ocean Coastal Manag.* 202:105506. doi: 10.1016/j.ocecoaman.2020.105506

Chavez, F. P., Pennington, J. T., Herlien, R., Jannasch, H., Thurmond, G., and Friederich, G. E. (1997). Moorings and drifters for real-time interdisciplinary oceanography. *J. Atmos. Ocean. Technol.* 14, 1199–1211. doi: 10.1175/1520-0426(1997)014andlt;1199:MADFRTandgt;2.0.CO;2

Cohen, M. J. (1993). Economic impact of an environmental accident: a time-series analysis of the exxon valdez oil spill in southcentral alaska. *Sociol. Spectrum* 13, 35–63. doi: 10.1080/02732173.1993.9982016

Cormack, D., and Nichols, J. A. (1977). The concentrations of oil in sea water resulting from natural and chemically induced dispersion of oil slicks. *Int. Oil Spill Conf. Proc.* 1977, 381–385. doi: 10.7901/2169-3358-1977-1-381

Cyr, F., Tedetti, M., Besson, F., Bhairy, N., and Goutx, M. (2019). A glider-compatible optical sensor for the detection of polycyclic aromatic hydrocarbons in the marine environment. *Front. Mar. Sci.* 6:110. doi: 10.3389/fmars.2019.00110

D'Andrea, M. A., and Reddy, G. K. (2014). Crude oil spill exposure and human health risks. *J. Occup. Environ. Med.* 56, 1029–1041. doi: 10.1097/JOM.0000000000000217

Delauney, L., Compare, C., and Lehaitre, M. (2010). Biofouling protection for marine environmental sensors. *Ocean Sci.* 6, 503–511. doi: 10.5194/os-6-503-2010

Engelhardt, F. (1987). "Assessment of the vulnerability of marine mammals to oil pollution," in *Fate and Effects of Oil in Marine Ecosystems*, eds J. Kuiper and W. Van den Brink (Dordrecht: Martinus Nijhoff Publishers), 101–115.

Farrington, J. W. (2014). Oil pollution in the marine environment II: Fates and effects of oil spills. *Environment* 56, 16–31. doi: 10.1080/00139157.2014.922382

Ferraro, G., Meyer-Roux, S., Muellenhoff, O., Pavliha, M., Svetak, J., Tarchi, D., et al. (2009). Long term monitoring of oil spills in European seas. *Int. J. Remote Sens.* 30, 627–645. doi: 10.1080/01431160802339464

F. I. M. R., and Olsonen, R. (2007). *FIMR Monitoring of the Baltic Sea Environment-Annual Report 2006*. Technical Report 59, The Finnish Institute of Marine Research.

Fingas, M., and Brown, C. E. (2018). A review of oil spill remote sensing. *Sensors* 18, 1–18. doi: 10.1007/978-1-4939-2493-6_732-4

Fox, C. H., O'Hara, P. D., Bertazzon, S., Morgan, K., Underwood, F. E., and Paquet, P. C. (2016). A preliminary spatial assessment of risk: Marine birds and chronic oil pollution on Canada's Pacific coast. *Sci. Total Environ.* 573, 799–809. doi: 10.1016/j.scitotenv.2016.08.145

Gade, M., Scholz, J., and von Viebahn, C. (2000). On the detectability of marine oil pollution in European marginal waters by means of ERS SAR imagery. *Int. Geosci. Remote Sens. Sympos.* 6, 2510–2512. doi: 10.1109/IGARSS.2000.859623

Green, D., Humphrey, B., and Fowler, B. (1983). The use of flow-through fluorometry for tracking dispersed oil. *Int. Oil Spill Conf.* 1983, 473–475. doi: 10.7901/2169-3358-1983-1-473

Green, D. R., Bucley, J., and Humphrey, B. (1982). *Fate of Chemically Dispersed Oil in the Sea, A Report on Two Field Experiments*. Environment Protection Service Report EPS 4-EC-82-5. Environmental Impact Control Directorate, Canada.

Groetsch, P. M. M., Simis, S. G. H., Eleveld, M. A., and Peters, S. W. M. (2014). Cyanobacterial bloom detection based on coherence between ferrybox observations. *J. Mar. Syst.* 140, 50–58. doi: 10.1016/j.jmarsys.2014.05.015

Groetsch, P. M. M., Simis, S. G. H., Eleveld, M. A., and Peters, S. W. M. (2016). Spring Blooms in the Baltic Sea have weakened but lengthened from 2000 to 2014. *Biogeosciences* 13, 4959–4973. doi: 10.5194/bg-13-4959-2016

Hayakawa, K. (2018). "Oil Spills and Polycyclic Aromatic Hydrocarbons," in *Polycyclic Aromatic Hydrocarbons*, ed K. Hayakawa (Singapore: Springer), 213–223. doi: 10.1007/978-981-10-6775-4_16

He, L. M., Kear-padilla, L. L., Lieberman, S. H., and Andrews, J. M. (2003). Rapid *in situ* determination of total oil concentration in water using ultraviolet fluorescence and light scattering coupled with artificial neural networks. *Anal. Chim. Acta* 478, 245–258. doi: 10.1016/S0003-2670(02)01471-X

HELCOM (2003). *The Baltic Marine Environment 1999–2002*. Technical Report 87, The Helsinki Commission. Available online at: https://www.helcom.fi/wp-content/uploads/2019/10/BSEP87.pdf (accessed September 2, 2021).

HELCOM (2013). *Risks of Oil and Chemical Pollution*. Technical report, HELCOM. Available online at: https://helcom.fi/media/publications/BRISK-BRISK-RU_SummaryPublication_spill_of_oil.pdf (accessed September 2, 2021).

HELCOM (2017). *Helcom Metadata Catalouge-2016 All Ship Types Ais Shipping Density*. Available online at: http://metadata.helcom.fi/geonetwork/srv/eng/catalog.search#/metadata/95c5098e-3a38-48ee-ab16-b80a99f50fef (accessed September 2, 2021).

HELCOM (2018a). *HELCOM Maritime Assesment 2018 - Maritime Activities in the Baltic Sea*. Technical report, The Helsinki Commission. Available online at: https://www.helcom.fi/wp-content/uploads/2019/08/BSEP152-1.pdf (accessed September 2, 2021).

HELCOM (2018b). *Helcom Metadata Catalouge-Illegal Oil Discharges*. Available online at: http://metadata.helcom.fi/geonetwork/srv/eng/catalog.search#/metadata/345c9b95-6e9c-44a4-b02a-ee4304cccffc (accessed September 2, 2021).

HELCOM (2018c). *Operational oil spills from ships - HELCOM core indicator report*. Technical report, HELCOM. Available online at: https://helcom.fi/media/core%20indicators/Operational-oil-spills-from-ships-HELCOM-core-indicator-2018.pdf (accessed September 2, 2021).

Henry, C. B., Roberts, P. O., and Overton, E. B. (1999). "A primer on *in situ* fluorometry to monitor dispersed oil," in *International Oil Spill Conference Proceedings* (Seattle, WA).

Honda, M., and Suzuki, N. (2020). Toxicities of polycyclic aromatic hydrocarbons for aquatic animals. *Int. J. Environ. Res. Public Health* 17, 1363. doi: 10.3390/ijerph17041363

Humphrey, B., Green, D. R., Fowler, B. R., Hope, D., and Boehm, P. D. (1987). The fate of oil in the water column following experimental oil spills in the arctic marine nearshore. *Arctic* 40, 124–132. doi: 10.14430/arctic1808

Hydes, D. J., Kelly-Gerreyn, B. A., Colijn, F., Petersen, W., Schroeder, F., Mills, D., et al. (2010). "The way forward in developing and integrating FerryBox technologies," in *Proceedings of OceanObs'09: Sustained Ocean Observations and Information for Society* (Venice), 503–510.

Hylland, K. (2006). Polycyclic aromatic hydrocarbon (PAH) ecotoxicology in marine ecosystems. *J. Toxicol. Environ. Health A* 69, 109–123. doi: 10.1080/15287390500259327

Jensen, H. V., Andersen, J. H., Daling, P. S., and Nøst, E. (2008). "Recent experience from multiple remote sensing and monitoring to improve oil spill response operations," in *International Oil Spill Conference-IOSC 2008, Proceedings* (Savannah, GA), 407–412.

Jenssen, B. M. (1994). Review article: Effects of oil pollution, chemically treated oil, and cleaning on thermal balance of birds. *Environ. Pollut.* 86, 207–215. doi: 10.1016/0269-7491(94)90192-9

Jha, M. N., Levy, J., and Gao, Y. (2008). Advances in remote sensing for oil spill disaster management: state-of-the-art sensors technology for oil spill surveillance. *Sensors* 8, 236–255. doi: 10.3390/s8010236

Jørgensen, K. S., Kreutzer, A., Lehtonen, K. K., Kankaanpää, H., Rytkönen, J., Wegeberg, S., et al. (2019). The EU Horizon 2020 project GRACE: integrated oil spill response actions and environmental effects. *Environ. Sci. Eur.* 31:44. doi: 10.1186/s12302-019-0227-8

Kahru, M., Elmgren, R., and Savchuk, O. P. (2016). Changing seasonality of the Baltic Sea. *Biogeosciences* 13, 1009–1018. doi: 10.5194/bg-13-1009-2016

Kahru, M., Savchuk, O. P., and Elmgren, R. (2007). Satellite measurements of cyanobacterial bloom frequency in the Baltic Sea: interannual and spatial variability. *Mar. Ecol. Prog. Ser.* 343, 15–23. doi: 10.3354/meps06943

Karlson, B., Andersson, L. S., Kaitala, S., Kronsell, J., Mohlin, M., Seppälä, J., et al. (2016). A comparison of FerryBox data vs. monitoring data from research vessels for near surface waters of the Baltic Sea and the Kattegat. *J. Mar. Syst.* 162, 98–111. doi: 10.1016/j.jmarsys.2016.05.002

Kikas, V., and Lips, U. (2016). Upwelling characteristics in the Gulf of Finland (Baltic Sea) as revealed by Ferrybox measurements in 2007-2013. *Ocean Sci.* 12, 843–859. doi: 10.5194/os-12-843-2016

Kim, M., Hyuk, U., Hee, S., Jung, J.-H., Choi, H.-W., An, J., et al. (2010). Hebei Spirit oil spill monitored on site by fluorometric detection of residual oil in coastal waters off Taean, Korea. *Mar. Pollut. Bull.* 60, 383–389. doi: 10.1016/j.marpolbul.2009.10.015

Krestenitis, M., Orfanidis, G., Ioannidis, K., Avgerinakis, K., Vrochidis, S., and Kompatsiaris, I. (2019). Oil spill identification from satellite images using deep neural networks. *Remote Sens.* 11, 1–22. doi: 10.3390/rs11151762

Lambert, P., Fingas, M., and Goldthorp, M. (2001). An evaluation of field total petroleum hydrocarbon (TPH) systems. *J. Hazard Mater.* 83, 65–81. doi: 10.1016/S0304-3894(00)00328-9

Lambert, P., Goldthorp, M., Fieldhouse, B., Wang, Z., Fingas, M., Pearson, L., et al. (2003). Field fluorometers as dispersed oil-in-water monitors. *J. Hazard Mater.* 102, 57–79. doi: 10.1016/S0304-3894(03)00202-4

Lichtenthaler, R. G., and Daling, P. S. (1983). "Dispersion of chemically treated crude oil in Norwegian offshore waters," in *Proceedings of the 1983 Oil Spill Conference* (San Antonio, TX), 7–14.

Lichtenthaler, R. G., and Daling, P. S. (1985). "Aerial application of dispersants comparison of slick behavior of chemically treated versus non-treated slicks," in *International Oil Spill Conference Proceedings (1985)* (Los Angeles, CA), 471–478.

Lips, U., Kikas, V., Liblik, T., and Lips, I. (2016). Multi-sensor *in situ* observations to resolve the sub-mesoscale features in the stratified Gulf of Finland, Baltic Sea. *Ocean Sci.* 12, 715–732. doi: 10.5194/os-12-715-2016

Liubartseva, S., De Dominicis, M., Oddo, P., Coppini, G., Pinardi, N., and Greggio, N. (2015). Oil spill hazard from dispersal of oil along shipping lanes in the Southern Adriatic and Northern Ionian Seas. *Mar. Pollut. Bull.* 90, 259–272. doi: 10.1016/j.marpolbul.2014.10.039

Lunel, T. (1995). Dispersant effectiveness at sea. *Int. Oil Spill Conf. Proc.* 1995, 147–155. doi: 10.7901/2169-3358-1995-1-147

Malkov, V., and Sievert, D. (2010). Oil-in-water fluorescence sensor in wastewater and other industrial applications. *Power Plant Chem.* 12, 144–154.

Manov, D. V., Chang, G. C., and Dickey, T. D. (2004). Methods for reducing biofouling of moored optical sensors. *J. Atmos. Ocean. Technol.* 21, 958–968. doi: 10.1175/1520-0426(2004)021andlt;0958:MFRBOMandgt;2.0.CO;2

Marghany, M. (2016). Automatic mexico gulf oil spill detection from radarsat-2 SAR satellite data using genetic algorithm. *Acta Geophys.* 64, 1916–1941. doi: 10.1515/acgeo-2016-0047

Mills, D. K., Laane, R., Rees, J. M., Rutgers van der Loeff, M., Suylen, J. M., Pearce, D. J., et al. (2003). Smartbuoy: a marine environmental monitoring buoy with a difference. *Elsevier Oceanogr. Ser.* 69, 311–316. doi: 10.1016/S0422-9894(03)80050-8

Mishra, A. K., and Kumar, G. S. (2015). Weathering of oil spill: modeling and analysis. *Aquatic Procedia* 4, 435–442. doi: 10.1016/j.aqpro.2015.02.058

Moroni, D., Pieri, G., Salvetti, O., Tampucci, M., Domenici, C., and Tonacci, A. (2016). Sensorized buoy for oil spill early detection. *Methods Oceanogr.* 17:221–231. doi: 10.1016/j.mio.2016.10.002

Nam, S., Kim, G., Kim, K.-,r., Kim, K., Cheng, L. O., Kim, K.-W., et al. (2005). Application of real-time monitoring buoy systems for physical and biogeochemical parameters in the coastal ocean around the korean peninsula. *Mar. Technol. Soc. J.* 39, 70–80. doi: 10.4031/002533205787444024

Papadimitrakis, I., Psaltaki, M., and Markatos, N. (2011). 3-D oil spill modelling. Natural dispersion and the spreading of oil-water emulsions in the water column. *Global Nest J.* 13, 325–338. doi: 10.30955/gnj.000726

Papoutsa, C., Kounoudes, A., Milis, M., Toulios, L., Retalis, A., Kyrou, K., et al. (2012). Monitoring turbidity in asprokremmos dam in cyprus using earth observation and smart buoy platform. *Eur. Water* 38, 25–32.

Petersen, W. (2014). FerryBox systems: State-of-the-art in Europe and future development. *J. Mar. Syst.* 140, 4–12. doi: 10.1016/j.jmarsys.2014.07.003

Petersen, W., Petschatnikov, M., and Schroeder, F. (2003). FerryBox systems for monitoring coastal waters. Building the European capacity in operational oceanography. *Proc. Third Int. Conf. EuroGOOS* 69, 325–333. doi: 10.1016/S0422-9894(03)80052-1

Petersen, W., Schroeder, F., and Bockelmann, F. D. (2011). FerryBox - Application of continuous water quality observations along transects in the North Sea. *Ocean Dyn.* 61, 1541–1554. doi: 10.1007/s10236-011-0445-0

Pikkarainen, A. L., and Lemponen, P. (2005). Petroleum hydrocarbon concentrations in Baltic Sea subsurface water. *Boreal Environ. Res.* 10, 125–134.

Polinov, S., Bookman, R., and Levin, N. (2021). Spatial and temporal assessment of oil spills in the Mediterranean Sea. *Mar. Pollut. Bull.* 167:112338. doi: 10.1016/j.marpolbul.2021.112338

Ribeiro, L. C. D. S., Souza, K. B. D., Domingues, E. P., and Magalh aes, A. S. (2021). Blue water turns black: economic impact of oil spill on

tourism and fishing in Brazilian Northeast. *Curr. Issues Tour.* 24, 1042–1047. doi: 10.1080/13683500.2020.1760222

Ridoux, V., Lafontaine, L., Bustamante, P., Caurant, F., Dabin, W., Delcroix, C., et al. (2004). The impact of the "Erika" oil spill on pelagic and coastal marine mammals: combining demographic, ecological, trace metals and biomarker evidences. *Aquat. Living Resour.* 17, 379–387. doi: 10.1051/alr:2004031

Rytkönen, J., Siitonen, L., Riipi, T., Sassi, J., and Sukselainen, J. (2002). *Statistical Analyses of the Baltic Maritime Traffic*. Technical Report VAL34-012344, VTT Technical research centre of Finland. Available online at: https://cris.vtt.fi/en/publications/statistical-analyses-of-the-baltic-maritime-traffic (accessed September 2, 2021).

Samiullah, Y. (1985). Biological effects of marine oil pollution. *Oil Petrochem. Pollut.* 2, 235–264. doi: 10.1016/S0143-7127(85)90233-9

Sandifer, P. A., Ferguson, A., Finucane, M. L., Partyka, M., Solo-Gabriele, H. M., Walker, A. H., et al. (2021). Human health and socioeconomic effects of the deepwater horizon oil spill in the gulf of Mexico. *Oceanography* 34, 174–191. doi: 10.5670/oceanog.2021.125

Sankaran, K. (2019). Protecting oceans from illicit oil spills: environment control and remote sensing using spaceborne imaging radars. *J. Electromag. Waves Appl.* 33, 2373–2403. doi: 10.1080/09205071.2019.1685409

Schneider, B., Gülzow, W., Sadkowiak, B., and Rehder, G. (2014). Detecting sinks and sources of CO_2 and CH4 by ferrybox-based measurements in the Baltic Sea: three case studies. *J. Mar. Syst.* 140, 13–25. doi: 10.1016/j.jmarsys.2014.03.014

Serra-Sogas, N., O'Hara, P. D., Canessa, R., Keller, P., and Pelot, R. (2008). Visualization of spatial patterns and temporal trends for aerial surveillance of illegal oil discharges in western Canadian marine waters. *Mar. Pollut. Bull.* 56, 825–833. doi: 10.1016/j.marpolbul.2008.02.005

Shultz, J. M., Walsh, L., Garfin, D. R., Wilson, F. E., and Neria, Y. (2015). The 2010 deepwater horizon oil spill: the trauma signature of an ecological disaster. *J. Behav. Health Serv. Res.* 42, 58–76. doi: 10.1007/s11414-014-9398-7

Sipelgas, L., and Uiboupin, R. (2007). "Elimination of oil spill like structures from radar image using MODIS data," in *International Geoscience and Remote Sensing Symposium (IGARSS)* (Barcelona), 429–431.

Solberg, A. H. (2012). Remote sensing of ocean oil-spill pollution. *Proc. IEEE* 100, 2931–2945. doi: 10.1109/JPROC.2012.2196250

Stephenson, R. (1997). Effects of oil and other surface-active organic pollutants on aquatic birds. *Environ. Conserv.* 24, 121–129. doi: 10.1017/S0376892997000180

Taleghani, N. D., and Tyagi, M. (2017). Impacts of major offshore oil spill incidents on petroleum industry and regional economy. *J. Energy Resour. Technol. Trans. ASME* 139, 1–7. doi: 10.1115/1.4035426

TalTech (2017). *M/S BALTIC QUEEN FerryBox Monitoring System*. Available online at: http://on-line.msi.ttu.ee/GRACEferry/ (accessed September 2, 2021).

Tarr, M. A., Zito, P., Overton, E. B., Olson, G. M., Adhikari, P. L., and Reddy, C. M. (2016). Weathering of oil spilled in the marine environment. *Oceanography* 29, 126–135. doi: 10.5670/oceanog.2016.77

Tedetti, M., Guigue, C., and Goutx, M. (2010). Utilization of a submersible UV fluorometer for monitoring anthropogenic inputs in the Mediterranean coastal waters. *Mar. Pollut. Bull.* 60, 350–362. doi: 10.1016/j.marpolbul.2009.10.018

Tuomi, L., Kahma, K. K., and Pettersson, H. (2011). Wave hindcast statistics in the seasonally ice-covered Baltic Sea. *Boreal Environ. Res.* 16, 451–472.

Uiboupin, R., Raudsepp, U., and Sipelgas, L. (2008). "Detection of oil spills on SAR images, identification of polluters and forecast of the slicks trajectory," in *US/EU-Baltic International Symposium: Ocean Observations, Ecosystem-Based Management and Forecasting - Provisional Symposium Proceedings, BALTIC* (Tallinn), 6–10.

Westerlund, A., Tuomi, L., Alenius, P., Miettunen, E., and Vankevich, R. E. (2018). Attributing mean circulation patterns to physical phenomena in the Gulf of Finland. *Oceanologia* 60, 16–31. doi: 10.1016/j.oceano.2017.05.003

WWF (2010). *Future Trends in the Baltic Sea. Baltic Ecoregion Programme–Future Trends in the Baltic Sea*, 1–40. Available online at: https://wwwwwfse.cdn.triggerfish.cloud/uploads/2019/01/wwf_future_trends_in_the_baltic_sea_2010_1_.pdf (accessed September 2, 2021).

Xiankun, L., Jing, L., and Shuzhu, C. (1993). Dynamic model for oil slick dispersion into a water column-a wind-driwen wave tank experiment. *Chin. J. Oceanol. Limnol.* 11, 161–170. doi: 10.1007/BF02850823

Xu, J., Wang, H., Cui, C., Zhao, B., and Li, B. (2020). Oil spill monitoring of shipborne radar image features using SVM and local adaptive threshold. *Algorithms* 13:69. doi: 10.3390/a13030069

Zanardi, E., Bícego, M. C., and Weber, R. R. (1999). Dissolved/dispersed petroleum aromatic hydrocarbons in the Sao Sebastiao Channel, São Paulo, Brazil. *Mar. Pollut. Bull.* 38, 410–413. doi: 10.1016/S0025-326X(97)00194-X

Zeng, K., and Wang, Y. (2020). A deep convolutional neural network for oil spill detection from spaceborne SAR images. *Remote Sens.* 12, 1015. doi: 10.3390/rs12061015

Conflict of Interest: The authors declare that the research was conducted in the absence of any commercial or financial relationships that could be construed as a potential conflict of interest.

Publisher's Note: All claims expressed in this article are solely those of the authors and do not necessarily represent those of their affiliated organizations, or those of the publisher, the editors and the reviewers. Any product that may be evaluated in this article, or claim that may be made by its manufacturer, is not guaranteed or endorsed by the publisher.

frontiers in Marine Science

ORIGINAL RESEARCH
published: 07 December 2021
doi: 10.3389/fmars.2021.754278

Distribution of Polychlorinated Naphthalenes in Sediment From Industrialized Coastal Waters of Korea With the Optimized Cleanup and GC-MS/MS Methods

*Ha-Hyun Lee[1], Sunggyu Lee[1], Jung Suk Lee[2] and Hyo-Bang Moon[1]**

[1] Department of Marine Sciences and Convergent Technology, College of Science and Convergence Technology, Hanyang University, Ansan, South Korea, [2] NeoEnBiz Co., Bucheon, South Korea

OPEN ACCESS

Edited by:
Kenneth Mei Yee Leung, City University of Hong Kong, Hong Kong SAR, China

Reviewed by:
Guijin Su, Research Center for Eco-Environmental Sciences, Chinese Academy of Sciences (CAS), China
Jinping Cheng, Hong Kong University of Science and Technology, Hong Kong SAR, China

***Correspondence:**
Hyo-Bang Moon
hbmoon@hanyang.ac.kr

Specialty section:
This article was submitted to Marine Pollution, a section of the journal Frontiers in Marine Science

Received: *06 August 2021*
Accepted: *11 November 2021*
Published: *07 December 2021*

Citation:
Lee H-H, Lee S, Lee JS and Moon H-B (2021) Distribution of Polychlorinated Naphthalenes in Sediment From Industrialized Coastal Waters of Korea With the Optimized Cleanup and GC-MS/MS Methods. Front. Mar. Sci. 8:754278. doi: 10.3389/fmars.2021.754278

Limited studies have been conducted on polychlorinated naphthalenes (PCNs) in the coastal environment worldwide. In this study, analytical methods were optimized for 18 PCN congeners in sediment using a multi-layer silica gel column and a gas chromatograph coupled to tandem mass spectrometry (GC-MS/MS). The optimized analytical methods of PCNs were employed for sediment samples from heavily industrialized bays of Korea to assess the occurrence, contamination, potential sources, and ecotoxicological concerns. PCNs were detected in all sediment samples, indicating ubiquitous contamination in industrialized coastal regions of Korea. Total concentrations and toxic equivalents (TEQs) of PCNs ranged from 0.99 to 21,500 (mean: 568) pg/g dry weight and from 1.72×10^{-5} to 18.8 (mean: 0.52) pg TEQ/g dry weight, respectively, which were within the ranges reported by other studies. A clear decreasing gradient was observed for the sedimentary PCNs from inner to outer parts of the bays, streams, and rivers. This result indicates that industrial activities are primary sources of PCNs. The highest PCN concentrations were observed in sediment close to non-ferrous and petrochemical industries, indicating potential sources. CNs 73 and 52 were predominant congeners of PCNs in all sediment samples. Diagnostic ratios and non-parametric multidimensional scaling analysis showed that the potential primary sources of PCNs are thermal-related emissions and the use of PCB technical mixtures. Although a few sediment samples exceeded the sediment quality guidelines of TEQs, the cumulative risks by dioxin-like contaminants may be caused for almost all coastal zones surveyed. This is the first report on PCNs in sediment from Korean coastal waters.

Keywords: TEQ, non-ferrous, sediment quality, dioxin-like, cumulative risk, PCB

INTRODUCTION

Polychlorinated naphthalenes (PCNs) comprise 75 congeners from mono- to octa-CNs, with differing numbers and positions of chlorine substituents based on naphthalene structure. PCNs were extensively produced for applications including insulating oils for capacitors and flame retardants in electrical cables beginning in the 1950s (Odabasi et al., 2017; Agunbiade et al., 2020).

The major PCN technical mixtures were branded as Halowax, Seekau, Clonacure waxes, and Wako-PCN, and were used in many countries (Falandysz et al., 2008). Although the consumption data of PCNs was not precisely recorded, the total PCN production from larger companies was estimated to be approximately 150,000 tons during the 1930s–1970s (Falandysz et al., 2014). Based on the structural similarities with polychlorinated biphenyls (PCBs) and polychlorinated dibenzo-*p*-dioxins and dibenzofurans (PCDD/Fs), PCNs showed similar dioxin-like toxicological effects binding with aryl-hydrocarbon (AhR) receptors (Falandysz et al., 2014). Previous *in vivo* and *in vitro* studies have reported that PCNs elicited mortality, embryotoxicity, hepatotoxicity, dermal lesions, teratogenicity, and carcinogenicity (Behnisch et al., 2003; Falandysz et al., 2014; Suzuki et al., 2020). The ecotoxicological data of PCNs have been reported for several species representing different trophic levels: algae, aquatic plants, invertebrates, fish, and birds (Noma et al., 2005; Helm et al., 2006). Because most studies used the Halowax technical mixtures, the ecotoxicological experiments could result in confusion due to possible toxicological interactions and dioxin impurities (Noma et al., 2005). Several acute toxicities of 1-chloronaphthalene have been reported on freshwater and saltwater species as 1,600, 2,300, and 690–2,500 μg/L for *Daphnia magna, Lepomis macrochirus*, and *Cyprinodon variegatus*, respectively (Falandysz, 1998; Helm et al., 2006). However, no data are available on ecotoxicological data for benthic organisms of PCNs.

Due to domestic and worldwide regulations on PCNs, the current PCN contamination is mostly emitted from thermal processes, accounting for over 80% of total PCN emissions in the environment (Bidleman et al., 2010). These include waste incineration, steel and coking industries, and chlor-alkali and copper smelting processes (Liu et al., 2010, 2014; Hu et al., 2013; Waheed et al., 2020). PCNs are also released from the use of PCB technical mixtures as impurities contained (Huang et al., 2015; Li et al., 2021). Although there has been no consumption of technical PCN mixtures (Park et al., 2010), several PCN congeners have been detected in multiple matrices, such as air, soil, freshwater biota, and human serum (Lee et al., 2007; Park et al., 2010; Kim et al., 2019a). However, no reports are available on the PCN contamination in the coastal environment of Korea.

Sediment acts as the last depositional reservoir for hydrophobic contaminants in the coastal environment (Liu et al., 2018; Dat et al., 2019; Lee et al., 2020). A previous study reported that PCNs are accumulated from sedimentary particles to marine species (Wang et al., 2012). It is prompted to survey the distribution and accumulation of organic contaminants in coastal sediments for evaluating the potential health risks of marine species (Moon et al., 2008a; Mahmood et al., 2014; Walker et al., 2015). Gu et al. (2021) predicted that PCN congeners are highly toxic at all the trophic positions in the food-web associated with joint toxicity mechanisms. To date, most previous studies have conducted the determination of PCN congeners in environmental and biota samples using a high-resolution mass spectrometer (HRMS) (Park et al., 2010, 2021; Liu et al., 2018; Kim et al., 2019a). Due to the enhanced sensitivity, chromatograph coupled to a tandem mass spectrometer (GC-MS/MS) has been partly utilized for PCN analysis in sediment samples (Li et al., 2016a; Wu et al., 2018). The challenge for an analytical method using a GC-MS/MS is the separation of individual PCN congeners because PCNs showed congener-specific toxicities (Falandysz et al., 2014; Suzuki et al., 2020). In our study, the analytical methods were optimized using a multi-layer silica gel column and a GC-MS/MS for the determination of major PCN congeners in sediment samples. Compared to the HRMS determination, the GC-MS/MS analysis could provide more cost-effective and comprehensive monitoring programs. In the present study, the PCN congeners were measured for the sediments collected from Ulsan and Onsan Bays surrounded by the "National Industrial Complexes" which have been developed since the 1970s. Our previous studies have reported severe pollution by unintentional and industrial contaminants, such as PCDD/Fs, dioxin-like PCBs, polybrominated diphenyl ethers (PBDEs), siloxanes, and plasticizers in the surveyed bays (Moon et al., 2007, 2008b; Lee et al., 2018, 2020; Kim et al., 2021). Therefore, the objectives of the present study are to assess the occurrence, contamination, source tracking, and ecotoxicological implications of PCNs in sediment from highly industrialized coastal waters. This is the first report on the congener-specific data on PCNs in Korean coastal waters.

MATERIALS AND METHODS

Sample Collection

The Ulsan and Onsan Bays, located in the southeastern part of Korea, are surrounded by heavily industrialized complexes and the largest commercial harbors in Korea (**Figure 1**). The industrial complexes, comprising petrochemical, iron and non-ferrous industries, automobiles, and shipyards, have produced approximately 32% of the commercial and industrial products consumed in Korea (Lee et al., 2020). Surface sediments (4 cm depth), representing the sedimentation record for recent 4–6 years (Lee et al., 2018), were collected from 49 locations in April 2020 using a Van Veen grab sampler. Samples were wrapped in an aluminum foil that had been pre-washed with a solvent and transported to the laboratory. All sediment samples were stored in a −20°C freezer and then freeze-dried. In our study, the closest locations to industries around streams and rivers were chosen for tracking and characterizing the contamination sources of PCNs using congener-specific analysis. The sampling locations were divided into streams, rivers, and bays, such as Gosa (G1–G4), Yeocheon (Y1–Y2), and Daejeong (D1–D4) Streams, Taehwa (T1–T4) and Woihwang (W1–W7) Rivers, and Ulsan (U1–U18) and Onsan (O1–O10) Bays to investigate the spatial distribution of PCN contamination.

Standards and Reagents

Among 75 PCN congeners, 18 congeners from mono- to octa-CNs (CNs 2, 6, 13, 27, 36/28, 46, 48, 50, 52, 53, 54, 63, 64/68, 66/67, 69, 72, 73, and 75) were measured for target contaminants, which were chosen based on toxic potency with

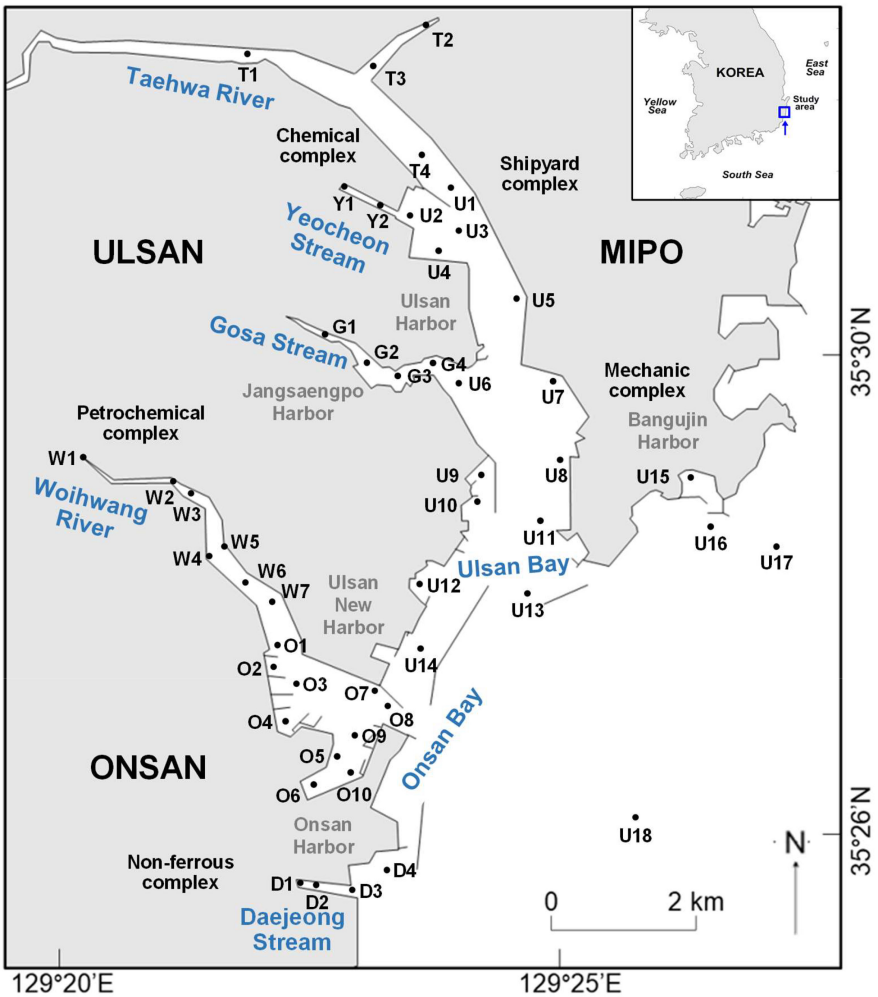

FIGURE 1 | Sampling locations of sediment collected from Ulsan and Onsan Bays and their inflowing rivers and streams, Korea. Sampling stations T, Y, G, U, W, D, and O represent Taehwa River, Yeocheon Stream, Gosa Stream, Ulsan Bay, Woihwang Stream, Daejeong Stream, and Onsan Bay, respectively.

AhR receptors and environmental occurrence (Falandysz et al., 2014; Pagano and Garner, 2021). All native standards of PCNs were purchased from Cambridge Isotope Laboratories (Andover, MA, United States) and Wellington Laboratories (Guelph, ON, Canada). Mass-labeled PCNs ($^{13}C_{10}$-CNs 27, 42, 52, 67, 73, and 75; ECN-5102, Wellington Laboratories) and native PCB congeners (CBs 103, 198, and 209) were used as internal and surrogate standards, respectively. Ultra-trace residue levels of hexane and dichloromethane (DCM) were purchased from J. T. Baker. Pesticide-analysis grade silica gel, nonane, anhydrous Na_2SO_4, and copper were purchased from GL Sciences, Kanto Chemical, Merck, and Sigma-Aldrich, respectively.

Optimization of a Clean-Up Method and Instrumental Parameters

Considering similar characteristics of PCNs with PCBs and PBDEs, a multi-layer silica gel column was applied for a clean-up method in the determination of PCN congeners in sediment samples (Moon et al., 2007, 2008a,b). A multi-layer silica column contained anhydrous Na_2SO_4 (0.5 g), activated silica gel (1 g), 22% H_2SO_4-impregnated silica gel (4 g), 44% H_2SO_4-impregnated silica gel (4 g), activated silica gel (1 g), 2% KOH-silica (3 g), and anhydrous Na_2SO_4 (0.5 g) from bottom to top in the class column (300 mm length, 15 mm inner diameter) (**Supplementary Figure 1**). Native and mass-labeled standards of PCNs were spiked into a sediment extractor to check for the efficacy and elution patterns of a multi-layer silica gel column. After the extractor was added to a multi-layer silica gel column, a mixture of 15% DCM in hexane (180 mL) was used as an elution solvent to remove the interferences and to fractionize the PCN congeners in sediment samples. The method optimized in our study is a minor modification of the method used for PCB and PBDE determinations in earlier studies (Moon et al., 2007, 2008a,b). Six eluted portions were fractionized every 30 mL of elution solvent. All 18 PCN congeners were eluted within 60 mL of a mixture of 15% DCM in hexane, which was used for a final cleanup method.

Sediment samples (∼10 g) were extracted using an accelerated solvent extractor (ASE 350, Dionex, Sunnyvale, CA, United States) with 60 mL of DCM and hexane (3:1) after spiking into surrogate standards (5 ng; CBs 103, 198, and 209), similar to the method for PCDD/Fs, PCBs, and PBDEs (Moon et al., 2007; Lee et al., 2020). Extracts were concentrated to 5 mL by TurboVap LV (Biotage, Uppsala, Sweden) and sulfur in extracts was removed using activated cooper. A multi-layer silica gel column optimized was used as a cleanup method with an elution with 60 mL of 15% DCM after spiking internal standards of mass-labeled PCNs (1 ng each). Eluant was concentrated and then dissolved in 100 μL of nonane.

A GC-MS/MS (7890GC/7000B, Agilent Technologies, Wilmington, DE, United States) and a DB-5MS UI capillary column (60 m length, 0.25 mm inner diameter, 0.25 μm film thickness; J&W Scientific, Palo Alto, CA, United States) were used for separation and quantification of 18 PCN congeners. The oven temperature was programed to increase from 90°C (1 min) to 160°C at 10°C/min (10 min), and then to 300°C (2 min). Inlet and ion source temperatures were maintained at 270°C and 330°C, respectively. Helium was used as a carrier gas at a constant flow rate of 1 mL/min. The MS/MS conditions were optimized for the accurate quantitation of PCN congeners under the multiple reaction monitoring (MRM) mode. Some congeners, such as CNs 36/28, 64/68, and 66/67, were co-eluted in our analytical method, similar to those described previously (Wu et al., 2018). Detailed information on quantification and confirmation *m/z* under the MRM mode and retention time for targeted PCN congeners are summarized in **Supplementary Table 1**.

Quality Control

In order to check for background contamination throughout whole experimental procedures, the procedural blank samples (n = 5; anhydrous Na_2SO_4) were processed every 10 samples as real samples. Only trace levels (CNs 2, 6, 13, 36/28, 46, and 48; 0.21 to 2.3 pg/g) were detected in the blank samples, which were subtracted from the measured concentrations in real samples. To check a crossover contamination of PCNs during a GC-MS/MS analysis, hexane was used before and after the injections of calibration standards and between every 15 samples. No crossover contamination was observed in our sample batch. The instrumental limit of quantifications (iLOQs) of 18 PCN congeners with a GC-MS/MS were calculated as ten times the standard deviation for seven replicate injections of the lowest acceptable level (0.1 ng/mL), which ranged from 0.1 to 1.4 pg/g dry weight (wt). All mass-labeled internal standards were detected without any interferences in all sediment samples. The recoveries of surrogate standards were 91% ± 11% (average ± standard deviation), 88% ± 14%, and 95% ± 8.3% for CBs 103, 198, and 209, respectively. Matrix-spiked samples were also employed to check for the influence of matrix effects for sediment samples. Recoveries of native and mass-labeled standards of PCNs for matrix-spiked samples ranged from 84 to 105% (mean: 93.6%) and 85 to 101% (mean: 95.3%), respectively. The detailed results of quality control conducted in our study are summarized in **Supplementary Table 2**. Total organic carbon (TOC) and nitrogen (TON) were measured using a CHN elemental analyzer. The accuracy and precision were 92 and 9.31% for TOC and 93 and 4.62% for TON, respectively.

Calculation of Toxic Equivalent Concentrations and Statistical Analysis

Unlike PCDD/Fs and dioxin-like PCBs, the toxic equivalent factors (TEFs) of PCNs are not provided from international agencies, such as the World Health Organization (WHO) (Van den Berg et al., 2006). In our study, the TEFs of PCN congeners were used from the values proposed by Falandysz et al. (2014), which was used for other studies (Pagano and Garner, 2021; Park et al., 2021). The toxic equivalent (TEQ) concentrations were calculated by multiplying the actual concentration of individual PCN congener and its TEF.

Total concentrations of PCNs (ΣPCN; the sum of 18 PCNs) and individual PCN detected > 60% in all sediment samples were only employed for statistical analyses. The concentration of individual PCN congener < iLOQ was treated as half iLOQ for the statistical analysis. For the calculation of ΣPCN concentrations, the concentration of individual PCN congener < iLOQ was treated as zero to avoid overestimation of the results. Because the PCN concentrations showed the log-normal distribution in our sediment samples, individual and total PCN concentrations were transformed to logarithm value for parametric analysis. Analysis of variance was used to assess differences in the concentrations and compositions of the sedimentary PCN congeners depending on the sampling locations. Pearson correlation analysis was conducted to assess the strength of relationships among PCN congeners or between PCN concentrations and TOC contents. All statistical analyses were performed using SPSS 18.0 software with a significance level at $p < 0.05$.

RESULTS AND DISCUSSION

Occurrence and Concentrations of Polychlorinated Naphthalenes in Industrialized Coastal Sediment

The sample characteristics and concentrations of PCN congeners detected in sediment from industrialized bays and their inflowing rivers and streams of Korea are summarized in **Table 1** and **Supplementary Table 3**. Contents of TOC and TON in all of the sediment samples varied widely depending on the sampling locations, with ranges of 0.22–6.63% (mean: 1.78%) and 0.01–0.55% (mean: 0.15%) for TOC and TON, respectively. The highest TOC contents were observed at locations from streams, such as Gosa Stream (G2; 6.63%), Yeocheon Stream (Y1; 6.36%), and Daejeong Stream (D2; 5.95%), which are surrounded by heavily industrial complexes. The TOC contents in sediments from Taehwa River (0.94% ± 0.52%) passing through the urbanized region were significantly ($p < 0.05$) lower than those found in other coastal zones. Similar to TOC, the highest and lowest contents of TON were observed at stations collected from streams (G2 and D3) and Taehwa River (T1–T4; mean: 0.07%), respectively. Previous studies have reported that the molar ratio of C/N is a proxy for organic matter sources, which are 5–7

TABLE 1 | Sediment characteristics and the concentrations of polychlorinated naphthalene (PCN) congeners in sediments collected from Ulsan and Onsan Bays and their inflowing streams and rivers, Korea.

	Detection rate (%)	Min–Max	Average ± SD[a]	TEQ[b] (Average)
Sediment characteristics				
Total organic carbon (%)		0.22–6.63	1.78 ± 1.38	
Total organic nitrogen (%)		0.01–0.55	1.15 ± 0.09	
Polychlorinated naphthalene (PCN) congeners (pg/g dry weight)				
CN 2	43	< iLOQ–111	3.56 ± 15.9	6.41×10^{-5}
CN 6	27	< iLOQ–202	6.11 ± 6.11	
CN 13	69	< iLOQ–304	9.06 ± 43.5	
CN 36/48	39	< iLOQ–625	16.6 ± 89.6	6.79×10^{-6}
CN 27	88	< iLOQ–1,140	24.4 ± 164	
CN 48	98	< iLOQ–1,180	31.1 ± 170	6.53×10^{-4}
CN 46	78	< iLOQ–1,520	39.1 ± 219	
CN 52	100	0.25–1,240	36.2 ± 177	1.24×10^{-4}
CN 50	59	< iLOQ–1,190	29.6 ± 170	2.46×10^{-3}
CN 54	27	< iLOQ–253	7.20 ± 36.3	1.22×10^{-3}
CN 53	84	< iLOQ–1,660	41.6 ± 238	7.49×10^{-5}
CN 66/67	67	< iLOQ–846	27.7 ± 121	1.08×10^{-1}
CN 64/68	43	< iLOQ–954	25.3 ± 137	5.05×10^{-4}
CN 69	45	< iLOQ–1,810	45.6 ± 260	9.12×10^{-2}
CN 63	29	< iLOQ–864	22.0 ± 124	4.41×10^{-4}
CN 72	33	< iLOQ–2,070	49.4 ± 297	2.96×10^{-3}
CN 73	100	0.74–3,270	90.7 ± 469	2.72×10^{-1}
CN 75	57	< ILOQ–2,190	63.2 ± 315	6.32×10^{-4}
ΣPCN[c]		0.99–21,400	568 ± 3,060	5.24×10^{-1}

[a] *SD, Standard deviation.*
[b] *TEQ, Toxic equivalent.*
[c] *ΣPCN, Sum of 18 PCN congeners detected in sediment samples.*

and > 15 for marine and terrestrial origins, respectively (Wu et al., 2020). In our study, the molar ration of C/N in sediment ranged from 6.88 to 36.1, with a mean value of 13.2, indicating that most sampling zones including the streams, rivers, and bays are influenced by the land-based organic matters. The highest C/N ratios were observed in sediments from inner part of streams and rivers, such as D1 (36.1), D2 (29.7), Y1 (27.6), and G1 (21.6) but were not significant ($p > 0.05$). Our findings suggest that industrial activities contributed to the high burden of organic matter into the bays through rivers and streams.

Although the consumption of PCN technical mixtures was restricted in industrial markets of Korea, PCNs were detected in all sediment samples from industrialized coastal waters of Korea. This indicates the presence of ongoing sources of PCNs from industrialized complexes. The ΣPCN concentrations in all sediment samples ranged from 0.99 to 21,400 (mean: 568) pg/g dry wt. CNs 73 and 52 were detected in all sediment samples among 18 PCN congeners. CNs 13, 27, 36/28, 46, 48, 53, and 73 were detected at > 60% of all sediment samples. For homolog patterns, penta-CN was predominant, whereas mono- and di-CNs, except CN 13, were detected < 20% in all sediment samples. The highest concentration of PCN congeners was observed for CN 73, ranging from 0.74 to 3,270 (mean: 90.7) pg/g dry wt. The concentrations of highly chlorinated congeners, such as CNs 75 and 72, were also significantly ($p < 0.05$) higher than the concentrations of the remaining PCN congeners. The concentrations of CNs 75 and 72 ranged from < iLOQ to 2,190 (mean: 63.2) and < iLOQ to 2,070 (mean: 49.4) pg/g dry wt, respectively. Halowax (e.g., Halowax 1000), a representative PCN technical mixture, is primarily composed of mono- and di-CN congeners (Falandysz et al., 2006), which is inconsistent with the congener patterns of PCNs observed in our study. This implies that PCN technical mixtures are not major contamination sources in Korean coastal waters. The higher concentrations of CNs 75 and 72 in the sediment samples could be caused by a preferential adsorption of highly chlorinated contaminants to sedimentary particles (Moon et al., 2008a,b; Lee et al., 2020). In our study, the TEQ concentrations in all of the sediment samples ranged from 0.002 to 18.8 (mean: 0.52) pg TEQ/g dry wt. The highest TEQ concentrations were observed for CN 73 (mean: 0.27 pg TEQ/g dry wt), CN 66/67 (0.11 pg TEQ/g dry wt), and CN 69 (0.09 pg TEQ/g dry wt), which collectively accounted for over 90% of total TEQ concentrations.

The PCN concentrations observed in our sediment samples are compared to those reported for other locations or countries (**Supplementary Table 4**). The PCN concentrations in sediment samples collected after 2010 were only used to prevent the effectiveness of time trends. The ΣPCN concentrations in sediment from Ulsan Bay (mean: 42.3 pg/g dry wt), Onsan Bay (17.4 pg/g dry wt), and Taehwa River (19.6 pg/g dry wt) measured in our study were similar to those reported from Feitsui Reservoir, Taiwan (mean: 29.2 pg/g dry wt; Dat et al., 2019). The ΣPCN concentrations in sediment from Woihwang River (mean: 268 pg/g dry wt) and Yeocheon Stream (333 pg/g dry wt) were a similar order of magnitude to those reported for the Laojie River, Taiwan (980 pg/g dry wt; Dat et al., 2019). The highest ΣPCN concentrations found in Daejeong Stream (mean: 5,970 pg/g dry wt) were within the ranges of those reported for the Yangtze River, China (3,270 pg/g dry wt; Zhang et al., 2015), Liaohe River, China (4,400 pg/g dry wt; Li et al., 2016b), Yellow River, China (7,100 pg/g dry wt; Li et al., 2017), and Chenab River, Pakistan (8,930 pg/g dry wt; Mahmood et al., 2014). East China Sea (77,000 pg/g dry wt; Liu et al., 2018) and Detroit River, the United States (264,000 pg/g dry wt; McGoldrick et al., 2018) were approximately 2–4 orders of magnitude higher than those observed in our study. The Detroit River is located close to the largest industrial complexes in the United States, including steel, petrochemical, and automobile industries (McGoldrick et al., 2018).

Significant correlations ($r = 0.315$–0.950, $p < 0.05$) were observed among the concentrations of individual PCN congeners in our sediment samples (**Supplementary Table 5**), implying the presence of common sources and environmental behavior of PCN congeners in the coastal environment. The highest correlation coefficients were observed for CN 52 with other congeners, such as CN 73 ($r = 0.923$, $p < 0.001$), CN 46 ($r = 0.861$, $p < 0.001$), and CN 64/68 ($r = 0.842$, $p < 0.001$). In our study, a significant correlation coefficient was found between ΣPCN

concentrations and TOC content ($r = 0.409$, $p < 0.01$). The higher correlation coefficients were observed for sediments collected from each coastal region, such as Gosa Stream (r = 0.541–0.990, $p < 0.05$), Daejeong Stream (r = 0.637–0.995, $p < 0.05$), and Woihwang River (r = 0.521–0.919, $p < 0.05$). These rivers and streams are surrounded by industrial complexes, which could expect the direct influences from industrial activities. In particular, the highest correlation coefficients were observed for sediments from Daejeong Stream, which is characterized by the highest contamination by PCNs observed in our study. This finding suggests that PCNs are primarily originated from the same sources, such as a specific industrial facility. Except for CNs 13 and 75, all PCN congeners showed significant correlations (r = 0.305–0.494, $p < 0.05$) with TOC content. This is likely due to greater hydrophobicity and K_{oc} values of PCNs. This result suggests that organic carbon is to be one of the primary factors governing the sedimentary distribution of PCNs. Similar results were reported for other hydrophobic contaminants in the coastal environments of Korea (Lee et al., 2018, 2020; Kim et al., 2021).

Spatial Distribution of Polychlorinated Naphthalenes in Sedimentary Environment

The spatial distribution of the actual and TEQ concentrations of ΣPCN in sediment collected from Ulsan and Onsan Bays and their inflowing rivers and streams are presented in **Figure 2**. The overall contamination of ΣPCN in sediment was higher in Ulsan Bay (42.7 ± 61.1 pg/g dry wt; mean ± standard deviation) than in Onsan Bay (17.6 ± 12.7 pg/g dry wt) without significance ($p > 0.05$). Our previous studies have reported the higher sedimentary contamination by flame retardants and plasticizers in Onsan Bay than Ulsan Bay (Lee et al., 2020; Kim et al., 2021), which was inconsistent with those observed in our study. This implies that sources and environmental behaviors are dependent on types of organic contaminants in the coastal environment. Sediment from Taehwa River showed relatively lower ΣPCN concentrations (22.3 ± 30.6 pg/g dry wt) than those found in Ulsan Bay, suggesting that urbanized activities are not a major contamination source of PCNs. However, the higher ΣPCN concentrations were observed in sediment from Yeocheon Stream (Y1–Y2; 350 ± 493 pg/g dry wt), close to non-ferrous industries (e.g., aluminum). Our findings indicate that the sedimentary contamination by PCNs is associated with the proximity to the industry producing PCNs. For Ulsan Bay, the ΣPCN concentrations in sediment collected from the inner part (U1–U4; 90.7 ± 65.7 pg/g dry wt) were significantly ($p < 0.05$) higher than those observed in the outer part of the bay (U5–U14; 12.9 ± 6.92 pg/g dry wt). Moreover, a clear decreasing trend was observed in the ΣPCN concentrations from inner to outer parts of the bay. Similarly, a clear decreasing trend in the ΣPCN concentrations was observed in sediment from inner to outer part of Gosa Stream. These results suggest that contamination sources of PCNs are present in inner parts of the bays and streams close to industrial complexes and harbors. In our study, the ΣPCN concentrations in sediment from Gosa Stream (G1–G4; 83.9 ± 63.6 pg/g dry wt) were significantly ($p < 0.05$) lower than those found in Yeocheon Stream. Unlike our findings, the highest contamination by siloxanes were observed in sediment from Gosa Stream (Lee et al., 2018), suggesting both chemical groups seem to have distinct contamination sources.

Although the ΣPCN concentrations in sediment from Onsan Bay were relatively lower than those observed in other coastal regions surveyed, the sediment from Woihwang River (W1–W7; 273 ± 417 pg/g dry wt) was highly contaminated by PCNs. In particular, the sediment from Station W1 close to non-ferrous and petrochemical industries showed higher concentration of ΣPCN (1,175 pg/g dry wt). This indicates that these industries could be primary sources of PCN contamination. Previous studies have reported that the metal and non-ferrous smelting processes are major contamination sources of PCNs in the environment (Yamamoto et al., 2018; Hu et al., 2021; Shen et al., 2021). In our study, the highest ΣPCN concentrations were observed in sediment from Daejeong Stream (D1–D4; 6,000 ± 10,400 pg/g dry wt), surrounded by non-ferrous (zinc, copper, and aluminum) industries. In particular, the sediment from Station D2 showed the highest ΣPCN concentration (21,000 pg/g dry wt) in all sediment samples. During the smelting processes of iron and non-ferrous materials (e.g., copper and aluminum), cutting oils could contain PCNs as impurities (Agunbiade et al., 2020; Shen et al., 2021).

The overall spatial distribution of TEQ concentrations in sediment was similar to those observed in the actual ΣPCN concentrations (**Figure 2B**). The highest TEQ concentrations were found in sediment from Daejeong Stream (5.32 ± 9.03 pg TEQ/g dry wt), which were 1–2 orders of magnitude higher ($p < 0.05$) than those observed in other coastal regions. Sediment from Station D2 showed the highest TEQ concentration (18.8 pg TEQ/g dry wt), followed by Station D3 (2.27 pg TEQ/g dry wt) from Daejeong Stream. Sediments from Yeocheon Stream (0.31 ± 0.43 pg TEQ/g dry wt) and Woihwang River (0.31 ± 0.48 pg TEQ/g dry wt) had higher TEQ concentrations than those observed in other regions.

Congener-Specific Profiles and Potential Sources of Polychlorinated Naphthalenes

The congener profiles of actual and TEQ concentrations of PCNs in sediment from Ulsan and Onsan Bays and their inflowing rivers and streams are presented **Figure 3**. For actual PCN concentrations, the predominant congeners were CNs 73 and 52 in all sediment samples, which accounted for 31 and 19% of the ΣPCN concentrations, respectively. The next highly contributed congeners were CNs 53 and 66/67, collectively accounting for 22% of the ΣPCN concentrations. The other PCN congeners contributed to < 10% of the ΣPCN concentrations. Previous studies reported the predominance of CNs 73, 52, and 60 in sediment samples (Castells et al., 2008; Zhao et al., 2011), consistent with those found in our study. Penta- and hexa-CNs were major homolog groups rather than less-chlorinated PCNs due to their hydrophobic characters in aquatic environment

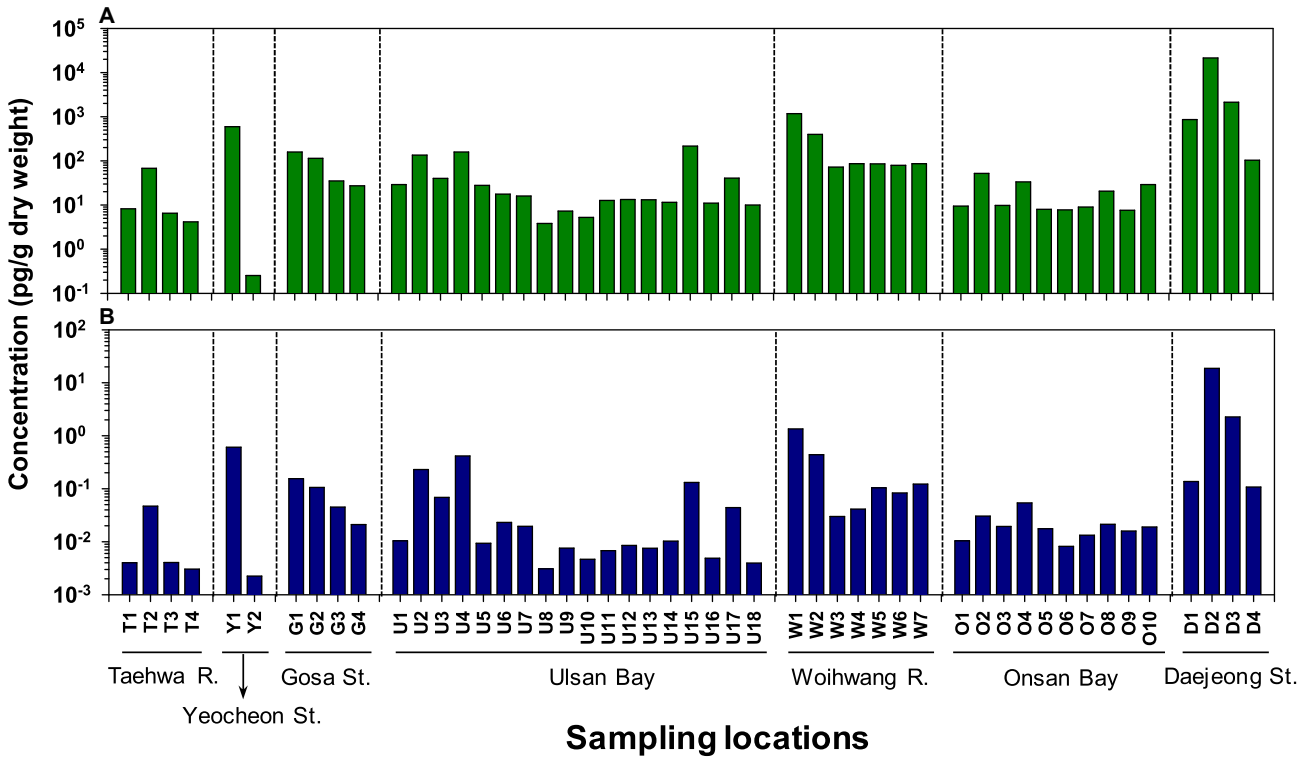

FIGURE 2 | Spatial distribution of **(A)** total and **(B)** toxic equivalent (TEQ) concentrations of polychlorinated naphthalenes (PCNs) in sediment collected from Ulsan and Onsan Bays and their inflowing rivers and streams, Korea.

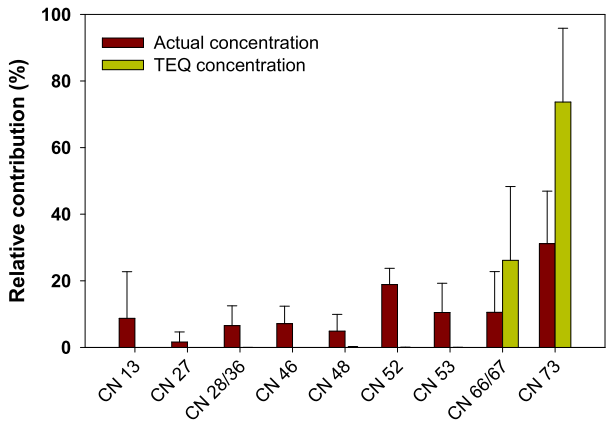

FIGURE 3 | Average relative contribution of PCN congeners for actual and TEQ concentrations in sediment from Ulsan and Onsan Bays and their inflowing rivers and streams, Korea. Vertical bars represent standard deviation.

(Meijer et al., 2001). For TEQ concentrations, CNs 73 (mean: 74%) and 66/67 (24%) only showed contributions of total TEQs. This could be explained by higher concentrations and 1–5 orders of magnitude higher TEFs of these congeners than those of the others. The congener patterns of predominant PCNs in our sediment samples were similar to those observed in marine biota. Reported data showed that highly toxic congeners of PCNs (CNs 66, 67, and 73) are prevalent in marine fish and mammals (e.g., polar bears) across the globe (Bidleman et al., 2010; Agunbiade et al., 2020). This similarity of congener patterns for PCNs in marine sediment and biota could be based on their persistence and bioaccumulation potentials. Comprehensive bioaccumulation studies are needed for protecting marine organisms and humans from the exposure of PCNs.

Earlier studies have utilized the diagnostic ratios of PCN congeners to track the potential sources of PCNs in sediment samples (Lee et al., 2007; Wang et al., 2012; Dat et al., 2019). The diagnostic ratio of CNs 66/67 to 71/72 has been applied to differentiate typical contamination sources of PCNs, such as thermal-related emission, technical PCB mixtures, and technical PCN mixtures (Dat et al., 2019). Ratio of CNs 66/67 and 71/72 $>$ 2.5 indicate thermal-related emissions, while that $<$ 2.5 indicates the consumption of PCB or PCN technical mixtures (Dat et al., 2019). The concentration ratio of ΣPCN with thermal-related congeners (CNs 13, 27, 36, 50, 52, 54, 66, 67, and 73) and ΣPCN was also employed to distinguish the contamination sources, which are $>$ 0.5 for thermal-related emissions and $<$ 0.11 for the use of technical mixtures (Lee et al., 2007). Some sediment samples (D1, W2, W4, W7, U2, G1, and T2) exceeded 2.5 for the diagnostic ratio of CNs 66/67 to 71/72 (**Figure 4**), indicating thermal-related emissions of PCNs. In contrast, sediments from W1, Y1, D2, D3, D4, G2, and U17 indicated the consumption of PCB or PCN technical mixtures for PCN contamination. In our study, most sediment

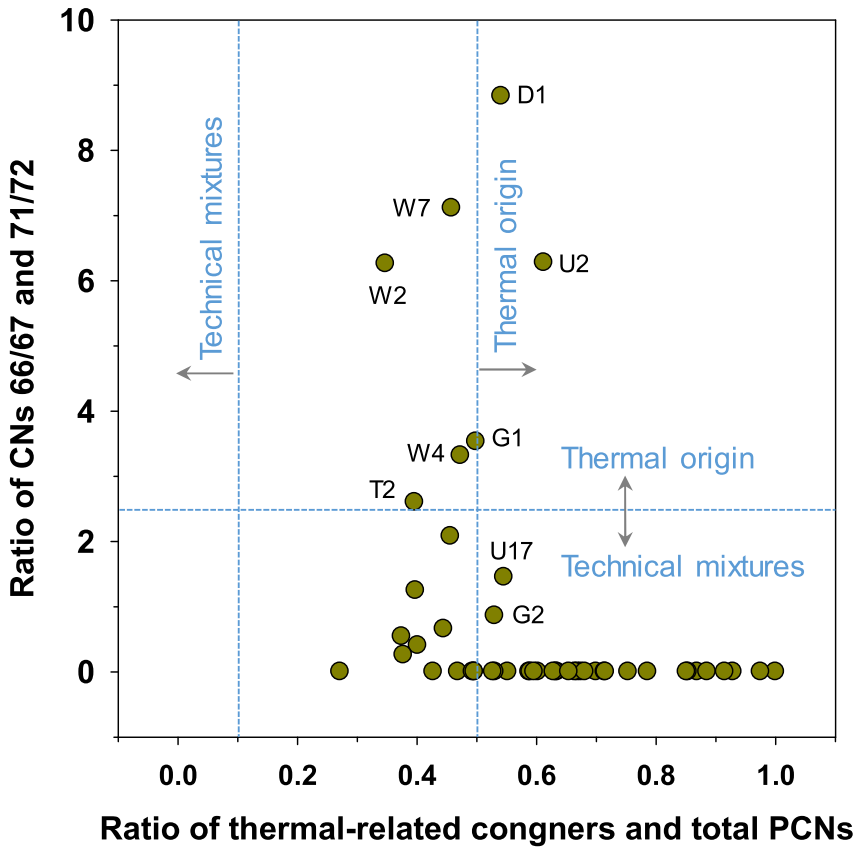

FIGURE 4 | Diagnostic ratios of the concentrations of PCN congeners in sediment from Ulsan and Onsan Bays and their inflowing streams and rivers, Korea.

samples from Ulsan and Onsan Bays did not contain CNs 71/72, precluding calculation of the diagnostic ratio of CNs 66/67 and 71/72. The diagnostic ratio between ΣPCN with thermal-related congeners and ΣPCN exceeded 0.5, indicating thermal-related contamination of PCNs. However, no sediment samples were included as an indication for the use of technical mixtures. Our findings suggest that the sedimentary contamination by PCNs in our study primarily originates from thermal-related emissions with a minor contribution from technical mixtures of PCBs as impurities. Considering no consumption of PCN technical mixtures in Korea, technical mixtures could be associated with the consumption of PCBs. Ulsan and Onsan industrial complexes are surrounded by industrial complexes for petrochemicals, ferrous and non-ferrous products, paints, plasticizers, and automobiles. These industries include the combustion processes and the use of industrial products containing PCBs, which are supported by the severe contamination by PCBs in Ulsan and Onsan Bays (Moon et al., 2008b).

In order to further characterize the contamination sources of PCNs, non-parametric multidimensional scaling (*n*MDS) analysis was performed with sedimentary PCN congeners using a PRIMER software (Plymouth, United Kingdom) (**Figure 5**). Four groups were clustered based on cluster analysis and a stress value of 0.01, indicating significance. All groups showed higher contribution of CN 73, which is an indicator for thermal emission of PCNs (Liu et al., 2018). This result indicates that thermal processes primarily contributed to PCN contamination in the coastal zones surveyed, consistent with the results from diagnostic ratios. Group A included almost all of the sampling locations. It was characterized by the dominance of CNs 73 and 52, collectively accounting for > 50% of the ΣPCN concentrations. These PCN congeners primarily originate from thermal-related activities (Lee et al., 2007; Liu et al., 2018). This suggests that PCNs are derived from thermal emission associated with industrial activities. As mentioned above, the Ulsan and Onsan industrial complexes are characterized by thermal-related activities, such as petrochemical and non-ferrous industries. Thus, thermal-related industrial activities could primarily contribute to sedimentary contamination by PCNs. Park et al. (2021) reported that combustion-related congeners are predominantly detected in agricultural soils near industrial cities of Korea. Group B, an innermost location (Station W1) from Woihwang River, was characterized by a higher contribution of tetra-CNs (44% of ΣPCN), such as CNs 28/36, 46, and 48, to the ΣPCN concentrations. Nadal et al. (2007, 2011) reported the dominance of tetra-CNs in environmental samples collected from chemical/petrochemical complexes. Woihwang River is surrounded by the largest petrochemical and non-ferrous industries, which could significantly affect PCN contamination in sediment. Although Groups C and D include the stations

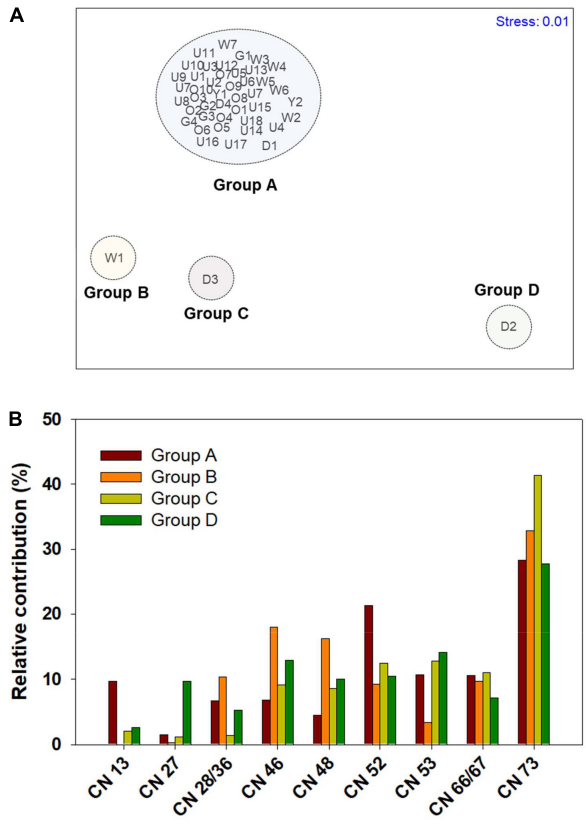

FIGURE 5 | (A) Plot of non-parametric multidimensional scaling (*n*MDS) ordination for polychlorinated naphthalene (PCN) congeners in sediment from industrialized bays and their surrounding rivers and streams of Korea. **(B)** Comparison of relative congener profiles of PCNs for each group (Groups A, B, C, and D) clustered by *n*MDS ordination.

(D2 and D3) from Daejeong Stream, the congener profiles of PCNs were different. Group C (Station D3) was characterized by the dominance of CN 73 (> 40% of ΣPCN) and similar contributions (∼10% of each) of CNs 46, 48, 52, 53, and 66/67 of the ΣPCN concentrations. Group D (Station D2), the highest PCN concentration (21,000 pg/g dry wt and 18.8 pg TEQ/g dry wt) recorded in our study, was characterized by similar contributions (10% ± 3.1%) for all tetra- to hexa-CN congeners (CNs 28/36, 46, 48, 52, 53, and 66/67) of the ΣPCN concentrations. Considering the location close to non-ferrous industries, discharges of cutting oils containing PCNs as impurities during non-ferrous smelting processes may affect the severe contamination by PCNs. Shen et al. (2021) reported that smelting processes are major sources of PCNs in the environment. Although the specific industrial facilities or processes were not suggested for PCN contamination sources in our study due to the limited accessibility for sample collection, the comprehensive survey on PCN contamination sources is required for effluents from different types of industrial complexes. Moreover, the additional analytical tools, such as stable carbon isotope fractionation, are needed to accurately identify the specific sources of PCNs in the sedimentary environment (Horii et al., 2005; Huang et al., 2020).

Ecotoxicological Implications

Several sediment quality guidelines (SGQs) have been developed for assessing the association between dioxin-like contaminant levels and biological significance (Canadian Council of Ministers of the Environment, 2014; Walker et al., 2015). The Canadian Council of Ministers of the Environment (CCME) has proposed the interim SQGs (ISQGs; 0.85 pg TEQ/g dry wt) and probable effect levels (PELs; 21.5 pg TEQ/g dry wt) as screening tools to assess the potential health risks to aquatic life derived from dioxin-like contaminants (Zhao et al., 2011; Walker et al., 2015). Due to the lack of available SQGs for only PCNs, the SQGs of PCDD/Fs expressed as TEQs were employed for the assessment of ecotoxicological concerns of PCNs. In our study, only three sediment samples from Daejeong Streams (D2; 18.6 and D3: 2.27 pg TEQ/g dry wt) and Woihwang River (W1; 1.35 pg TEQ/g dry wt) exceeded the ISQGs, implying limited health risks to benthic organisms (**Supplementary Figure 2**). Moreover, no sediments exceeded the PELs. Despite this, our previous studies have reported higher levels of TEQs by PCDD/Fs and dioxin-like PCBs in Ulsan Bay sediments, which showed 3.01 ± 0.95 and 5.40 ± 8.11 pg TEQ/g dry wt for PCDD/Fs and dioxin-like PCBs, respectively (Moon et al., 2008b). The study surveyed the dioxin-like contaminants in the sediments from only central parts of Ulsan Bay. Thus, the higher concentrations of PCDD/Fs and dioxin-like PCBs are expected in sediments from inner parts of bays, rivers, and streams. Kim et al. (2019b) also reported the newly identified dioxin-like contaminants, such as new polycyclic aromatic hydrocarbons, in sediments from tributaries of Ulsan and Onsan Bays. Our findings indicate the cumulative risks of dioxin-like contaminants to inhabiting species in the sedimentary environments surveyed.

CONCLUSION

Analytical methods for the determination of 18 PCN congeners in sediment samples were optimized with a multi-layer silica gel column and a GC-MS/MS. PCNs were detectable in all sediment samples from the industrialized coastal zone, indicating widespread contamination by PCNs in the coastal environments. The concentrations of PCNs and TEQs were within the ranges of those reported for other countries. Gradual decrease in concentrations of PCNs were observed from inner to outer parts of the streams, rivers, and bays, indicating that sedimentary PCN distribution is influenced by proximity to industrial complexes. The highest concentrations of PCNs were observed in sediment close to non-ferrous and petrochemical industries. Predominant congeners, diagnostic ratios, and multivariate statistical analysis showed that PCNs primarily originate from thermal-related emission and the use of PCB technical mixtures. The concentrations of PCNs in sediment could be contributed to the cumulative risks by dioxin-like contaminants, which may exceed the SQGs.

A comprehensive ecotoxicological investigation on dioxin-like toxicity is required to protect inhabiting species in the coastal environments surveyed.

DATA AVAILABILITY STATEMENT

The original contributions presented in the study are included in the article/**Supplementary Material**, further inquiries can be directed to the corresponding author/s.

AUTHOR CONTRIBUTIONS

H-HL collected the sediment samples in the field, measured target contaminants in the samples, and wrote the draft of the manuscript. SL developed and validated the analytical methods of target contaminants. JSL processed and analyzed the chemical data and critically reviewed the draft of the manuscript. H-BM processed all analytical data and edited the manuscript for journal submission. All authors contributed to the article and approved the submitted version.

FUNDING

This study was supported by the projects entitled "Development of Techniques for Assessment and Management of Hazardous Chemicals in the Marine Environment" and "Development of Technology for Impact Assessment and Management of HNS Discharged from Marine Industrial Facilities" funded by the Ministry of Oceans and Fisheries (MOF), Korea.

SUPPLEMENTARY MATERIAL

The Supplementary Material for this article can be found online at: https://www.frontiersin.org/articles/10.3389/fmars.2021.754278/full#supplementary-material

REFERENCES

Agunbiade, I. V., Adeniji, A. O., Okoh, A. I., and Okoh, O. O. (2020). A review on occurrence and analytical procedures for the evaluation of polychlorinated naphthalenes in human and environmental matrices. *Environ. Pollut. Bioavailab.* 32, 154–174.

Behnisch, P. A., Hosoe, K., and Sakai, S. I. (2003). Brominated dioxin-like compounds: *In vitro* assessment in comparison to classical dioxin-like compounds and other polyaromatic compounds. *Environ. Int.* 29, 861–877. doi: 10.1016/s0160-4120(03)00105-3

Bidleman, T. F., Helm, P. A., Braune, B. M., and Gabrielsen, G. W. (2010). Polychlorinated naphthalenes in polar environments–A review. *Sci. Total Environ.* 408, 2919–2935. doi: 10.1016/j.scitotenv.2009.09.013

Canadian Council of Ministers of the Environment (2014). *Sediment quality guidelines for the protection of aquatic life*. Winnipeg: Canadian Council of Ministers of the Environment.

Castells, P., Parera, J., Santos, F. J., and Galceran, M. T. (2008). Occurrence of polychlorinated naphthalenes, polychlorinated biphenyls and short-chain chlorinated paraffins in marine sediments from Barcelona (Spain). *Chemosphere* 70, 1552–1562. doi: 10.1016/j.chemosphere.2007.08.034

Dat, N. D., Chang, K. S., Wu, C. P., Chen, Y. J., Tsai, C. L., Chi, K. H., et al. (2019). Measurement of PCNs in sediments collected from reservoir and river in northern Taiwan. *Ecotoxicol. Environ. Saf.* 174, 384–389. doi: 10.1016/j.ecoenv.2019.02.087

Falandysz, J. (1998). Polychlorinated naphthalenes: An environmental update. *Environ. Pollut.* 101, 77–90. doi: 10.1016/s0269-7491(98)00023-2

Falandysz, J., Chudzyński, K., Takekuma, M., Yamamoto, T., Noma, Y., Hanari, N., et al. (2008). Multivariate analysis of identity of imported technical PCN formulation. *J. Environ. Sci. Health C* 43, 1381–1390. doi: 10.1080/10934520802232022

Falandysz, J., Fernandes, A., Gregoraszczuk, E., and Rose, M. (2014). The toxicological effects of halogenated naphthalenes: a review of aryl hydrocarbon receptor-mediated (dioxin-like) relative potency factors. *J. Environ. Sci. Health. C* 32, 239–272. doi: 10.1080/10590501.2014.938945

Falandysz, J., Nose, K., Ishikawa, Y., Łukaszewicz, E., Yamashita, N., and Noma, Y. (2006). HRGC/HRMS analysis of chloronaphthalenes in several batches of Halowax 1000, 1001, 1013, 1014 and 1099. *J. Environ. Sci. Health A* 41, 2237–2255. doi: 10.1080/10934520600872748

Gu, W., Li, X., Du, M., Ren, Z., Li, Q., and Li, Y. (2021). Identification and regulation of ecotoxicity of polychlorinated naphthalenes to aquatic food Chain (green algae-*Daphnia magna*-fish). *Aquat. Toxicol.* 233:105774. doi: 10.1016/j.aquatox.2021.105774

Helm, P. A., Kannan, K., and Bidleman, T. F. (2006). "Polychlorinated naphthalenes in the Great Lakes," in *Persistent Organic Pollutants in the Great Lakes*, ed. R. A. Hites (Berlin: Springer), 267–306. doi: 10.1007/698_5_043

Horii, Y., Kannan, K., Petrick, G., Gamo, T., Falandysz, J., and Yamashita, N. (2005). Congener-specific carbon isotopic analysis of technical PCB and PCN mixtures using two-dimensional gas chromatography-isotope ratio mass spectrometry. *Environ. Sci. Technol.* 39, 4206–4212. doi: 10.1021/es050133q

Hu, J. C., Wu, J., Xu, C. Y., and Jin, J. (2021). Characterization and health risks of PCDD/Fs, PCBs, and PCNs in the soil around a typical secondary copper smelter. *Huan. Jing. Ke. Xue.* 42, 1141–1151. doi: 10.13227/j.hjkx.202009052

Hu, J., Zheng, M., Liu, W., Li, C., Nie, Z., Liu, G., et al. (2013). Characterization of polychlorinated naphthalenes in stack gas emissions from waste incinerators. *Environ. Sci. Pollut. Res.* 20, 2905–2911. doi: 10.1007/s11356-012-1218-0

Huang, C., Zeng, Y., Luo, X., Ren, Z., Lu, Q., Tian, Y., et al. (2020). Tracing the sources and microbial degradation of PCBs in field sediments by a multiple-line-of-evidence approach including compound-specific stable isotope analysis. *Wat. Res.* 182:115977. doi: 10.1016/j.watres.2020.115977

Huang, J., Yu, G., Yamaguchi, M., Matsumura, T., Yamazaki, N., and Weber, R. (2015). Congener-specific analysis of polychlorinated naphthalenes (PCNs) in the major Chinese technical PCB formulation from a stored Chinese electrrical capacitor. *Envrion. Sci. Pollut. Res.* 22, 14471–14477. doi: 10.1007/s11356-014-3677-y

Kim, J., Hong, S., Cha, J., Lee, J., Kim, T., Lee, S., et al. (2019b). Newly identified AhR-active compounds in the sediments of an industrial area using effect-directed analysis. *Environ. Sci. Technol.* 53, 10043–10052. doi: 10.1021/acs.est.9b02166

Kim, K. W., Choo, G., Cho, H. S., Lee, B. C., Park, K., and Oh, J. E. (2019a). The occurrence and distribution of polychlorinated naphthalenes (PCNs), focusing on tissue-specific bioaccumulation in crucian carp in South Korea. *Sci. Total Environ.* 665, 484–491. doi: 10.1016/j.scitotenv.2019.01.238

Kim, S., Kim, Y., and Moon, H.-B. (2021). Contamination and historical trends of legacy and emerging plasticizers in sediment from highly industrialized bays of Korea. *Sci. Total Environ.* 765:142751. doi: 10.1016/j.scitotenv.2020.142751

Lee, H.-K., Lee, S., Lim, J.-E., and Moon, H.-B. (2020). Legacy and novel flame retardants in water and sediment from highly industrialized bays of Korea: Occurrence, source tracking, decadal time trend, and ecological risks. *Mar. Pollut. Bull.* 160:111639. doi: 10.1016/j.marpolbul.2020.111639

Lee, S. C., Harner, T., Pozo, K., Shoeib, M., Wania, F., Muir, D. C., et al. (2007). Polychlorinated naphthalenes in the global atmospheric passive sampling (GAPS) study. *Environ. Sci. Technol.* 41, 2680–2687. doi: 10.1021/es062352x

Lee, S.-Y., Lee, S., Choi, M., Kannan, K., and Moon, H.-B. (2018). An optimized method for the analysis of cyclic and linear siloxanes and their distribution in surface and core sediments from industrialized bays in Korea. *Environ. Pollut.* 236, 111–118. doi: 10.1016/j.envpol.2018.01.051

Li, C., Li, J., Lyu, B., Wu, Y., Yang, L., Zheng, M., et al. (2021). Burden and risk of polychlorinated naphthalenes in Chinese human milk and a global comparison of human exposure. *Environ. Sci. Technol.* 55, 6804–6813. doi: 10.1021/acs.est.1c00605

Li, F., Jin, J., Gao, Y., Geng, N., Tan, D., Zhang, H., et al. (2016b). Occurrence, distribution and source apportionment of polychlorinated naphthalenes (PCNs) in sediments and soils from the Liaohe River Basin. *China Environ. Pollut.* 211, 226–232. doi: 10.1016/j.envpol.2015.09.055

Li, F., Jin, J., Tan, D., Xu, J., Dhanjai, N. Y., Zhang, H., et al. (2016a). High performance solid-phase extraction cleanup method coupled with gas chromatography-triple quadrupole mass spectrometry for analysis of polychlorinated naphthalenes and dioxin-like polychlorinated biphenyls in complex samples. *J. Chromato. A* 1448, 1–8. doi: 10.1016/j.chroma.2016.04.037

Li, Q., Cheng, X., Wang, Y., Cheng, Z., Guo, L., Li, K., et al. (2017). Impacts of human activities on the spatial distribution and sources of polychlorinated naphthalenes in the middle and lower reaches of the Yellow River. *Chemosphere* 176, 369–377. doi: 10.1016/j.chemosphere.2017.02.130

Liu, A., Jia, J., Lan, J., Zhao, Z., and Yao, P. (2018). Distribution, composition, and ecological risk of surface sedimental polychlorinated naphthalenes in the East China Sea. *Mar. Pollut. Bull.* 135, 90–94. doi: 10.1016/j.marpolbul.2018.07.017

Liu, G., Cai, Z., and Zheng, M. (2014). Sources of unintentionally produced polychlorinated naphthalenes. *Chemosphere* 94, 1–12. doi: 10.1016/j.chemosphere.2013.09.021

Liu, G., Zheng, M., Lv, P., Liu, W., Wang, C., Zhang, B., et al. (2010). Estimation and characterization of polychlorinated naphthalene emission from coking industries. *Environ. Sci. Technol.* 44, 8156–8161. doi: 10.1021/es102474w

Mahmood, A., Malik, R. N., Li, J., and Zhang, G. (2014). Congener specific analysis, spatial distribution and screening-level risk assessment of polychlorinated naphthalenes in water and sediments from two tributaries of the River Chenab. *Pakis. Sci. Total Environ.* 485, 693–700. doi: 10.1016/j.scitotenv.2014.03.118

McGoldrick, D. J., Pelletier, M., De Solla, S. R., Marvin, C. H., and Martin, P. A. (2018). Legacy of legacies: Chlorinated naphthalenes in Lake Trout, Walleye, Herring Gull eggs and sediments from the Laurentian Great Lakes indicate possible resuspension during contaminated sediment remediation. *Sci. Total Environ.* 634, 1424–1434. doi: 10.1016/j.scitotenv.2018.04.077

Meijer, S. N., Harner, T., Helm, P. A., Halsall, C. J., Johnston, A. E., and Jones, K. C. (2001). Polychlorinated naphthalenes in UK soils: time trends, markers of source, and equilibrium status. *Environ. Sci. Technol.* 35, 4205–4213. doi: 10.1021/es010071d

Moon, H.-B., Choi, H.-G., Lee, P.-Y., and Ok, G. (2008b). Congener-specific characterization and sources of polychlorinated dibenzo-*p*-dioxins, dibenzofurans and dioxin-like polychlorinated biphenyls in marine sediments from industrialized bays of Korea. *Environ. Toxicol. Chem.* 27, 323–333. doi: 10.1897/07-337R.1

Moon, H.-B., Kannan, K., Lee, S.-J., and Choi, M. (2007). Polybrominated diphenyl ethers (PBDEs) in marine sediments from industrialized bays of Korea. *Mar. Pollut. Bull.* 54, 1402–1412. doi: 10.1016/j.marpolbul.2007.05.024

Moon, H.-B., Yoon, S.-P., Jung, R.-H., and Choi, M. (2008a). Wastewater treatment plants (WWTPs) as a source of sediment contamination by toxic organic pollutants and fecal sterols in a semi-enclosed bay in Korea. *Chemosphere* 73, 880–889. doi: 10.1016/j.chemosphere.2008.07.038

Nadal, M., Schuhmacher, M., and Domingo, J. L. (2007). Levels of metals, PCBs, PCNs and PAHs in soils of a highly industrialized chemical/petrochemical area: Temporal trend. *Chemosphere* 66, 267–276. doi: 10.1016/j.chemosphere.2006.05.020

Nadal, M., Schuhmacher, M., and Domingo, J. L. (2011). Long-term environmental monitoring of persistent organic pollutants and metals in a chemical/petrochemical area: Human health risks. *Environ. Pollut.* 159, 1769–1777. doi: 10.1016/j.envpol.2011.04.007

Noma, Y., Minetomatsu, K., Falandysz, J., Swietojańska, A., Flisak, M., Miyaji, K., et al. (2005). By-side impurities in chloronaphthalene mixtures of the Halowax series: All 75 chlorodibenzo-*p*-dioxins. *J. Environ. Sci. Health A Toxicol. Hazard. Subst. Environ. Eng.* 40, 77–89. doi: 10.1081/ese-200033581

Odabasi, M., Dumanoglu, Y., Kara, M., Altiok, H., Elbir, T., and Bayram, A. (2017). Polychlorinated naphthalene (PCN) emissions from scrap processing steel plants with electric-arc furnaces. *Sci. Total Environ.* 574, 1305–1312. doi: 10.1016/j.scitotenv.2016.08.028

Pagano, J. J., and Garner, A. J. (2021). Polychlorinated naphthalenes across the great lakes: Lake trout and walleye concentrations, trends, and teq assessment-2004-2018. *Environ. Sci. Technol.* 55, 2411–2421. doi: 10.1021/acs.est.0c07507

Park, H., Kang, J.-H., Baek, S.-Y., and Chang, Y.-S. (2010). Relative importance of polychlorinated naphthalenes compared to dioxins, and polychlorinated biphenyls in human serum from Korea: Contribution to TEQ and potential sources. *Environ. Pollut.* 158, 1420–1427. doi: 10.1016/j.envpol.2009.12.039

Park, M.-K., Cho, H.-K., Cho, I.-G., Lee, S.-E., and Choi, S.-D. (2021). Contamination characteristics of polychlorinated naphthalenes in the agricultural soil of two industrial cities in South Korea. *Chemosphere* 273:129721. doi: 10.1016/j.chemosphere.2021.129721

Shen, J., Yang, L., Liu, G., Zhao, X., and Zheng, M. (2021). Occurrence, profiles, and control of unintentional POPs in the steelmaking industry: A review. *Sci. Total Environ.* 773:145692. doi: 10.1016/j.scitotenv.2021.145692

Suzuki, G., Michinaka, C., Matsukami, H., Noma, Y., and Kajiwara, N. (2020). Validity of using a relative potency factor approach for the risk management of dioxin-like polychlorinated naphthalenes. *Chemosphere* 244:125448. doi: 10.1016/j.chemosphere.2019.125448

Van den Berg, M., Birnbaum, L. S., Denison, M., De Vito, M., Farland, W., Feeley, M., et al. (2006). The 2005 World Health Organization reevaluation of human and mammalian toxic equivalency factors for dioxins and dioxin-like compounds. *Toxicol. Sci.* 93, 223–241. doi: 10.1093/toxsci/kfl055

Waheed, S., Khan, M. U., Sweetman, A. J., Jones, K. C., Moon, H.-B., and Malik, R. N. (2020). Exposure of polychlorinated naphthalenes (PCNs) to Pakistani populations via non-dietary sources from neglected e-waste hubs: A problem of high health concern. *Environ. Pollut.* 259:113838. doi: 10.1016/j.envpol.2019.113838

Walker, T. R., Willis, R., Gray, T., McClean, B., McMillan, S., Leroy, M., et al. (2015). Ecological risk assessment of sediments in Sydney Harbour, Nova Scotia, Canada. *Soil Sed. Contam.* 24, 471–493. doi: 10.1080/15320383.2015.982244

Wang, Y., Cheng, Z., Li, J., Luo, C., Xu, Y., Li, Q., et al. (2012). Polychlorinated naphthalenes (PCNs) in the surface soils of the Pearl River Delta, South China: Distribution, sources, and air-soil exchange. *Environ. Pollut.* 170, 1–7. doi: 10.1016/j.envpol.2012.06.008

Wu, J., Hu, J., Wang, S., Jin, J., Wang, R., Wang, Y., et al. (2018). Levels, sources, and potential human health risks of PCNs, PCDD/Fs, and PCBs in an industrial area of Shandong Province, China. *Chemosphere* 199, 382–389. doi: 10.1016/j.chemosphere.2018.02.039

Wu, X., Wu, B., Jiang, M., Chang, F., Nan, Q., Yu, X., et al. (2020). Distribution, sources and burial flux of sedimentary organic matter in the East China Sea. *J. Oceanol. Limnol.* 38, 1488–1501. doi: 10.1007/s00343-020-0037-2

Yamamoto, T., Higashino, K., Abe, T., Takasuga, T., Takemori, H., Weber, R., et al. (2018). PCDD/PCDF formation in the chlor-alkali process-Laboratory study and comparion with patterns from contaminated sites. *Envrion. Sci. Pollut. Res.* 25, 31874–31884. doi: 10.1007/s11356-017-0777-5

Zhang, L., Zhang, L., Dong, L., Huang, Y., and Li, X. (2015). Concentrations and patterns of polychlorinated naphthalenes in surface sediment samples from Wuxi, Suzhou, and Nantong, in East China. *Chemosphere* 138, 668–674. doi: 10.1016/j.chemosphere.2015.07.045

Zhao, X., Zhang, H., Fan, J., Guan, D., Zhao, H., Ni, Y., et al. (2011). Dioxin-like compounds in sediments from the Daliao River estuary of Bohai Sea: Distribution and their influencing factors. *Mar. Pollut. Bull.* 62, 918–925. doi: 10.1016/j.marpolbul.2011.02.054

Conflict of Interest: JSL was employed by the company NeoEnBiz Co.

The remaining authors declare that the research was conducted in the absence of any commercial or financial relationships that could be construed as a potential conflict of interest.

Publisher's Note: All claims expressed in this article are solely those of the authors and do not necessarily represent those of their affiliated organizations, or those of the publisher, the editors and the reviewers. Any product that may be evaluated in this article, or claim that may be made by its manufacturer, is not guaranteed or endorsed by the publisher.

frontiers in Marine Science

REVIEW
published: 15 December 2021
doi: 10.3389/fmars.2021.760649

Evidence of Microplastic Size Impact on Mobility and Transport in the Marine Environment: A Review and Synthesis of Recent Research

*Arefeh Shamskhany, Zhuoran Li, Preet Patel and Shooka Karimpour**

Department of Civil Engineering, Lassonde School of Engineering, York University, Toronto, ON, Canada

Marine Microplastics (MPs) exhibit a wide range of properties due to their variable origins and the weathering processes to which they are exposed. MP's versatile properties are connected to their dispersal, accumulation, and deposition in the marine environment. MP transport and dispersion are often explained by analogy with sediments. For natural sediments, one of the key features linked to transport and marine morphology is particle size. There is, however, no size classification defined for MP particles and MPs constitute all plastic particles sized smaller than the threshold of 5 mm. In this study, based on existing knowledge in hydrodynamics and natural sediment transport, the impact of MP size on turbulent entrainment, particle settling, and resuspension is described. Moreover, by analyzing several quantitative studies that have provided size distribution, size-selective accumulation of MPs in various regions of the marine environment is reported on. The preferential presence of MPs based on their size in different marine compartments is discussed based on the governing hydrodynamic parameters. Furthermore, the linkage between polymer properties and MP shape and size is explored. Despite the evident connection between hydrodynamic transport and MP size presented, classification of MP size presents challenges. MP size, shape, and density appear simultaneously in the definition of many hydrodynamic parameters described in this study. Unlike mineral sediments that possess a narrow range of density and shape, plastics are manufactured in a wide variety of densities and marine MPs are versatile in shape. Classification for MP size should incorporate particle variability in terms of polymer density and shape.

Keywords: marine microplastic pollution, particle size, hydrodynamics, entrainment and mixing, sediment transport

OPEN ACCESS

Edited by:
Allyson O'Brien,
The University of Melbourne, Australia

Reviewed by:
Conrad Sparks,
Cape Peninsula University of Technology, South Africa
Jinping Cheng,
Hong Kong University of Science and Technology, Hong Kong SAR, China

****Correspondence:***
Shooka Karimpour
shooka.karimpour@lassonde.yorku.ca

Specialty section:
This article was submitted to Marine Pollution, a section of the journal Frontiers in Marine Science

Received: *18 August 2021*
Accepted: *22 November 2021*
Published: *15 December 2021*

Citation:
Shamskhany A, Li Z, Patel P and Karimpour S (2021) Evidence of Microplastic Size Impact on Mobility and Transport in the Marine Environment: A Review and Synthesis of Recent Research. Front. Mar. Sci. 8:760649. doi: 10.3389/fmars.2021.760649

INTRODUCTION

Plastics are used for a wide spectrum of products and their production has increased drastically over the past decades. Due to improper or lack of end-of-life plastic management, plastic wastes appear globally from mountaintops (Napper et al., 2020) to seafloors (e.g., Van Cauwenberghe et al., 2013). Plastic emission to freshwater and marine environments occurs through various pathways such as stormwater runoffs, rivers, wastewater discharge, and wind. Once plastic debris reaches a body of

water, water acts as a transport vehicle and distributes and spreads the particles. Due to their slow decomposition processes, plastics can last in aquatic environments for centuries, if not millennia. In the past decade, concerns about Microplastics (MPs), plastic debris sized smaller than 5 mm, have emerged due to MP pollution impacts on the health of aquatic animals and humans. MPs can be ingested by various animals, ranging from microsized zooplankton (Cole et al., 2013) to whales (Fossi et al., 2012), and move up into the food chain. Furthermore, once ingested, toxins and microbes absorbed by MPs or accumulated on the surface can affect the host organism's health (Rochman et al., 2013; Lusher, 2015).

In marine and freshwater ecosystems, MPs have been reported in high concentrations both in the vicinity of their emission source, for instance, downstream of wastewater treatment plants (Murphy et al., 2016; Dalu et al., 2021), as well as in remote areas distant from the source (Huntington et al., 2020). Quantitative site-based studies in different water bodies have shown a varied assembly of MP properties in terms of their polymer, density, shape, and size (e.g., Morét-Ferguson et al., 2010; Naidoo et al., 2015). Many studies have identified the preferential presence of MPs based on their numerous properties in different compartments of aquatic systems (Thompson et al., 2004; Ryan, 2015; Baldwin et al., 2016; Cózar et al., 2017; Schwarz et al., 2019). Marine and freshwater MP particles are transported and dispersed by physical hydrodynamic processes. The importance and role of each process in MP mobility and deposition vary from site to site and are also dependent on MP properties (e.g., Zhang, 2017; Van Sebille et al., 2020).

One of the physical properties frequently associated with the distribution and mobility of MPs is density. Plastic density in freshwater and marine environments depends on the type of polymers and can be significantly affected by biofouling, that is the formation of biofilms on particles' surfaces (e.g., Long et al., 2015; Lagarde et al., 2016). Plastics with densities higher than the density of the ambient water are negatively buoyant and tend to sink, while plastics lighter than the ambient fluid are positively buoyant and tend to rise and float in a quiescent fluid (see **Figure 1**). For accumulation in surface water, for instance, some studies have found substantial quantities of polyethylene (PE) and polypropylene (PP) (e.g., Suaria et al., 2016), whereas others have identified polymers such as polystyrene (PS) to be abundantly present (e.g., Di and Wang, 2018). Review studies by Erni-Cassola et al. (2019) and Schwarz et al. (2019) have found PE and PP to be predominant in surface water, followed by PS. The overall data suggests that low-density polymers, PE and PP, both lighter than water, and PS, with densities only marginally different from that of water (**Table 1**), are predominant in surface water.

Similarly, MP shape is also linked to its mobility. MPs are either engineered as small-sized plastics, primary MPs, or they are the by-product of fragmentation of larger plastic debris, secondary MPs. While primary MPs are often in the form of spheres or pellets, secondary aquatic MPs exist in different shapes depending on their origin and exposure to fragmentation processes (Hidalgo-Ruz et al., 2012). Tanaka and Takada (2016), among others, presented shapes for MPs, from fragments and

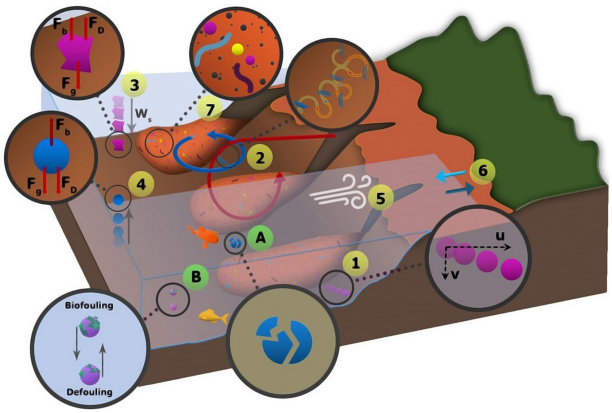

FIGURE 1 | Range of physical processes that affect the transport and distribution of marine MPs (modified from Karimpour et al., 2021a): (1) advection; (2) entrainment by turbulent structures; (3) sinking of negatively buoyant or biofouled MPs, and vertical forces including drag force, F_d, gravity, F_g, and buoyant force, F_b; (4) rising of positively buoyant or defouled MPs; (5) transport by wind; (6) coastal beaching and wash off; (7) transport with sediment gravity flow. A and B present fragmentation and biofouling, respectively. These two processes are assumed to play significant roles in altering MP transport (Waldschläger et al., 2020).

microbeads to sheets, films, and fibers. MP shape affects the particle's drag force, F_D, shown in **Figure 1**, and their rise and fall velocity (Kowalski et al., 2016; Khatmullina and Isachenko, 2017). The biofouling rate is also strongly linked to particle shape and the particles' exterior surface to volume ratio (Teuten et al., 2007; Kooi et al., 2017). Furthermore, sedimentary records have shown a higher presence of a specific MP shape, microfibers (Kane and Clare, 2019).

Another characteristic that can strongly impact MP dispersal is size. MPs are reported in a wide range of sizes across freshwater and marine compartments, varying from 10 μm to 5 mm (e.g., Reisser et al., 2015; Bergmann et al., 2017). Compared to natural sediments, the particle size of 5 mm, the upper size limit for MPs, is equivalent to the size of fine gravel, while the size of 10 μm is equivalent to that of silt. Among sediment properties, size classification is one of the most important sediment features affecting hydrodynamic transport and aquatic morphology (e.g., Heitmuller and Hudson, 2009; Yang and Shi, 2019). Despite its importance, a limited number of quantitative studies have sorted MPs based on size. In addition, in site-based quantitative studies that have provided size distributions, size classification and categories are inconsistent due to varying objectives, sampling locations and techniques, preparation, and analytical limitations. Filella (2015) has first highlighted the lack of attention to standardized size classification and its importance, using the sediment analogy. MP ingestion and ecological impacts are also tied to their size. Lehtiniemi et al. (2018) suggested that the size of MP fragments is a crucial factor, influencing the number of plastic particles ingested by small predators. In their study off the coast of South Africa for larger plastic debris, Ryan (2015) stressed the importance of plastic size in their long-distance transport. Furthermore, Kooi et al. (2017) noted the importance

TABLE 1 | Density of high-demand plastics (Harper and Petrie, 2003), seawater (25°C, salinity of 35 g/kg, 1 atm pressure), freshwater (4°C), and common range for mineral sediments.

Polymer type	Min (g/cm^3)	Max (g/cm^3)	Global plastic demand and distribution, 2019 (Plastics Europe, 2020)
Polyethylene (PE: LDPE, HDPE, LLDPE, MDPE)	0.88	0.97	29.8%
Polypropylene (PP)	0.90	0.92	19.4%
Polyvinyl chloride (PVC)	1.15	1.58	10.0%
Polyurethane (PUR)	0.01	1.26	7.9%
Polyethylene terephthalate (PET/PETE)	1.37	1.45	7.9%
Polystyrene (PS/EPS)	1.04	1.10	6.2%
Others	0.10	2.20	18.8%
Freshwater	1.000		–
Seawater	1.025		–
Mineral sand/silt/clay	2.50	2.80	–

The last column provides the global demand for each plastic polymer.

of size in MP biofouling and defouling. They have attributed size-dependent biofouling to the absence of finer MPs from the surface layers, reported by Cózar et al. (2014). Although the impact of MP size on some transport mechanisms has been discussed in several recent studies, a comprehensive understanding of this MP feature and its role in the mobility of MPs is still required.

In this study, some of the hydro-environmental factors that affect the transport of MPs are critically discussed. The impact of particle size and its linkage to these physical processes are explored in-depth. Furthermore, by consolidating the data on MP size distribution from different regions of the marine environment including sediments, the interconnections of size to transport process and accumulation are assessed. Evidence based on plastic composition and polymer types is also presented when reviewing the impact of polymer type and associated fragmentation rate on MP mobility. The objective is to provide a new narrative for MP size based on existing knowledge in sedimentology and to identify existing gaps in this area.

MICROPLASTIC SIZE IMPACT ON HYDRODYNAMIC PARAMETERS

Owing to the unique set of characteristics including their density, range, shape and morphology, MPs' behavior is different from that of natural sediments and other contaminants. Knowledge regarding the transport of natural sediments, however, can be utilized to formulate the unique hydrodynamic behavior of MP particles. In this section, the role of selected hydrodynamic processes in MP transport and their relation to particle size are discussed. **Figure 2** illustrates the role of particle size in MP response to the physical processes discussed in this section.

Effect of Size on Turbulent Mixing and Marine Microplastic Entrainment

In turbulent flow, the particle entrainment process is an interplay of turbulence features, gravitational effects, and particle morphology. This interaction between the turbulent flow and gravitational effects of particles appears in different scales of the flow, from larger integral-scale eddies to small dissipative Kolmogorov's scale. The energy-containing eddies are presented by the integral scale, while the viscous range is presented by the Kolmogorov's scale. In formulating this interaction, parameters associated with turbulence length and time scales must be accounted for. The larger scale of turbulence is presented by integral length, l, and turnover time scale, τ_l. The small Kolmogorov's time, τ_υ, and length scale, η, are defined as (e.g., Good et al., 2014):

$$\tau_\upsilon = \left(\frac{\upsilon}{\varepsilon}\right)^{1/2};\ \eta = \left(\frac{\upsilon^3}{\varepsilon}\right)^{1/4} \tag{1}$$

where υ is the kinematic viscosity of the fluid and ε is the dissipation rate per unit mass. Particle engagement also depends on particle size and density, as well as the density of the ambient fluid (Dey et al., 2019). These factors are reflected in particle relaxation time, τ_p:

$$\tau_p = \frac{d^2\left(\rho_p - \rho_w\right)}{18\mu} \tag{2}$$

where d is the particle diameter, ρ_p is the particle density, ρ_w the density of the ambient water, and μ is the dynamic viscosity of fluid. The particle relaxation time is sometimes defined by the absolute density (e.g., Wang and Maxey, 1993); however, the more general equation considers the density difference between the particle and the ambient fluid, as demonstrated in Eq. (2) (Wang et al., 2018). Two dimensionless parameters, based on turbulent time scales and particle relaxation time, can be defined to describe the relative significance of natural vertical movements of particles due to gravity and buoyancy, compared to turbulent-induced particle entrainment. The effects of small-scale turbulence on particle motion are ascertained by the Stokes number as defined by Kolmogorov's time scale:

$$St_\upsilon = \frac{\tau_p}{\tau_\upsilon} \tag{3}$$

The integral time and length scale are dependent on the magnitude of the geometry of the problem, as well as the initial instability conditions (e.g., Karimpour and Chu, 2019;

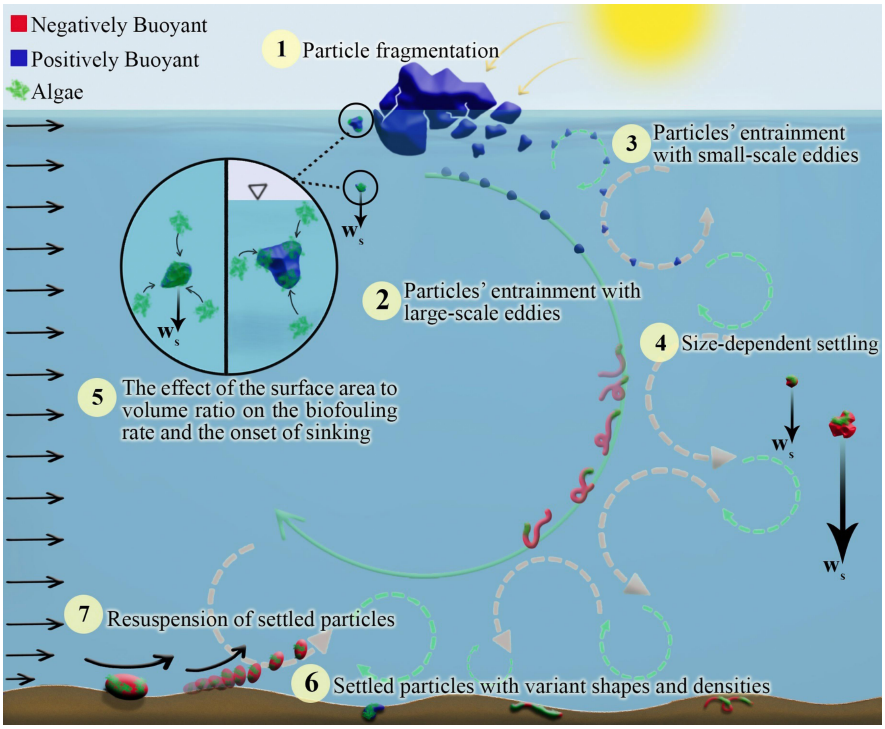

FIGURE 2 | Schematic representation of MP size linkage to different processes: from entrainment and sinking to resuspension. In this figure, MPs of different shapes are illustrated, where red and blue colors present negatively and positively buoyant plastics, respectively.

Karimpour et al., 2021b). The effect of integral scale eddies on entrainment is formulated using the integral time scale:

$$St_l = \frac{\tau_p}{\tau_l} \tag{4}$$

Large Stokes numbers associate with higher particle relaxation time or smaller turbulence time scales. In such conditions, particle engagement with the ambient structure lags, and particles move following their natural sinking or rising behavior. For suspended sediments, large Stokes numbers lead to sinking and deposition to bed. On the contrary, for small Stokes numbers, particles are entrained in the flow and when the Stokes number is very low, particle behavior will be similar to that of a passive scalar. The relevance of these two dimensionless Stokes numbers depends on the particle's size compared to integral and Kolmogorov's length scales (e.g., Gorokhovski and Zamansky, 2018).

As can be seen in Eq. (2), particle relaxation time, τ_p, is a function of the particle size, d, as well as the particle's marginal density from that of ambient water, $(\rho_p - \rho_w)$. Sediment particle density, composed of minerals, is typically between 2.50 to 2.80 g/cm^3. Plastics, on the other hand, possess a wide range of densities: density of foamed PS is a fraction of the density of water, PS can be marginally heavier or lighter than water, whereas PVC can be up to 60% heavier than seawater and freshwater. About 50% of plastics have densities within the 20% margin of seawater and freshwater densities (**Table 1**). The most common polymer types, PE and PP, are marginally lighter than seawater.

Figure 3 is the plot of relaxation time for sediment particles with density of $\rho_p = 2.65$ g/cm^3, positively buoyant plastics with densities between 0.88 and 0.97 g/cm^3, and negatively buoyant plastics with densities of 1.15 and 1.37 g/cm^3. These densities are selected as they represent the minimum and maximum ranges of some of the most common polymer types listed in **Table 1**. Particles with smaller marginal density compared to that of seawater, e.g., 0.97 g/cm^3, correspondingly have a very low overall relaxation time.

A sand particle with a diameter of 0.2 mm, has a relaxation time of about $\tau_p = 0.0036$ s. This relaxation time is attributed to the small particle diameter and marginal density, $(\rho_p - \rho_w)$. Particles smaller than fine sands (including silt and clay) are often entrained with the ambient flow and are transported to distant areas where samples from deep sediments often include silt, clay, and fine sands (e.g., Cunningham et al., 2020). However, MPs have a lower marginal density compared to natural sediments. Therefore, for a turbulent flow with an integral time scale of τ_l and Kolmogorov's time scale of τ_v , MP particles identical to sediments in terms of size and shape exhibit lower Stokes numbers. Due to the lower marginal density of MPs, larger MP particles may entrain in various scales of the turbulent flow. For instance, for a density of 0.88 g/cm^3 and 1.37 g/cm^3, MPs with diameters of 0.7 and 0.4 mm, respectively, exhibit the same relaxation time as sand particles with a diameter of 0.2 mm. For a MP particle, made of heavy PE with a density of 0.97 g/cm^3, particles with a diameter of 1.15 mm exhibit a similar range of relaxation time as fine sand particles. Due to their smaller

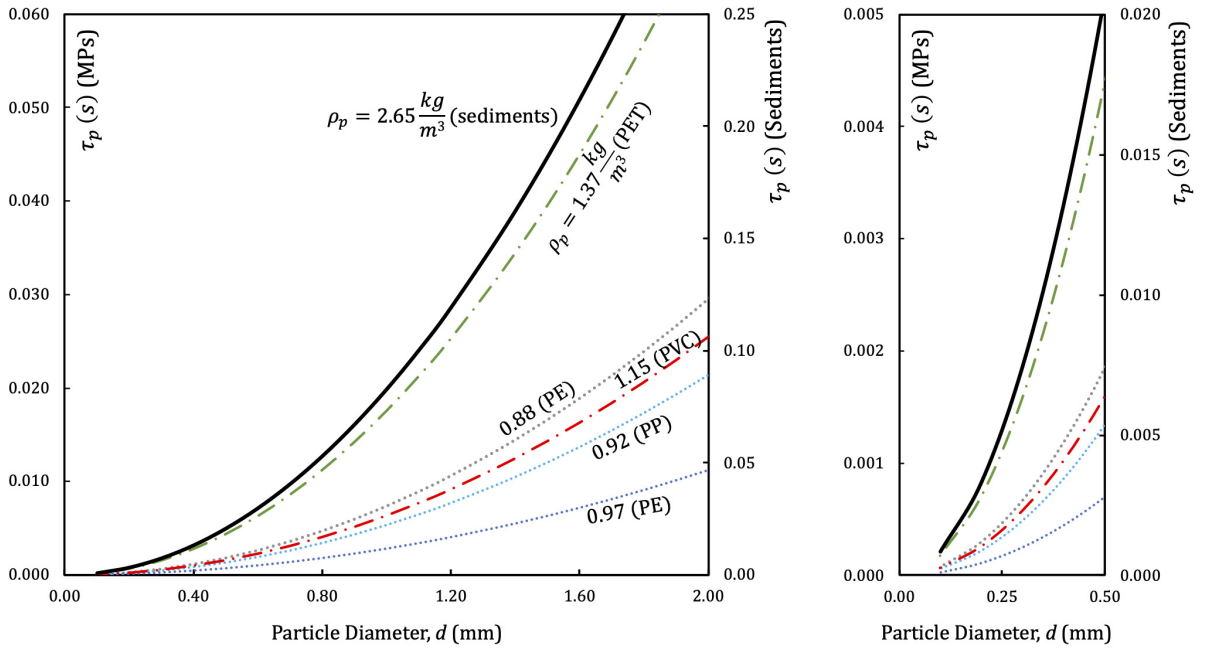

FIGURE 3 | Relaxation time, τ_p, for sediment particles (ρ_p = 2.65 g/cm^3) and microplastic particles (ρ_p = 0.88–1.37 g/cm^3). Figure on the left shows τ_p for particle sizes ranging from 0.1 to 2 mm, whereas figure on the right highlights the range for smaller sizes of 0.1–0.5 mm.

marginal density in turbulent flow, MP particles deviate from their natural sinking or rising behaviors as defined by their density. A combination of MP's marginal density and size will govern the process. As demonstrated in **Figure 2**, small size MP particles with small marginal density can be entrained and transported to areas distant from MP emission sources.

Rising and Settling Velocities of Microplastics

MP particles can either be positively or negatively buoyant, leading to the rising or settling of these contaminants in a motionless water column (**Figure 1**). The rising and settling velocities of MP particles are often assumed to be calculated similarly to those of natural sediments with similar characteristics (e.g., Waldschläger and Schüttrumpf, 2019). However, MP particles have shapes that exhibit complex sinking or rising behaviors (Tanaka and Takada, 2016). In motionless fluid, assuming that vertical forces are limited to gravity, buoyancy, and drag, the steady state particle velocity, w_p, can be estimated based on the following equation:

$$\frac{1}{2} C_D \rho_w A_p w_p^2 = |\rho_p - \rho_w| g V \quad (5)$$

where C_D is the drag coefficient and depends on particle shape and flow regime (e.g., Clift et al., 1978; Chubarenko et al., 2018), A_p is the particle projected area resisting the relative fluid motion, and V is the volume of the particle. Re-arranging Eq. (5) yields:

$$w_p = \sqrt{\frac{2g}{C_D} \frac{|\rho_p - \rho_w|}{\rho_w} \frac{V}{A_p}} \quad (6)$$

In Eq. (6), the volume to projected area ratio, V/A_p, is affected by particle shape which plays a key role in the settling pattern of MPs as it influences the drag coefficient as well as the volume to projected area ratio. MP shape can further affect the sinking or rising behavior of particles in favorable biofouling conditions (see section "Biofouling"). The volume to projected area ratio additionally signifies the role of particle size on settling and rising velocities. The particle size also affects the flow regime that is surrounding the MP particle by impacting the particle's Reynolds number:

$$\mathrm{Re}_p = \frac{w_p d}{\upsilon} \quad (7)$$

For laminar particle Reynolds number, the drag coefficient is larger for smaller particles. Along with a smaller volume to projected area ratio, V/A_p, this leads to a smaller steady state rising or settling velocity for finer particles. For MPs, Kooi et al. (2017) have shown the sinking velocity variability with size. Similar to Eq. (2) for particle relaxation time, Eq. (6) for settling and rising velocity is derived from the particle's force balance, therefore, marginal density, $(\rho_p - \rho_w)$, also appears in this equation. Due to a smaller marginal density in comparison to mineral sediment particles, MPs exhibit smaller settling velocities. The settling velocity of an MP particle with a density of 1.30 g/cm^3 is about 2.3 times slower than the settling velocity of a similarly sized and shaped sediment particle. The ratio for an MP particle of a density of 1.10 g/cm^3 is about 4.0. This leads to longer exposure of small MP particles to in-depth currents and mixing induced by waves, roller, and other wind-induced structures, as well as structures such as thermohaline circulations.

Such entrainment and mixing of MP particles, as evidenced by the Stokes number, results in inhibited sinking and rising.

Biofouling

Biofouling is an important mechanism that impacts the buoyancy of MPs in aquatic systems. The growth and accumulation of microbes, algae, and invertebrates alter the density of MPs, affecting their buoyancy and sinking or rising patterns (Ye and Andrady, 1991; Long et al., 2015). Some of the environmental parameters that affect biofilm formation, growth rate, and composition are depth profiles of light extinction, salinity, density, and viscosity (Kooi et al., 2017). Due to the variability of these environmental factors, the biofouling effect on MP vertical transport is reported to vary in different marine regions and seasons (e.g., Artham et al., 2009; Kaiser et al., 2017). Biofouling formation also depends on polymer composition, surface energy, and the particle's surface roughness (Artham et al., 2009; Andrady, 2011).

For naturally buoyant particles, biofouling results in an increase in apparent density and ultimate sinking. Biofouling also affects the settling behavior of negatively buoyant and naturally sinking particles (Rummel et al., 2017). The change in apparent density of biofouled MPs is directly related to the exterior surface area to volume ratio. This exterior surface area to volume ratio is affected by MP shape (e.g., Ballent et al., 2016; Fazey and Ryan, 2016) and size (Kooi et al., 2017). Based on the exterior surface to volume ratio analysis, Chubarenko et al. (2016) suggested that, for MP shapes of smaller characteristic length in similar environmental conditions, the impact of biofouling progression on density appears faster. Therefore, among different MP shape categories, those with a larger exterior surface area to volume ratio, such as fibers and filaments, will sink faster when exposed to biofouling in contrast to fragments and beads which are slower to respond to biofouling. Kaiser et al. (2017) suggested, however, that even in similar environments, the biofilm composition may be dependent on MP shape. Especially in microfibers, small exterior surface areas and characteristic length may prevent the attachment of some macro-foulants.

For MP particles of similar shapes, when particles are small, due to their large exterior surface area to volume ratio, the buoyancy changes immediately after the particle is exposed to biofouling. On the other hand, for larger particles, the impact of biofouling on particles' buoyancy only emerges after longer exposure, as illustrated in **Figure 2**. Kooi et al. (2017) evaluated settling onset time with different particle radii and densities. For spherical particles of different buoyant polymer types, the sinking onset was estimated at about 26 days for those with a radius of 1–10 mm, while the onset for smaller particles was estimated to occur more rapidly.

Moreover, the impact of biofouling on MP sinking behavior is complex and not solely due to the change in the particle's density. The accumulation of biofilm may alter the overall shape of the particles and affect their roughness. Furthermore, biofilm aggregates can be permeable, affecting the vertical transport patterns (Xiao et al., 2012; Long et al., 2015). Change of buoyancy due to biofouling is evidently affected by the plastic size, where smaller buoyant MPs change buoyancy faster. However, further studies will be required to examine the sinking behaviors of various sized and shaped MPs with different fouling conditions.

Critical Velocity for Resuspension

Negatively buoyant particles that have settled experience shear stress caused by flow velocity. The shear stress exerted on settled particles eventually reaches a value that will force the particles to resuspend, get entrained with the ambient flow, and be transported. A major advancement in sediment resuspension threshold determination was provided by the Shields diagram (Shields, 1936). The threshold developed by Shields (1936) is based on dimensional analysis where:

$$\text{Threshhold} = f\left(\upsilon, d_s, \tau_o, \rho_s, \rho_w, g\right) \tag{8}$$

which yields:

$$\frac{\tau_o}{(\rho_s-\rho_w)gd_s} = f\left(\frac{u_* d_s}{\upsilon}\right) = f\left(\frac{d_s}{\delta}\right) \tag{9}$$

where δ is the thickness of the viscous sublayer, d_s is the sediment size, ρ_s is sediment particle density, and τ_o is the shear stress. The ratio of particle to viscous sub-layer thickness on the right-hand side of Eq. (9), d_s/δ, is defined as the boundary layer Reynolds number, Re_*. Based on the shear stress, τ_o, shear velocity is defined as $u_* = \sqrt{\tau_o/\rho_w}$, which is a measure of the shear stress in the flow. The dimensionless variable on the left-hand-side denotes the ratio of forces acting on a particle affecting its motion and is recognized as Shields number, θ. The Shields diagram identifies the motion threshold based on the Shields number, θ, as a function of the boundary layer Reynolds number, Re_*. The Shields diagram and its variants are discussed in Miller et al. (1977). Similar to sediment particles, MPs that have settled in sediments are prone to resuspension. Chubarenko et al. (2018) have plotted experiments by Ballent et al. (2012) for MP pellets on the Shields diagram and identified the discrepancies in behavior observed between Shields material and MPs. Kane et al. (2020) have used the Shields number to assess the mobility of sedimentary MPs. Re-writing dimensional analysis and incorporating MP particle density, ρ_p, and size, d_p, the MP resuspension threshold becomes:

$$\text{Threshhold for MP Particles} = g\left(\upsilon, d_s, \tau_o, \rho_s, \rho_w, g, d_p, \rho_p\right) \tag{10}$$

which yields:

$$\frac{\tau_o}{\left(\rho_p-\rho_w\right)gd_p} = g\left(\frac{u_* d_s}{\upsilon}, \frac{d_s}{d_p}\right) \tag{11}$$

In Eq. (11), the Shields number, θ, is defined based on MP density, ρ_p, and size, d_p, as this dimensionless number denotes the forces on a MP particle. On the other hand, the boundary layer Reynolds number, Re_*, is governed by bed roughness size, for sediments denoted by d_s, and δ that is the thickness of the viscous sublayer. The impact of sediment to settled MP particle size ratio, d_s/d_p, on boundary layer development is not clear. However, in a few studies on sedimentary MPs, authors have reported sediment aggregate size and alluded to its potential impact on boundary

layer development and resuspension thresholds (Cunningham et al., 2020; Kane et al., 2020).

The impact of MP size on resuspension is clearly demonstrated in Eq. (11). MPs with a smaller characterized dimension, d_p, possess a higher Shields number, and are of greater probability to exceed the threshold of motion. The fine settled particles are more likely to resuspend in a weak flow field and surrender to long-distance transport. The particle's marginal density, $(\rho_p - \rho_w)$, also appears in the definition of this hydrodynamic parameter. With a marginal density difference between the ambient water and MP, smaller shear stresses and shear velocities lead to the resuspension of MPs.

EVIDENCE OF SIZE-SELECTIVE DISTRIBUTION AND TRANSPORT

For this section, literature on marine MP presence and detection is systematically reviewed, focusing on studies that have investigated size and density in various marine compartments. Among more than 200 reviewed studies, although many have reported the size range, only 15 provided size distribution for MP particles. These studies are summarized in **Table 2** and categorized on the basis of the region of the study and vicinity to nearshore for both sediments and surface water. The depth of the sampling is governed by the sampling method. In studies listed for surface water, a variety of sampling techniques, including bulk and volume-reduced sampling methods, were used. In volume-reduced methods employing manta and neuston nets listed in **Table 2**, the depth of the sampling did not exceed 75 cm from the free surface. While for the bulk sampling employed by Enders et al. (2015), the inlet of the pump was submerged to a depth of 3.0 m below the free surface. For studies in sediments, the depth of sampling was measured from the bed and was limited to 65 cm.

The reported abundance, concentration, and polymer type depend on source vicinity, discharge routes, and locally used plastics. The size distribution, however, is an indication of flow hydrodynamics dominating the MP spread and dispersal. Despite the provision of the size range in many reviewed studies, the size distribution is not widely available. In studies that have provided size distribution, there is no standardized size classification as observed by Filella (2015). Furthermore, the lower and upper size limits are bounded by sampling and analytical methods, as well as the objective of the study (see **Table 2** for size range). The lack of a unified and standardized approach amongst different studies has limited the analysis presented in this paper. However, the size distribution in these studies provides insight into the frequency and concentration of various size categories and qualitative descriptions of size distribution profiles.

Impact of Marine Microplastic Size on Surface Water Presence

Waves and currents in coastal regions are the most important factors in the transport, erosion, and deposition of sediments (Inman and Masters, 1991). In nearshore areas, the effect of breaking waves along with the presence of longitudinal currents generated by waves creates a size-selective distribution of sediments. This leads to a heterogeneous sediment distribution, with coarse material remaining on the beach and fine material being washed away. Inman and Bagnold (1963) were among the first to examine nearshore sand distribution based on their size. Finn et al. (2016) analyzed the motion of coarse and fine sand particles under passing surface waves, and found strong spatiotemporal particle size sorting patterns, where vertical size sorting of grains in suspension has been reported. Correspondingly, for microplastics, transport and entrainment induced by coastal sub-surface currents and vortices are size-dependent.

Ryan (2015) has reported the size distribution for plastic debris in nearshore and offshore sites for plastic pieces sized smaller than 60 cm. In the coastal areas, the results indicate that about 60% of plastic pieces were sized smaller than 5 cm. While in offshore regions, about 65% of plastics were sized between 5 to 30 cm. This shows a preferential abundance of larger floating plastic pieces offshore in surface water.

Figure 4 reports the size characteristics for studies in **Table 2** that provided size distribution for surface water in nearshore and offshore regions. In this figure a few features are extracted from the size distribution reported in the original studies: peak size distribution and D_{50}, or vicinity thereof. The peak size boxes in **Figure 4** have variable sizes as the bin sizes vary in different studies. D_{50} is the particle diameter at 50% in the cumulative distribution, demonstrated by a horizontal line for each study. Chae et al. (2015), Qu et al. (2018), and Sagawa et al. (2018) are among the studies that investigated the size distribution of microplastics in coastal areas. The peak size bins in all three studies lie between 100 and 750 μm, whereas D_{50} is approximately smaller than 1,200 μm as shown in **Figure 4A**.

Offshore studies, shown in **Figure 4B**, reported peak frequency or concentration at larger size categories. The peak size bin varies from Reisser et al. (2015), who have reported a peak size of 500–1,000 μm, to Morét-Ferguson et al. (2010) with a peak of 3,000–4,000 μm. Morét-Ferguson et al. (2010) have also used larger bin sizes to provide size distribution. The peak of the distribution, however, lies at a larger size. Furthermore, the vicinity of D_{50} is also identified at a larger size range. Enders et al. (2015) have looked at individual MP particle and fiber size. The mean size reported for particles with shapes other than fibers was notably smaller for both nearshore and offshore regions compared to other studies, as demonstrated in **Figure 4C**. They, however, reported mean size values from nearshore samples that were smaller compared to samples extracted from offshore, open ocean, and subtropical gyres.

For low-density buoyant MPs, with apparent density lower than that of seawater, particle size affects the relaxation time. Smaller MPs have smaller particle relaxation times. Therefore, as buoyant plastics and MPs reach coastal areas, small-sized particles are more likely to separate from the surface layer and get entrained with wave-, wind-, or thermal-induced currents and subsequently get advected and transported offshore. Additionally, small MPs have a larger exterior surface area to volume ratio and therefore, when exposed to biofouling, their onset of sinking is shorter. Due to the combined influence

TABLE 2 | Studies that have identified the size distribution of MPs in nearshore (NS) and offshore (OS) water and offshore sediments.

	Source	Location	Sampling depth (cm)	Sampling technique	Size range (μm)	Dominant shape
Surface water–NS	Qu et al. (2018)	Coastal waters of China	not available	Volumetric steel samplers	[20, 5,000]	Fibers
	Sagawa et al. (2018)	Hiroshima Bay, Japan	0.00–75.00[A]	Neuston net; 75 × 75 × 300 cm^3	(355, 5,000)	–
	Chae et al. (2015)	Korean West Coast	0.00–0.04	Stainless steel sieve; 20 cm diameter	[50, 1,000)	–
	Enders et al. (2015)	Atlantic European Coastal	0.00–300.00	Volumetric sampling using pump	[10, 10,000]	Other than fibers
Surface water–OS	Cózar et al. (2017)	Mediterranean Sea		Manta net; 86 cm width	[320, 860]	
		Arctic Ocean	0.00–15.00			Fragments
		Subtropical Gyres				
	Enders et al. (2015)	North Atlantic Subtropical Gyre	0.00–300.00	Volumetric sampling using pump	[10, 10,000]	Other than fibers
		Atlantic Open Ocean				–
		Atlantic European offshore				–
	Reisser et al. (2015)	North Atlantic sub-tropical gyre	0.00–50.00	Filter net	[500, 5,500)	Fragments
	Cózar et al. (2014)	Malaspina Circumnavigation	0.00—-50.00[A]	Neuston net; 50 × 100 cm^2	[200, 10,000]	Fragments and Sheets
	Morét-Ferguson et al. (2010)	Atlantic Ocean	0.00–25.00	Neuston net; 50 × 100 cm^2	[335, 15,000)	Fragments
	Moore et al. (2001)	North Pacific Central Gyre	0.00–15.00[A]	Manta trawl; 15 × 90 × 350 cm^3	[355, 4,760]	Fragments
Sediment–OS	Courtene-Jones et al. (2020)	Rockall Trough, North Atlantic Ocean	0.00–60.00	Sediment core samples; 60 cm height and 10 cm diameter	[52, 6,500)	Fibers
	Zhang et al. (2020)	Western Pacific Ocean	0.00–5.00	Stainless-steel box corer	[100, 5,000)	Fibers
	Cordova and Wahyudi (2016)	Eastern Indian Ocean	0.00–60.00[B]	Main samples: box corer; 60 × 40 × 50 cm^3; Sub-samples: stainless steel shovel	(20, 500)	Granules
Arctic Sediment–OS	Tekman et al. (2020)	Arctic Ocean	0.00–5.00	A video-guided multiple corer with eight cores of 100 mm diameter	[11, 100)	Fibers
	Mu et al. (2019)	Arctic Ocean	0.00–65.00[B]	Stainless-steel box corer; 50 × 50 × 65 cm^3	[100, 2,000)	Fibers
	Bergmann et al. (2017)	Arctic Ocean	0.00–5.00	A video-guided multiple corer with eight cores of 100 mm diameter	[11, 500)	–

In surface water sampling, depth indicates the depth from the free surface, while in sediments, depth is measured from the bed. Size limitation indicates the minimum threshold dictated by sampling and/or characterization method. Square brackets in size range indicate that the size range is limited to the endpoint, whereas round parentheses mean size range contains values beyond the endpoint.

[A]Water depth was not explicitly provided. Therefore, the maximum net mouth dimension is assumed as the depth.

[B]Sediment depth was not available. Therefore, the maximum core dimension is assumed as the depth.

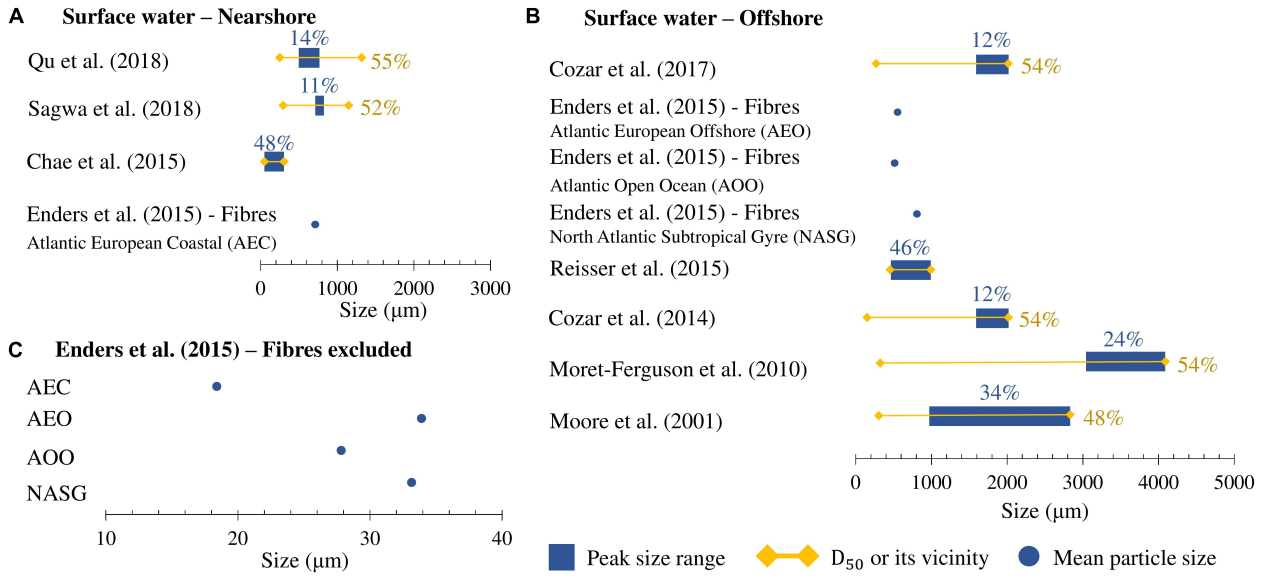

FIGURE 4 | Size distribution characteristics for surface water sample **(A)** nearshore and **(B)** offshore. **(C)** The mean size for MP particles excluding fibers by Enders et al. (2015). The box in each study identifies the size bin with the highest concentration. The size of the box is unique in each study and is consistent with the bin size reported. The horizontal bar in each study is the D_{50} or its proximity. Since bin sizes vary among these studies, D_{50} is determined within ± 5%. The circles are the average MP size presented by selected studies, where size distribution was available but could not be extracted.

of biofouling effect and higher potential for entrainment, they appear less abundant in offshore surface water samples.

Similarly, for fine negatively buoyant MPs, biofouled or pristine, entrainment with in-depth vortices and their offshore transport can be induced by weaker currents. This is further reinforced as smaller negatively buoyant particles sink gradually. Therefore, the presence of small-sized high-density MPs, both biofouled and pristine, in the water column is prolonged. This increases the likelihood of entrainment over time. While, for larger sinking MPs, only strong currents can entrain the particles and lead to offshore transport. Furthermore, the resuspension and mobility of settled MPs are also size dependant. Smaller sized MPs that have settled have a higher Shields number, θ, which leads to a lower resuspension threshold, and a higher likelihood of resuspension.

Deep-Sea Marine Microplastic Presence

Once sediments are transported by fluvial means into marine environments, larger sediments, such as sand, settle in shallower marine environments in nearshore areas. Smaller sediments, such as silt and clay, remain entrained in the currents and are transported offshore. These particles are carried to regions with lower velocity currents and, with a very slow rate, are deposited to the bed. Another main mechanism leading to the bed deposition of sediments is turbidity currents. Turbidity currents originate over continental shelves, where high-density sediment-laden flow plunges down to the seabed. These currents are the primary processes for carrying fine sand to deep-sea sediments. Similarly, MP debris accumulates in seafloor sediments either directly by sinking through the water column, or *via* currents and sediments transported from the fluvial regions (Clark et al., 2016; Kane and Clare, 2019). Some studies suggest that deep-sea sediments can be the sink for lost MPs (e.g., Anderson et al., 2016; Chiba et al., 2018). However, Barrett et al. (2020) have shown the contrary, where the sedimentary deep-sea MPs account for only a small portion of lost MPs. Nevertheless, our analysis of the existing studies on size distribution in nearshore and offshore areas on surface water shows that smaller MPs are missing from the water surface. This corroborates findings by Cózar et al. (2014) that have shown a size-selective absence of MPs from the ocean surface.

Figure 5A shows the peak bin size with the highest concentration and D_{50}, or its proximity, for deep-sea sediments. D_{50} in all cases falls below 1,000 µm, and this value never exceeds the peak bin size. This signifies the abundance of narrow particle size distribution that is limited to very fine MPs in deep-sea sediments. For nearshore surface water samples, although the peak size bin was also reported to be small, D_{50} extended beyond this size showing a wider spread of size distribution. This is attributed to the impact of size in hydrodynamic processes outlined in section "Microplastic Size Impact on Hydrodynamic Parameters." Intrusion of fine MPs in deep-sea sediments can partly explain the absence of these MPs from the water surface in offshore regions.

Remote Areas and Size Distribution

In recent years, the prevalence of MPs in remote Arctic and Antarctic regions has drawn the attention of researchers around the world. MP particles have been found in Arctic and Antarctic surface water (Cózar et al., 2017; Huntington et al., 2020; Tekman et al., 2020) as well as in deep-sea sediment samples (Bergmann et al., 2017; Mu et al., 2019; Huntington et al., 2020;

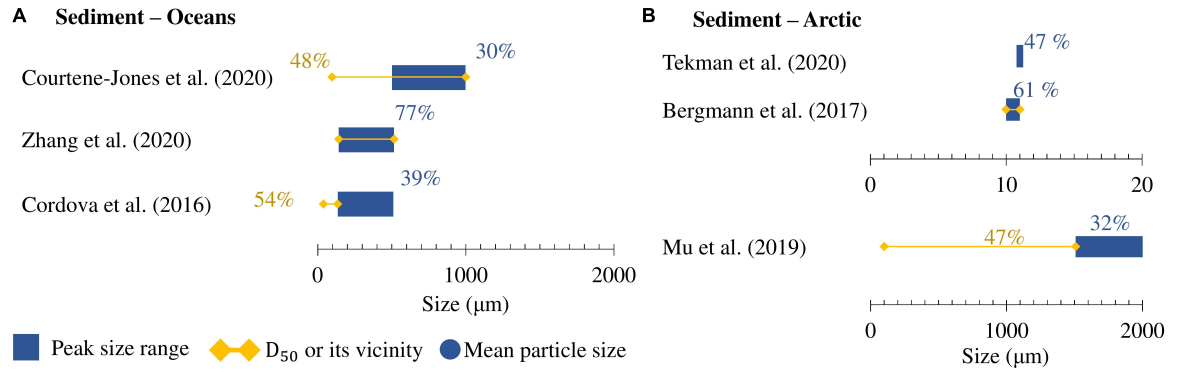

FIGURE 5 | Size distribution characteristics for sediment samples for **(A)** offshore and **(B)** the Arctic. The box in each study identifies the size bin with the highest concentration. The horizontal bar in each study is the D_{50}, or its proximity. The circles are the average MP size presented by selected studies, where size distribution was available but could not be extracted.

Tekman et al., 2020; Adams et al., 2021). The high abundance reported had no correlation with upstream population and was associated with long-distance transport from remote sources (Huntington et al., 2020). Thermohaline currents are among the important processes in the transport of deep fine sediments (Rebesco et al., 2014), and Cózar et al. (2017) attributed the prevalence of MPs in Arctic remote areas to these global currents. The shallow thermohaline currents can redistribute floating plastics from different latitudes (Cózar et al., 2017). On the other hand, deep thermohaline currents will interact with deep-sea sediments and sediment currents, and transport settled, settling, and neutrally buoyant MP pieces (Kane and Clare, 2019).

A few studies have provided the size distribution of MPs in the sediments extracted from Arctic regions (**Figure 5**). All these studies have noted the abundance of fine MPs in sediment samples. In fact, Bergmann et al. (2017) have reported that about 80% of MP particles were sized smaller than 25 μm. The mobility of MP particles induced by the thermohaline currents is dependent on their size. The shear velocity imposed by deep thermohaline currents can lead to resuspension of fine sediments, as well as fine MPs. The turbulent structures induced by this velocity gradient in a thermohaline current (Radko, 2019) can lead to the entrainment and long-distance transport of sediment and MP particles, depending on their size and relaxation time.

POLYMER TYPE AND RELATION TO PARTICLE SIZE AND SHAPE

Plastics are made of different polymers with a wide variety of properties. Plastic density has been highlighted as one of the important properties affecting transport and distribution. Density evidently impacts aquatic MP distribution as it affects the buoyancy of the particle in quiescent fluid. In recent years, Erni-Cassola et al. (2019) and Schwarz et al. (2019) have looked at plastic distribution in different freshwater and marine regions. Schwarz et al. (2019) have consolidated literature on marine sediments, while Erni-Cassola et al. (2019) have gathered evidence on polymer type accumulation in intertidal, subtidal, and deep-sea sediments separately. Both studies have discussed the selectiveness of MP distribution based on density.

Plastics, however, possess other properties that affect their distribution; among these properties are brittleness and flexibility. **Table 3** presents two material properties: Young's Modulus of elasticity, in MPa, and Elongation, in percentage. Young's Modulus is a measure of the ability of a material, plastics in this case, to withstand changes in length when it undergoes tension or compression. Elongation, on the other hand, is a measure of deformation before a material breaks if subjected to a tensile load. Plastic polymers such as HDPE, LDPE, PUR, and PP, have high elongation and can be categorized as ductile, while hard plastics such as PVC, PS, and PET have relatively lower elongation. All three polymers also have high Young's Modulus of elasticity and are more brittle than other plastics listed. This is consistent with the study by Efimova et al. (2018) that examined the fragmentation rate for PS, PS foam, LDPE, and PP. They reported that PS, listed with the lowest elongation in **Table 3**, has the highest fragmentation rate and after 15–18 days of mixing with sediment and water it reached about 80% fragmentation in the form of MPs, in terms of its original mass. Whereas, for PP, a ductile plastic polymer, only 0.07% of the original mass was fragmented into MPs after about 24 days of mixing. Due to their low brittleness, HDPE, LDP, PUR, and PP are resistant to fragmentation. Whereas fast fragmentation to smaller plastics and eventually to smaller-sized MPs is anticipated for PVC, PS, and PET.

As described in section "Microplastic Size Impact on Hydrodynamic Parameters," long-distance transport is size-selective. Given that PVC, PS, and PET are fragmented rapidly, under favorable conditions, they will most likely be entrained and transported farther. The meta-analysis by Erni-Cassola et al. (2019), clearly demonstrated this polymer selectiveness, established by a combination of fast fragmentation, density, and impact of size on transport. In their analysis for subtidal and intertidal sediments, they reported a concentration of between 25 and 40% for polyester, polyamide, and acrylic. Whereas, in deep-sea marine sediments their compilation yielded a higher

TABLE 3 | Young's modulus of elasticity and elongation for selected polymer types (Harper and Petrie, 2003).

Polymer type	Young's modulus (MPa)	Elongation (%)
Polyethylene, HDPE	1,069–1,089	10–1,200
Polyethylene, LDPE	172–282	100–650
Polypropylene (PP)	1,138–1,551	100–600
Polyvinyl chloride (PVC), hard	2,413–4,137	40–80
Polyurethane (PUR)	0.17–34.47	250–800
Polyethylene terephthalate (PET/PETE)	2,758–4,137	30–300
Polystyrene (PS/EPS)	2,275–3,275	1.2–2.5
Polyamide (PA6)	2,000	65–150
Polyamide (PA66)	1,586–3,447	150–300

concentration of roughly 75% for polyester, polyamide, and acrylic. The demand for polyester, made of PET, is about 8% and demand for polyamide is 2%. If the density is considered as the sole plastic property governing the distribution, all land-based debris pieces composed of PET, polyamide, and acrylic should settle nearshore as these polymers have densities higher than those of both seawater and freshwater. Due to their high fragmentation rate and smaller size, particles made of these polymers can be transported offshore and settle in areas with slow ambient velocities. The high concentration of polyester, polyamide, and acrylic in deep-sea sediment is due to the combination of polymer properties, including their brittleness, measured by elongation and density, as well as particle's shape. The presence of small-sized MPs, based on the evidence presented in this paper, along with the abundance of polyester, polyamide, and acrylic in deep-sea sediments conform with observations reported for MP shape in this compartment. All the studies listed in **Table 2** for deep-sea sediments have reported MP shape categories. Courtene-Jones et al. (2020) and Zhang et al. (2020) have distinctly reported fibers as the dominant shape. Microfibers are also found in higher percentages in other studies conducted for deep-sea sediments (e.g., Woodall et al., 2014). The abundance of microfibers is consistent with the reported polymer types, as microfibers used in textiles are commonly made of polyester, polyamide, and acrylic (Henry et al., 2019). Other factors have also been linked with the abundance of microfibers in deep-sea sediments. Owing to their distinct shape, Kane and Clare (2019) suggested that microfibers can be transported by gravity currents to deeper sediments. Furthermore, as discussed in this paper, microfibers possess a larger exterior surface to volume ratio, which would lead to fast alteration in buoyancy if exposed to biofouling. The combination of brittleness and density of these polymers with the unique shape of microfibers leads to their intrusion into deep-sea sediments.

For offshore surface water, a compilation by Erni-Cassola et al. (2019) shows that more than 75% of polymers present are either PP or PE, while the demand for these 2 polymers combined is about 50%. These polymers are ductile and are not easily fragmented. As described in this study, in this compartment, MPs have a larger mean particle size. Due to their size, stemming from their slow fragmentation, these plastics remain afloat as they are associated with larger Stokes numbers. Moreover, among the studies compiled here for surface water offshore, all have provided shape categories. Aside from Enders et al. (2015), all studies in this category have identified fragments as the dominant shape which was also reported by Woodall et al. (2014), among others. The combination of buoyancy and slow fragmentation rate leads to the presence of PP and PE particles in the surface, which is also related to a higher concentration of larger fragments in this compartment.

In nearshore surface water, however, authors did not find a consistently dominant shape in various studies. While Qu et al. (2018) reported fibers as the dominant shape, other studies such as Song et al. (2014) have reported fragments to be dominant. Furthermore, polymer analysis, conducted by Erni-Cassola et al. (2019) in the intertidal region, has shown the presence of multiple polymer types. This is likely due to the closer proximity of nearshore water to both marine and terrestrial plastic sources. Due to source variability in different geographical regions, plastic shapes and polymers found in studies conducted in the nearshore water are diverse.

As noted by Schwarz et al. (2019), the abundance of PVC in all freshwater and marine compartments is very low, while its production comprises about 10% of plastic demand. PVC is mainly used in building and construction (Plastics Europe, 2020) and, due to its extended life-cycle and better end-of-life waste management, provides a smaller contribution to freshwater and marine plastic pollution. Similarly, PUR is highly used in automotive and building and construction sectors, hence they also have not been reported in high concentrations in aquatic systems. PS is the polymer with the smallest elongation listed in **Table 2**. This polymer has been reported in various environmental compartments in both freshwater and marine surface and sediment samples (Erni-Cassola et al., 2019; Schwarz et al., 2019). This is due to the small marginal density of this polymer, $\left(\rho_p - \rho_w\right)$, combined with fast fragmentation. Once broken down into fine MPs, PS particles behave similarly to a passive scalar and disperse easily with the flow.

DISCUSSION AND RECOMMENDATION FOR FUTURE WORK

Aside from hydrodynamic and environmental factors, MPS' mobility is affected by their properties. These properties include polymer density, particle shape, and size. Motion of a MP particle, even in a quiescent fluid, is affected by all three properties: density dominates the buoyancy of the particle, shape affects the drag force, and size affects the magnitude of buoyant and gravitational forces as well as the magnitude of the drag force. Significant emphasis has been put on plastic density in the literature, as it is undeniably a critical factor in the distribution of plastics. Furthermore, to understand the mobility of MPs in terms of natural sediment particles, efforts have been made to define MPs by shape categories and, accordingly, define shape factors (Camenen, 2007; Kowalski et al., 2016). MP shape is also strongly linked to biofouling. The analogy with sediment particles infers that MP size is another important driver in MP distribution and mobility. Our assessment of several hydrodynamic factors,

namely relaxation time, settling and rise velocity, and Shields parameter indicates that MP particle size is directly tied to these parameters. Smaller-sized MPs exhibit lower relaxation time, lower settling velocity, faster onset of sinking if exposed to biofouling, and a lower Shields number.

These parameters affect the mobility of MP particles and their transport to regions distant from their source of emission. Our analysis of 15 studies that have provided size distribution for different regions of marine systems, also confirms this correlation. Nearshore surface water samples that are often closer to the emission source have exhibited a smaller D_{50}, while offshore surface water samples have shown a larger D_{50}, where aged plastics have undergone weathering and smaller MPs should be more abundant. This trend has been previously attributed to biofouling and faster onset of sinking for small MPs (Kooi et al., 2017). Our analysis suggests that other factors may contribute to the absence of small-sized MPs from the surface in offshore areas. Entrainment and in-depth mixing lead to the entrainment and long-distance transport of fine MPs. Similarly, small MPs can be entrained and advected with thermohaline circulation resulting in their deposit in remote Arctic areas. Furthermore, polymer fragmentation rates affect plastic size and, ultimately, its transport. Brittle polymers are fragmented into smaller MPs and are more abundant in far and remote areas. Along with microfibers' unique shape, this supports the presence of fibers in deep-sea sediments. On the other hand, polymers with slow fragmentation rates are found in larger fragment shapes in the offshore water surface. The studies that were presented in **Table 2** and analyzed in **Figures 4**, **5** were selected based on size distribution availability. However, these studies did not employ a standardized sampling, separation, and identification method or protocol. For in-depth and meaningful comparison and monitoring, it is critical to define and implement a standard method for all three steps to estimate the abundance, distribution, and composition of MPs. The size distribution range and bin sizes reported, therefore, were different since authors used different approaches. This has limited our analysis of existing literature and adds uncertainty to the analysis. Hence, we have limited our discussion and examination of these studies to qualitative analysis and have not provided aggregated size ranges herein.

This study highlights the importance of MP size, along with polymer composition and shape, in their mobility. Given the lack of data in size distribution, future quantitative studies should carefully examine the size distribution and limitations imposed by sampling and analysis. In using the analogy with natural sediments in terms of MP size, further research is required to investigate the linkage between MP shape, size, and density. Unlike mineral sediments, MPs are versatile in terms of their density and shape. As outlined in this study, marginal density, shape, and size appear in most hydrodynamic parameters, therefore, the definition of size categories for MPs should include consideration for other MP properties.

AUTHOR CONTRIBUTIONS

AS contributed to the core concept, conducted literature review, prepared the figures and tables, and contributed to the manuscript. ZL conducted literature review and contributed to the manuscript. PP conducted literature review, prepared tables, and contributed to the manuscript. SK contributed to ideation and core concept, supervised students, and wrote the manuscript. All authors contributed to the article and approved the submitted version.

FUNDING

This work was supported by the Natural Sciences and Engineering Research Council of Canada (Grant#: RGPIN-2020-06101) and the Social Sciences and Humanities Research Council (Grant#: 872-2019-1030).

REFERENCES

Adams, J. K., Dean, B. Y., Athey, S. N., Jantunen, L. M., Bernstein, S., Stern, G., et al. (2021). Anthropogenic particles (including microfibers and microplastics) in marine sediments of the Canadian Arctic. *Sci. Total Environ.* 784:147155. doi: 10.1016/j.scitotenv.2021.147155

Anderson, J. C., Park, B. J., and Palace, V. P. (2016). Microplastics in aquatic environments: implications for Canadian ecosystems. *Environ. Pollut.* 218, 269–280. doi: 10.1016/j.envpol.2016.06.074

Andrady, A. L. (2011). Microplastics in the marine environment. *Mar. Pollut. Bull.* 62, 1596–1605.

Artham, T., Sudhakar, M., Venkatesan, R., Nair, C. M., Murty, K. V. G. K., and Doble, M. (2009). Biofouling and stability of synthetic polymers in sea water. *Int. Biodeterior. Biodegradation* 63, 884–890.

Baldwin, A. K., Corsi, S. R., and Mason, S. A. (2016). Plastic debris in 29 Great Lakes tributaries: relations to watershed attributes and hydrology. *Environ. Sci. Technol.* 50, 10377–10385. doi: 10.1021/acs.est.6b02917

Ballent, A., Corcoran, P. L., Madden, O., Helm, P. A., and Longstaffe, F. J. (2016). Sources and sinks of microplastics in Canadian Lake Ontario nearshore, tributary and beach sediments. *Mar. Pollut. Bull.* 110, 383–395. doi: 10.1016/j.marpolbul.2016.06.037

Ballent, A., Purser, A., de Jesus Mendes, P., Pando, S., and Thomsen, L. (2012). Physical transport properties of marine microplastic pollution. *Biogeosci. Discuss.* 9, 18755–18798.

Barrett, J., Chase, Z., Zhang, J., Holl, M. M. B., Willis, K., Williams, A., et al. (2020). Microplastic pollution in deep-sea sediments from the great Australian bight. *Front. Mar. Sci.* 7:576170. doi: 10.3389/fmars.2020.576170

Bergmann, M., Wirzberger, V., Krumpen, T., Lorenz, C., Primpke, S., Tekman, M. B., et al. (2017). High quantities of microplastic in Arctic deep-sea sediments from the HAUSGARTEN observatory. *Environ. Sci. Technol.* 51, 11000–11010. doi: 10.1021/acs.est.7b03331

Camenen, B. (2007). Simple and general formula for the settling velocity of particles. *J. Hydraulic Eng.* 133, 229–233. doi: 10.1061/(ASCE)0733-9429(2007)133:2(229)

Chae, D. H., Kim, I. S., Kim, S. K., Song, Y. K., and Shim, W. J. (2015). Abundance and distribution characteristics of microplastics in surface seawaters of the Incheon/Kyeonggi coastal region. *Arch. Environ. Contam. Toxicol.* 69, 269–278. doi: 10.1007/s00244-015-0173-4

Chiba, S., Saito, H., Fletcher, R., Yogi, T., Kayo, M., Miyagi, S., et al. (2018). Human footprint in the abyss: 30 year records of deep-sea plastic debris. *Mar. Policy* 96, 204–212.

Chubarenko, I., Bagaev, A., Zobkov, M., and Esiukova, E. (2016). On some physical and dynamical properties of microplastic particles in marine environment. *Mar. Pollut. Bull.* 108, 105–112.

Chubarenko, I., Esiukova, E., Bagaev, A., Isachenko, I., Demchenko, N., Zobkov, M., et al. (2018). "Behavior of microplastics in coastal zones," in *Microplastic Contamination In Aquatic Environments*, ed. E. Y. Zeng (Amsterdam: Elsevier), 175–223.

Clark, J. R., Cole, M., Lindeque, P. K., Fileman, E., Blackford, J., Lewis, C., et al. (2016). Marine microplastic debris: a targeted plan for understanding and quantifying interactions with marine life. *Front. Ecol. Environ.* 14:317–324. doi: 10.1002/fee.1297

Clift, R., Grace, J. R., and Weber, M. E. (1978). "Nonspherical rigid particles at higher Reynolds numbers," in *Bubbles Drops and Particles*, eds R. Clift, J. R. Grace, M. E. Weber, and M. F. Weber (Cambridge, MA: Academic Press), 142–168.

Cole, M., Lindeque, P., Fileman, E., Halsband, C., Goodhead, R., Moger, J., et al. (2013). Microplastic ingestion by zooplankton. *Environ. Sci. Technol.* 47, 6646–6655.

Cordova, M. R., and Wahyudi, A. (2016). Microplastic in the deep-sea sediment of Southwestern Sumatran Waters. *Mar. Res. Indones.* 41, 27–35.

Courtene-Jones, W., Quinn, B., Ewins, C., Gary, S. F., and Narayanaswamy, B. E. (2020). Microplastic accumulation in deep-sea sediments from the Rockall Trough. *Mar. Pollut. Bull.* 154:111092. doi: 10.1016/j.marpolbul.2020.111092

Cózar, A., Echevarría, F., González-Gordillo, J. I, Irigoien, X., Úbeda, B., Hernández-León, S., et al. (2014). Plastic debris in the open ocean. *Proc. Natl. Acad. Sci. U.S.A.* 111, 10239–10244.

Cózar, A., Martí, E., Duarte, C. M., García-de-Lomas, J., Van Sebille, E., Ballatore, T. J., et al. (2017). The Arctic Ocean as a dead end for floating plastics in the North Atlantic branch of the Thermohaline Circulation. *Sci. Adv.* 3:e1600582. doi: 10.1126/sciadv.1600582

Cunningham, E. M., Ehlers, S. M., Dick, J. T., Sigwart, J. D., Linse, K., Dick, J. J., et al. (2020). High abundances of microplastic pollution in deep-sea sediments: evidence from Antarctica and the Southern Ocean. *Environ. Sci. Technol.* 54, 13661–13671. doi: 10.1021/acs.est.0c03441

Dalu, T., Banda, T., Mutshekwa, T., Munyai, L. F., and Cuthbert, R. N. (2021). Effects of urbanisation and a wastewater treatment plant on microplastic densities along a subtropical river system. *Environ. Sci. Pollut. Res.* 28, 36102–36111. doi: 10.1007/s11356-021-13185-1

Dey, S., Zeeshan Ali, S., and Padhi, E. (2019). Terminal fall velocity: the legacy of Stokes from the perspective of fluvial hydraulics. *Proc. R. Soc. A* 475:20190277. doi: 10.1098/rspa.2019.0277

Di, M., and Wang, J. (2018). Microplastics in surface waters and sediments of the Three Gorges Reservoir, China. *Sci. Total Environ.* 616, 1620–1627.

Efimova, I., Bagaeva, M., Bagaev, A., Kileso, A., and Chubarenko, I. P. (2018). Secondary microplastics generation in the sea swash zone with coarse bottom sediments: laboratory experiments. *Front. Mar. Sci.* 5:313. doi: 10.3389/fmars.2018.00313

Enders, K., Lenz, R., Stedmon, C. A., and Nielsen, T. G. (2015). Abundance, size and polymer composition of marine microplastics $\geq$ 10 μm in the Atlantic Ocean and their modelled vertical distribution. *Mar. Pollut. Bull.* 100, 70–81. doi: 10.1016/j.marpolbul.2015.09.027

Erni-Cassola, G., Zadjelovic, V., Gibson, M. I., and Christie-Oleza, J. A. (2019). Distribution of plastic polymer types in the marine environment; a meta-analysis. *J. Hazard. Mater.* 369, 691–698. doi: 10.1016/j.jhazmat.2019.02.067

Fazey, F. M., and Ryan, P. G. (2016). Biofouling on buoyant marine plastics: an experimental study into the effect of size on surface longevity. *Environ. Pollut.* 210, 354–360. doi: 10.1016/j.envpol.2016.01.026

Filella, M. (2015). Questions of size and numbers in environmental research on microplastics: methodological and conceptual aspects. *Environ. Chem.* 12, 527–538.

Finn, J. R., Li, M., and Apte, S. V. (2016). Particle based modelling and simulation of natural sand dynamics in the wave bottom boundary layer. *J. Fluid Mech.* 796, 340–385.

Fossi, M. C., Panti, C., Guerranti, C., Coppola, D., Giannetti, M., Marsili, L., et al. (2012). Are baleen whales exposed to the threat of microplastics? A case study of the Mediterranean fin whale (*Balaenoptera physalus*). *Mar. Pollut. Bull.* 64, 2374–2379. doi: 10.1016/j.marpolbul.2012.08.013

Good, G. H., Ireland, P. J., Bewley, G. P., Bodenschatz, E., Collins, L. R., and Warhaft, Z. (2014). Settling regimes of inertial particles in isotropic turbulence. *J. Fluid Mech.* 759:R3. doi: 10.1103/PhysRevLett.117.064501

Gorokhovski, M., and Zamansky, R. (2018). Modeling the effects of small turbulent scales on the drag force for particles below and above the Kolmogorov scale. *Phys. Rev. Fluids* 3:034602.

Harper, C. A., and Petrie, E. M. (2003). *Plastics Materials And Processes: A Concise Encyclopedia*. Hoboken, NJ: John Wiley & Sons.

Heitmuller, F. T., and Hudson, P. F. (2009). Downstream trends in sediment size and composition of channel-bed, bar, and bank deposits related to hydrologic and lithologic controls in the Llano River watershed, central Texas, USA. *Geomorphology* 112, 246–260.

Henry, B., Laitala, K., and Klepp, I. G. (2019). Microfibres from apparel and home textiles: prospects for including microplastics in environmental sustainability assessment. *Sci. Total Environ.* 652, 483–494. doi: 10.1016/j.scitotenv.2018.10.166

Hidalgo-Ruz, V., Gutow, L., Thompson, R. C., and Thiel, M. (2012). Microplastics in the marine environment: a review of the methods used for identification and quantification. *Environ. Sci. Technol.* 46, 3060–3075.

Huntington, A., Corcoran, P. L., Jantunen, L., Thaysen, C., Bernstein, S., Stern, G. A., et al. (2020). A first assessment of microplastics and other anthropogenic particles in Hudson Bay and the surrounding eastern Canadian Arctic waters of Nunavut. *Facets* 5, 432–454.

Inman, D. L., and Bagnold, R. A. (1963). "Beach and nearshore processes. Part II. Littoral processes," in *The Sea: Ideas and Observations*, ed. M. N. Hille (Cambridge, MA: Harvard University Press), 529–553.

Inman, D. L., and Masters, P. M. (1991). "Coastal sediment transport concepts and mechanisms," in *Coast of California Storm and Tidal Waves Study: State of the Coast Report*, (Los Angeles, CA: U.S. Army Corps of Engineers). Available online at: https://escholarship.org/uc/item/8tc9x82q

Kaiser, D., Kowalski, N., and Waniek, J. J. (2017). Effects of biofouling on the sinking behavior of microplastics. *Environ. Res. Lett.* 12:124003.

Kane, I. A., and Clare, M. A. (2019). Dispersion, accumulation, and the ultimate fate of microplastics in deep-marine environments: a review and future directions. *Front. Earth Sci.* 7:80.

Kane, I. A., Clare, M. A., Miramontes, E., Wogelius, R., Rothwell, J. J., Garreau, P., et al. (2020). Seafloor microplastic hotspots controlled by deep-sea circulation. *Science* 368, 1140–1145. doi: 10.1126/science.aba5899

Karimpour, S., and Chu, V. H. (2019). The role of waves on mixing in shallow waters. *Can. J. Civil Eng.* 46, 134–147.

Karimpour, S., Wang, T., and Chu, V. H. (2021b). The exchanges between the mainstream in an open channel and a recirculating flow on its side at large Froude numbers. *J. Fluid Mech.* 920:A8.

Karimpour, S., Brar, S. K., and Shirkhani, H. (2021a). *The Fate And Transport Of Microplastics In Aquatic Ecosystems: Synthesis And Directions For Future Research*. Ottawa, ONT: Social Sciences and Humanities Research Council (SSHRC) of Canada.

Khatmullina, L., and Isachenko, I. (2017). Settling velocity of microplastic particles of regular shapes. *Mar. Pollut. Bull.*114, 871–880. doi: 10.1016/j.marpolbul.2016.11.024

Kooi, M., Nes, E. H. V., Scheffer, M., and Koelmans, A. A. (2017). Ups and downs in the ocean: effects of biofouling on vertical transport of microplastics. *Environ. Sci. Technol.* 51, 7963–7971. doi: 10.1021/acs.est.6b04702

Kowalski, N., Reichardt, A. M., and Waniek, J. J. (2016). Sinking rates of microplastics and potential implications of their alteration by physical, biological, and chemical factors. *Mar. Pollut. Bull.* 109, 310–319. doi: 10.1016/j.marpolbul.2016.05.064

Lagarde, F., Olivier, O., Zanella, M., Daniel, P., Hiard, S., and Caruso, A. (2016). Microplastic interactions with freshwater microalgae: hetero-aggregation and changes in plastic density appear strongly dependent on polymer type. *Environ. Pollut.* 215, 331–339. doi: 10.1016/j.envpol.2016.05.006

Lehtiniemi, M., Hartikainen, S., Näkki, P., Engström-Öst, J., Koistinen, A., and Setälä, O. (2018). Size matters more than shape: ingestion of primary and secondary microplastics by small predators. *Food Webs* 17:e00097.

Long, M., Moriceau, B., Gallinari, M., Lambert, C., Huvet, A., Raffray, J., et al. (2015). Interactions between microplastics and phytoplankton aggregates: impact on their respective fates. *Mar. Chem.* 175, 39–46.

Lusher, A. (2015). "Microplastics in the marine environment: distribution, interactions and effects," in *Marine Anthropogenic Litter*, eds M. Bergmann, L. Gutow, and M. Klages (Cham: Springer), 245–307.

Miller, M. C., McCave, I. N., and Komar, P. (1977). Threshold of sediment motion under unidirectional currents. *Sedimentology* 24, 507–527.

Moore, C. J., Moore, S. L., Leecaster, M. K., and Weisberg, S. B. (2001). A comparison of plastic and plankton in the North Pacific central gyre. *Mar. Pollut. Bull.* 42, 1297–1300. doi: 10.1016/s0025-326x(01)00114-x

Morét-Ferguson, S., Law, K. L., Proskurowski, G., Murphy, E. K., Peacock, E. E., and Reddy, C. M. (2010). The size, mass, and composition of plastic debris in the western North Atlantic Ocean. *Mar. Pollut. Bull.* 60, 1873–1878. doi: 10.1016/j.marpolbul.2010.07.020

Mu, J., Qu, L., Jin, F., Zhang, S., Fang, C., Ma, X., et al. (2019). Abundance and distribution of microplastics in the surface sediments from the northern Bering and Chukchi Seas. *Environmental Pollution* 245, 122–130. doi: 10.1016/j.envpol.2018.10.097

Murphy, F., Ewins, C., Carbonnier, F., and Quinn, B. (2016). Wastewater treatment works (WwTW) as a source of microplastics in the aquatic environment. *Environ. Sci. Technol.* 50, 5800–5808.

Naidoo, T., Glassom, D., and Smit, A. J. (2015). Plastic pollution in five urban estuaries of KwaZulu-Natal, South Africa. *Mar. Pollut. Bull.* 101, 473–480. doi: 10.1016/j.marpolbul.2015.09.044

Napper, I. E., Davies, B. F., Clifford, H., Elvin, S., Koldewey, H. J., Mayewski, P. A., et al. (2020). Reaching new heights in plastic pollution—preliminary findings of microplastics on Mount Everest. *One Earth* 3, 621–630.

Plastics Europe (2020). *Plastics – The Facts 2020: An Analysis Of European Plastics Production, Demand And Waste Data*. Brussels: Plastic Europe.

Qu, X., Su, L., Li, H., Liang, M., and Shi, H. (2018). Assessing the relationship between the abundance and properties of microplastics in water and in mussels. *Sci. Total Environ.* 621, 679–686.

Radko, T. (2019). Thermohaline-shear instability. *Geophys. Res. Lett.* 46, 822–832.

Rebesco, M., Hernández-Molina, F. J., Van Rooij, D., and Wåhlin, A. (2014). Contourites and associated sediments controlled by deep-water circulation processes: state-of-the-art and future considerations. *Mar. Geol.* 352, 111–154.

Reisser, J., Slat, B., Noble, K., Du Plessis, K., Epp, M., Proietti, M., et al. (2015). The vertical distribution of buoyant plastics at sea: an observational study in the North Atlantic Gyre. *Biogeosciences* 12, 1249–1256.

Rochman, C. M., Hoh, E., Kurobe, T., and Teh, S. J. (2013). Ingested plastic transfers hazardous chemicals to fish and induces hepatic stress. *Sci. Rep.* 3, 1–7. doi: 10.1038/srep03263

Rummel, C. D., Jahnke, A., Gorokhova, E., Kühnel, D., and Schmitt-Jansen, M. (2017). Impacts of biofilm formation on the fate and potential effects of microplastic in the aquatic environment. *Environ. Sci. Technol. Lett.* 4, 258–267.

Ryan, P. G. (2015). Does size and buoyancy affect the long-distance transport of floating debris? *Environ. Res. Lett.* 10:084019.

Sagawa, N., Kawaai, K., and Hinata, H. (2018). Abundance and size of microplastics in a coastal sea: comparison among bottom sediment, beach sediment, and surface water. *Mar. Pollut. Bull.* 133, 532–542. doi: 10.1016/j.marpolbul.2018.05.036

Schwarz, A. E., Ligthart, T. N., Boukris, E., and Van Harmelen, T. (2019). Sources, transport, and accumulation of different types of plastic litter in aquatic environments: a review study. *Mar. Pollut. Bull.* 143, 92–100. doi: 10.1016/j.marpolbul.2019.04.029

Shields, A. (1936). *Application Of Similarity Principles And Turbulence Research To Bed-Load Movement*. Pasadena, CA: California Institute of Technology.

Song, Y. K., Hong, S. H., Jang, M., Kang, J. H., Kwon, O. Y., Han, G. M., et al. (2014). Large accumulation of micro-sized synthetic polymer particles in the sea surface microlayer. *Environ. Sci. Technol.* 48, 9014–9021. doi: 10.1021/es501757s

Suaria, G., Avio, C. G., Mineo, A., Lattin, G. L., Magaldi, M. G., Belmonte, G., et al. (2016). The mediterranean plastic soup: synthetic polymers in mediterranean surface waters. *Sci. Rep.* 6, 1–10. doi: 10.1038/srep37551

Tanaka, K., and Takada, H. (2016). Microplastic fragments and microbeads in digestive tracts of planktivorous fish from urban coastal waters. *Sci. Rep.* 6, 1–8. doi: 10.1038/srep34351

Tekman, M. B., Wekerle, C., Lorenz, C., Primpke, S., Hasemann, C., Gerdts, G., et al. (2020). Tying up loose ends of microplastic pollution in the Arctic: distribution from the sea surface through the water column to deep-sea sediments at the Hausgarten observatory. *Environ. Sci. Technol.* 54, 4079–4090. doi: 10.1021/acs.est.9b06981

Teuten, E. L., Rowland, S. J., Galloway, T. S., and Thompson, R. C. (2007). Potential for plastics to transport hydrophobic contaminants. *Environ. Sci. Technol.* 41, 7759–7764.

Thompson, R. C., Olsen, Y., Mitchell, R. P., Davis, A., Rowland, S. J., John, A. W., et al. (2004). Lost at sea: where is all the plastic? *Science (Washington)* 304, 838.

Van Cauwenberghe, L., Vanreusel, A., Mees, J., and Janssen, C. R. (2013). Microplastic pollution in deep-sea sediments. *Environ. Pollut.* 182, 495–499.

Van Sebille, E., Aliani, S., Law, K. L., Maximenko, N., Alsina, J. M., Bagaev, A., et al. (2020). The physical oceanography of the transport of floating marine debris. *Environ. Res. Lett.* 15:023003.

Waldschläger, K., and Schüttrumpf, H. (2019). Effects of particle properties on the settling and rise velocities of microplastics in freshwater under laboratory conditions. *Environ. Sci. Technol.* 53, 1958–1966. doi: 10.1021/acs.est.8b06794

Waldschläger, K., Born, M., Cowger, W., Gray, A., and Schüttrumpf, H. (2020). Settling and rising velocities of environmentally weathered micro-and macroplastic particles. *Environ. Res.* 191:110192. doi: 10.1016/j.envres.2020.110192

Wang, L. P., and Maxey, M. R. (1993). Settling velocity and concentration distribution of heavy particles in homogeneous isotropic turbulence. *J. Fluid Mech.* 256, 27–68.

Wang, Y., Lam, K. M., and Lu, Y. (2018). Settling velocity of fine heavy particles in turbulent open channel flow. *Phys. Fluids* 30:095106.

Woodall, L. C., Sanchez-Vidal, A., Canals, M., Paterson, G. L., Coppock, R., Sleight, V., et al. (2014). The deep sea is a major sink for microplastic debris. *R. Soc. Open Sci.* 1:140317.

Xiao, F., Li, X., Lam, K., and Wang, D. (2012). Investigation of the hydrodynamic behavior of diatom aggregates using particle image velocimetry. *J. Environ. Sci.* 24, 1157–1164. doi: 10.1016/s1001-0742(11)60960-1

Yang, H., and Shi, C. (2019). Sediment grain-size characteristics and its sources of ten wind-water coupled erosion tributaries (the Ten Kongduis) in the Upper Yellow River. *Water* 11:115.

Ye, S., and Andrady, A. L. (1991). Fouling of floating plastic debris under Biscayne Bay exposure conditions. *Mar. Pollut. Bull.* 22, 608–613.

Zhang, D., Liu, X., Huang, W., Li, J., Wang, C., Zhang, D., et al. (2020). Microplastic pollution in deep-sea sediments and organisms of the Western Pacific Ocean. *Environ. Pollut.* 259:113948. doi: 10.1016/j.envpol.2020.113948

Zhang, H. (2017). Transport of microplastics in coastal seas. *Estuar. Coast. Shelf Sci.* 199, 74–86.

Conflict of Interest: The authors declare that the research was conducted in the absence of any commercial or financial relationships that could be construed as a potential conflict of interest.

Publisher's Note: All claims expressed in this article are solely those of the authors and do not necessarily represent those of their affiliated organizations, or those of the publisher, the editors and the reviewers. Any product that may be evaluated in this article, or claim that may be made by its manufacturer, is not guaranteed or endorsed by the publisher.

frontiers | Frontiers in Marine Science

ORIGINAL RESEARCH
published: 04 April 2022
doi: 10.3389/fmars.2022.849819

Long-Term Harmful Algal Blooms and Nutrients Patterns Affected by Climate Change and Anthropogenic Pressures in the Zhanjiang Bay, China

Peng Zhang[1], Conghui Peng[1], Jibiao Zhang[1], Junxiao Zhang[2,3], Jiyu Chen[2,3] and Hui Zhao[1]*

[1] College of Chemistry and Environmental Science, Guangdong Ocean University, Zhanjiang, China, [2] South China Sea Marine Technology and Survey Center, State Oceanic Administration, Guangzhou, China, [3] Key Laboratory of Marine Environmental Survey Technology and Application, Ministry of Natural Resources, Guangzhou, China

OPEN ACCESS

Edited by:
Kenneth Mei Yee Leung, City University of Hong Kong, Hong Kong SAR, China

Reviewed by:
Xingyu Song, South China Sea Institute of Oceanology (CAS), China
Yongyu Zhang, Qingdao Institute of Bioenergy and Bioprocess Technology (CAS), China

***Correspondence:**
Jibiao Zhang
zhangjb@gdou.edu.cn

Specialty section:
This article was submitted to Marine Pollution, a section of the journal Frontiers in Marine Science

Received: *06 January 2022*
Accepted: *24 February 2022*
Published: *04 April 2022*

Citation:
Zhang P, Peng C, Zhang J, Zhang J, Chen J and Zhao H (2022) Long-Term Harmful Algal Blooms and Nutrients Patterns Affected by Climate Change and Anthropogenic Pressures in the Zhanjiang Bay, China. Front. Mar. Sci. 9:849819. doi: 10.3389/fmars.2022.849819

Climate change and anthropogenic pressures have significantly affected coastal environments. This study obtained historical data on harmful algal blooms (HABs) and nutrient patterns over a 30-year period to explore responses to long-term climate change and anthropogenic pressure indicators. Although the surrounding area has achieved great economic success over the past 30 years, the Zhanjiang Bay (ZJB) has been seriously affected by various pollutants and is threatened by increasing eutrophication and HABs due to climate change and anthropogenic pressures. In the ZJB, HABs rarely occurred before the 1980s but have occurred periodically and frequently since the 2000s. The largest HAB covered a cumulative area of 310 km^2 in 2005. Most of the HABs occurred during spring. Additionally, the dominant phytoplankton species were *Skeletonema costatum* and *Phaeocystis globosa*, accounting for 37.50 and 43.75% of the HABs observed, respectively. Anthropogenic pressures have caused the nutrient regime to significantly increased in the ZJB over the past three decades ($P < 0.05$). Specifically, the concentration of dissolved inorganic nitrogen (DIN) increased threefold from the beginning of the 1990 to 2019 period, while the dissolved inorganic phosphorus (DIP) concentration increased 21-fold. Unsynchronized variation in nutrient patterns has led to changes in the composition of nutrients, and the ZJB ecosystem has shifted from a P-limited oligotrophic state before the 2000s to an N-limited eutrophic state. Anthropogenic pressure indicators showed a significant linear correlation with nutrients ($P < 0.05$), but climate change indicators did not play a direct role in the eutrophication problem in the ZJB during this period ($P > 0.05$). Therefore, integrated land-ocean environment management should be introduced to reduce land-based pollution sources, mitigate eutrophication, and curb the blooms of harmful algae in the ZJB.

Keywords: long-term trends, harmful algal blooms, nutrient regimes, climate change, anthropogenic pressures, coastal water

INTRODUCTION

Blooms of toxic or harmful microalgae are commonly called "harmful algal blooms" (HABs) and occur in many forms, ranging from massive accumulations of cells that discolor water to dilute, inconspicuous, but highly toxic populations (Anderson et al., 2000). HABs cannot only change the structure and function of marine ecosystems and destroy fishery resources and marine environments (Mohamed and Al-Shehri, 2012; Yu et al., 2017), but can also result in toxic seafood and toxicity to human health (Song et al., 2018; Svirčev et al., 2019; Chen et al., 2021). In recent decades throughout the world, the increasing occurrence of HABs suggests an unsettling trend that has become a serious ecological issue (Zhou et al., 2001; Anderson et al., 2012; Liu et al., 2013; Mohamed, 2018).

Although determining the causative factors for HAB events are complex (Davidson et al., 2014), there is no doubt that the changes in climate and anthropogenic nutrient inputs contribute to global eutrophication and expanding global footprint of HABs (Glibert, 2020). Eutrophication, which results from the increased input of nutrients to marine waters (Wang, 2006; Liang et al., 2015), is now recognized as an important factor contributing to the geographical and temporal expansion of several HAB species (Smayda, 1990; Anderson et al., 2002). Shifts in species composition have often been attributed to changes in the nutrient supply ratios (Anderson et al., 2002). To govern the biogeography and formation of HABs, it is generally accepted that the availability of dissolved inorganic nutrients likely mediates phytoplankton growth in most coastal waters (Howarth and Marino, 2006). However, the mode of delivery of inorganic nutrients (especially nitrogen) is not restricted to aquatic sources; atmospheric input is also important (Glibert et al., 2005). In many estuarine and coastal waters, the atmosphere may contribute up to 40% of the total inorganic and organic nitrogen inputs (Howarth et al., 2002; Glibert et al., 2005). Climate effects on hydrology impart high variability to properties controlling water quality, including nutrient loadings, concentrations, and phytoplankton biomass in estuarine and coastal ecosystems (Harding et al., 2016). Anticipated future changes in climatic conditions are likely to increase the threats of HABs. Among these climatic threats are increases in the intensity and duration of hurricanes and El Niño periods (Emanuel, 2005; Webster et al., 2005; Fasullo et al., 2018). The increase in high rainfall and winds associated with hurricanes and El Niño results in enhanced nutrient loads which drive HABs (Mallin and Corbett, 2006; Miller et al., 2006; Dybas, 2018; Gomez et al., 2019; Phlips et al., 2020). Furthermore, the pollution of coastal waters by nutrients is a result of anthropogenic pressures (population growth, food production, and energy production and consumption) and is considered one of the largest global pollution problems (Howarth et al., 2002). Anthropogenic pressures severely impact aquatic ecosystems, which are also increasingly affected by global change, urban development, industrialization, and the unsustainable exploitation of aquatic resources. Increasing coastal human populations, industrialization, and the intensification of agriculture have elevated the supply of nitrogen (N) and phosphorus (P) to coastal waters (Ferreira et al., 2011). Importantly, there is consensus that HABs are complex events, typically not caused by a single environmental driver but rather by multiple factors occurring simultaneously (Heisler et al., 2008). For example, the agricultural fertilizer utilization, industrial development, and human activities associated nutrient discharge were the key drivers of HAB events in the Beibu Gulf, Yangze River estuary, Atlantic coast of Europe, and Tampa Bay, Florida (Greening et al., 2014; Yu et al., 2017; Desmit et al., 2018; Xu et al., 2019). In addition, recent study has found that terrestrial input of herbicides plays a significant role on phytoplankton and bacterioplankton communities in coastal waters (Yang et al., 2021). Furthermore, the climate change also impacted on the HABs development in the magnitude and frequency of these events (O'Neil et al., 2012; Phlips et al., 2020). It is important to clarify the combined effects of eutrophication and climate change. Therefore, recent reviews on HABs, eutrophication and climate have focused on the complex nature of this nexus (Glibert, 2020).

The Zhanjiang Bay (ZJB) is a semi-enclosed bay in China, with a total area of 193 km^2 and an average depth of 18 m (Chen and Yan, 2006). It is connected to the South China Sea through the ZJB mouth (**Figure 1**). There are several seasonal rivers, including three major rivers (the Suixi, Nanliu, and Lvtang rivers) that flow into its coastal waters. In recent decades, with the rapid expansion of industry, agriculture, and mariculture, nutrient fluxes from rivers, atmospheric deposition, and wastewater discharge have increased substantially (Zhang et al., 2019). Eutrophication—a result of human-induced nutrient enrichment—has become a concern in the ZJB (Shi et al., 2015). Over the past several decades, many industrial facilities have been built along the coast and tons of industrial wastewater and agricultural or aquacultural pollutants have been discharged into the bay, which has led to eutrophication (Zhang et al., 2019). In 2016, HABs occurred in the aquacultural area of the ZJB, which caused a large number of deaths of farmed fish and serious economic losses (Yu and Chen, 2019). However, the combined effect and possible synergies can be difficult to distinguish and require comprehensive studies of the entire ecosystem on long time scales (Frigstad et al., 2013). Time-series data for several ecosystems reveal high spatiotemporal variability superimposed on secular trends that are traceable to nutrient over-enrichment (Harding et al., 2019). Long-term nutrient variations have potential ecological impacts on the frequencies, affected areas, and diversity of dominant species of these local HABs (Wang et al., 2018). However, historical data for the earlier periods in the ZJB, which were less affected by anthropogenic eutrophication, are not included. To date, the patterns of the long-term variation in the nutrients in the ZJB remain unclear.

Therefore, there is an urgent need to clarify the mechanism of HABs in the ZJB and their relationship with nutrient patterns influenced by climate change and anthropogenic pressures. In this study, we performed a retrospective analysis of the long-term variations in HABs and nutrient patterns in the ZJB based on historical data. The objectives of this study is to (1) clarify the long-term HABs in the ZJB coastal waters, (2) identify the long-term nutrient patterns in the ZJB coastal waters, and (3) discuss the impacts of climate change and anthropogenic pressures. By

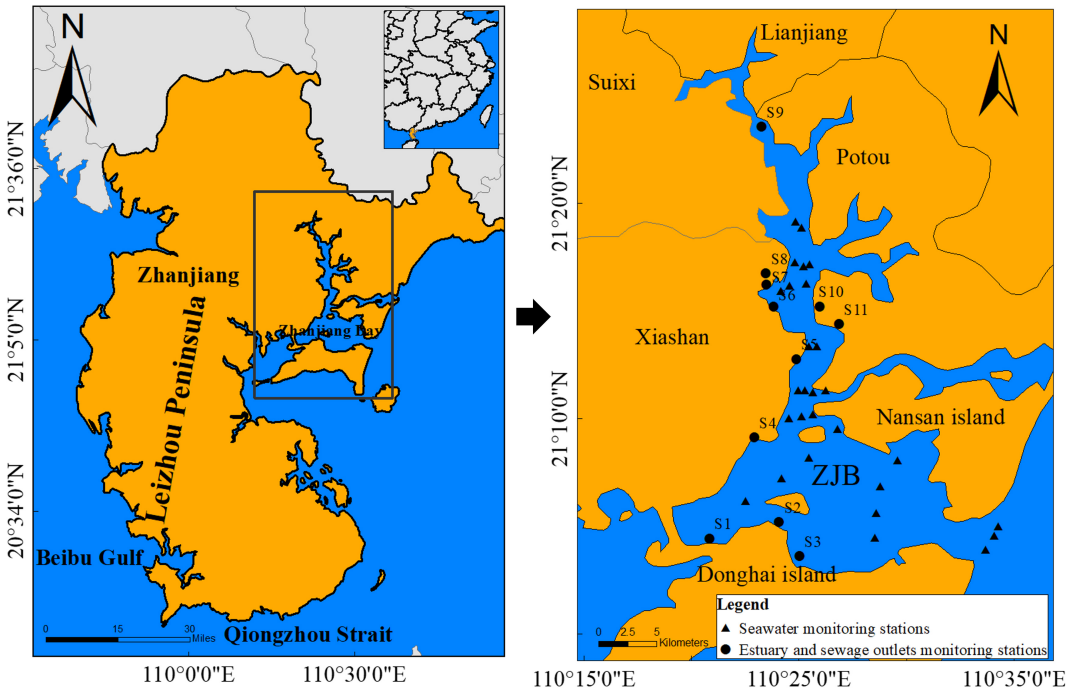

FIGURE 1 | Geographic location and seawater monitoring stations of 2019 in the Zhanjiang Bay.

highlighting the long-term HABs and nutrients patterns affected by climate change and anthropogenic pressures in the ZJB, we hope to reveal the characteristics of HABs and provide a framework for integrated land–ocean environment management and water quality improvement in the ZJB in the future.

MATERIALS AND METHODS

Study Areas

According to its geographical location, the ZJB is located in the southernmost part of the Chinese mainland—Guangdong Province. The ZJB is a semi-enclosed bay with poor hydrodynamic conditions and is surrounded by the Leizhou Peninsula, Donghai Island, Nansan Island, and South China Sea. Due to land reclamation within the ZJB, and the decreasing water-exchange ability corresponds to an increasing average residence time over the past decades, which had influenced the hydrodynamic conditions and pollutants transport (Li X. B. et al., 2012; Zhang et al., 2020a). It has a length of 54 km from south to north and a width of 24 km, covering an area of 193 km^2 (Zhang J. et al., 2021). The deep channel (>10 m) is 40 km long, and the mouth is about 2 km wide (Shi et al., 2015). With the rapid development of the economy and the increasing population in Zhanjiang, modern industrial facilities, marine aquaculture functional areas, and agricultural functional areas were built in the bay by the government. In recent years, rivers flowing through urban areas along the coastline contribute to the load input of various land-based pollution sources (**Figure 1**). This situation causes serious marine ecological environmental problems, such as water quality deterioration and HABs (Zhang et al., 2019, 2020a,b).

Data Sources and Treatment

The data on the frequency, area, and phytoplankton species composition of HABs for 1980–2004 were from Li and Lv (2009), for the period from 2005 to 2011 the data were from the Guangdong Oceanic and Fishery Bureau (2005-2012), and for the period from 2012–2020 the data were from the Department of Natural Resources of Guangdong Province (2013–2020). Dissolved inorganic nitrogen (DIN) and dissolved inorganic phosphorous (DIP) are the indicators of Chinese national seawater quality standards (GB3097- 1997) (AQSIQ, 1997). In GB3097- 1997, the grade IV seawater quality standard is applicable to the seawater of marine port or marine exploitation operation areas. The DIN and DIP concentration of the grade IV seawater quality standard was 35.71 and 1.45 μmol/L, respectively (AQSIQ, 1997). The yearly averaged data of nutrients (DIN and DIP) were used to represent the long-term nutrient variations. The nutrient data for 1990 were obtained from the Compiling Committee of Records of China Bays (1999). The nutrient data for the period from 1998 to 2001 were from Lv et al. (2002), for the period from 2006 to 2010 the data were from the Zhanjiang Oceanic and Fishery Bureau (2007–2011), and for the period 2011–2015 the data were from Yuan et al. (2016). The mean nutrient data for 2019 were obtained from the field monitoring data in this study. The data on anthropogenic pressures, such as gross domestic product (GDP), population, fertilizer use, industrial wastewater discharge, and the total output of marine products during this investigation period,

were from the Zhanjiang Municipal Statistics Bureau (2007–2011). The annual precipitation and air temperature data for the ZJB were obtained from the Guangdong Municipal Statistics Bureau (2019) (**Table 1**). To concentrate on long-term HABs and nutrients patterns affected by climate change and anthropogenic pressures, the annual mean data values, based on pooled samples, were determined in the analysis (McQuatters-Gollop et al., 2007; Zhang et al., 2017). In addition, to avoid long-term data sources of error in the method of monitoring HABs and nutrients patterns, climate change and anthropogenic pressures indicators, the analyses were in accordance with the investigation criteria of China and aimed to ensure the consistency of methods as far as possible (Zhang et al., 2017). Furthermore, for the accuracy of the datasets of all long-term indicators, we cited government administration reports and references that had confirmed the comparability of the long-term data (Yuan et al., 2016; Zhang et al., 2017). Thus, the information regarding the long-term annual mean data obtained in the ZJB were deemed relatively accurate and reliable.

Statistical Method

The geographic information system ArcGIS (10.2) (Esri Corporation, New York, NY, United States) was used to map the monitoring stations of the ZJB coastal waters and land-based pollution sources. The maps of HABs, DIN, and DIP, and climate and anthropogenic pressures in the ZJB were drawn using Origin 9.0 software (Origin Lab Corporation, Northampton, MA, United States). The linear regression analysis described the linear relationship between HABs, nutrients, and the climate and anthropogenic pressures indicators and determined how much of the variation can be explained by the linear relationship with indicators and how much of this variation remains unexplained (Zhang et al., 2017). The linear regression analysis between variables was determined among the HABs, nutrients, climate change, and anthropogenic pressures indicators using Origin 9.0 software (Origin Lab Corporation, Northampton, MA, United States). A probability level of 0.05 was used to determine significance.

TABLE 1 | Meteorological and physico-chemical data references used in this study.

Time period	Variables	Data sources
1980–2019	Frequency and duration of HABs and the phytoplankton species composition of HABs	Li and Lv, 2009; Department of Natural Resources of Guangdong Province, 2013–2020
1990	DIN and DIP	Compiling Committee of Records of China Bays, 1999
1998–2001	DIN and DIP	Lv et al., 2002
2006–2010	DIN and DIP	Zhanjiang Oceanic and Fishery Bureau, 2007–2011
2011–2015	DIN and DIP	Yuan et al., 2016
2019	DIN and DIP	This study
1980–2019	Fertilizer use, gross domestic product, population, industrial wastewater discharge, and the total output of marine products	Zhanjiang Oceanic and Fishery Bureau, 2000–2020
1980–2019	Precipitation and air temperature	Guangdong Municipal Statistics Bureau, 2019

Change data sources.

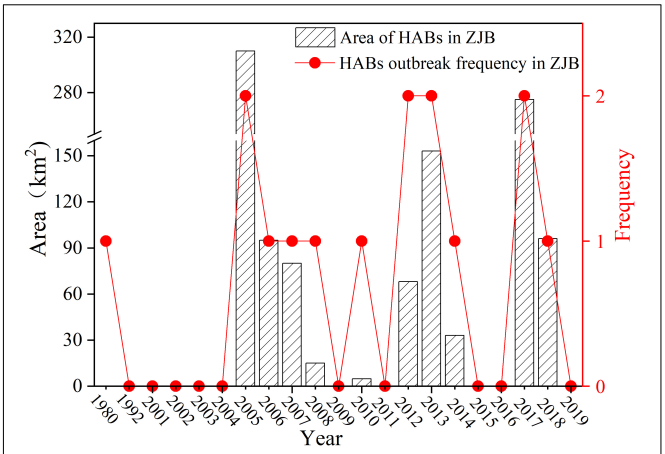

FIGURE 2 | Number of HAB events and their extension (km^2) from 1980 to 2020 in Zhanjiang Bay, China.

RESULTS

Long-Term Harmful Algal Blooms Variation in the Zhanjiang Bay Coastal Water

Long-Term Harmful Algal Blooms Variation of Frequency and Areas in the Zhanjiang Bay

During the period 1980–2019, HABs occurred 15 times in the ZJB (**Figure 2**). However, there was no significant change in the frequency of HABs in the ZJB; they occurred at a frequency of once or twice in the outbreaking year. Before the 2000s, HAB events were not typically observed, occurring only once in 1980. From 2001 to 2004, no HAB events were registered. Afterward, the frequency of HABs reached twice per year in 2005, during which the largest area of HABs were observed with an extent of more than 300 km^2. From 2006 to 2008 only one HAB was registered per year, and the extent of these events also showed a decreasing trend. The frequency of HABs in 2010 decreased to one event with an area of 4.8 km^2, which was the smallest area observed during this period. In 2012, the frequency of HABs increased to two events per year, and again decreased in the following years, with no HAB events in 2015 and 2016. However, the area of HABs increased in 2017, with the second largest observed area of 275 km^2 during these years, and the frequency of HABs increased up to twice per year. With the decrease in the area o HABs, the frequency decreased once in 2018.

Long-Term Harmful Algal Blooms Variation of Phytoplankton Species Composition in the Zhanjiang Bay

Five phytoplankton species bloomed in the ZJB during the three decades of the investigation period (**Figure 3**). It was evident

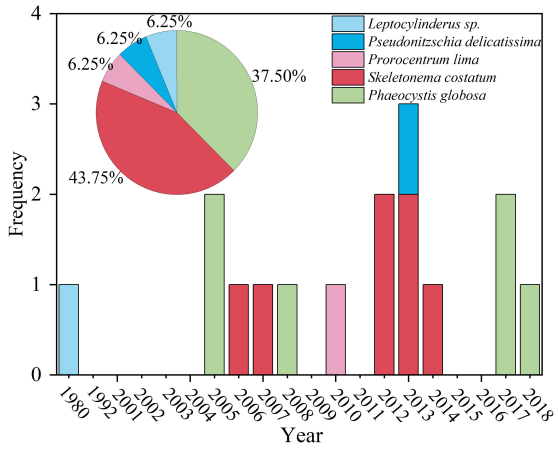

FIGURE 3 | Phytoplankton species that formed HABs in the Zhanjiang Bay, China from 1980 to 2020.

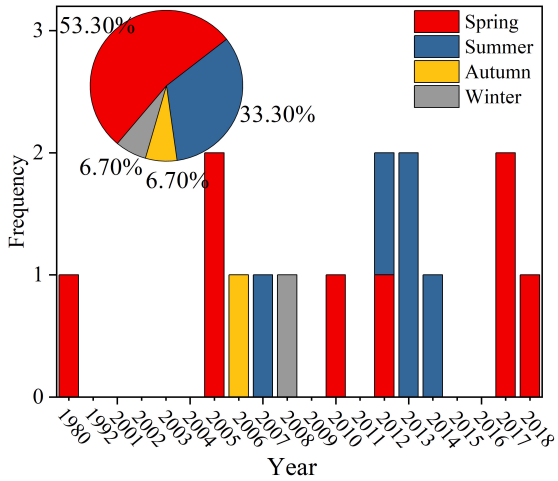

FIGURE 4 | Long-term HABs period and duration.

that *Skeletonema costatum* had the highest bloom frequency, accounting for 43.75%. Following by *Phaeocystis globosa* with a frequency of 37.50%. *Leptocylinderus* sp., *Pseudonitzschia delicatissima,* and *Prorocentrum lima* had the same bloom frequencies, accounting for 6.25%. The bloom frequency of *Phaeocystis globosa* doubled in 2005 and 2017. Moreover, *Skeletonema costatum* occurred twice in 2012 and 2013. In 2013, two phytoplankton species, *Skeletonema costatum* and *Pseudoitzschia delicatissima*, occurred in the ZJB. During the investigation period, the dominant phytoplankton species of the HABs were *Skeletonema costatum* and *Phaeocystis globosa*.

Long-Term Harmful Algal Blooms Seasonal Occurrence in the Zhanjiang Bay

To determine long-term seasonal variation of HABs in ZJB, four seasons of 12 months each were defined as spring (March, April, May), summer (June, July, August), autumn (September, October, November), winter (December, January, February). The seasons and durations of the HABs in different years varied (**Figure 4**). The month with the highest record of bloom events was March. There were six occurrences of HABs in March, accounting for 30.00% of the total frequency. Following April and March that accounted for 15.00% of the total frequency during these decades. The period of the HABs occurred in August in 2012 and 2013. Additionally, the period of the HABs occurred in March and April in 2017 and 2018. However, HABs did not occur in November or December. The longest duration of HABs lasted 4 months in 2005. Overall, HABs became more frequent after the 1990s. Moreover, HAB events were focused in spring, including the months of March, April, and May, accounting for 53.30% of the total percentage of occurrences.

Long-Term Nutrients Variation in the Zhanjiang Bay Coastal Water

In the last three decades, nutrients in the coastal seawater of the ZJB have experienced a significant change ($P < 0.01$). The annual mean DIN concentration in the ZJB seawater increased threefold during this period, from 9.87 to 40.06 μmol/L. The concentration of DIN increased slowly at the beginning of the 1990s and then decreased slowly from the mid-1990s to the mid-2000s. Then, it increased rapidly, achieving a value of 58.43 μmol/L in 2009. Thereafter, it maintained a high level of fluctuation and showed a fluctuating downward trend (**Figure 5**). The annual mean DIP concentration increased by 21-fold and ranged from 0.13 to 3.74 μmol/L. Changed from lower concentration in the early1990s to higher concentrations in the mid-2000s. Subsequently, the DIP concentration maintained high-level fluctuations and exhibited an increase in the early 2010s. The highest DIP concentration was 3.74 μmol/L in 2015. Before 2008, the concentrations of DIN and DIP did not exceed the grade IV seawater quality standard. The concentration of DIN exceeded the standard in 2009, 2010, 2013, 2014, and 2019, respectively. From 2009 to 2015 and 2019, the concentrations of DIP exceeded the grade IV seawater quality standard. Conversely, it seems that the value of DIN/DIP exhibited a drastic decrease during these decades. Compared to 2019, the value of DIN/DIP in 1990 decreased fourfold. A significant decrease of 74.10–18.00 was observed from the early to the end of the 1990s. In the early 2000s, the value of DIN/DIP seemed to remain stable but still maintained a slowly fluctuating decline with a minimum value of 9.00 in 2015. The value of DIN/DIP exceeded 16:1 (Redfield Ratio) in most of the years, except in 2008, 2012, 2015, and 2019. The nutrient regime in the ZJB shifted from an oligotrophic state with P-limitation to a eutrophic state with N-limitation.

Long-Term Variation of the Climate Change in the Zhanjiang Bay

During the investigation period, the annual average air temperature ranged from 22.4 to 24.5°C. The phases of temperature variation presented an uneven "M" shape from 1995 to 2005 and presented an uneven "W" shape from 2005 to 2015 (**Figure 6**). Precipitation exhibited an irregularly changing trend and maintained high-level fluctuations during these years.

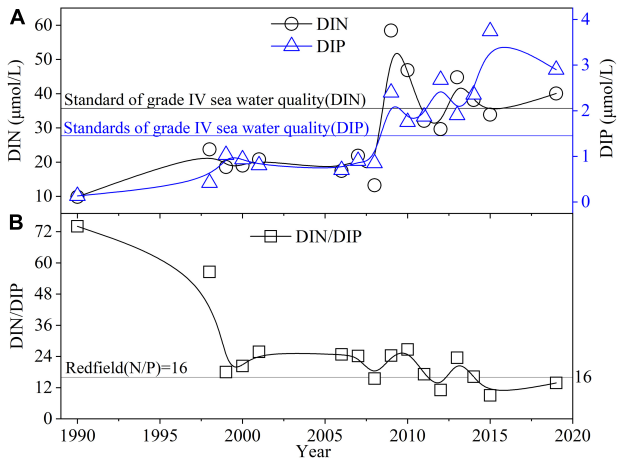

FIGURE 5 | Long-term nutrients' concentration **(A)** and composition **(B)** variation in the Zhanjiang Bay coastal water.

The highest value of precipitation was 2411.3 mm in 1985, and the lowest value was 1068.5 mm in 2004. Precipitation had a significant decreasing trend from the early 2000s to the mid-2000s and increased slowly in the following years.

Long-Term Variation of the Anthropogenic Pressures in the Zhanjiang Bay

During the investigation period, the population, industrial facilities, and agricultural intensity grew rapidly with the rapid development of the economy and society in Zhanjiang (**Figure 7**). According to the statistics, the gross domestic product (GDP) and population grew at a steadily increasing rate. Simultaneously, fertilizer use in Zhanjiang reached 445,720 tons in 2018. Although this was lower than in 2017, it was a 10-fold increase compared to the early 1980s. There were drastic changes in the amount of industrial wastewater discharge. The volume also increased from the early 1980s to 1990 and showed a fluctuating decrease during the 1990s and 2000s. At the beginning of the 2010s, it increased rapidly and then decreased slowly over the next few years. Overall, industrial wastewater discharge was 4.98×10^7 tons in 2018, which was 17% lower than that in 1980. In contrast, Zhanjiang is also a major marine aquaculture city. The number of marine products increased steadily during this period and was 8.8 times more than that in 1980.

DISCUSSION

Causes of Harmful Algal Blooms Events in Zhanjiang Bay Coastal Water

HABs damage ecosystems and threaten human health worldwide (Corcoran and Hunt, 2021). To strengthen the prediction and mitigation of HABs, further studies on the role of nutrients in HAB expressions are critical (Heisler et al., 2008). There are numerous clear examples of the relationship between HAB frequency and increased total nutrient loading in the coastal waters of China (Glibert et al., 2005). Previous research has found that the intracellular and extracellular balance of nutrients is central to phytoplankton growth and competition (Tilman, 1977). Using the recorded data, the link between nutrient concentrations and HAB characteristics, including the occurrence area, frequency, and bloom timing, was analyzed for the ZJB. During this long-term investigation, the frequency and area of HAB events in the ZJB increased after the 1990s and reached an explosive trend, with the largest total area of HABs (310 km^2) occurring in 2005. However, due to the insufficient data, the frequency and area of HABs in the ZJB are not linearly correlated with the inorganic nutrient concentration of seawater ($P > 0.05$) (**Figure 8**). Therefore, eutrophication (inorganic) may not have a direct relationship with HABs in

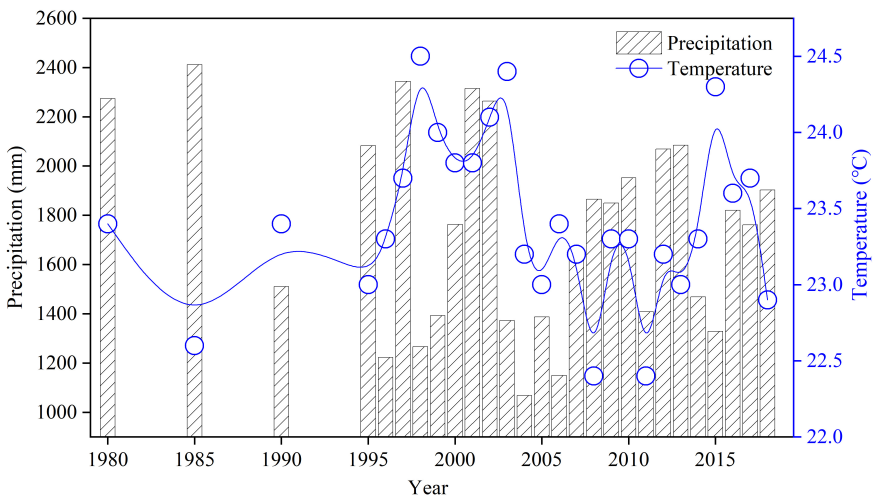

FIGURE 6 | Long-term annual precipitation and temperature in the Zhanjiang Bay coastal water.

the ZJB from a long-term perspective, which is similar to conditions in the Pearl River Estuary (Anderson et al., 2002). The Pearl River estuary discharges a significant volume of polluted waters into South China Sea, including the western waters of Hong Kong, yet the occurrence of HABs is low compared to the conditions in Victoria Harbor and areas to the east (Anderson et al., 2002). It was that low nutrient values may occur due to phytoplankton uptaking during HABs events. While most studies have focused on the inorganic nutrients, they are not the only the nutrient source for many HABs. Major pools of dissolved organic matter, such as dissolved organic nitrogen (DON) and dissolved organic phosphorus (DOP), originate from both allochthonous and autochthonous sources (Antia et al., 1991; Glibert et al., 2005; Davidson et al., 2007, 2014; Pete et al., 2010). Organic nutrients play an important role in the development of blooms of various HAB species, and the importance of this phenomenon has been globally documented (Glibert et al., 2001, 2005). Many HAB species rely strictly on photosynthesis for their energy and use inorganic nutrients. At the same time, the appreciation of the importance of mixotrophy of HABs species also affects which nutrient forms should be considered in water management strategies (Burkholder et al., 2008; Flynn et al., 2018). In addition, the dissolved or particulate organic nutrients for several or all of their nutrient demands can be also available for the HAB species during photosynthesis process or mixotrophy (Granéli et al., 1999; Stoecker, 1999; Glibert et al., 2005; Burkholder et al., 2008). Additionally, five phytoplankton species of HABs were identified in the ZJB. Among all the bloom frequencies of the phytoplankton species, *Skeletonema costatum* and *Phaeocystis globosa* accounted for 37.50 and 43.75% of the total, respectively. Simultaneously, *Skeletonema costatum* and *Phaeocystis globosa* bloomed during the 2000s and 2010s. However, *Skeletonema costatum* was the dominant phytoplankton species observed in the 2000s and *Phaeocystis globosa* is the dominant phytoplankton species observed in 2010s. Laboratory research results showed that phosphate and nitrate were the main limiting factors for the growth of *Phaeocystis globosa* strains, and their tolerance to phosphate ranged from 0 to 180 μmol/L. In the lower N/P range (5.9–19.6), the growth rate of *Phaeocystis globosa* is higher (Guo et al., 2007; Shen et al., 2018). Therefore, this may be why the dominant phytoplankton species of the HABs in the ZJB changed from *Skeletonema costatum* to *Phaeocystis globosa* during the 2000–2010s. March, April, and May, which were spring in the ZJB, were the months with the highest frequencies of HABs. The temperature initially increases in spring. The suitable temperature of *Phaeocystis globosa* ranged from 15 to 27°C (He et al., 2019). Comparatively, the most growth temperature of *Skeletonema costatum* was 24–28°C (Huo et al., 2001). Temperature variations may affect the habitat for HABs and the community of organisms within which the harmful algal species may live (Anderson, 2000; Wells et al., 2015; Glibert, 2020). For example, climate warming leads to longer growing seasons of two harmful algal species (*Prorocentrum minimum* and *Karlodinium veneficum*) in eutrophic Chesapeake Bay, but may suppress bloom habitat (Li et al., 2020). In future, for better understanding climate change-driven by temperature variations, the dynamic mathematical model and field experimental observation should be conducted in the ZJB (Lin et al., 2018).

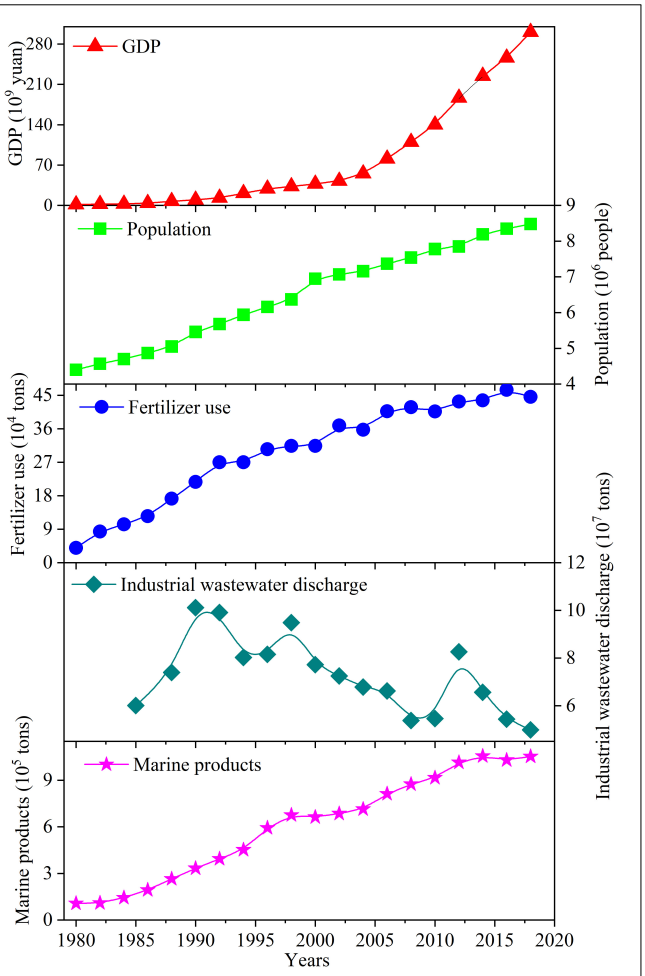

FIGURE 7 | Long-term anthropogenic pressures' variation in Zhanjiang city.

Nutrients Change and the Eutrophication Trend in Zhanjiang Bay

In recent decades, anthropogenic activities have substantially increased the nutrient inputs to waters and changed the nutrient composition. Eutrophication is the over-enrichment of nutrients in a water body, causing an advanced production of organic matter, particularly algae (Wang et al., 2018). The reasons for the occurrence of HAB events in the ZJB may be complex. Through the analysis of the long-term nutrient variation in the ZJB and previous studies, it was found that the water quality of the ZJB has seriously exceeded the standard, and the nutrient concentration in most of the sea areas also exceeded the grade IV national seawater quality standard (Lv et al., 2002; Zhang et al., 2009, 2019; Shi et al., 2015; Yuan et al., 2016). Excessive accumulation of nutrients had led to the eutrophication issue in the ZJB. In marine systems, the concept of the "Redfield Ratio" has been central to the debate surrounding resource competition (Davidson et al., 1992). Redfield demonstrated that the chemical composition

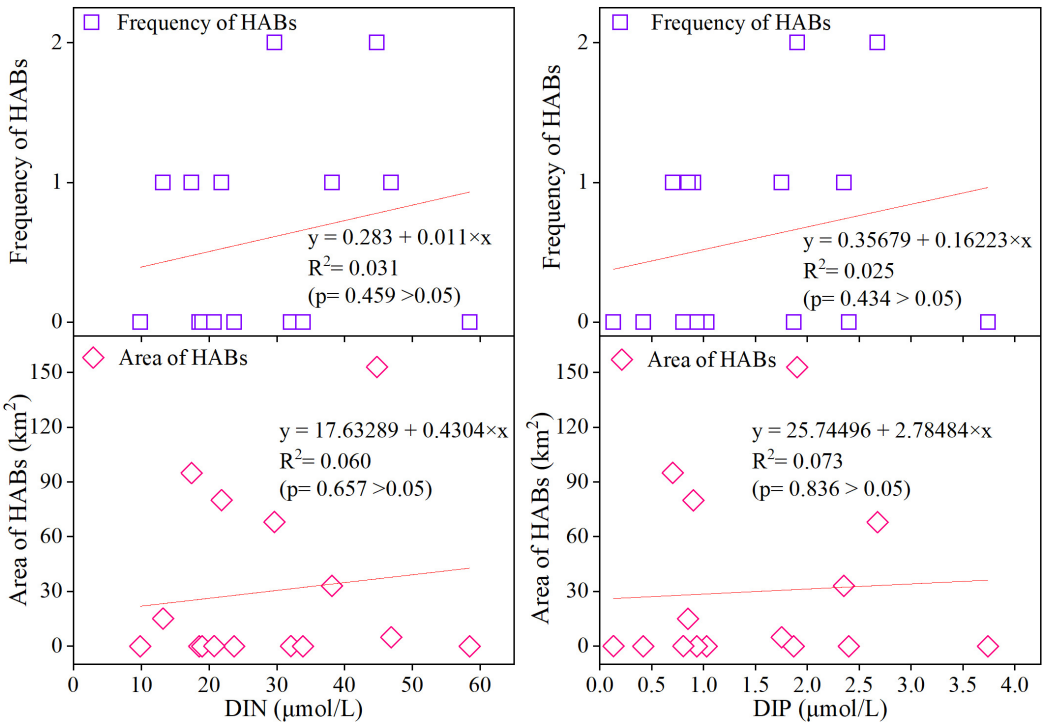

FIGURE 8 | Relationship between DIN, DIP and frequency and extension of HABs. Data from 1980 to 2020.

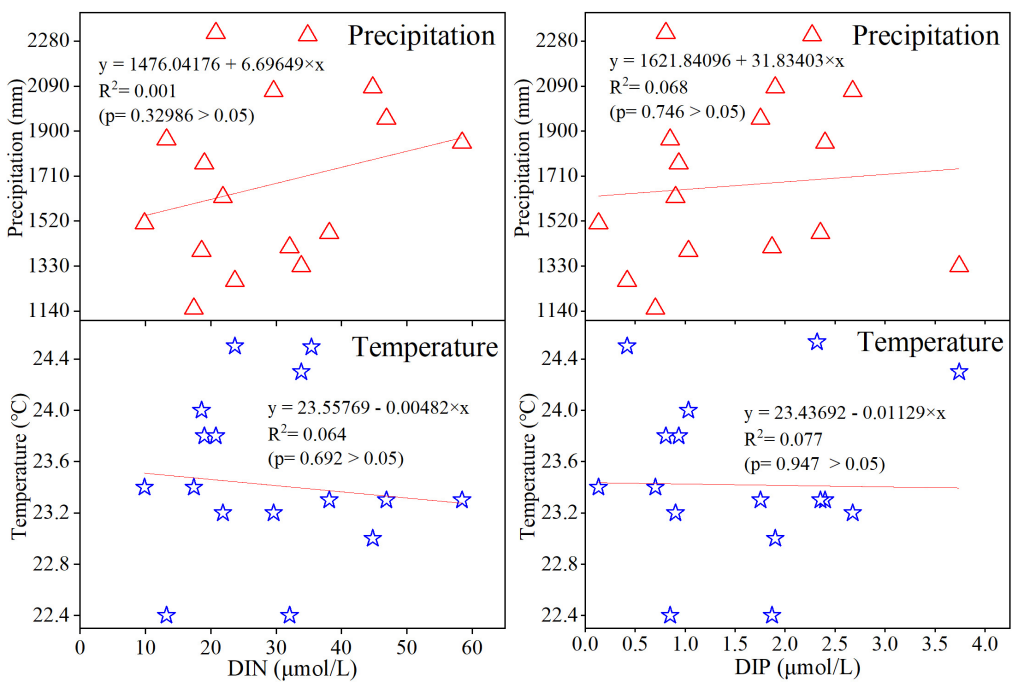

FIGURE 9 | Relationships between DIN, DIP, temperature and precipitation in Zhanjiang Bay, China. Data from 1990 to 2020.

of plankton tends toward an average atomic C:N:P ratio of 106:16:1. The nutrient in least supply relative to the requirements for growth (determined by their biochemical composition) is deemed the "limiting" nutrient. Therefore, an important problem related to HABs is the role of nutrient ratios in governing bloom formation (Davidson et al., 1992, 2014). Based on the

long-term analysis of DIN/DIP, the N/P ratio exceeds the normal range of the Redfield Ratio. With the asymmetric increasing of DIN and DIP in these decades, the rate of DIP increase is much faster than DIN in ZJB. The results showed that the concentration of DIN increased threefold from the beginning of the 1990 to 2019 period, while the DIP concentration increased 21-fold. On one hand, the decline of DIN/DIP may be caused by phosphorus fertilizer in the biggest Suixi river watershed. In the watershed, the non-point source of phosphorus fertilizer was widely used in copland and finally entered adjacent coastal water due to the heavy rainfall influence in summer (Zhang P. et al., 2021). On the other hand, the surrounding factories, including fertilizer manufacturing, and large amount of wastewater with high concentrations of phosphorus was also discharged into the rivers entering coastal water (Zhang et al., 2019). The severe imbalance between the N/P ratio caused the nutrient regime in the ZJB to shift from P-limitation to N-limitation, which had great impact on the growth of phytoplankton. Continued nutrient enrichment and the decline of N:P ratio have increased the risk of nutrient-enhanced algal bloom (Chen et al., 2013). Both N and P are of concern in eutrophication, but N has received more attention because it is used to limit primary production in estuaries and coastal waters (Glibert et al., 2005). Under the environment of increasingly serious nitrogen pollution in the sea, sufficient nitrogen sources have become an important reason for the frequent occurrence of coastal HABs in China in recent years (Liang, 2010). Additionally, compared to inorganic nutrients, the organic nutrients (such as urea) in the seawater of the ZJB may have a more signification relationship with HABs. Urea, which has been identified as a source of organic nitrogen, has been used as a nitrogen fertilizer and feed additive, increasing in use by more than 50% over the past decade (Glibert et al., 2005, 2006). Since the 1970s, when the escalation in the use of chemical fertilizer began in China, the number of HABs has increased by 20 times, with blooms that are now of greater geographic extent, more toxic, and more prolonged (Anderson et al., 2002). A previous study has found that urea, originating from land-based input, in the ZJB may have a bioavailable DON source (Zhang et al., 2020a). Thus, organic nutrients in the ZJB could have a significant effect on the HAB events. However, according to other coastal regions (Davidson et al., 2014), it was shown that an anthropogenic nutrient-HABs link is a typical, with insufficient evidence to draw definitive conclusions. Nutrient enrichment has been strongly linked to the stimulation of several harmful species, but for others it has not been an apparent contributing factor (Anderson et al., 2002). Although nutrient pollution is the primary driver of eutrophication, many studies have recognized that the relationship between nutrient pollution and HABs is more complex than previously thought (Glibert et al., 2005; Heisler et al., 2008): not all nutrient loads result in HABs, and not all nutrient effects that result in HABs cause other eutrophication impacts (Glibert and Burford, 2017). The mode of delivery of both inorganic and organic nutrients, especially nitrogen, is not restricted to aquatic sources, while the atmospheric input is also important (Glibert et al., 2005). In, Howarth et al. (2002) found that the atmosphere may contribute up to 40% of the total inorganic and organic nitrogen inputs in many estuarine and coastal waters. Analyzes of the data related to nutrients and climate indicators in the ZJB showed that there were no significant linear relationships between the long-term climate change indicators and nutrient concentration in seawater ($P > 0.05$) (**Figure 9**). Previous field studies showed that the land-based nutrients flux input was much greater than atmospheric wet deposition in the ZJB (Chen et al., 2017; Zhang et al., 2019). Therefore, in comparison with land-based nutrient sources input, atmospheric wet deposition may not have a remarkable effect on the nutrient concentration change in the ZJB. Thus, the eutrophication problems in the ZJB may be induced by land-based sources. However, the short-term extreme climate events, such as hydrological change driven by tropical typhoon, cannot be neglected in the contribution of nutrients load from land-based and atmospheric sources input in the tropical coastal eutrophication (O'Neil et al., 2012; Chen et al., 2017; Phlips et al., 2020; Zhang et al., 2020c).

Land-Based Sources of Pollutant Input Affecting the Water Quality

Eutrophication originates from the significant increase in the utilization of chemical fertilizers that began in the 1950s and is projected to continue to escalate in the coming decades (Smil, 2001; Glibert et al., 2005). Eutrophication in the ZJB ecosystem may result from a combined influence and change in the relative importance, of several factors, including external nutrient input cycles (primarily the anthropogenic pressures). With the development of Zhanjiang's social economy in recent years, the government has promoted an industry-oriented development strategy, which allowed the industry to develop rapidly (Shi et al., 2015). Imported projects within the heavy industry have brought tremendous pressure upon the ecological environment of the ZJB (Shi et al., 2015). An environment of estuaries and coastal areas, such as the ZJB, is always influenced by the anthropogenic activity indicators and river runoff (agriculture, industrial wastewater input, etc.) (Zhang J. et al., 2021). Through the correlation analysis of these factors and the nutrients, it was found that these influencing factors had significant impacts on the nutrient concentration in the ZJB coastal seawater, except for industrial wastewater discharge (**Figure 10**). With the treatment of domestic and industrial wastewater according to the national standard of wastewater discharge in Zhanjiang in recent years, the nutrients discharge load from wastewater has gradually decreased, but the concentration of nutrients still shows an increasing trend in ZJB coastal water. Therefore, the point source (industrial wastewater) is not the predominant influencing factor in the nutrient enrichment of the ZJB. However, the most complex nutrient sources for understanding and regulation are non-point source inputs, such as agricultural runoff, groundwater, and atmospheric deposition (Heisler et al., 2008). Non-point sources are the major sources of the ZJB coastal waters. Land-based source inputs, especially agricultural fertilizer runoff, might be the major means of non-point sources pollution in the ZJB. This situation is caused by the rapid development of the society and the economy around the ZJB, which has led to a continuous increase in nitrogen pollutant

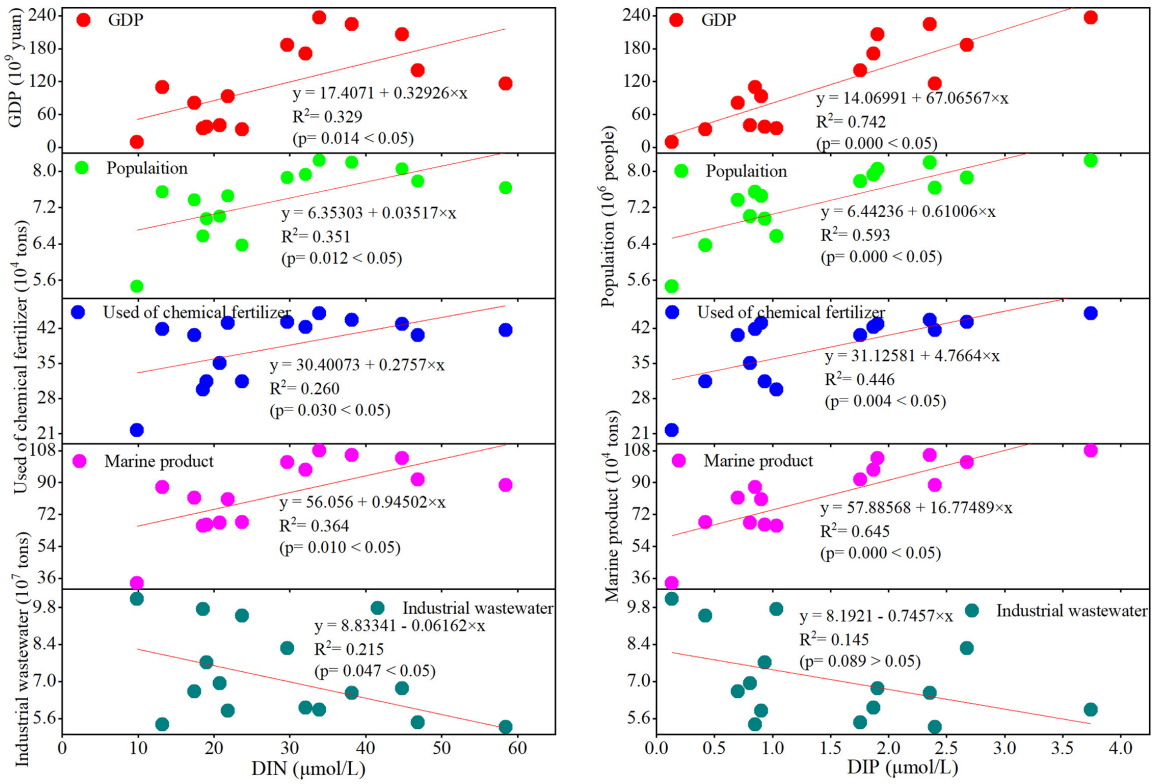

FIGURE 10 | Relationship between water quality and anthropogenic pressures.

emissions and water quality deterioration (Zhang et al., 2019). Similarly, marine aquaculture has accelerated the development of phytoplankton communities (Chen et al., 2001). Zhanjiang has large-scale aquaculture industries, including freshwater and seawater (Zhang et al., 2020a). A previous study has shown that aquaculture pollution in the ZJB seriously threatens the health of the bay's ecosystem (Li Z. Y. et al., 2012). Simultaneously, the evaluation results revealed that the value of the pollutant treatment function in the ZJB is very limited, and reducing the discharge of land-based pollutants into the bay is the key to the construction of an ecological bay city in Zhanjiang (Li Z. Y. et al., 2012). As the higher rate of DIP increased, governments need to pay more attention on policy about the limiting of the use of P in domestic and agricultural application. Protection of estuarine–coastal ecosystems from the eutrophication syndrome has proven to be a difficult policy challenge, partly because of the diverse sources of nutrients delivered to the coastal waters from urban and agricultural runoff, atmospheric deposition, and point sources such as municipal wastewater treatment plants.

Integrated Land-Ocean Environment Management in the Zhanjiang Bay

The long-term relationships between eutrophication and anthropogenic pressure indicators in the ZJB suggest that anthropogenic pressures have become a serious threat leading to eutrophication in the ZJB. Rapid increases in population, economic growth, and aquaculture development in the ZJB have resulted in the massive mobilization of bioactive nutrients, such as DIN and DIP, in recent decades. If the effective measures were not taken in coastal water quality protection, the increasing trends are not expected to cease in the next years. Future shared socioeconomic pathways show that high N/P ratios are likely to persist for decades to come, even worsening in a future oriented toward sustainability, and indicate that HABs may be a persistent problem in China's coastal waters (Wang et al., 2021). Liu et al. (2012) also predicted future trends in water pollution by nitrogen and phosphorus in major rivers worldwide. These results indicate that the ZJB is likely to encounter severe DIN and DIP discharge problems with considerable increases in agricultural activity over the next two decades compared to other major rivers worldwide (Li et al., 2014). The annual discharge of pollutants into the ZJB from the land-based source inputs has greatly exceeded its environmental capacity requirements (Li X. B. et al., 2012). Additionally, based on the numerical modeling systems, a previous study has calculated the environmental capacity of the inner ZJB and proposed land-based source pollution control measures to improve water quality (Shi et al., 2021). Strategies to limit sewage and agricultural and industrial discharges to coastal waters are being implemented in many countries by N and P removal from waste and the control of fertilizer application (Davidson et al., 2014). Therefore, both point and non-point sources in the coastal water environment should be further reduced. Additionally, the land-based pollutants load

reduction mismatched the coastal water quality indicator and environmental capacity in ZJB at present (Zhang et al., 2019, 2020a). For example, the nutrients criteria of total nitrogen and phosphorus could be developed for efficiently nutrients load management (Yang et al., 2019). Furthermore, to identify and quantify the critical pollutants source areas and load in the surrounding watersheds, the integrated land–ocean environment management based on environmental capacity of pollutants should be introduced to reduce land-based pollution sources, mitigate eutrophication, and curb the HABs in the ZJB.

CONCLUSION

Based on a long-term survey in ZJB, carried out over the last three decades, the problems of HABs and eutrophication have been highlighted. HABs rarely occurred before the 1990s but have occurred periodically and frequently since the 2000s. The frequency of HABs was once or twice per year in the ZJB, and the largest area of HABs observed during the study period was 310 km^2 in 2005. Most HAB events occur in spring. Additionally, the dominant phytoplankton species were *Skeletonema costatum* and *Phaeocystis globosa*, which accounted for 37.50 and 43.75% of the total, respectively. During these years, the concentration of DIN increased by approximately 9.87–58.43 μmol/L, while the concentration of DIP increased by 0.13–3.74 μmol/L. After 2008, the concentrations of DIN and DIP both exceeded the grade IV seawater quality standard. However, the N/P ratio showed decreasing trend from 74.31 to 9.00. This situation caused the ZJB ecosystem to shift from a P-limited oligotrophic state before the 1990s to an N-limited eutrophic state. The significant changes in the composition of the nutrients in the seawater are likely to play an important role in the future development and construction near the ZJB. With the rapid development of society and the economy in Zhanjiang, anthropogenic pressures may be driving the changes in water quality. Integrated land–ocean environment management in the ZJB should be introduced to curb the HABs and improve water quality. In addition, given HAB occurrence and the event response nature of coastal water affected by climate change and anthropogenic pressures in China and worldwide, the long-term integrated monitoring programs should be available for the healthy and sustainable marine environment in the future.

DATA AVAILABILITY STATEMENT

The raw data supporting the conclusions of this article will be made available by the authors, without undue reservation.

AUTHOR CONTRIBUTIONS

PZ: conceptualization, project administration, and writing—original draft preparation. PZ and JiZ: methodology, funding acquisition. CP: visualization and software. CP and JC: validation. PZ and CP: formal analysis. PZ, CP, and HZ: writing—review and editing. JuZ and JC: supervision. All authors listed have made a substantial, direct, and intellectual contribution to the work, and approved it for publication.

FUNDING

This research was financially supported by the Research and Development Projects in Key Areas of Guangdong Province (2020B1111020004), the Guangdong Basic and Applied Basic Research Foundation (2020A1515110483), the Guangdong Ocean University Fund Project (R18021), the Science and Technology Special Project of Zhanjiang City (2019B01081), the First-Class Special Fund (231419018), the Innovation Strong School Project (230420021) of Guangdong Ocean University.

ACKNOWLEDGMENTS

We are grateful for the reviewers' careful review and valuable suggestions to improve the manuscript.

REFERENCES

Anderson, D. M., Cembella, A. D., and Hallegraeff, G. M. (2012). Progress in understanding harmful algal blooms: paradigm shifts and new technologies for research, monitoring, and management. *Annu. Rev. Mar. Sci.* 4, 143–176. doi: 10.1146/annurev-marine-120308-081121

Anderson, D. M., Glibert, P. M., and Burkholder, J. M. (2002). Harmful algal blooms and eutrophication: nutrient sources, composition, and consequences. *Estuaries* 25, 704–726. doi: 10.1007/BF02804901

Anderson, D. M., Hoagland, P., Kaoru, Y., and White, A. W. (2000). *Estimated Annual Economic Impacts from Harmful Algal Blooms (HABs) in the United States*. Woods Hole, MA: Woods Hole Oceanographic Institution. doi: 10.1575/1912/96

Anderson, N. J. (2000). Diatoms, temperature and climate change. *Eur. J. Phycol.* 35, 307–314. doi: 10.1017/S0967026200002857

Antia, N., Harrison, P. J., and Oliveira, L. (1991). The role of dissolved organic nitrogen in phytoplankton nutrition, cell biology and ecology. *Phycologia* 30, 1–89. doi: 10.2216/i0031-8884-30-1-1.1

AQSIQ (1997). *Seawater Quality Standard (GB3097-1997)*. Beijing: Standards Press of China.

Burkholder, J. M., Glibert, P. M., and Skelton, H. (2008). Mixotrophy: a major mode of nutrition for harmful algal species in eutrophic waters. *Harmful Algae* 8, 77–93. doi: 10.1016/j.hal.2008.08.010

Chen, B. H., Wang, K., Dong, X., and Lin, H. (2021). Long-term changes in red tides outbreaks in Xiamen Bay in China from 1986 to 2017. *Estuar. Coast. Shelf Sci.* 249:107095. doi: 10.1016/j.ecss.2020.107095

Chen, D. S., and Yan, J. H. (2006). A characteristic and impact on water environment current in the gulf sea area of Zhanjiang. *Sci. Technol. Eng.* 14, 2100–2103.

Chen, F. J., Chen, C. Q., Zhou, F. X., Lao, Q. B., Zhu, F. M., and Zhang, S. W. (2017). Nutrients in atmospheric wet deposition in the Zhanjiang Bay. *China Environ. Sci.* 37, 2055–2063.

Chen, N. W., Peng, B. R., Hong, H. S., Turyaheebwa, N., Cui, S. H., and Mo, X. J. (2013). Nutrient enrichment and N:P ratio decline in a coastal bay-river system un southeast China: the need for a dual nutrient (N and P) management strategy. *Ocean Coast. Manage.* 81, 7–13. doi: 10.1016/j.ocecoaman.2012.07.013

Chen, Y. H., Yang, Y. F., and Jiao, N. Z. (2001). Effect of mariculture on the planktonic community and water environments: a review. *Mar. Sci.* 25, 20–22.

Compiling Committee of Records of China Bays (1999). *Records of China Bays 10th Fascicule*. Beijing: Ocean Press.

Corcoran, A. A., and Hunt, R. W. (2021). Capitalizing on harmful algal blooms: from problems to products. *Algal Res.* 55:102265. doi: 10.1016/j.algal.2021.102265

Davidson, K., Flynn, K. J., and Cunningham, A. (1992). Non-steady state ammonium-limited growth of the marine phytoflagellate, *Isochrysis galbana* Parke. *New Phytol.* 122, 433–438. doi: 10.1111/j.1469-8137.1992.tb00070.x

Davidson, K., Gilpin, L. G., Hart, M. C., Fouilland, E., Mitchell, E., Calleja, L. A., et al. (2007). The influence of the balance of inorganic and organic nitrogen on the trophic dynamics of microbial food webs. *Limnol. Oceanogr.* 52, 2147–2163. doi: 10.4319/lo.2007.52.5.2147

Davidson, K., Gowen, R. J., Harrison, P. J., Fleming, L. E., Hoagland, P., and Moschonas, G. (2014). Anthropogenic nutrients and harmful algae in coastal waters. *J. Environ. Manage.* 146, 206–216. doi: 10.1016/j.jenvman.2014.07.002

Department of Natural Resources of Guangdong Province (2013-2020). *Guangdong Marine Disaster Bulletin*. Guangzhou: Department of Natural Resources of Guangdong Province.

Desmit, X., Thieu, V., Billen, G., Campuzano, F., Dulière, V., Garnier, J., et al. (2018). Reducing eutrophication may require a paradigmatic change. *Sci. Total Environ.* 635, 1444–1466. doi: 10.1016/j.scitotenv.2018.04.181

Dybas, C. (2018). *Two Decades of Hurricanes Change Coastal Ecosystems: Increase Algae Blooms, Fish Kills, Dead Zones*. Available Online at: https://phys.org/news/2018-05-decades-hurricanes-coastal-ecosystemsincrease-algae.html [accessed May 3, 2018].

Emanuel, K. (2005). Increasing destructiveness of tropical cyclones over the past 30 years. *Nature* 436, 686–688. doi: 10.1038/nature03906

Fasullo, J. T., Otto-Bliesner, B. L., and Stevenson, S. (2018). ENSO's changing influence on temperature, precipitation and wildfire in a warming climate. *Geophys. Res. Lett.* 45, 9216–9225. doi: 10.1029/2018GL079022

Ferreira, J. G., Andersen, J. H., Borja, A., Bricker, S. B., Camp, J., Cardoso da Silva, M., et al. (2011). Overview of eutrophication indicators to assess environmental status within the European marine strategy framework directive. *Estuar. Coast. Shelf Sci.* 93, 117–131. doi: 10.1016/j.ecss.2011.03.014

Flynn, K. J., Mitra, A., Glibert, P. M., and Burkholder, J. M. (2018). "Mixotrophy in harmful algal blooms: by whom, on whom, when, why, and what next," in *Global Ecology and Oceanography of Harmful Algal Blooms*, eds P. M. Glibert, E. Berdalet, M. A. Burford, G. C. Pitcher, and M. Zhou (Cham: Springer), 113–132. doi: 10.1007/978-3-319-70069-4_7

Frigstad, H., Andersen, T., Hessen, D. O., Jeansson, E., Skogen, M. D., Naustvoll, L. J., et al. (2013). Long-term trends in carbon, nutrients and stoichiometry in Norwegian coastal waters: evidence of a regime shift. *Prog. Oceanogr.* 111, 113–124. doi: 10.1016/j.pocean.2013.01.006

Glibert, P. M., and Burford, M. A. (2017). Globally changing nutrient loads and harmful algal blooms. *Oceanography* 30, 58–69. doi: 10.5670/oceanog.2017.110

Glibert, P. M., Seitzinger, S. P., Heil, C. A., Burkholder, J. M., Parrow, M. W., Codispoti, L. A., et al. (2005). The role of eutrophication in the global proliferation of harmful algal blooms. *Oceanography* 18, 198–209. doi: 10.5670/oceanog.2005.54

Glibert, P. M. (2020). Harmful algae at the complex nexus of eutrophication and climate change. *Harmful Algae* 91:101583. doi: 10.1016/j.hal.2019.03.001

Glibert, P. M., Harrison, J., Heil, C., and Seitzinger, S. (2006). Escalating worldwide use of urea- a global change contributing to coastal eutrophication. *Biogeochemistry* 77, 441–463. doi: 10.1007/s10533-005-3070-5

Glibert, P. M., Magnien, R., Lomas, M. W., Alexander, J., Fan, C., Haramoto, E., et al. (2001). Harmful algal blooms in the Chesapeake and coastal bays of Maryland, USA: comparison of 1997, 1998, and 1999 events. *Estuaries* 24, 875–883. doi: 10.2307/1353178

Gomez, F. A., Lee, S. K., Hernandez, F. J. Jr., Chiaverano, L. M., Muller-Karger, F. E., Liu, Y. Y., et al. (2019). ENSO-induced co-variability of salinity, plankton biomass and coastal currents in the northern Gulf of Mexico. *Sci. Rep.* 9:178. doi: 10.1038/s41598-018-36655-y

Granéli, E., Carlsson, P., and Legrand, C. (1999). The role of C, N and P in dissolved and particulate organic matter as a nutrient source for phytoplankton growth, including toxic species. *Aquat. Ecol.* 33, 17–27. doi: 10.1023/A:1009925515059

Greening, H., Janicki, A., Sherwood, E. T., Pribble, R., and Johansson, J. O. R. (2014). Ecosystem responses to long-term nutrient management in an urban estuary: Tampa Bay, Florida, USA. *Estuar. Coast. Shelf Sci.* 151, A1–A16. doi: 10.1016/j.ecss.2014.10.003

Guangdong Municipal Statistics Bureau (2019). *Guangdong Statistical Yearbook, 2018*. Guangzhou: Guangdong Bureau of Statistics.

Guangdong Oceanic and Fishery Bureau (2005-2012). *Marine Environment Quality Bulletin of Guangdong Province*. Guangzhou: Guangdong Oceanic and Fishery Bureau.

Guo, J., Yang, W. D., Liu, J. S., and Fan, Z. H. (2007). Effects of salinity, temperature and light intensity on the growth and toxin production of *Phaeocystis globosa*. *Acta Sci. Circumstantiae* 27, 1341–1346.

Harding, L. W., Gallegos, C. L., Perry, E. S., Miller, W. D., Adolf, J. E., Mallonee, M. E., et al. (2016). Long-term trends of nutrients and phytoplankton in Chesapeake Bay. *Estuaries Coast.* 39, 664–681. doi: 10.1007/s12237-015-0023-7

Harding, L. W., Mallonee, M. E., Perry, E. S., Miller, W. D., Adolf, J. E., Gallegos, C. L., et al. (2019). Long-term trends, current status, and transitions of water quality in Chesapeake Bay. *Sci. Rep.* 9:6709. doi: 10.1038/s41598-019-43036-6

He, C., Song, S. Q., and Li, C. W. (2019). The spatial-temporal distribution of *Phaeocystis globose* colonies and related affecting factors in Guangxi Beibu Gulf. *Oceanol. Limnol. Sin.* 50, 630–643.

Heisler, J., Glibert, P. M., Burkholder, J. M., Anderson, D. M., Cochlan, W., Dennison, W. C., et al. (2008). Eutrophication and harmful algal blooms: a scientific consensus. *Harmful Algae* 8, 3–13. doi: 10.1016/j.hal.2008.08.006

Howarth, R. W., and Marino, R. (2006). Nitrogen as the limiting nutrient for eutrophication in coastal marine ecosystems: evolving views over three decades. *Limnol. Oceanogr.* 51, 364–376. doi: 10.4319/lo.2006.51.1_part_2.0364

Howarth, R. W., Sharpley, A., and Walker, D. (2002). Sources of nutrient pollution to coastal waters in the United States: implications for achieving coastal water quality goals. *Estuaries* 25, 656–676. doi: 10.1007/BF02804898

Huo, W. Y., Yu, Z. M., Zou, J. Z., Song, X. X., and Hao, J. H. (2001). Outbreak of *Skeletonema costatum* red tide and its relation to environment al factors in the Jiaozhou Bay. *Oceanol. Limnol. Sin.* 32, 312–317.

Li, H. M., Tang, H. J., Shi, X. Y., Zhang, C. S., and Wang, X. L. (2014). Increased nutrient loads from the Changjiang (Yangtze) River have led to increased harmful algal blooms. *Harmful Algae* 39, 92–101. doi: 10.1016/j.hal.2014.07.002

Li, L., and Lv, S. H. (2009). A 30-year retrospective analysis over the detrimental algal blooms in Guangdong coastal areas. *J. Safe Environ.* 9, 83–86.

Li, M., Ni, W., Zhang, F., Glibert, P. M., and Lin, C. H. M. (2020). Climate-induced interannual variability and projected change of two harmful algal bloom taxa in Chesapeake Bay, USA. *Sci. Total Environ.* 744:140947. doi: 10.1016/j.scitotenv.2020.140947

Li, X. B., Sun, X. Y., Niu, F. X., and Song, J. (2012). Numerical study on the water exchange of a semi-closed bay. *Mar. Sci. Bull.* 31, 248–254.

Li, Z. Y., Xu, S. J., Xu, H. Y., and Cai, X. (2012). Value assessment of marine ecosystem service in Zhanjiang Bay. *Mar. Environ. Sci.* 31, 567–571.

Liang, S. K., Pearson, S., Wu, W., Ma, Y. J., Qiao, L. L., Wang, X. H., et al. (2015). Reseach and integrated coastal zone management in rapidly developing estuarine harbours: a review to inform sustainment of functions in Jiaozhou Bay, China. *Ocean Coast. Manage.* 116, 470–477. doi: 10.1016/j.ocecoaman.2015.09.014

Liang, Y. (2010). *Response of Typical HABs Microalgaes to Nitrogen and Phosphorus*. Guangzhou: Jinan University.

Lin, C. H., Flynn, K. J., Mitra, A., and Glibert, P. M. (2018). Simulating effects of variable stoichiometry and temperature on mixotrophy in the harmful dinoflagellate *Karlodinium veneficum*. *Front. Mar. Sci.* 5:320. doi: 10.3389/fmars.2018.00320

Liu, C., Kroeze, C., Hoekstra, A. Y., and Gerbens-Leenes, W. (2012). Past and future trends in grey water footprints of anthropogenic nitrogen and phosphorus inputs to major world rivers. *Ecol. Indic.* 18, 42–49. doi: 10.1016/j.ecolind.2011.10.005

Liu, L. S., Zhou, J., Zheng, B. H., Cai, W. Q., Lin, K. X., and Tang, J. L. (2013). Temporal and spatial distribution of red tide outbreaks in the Yangtze River Estuary and adjacent waters, China. *Mar. Pollut. Bull.* 72, 213–221. doi: 10.1016/j.marpolbul.2013.04.002

Lv, J., Fang, H. P., Li, K. J., Zhang, L. Z., and Li, Q. (2002). Water quality investigation and assessment on seawater in Zhanjiang Port-Bay. *Environ. Prot. Transport* 23, 16–18, 24.

Mallin, M. A., and Corbett, C. A. (2006). How hurricane attributes determine the extent of environmental effects: multiple hurricanes and different coastal systems. *Estuaries Coast.* 29, 1046–1061. doi: 10.1007/BF02798667

McQuatters-Gollop, A., Raitsos, D., Edwards, M., Pradhan, Y., Mee, L., and Lavender, S. (2007). A long-term chlorophyll dataset reveals regime shift in North Sea phytoplankton biomass unconnected to nutrient levels. *Limnol. Oceanogr.* 52, 635–648. doi: 10.4319/lo.2007.52.2.0635

Miller, W. D., Harding, L. W., and Adolf, J. E. (2006). Hurricane Isabel generated an unusual fall bloom in Chesapeake Bay. *Geophys. Res. Lett.* 33:LO6612. doi: 10.1029/2005GL025658

Mohamed, Z. A. (2018). Potentially harmful microalgae and algal blooms in the Red Sea: current knowledge and research needs. *Mar. Environ. Res.* 140, 234–242. doi: 10.1016/j.marenvres.2018.06.019

Mohamed, Z. A., and Al-Shehri, A. M. (2012). The link between shrimp farm runoff and blooms of toxic *Heterosigma akashiwo* in Red Sea coastal waters. *Oceanologia* 54, 287–309. doi: 10.5697/oc.54-2.287

O'Neil, J. M., Davis, T. W., Burford, M. A., and Gobler, C. J. (2012). The rise of harmful cyanobacteria blooms: the potential roles of eutrophication and climate change. *Harmful Algae* 14, 313–334. doi: 10.1016/j.hal.2011.10.027

Pete, R., Davidson, K., Hart, M. C., Gutierrez, T., and Miller, A. E. J. (2010). Diatom derived dissolved organic matter as a driver of bacterial productively: the role of nutrient limitation. *J. Exp. Mar. Biol. Ecol.* 391, 20–26. doi: 10.1016/j.jembe.2010.06.002

Phlips, E. J., Badylak, S., Nelson, N. G., and Havens, K. E. (2020). Hurricanes, El Niño and harmful algal blooms in two sub-tropical Florida estuaries: direct and indirect impacts. *Sci. Rep.* 10:1910. doi: 10.1038/s41598-020-58771-4

Shen, P. P., Qi, Y. Z., and Ou, L. J. (2018). *Phaeocystis globosa* in coastal China: taxonomy, distribution, and its blooms. *Mar. Sci.* 10, 146–162.

Shi, Y. H., Jia, L. W., and Lin, Y. T. (2021). Environmental capacity calculation and sewage treatment in the inner Zhanjiang Bay. *J. Trop. Oceanogr.* 40, 134–142.

Shi, Y. Z., Zhang, Y. B., and Sun, S. L. (2015). Spatiotemporal distribution of eutrophication and its relationship with environmental factors in Zhanjiang Sea Bay Area. *J. Environ. Sci. Technol.* 38, 90–96, 122.

Smayda, T. J. (1990). "Novel and nuisance phytoplankton blooms in the sea: evidence for a global epidemic," in *Toxic Marine Phytoplankton*, eds E. Granéli, B. Sundström, L. Edler, and D. M. Anderson (New York, NY: Elsevier), 29–40.

Smil, V. (2001). *Enriching the Earth: Fritz Haber, Carl Bosch, and the Transformation of World Food*. Cambridge: The MIT Press. doi: 10.7551/mitpress/2767.001.0001

Song, N., Wang, N., Wu, N., and Lin, W. N. (2018). Temporal and spatial distribution of harmful algal blooms in the Bohai Sea during 1952-2016 based on GIS. *China Environ. Sci.* 38, 1142–1148.

Stoecker, D. K. (1999). Mixotrophy among dinoflagellates. *J. Eukaryot. Microbiol.* 46, 397–401. doi: 10.1111/j.1550-7408.1999.tb04619.x

Svirčev, Z., Lalić, D., Savić, G. B., Tokodi, N., Backović, D. D., Chen, L., et al. (2019). Global geographical and historical overview of cyanotoxin distribution and cyanobacterial poisonings. *Arch. Toxicol.* 93, 2429–2481. doi: 10.1007/s00204-019-02524-4

Tilman, D. (1977). Resource competition between plankton algae: an experimental and theoretical approach. *Ecology* 58, 338–348. doi: 10.2307/1935608

Wang, B. D. (2006). Cultural eutrophication in the Changjiang (Yangtze River) plume: history and perspective. *Estuar. Coast. Shelf Sci.* 69, 474–477. doi: 10.1016/j.ecss.2006.05.010

Wang, B. D., Xin, M., Wei, Q. S., and Xie, L. P. (2018). A historical overview of coastal eutrophication in China Seas. *Mar. Pollut. Bull.* 136, 394–400. doi: 10.1016/j.marpolbul.2018.09.044

Wang, J. J., Bouwman, A. F., Liu, X. C., Beusen, A. H. W., Dingenen, R. V., Dentener, F., et al. (2021). Harmful algal blooms in Chinese coastal waters will persist due to perturbed nutrient ratios. *Environ. Sci. Technol. Lett.* 8, 276–284. doi: 10.1021/acs.estlett.1c00012

Webster, P. J., Holland, G. J., Curry, J. A., and Chang, H. R. (2005). Changes in tropical cyclone number, duration, and intensity in a warming environment. *Science* 309, 1844–1846. doi: 10.1126/science.1116448

Wells, M. L., Trainer, V. L., Smayda, T. J., Karlson, B. S., Trick, C. G., Kudela, R. M., et al. (2015). Harmful algal blooms and climate change: learning from the past and present to forecast the future. *Harmful Algae* 49, 68–93. doi: 10.1016/j.hal.2015.07.009

Xu, Y., Zhang, T., and Zhou, J. (2019). Historical occurrence of algal blooms in the northern Beibu Gulf of China and implications for future trends. *Front. Microbiol.* 10:451. doi: 10.3389/fmicb.2019.00451

Yang, F., Mi, T., Chen, H., and Yao, Q. (2019). Developing numeric nutrient criteria for the Yangtze River Estuary and adjacent waters in China. *J. Hydrol.* 579:124188. doi: 10.1016/j.jhydrol.2019.124188

Yang, L. Q., Mou, S. L., Li, H. M., Zhang, Z. H., Jiao, N. Z., and Zhang, Y. Y. (2021). Terrestrial input of herbicides has significant impacts on phytoplankton and bacterioplankton communities in coastal waters. *Limnol. Oceanogr.* 66, 4028–4045. doi: 10.1002/lno.11940

Yu, R. C., Zhang, Q. C., Kong, F. Z., Zhou, Z. X., Chen, Z. F., Zhao, Y., et al. (2017). Status, impacts and long changes of harmful algae blooms in the sea area adjacent to the Changjiang River estuary. *Oceanol. Limnol. Sin.* 48, 1178–1186.

Yu, Z. M., and Chen, N. S. (2019). Emerging trends in red tide and major research processes. *Oceanol. Limnol. Sin.* 50, 474–486.

Yuan, Q., Xu, Z. Y., Peng, H. Q., Lu, J. M., Huang, L. C., Liang, X. J., et al. (2016). Research on nitrogen and phosphorus variation trend in Zhanjiang harbor and its near waters in recent five years. *J. Green Sci. Technol.* 24, 41–45.

Zhang, J., Zhang, Y., Zhang, P., Li, Y., Li, J., Luo, X., et al. (2021). Seasonal phosphorus variation in coastal water affected by the land-based sources input in the eutrophic Zhanjiang Bay, China. *Estuar. Coast. Shelf Sci.* 252:107277. doi: 10.1016/j.ecss.2021.107277

Zhang, P., Dai, P., Zhang, J., Li, J., Zhao, H., and Song, Z. (2021). Spatiotemporal variation, speciation, and transport flux of TDP in Leizhou Peninsula coastal waters, South China Sea. *Mar. Pollut. Bull.* 167:112284. doi: 10.1016/j.marpolbul.2021.112284

Zhang, L. Z., Yu, L., and Tang, M. S. (2009). Eutrophication and red tide in coastal waters of Zhanjiang port. *Water Resour. Prot.* 25, 50–54.

Zhang, P., Peng, C. H., Zhang, J. B., Zou, Z. B., Shi, Y. Z., Zhao, L. R., et al. (2020a). Spatiotemporal urea distribution, sources, and indication of DON bioavailability in Zhanjiang Bay, China. *Water* 12:633. doi: 10.3390/w12030633

Zhang, P., Xu, J. L., Zhang, J. B., Li, J. X., Zhang, Y. C., Li, Y., et al. (2020b). Spatiotemporal dissolved silicate variation, sources, and behavior in the eutrophic Zhanjiang Bay, China. *Water* 12:3586. doi: 10.3390/w12123586

Zhang, P., Ruan, H. M., Dai, P. D., Zhao, L. R., and Zhang, J. B. (2020c). Spatiotemporal river flux and composition of nutrients affecting adjacent coastal water quality in Hainan Island, China. *J. Hydrol.* 591:125293. doi: 10.1016/j.jhydrol.2020.125293

Zhang, P., Su, Y., Liang, S. K., Li, K. Q., Li, Y. B., and Wang, X. L. (2017). Assessment of long-term water quality variation affected by high-intensity land-based inputs and land reclamation in Jiaozhou Bay, China. *Ecol. Indic.* 75, 210–219. doi: 10.1016/j.ecolind.2016.12.035

Zhang, P., Wei, L. R., Lai, J. Y., Dai, P. D., and Zhang, J. B. (2019). Concentration, composition and fluxes of terrestrial nitrogen and phosphorus source pollutants input into Zhanjiang Bay in summer. *J. GDOU* 39, 46–55.

Zhanjiang Municipal Statistics Bureau (2007-2011). *Bulletin of Marine Environmental Status of Zhanjiang*. Zhanjiang: Zhanjiang Oceanic and Fishery Bureau.

Zhanjiang Oceanic and Fishery Bureau (2000-2020). *Bulletin of Marine Environmental Status of Zhanjiang*. Zhanjiang: Zhanjiang Oceanic and Fishery Bureau.

Zhanjiang Oceanic and Fishery Bureau (2007-2011). *Bulletin of Marine Environmental Status of Zhanjiang*. Zhanjiang: Zhanjiang Oceanic and Fishery Bureau.

Zhou, M., Zhu, M., and Zhang, J. (2001). Status of harmful algal blooms and related research activities in China. *Chin. Bull. Life Sci.* 13, 53–59.

Conflict of Interest: The authors declare that the research was conducted in the absence of any commercial or financial relationships that could be construed as a potential conflict of interest.

Publisher's Note: All claims expressed in this article are solely those of the authors and do not necessarily represent those of their affiliated organizations, or those of the publisher, the editors and the reviewers. Any product that may be evaluated in this article, or claim that may be made by its manufacturer, is not guaranteed or endorsed by the publisher.

frontiers | Frontiers in Marine Science

ORIGINAL RESEARCH
published: 13 May 2022
doi: 10.3389/fmars.2022.863629

Bioaccumulation of Mercury and Other Trace Elements in the Edible Holothurian *Holothuria* (*Halodeima*) *atra* in Relation to Gold Mining Activities in North Sulawesi, Indonesia

Marco Tamburini[1†], Denis Badocco[2†], Riccardo Ercadi[3], Eva Turicchia[3,4,5,6,7†], Greta Zampa[3†], Fabio Gasparini[8†], Loriano Ballarin[8†], Roberta Guerra[9†], Markus T. Lasut[10†], Daisy M. Makapedua[10†], Jane Mamuaja[10†], Paolo Pastore[2†] and Massimo Ponti[3,5,6,7†]*

[1] Dipartimento di Scienze della Terra e dell'Ambiente, Università degli Studi di Pavia, Pavia, Italy, [2] Dipartimento di Scienze Chimiche, Università degli Studi di Padova, Padova, Italy, [3] Dipartimento di Scienze Biologiche, Geologiche e Ambientali, Alma Mater Studiorum Università di Bologna, Ravenna, Italy, [4] Dipartimento di Beni Culturali, Alma Mater Studiorum Università di Bologna, Ravenna, Italy, [5] Centro Interdipartimentale di Ricerca Industriale Fonti Rinnovabili, Ambiente, Mare ed Energia, Università degli studi di Bologna, Ravenna, Italy, [6] Reef Check Italia onlus, Ancona, Italy, [7] Consorzio Nazionale Interuniversitario per le Scienze del Mare, Roma, Italy, [8] Dipartimento di Biologia, Università degli Studi di Padova, Padova, Italy, [9] Dipartimento di Fisica e Astronomia, Alma Mater Studiorum Università di Bologna, Ravenna, Italy, [10] Faculty of Fisheries and Marine Science, Sam Ratulangi University, Manado, North Sulawesi, Indonesia

Artisanal and small-scale gold mines (ASGMs) have been accompanied by widespread usage of mercury amalgamation to extract gold from ores, putting Indonesia among the top three global emitters of this pollutant and posing potential risks to the marine ecosystem and human health. Although the use of mercury has been largely eliminated following the signature of the Minamata Convention on Mercury, the practice of mercury amalgamation in ASGM has persisted in several regions, including the North Sulawesi. This study assesses how on the contamination of mercury and other trace elements coming from both industrial mines and ASGMs affects marine sediments and their bioaccumulation in two tissues (body wall and guts) of the edible holothurian *Holothuria* (*Halodeima*) *atra*, by comparing samples collected downstream of four mining areas to four control sites in the North Sulawesi province, Indonesia. In sediments, mean concentrations of arsenic, gold, cobalt, chromium, copper, mercury, nickel, lead, antimony, and zinc were significantly higher at sites receiving mine discharges than at control sites. Downstream to gold mines, compared to control sites, significant higher concentrations of As, Au, Cr, Hg, and Ni in holothurians body walls and of As, Au, Co, Cr, Cu, Hg, Pb, Sb, Sn, and Zn in holothurians guts were found. In general, higher contaminations in sediments and tissues were found at the site near the oldest artisanal mine. Trace element levels in *H. atra* specimens in North Sulawesi were generally higher than those reported in other regions. In the study area, these holothurians significantly

OPEN ACCESS

Edited by:
Elisabeth Marijke Anne Strain, University of Tasmania, Australia

Reviewed by:
Alberto Sánchez-González, Instituto Politécnico Nacional (IPN), Mexico
Patrícia Pereira, University of Aveiro, Portugal

***Correspondence:**
Eva Turicchia
eva.turicchia2@unibo.it

†ORCID:
Marco Tamburini
orcid.org/0000-0001-7802-3761
Denis Badocco
orcid.org/0000-0001-6270-7966
Eva Turicchia
orcid.org/0000-0002-8952-9028
Greta Zampa
orcid.org/0000-0003-0217-8972
Fabio Gasparini
orcid.org/0000-0002-7574-0834
Loriano Ballarin
orcid.org/0000-0002-3287-8550
Roberta Guerra
orcid.org/0000-0002-7151-6616
Markus T. Lasut
orcid.org/0000-0003-2087-1877
Daisy M. Makapedua
orcid.org/0000-0003-4334-6020
Jane Mamuaja
orcid.org/0000-0002-6496-7582
Paolo Pastore
orcid.org/0000-0003-1448-0175
Massimo Ponti
orcid.org/0000-0002-6521-1330

Specialty section:
This article was submitted to Marine Pollution, a section of the journal Frontiers in Marine Science

Received: *27 January 2022*
Accepted: *06 April 2022*
Published: *13 May 2022*

bioaccumulate Hg, As, Zn, Cd, Cu, Sn, and biota-sediment accumulation factors were higher in guts than in body walls. From an environmental and human health perspective, Hg is resulted the most concerning element in surface sediment and *H. atra* specimens. Based on this evidence, further studies are urgently needed to understand better the effect of mercury and other potentially toxic trace elements in marine ecosystems and food webs in mining areas both in North Sulawesi and in many still poorly investigated southeast Pacific areas.

Keywords: heavy metals, pollution, lollyfish, trepang, sea cucumbers, artisanal mines, coral reef, coral triangle

INTRODUCTION

Toxic trace elements including arsenic (As), cadmium (Cd), cobalt (Co), chromium (Cr), copper (Cu), mercury (Hg), nickel (Ni), lead (Pb), antimony (Sb), tin (Sn) and zinc (Zn) can accumulate in marine and coastal environments, derived from natural processes, including rock weathering, volcanic emissions, and aeolian transport, and human activities. Swift industrialization, economic development, and urbanization in coastal regions has contributed to an increase of trace elements in seas, in estuarine and coastal habitats (Jiang et al., 2014). This increasing spread of trace elements and other pollutants from anthropogenic activities threatens local species and humans and has assumed global relevance (Long and Chapman, 1985; Ponti et al., 2021).

Mining activities are among the main causes of mobilization and release of trace elements into the environment (Marmolejo-Rodríguez et al., 2011). In the North Sulawesi province (Indonesia), as in many other areas of the Coral Triangle (*sensu* Veron et al., 2009), industrial and artisanal gold mining activities are widespread. While industrial gold mines generally use the cyanidation method, artisanal and small-scale gold mines (hereafter ASGMs) still employ Hg amalgamation to extract gold from ores (Bose-O'Reilly et al., 2010; Edinger, 2012). ASGMs are considered a major source for emission and release of Hg worldwide (Velásquez-López et al., 2010; Cordy et al., 2011; Odumo et al., 2014; González-Merizalde et al., 2016; Oke and Vermeulen, 2016), with 410-1040 tons of employed Hg per year corresponding to ca. 37% of total anthropogenic Hg emissions (Futsaeter and Wilson, 2013). Moreover, Hg (as cinnabar, a form of mercury sulfide), As, and Sb can be present in many gold deposits (Edinger, 2012). Mine tailings, even when stored in artificial closed ponds, as occurs in industrial mines, may be dispersed in the catchment basin due to heavy rain and flooding events, frequent in tropical areas (González-Valoys et al., 2022).

After the discovery of the Minamata neurological disease, caused by severe Hg poisoning in the Minamata Bay (Japan) from a local chemical factory in the 1956 (Eto et al., 2010), numerous studies were carried out on the bioaccumulation and marine food web transfers of potentially toxic trace elements (e.g., Bryan and Langston, 1992; Wang, 2002; Gao and Chen, 2012; Li et al., 2017; Murillo-Cisneros et al., 2019). A large number of chemical and biological mediated processes can contribute to trace element mobilization from rocks and soils (e.g., Carrillo-González et al., 2006; Sessitsch et al., 2013; Sánchez-Donoso et al., 2021). After being released from natural or anthropogenic sources like factories, mines, shipping, dumping, or harbors to the marine environment, soluble trace metal species are accumulated in sediments through physical, chemical, and biological processes. For example, bacterially mediated processes can methylate Hg once it is available at the sediment-water interface as metallic Hg or in metastable phases. Then methylmercury (MeHg) is acutely toxic and readily biomagnifies up marine food webs (Edinger, 2012). The sedimentation of trace elements is quickened thanks to the high salinity of seawater that enhances the aggregation of suspended particles; therefore, sediment is considered the main sink for trace elements (and other pollutants) in urbanized coastal ecosystems (e.g., Du Laing et al., 2009; Jonathan et al., 2011; Qian et al., 2015; Birch et al., 2020).

Given their bioaccumulation and toxic effects on aquatic organisms, trace metals analyses are usually included in marine environmental monitoring programs (e.g., Badr et al., 2009; Greggio et al., 2021). Benthic communities involved in detrital-based food webs are frequently subjected to effluent waste from anthropogenic sources: high levels of trace elements in sediments might mean an ecotoxicological threat for benthic invertebrates (e.g., Bryan and Langston, 1992; Rainbow, 2002; O'Brien and Keough, 2014). In particular, being deposit-feeders and scavengers, many holothurians represent a relevant step in transferring of pollutants from sediments to marine food webs (Aydın et al., 2017). They play major roles in sediment bioturbation (Uthicke, 1999) and are preyed upon by many taxa, thereby transferring accumulated toxic elements to higher trophic levels (Purcell et al., 2016). Some holothurians are also food for humans. They are mainly eaten in Asia, where are regarded as traditional medicine, delicacies and aphrodisiacs (Aydın et al., 2017).

The target species of the present study is *Holothuria* (*Halodeima*) *atra*, commonly known as black sea cucumber or lollyfish. It is an intertidal and shallow-water species widely distributed in the tropical Indo-Pacific region and one of the most frequently encountered in Indonesia (Conand, 1998; Bellchambers et al., 2011). Inshore shallow-water populations are often dense and composed of small individuals (about 20 cm and 0.2 kg live weight, on average) that reproduce mostly by transversal fission (Hartati et al., 2019; Hartati et al., 2020). Individuals of deeper or outer reef populations are more

scattered and larger (up to 45 cm and 1 kg live weight) and reproduce sexually more frequently (Conand, 1998). Preferring habitats rich in organic matter, this species plays a relevant role in nutrients recycling and sediment reworking in tropical sea bottom (Conand, 2004). It is considered a deposit-feeders and scavenger species that feeds on bacteria and detritus but may digest microalgae and cyanobacteria as well (Uthicke, 1999; Retno et al., 2020). *H. atra* also has relevant commercial importance for the Asian markets (Toral-Granda et al., 2008; Purcell et al., 2012; Setyastuti and Purwati, 2015). According to the Red List of threatened species provided by the International Union for the Conservation of Nature (IUCN), the conservation of this species is considered of least concern (Conand et al., 2013).

This study focuses on the contamination of mercury and other trace elements coming from both industrial mines and ASGMs in marine sediments and their bioaccumulation in two tissues (body wall and guts) of the edible holothurian *Holothuria* (*Halodeima*) *atra*, by comparing samples collected in coastal areas downstream of four mines and at four control sites in the North Sulawesi province, Indonesia. Overall, 12 potentially toxic trace elements were investigated (As, Au, Cd, Co, Cr, Cu, Hg, Ni, Pb, Sb, Sn, and Zn), of these four are particularly linked to gold mining and therefore should be more abundant in sediments and holothurian tissues at sites close to the four mines than at the control sites: Hg, used in ASGMs for gold extraction and often associated to gold deposits; As and Sb, abundant in gold deposits in the region; and Au, the target of mining activities.

MATERIALS AND METHODS

Study Area and Watershed Analysis

The present study was carried out in the North Sulawesi (Indonesian: Sulawesi Utara) province and included four putatively impact sites and four control sites randomly interspersed among the impact ones (**Figure 1**; **Supplementary Material S1; Table S1.1**; **Figure S1.1**). This tropical area is affected by monsoon winds and uneven rainfall (mainly from November to April), with annual rates ranging from 1,000 to 5,000 mm. Air temperature ranges from 22 to 30°C (25°C on average), while sea surface temperature ranges from 27 to 29°C[1].

Impact sites were chosen as closest as possible to the mouth of streams or rivers flowing through mining areas, identified based on a watershed analysis performed with the GRASS' "r.watershed" algorithm in QGIS 3.16 (QGIS Development Team, 2021) using the digital elevation model by the Shuttle Radar Topography Mission (SRTM 4.1; horizontal resolution of 90 m at the equator). Maps resulting from the watershed analysis are reported in **Supplementary Material S1**. These impact sites correspond to different types and periods of gold mining activities.

The first impact site was chosen at Totok Bay (labeled as TB; **Figures S1.1a, S1.2**), where ASGMs were established in the mid-19th century. Totok Bay and the nearby Buyat Bay (Buyat-Ratatotok district; Turner et al., 1994) are areas already known for pollution from gold mines. From 1996 to 2004, Buyat Bay was affected by a submarine tailing disposal of an industrial gold mine (Blackwood and Edinger, 2007; Lasut and Yasuda, 2008; Edinger, 2012). Totok Bay, separated by a discontinuous peninsula, is mainly affected by the wastewater and surface percolation from the ASGM (Blackwood and Edinger, 2007). Lasut et al. (2010) sampled surface sediments from the beach, river estuary, and marine shallow bottom, and some specimens of soft corals, seaweeds, seagrasses, mollusks, crabs, and fishes from both bays, as well as the scalp hair of residents in the area. Total mercury and MeHg were detected in all samples, with the highest concentrations at Totok Bay and intermediate concentrations at Buyat Bay compared to the control area. The second impact site was chosen at the mouth of Talawaan River (TR; **Figures S1.1b, S1.3**) downstream of the Talawaan-Tatelu ASGMs, established in 1997. Here, Kambey et al. (2001) found that fish from the affected area had a mercury content 30 times higher than those from the reference site. The third impact site was chosen at Pantai Surabaya (PS; **Figures S1.1c, S1.4**), downstream to the Toka Tindung industrial mine, operating since 2010. There are no published pollution studies for this area. The fourth impact site was chosen at the mangroves (M1; **Figures S1.1d, S1.5**) between the Coral Eye resort and an industrial mining site under preparation on the west side of Bangka Island, whose soil handling works started in 2014. The start of mining activities immediately raised concern for local coral reefs' health (Ponti et al., 2016). The mine was officially closed in 2017 after the Supreme Court of Jakarta accepted a lawsuit filed by residents and tour operators.

Control sites were randomly located at Lihunu Bay (LB; **Figure S1.1e**), at the North-west Bangka Island mangroves (M2; **Figure S1.1f**), at Tumbak Island (TI; **Figure S1.1g**), and close to the Tasik Ria Resort (TR; **Figure S1.1h**).

Sampling and Sample Processing

All sampling activities took place from June to August 2017, at times chosen around the peak of low tide in a range of depth between -0.9 and 2.8 m below the mean lower low water (**Table S1.1**). Tide levels were calculated by the freeware software WXTide[2], using the closest subordinate harmonic data station available (i.e., Manado or Lembeh Strait).

Three replicate samples of undisturbed surface sediment (top 5 cm) were randomly taken by a plastic scoop at each site to measure grain size and trace element concentration in the sediments. The sampler was washed in deionized water to avoid any contamination after every sampling. Each sample was collected and stored in new low-density polyethylene (LDPE) grip seal bags. All sediment samples were oven-dried at 50°C for 24 h. After a pre-sieving at 2000 μm to remove coral rubbles and large shells, a portion of 10 g from each sample was taken for further chemical analysis. Medium and coarse sand (2000 – 250 μm), fine sand (250 – 63 μm), and mud (silt and clay, < 63 μm)

[1] Climate date from the NOAA Climate.gov.

[2] http://www.wxtide32.com

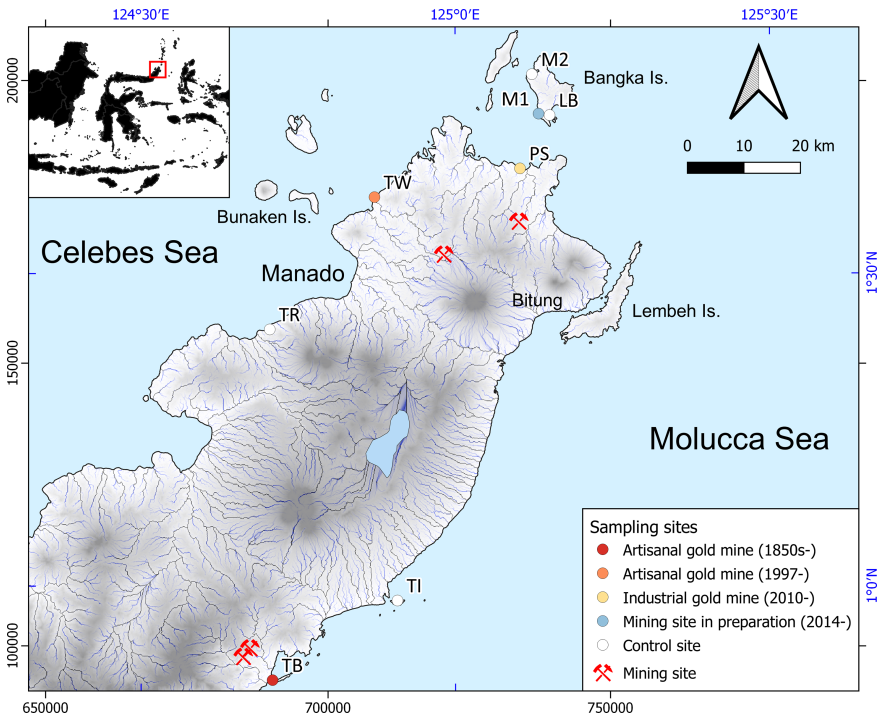

FIGURE 1 | Map of the study area and sampling sites (Datum WGS84, Projection UTM zone 51). Included active gold mines: Totok Bay (TB); Talawaan River (TW); Pantai Surabaya (PS); Mining site in preparation: West Bangka mangroves (M1); Control sites: Lihunu Bay (LB); North-west Bangka mangroves (M2); Tumbak Island (TI); Tasik Ria Resort (TR).

sediment content was measured as dry weight percentage after sieving using certified stainless-steel sieves (Guerra et al., 2009).

At each sites, the population density of *H. atra* was estimated by counting individuals along three belt transects (100 × 4 m, i.e., 400 m^2), carried out at least 10 m apart either by snorkeling or on foot, depending on the depth and tide conditions (Bellchambers et al., 2011). Then, eight specimens of *H. atra* were collected in the intertidal zone to measure trace element concentrations. To avoid differences in bioconcentration among individuals due to different ages, and therefore time exposures, the collected individuals were of similar size (~ 20 cm in length; mean wet weight: 103.7 ± 8.7 g) (Denton et al., 2009). Specimens were transported alive in plastic grip seal bags with seawater until they were placed in 20-liter aquariums with aerators, four specimens per aquarium, to purge their intestinal sediment. After 24-48 hours in the aquarium, the specimens were put in large beakers with a solution of 8% $MgCl_2$ in seawater for 30 min for tissue relaxing. Later, the samples were washed with tap water and dried on the surface with paper towels, weighted (for wet mass measures), and dissected by a longitudinal incision from the anus to the mouth, in order to separately analyze the body wall (about 4 mm thick; Conand, 1998) and guts (Xing and Chia, 1997). Tissue samples were washed in a stream of distilled water to remove the salt, then they were dried at no more than 50°C for 24 h and individually stored in new LDPE grip seal bags until chemical analysis.

Chemical Analysis

Both dried sediment samples and holothurian tissues were grinded in the laboratory after additional drying for 24 h at no more than 50°C. Approximately 1 g of each sample was powdered in a ceramic mortar and put in a plastic screw-top vial. A sediment subsample (about 0.075 g) was added with 0.35 g of HNO_3 (69%) and 0.75 g of HCl (37%, Analytical Reagent). A microwave digestion system (CEM EXPLORER SP-D PLUS) was used for the acid digestion, according to the following protocol: ramp temperature from ambient to 200°C for 4 min, then 200°C for 2 min, and 300 W power with medium stirring and 300 PSI of pressure. Tissue samples (about 0.075 g) were heated in closed polypropylene vials for 3 hours at 100°C and then diluted with Milli-Q water to obtain 5% by weight. All tools, vials and jars were cleaned before every use with 20% nitric acid and deionized water to avoid cross-contamination among samples.

Twelve elements (As, Au, Cd, Co, Cr, Cu, Hg, Ni, Pb, Sb, Sn, and Zn) important for the results of the present study were quantified both in sediment and holothurian tissues by using inductively coupled plasma coupled to a mass spectrometer (ICP-MS, Agilent Technologies 7700x. Agilent Technologies International Japan, Ltd., Tokyo, Japan). In addition, the main rock-forming elements (Ca, Mg, Na, S, Al, Fe, Si, K, Ti) and Li, Ba, and Sr were also quantified to characterize the origin of the sediments. The instrument was equipped with an octupole collision cell operating in kinetic energy discrimination mode,

which was used to remove polyatomic and argon-based interferences. The operating conditions and data acquisition parameters were the same as reported in Badocco et al. (2015a). Multielement standard solutions for calibration were prepared in aqua regia (5%) by gravimetric serial dilution at twelve different concentrations - from a minimum of 1 ng L^{-1} to a maximum of 100 mg L^{-1}. All solutions were prepared in Milli-Q ultrapure water obtained using a Millipore Plus System (Milan, Italy, resistivity 18.2 MOhm cm^{-1}). All regressions were linear with a determination coefficient (R^2) larger than 0.9999. The ICP-MS was tuned daily using a tuning solution containing 1 µg L^{-1} of 140Ce, 7Li, 205Tl, and 89Y (Agilent Technologies, UK). The internal standard mixture (Agilent, 5183-4681) containing Bi, Ge, In, Sc, Tb, Y, and Li (6) at 10 µg mL^{-1}, each in 5% HNO_3 was used. The internal standard was added to the sample solution *via* a T-junction. The Critical Limit (CL), Limit of Detection (LOD) and Limit of Quantification (LOQ) of each element were computed based on the methods described in Lavagnini et al. (2011) and Badocco et al. (2014; 2015a; 2015b; 2015c).

In tissues analysis, the recovery value was assessed using a standard reference material (SRM) 2976 specifically intended for use for the determination of trace elements in marine mollusk tissue or similar matrices. The average recovery obtained from the repetition of 5 measurements was between 93% and 104% for all the elements investigated. The recovery of Au equal to 96% was evaluated by spiking the matrix with suitable amounts of Au solutions. Since the obtained recovery was always close to 100%, the analytical results were not corrected for holothurian tissues as suggested in other works citing recoveries between 80 and 120% as acceptable (Chen and Ma, 2001). In sediment analysis, the recovery of the elements is a variable parameter linked to the nature of the type of rock that originates the sediment. The SRM 2702 Inorganics in Marine Sediment was used as a reference for the tested sediments. The recovery of the elements of interest was between 82% and 112%. The recoveries of Si and Al were lower than 50%. However, the quantification of these elements was used only as an indication of the nature of the sediment.

Data Analysis

Trace element concentration values below Critical Limit (CL) were replaced by one-half of the minimum Limit of Detection (LODmin) only for statistical purposes (Paschal et al., 1998). Since there were no reasons to hypothesize that the concentrations of trace elements in sediment and holothurian tissues were affected in the same way in the different basins subject to gold mines, each putatively impacted site was individually compared to the control sites (as in Guerra et al., 2009 and Ponti et al., 2009). To this end, two-way asymmetrical permutational analysis of variance (PERMANOVA; $\alpha = 0.05$), based on Euclidean distances, was applied to assess the differences in mean concentrations in sediments and tissues (body wall and guts) between Impact and Control, and among sites nested in the interaction Impact × Control, where Impact is represented by a single site while Control has four sites (Anderson and Robinson, 2008). When less than 100 unique permutations were available, the asymptotic Monte Carlo *p*-value was used instead of the permutational one. When no significant differences in mean trace element concentrations were found among control sites ($p > 0.25$), site data were pooled to improve the power of the test for differences between Impact and Control (Anderson et al., 2008).

Possible correlations between the concentrations of trace elements in the body wall and guts of individuals of *H. atra* (n = 64) and between the mean concentrations in the sediments of the different sites and those in the body walls and guts of *H. atra* (n = 64) were estimated with Pearson's moment-product correlation coefficient (*r*), whose difference from zero were assessed by *t*-test ($\alpha = 0.05$).

Bioaccumulation is the concentration in the organism of a chemical resulting from the dynamic equilibrium between the uptake rate (by all possible means, including contact, respiration and ingestion) and the elimination rate (Chojnacka and Mikulewicz, 2014). Since *H. atra* mainly feeds on sediment, for each element, the bioaccumulation in the field can be assessed by the biota-sediment accumulation factor (BSAF), calculated as the ratio between the mean concentrations in tissues (body walls and guts) and sediments at a given site (Thomann et al., 1995). Bioaccumulation in the study area was confirmed when mean BSAF across sites was significantly greater than 1 according to a *t*-test ($\alpha = 0.05$, n = 8).

PERMANOVA analyses were done using PRIMER 6 with PERMANOVA+ addon package (Anderson et al., 2008), while linear correlations and *t*-tests were conducted with the computational language R (R Core Team, 2021). Mean values were reported with their standard errors.

RESULTS

Sediment Features and Contamination

Sandy sediments characterized all sampling sites, but with large variability in medium/coarse sand (12.11-94.83%) and fine sand (5.01-86.16%) contents, while the fraction of mud (silt and clay) was always very low (0.08%-2.59%). Overall, mean grain size at control sites covered the entire range of the putatively impacted sites; however, control M2, TI, and TR sites and the impact site TW showed a higher percentage of medium/coarse sand and a low percentage of fine sand, compared to the other sites (**Supplementary Material S2**, **Figure S2.1**). Mean composition of the main rock-forming elements in the sampled sediments reveals a high percentage of calcium (34-43%) at all sites but TB and PS (1.7% and 11.7%, respectively); here, the sediments resulted comparatively richer in aluminum and iron (**Supplementary Material S2**, **Figure S2.2**).

Mercury and Other Trace Elements Contamination in Surface Sediments

Mean concentrations of trace elements in sediment at impact and control sites are shown by bar plots in **Figure 2**, while tests for significance of differences between mean concentrations at each single impact site to the control ones are reported in the Supplementary Materials (**Tables S3.1–4**). Mean concentrations

of Hg in sediments ranged from below the CL, as occurred at all control sites, to 1.25 ± 0.60 μg g^{-1} at TB (**Figure 2A**). At all putatively impacted sites, including M1, where gold extractions should never have started, the mean Hg concentrations in sediments were significantly higher than at the control sites. Mean concentrations of As ranged from 1.53 ± 0.15 μg g^{-1} at LB to 34.08 ± 3.51 μg g^{-1} at TB, and at TB and PS they were significantly higher than at the control sites (**Figure 2B**). Mean Au concentrations were below CL at all sites except TB, where it was 0.07 ± 0.02 μg g^{-1}, clearly significantly higher than at the control sites (**Figure 2C**). Mean concentrations of Sb ranged from 0.0524 ± 0.0004 μg g^{-1} at LB to 1.16 ± 0.15 μg g^{-1} at TB, and at TB and PS they were significantly higher than at the control sites (**Figure 2D**). Mean concentrations of Cd ranged from 0.023 ± 0.003 μg g^{-1} at PS to 0.047 ± 0.002 μg g^{-1} at LB (**Figure 2E**), resulting significantly heterogeneous between control sites (p <

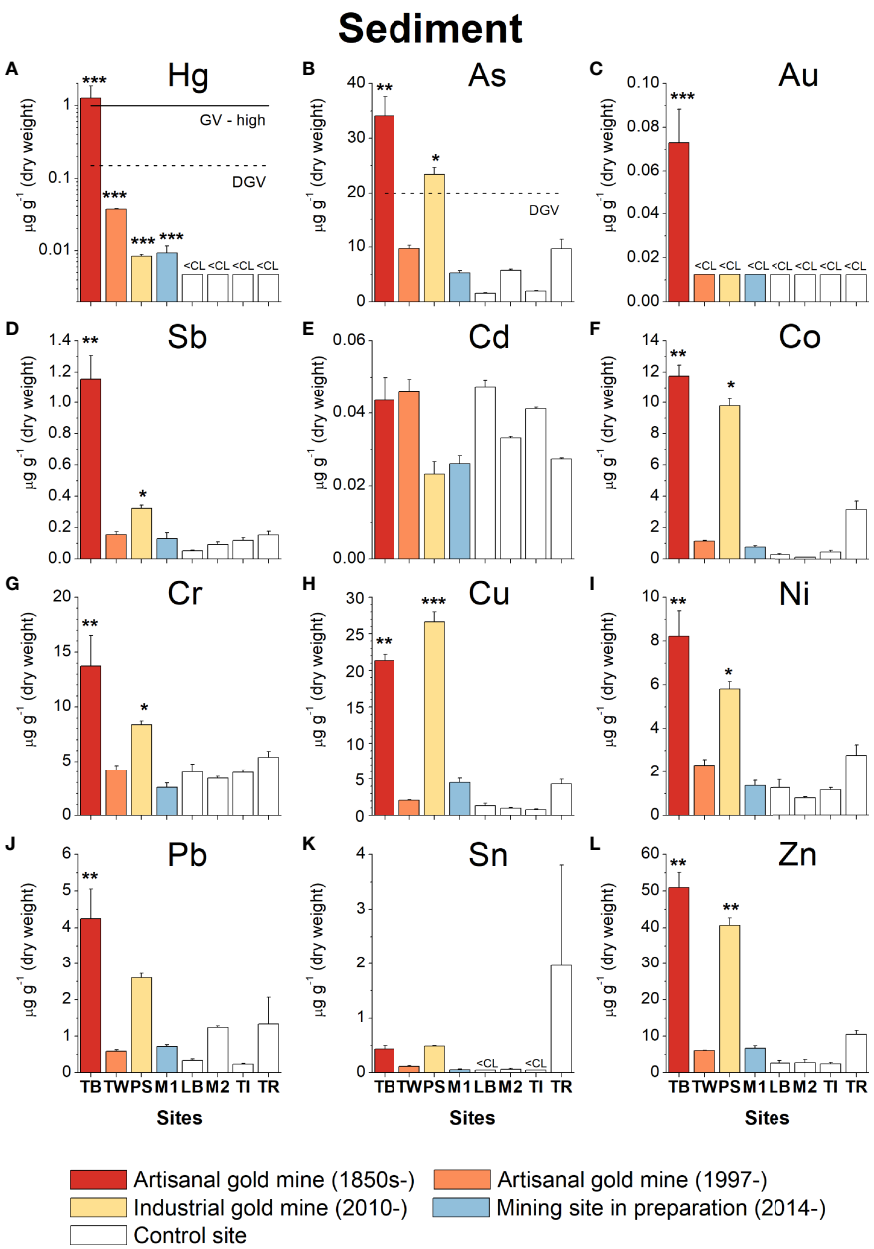

FIGURE 2 | Mean concentrations (± s.e.) of Hg **(A)**, As **(B)**, Au **(C)**, Sb **(D)**, Cd **(E)**, Co **(F)**, Cr **(G)**, Cu **(H)**, Ni **(I)**, Pb **(J)**, Sn **(K)** and Zn **(L)** in surface sediment at each study site (TB, Totok Bay; TW, Talawaan River; PS, Pantai Surabaya; M1, West Bangka mangroves; LB, Lihunu Bay; M2, North-west Bangka mangroves; TI, Tumbak Island; TR, Tasik Ria Resort). Whenever possible, the default guideline value (DGV), i.e., the concentration below which there is a low risk of unacceptable effects occurring, and the 'upper' guideline value (GV-high), i.e., the concentration over which adverse effects are expected, from Simpson et al. (2013), were reported (CL, critical limit). Impact sites that differ significantly from controls are marked with asterisks: *p < 0.05; **p < 0.01; ***p < 0.001.

0.001); since this variability, the concentrations at the impact sites were not significantly different from those of the controls.

Mean concentrations of Co ranged from 0.13 ± 0.01 μg g^{-1} at M2 to 11.74 ± 0.70 μg g^{-1} at TB (**Figure 2F**). Mean concentrations of Cr ranged from 2.55 ± 0.41 μg g^{-1} at M1 to 13.72 ± 2.80 μg g^{-1} at TB (**Figure 2G**). Mean concentrations of Cu ranged from 0.76 ± 0.11 μg g^{-1} at TI to 26.64 ± 1.35 μg g^{-1} at PS (**Figure 2H**). Mean concentrations of Ni ranged from 0.80 ± 0.04 μg g^{-1} at M2 to 8.22 ± 1.16 μg g^{-1} at TB (**Figure 2I**). Although with different levels of significance, Co, Cr, Cu, and Ni were all significantly higher at TB and PS than at the control sites.

Mean concentrations of Pb ranged from 0.23 ± 0.02 μg g^{-1} at TI to 4.25 ± 0.81 μg g^{-1} at TB, which was the only impact site with significantly enriched compared the control sites (**Figure 2J**). Mean concentrations of Sn ranged from below the CL at LB and TI to 1.97 ± 1.84 μg g^{-1} at TR, where it was very variable (**Figure 2K**). Given this variability, it was not possible to detect significant differences between the individual impact sites and the control sites. Finally, mean concentrations of Zn ranged from 2.49 ± 0.40 μg g^{-1} at TI to 50.98 ± 4.15 μg g^{-1} at TB, and, as for many other trace elements, at TB and PS they were significantly higher than at the control sites (**Figure 2L**).

Mercury and Other Trace Elements Concentration in Holothurian Tissues

The mean densities of holothurians ranged from 0.08 ± 0.08 to 3.08 ± 1.18 individuals of *H. atra* per 100 m^2 (**Figure 3**). The density of holothurians was very variable across control and impact sites. Only at the PS impact site the density was significantly higher (ANOVA $p < 0.01$) than the average of the control sites.

Mean concentrations of trace elements in body walls and guts, at impact and control sites, are shown by bar plots in **Figures 4, 5**, respectively, while tests for significance of differences between mean concentrations at each single impact site to the control ones are reported in the Supplementary Materials (**Tables S3.5–12**). Mean concentrations of Hg in body walls of *H. atra* specimens ranged from 0.015 ± 0.001 μg g^{-1} at M2 to 0.25 ± 0.03 μg g^{-1} at TB, and they were significantly higher at the impact sites TB and TW than at the control sites (**Figure 4A**). In guts, mean concentrations of Hg ranged from 0.10 ± 0.02 μg g^{-1} at TR to 1.72 ± 0.37 μg g^{-1} at TB, and they were significantly higher at all active gold mine sites (TB, TW, and PS) than at the control sites (**Figure 5A**). Mean concentrations of As in body walls ranged from 10.38 ± 0.59 μg g^{-1} at TB to 118.72 ± 10.22 μg g^{-1} at the industrial mine site PS, where it was significantly higher than at the control sites (**Figure 4B**). In guts, mean concentrations of As ranged from 24.65 ± 1.92 μg g^{-1} at TB to 219.68 ± 29.09 μg g^{-1} at PS, and they were significantly higher at TW and PS than at the control sites (**Figure 5B**). Mean concentrations of Au in body walls ranged from 0.006 ± 0.001 μg g^{-1} at TR to 0.050 ± 0.002 μg g^{-1} at PS, where it was significantly higher than at the control sites (**Figure 4C**). In guts, mean concentrations of Au ranged from below the CL, at control sites M2 and TR, to 0.51 ± 0.06 μg g^{-1} at PS, and they were significantly higher at all active gold mine sites (TB, TW, and PS) than at the control sites (**Figure 5C**). Mean concentrations of Sb in body walls ranged from 0.021 ± 0.002 μg g^{-1} at TB to 0.05 ± 0.001 μg g^{-1} at PS; however, the mean value at each impact site did not differ significantly from those of the controls (**Figure 4D**). In guts, mean concentrations of Sb ranged from 0.033 ± 0.004 μg g^{-1} at M1 to 0.16 ± 0.02 μg g^{-1} at TB, and they were significantly higher at TB and PS than at the control sites

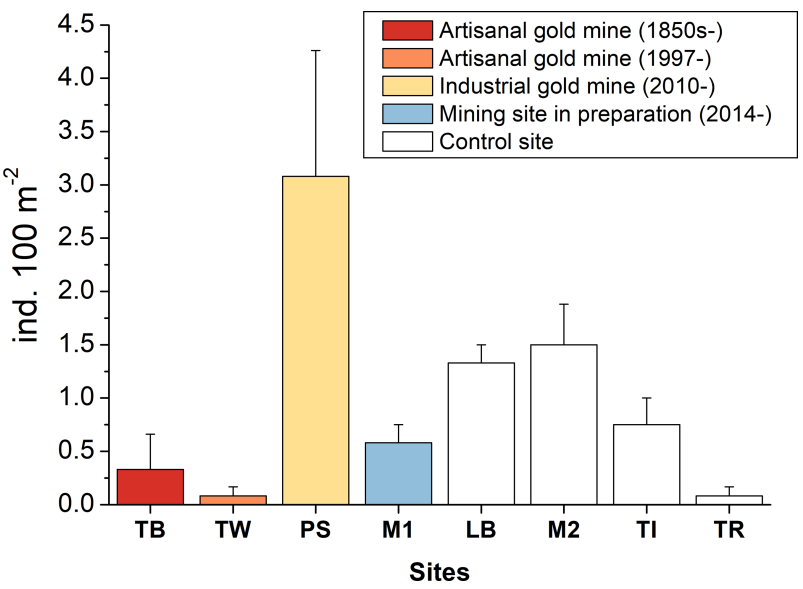

FIGURE 3 | Mean density (± s.e.) of *H. atra* at each study site: TB, Totok Bay; TW, Talawaan River; PS, Pantai Surabaya; M1, West Bangka mangroves; LB, Lihunu Bay; M2, North-west Bangka mangroves; TI, Tumbak Island; TR, Tasik Ria Resort.

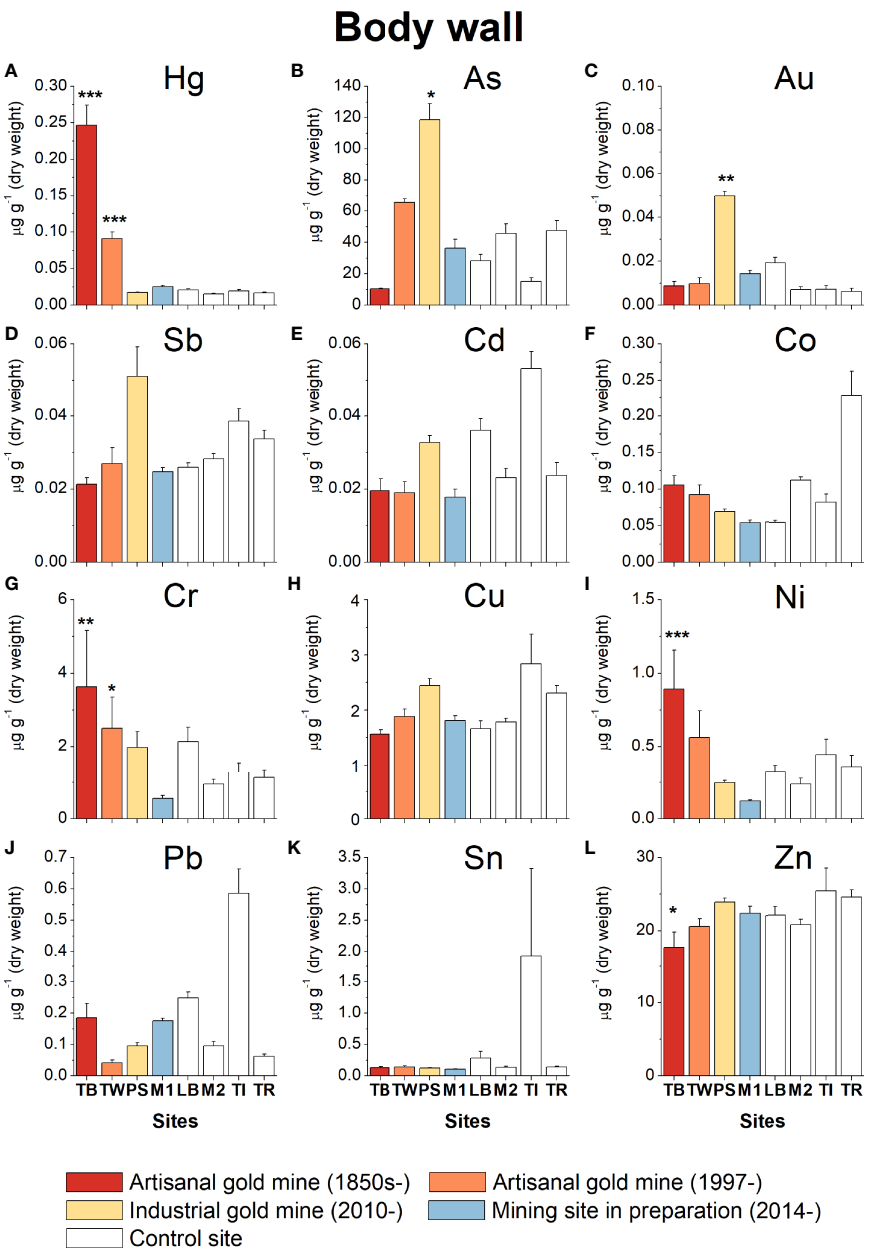

FIGURE 4 | Mean concentrations (± s.e.) in *H. atra* body wall of Hg **(A)**, As **(B)**, Au **(C)**, Sb **(D)**, Cd **(E)**, Co **(F)**, Cr **(G)**, Cu **(H)**, Ni **(I)**, Pb **(J)**, Sn **(K)** and Zn **(L)** at each study site (TB, Totok Bay; TW, Talawaan River; PS, Pantai Surabaya; M1, West Bangka mangroves; LB, Lihunu Bay; M2, North-west Bangka mangroves; TI, Tumbak Island; TR, Tasik Ria Resort). Impact sites that differ significantly from controls are marked with asterisks: $^{*}p < 0.05$; $^{**}p < 0.01$; $^{***}p < 0.001$.

(**Figure 5D**). Mean concentrations of Cd in body walls ranged from 0.018 ± 0.002 µg g^{-1} at M1 to 0.053 ± 0.005 µg g^{-1} at TI (**Figure 4E**), while in guts, they ranged from 0.25 ± 0.05 µg g^{-1} at TR to 1.06 ± 0.09 µg g^{-1} at PS (**Figure 5E**). Concentrations of this element in holothurian tissues were highly variable between sites, and no impact sites showed mean values significantly higher than controls. Mean concentrations of Co in body walls ranged from 0.054 ± 0.004 µg g^{-1} at M1 to 0.23 ± 0.03 µg g^{-1} at TR (**Figure 4F**), while in guts, they ranged from 0.14 ± 0.01 µg g^{-1} at LB to 1.14 ± 0.20 µg g^{-1} at TB (**Figure 5F**). Only at the old ASGM site TB, the mean concentration in the guts was significantly higher than at the controls. Mean concentrations of Cr in body walls ranged from 0.56 ± 0.08 µg g^{-1} at M1 to 3.63 ± 1.53 µg g^{-1} at TB, and they were significantly higher at ASGM sites, TB and TW, than at the control sites (**Figure 4G**). In guts, mean concentrations of Cr ranged from 1.84 ± 0.38 µg g^{-1} at M2 to 9.21 ± 1.92 µg g^{-1} at PS, and they were significantly higher at TB and PS than at the control sites (**Figure 5G**).

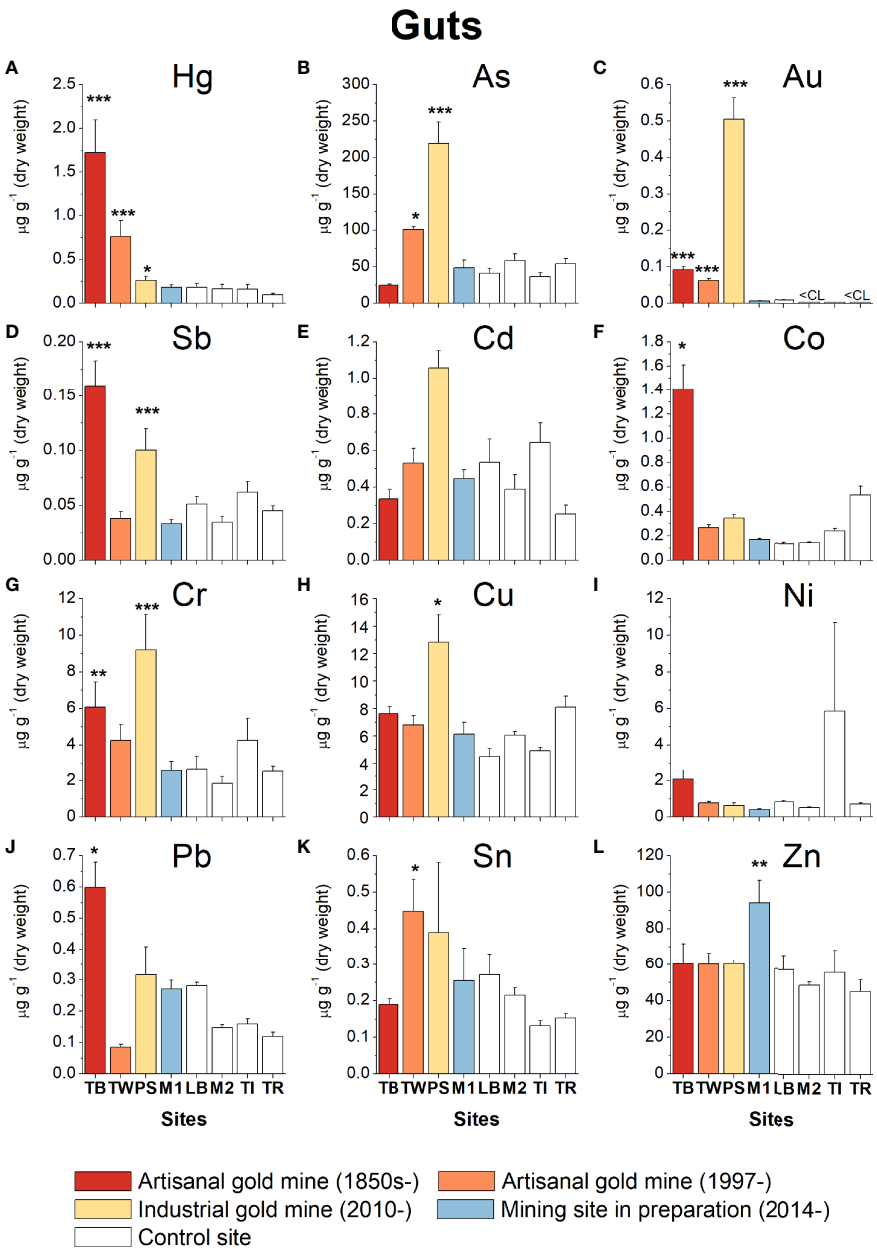

FIGURE 5 | Mean concentrations (± s.e.) in *H. atra* guts of Hg **(A)**, As **(B)**, Au **(C)**, Sb **(D)**, Cd **(E)**, Co **(F)**, Cr **(G)**, Cu **(H)**, Ni **(I)**, Pb **(J)**, Sn **(K)** and Zn **(L)** at each study site (TB, Totok Bay; TW, Talawaan River; PS, Pantai Surabaya; M1, West Bangka mangroves; LB, Lihunu Bay; M2, North-west Bangka mangroves; TI, Tumbak Island; TR, Tasik Ria Resort). Impact sites that differ significantly from controls are marked with asterisks: *$p < 0.05$; **$p < 0.01$; ***$p < 0.001$.

Mean concentrations of Cu in body walls ranged from 1.56 ± 0.08 µg g^{-1} at TB to 2.84 ± 0.54 µg g^{-1} at TI (**Figure 4H**), while in guts, they ranged from 4.50 ± 0.60 µg g^{-1} at LB to 12.84 ± 2.00 µg g^{-1} at PS (**Figure 5H**). Only at the industrial mine site PS, the mean concentration in the guts was significantly higher than at the controls. Mean concentrations of Ni in body walls ranged from 0.12 ± 0.01 µg g^{-1} at M1 to 0.89 ± 0.26 µg g^{-1} at TB, where the mean value was significantly higher than at the control sites (**Figure 4I**). In guts, mean concentrations of Ni ranged from 0.40 ± 0.04 µg g^{-1} at M1 to 5.86 ± 4.87 µg g^{-1} at control site TI, and no impact sites showed mean values significantly higher than controls (**Figure 5I**). Mean concentrations of Pb in body walls ranged from 0.04 ± 0.01 µg g^{-1} at TW to 0.59 ± 0.08 µg g^{-1} at control site TI (**Figure 4J**), while in guts, they ranged from 0.08 ± 0.01 µg g^{-1} at TW to 0.60 ± 0.08 µg g^{-1} at TB (**Figure 5J**). Only at the old ASGM site TB, the mean concentration in the guts was significantly higher than at the controls. Mean concentrations of Sn in body walls ranged from 0.11 ± 0.01 µg g^{-}

^{1} at M1 to 1.93 ± 1.40 μg g^{-1} at control site TI (**Figure 4K**), while in guts, they ranged from 0.13 ± 0.01 μg g^{-1} at TI to 0.45 ± 0.09 μg g^{-1} at TW (**Figure 5K**). Only at the ASGM site TW, the mean concentration in the guts was significantly higher than at the controls. Finally, mean concentrations of Zn in body walls ranged from 17.72 ± 2.09 μg g^{-1} at site TB to 25.36 ± 3.15 μg g^{-1} at TI, and at TB, the mean value was significantly lower than at the controls (**Figure 4L**). In guts, mean concentrations of Zn ranged from 45.62 ± 6.45 μg g^{-1} at TR to 94.16 ± 12.34 μg g^{-1} at M1, where was significantly higher than at the control sites (**Figure 5L**).

Trace Elements Bioaccumulation

The relationships between the mean concentrations of trace elements in sediments and holothurian tissues (body wall and guts) are shown in **Figure 6**, while Pearson's product-moment correlation coefficients (r) and corresponding t-tests for difference from zero are reported in **Table 1**. Significant positive correlations were found for the concentrations in the sediment and in *H. atra* tissues, body walls and guts, both for Hg and Cr, with very high correlation coefficients for Hg. Ni showed a significant, albeit weak, positive correlation between sediments and body walls, but not guts. As, Sb, Co and Cu exhibited

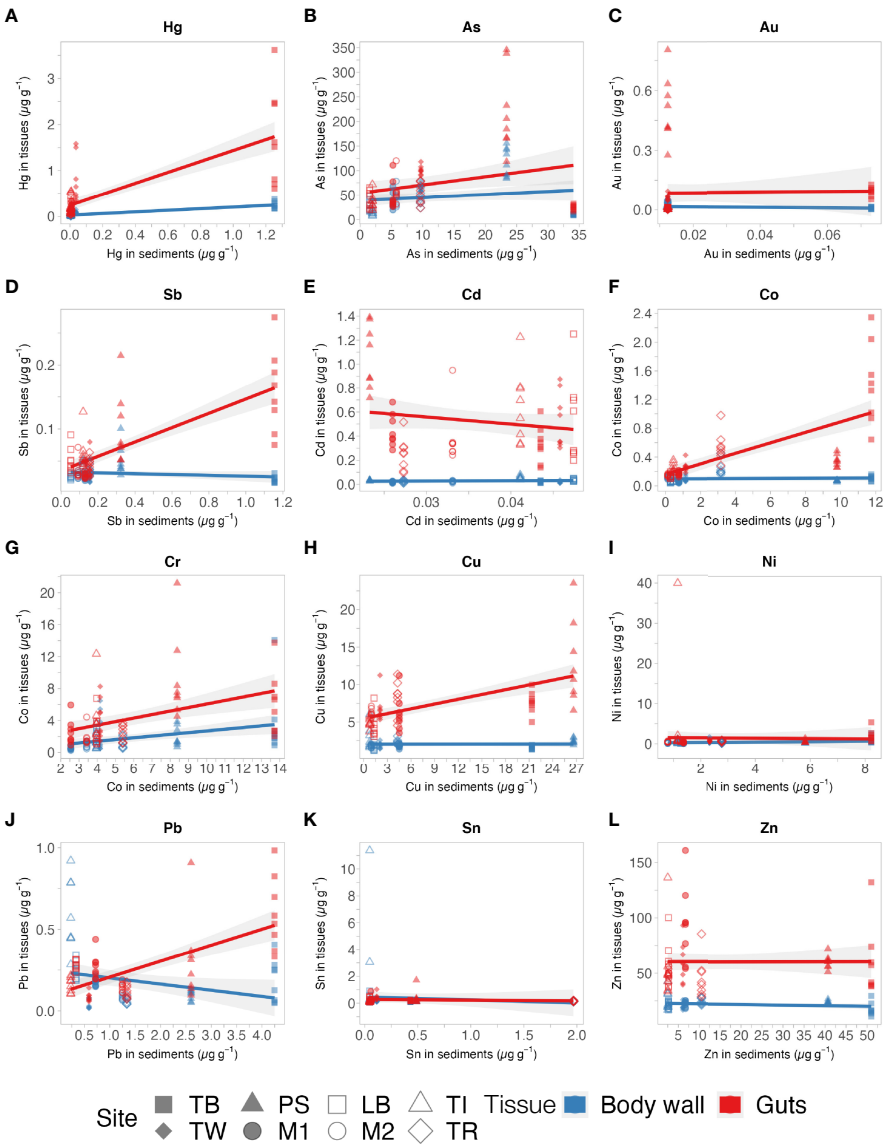

FIGURE 6 | Relations between the mean concentrations of Hg **(A)**, As **(B)**, Au **(C)**, Sb **(D)**, Cd **(E)**, Co **(F)**, Cr **(G)**, Cu **(H)**, Ni **(I)**, Pb **(J)**, Sn **(K)** and Zn **(L)** in sediments and their accumulation in holothurian tissues (blue: body wall, red: guts). Impact sites are represented by solid symbols (TB, Totok Bay; TW, Talawaan River; PS, Pantai Surabaya; M1, West Bangka mangroves), while control sites by open symbols (LB, Lihunu Bay; M2, North-west Bangka mangroves; TI, Tumbak Island; TR, Tasik Ria Resort). Lines indicate the linear tendencies, and the grey shadow areas the corresponding 95% confidence intervals.

significant positive correlations between sediments and guts, but not body walls. Pb had a weak but significant negative correlation between sediment and body wall, and a significant positive correlation between sediments and guts. The correlation between the concentration of gold between sediments and tissues was not significant, probably due to the finding in the sediments only at Totok Bay. Comparing the concentrations of trace elements in body walls and guts of single individuals, strong positive correlations were found for Hg, As, Au; moreover, weak but significant positive correlations were also detected for Sb, Cd, Co, and Ni (**Table 1**).

Bioaccumulation, assessed in terms of BSAF, largely varied among elements, sites, and tissues from 0.01 to 45.45 (**Table 2**). In general, higher values were obtained for guts compared to body walls. The most bioaccumulated element was Hg, whose BSAF resulted in greater than 1 at all sites except for body walls at Totok Bay. The second most accumulated element is As, with a BSAF greater than one at all sites except Totok Bay. The highest calculated BSAF is that of Cd in guts at Pantai Surabaya. BSAFs greater than 1 have also generally been found for Zn, especially in guts, and for Sn. The site showing lower BSAFs for the different elements was Totok Bay, while the sites with the highest ones were Tumbak Island for body walls and Pantai Surabaya for guts.

By averaging the BSAF values of each element across sites (**Table 2**; **Figure 7**), Hg, As and Zn significantly were bioaccumulated both in body walls and in guts in the study region. In addition, cadmium and copper were significantly bioaccumulated in the guts.

DISCUSSION

This study provides the first data on the concentration of trace elements in surface sediments and their bioaccumulation in *Holothuria* (*Halodeima*) *atra* in relation to different gold mining activities in North Sulawesi, Indonesia. Impact and control sites were chosen along the coast, analyzing drainage basins with and without mining activities. In particular, Totok Bay was affected by one of the oldest artisanal gold mines in the region, dating back to 1850's; the mouth of the Talawaan River was downstream to recent and active artisanal gold mines; Pantai Surabaya received drainage waters from a recent industrial gold mine; while the mangroves site at West Bangka was near a mine in preparation, officially closed the year the sampling was carried out, 2017.

At all study sites, surface sediments were mainly sandy with a high content of calcium, which may indicate a prevalent biogenic origin from surrounding coral reefs; however, at Totok Bay and Pantai Surabaya, chemical composition and finer particle size indicate a relevant terrigenous contribution. Control sites, randomly interspersed among impact ones, well represent the variety of sedimentary conditions and coastal habitats in the region. Origin, local depositional environment and mean grain size may have influenced the trace elements regimes in sediments (Li et al., 2017). In general, finer sediments can contain higher concentrations of trace elements than the coarser ones because of the larger surface-to-volume ratio (Amin et al., 2009). Nevertheless, the distribution patterns of some trace elements in the sediment appeared well related to mining activities; contamination generally ranking Totok Bay first, Pantai Surabaya second, Talawaan River third (but see high Hg values here), the mining site in preparation at Bangka Island fourth.

The trace element that deserves more attention and of greatest environmental concern is certainly mercury. Not detectable in the sediments at the control sites, it was found at all impact sites. The most polluted site was Totok Bay, downstream one of the oldest and active ASGM in the area. Here, the mean concentration exceeded that beyond which adverse biological effects on marine life are likely according to Australian guidelines on sediment quality (GV-high in Simpson et al., 2013), which are mostly based on the effects-range median (ERM) values proposed by Long et al. (1995). Lasut et al. (2010) found similar or even higher concentrations in the surface sediments sampled in this area in 2004.

The second site in order of sediment mercury pollution was at the Talawaan River mouth, downstream of a more recent ASGM.

TABLE 1 | Pearson's product-moment correlation coefficients (*r*) and corresponding *t*-tests for difference from zero of trace element concentrations between sediment (Sed) and body walls (BW) or guts (GU), and between body wall (BW) and guts (GU) (n = 64).

	Sed *vs* BW		Sed *vs* GU		BW *vs* GU	
	r	*t*-test	*r*	*t*-test	*r*	*t*-test
Hg	0.90	***	0.74	***	0.64	***
As	0.18	ns	0.27	**	0.91	***
Au	-0.17	ns	0.01	ns	0.85	***
Sb	-0.17	ns	0.74	***	0.21	*
Cd	0.16	ns	-0.17	ns	0.31	**
Co	0.05	ns	0.71	***	0.24	*
Cr	0.37	**	0.42	***	0.13	ns
Cu	0.01	ns	0.60	***	0.14	ns
Ni	0.36	**	-0.02	ns	0.23	*
Pb	-0.26	**	0.64	***	0.07	ns
Sn	-0.10	ns	-0.13	ns	-0.07	ns
Zn	-0.20	ns	0.00	ns	0.07	ns

*Significant levels were indicated by the following symbols: ns, not significant; *p < 0.05; **p < 0.01; ***p < 0.001.*

TABLE 2 | Biota-sediment accumulation factors (BSAFs) for each element in body wall (BW) and guts (GU) at each site: Totok Bay (TB); Talawaan River (TW); Pantai Surabaya (PS); West Bangka mangroves (M1); Lihunu Bay (LB); North-west Bangka mangroves (M2); Tumbak Island (TI); Tasik Ria Resort (TR).

Tissue	Site	Hg	As	Au	Sb	Cd	Co	Cr	Cu	Ni	Pb	Sn	Zn
BW	**TB**	0.20	0.30	0.12	0.02	0.45	0.01	0.26	0.07	0.11	0.04	0.30	0.35
	TW	2.51	6.75	0.79	0.17	0.41	0.08	0.60	0.91	0.24	0.07	1.27	3.38
	PS	2.07	5.08	4.01	0.16	1.41	0.01	0.24	0.09	0.04	0.04	0.25	0.59
	M1	2.71	6.91	1.15	0.19	0.68	0.07	0.22	0.40	0.09	0.24	1.92	3.35
	LB	4.37	18.41	1.56	0.50	0.76	0.20	0.54	1.28	0.26	0.75	6.04	8.31
	M2	3.24	7.94	0.57	0.31	0.70	0.89	0.28	1.85	0.30	0.08	2.17	7.64
	TI	4.07	7.69	0.58	0.32	1.30	0.19	0.32	3.76	0.38	2.53	41.17	10.18
	TR	3.52	4.93	0.50	0.22	0.87	0.07	0.21	0.54	0.13	0.05	0.07	2.33
Mean		**2.83**	**7.25**	1.16	0.24	0.82	0.19	0.33	1.11	0.19	0.47	6.65	**4.52**
***p*-value**		**0.003**	**0.005**	0.362	1.000	0.897	1.000	1.000	0.402	1.000	0.935	0.147	**0.016**
Tissue	**Site**	**Hg**	**As**	**Au**	**Sb**	**Cd**	**Co**	**Cr**	**Cu**	**Ni**	**Pb**	**Sn**	**Zn**
GU	**TB**	1.38	0.72	1.26	0.14	7.70	0.12	0.44	0.36	0.25	0.14	0.44	1.18
	TW	20.96	10.42	5.02	0.24	11.58	0.23	1.02	3.30	0.33	0.14	3.95	9.89
	PS	31.28	9.39	40.65	0.31	45.45	0.04	1.10	0.48	0.11	0.12	0.80	1.49
	M1	19.41	9.25	0.51	0.26	17.14	0.22	1.00	1.36	0.29	0.38	4.46	14.07
	LB	38.07	26.87	0.74	0.98	11.27	0.50	0.68	3.45	0.66	0.85	5.79	21.75
	M2	34.74	10.18	0.24	0.38	11.72	1.18	0.54	6.27	0.65	0.12	3.39	18.07
	TI	33.44	18.54	0.27	0.52	15.66	0.55	1.08	6.52	5.07	0.69	2.81	22.53
	TR	20.67	5.59	0.24	0.29	9.22	0.17	0.46	1.89	0.26	0.09	0.08	4.33
Mean		**24.99**	**11.37**	6.12	0.39	**16.22**	0.38	0.79	**2.95**	0.95	0.32	**2.72**	**11.67**
***p*-value**		**<0.001**	**0.004**	0.169	1.000	**0.005**	0.999	0.961	**0.028**	0.531	1.000	**0.026**	**0.005**

Mean among sites and p-values, under the null hypothesis that the mean is not greater than 1, are reported (significant values in bold).

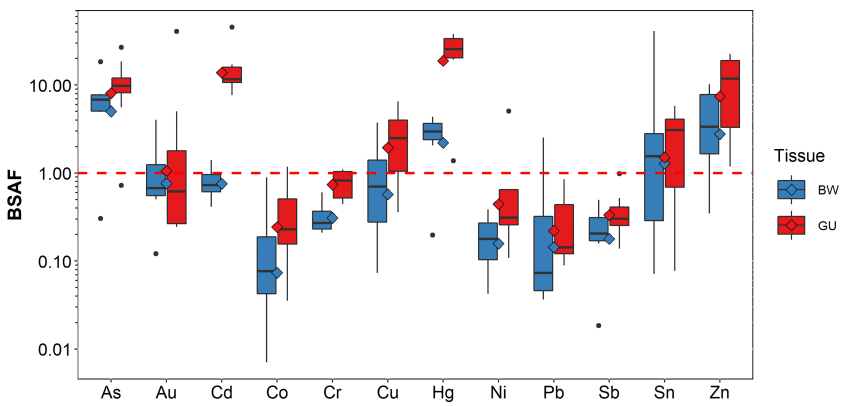

FIGURE 7 | Boxplots (median, interquartile, 1.5 interquartile and outliers) of the biota-sediment accumulation factors (BSAFs) for each element in body wall (BW, in blue) and guts (GU, in red) among sites. Mean values are also shown (diamond symbol).

In this case, the concentrations seem less concerning because lower than the default guideline value, therefore with a low risk of unacceptable effects on marine life. However, a previous study conducted along the Talawaan River in 2001 reported a sediment Hg concentration at the river mouth up to 200 times higher than in the present survey (Limbong et al., 2003), suggesting great spatial and/or temporal variability in this area. For both these sites, the release of mercury into the environment is most likely related to the artisanal method of gold mining, which employs Hg amalgamation. Although with lower concentrations than at the sites affected by ASGMs, high levels of mercury were also found in sediments at Pantai Surabaya, downstream of the industrial mine, and at the west Bangka mangroves, the mining site under preparation. Here, not using amalgamation, the mercury could be easily mobilized from the disposal of mining tailings and leaching of soil, probably rich in cinnabar (HgS) often associated with gold deposits in the region (Turner et al., 1994).

Mercury was always found in the holothurian tissues, both body walls and guts, at all study sites, including at the control sites, even where it was not detectable in the sediment. This suggests a high bioaccumulation capacity by *H. atra*, even at very low environmental concentrations, especially in guts, where the concentrations resulted about an order of magnitude higher than

in the body walls. On the other hand, BSAFs values were everywhere greater than 1, except in body walls at Totok Bay, and very high (usually > 20) for guts.

The second trace element of environmental concern is arsenic. Significant sediment enrichments, with values compatible with unacceptable negative biological effects on marine life according to the Australian guidelines on sediment quality (Simpson et al., 2013), primarily adapted from the original effects range-low (ERL) values provided by Long et al. (1995), were found at Totok Bay and Pantai Surabaya, downstream the two most active mines. Arsenic found in sediment may come from weathering of rocks associated with gold deposits in North Sulawesi, which are often rich in this element (Turner et al., 1994; Edinger et al., 2007). Ore processing for gold extraction can bring rocks disaggregation and the release of As in the river and eventually into the sea. In *H. atra*, higher concentrations than controls were measured in body walls at Pantai Surabaya and guts at Pantai Surabaya and Talawaan River. In this case, despite a strong correlation between the concentrations of the two tissues, with those of the guts about double, the concentrations in the tissues were not well correlated with those in the sediments, and it was found to be particularly low in the most polluted site (i.e., Totok Bay). Indeed, in terms of BSAF, bioaccumulation was largely greater than 1 both in body walls and guts at all sites except Totok Bay. Again, the bioaccumulation factors are always higher in guts than in body walls.

Although gold is the main target element of mining activities, small quantities can leak into the environment, especially where the extraction processes are less effective and/or have taken place longer. Not surprisingly, gold was found in detectable concentrations only in sediments from Totok Bay. However, *H. atra* has demonstrated a capacity for gold bioaccumulation in guts at all active mining sites (BSAF up to 40 at Pantai Surabaya), albeit without any correlation between tissue and sediment concentrations and no significant mean bioaccumulation across sites.

Antimony, cobalt, chromium, copper, nickel, and zinc are all consistently associated with gold deposits in North Sulawesi (Turner et al., 1994; Edinger et al., 2007). Significant sediment enrichments of these trace elements were found both at Totok Bay and Pantai Surabaya, downstream the two most active mines. Despite this, none of these trace elements showed concentrations above the Australian guideline values for sediment quality (Simpson et al., 2013), therefore no adverse biological effects on marine life are expected. Their concentration in *H. atra* tissues was always higher in guts than in body walls but variable case by case. Although Sb, Co, and Cr concentrations in guts were well correlated to those in sediments, they did not show bioaccumulation in the tissues. Ni was also not significantly bioaccumulated, while Cu showed some net bioaccumulation, especially in guts, regardless of mining activities in the area. Although with no correlations among concentrations in sediments and tissues, Zn showed significant bioaccumulation with locally very high BSAF values in guts, disregarding the presence of gold mines. Cadmium and tin didn't show any distribution pattern in sediment and tissues in relation to mine activities; however, Cd showed net bioaccumulation in guts at all sites with BSAF higher than 45 at Pantai Surabaya, downstream the industrial gold mine. Finally, although relatively abundant at Totok Bay and with concentrations in tissues well correlated with those in sediments, lead was not significantly bioaccumulated either in the body walls or in the guts.

H. atra, like many other holothurians, plays an essential ecological role in sediment bioturbation and mineralization, in the food web, and as a host of several organisms in symbiotic relationships (Purcell et al., 2016). Uthicke (1999) found that a single individual of *H. atra* daily ingests, on average, 67 g dry wt. of sediment. The author also estimated that a mixed population of *H. atra* and *Stichopus chloronotus* Brandt, 1835 was able to rework annually about 4600 kg dry wt. of sediment in 1000 m^2, mainly contributing to trace elements mobilization. At the study sites, the densities of *H. atra* (max 3 individual per 100 m^{-2}) were on average low when compared with other populations reported in Indonesia (up to 15 individual per 100 m^{-2}; Hartati et al., 2020; Luhulima et al., 2020), likely a result of intense local fishing. Holothurians, thanks to their feeding ecology and sediment bioturbation role (Purcell et al., 2016), low-mobility, large size, long lifespan, high abundance, and large geographical distribution, have been proposed as bioindicators and/or biomonitoring species (Storelli et al., 2001; Jinadasa et al., 2014; Aydın et al., 2017). Nevertheless, trace element contamination in holothurian species has been little investigated (see also Laboy-Nieves and Conde, 2001; Noël et al., 2011). This study and the previous ones agree that trace elements concentrations in guts were generally higher than in body walls (Denton et al., 2006; Denton et al., 2009; Ahmed et al., 2017; Gajdosechova et al., 2020). The concentrations of trace elements found in *H. atra* tissues at the impact sites of this study were higher than in the same tissues of the same species in other areas of the world, subject to different types of pollution (Denton et al., 2006; Denton et al., 2009).

Regardless of the presence of gold mines and sediment pollution levels, in the present study, *H. atra* has been shown to bioaccumulate some trace elements, mainly mercury, arsenic and zinc, and copper and cadmium in the guts, which had higher overall bioaccumulation factors. The large variability of bioaccumulation factors between sites suggests differences in the bioavailability of the trace elements, which is primarily due to local environmental conditions, water chemistry, and sedimentary regimes, but also the geochemical form of the elements (Thomann et al., 1995; McAloon and Mason, 2003; Sánchez-Donoso et al., 2021). The transport of trace elements from the substrate to the body wall and guts in holothurian is mainly unknown. Holothurian intestines have solubilization and bioaccumulation roles (McAloon and Mason, 2003); a generally lesser degree of accumulations of metals with different profiles in the body wall, compared to guts, could be due to a limited amount of metal-binding proteins (Tunca et al., 2016). Mercury intake in holothurians is probably a complexation process instead of an enzymatic one due to free amino acids produced by guts (Zhong and Wang, 2006). Although there is very little information on the

contribution of certain free amino acids to the overall intake by gut fluids of holothurians, cysteine was found to be a predominant binding ligand for Hg, because it extracts far more Hg from ingested sediment than any other amino acid (Zhong and Wang, 2006). Further investigations on the molecular transport pathways in *H. atra* could highlight the bioaccumulation mechanisms of trace elements in different tissues.

Possible Implications for Human Health

Through bioturbation and being the prey to many marine invertebrates and vertebrates (Purcell et al., 2016), holothurians can play a fundamental role in the transfer of trace elements from sediments to marine organisms, contributing to the biomagnification process in the upper levels of the food web, in which also human sooner or later is involved. In particular, *H. atra*, even though it has a comparatively low economic value, belongs to Indonesian commercial species (*trepang* or *trīpang*, in Indonesian; Purcell et al., 2012; Setyastuti and Purwati, 2015). In a few Pacific Island countries, the body wall, intestines and/or gonads are consumed in traditional diets or in times of hardship. However, most organisms are processed and exported for consumption, above all by Asians (Purcell et al., 2012). The main target markets are China and Hong Kong, but also Ho Chi Minh City in Viet Nam for further export to China. Although it trades at USD 2-20 per dried kg in the countries of origin, its retail price can be up to USD 210 per dried kg in Hong Kong (Purcell et al., 2012).

Although sea cucumbers usually have trace elements concentrations acceptable for human consumption at nutritional and toxicological levels (Wen and Hu, 2010), individuals of *H. atra* coming from coastal areas of the North Sulawesi impacted by inland mining activities might pose some risks. The toxicity of mercury largely depends on the chemical form in which it is taken; however, the World Health Organization (WHO) guidelines indicate a tolerable human intake of total mercury of 2 μg kg^{-1} body weight per day (Fisher, 2003), while the Europe Union sets a maximum level of 500 μg kg^{-1} wet weight in fishery products (Commission Regulation (EC) No 1881/2006). The mean Hg content in guts in individuals of *H. atra* from Totok Bay and Talawaan River exceeded these values, albeit in terms of dry weight. Unfortunately, neither the FAO/WHO (Codex Alimentarius Commission, 1995) nor the European Commission (EC) has human health-based standards or guidelines for arsenic in seafood. Australia and New Zealand have health-based guidelines providing maximum levels for inorganic arsenic in mollusks and fish (respectively 1000 and 2000 μg kg^{-1} wet weight; Stewart and Turnbull, 2015), while the US Food and Drug Administration (USFDA) set a less conservative limit of 76000 μg kg^{-1} dry weight (Wen and Hu, 2010). The mean arsenic content both in body walls and guts in individuals of *H. atra* exceeded the USFDA values at Pantai Surabaya and Talawaan River. The Europe Union (Commission Regulation (EC) No 1881/2006) also sets maximum levels in different fishery products for lead (500-1500 μg kg^{-1} wet weight) and cadmium (500-1000 μg kg^{-1} wet weight), which are higher than concentrations found in the present study. For the North Sulawesi populations, the greatest concern relates to the intake of mercury and arsenic from fish consumption (Bentley and Soebandrio, 2017); however, the risks of consuming other fishery products, including holothurians, should not be overlooked.

CONCLUSIONS

In the North Sulawesi, mercury resulted in the most concerning element found in surface sediment and *H. atra* specimens, followed by arsenic. Both were related to gold mining activities in the region, especially the oldest ASGMs, and were significantly bioaccumulated in the holothurian tissues, mainly in guts. However, further studies are needed to understand better the effect of mercury and other potentially toxic elements in marine ecosystems and trophic chains of impacted areas of North Sulawesi.

Indonesia is recognized by United Nations as the third country globally (after China and India) for Hg emission, with reports warning on mercury usage in ASGMs, which has significantly increased over the past two decades (Spiegel et al., 2018). A global treaty to protect human health and the environment from the adverse effects of Hg was agreed in 2013 – The Minamata Convention on Mercury (http://www.mercuryconvention.org). Indonesia signed this convention in 2013 and ratified it in 2017. However, recent increases in domestic Hg supplies through new cinnabar mining developments have made Hg less expensive and more available in Indonesia, increasing obstacles to implementing the Minamata Convention (Spiegel et al., 2018). Phasing out mercury amalgamation for gold extraction, regulating artisanal mining, and enforcing environmental regulations and regular seafood contamination monitoring must be a priority objective for Indonesia. In this regard, measuring trace elements in *H. atra* could be adopted in biomonitoring across the Indo-Pacific region.

DATA AVAILABILITY STATEMENT

The raw data supporting the conclusions of this article will be made available by the authors, without undue reservation.

AUTHOR CONTRIBUTIONS

Conceptualization: MP, ET; Formal analysis: MT, DB, ET, FG, LB, RG, PP, MP; Funding acquisition: MP, DB, PP, ML; Resources: MP, DB, PP, ML, FG, LB, RG, DM, JM; Visualization: ET, MT, MP; Writing – original draft: MT, ET, MP; Writing- review & editing: all authors. All authors contributed to the article and approved the submitted version.

FUNDING

ET benefited from a EuroMarine Young Scientist Fellowship by the OYSTER group within its programme for training.

ACKNOWLEDGMENTS

We would like to thank the staff at the Faculty of Fisheries and Marine Science, Sam Ratulangi University (UNSRAT, Manado, Indonesia), who supervised the research activities in Indonesia and supported visa applications for foreign colleagues. In addition, we would like to thank the staff of the Coral Eye (dive resort and marine outpost on Bangka Island) who assisted in the fieldwork. Research was carried out under the research permits from the Ministry of Research, Technology, and Higher Education in Indonesia to MP (n° 357/SIP/FRP/E5/Dit.KI/X/2018), ET (n° 358/SIP/FRP/E5/Dit.KI/X/2018) and GZ (n° 204/SIP/FRP/E5/Dit.KI/VII/2018). We kindly acknowledge the reviewers and the editor for the constructive comments that improved the quality of the manuscript.

SUPPLEMENTARY MATERIAL

The Supplementary Material for this article can be found online at: https://www.frontiersin.org/articles/10.3389/fmars.2022.863629/full#supplementary-material

REFERENCES

Ahmed, Q., Mohammad Ali, Q., and Bat, L. (2017). Assessment of Heavy Metals Concentration in Holothurians, Sediments and Water Samples From Coastal Areas of Pakistan (Northern Arabian Sea). *J. Coast.* 5 (5), 191–201. doi: 10.12980/jclm.5.2017J7-56

Amin, B., Ismail, A., Arshad, A., Yap, C. K., and Kamarudin, M. S. (2009). Anthropogenic Impacts on Heavy Metal Concentrations in the Coastal Sediments of Dumai, Indonesia. *Environ. Monit. Assess.* 148 (1-4), 291–305. doi: 10.1007/s10661-008-0159-z

Anderson, M. J., Gorley, R. N., and Clarke, K. R. (2008). *PERMANOVA+ for PRIMER: Guide to Software and Statistical Methods* (Plymouth, UK: PRIMER-E Ltd).

Anderson, M. J., and Robinson, J. (2008). Permutation Tests for Linear Models. *Aust. N. Z. J. Stat.* 43 (1), 75–88. doi: 10.1111/1467-842x.00156

Aydın, M., Tunca, E., and Alver Şahin, Ü. (2017). Effects of Anthropological Factors on the Metal Accumulation Profiles of Sea Cucumbers in Near Industrial and Residential Coastlines of İzmir, Turkey. *Int. J. Environ. Anal. Chem.* 97 (4), 368–382. doi: 10.1080/03067319.2017.1315112

Badocco, D., Lavagnini, I., Mondin, A., Favaro, G., and Pastore, P. (2015a). Definition of the Limit of Quantification in the Presence of Instrumental and non-Instrumental Errors. Comparison Among Various Definitions Applied to the Calibration of Zinc by Inductively Coupled Plasma–Mass Spectrometry. *Spectrochim. Acta B* 114, 81–86. doi: 10.1016/j.sab.2015.10.004

Badocco, D., Lavagnini, I., Mondin, A., and Pastore, P. (2014). Estimation of the Uncertainty of the Quantification Limit. *Spectrochim. Acta B* 96, 8–11. doi: 10.1016/j.sab.2014.03.013

Badocco, D., Lavagnini, I., Mondin, A., and Pastore, P. (2015b). Effect of Multiple Error Sources on the Calibration Uncertainty. *Food Chem.* 177, 147–151. doi: 10.1016/j.foodchem.2015.01.020

Badocco, D., Lavagnini, I., Mondin, A., Tapparo, A., and Pastore, P. (2015c). Limit of Detection in the Presence of Instrumental and non-Instrumental Errors: Study of the Possible Sources of Error and Application to the Analysis of 41 Elements at Trace Levels by Inductively Coupled Plasma-Mass Spectrometry Technique. *Spectrochim. Acta B* 107, 178–184. doi: 10.1016/j.sab.2015.03.009

Badr, N. B. E., El-Fiky, A. A., Mostafa, A. R., and Al-Mur, B. A. (2009). Metal Pollution Records in Core Sediments of Some Red Sea Coastal Areas, Kingdom of Saudi Arabia. *Environ. Monit. Assess.* 155 (1-4), 509–526. doi: 10.1007/s10661-008-0452-x

Bellchambers, L. M., Meeuwig, J. J., Evans, S. N., and Legendre, P. (2011). Modelling Habitat Associations of 14 Species of Holothurians From an Unfished Coral Atoll: Implications for Fisheries Management. *Aquat. Biol.* 14 (1), 57–66. doi: 10.3354/ab00381

Bentley, K., and Soebandrio, A. (2017). Dietary Exposure Assessment for Arsenic and Mercury Following Submarine Tailings Placement in Ratatotok Sub-District, North Sulawesi, Indonesia. *Environ. Pollut.* 227, 552–559. doi: 10.1016/j.envpol.2017.04.081

Birch, G. F., Lee, J. H., Tanner, E., Fortune, J., Munksgaard, N., Whitehead, J., et al. (2020). Sediment Metal Enrichment and Ecological Risk Assessment of Ten Ports and Estuaries in the World Harbours Project. *Mar. Pollut. Bull.* 155, 111129. doi: 10.1016/j.marpolbul.2020.111129

Blackwood, G. M., and Edinger, E. N. (2007). Mineralogy and Trace Element Relative Solubility Patterns of Shallow Marine Sediments Affected by Submarine Tailings Disposal and Artisanal Gold Mining, Buyat-Ratototok District, North Sulawesi, Indonesia. *Environ. Geol.* 52 (4), 803–818. doi: 10.1007/s00254-006-0517-5

Bose-O'Reilly, S., McCarty, K. M., Steckling, N., and Lettmeier, B. (2010). Mercury Exposure and Children's Health. *Curr. Probl. Pediatr. Adolesc. Health Care* 40 (8), 186–215. doi: 10.1016/j.cppeds.2010.07.002

Bryan, G. W., and Langston, W. J. (1992). Bioavailability, Accumulation and Effects of Heavy Metals in Sediments With Special Reference to United Kingdom Estuaries: A Review. *Environ. Pollut.* 76 (2), 89–131. doi: 10.1016/0269-7491(92)90099-v

Carrillo-González, R., Šimůnek, J., Sauvé, S., and Adriano, D. (2006). Mechanisms and Pathways of Trace Element Mobility in Soils. *Adv. Agron.* 91, 111–178. doi: 10.1016/S0065-2113(06)91003-7

Chen, M., and Ma, L. Q. (2001). Comparison of Three Aqua Regia Digestion Methods for Twenty Florida Soils. *Soil Sci. Soc. Am. J.* 65 (2), 491–499. doi: 10.2136/sssaj2001.652491x

Chojnacka, K., and Mikulewicz, M. (2014). "Bioaccumulation," in *Encyclopedia of Toxicology, 3rd ed.* Ed. P. Wexler (Oxford: Academic Press), 456–460.

Codex Alimentarius Commission (1995). *General Standard for Contaminants and Toxins in Food and Feed. CXS 193-1995* (Rome: Food and Agriculture Organization & World Health Organization of the United Nations).

Conand, C. (1998). "Holothurians (Sea Cucumbers, Class Holothuroidea)," in *FAO Species Identification Guide for Fishery Purposes. The Living Marine Resources of the Western Central Pacific. Vol. 2. Cephalopods, Crustaceans, Holothurians and Sharks*. Eds. K. E. Carpenter and V. H. Niem (Rome: International Union for Conservation of Nature - IUCN), 1157–1190.

Conand, C. (2004). Monitoring a Fissiparous Population of *Holothuria Atra* on a Fringing Reef on Reunion Island (Indian Ocean). *SPC Beche-de-mer Inf. Bull.* 20, 22–25.

Conand, C., Gamboa, R., and Purcell, S. (2013). *Holothuria Atra. The IUCN Red List of Threatened Species* (Rome: International Union for Conservation of Nature - IUCN).

Cordy, P., Veiga, M. M., Salih, I., Al-Saadi, S., Console, S., Garcia, O., et al. (2011). Mercury Contamination From Artisanal Gold Mining in Antioquia, Colombia: The World's Highest Per Capita Mercury Pollution. *Sci. Total Environ.* 410-411, 154–60. doi: 10.1016/j.scitotenv.2011.09.006

Denton, G. R. W., Concepcion, L. P., Wood, H. R., and Morrison, R. J. (2006). Trace Metals in Marine Organisms From Four Harbours in Guam. *Mar. Pollut. Bull.* 52 (12), 1784–1804. doi: 10.1016/j.marpolbul.2006.09.010

Denton, G. R. W., Morrison, R. J., Bearden, B. G., Houk, P., Starmer, J. A., and Wood, H. R. (2009). Impact of a Coastal Dump in a Tropical Lagoon on Trace Metal Concentrations in Surrounding Marine Biota: A Case Study From Saipan, Commonwealth of the Northern Mariana Islands (CNMI). *Mar. Pollut. Bull.* 58 (3), 424–431. doi: 10.1016/j.marpolbul.2008.11.029

Du Laing, G., Rinklebe, J., Vandecasteele, B., Meers, E., and Tack, F. M. G. (2009). Trace Metal Behaviour in Estuarine and Riverine Floodplain Soils and Sediments: A Review. *Sci. Total Environ.* 407 (13), 3972–3985. doi: 10.1016/j.scitotenv.2008.07.025

Edinger, E. (2012). Gold Mining and Submarine Tailings Disposal Review and Case Study. *Oceanography* 25 (2), 184–199. doi: 10.5670/oceanog.2012.54

Edinger, E. N., Siregar, P. R., and Blackwood, G. M. (2007). Heavy Metal Concentrations in Shallow Marine Sediments Affected by Submarine Tailings Disposal and Artisanal Gold Mining, Buyat-Ratototok District,

North Sulawesi, Indonesia. *Environ. Geol.* 52 (4), 701–714. doi: 10.1007/s00254-006-0506-8

Eto, K., Marumoto, M., and Takeya, M. (2010). The Pathology of Methylmercury Poisoning (Minamata Disease). *Neuropathology* 30 (5), 471–479. doi: 10.1111/j.1440-1789.2010.01119.x

Fisher, J. F. (2003). *Elemental Mercury and Inorganic Mercury Compounds: Human Health Aspects* (Geneva: World Health Organization & International Programme on Chemical Safety).

Futsaeter, G., and Wilson, S. (2013). The UNEP Global Mercury Assessment: Sources, Emissions and Transport. *E3S Web Conf.* 1, 36001. doi: 10.1051/e3sconf/20130136001

Gajdosechova, Z., Palmer, C. H., Dave, D., Jiao, G., Zhao, Y., Tan, Z., et al. (2020). Arsenic Speciation in Sea Cucumbers: Identification and Quantitation of Water-Extractable Species. *Environ. Pollut.* 266, 115190. doi: 10.1016/j.envpol.2020.115190

Gao, X., and Chen, C.-T. A. (2012). Heavy Metal Pollution Status in Surface Sediments of the Coastal Bohai Bay. *Water Res.* 46 (6), 1901–1911. doi: 10.1016/j.watres.2012.01.007

González-Merizalde, M. V., Menezes-Filho, J. A., Cruz-Erazo, C. T., Bermeo-Flores, S. A., Sánchez-Castillo, M. O., Hernández-Bonilla, D., et al. (2016). Manganese and Mercury Levels in Water, Sediments, and Children Living Near Gold-Mining Areas of the Nangaritza River Basin, Ecuadorian Amazon. *Arch. Environ. Con. Tox.* 71 (2), 171–182. doi: 10.1007/s00244-016-0285-5

González-Valoys, A. C., Arrocha, J., Monteza-Destro, T., Vargas-Lombardo, M., Esbrí, J. M., Garcia-Ordiales, E., et al. (2022). Environmental Challenges Related to Cyanidation in Central American Gold Mining; the Remance Mine (Panama). *J. Environ. Manage.* 302, 113979. doi: 10.1016/j.jenvman.2021.113979

Greggio, N., Capolupo, M., Donnini, F., Birke, M., Fabbri, E., and Dinelli, E. (2021). Integration of Physical, Geochemical and Biological Analyses as a Strategy for Coastal Lagoon Biomonitoring. *Mar. Pollut. Bull.* 164, 112005. doi: 10.1016/j.marpolbul.2021.112005

Guerra, R., Pasteris, A., and Ponti, M. (2009). Impacts of Maintenance Channel Dredging in a Northern Adriatic Coastal Lagoon. I: Effects on Sediment Properties, Contamination and Toxicity. *Estuar. Coast. Shelf Sci.* 85 (1), 134–142. doi: 10.1016/j.ecss.2009.05.021

Hartati, R., Zainuri, M., Ambariyanto, A., Redjeki, S., Riniatsih, I., Azizah, R., et al. (2019). Aseksual Reproduction of Black Sea Cucumber From Jepara Waters. *ILMU KELAUTAN: Indonesian J. Marine Sci.* 24 (3), 121. doi: 10.14710/ik.ijms.24.3.121-126

Hartati, R., Zainuri, M., Ambariyanto, A., Riniatsih, I., Endrawati, H., Redjeki, S., et al. (2020). Density and Population Growth of the Black Sea Cucumber, *Holothuria* (*Halodeima*) *Atra* (Jaege) in Two Different Microhabitats of Jepara Waters, Indonesia. *Eco. Env. Cons.* 26 (3), 1222–1227.

Jiang, X., Teng, A., Xu, W., and Liu, X. (2014). Distribution and Pollution Assessment of Heavy Metals in Surface Sediments in the Yellow Sea. *Mar. Pollut. Bull.* 83 (1), 366–375. doi: 10.1016/j.marpolbul.2014.03.020

Jinadasa, B. K. K. K., Samanthi, R. I., and Wicramsinghe, I. (2014). Trace Metal Accumulation in Tissue of Sea Cucumber Species; North-Western Sea of Sri Lanka. *Am. J. Public Health Res.* 2 (5A), 1–5. doi: 10.12691/ajphr-2-5A-1

Jonathan, M. P., Roy, P. D., Thangadurai, N., Srinivasalu, S., Rodríguez-Espinosa, P. F., Sarkar, S. K., et al. (2011). Metal Concentrations in Water and Sediments From Tourist Beaches of Acapulco, Mexico. *Mar. Pollut. Bull.* 62 (4), 845–850. doi: 10.1016/j.marpolbul.2011.02.042

Kambey, J. L., Farrell, A. P., and Bendell-Young, L. I. (2001). Influence of Illegal Gold Mining on Mercury Levels in Fish of North Sulawesi's Minahasa Peninsula, (Indonesia). *Environ. Pollut.* 114 (3), 299–302. doi: 10.1016/s0269-7491(01)00163-4

Laboy-Nieves, E. N., and Conde, J. E. (2001). Metal Levels in Eviscerated Tissue of Shallow-Water Deposit-Feeding Holothurians. *Hydrobiologia* 459 (1/3), 19–26. doi: 10.1023/a:1012589009243

Lasut, M. T., and Yasuda, Y. (2008). Accumulation of Mercury in Marine Biota of Buyat Bay, North Sulawesi, Indonesia. *Coast. Mar. Sci.* 32, 33–38.

Lasut, M. T., Yasuda, Y., Edinger, E. N., and Pangemanan, J. M. (2010). Distribution and Accumulation of Mercury Derived From Gold Mining in Marine Environment and its Impact on Residents of Buyat Bay, North Sulawesi, Indonesia. *Water Air Soil Pollut.* 208 (1-4), 153–164. doi: 10.1007/s11270-009-0155-0

Lavagnini, I., Badocco, D., Pastore, P., and Magno, F. (2011). Theil–Sen Nonparametric Regression Technique on Univariate Calibration, Inverse Regression and Detection Limits. *Talanta* 87, 180–188. doi: 10.1016/j.talanta.2011.09.059

Li, H., Kang, X., Li, X., Li, Q., Song, J., Jiao, N., et al. (2017). Heavy Metals in Surface Sediments Along the Weihai Coast, China: Distribution, Sources and Contamination Assessment. *Mar. Pollut. Bull.* 115 (1-2), 551–558. doi: 10.1016/j.marpolbul.2016.12.039

Limbong, D., Kumampung, J., Rimper, J., Arai, T., and Miyazaki, N. (2003). Emissions and Environmental Implications of Mercury From Artisanal Gold Mining in North Sulawesi, Indonesia. *Sci. Total Environ.* 302 (1), 227–236. doi: 10.1016/s0048-9697(02)00397-2

Long, E. R., and Chapman, P. M. (1985). A Sediment Quality Triad: Measures of Sediment Contamination, Toxicity and Infaunal Community Composition in Puget Sound. *Mar. Pollut. Bull.* 16 (10), 405–415. doi: 10.1016/0025-326x(85)90290-5

Long, E. R., Macdonald, D. D., Smith, S. L., and Calder, F. D. (1995). Incidence of Adverse Biological Effects Within Ranges of Chemical Concentrations in Marine and Estuarine Sediments. *Environ. Manage.* 19 (1), 81–97. doi: 10.1007/bf02472006

Luhulima, Y., Zamani, N. P., and Bengen, D. G. (2020). Density and Growth Pattern of Sea Cucumbers Holothuria Scabra, Holothuria Atra and Bohadchia Marmorata and Their Association With Seagrass in Coastal Area of Ambon, Saparua, Osi and Marsegu Island, Maluku Province. *Jurnal Ilmu Dan Teknol Kelautan Tropis* 12 (2), 541–554. doi: 10.29244/jitkt.v12i2.23454

Marmolejo-Rodríguez, A. J., Sánchez-Martínez, M. A., Romero-Guadarrama, J. A., Sánchez-González, A., and Magallanes-Ordóñez, V. R. (2011). Migration of As, Hg, Pb, and Zn in Arroyo Sediments From a Semiarid Coastal System Influenced by the Abandoned Gold Mining District at El Triunfo, Baja California Sur, Mexico. *J. Environ. Monit.* 13 (8), 2182. doi: 10.1039/c1em10058k

McAloon, K. M., and Mason, R. P. (2003). Investigations Into the Bioavailability and Bioaccumulation of Mercury and Other Trace Metals to the Sea Cucumber, *Sclerodactyla Briareus*, Using *In Vitro* Solubilization. *Mar. Pollut. Bull.* 46 (12), 1600–1608. doi: 10.1016/s0025-326x(03)00326-6

Murillo-Cisneros, D. A., O'Hara, T. M., Elorriaga-Verplancken, F. R., Sánchez-González, A., Marín-Enríquez, E., Marmolejo-Rodríguez, A. J., et al. (2019). Trophic Structure and Biomagnification of Total Mercury in Ray Species Within a Benthic Food Web. *Arch. Environ. Con. Tox.* 77 (3), 321–329. doi: 10.1007/s00244-019-00632-x

Noël, L., Testu, C., Chafey, C., Velge, P., and Guérin, T. (2011). Contamination Levels for Lead, Cadmium and Mercury in Marine Gastropods, Echinoderms and Tunicates. *Food Control* 22 (3-4), 433–437. doi: 10.1016/j.foodcont.2010.09.021

O'Brien, A. L., and Keough, M. J. (2014). Ecological Responses to Contamination: A Meta-Analysis of Experimental Marine Studies. *Environ. Pollut.* 195, 185–191. doi: 10.1016/j.envpol.2014.09.005

Odumo, B. O., Carbonell, G., Angeyo, H. K., Patel, J. P., Torrijos, M., and Rodríguez Martín, J. A. (2014). Impact of Gold Mining Associated With Mercury Contamination in Soil, Biota Sediments and Tailings in Kenya. *Environ. Sci. Pollut. Res.* 21 (21), 12426–12435. doi: 10.1007/s11356-014-3190-3

Oke, S., and Vermeulen, D. (2016). Geochemical Modeling and Remediation of Heavy Metals and Trace Elements From Artisanal Mines Discharge. *Soil Sediment Contam.* 26 (1), 84–95. doi: 10.1080/15320383.2017.1241216

Paschal, D. C., Ting, B. G., Morrow, J. C., Pirkle, J. L., Jackson, R. J., Sampson, E. J., et al. (1998). Trace Metals in Urine of United States Residents: Reference Range Concentrations. *Environ. Res.* 76 (1), 53–59. doi: 10.1006/enrs.1997.3793

Ponti, M., Fratangeli, F., Dondi, N., Segre Reinach, M., Serra, C., and Sweet, M. J. (2016). Baseline Reef Health Surveys at Bangka Island (North Sulawesi, Indonesia) Reveal New Threats. *PeerJ* 4, e2614. doi: 10.7717/peerj.2614

Ponti, M., Linares, C., Cerrano, C., Rodolfo-Metalpa, R., and XXXW, H. B. (2021). Editorial: Biogenic Reefs at Risk: Facing Globally Widespread Local Threats and Their Interaction With Climate Change. *Front. Mar. Sci.* 8. doi: 10.3389/fmars.2021.793038

Ponti, M., Pasteris, A., Guerra, R., and Abbiati, M. (2009). Impacts of Maintenance Channel Dredging in a Northern Adriatic Coastal Lagoon. II: Effects on

Macrobenthic Assemblages in Channels and Ponds. *Estuar. Coast. Shelf Sci.* 85 (1), 143–150. doi: 10.1016/j.ecss.2009.06.027

Purcell, S., Conand, C., Uthicke, S., and Byrne, M. (2016). Ecological Roles of Exploited Sea Cucumbers. *Oceanogr. Mar. Biol.* 54, 367–386. doi: 10.1201/9781315368597

Purcell, S. W., Samyn, Y., and Conand, C. (2012). "Commercially Important Sea Cucumbers of the World," in *FAO Species Catalogue for Fishery Purposes No. 6* (Rome: FAO).

QGIS Development Team (2021) *QGIS Geographic Information System Version 3.16.5 LTR*. Available at: http://qgis.osgeo.org (Accessed March 15, 2021).

Qian, Y., Zhang, W., Yu, L., and Feng, H. (2015). Metal Pollution in Coastal Sediments. *Curr. Pollut. Rep.* 1 (4), 203–219. doi: 10.1007/s40726-015-0018-9

Rainbow, P. S. (2002). Trace Metal Concentrations in Aquatic Invertebrates: Why and So What? *Environ. Pollut.* 120 (3), 497–507. doi: 10.1016/S0269-7491(02)00238-5

R Core Team (2021) *R: A Language and Environment for Statistical Computing Version 4.0.5*. Available at: https://www.r-project.org/ (Accessed March 31, 2021).

Retno, H., Ambariyanto, A., Widianingsih, W., and Muhammad, Z. (2020). Feeding Selectivity of *Holothuria Atra* in Different Microhabitat in Panjang Island, Jepara (Java, Indonesia). *Biodiversitas* 21 (5), 2233–2239. doi: 10.13057/biodiv/d210552

Sánchez-Donoso, R., García Lorenzo, M. L., Esbrí, J. M., García-Noguero, E. M., Higueras, P., and Crespo, E. (2021). Geochemical Characterization and Trace-Element Mobility Assessment for Metallic Mine Reclamation in Soils Affected by Mine Activities in the Iberian Pyrite Belt. *Geosciences* 11 (6), 233. doi: 10.3390/geosciences11060233

Sessitsch, A., Kuffner, M., Kidd, P., Vangronsveld, J., Wenzel, W. W., Fallmann, K., et al. (2013). The Role of Plant-Associated Bacteria in the Mobilization and Phytoextraction of Trace Elements in Contaminated Soils. *Soil Biol. Biochem.* 60, 182–194. doi: 10.1016/j.soilbio.2013.01.012

Setyastuti, A., and Purwati, P. (2015). Species List of Indonesian Trepang. *SPC Beche-de-mer Inf. Bull.* 35, 19–25.

Simpson, S. L., Batley, G. B., and Chariton, A. A. (2013). "Revision of the ANZECC/ARMCANZ Sediment Quality Guidelines," in *CSIRO Land and Water Science Report 08/07*. (Canberra:CSIRO Land and Water)

Spiegel, S. J., Agrawal, S., Mikha, D., Vitamerry, K., Le Billon, P., Veiga, M., et al. (2018). Phasing Out Mercury? Ecological Economics and Indonesia's Small-Scale Gold Mining Sector. *Ecol. Econ.* 144, 1–11. doi: 10.1016/j.ecolecon.2017.07.025

Stewart, I., and Turnbull, A. (2015). *Arsenic in Australian Seafood: A Review and Analysis of Monitoring Data 2000 - 2013* (Adelaide, Australia: South Australian Research and Development Institute).

Storelli, M. M., Storelli, A., and Marcotrigiano, G. O. (2001). Heavy Metals in the Aquatic Environment of the Southern Adriatic Sea, Italy: Macroalgae, Sediments and Benthic Species. *Environ. Int.* 26 (7-8), 505–509. doi: 10.1016/s0160-4120(01)00034-4

Thomann, R. V., Mahony, J. D., and Mueller, R. (1995). Steady-State Model of Biota Sediment Accumulation Factor for Metals in Two Marine Bivalves. *Environ. Toxicol. Chem.* 14 (11), 1989–1998. doi: 10.1002/etc.5620141121

Toral-Granda, V., Lovatelli, A., and Vasconcellos, M. (2008). "Sea Cucumbers. A Global Review of Fisheries and Trade," in *FAO Fisheries and Aquaculture Technical Paper. No. 516* (Rome: FAO).

Tunca, E., Aydın, M., and Şahin, Ü. (2016). Interactions and Accumulation Differences of Metal(Loid)s in Three Sea Cucumber Species Collected From the Northern Mediterranean Sea. *Environ. Sci. Pollut. Res.* 23 (20), 21020–21031. doi: 10.1007/s11356-016-7288-7

Turner, S. J., Flindell, P. A., Hendri, D., Hardjana, I., Lauricella, P. F., Lindsay, R. P., et al. (1994). Sediment-Hosted Gold Mineralisation in the Ratatotok District, North Sulawesi, Indonesia. *J. Geochem. Explor.* 50 (1-3), 317–336. doi: 10.1016/0375-6742(94)90029-9

Uthicke, S. (1999). Sediment Bioturbation and Impact of Feeding Activity of *Holothuria* (*Halodeima*) *Atra* and *Stichopus Chloronotus*, Two Sediment Feeding Holothurians, at Lizard Island, Great Barrier Reef. *Bull. Mar. Sci.* 64 (1), 129–141.

Velásquez-López, P. C., Veiga, M. M., and Hall, K. (2010). Mercury Balance in Amalgamation in Artisanal and Small-Scale Gold Mining: Identifying Strategies for Reducing Environmental Pollution in Portovelo-Zaruma, Ecuador. *J. Clean. Prod.* 18 (3), 226–232. doi: 10.1016/j.jclepro.2009.10.010

Veron, J. E. N., Devantier, L. M., Turak, E., Green, A. L., Kininmonth, S., Stafford-Smith, M., et al. (2009). Delineating the Coral Triangle. *Galaxea* 11 (2), 91–100. doi: 10.3755/galaxea.11.91

Wang, W. X. (2002). Interactions of Trace Metals and Different Marine Food Chains. *Mar. Ecol. Prog. Ser.* 243, 295–309. doi: 10.3354/meps243295

Wen, J., and Hu, C. (2010). Elemental Composition of Commercial Sea Cucumbers (Holothurians). *Food Addit. Contam. B* 3 (4), 246–252. doi: 10.1080/19393210.2010.520340

Xing, J., and Chia, F.-S. (1997). Heavy Metal Accumulation in Tissue/Organs of a Sea Cucumber, *Holothuria Leucospilota*. *Hydrobiologia* 352 (1/3), 17–23. doi: 10.1023/a:1003028601518

Zhong, H., and Wang, W.-X. (2006). Sediment-Bound Inorganic Hg Extraction Mechanisms in the Gut Fluids of Marine Deposit Feeders. *Environ. Sci. Technol.* 40 (19), 6181–6186. doi: 10.1021/es061195z

Conflict of Interest: The authors declare that the research was conducted in the absence of any commercial or financial relationships that could be construed as a potential conflict of interest.

Publisher's Note: All claims expressed in this article are solely those of the authors and do not necessarily represent those of their affiliated organizations, or those of the publisher, the editors and the reviewers. Any product that may be evaluated in this article, or claim that may be made by its manufacturer, is not guaranteed or endorsed by the publisher.

Citation: *Tamburini M, Badocco D, Ercadi R, Turicchia E, Zampa G, Gasparini F, Ballarin L, Guerra R, Lasut MT, Makapedua DM, Mamuaja J, Pastore P and Ponti M (2022) Bioaccumulation of Mercury and Other Trace Elements in the Edible Holothurian Holothuria (Halodeima) atra in Relation to Gold Mining Activities in North Sulawesi, Indonesia.*
Front. Mar. Sci. 9:863629. doi: 10.3389/fmars.2022.863629

Advantages of publishing in Frontiers

OPEN ACCESS
Articles are free to read for greatest visibility and readership

FAST PUBLICATION
Around 90 days from submission to decision

HIGH QUALITY PEER-REVIEW
Rigorous, collaborative, and constructive peer-review

TRANSPARENT PEER-REVIEW
Editors and reviewers acknowledged by name on published articles

Frontiers
Avenue du Tribunal-Fédéral 34
1005 Lausanne | Switzerland

Visit us: www.frontiersin.org
Contact us: frontiersin.org/about/contact

REPRODUCIBILITY OF RESEARCH
Support open data and methods to enhance research reproducibility

DIGITAL PUBLISHING
Articles designed for optimal readership across devices

FOLLOW US
@frontiersin

IMPACT METRICS
Advanced article metrics track visibility across digital media

EXTENSIVE PROMOTION
Marketing and promotion of impactful research

LOOP RESEARCH NETWORK
Our network increases your article's readership